University of Southampton

Faculty of Environmental and Life Sciences

School of Biological Sciences

Factors Influencing the Three-Dimensional Structure of Urinary Biofilms

by

Nany Malissa binti Rahimi

ORCID ID 0000-0003-1970-2128

Thesis for the degree of Doctor of Philosophy

August 2019

University of Southampton

Abstract

Faculty of Environmental and Life Sciences

School of Biological Sciences

Thesis for the degree of Doctor of Philosophy

Factors Influencing the Three-Dimensional Structure of Urinary Biofilms

by

Nany Malissa binti Rahimi

Catheter-associated urinary tract infection is the most common type of urinary tract infection among healthcare-associated infections that are caused by biofilms developing on the catheter. The study aims to investigate the urinary biofilm characteristics and the genes associated with the biofilm formation on the urinary catheter.

Rapid cell attachment occurred as early as 1 h showed that the artificial urine medium supports biofilm growth of uropathogens. AUBK is the most physicochemically similar artificial urine media to urine that promoted better biofilm development on the urinary catheter compared to other laboratory media. *Pseudomonas aeruginosa* PAO1 is studied as a model organism for urinary biofilm to describe the biofilm development common traits, including the initial attachment, aggregation of cells, and the build-up of microcolonies surrounded by the extracellular polymeric substances. Screening of urease, quorum-sensing, polysaccharide and attachment/motility gene mutants showed that the involvement of the genes differs at different stages of biofilm development.

Mutants of *rhlB*, *pelA*, *pslD*, *fliC*, *fliM*, *pilA* biofilm were affected at 1 h during essential initial cell adherence that prevents cells from returning to the planktonic state. Mutants with *lasI*, *rhlI*, *pqsA*, *pqsE* and *fliC* produced flat biofilms instead of the characteristic three-dimensional mature biofilm at 24 h, showingthat biofilm was unable to differentiate into mature biofilms without cell-signalling and flagella-mediated motility. Biofilms of urease and alginate gene-deficient mutants were not affected and had no significant role in urinary biofilm. We also discovered a new, unreported unique feature in the *P. aeruginosa* PAO1 urinary biofilm formation that mediates cell translocation to the nearest microcolony, observed at 1 h and 3 h timepoints.

This study highlights the roles of essential genes in biofilm formation as well as the need to use appropriate artificial urine medium in the urinary biofilm studies as nutrient availability impacts profoundly on urinary biofilm growth and development.

Table of Contents

Table of Tables

Table of Tables

Table of Figures

Table of Figures

Table of Figures

Table of Figures

Research Thesis: Declaration of Authorship

Print name:	Nany Malissa binti Rahimi

Title of thesis:	Factors influencing the three-dimensional structure of urinary biofilms

I declare that this thesis and the work presented in it are my own and has been generated by me as the result of my own original research.

I confirm that:

1. This work was done wholly or mainly while in candidature for a research degree at this University;
2. Where any part of this thesis has previously been submitted for a degree or any other qualification at this University or any other institution, this has been clearly stated;
3. Where I have consulted the published work of others, this is always clearly attributed;
4. Where I have quoted from the work of others, the source is always given. With the exception of such quotations, this thesis is entirely my own work;
5. I have acknowledged all main sources of help;
6. Where the thesis is based on work done by myself jointly with others, I have made clear exactly what was done by others and what I have contributed myself;
7. None of this work has been published before submission

Signature:		Date:	

Acknowledgements

Firstly, I would like to express my highest praise, and sincerest gratitude to the Almighty for all the blessing received throughout my life and for giving me the efforts to finish this thesis successfully. Additionally, I would like to gratefully acknowledge the funding received towards my PhD from the Commonwealth Scholarship Commission in the UK (CSC).

My highest appreciation is dedicated to my two respected supervisors, Professor Bill Keevil and Dr Sandra Wilks, for their expertise, wisdom, and patience throughout each stage, not to mention the invaluable guidance, suggestions, continued support and constant encouragement that has substantially helped me with my studies as well as in other aspects of my life throughout these years. I am eternally grateful to receive this profound learning experience as well as an honour to have worked under their supervision.

I am greatly indebted and thankful to the brilliant Dr Catherine Bryant, who has been kind, encouraging, and helped me in the lab as well as during the completion of my thesis. To the people who have made this PhD an enjoyable journey; my friends and colleagues at the University of Southampton, especially the excellent company from Keevil group and Webb group that provide great fun to work and play with during the duration of my PhD.

Next, is the most important group of people that I wish to immortalise in this acknowledgement, which is my family.

I am forever grateful to my wonderful husband, Suhaimi, who have gone above and beyond in supporting me pursuing my studies. I am lucky to have the most excellent companion beside me in my eventful PhD journey, at the same time providing me love and endless care. Thank you for being patient, understanding, and sacrificing a lot for our family and me. It will be my lifelong promise to payback for the times you had to endure all the sufferings these past years due to my studies. I can never imagine being able to reach this stage without you in my life. To my children Dahlia, Azhar and Ishaq, I am thankful for all the prayers you made for me, your patience and understanding in my inadequacies in your growing years. You have been my source of motivation to work harder, and it has always been a joy to have you as a blessing in my life.

To my beloved Ibu and Papa, of which I cherish, for all the love and care you have given that made me who I am today. Your selflessness in providing constant support, as well as your unfaltering belief in me, which gave me wings to achieve my dreams.

To my in-laws; Mama Noridah, Maryam, Hazwan, Aida, Norita and Hazwan, for being understanding in our lack of presence in family events, and for being the pillars of strength to my husband and me, for always supported me in all my endeavours.

To my extended families; Mama Roseniah, Ummi, Mama Uda, Pakwe, Rozeleen Rahim, and Nadiah Umno for always believing in me, motivating me and praying for my success.

I want to give my exceptional thanks to the amazing people in my life; Professor Halimaton Hamdan, Daud Oi, Haziqah Zulaikha, Melissa Mohamed, Azura Dahalan, Nureen Sudirman and Nur Albi Shahrir. I am indebted with all their continuous support, encouragement and companionship during all these times and for everything.

I would like to express my appreciation to all the people that I might not mention, from the bottom of my heart, thank you so much for all your help to my family and me.

Finally, I would like to say my thanks to the people who have left this world. To my late father, Ayah, for your constant love and consent in allowing me to pursue my dreams; my late father-in-law, Bapak, for his encouragement and blessing; and lastly to my grandmother, Atuk, my voice of reason, which not a day goes by without me thinking about you. You are missed more than you could imagine.

Definitions and Abbreviations

HCAI	Healthcare-associated Infection
CAUTI	Catheter-associated Urinary Tract Infection
UTI	Urinary Tract Infection
AUR	Acute urinary retention
UPEC	Uropathogenic *Escherichia coli*
cfu	Colony forming unit
EPS	Extracellular polymeric substances
SEM	Scanning electron microscopy
ESEM	Environmental scanning electron microscopy
CLSM	Confocal laser scanning microscopy
DIC	Differential interference contrast
EDIC	Episcopic differential interference contrast
EF	Epifluorescence
SCLM	Scanning Confocal Laser Microscopy
QS	Quorum-sensing
AHL	N-Acyl-homoserine lactones
eDNA	extracellular DNA
CF	Cystic fibrosis
DAPI	4,6-diamidino-2-phenylindole
ConA	Concanavalin A
UF	Ultrafiltered
AUM	Artificial Urine Medium
LB	Luria Bertani Broth
NB	Nutrient Broth
TSB	Trypticase Soy Broth
TSA	Tryptone Soya Agar
CLED	Cystine Lactose Electrolyte Deficient
AUBK	Artificial Urine Medium Brooks & Keevil, 1997
AUG	Artificial Urine Medium Griffiths *et al*., 1976
PBS	Phosphate-Buffered Saline
dsDNA	Double strand DNA
PI	Propidium iodide
ADI	Arginine Deiminase pathway
PS	polysaccharide
AI	Autoinducers

Chapter 1 Introduction

1.1 Thesis outline structure

The research was undertaken in the pursuit to understand the factors influencing the three-dimensional structure in contaminating urinary biofilms. The outline of this thesis is structured, as shown in Figure 1-1 below.

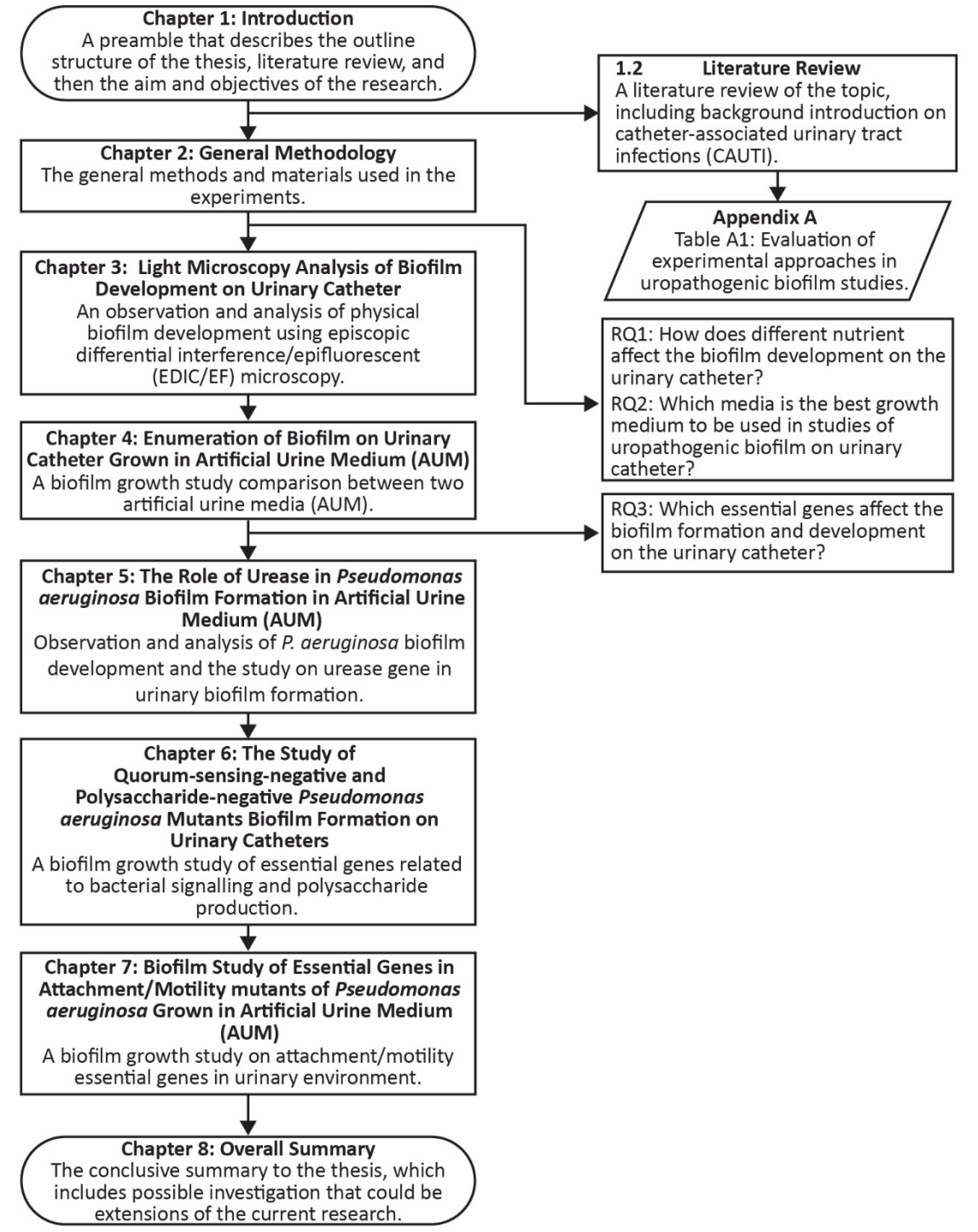

Figure 1-1 Structure of this thesis (RQ = research questions).

Chapter 1 consists of an outline structure of this thesis (Figure 1-1), presents the aim and objectives, and a literature review of the research. The literature review includes background information on healthcare-associated infections (HCAI); catheter-associated urinary tract infection (CAUTI); an introduction to biofilm and urinary biofilm development; commonly used growth media; and lastly, *Pseudomonas aeruginosa* as a model organism in urinary biofilms past studies.

General methods and the materials used in this research are described in Chapter 2, which describes the culture maintenance and inocula preparation; preparation of relevant media used; the sample preparation for microscopy, and the experimental design of static biofilm growth method using 6-well plates.

Chapter 3 and Chapter 4 contain the preliminary background work done in this study. It consists of microscopy observations and biofilm enumeration analysis to study the temporal development of common uropathogens, *Escherichia coli*, *Proteus mirabilis* and *P. aeruginosa* biofilms on the urinary catheter.

By using *P. aeruginosa* as a model organism, the roles of different essential genes in biofilm formation are studied and conducted as a three-part series in Chapter 5, Chapter 6, and Chapter 7. Chapter 8 presents the overall summary of our findings, as well as discussing the research limitations and future research plans following this study. This chapter ends with the concluding remarks for the thesis.

1.2 Literature review

1.2.1 Introduction to healthcare-associated infections (HCAI)

Healthcare-associated infection is a severe prevalent healthcare problem happening worldwide (World Health Organization 2011). The term healthcare-associated infection (HCAI) is commonly used compared to the previously adopted term nosocomial infections. HCAI includes infection-related incidents from various healthcare facilities other than the hospital, including hospices and elderly care homes (Cardoso *et al.* 2014).

Patients staying at these healthcare facilities are exposed to the risk of contracting HCAI through treatment procedures, improper healthcare management, inadequate training, or poor environmental setting (Collins 2008). Instead of benefiting from the treatment received at these facilities, some patients have acquired HCAI during their admission. Contracting HCAI poses further threat to patients' health by offsetting their recovery process and often complicates the treatment course (World Health Organization 2011).

HCAI is a notable financial burden to patients and the government as it increases the direct and secondary cost of therapy. The direct cost refers to medical related treatment during the admission of the patients such as medication and the length of stay. Indirect cost would be the non-medical cost of excess treatment in ineffective antibiotic in resistant bacteria infection and extended length of stay(Saint 2000; Jacobsen *et al.* 2008; Mittal *et al.* 2010). The cost implicated by HCAI is approximately 5 billion pounds per annum in the United States, and the estimated cost in the United Kingdom is 1 billion pounds per annum (National Patient Safety Agency 2004; World Health Organization 2011). This is due to the excessive bed-days and the additional procedures or medication prescribed to treat or prevent the HCAI infection (Tambyah *et al.* 1999; World Health Organization 2011; King *et al.* 2012).

The alarming global occurrences of HCAI have been reported by World Health Organization (2011) to have higher incidences in middle to low-income countries compared to high-income countries (Figure 1-2). The increasing incidences of HCAI are closely associated with the use of invasive medical devices due to biofilm formation on the medical devices' surface (Costerton *et al.* 1999; Collins 2008; Denstedt and Cadieux 2009; Azevedo *et al.* 2014). The most significant and leading contributor of HCAI cases worldwide is the use of indwelling urinary catheters. Long-term patients, patients with acute urinary retention (AUR), or patients with neurological illness often use the indwelling urinary catheters, which then put them at risk of getting urinary tract infections (UTI) (Saint 2000; Greene *et al.* 2008; King *et al.* 2012).

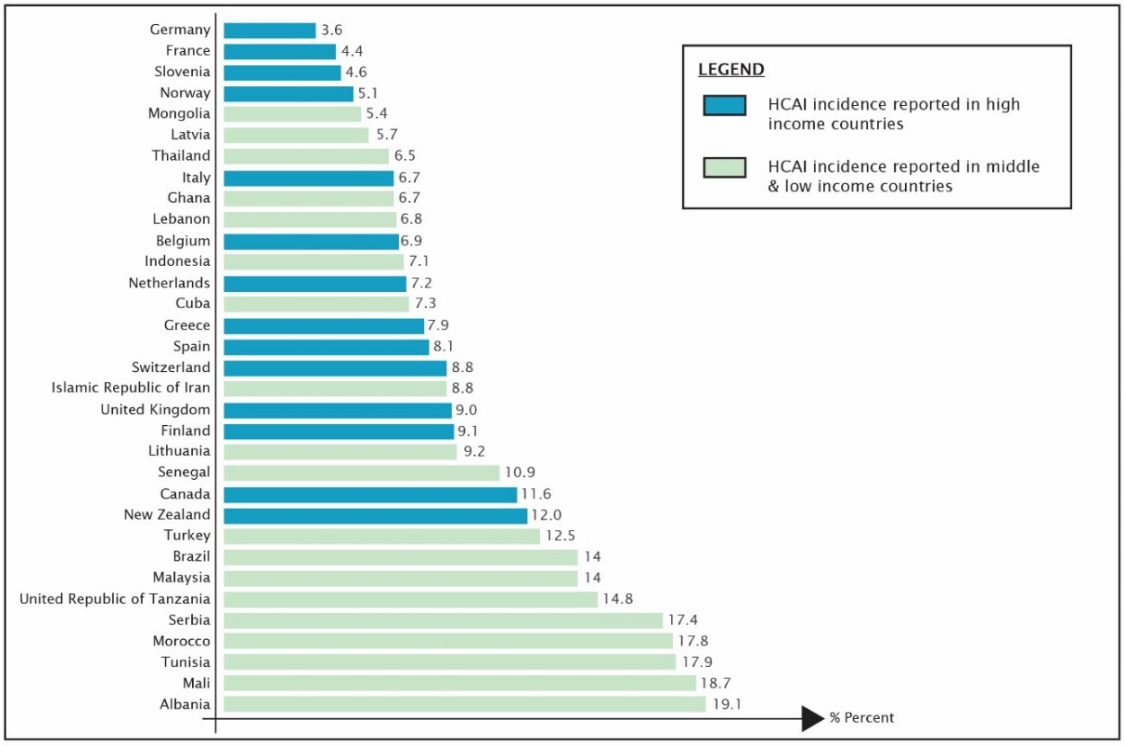

Figure 1-2 Ascending order of HCAI incidences reported in high (blue) and middle to low-income countries (green).

1.2.2 Urinary tract infection (UTI)

Urinary tract infection (UTI) is one of the most common bacterial infections and is a serious health problem in public health that affects millions of people each year (Stamm and Norrby 2001; Greene *et al.* 2008). At twenty per cent (20 %), it is the second-highest contributor of HCAI cases in the United Kingdom, costing 68 million pounds with about 66 160 cases annually (King *et al.* 2012). The annual estimation of UTI is 150 million cases worldwide (Stamm and Norrby 2001).

The differences between the two classifications of UTI, which are complicated UTI and uncomplicated UTI, depend on various factors contributing to the disease and the well-being of the patient (Flores-Mireles *et al.* 2015). Figure 1-3 is a pie chart of common uropathogens found in complicated and uncomplicated UTI and the risk factors associated with it.

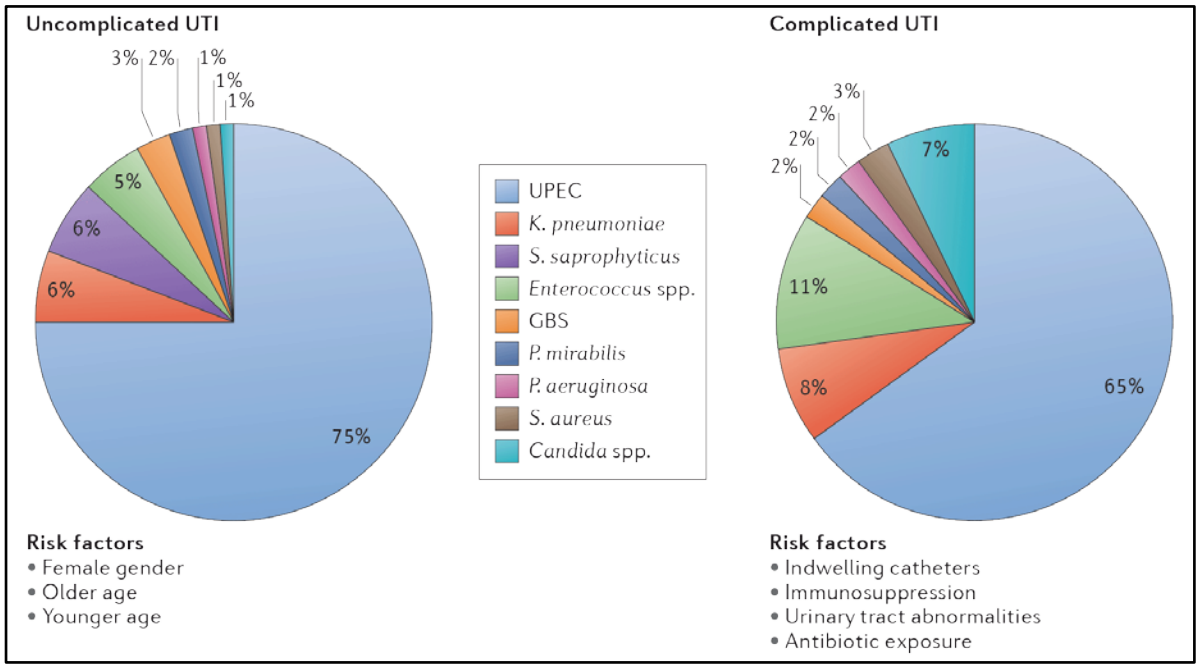

Figure 1-3 Epidemiology of urinary tract infections. Adapted from Flores-Mireles *et al.* (2015)

The uropathogenic *Escherichia coli* (UPEC) is the most common species found in both complicated and uncomplicated UTI, with sixty-five per cent (65 %) and seventy-five per cent (75 %) of infections, respectively. Uncomplicated UTI is associated with both older or younger patients and present more risk to female patients compared to male. Complicated UTI increases health risk to patients with indwelling catheters in place, or immunocompromised patients, among other factors (Kohler-Ockmore and Feneley 1996; Greene *et al.* 2008; Ramanathan and Duane 2014; Flores-Mireles *et al.* 2015).

UTI interaction between pathogen and host usually occur asymptomatically, but often result in severe symptomatic bacteriuria. The common symptoms are fever, frequent urge to urinate or frequent urination (which also includes uncontrollable urination) and burning sensation or painful urination. Asymptomatic UTI often occurs in healthy people, diagnosed through the presence of

abnormal numbers of microorganisms in urine sample cultures. While asymptomatic UTI patients may appear physically well, the infection can cause serious kidney complication if left untreated (Flores-Mireles *et al.* 2015).

1.2.3 Catheter-associated urinary tract infection (CAUTI)

A urinary catheter is an invasive medical device that was designed to help in emptying the patients' bladder and monitor urine output (Rosdahl and Kowalski 2011). Healthcare-associated catheter-associated urinary tract infections (CAUTI) are UTI that was promoted by the catheterisation of the patients' urinary bladder during their stay at the healthcare facility (Velraeds *et al.* 1998; Simhi *et al.* 2000; Stickler 2002; Armbruster *et al.* 2017).

The procedure increases the risk of microbial colonisation in the lower urinary tract of the patients that potentially develops into biofilm (Wang *et al.* 2010; Stahlhut *et al.* 2012). Biofilm contamination on the urinary catheter is one of the major contributors in CAUTI (Tambyah *et al.* 1999; Pratt *et al.* 2007; Stickler 2008; Azevedo *et al.* 2016b). The bacterial contamination that later develops into biofilm on the catheter leads to subsequent adverse events, as shown in Figure 1-4.

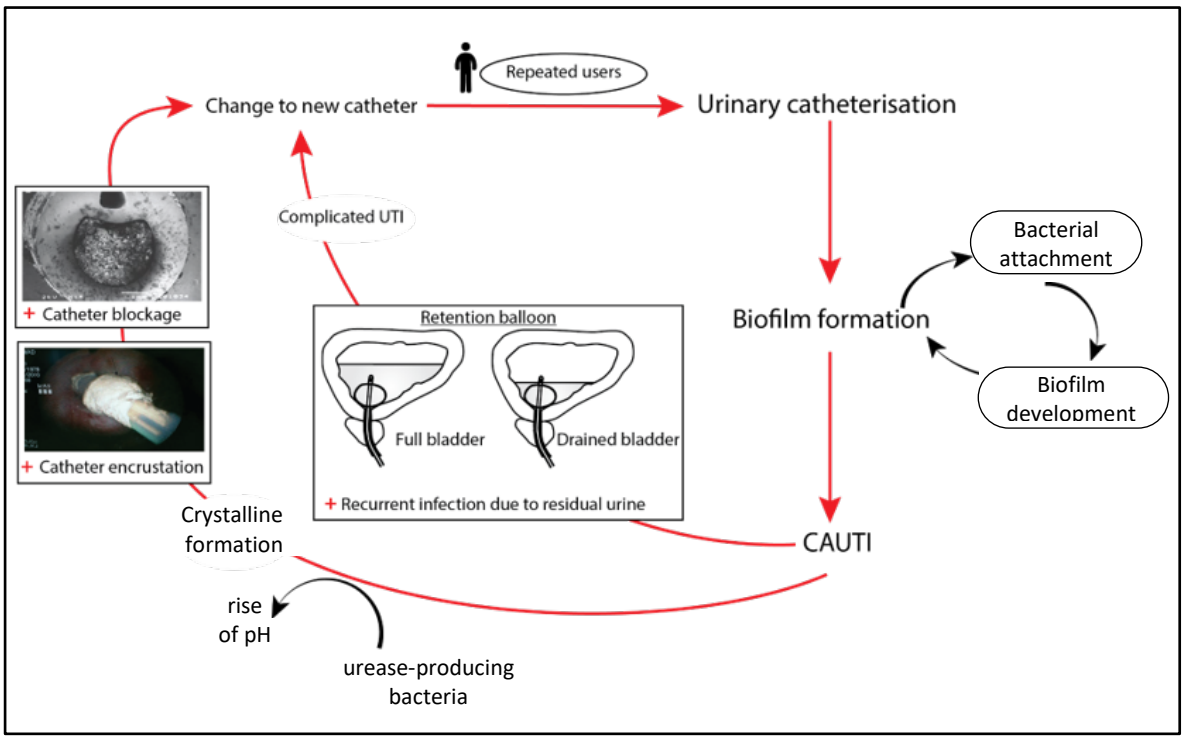

Figure 1-4 Typical flow of incidences related to biofilm with the use of urinary catheters.

The increase of CAUTI cases every year is at an alarming rate as the procedure of urinary catheterisation increases the risk of UTI (Maki and Tambyah 2001). Indwelling urinary catheters contribute to approximately eighty per cent (80 %) of all UTI cases worldwide (King *et al.* 2012; Flores-Mireles *et al.* 2015; Lim *et al.* 2015). There are more than 900 000 episodes of CAUTI reported happening in acute-care hospitals in the United States every year (Johnson *et al.* 1993;

Greene *et al.* 2008). Nearly forty per cent (40 %) of nosocomial infection in the United Kingdom occurs from catheterisation, and one out of four patients requires urinary catheterisation when admitted to the hospital in the US (Saint 2000; Stamm and Norrby 2001; Schumm and Lam 2008).

Patients of any age may need long-term urinary catheterisation due to post-operation procedures and medical complications, but it is more commonly observed in spinal surgery patients or older patients (geriatric) after hip arthroplasty procedure (Stamm and Norrby 2001; Ramakrishnan and Mold 2004; King *et al.* 2012). Patients that contracted CAUTI during their hospital stay often causes excessive bed-days that increases the cost per patient and reduces available bed in the hospital (Beattie and Taylor 2011; King *et al.* 2012; Lehman and Donlan 2015).

Table 1-1 Risk factors and preventive measures associated with CAUTI. Adapted from Ramakrishnan and Mold (2004).

Risk factors associated with catheter-associated infection	**Preventive measures against ascending CAUTI**
• Duration of catheterisation • Female gender • Diabetes mellitus • Lack of systemic antibiotics during short catheterisation • Not incorporating a urine meter (a measuring device to measure hourly urine output) • Microbial colonisation of the drainage bag • Serum creatinine greater than 2mg/dl at the time of catheterisation • Use of catheters with sealed collection junctions when no antibiotic is administered	• Early catheter removal • Using a closed drainage system • Intermittent catheterisation (every 4 h) • Smaller bore catheters • Optimal hygiene techniques (handwashing, sterile catheterisation techniques) • Silicone, antibiotic-impregnated catheters • Catheter removal when infection suspected

Table 1-1 lists the risk factors and preventive measures associated with CAUTI (Ramakrishnan and Mold 2004). The factors affecting the onset of CAUTI are such as duration of catheterisation, gender or health condition of the patient, appropriate usage of the catheter, and the quality of catheter care. These factors have been similarly highlighted previously in the report by Platt *et al.* (1986), Maki and Tambyah (2001) and Pratt *et al.* (2007). The risk of bacterial contamination is highest and more anticipated among patients with an indwelling catheter.

The risk of contracting CAUTI increases five per cent (5 %) for each day the catheter remains in place, putting patients with prolonged catheterisation of more than six days at the highest risks

(Maki and Tambyah 2001). Long-term catheterisation is a huge concern in elderly and nursing care homes where at least ten per cent (10 %) of occupants will have a catheter fitted throughout the year. They are more prone to bacteriuria and pose three times more risk of mortality within a year of being catheterised (Kunin *et al.* 1992).

Female patients are the second-highest risk factor for CAUTI due to the short length of the female urethra (Maki and Tambyah 2001; Ramakrishnan and Mold 2004; Greene *et al.* 2008; Ramanathan and Duane 2014). However, certain circumstances such as acute urinary retention (AUR) patients are affecting men ten times more than women. AUR is the sudden inability to pass urine, which often requires long-term catheterisation as a treatment. AUR is common among postoperative patients and it affects approximately three in every 1,000 men per annum in the United Kingdom (Cathcart *et al.* 2006; Newman and Willson 2011). Earlier technology uses open system drainage bag, which appears to be a source for contamination, among other factors for CAUTI. However, the open system drainage bag has been replaced with a closed drainage system that lowers the risk of infection since it has been adapted (Ramakrishnan and Mold 2004).

In the United Kingdom, a clear guideline by Pratt *et al.* (2007) suggests four main interventions in reducing CAUTI; which are i) assessing the need for catheterisation, ii) selecting the appropriate catheter type, iii) inserting the catheter using an aseptic technique, and iv)proper management of the catheter. If a patient is suspected of contracting a UTI due to catheterisation, the current practice is to replace the catheter with a new one immediately (Ramakrishnan and Mold 2004). A sudden drop in UTI level confirms that the bacterial colonisation on the catheter had caused the infection. The surveillance system for CAUTI management in middle-to-low income countries is poorly developed or non-existent compared to high-income countries.

Other than the presence of clinical symptoms, the usual definition of UTI is the diagnosis of bacterial (or fungal) growth detected in urine at 10^5 colony-forming unit per millilitre, cfu/ml. However, the prognosis is defined as CAUTI when the patients are catheterised or were catheterised previously, and have a urine diagnosis of microbial growth reaching 10^3 cfu/ml (Barford *et al.* 2008; Schmiemann *et al.* 2010). Current diagnosis is by standard urine culture protocol, which is the gold standard in determining bacterial growth in the laboratory. The standard urine culture protocol involves taking 1 µ of urine to be plated in the laboratory and grown overnight. Each colony grown represents 10^3 cfu/ml, making it a positive urine culture and a “no growth” would indicate a negative urine culture (Tambyah *et al.* 1999).

It is a common medical practice to avoid overmedication of CAUTI bacteraemia to prevent promoting bacterial antibiotic resistance. However, medical practices in some developing

countries have increased the numbers of antibiotic prescriptions to treat CAUTI despite various prevention methods and procedures advocated by WHO (World Health Organization 2011).

1.2.3.1 The urinary catheter

The urological catheter is the most commonly utilised medical device with an annual estimation of 100 million pieces being used worldwide. The most popular urinary catheters are the Foley catheters, named after the famous American urologist Frederic Foley (Figure 1-5). He designed the first flexible urinary catheter that was later manufactured and made famous by Bard (Tatem *et al.* 2013).

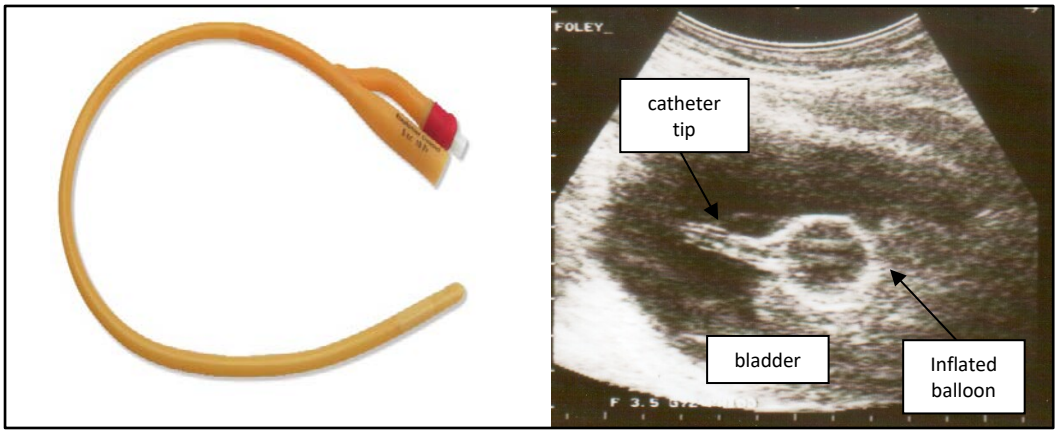

Figure 1-5 Silicone-coated latex Foley catheter (left) and an ultrasound scan image showing a ballooned catheter inside the bladder (right). Image (left) from http://www.vygon.com (last accessed 16th January 2017), and ultrasound image (right) by Nevit Dilmen (1997).

1.2.3.1.1 Catheter design

The catheter design has not evolved much in eighty years since its invention in 1937 (Prinjha and Chapple 2013). There is similarity in shape of the first Foley catheter, which was made of latex in Figure 1-6, with the earlier mentioned example of catheter used currently shown in features the typical design of urinary catheter that is widely used today. It is a long tube made from flexible and durable material with options for different tip shape and number of channels. These current modifications to the original Foley design were essential to suit the needs of the treatment to patients.

The tip of the urinary catheter has either the common basic straight tip or a modified tip. The curved (or coude) tip, which was used for male patients to help facilitate passage through the prostate due to urethra stricture problems from the previous usage of catheters (Newman and Willson 2011).

Another example is the Whistle-tipped catheter that has an additional eyelet hole positioned closer above the balloon that functions to help with the drainage of accumulated blood clots and other debris (Getliffe 2004; Ramakrishnan and Mold 2004; Jacobsen *et al.* 2008).

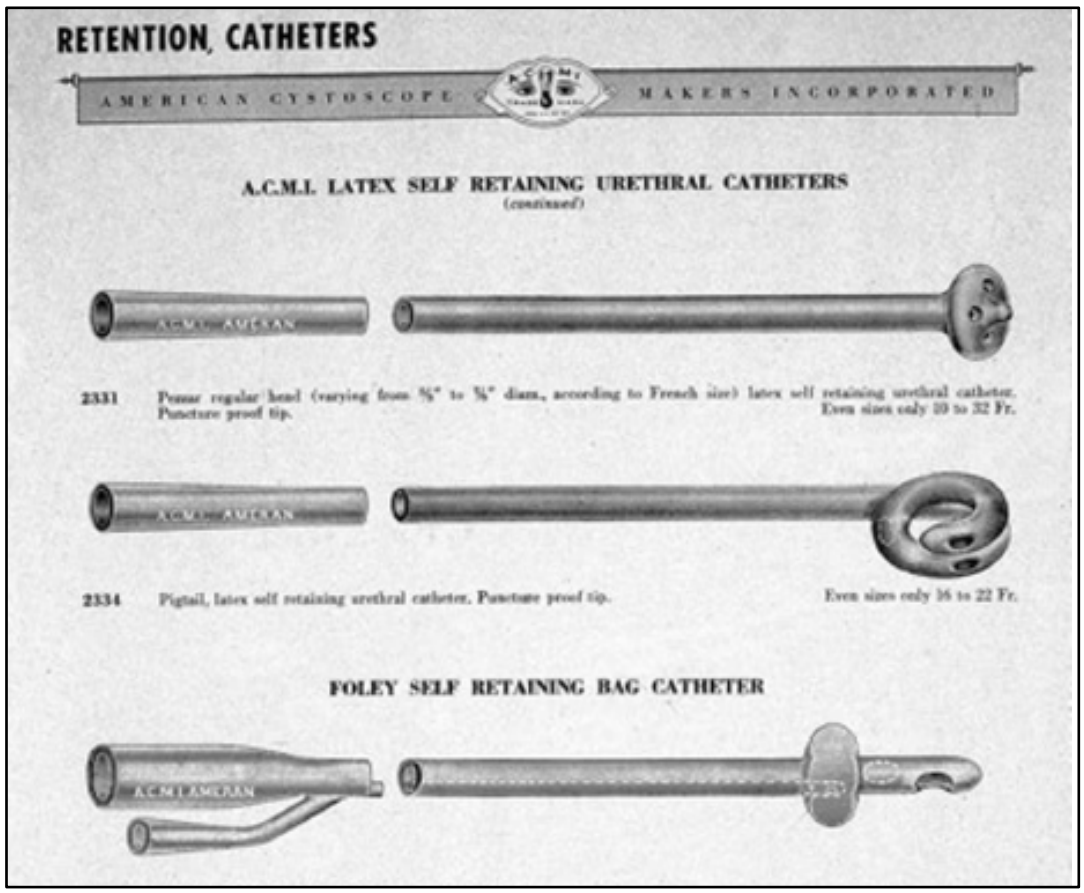
RETENTION CATHETERS

AMERICAN CYSTOSCOPE MAKERS INCORPORATED

A.C.M.I. LATEX SELF RETAINING URETHRAL CATHETERS
(continued)

2331 Pezzer regular head (varying from 5/64" to 3/16" diam., according to French size) latex self retaining urethral catheter. Puncture proof tip. Even sizes only 10 to 32 Fr.

2334 Pigtail, latex self retaining urethral catheter. Puncture proof tip. Even sizes only 16 to 22 Fr.

FOLEY SELF RETAINING BAG CATHETER

Figure 1-6 A catalogue page of the first Foley latex catheter supplied by the American Cystoscope Makers, Inc. Adapted from Tatem *et al.* (2013).

In two-way or three-way channel urinary catheters, the main channel's function is to drain the urine from the bladder, and the second channel is used to inflate the balloon to ensure the eyelet of the catheter remains in the bladder. The third channel from the three-way channel urinary catheter is used for bladder irrigation which usually is an elective post-operative procedure after prostate surgery (Ramakrishnan and Mold 2004; Feneley *et al.* 2015). The beneficial effects of bladder irrigation to reduce CAUTI are still questionable and unsupported (Maki and Tambyah 2001; Pratt *et al.* 2007).

Knowing the suitable size of the catheter is important as improper sizing might cause unnecessary discomfort to patients. The catheters are commonly sized using Charrier (Ch) units, where one Ch is equivalent to one-third (1/3) of the diameter in millimetre (mm). The sizing differs and related to the material used for the catheter as the silicone and latex catheter are designed differently (Figure 1-8). The smallest size diameter catheter suitable for patients is preferred to minimise the urethral tissue trauma (Nicolle 2014).

A bigger or wider diameter catheter might cause urethral trauma and spasm of the urethra and bladder (Ramakrishnan and Mold 2004; Rosdahl and Kowalski 2011). While current latex-free materials used for catheters such as silicon, PVC, and PTFE reduce the hypersensitivity in patients, this causes a slight increase to the catheter diameter to improve pliability of the catheter (Newman and Willson 2011). The change from silicon catheters in chronic patients were mostly responsible for the decrease of catheter blockage incidence because it has larger lumen size compared to latex catheters (Nicolle 2014).

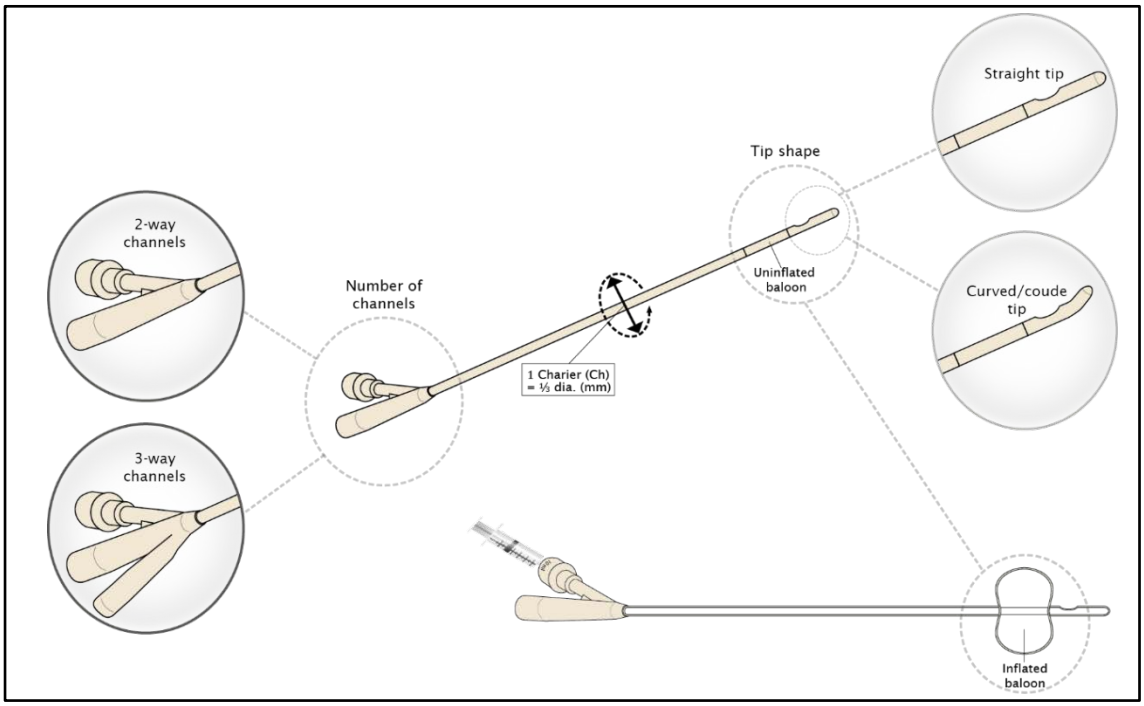

Figure 1-7 A urinary catheter with several option modifications according to manufacturer design and function.

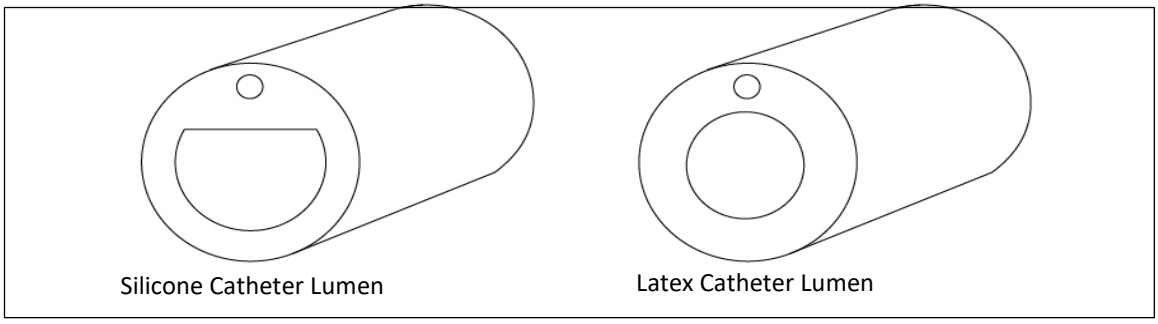

Figure 1-8 Difference of lumen shape between silicone and latex catheter.

The tip of the catheter acts as the lead of the insertion through the urethra and the catheter is pushed further until the tip reaches the bladder. The retention balloon is inflated after the catheter tip has reached into the bladder area (Figure 1-9). A volume of 10 ml to 15 ml saline or water is pumped into the second channel to inflate the balloon and ensuring the catheter tip (and eyelet) is in place (Pomfret 2007; Rosdahl and Kowalski 2011).

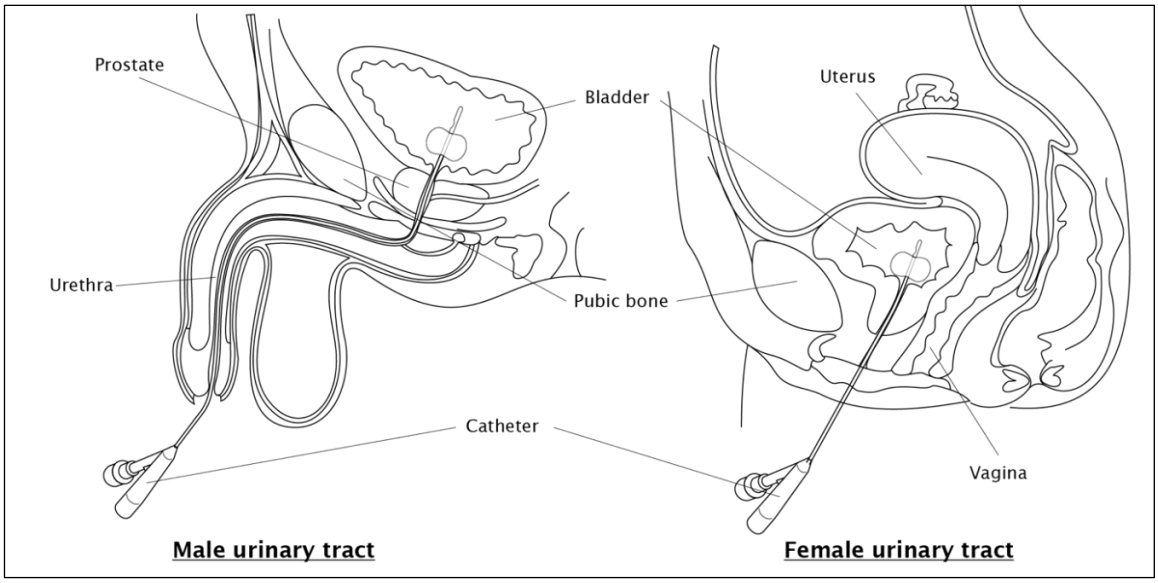

Figure 1-9 Representation image of male and female lower urinary tract with a (ballooned) catheter in place.

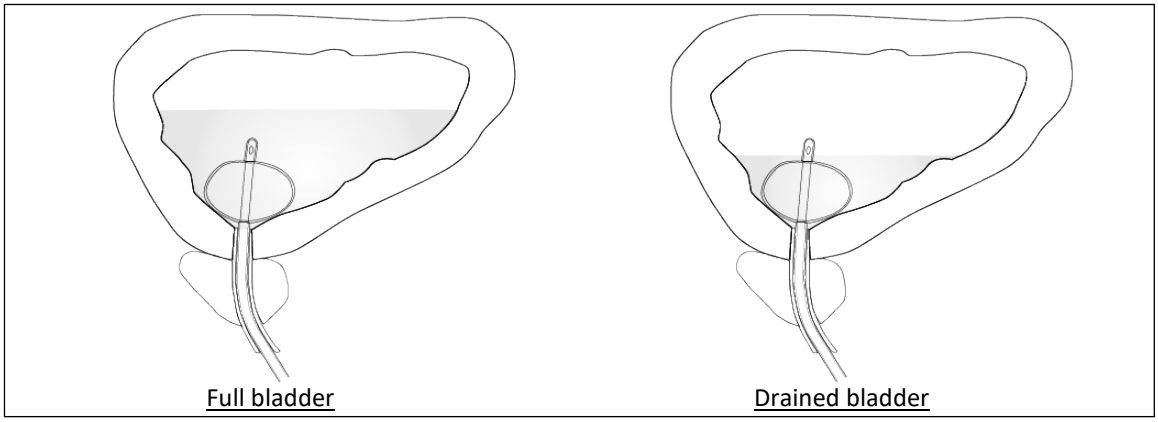

Figure 1-10 Representation of how residual urine accumulates in the bladder due to the retention balloon. Urine collects until below the drainage eyelet of the catheter tip.

The retention balloon is a great factor in CAUTI, as a large balloon capacity will leave a significant amount of accumulated residual urine in the bladder. Residual urine is the remaining urine left in the bladder when a urinary catheter is used, as the drainage eye of the catheter is usually placed above the balloon, and it sets the level where any urine below cannot be drained out (Figure 1-10). It is among the reasons contributing to CAUTI and an important risk factor for recurrent infection (Choong *et al.* 2001; Stamm and Norrby 2001; Cathcart *et al.* 2006; Feneley *et al.* 2012; Siddiq and Darouiche 2012). This residual urine volume has been observed in UTI and investigated in the laboratory since 1976 (Greenwood 1976). Greenwood (1976) pioneered the use of a laboratory bladder model to study the effect of antibiotics on bacteria in bladders and reported that residual urine is causing the complications in treating UTI. The underlying problem was that the retention balloon prevents the bladder from being drained out completely and increases the amount of urine reservoir in the bladder.

The residual urine acts as an inoculum in the bladder that is intermittently replenished with fresh urine and continuously recultivates the urinary catheter (Trautner and Darouiche 2004a). Many studies incorporated residual urine in reproducing investigations related to UTI and the use of the urinary catheter with laboratory bladder model (Anderson *et al.* 1980; Stickler *et al.* 1999a; Broomfield *et al.* 2009; Malic *et al.* 2014; Nzakizwanayo *et al.* 2015).

The design for indwelling urinary catheters, especially the ones used by patients with chronic illness, includes the attachment of reservoir urine bag to store the drained urine. While a closed urinary system is critical to ensure CAUTI risk is minimised, the outlets on the drainage bag are possible entry points for bacterial contamination, as shown in Figure 1-11. Studies shown that bacteria contamination may originate from either the sampling port or the valve, which makes the closed urinary system ineffective (Siddiq and Darouiche 2012).

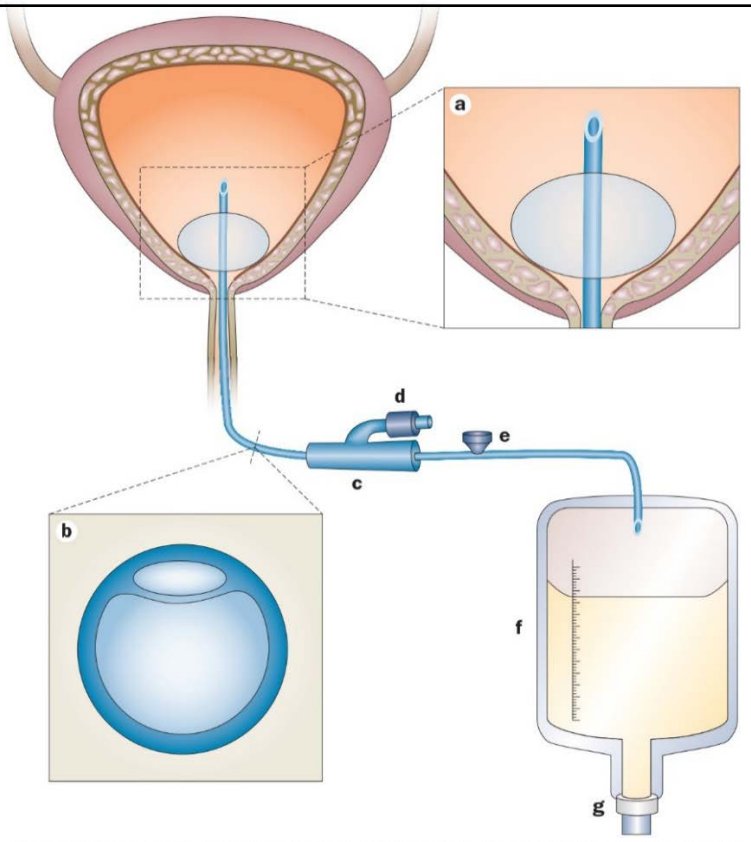

a | An eyelet at the proximal end of the catheter allows drainage of urine from the bladder. The reservoir balloon is routinely filled with sterile saline.
b | Cross-section of the commonly used double-lumen indwelling urinary catheter is shown. The large lumen is for urinary drainage; the small lumen is connected to the port.
c | The preconnected, presealed junction of the indwelling catheter and the drainage system should not be broken.
d | This port is connected to the small lumen of the catheter and is used to inflate the resevoir balloon with sterile saline.
e | This port is a one-way sampling port through which urine specimens for microbiological testing are collected.
f | Draining urine accumulates in the collection bag.
g | Urine is ultimately emptied into the external environment via the outlet valve. Thus, 'closed urinary system' is a misnomer.

Figure 1-11 Urinary bladder with an indwelling urinary catheter. Adapted from Siddiq and Darouiche (2012).

1.2.3.1.2 Catheter material

Dr Frederic Foley invented the Foley catheter in 1937 and used latex from natural rubber as the catheter material (Prinjha and Chapple 2013; Tatem *et al.* 2013). Currently, the use of latex catheter has become uncommon compared to other catheter materials. Even though latex is very flexible, cheap, and easy to obtain, latex catheter is unpopular as it can cause hypersensitivity to patients and increase the risk of infection (Schumm and Lam 2008).

Currently there are many variations of catheters from improved materials, such as silicone-coated latex, silicone, PTFE-coated, hydrogel-coated, and even antimicrobial-coated and metal-coated catheters. (Ramakrishnan and Mold 2004; Lawrence and Turner 2005; Jahn *et al.* 2007). Silicone-coated latex catheters have silicone coating on the outer layer that acts as a barrier for the latex from being in contact with the urethra mucosal tissue to overcome the hypersensitivity problems (Tatem *et al.* 2013). Although it retains the same pliability to latex catheters, the silicone coating is prone to degradation after long-term use that consequently reveals the underlying layer of latex.

The silicone-coated latex catheters are suitable for short-term use of less than two weeks before it is advisable to replace it with a new one (Jahn *et al.* 2007; Schumm and Lam 2008). The hydrogel-coated catheter was then invented as an alternative to silicone-coated latex catheters, but has similar limitations for long-term use (Lawrence and Turner 2005). Nowadays, catheters are commonly made of silicone, which made the catheters more rigid than the latex catheter, to ensure durability for longer usage life (Newman and Willson 2011; Prinjha and Chapple 2013).

All-silicone catheters are much more costly to produce compared to their predecessor latex catheters. However, mass production and increased demand for all-silicone catheters has significantly reduced the relative cost (Lawrence and Turner 2005; Schumm and Lam 2008). Silicone possesses hydrophobic properties on its surface that repel water. Nonetheless, this does not hinder the bacterial attachment of freshwater and soil biofilm, which can still occur regardless of surface material (Gich *et al.* 2012). There is no significant difference in the risk of bacterial infection between catheter material made of silicone, latex, or even with hydrogel coating, regardless of its cost (Nicolle 2014).

The urinary catheter allows route for entry and transportation for opportunistic and harmful pathogens travel into our bladder, which possess abundant inert surfaces that are susceptible to bacterial attachment and biofilm formation (Trautner *et al.* 2012). Many studies have been conducted on the improved materials for urinary catheter but the significant effectiveness in reducing CAUTI is still questionable as biofilms persist to be a global healthcare problem (Schumm and Lam 2008; Beattie and Taylor 2011; Shunmugaperumal *et al.* 2015).

The most desirable solution for catheter material would be one that prevents or reduces infection in patients. Morris *et al.* (1997) concluded in his study of various catheter against *Proteus mirabilis* encrustation that the ideal characteristics that a catheter should have are surfaces that repel colonisation of bacteria and prevent crystal formation and deposition, in addition to having wider lumen and eyeholes. However, current breakthroughs for improved materials such as the antimicrobial-coated catheter shows that it was only able to delay the onset of the urinary tract infection but is not able to prevent it from happening (Desai *et al.* 2010; Pickard *et al.* 2012; Shunmugaperumal *et al.* 2015).

The production of antimicrobial urinary catheters has yet to become cost-friendly, as the surface needs to yield high concentrations of antimicrobials for it to become effective enough to fight off biofilm contamination. This is because of poor penetration of antimicrobials across the extracellular polymeric substances (EPS) matrix and partly due to the increase of antimicrobial resistance among clinical strains (Dave *et al.* 2011). It is vital to combat the issue of contaminating biofilm from every angle, but the focus should be on antifouling materials that either repel bacterial attachment or limits the bacteria or biofilm growth (Table 1-2).

Use of metals to interfere with biofilm formation has been widely studied to develop new catheter technologies. Certain metal ions concentrate in the biofilm environment to serve as either important virulence or fitness factors for bacteria. *E. coli* has previously been shown to limit their biofilm development with iron chelator but increased growth when iron is included as a growth medium nutrient (Hancock *et al.* 2010). Desai *et al.* (2010) showed that impregnated catheters might help for short-term catheter users, but long-term users of indwelling catheter were still at risk of getting an infection. They found that silver-impregnated catheters had minimal effect on bacterial adherence, and nitrofurazone impregnation had significant effect only for the first five days. Silver-impregnated catheters are more preferred and efficient than standard silicone and latex catheters (Beattie and Taylor 2011). However, Pickard *et al.* (2012) have reported that neither silver nor nitrofurazone impregnation was significantly effective in reducing symptomatic CAUTI.

Currently, commercially available silver-coated Dover^{TM} catheters are able to prevent encrustation for up to 6 days (Wang *et al.* 2015). Wang *et al.* (2015) also reported that modified pre-treated silicone catheters with silver nanoparticles immobilised on polydopamine bilayers (AgNP-PDA) were able to resist *Proteus mirabilis* encrustation for 12 days for single layer and up to 45 days for double layers of polydopamine bilayers. These studies present promising result of using silver as antifouling material in catheters, but this could significantly increase the catheter cost. A feasibility study for using antifouling materials in catheters is required to ensure that the benefit outweighs the cost of manufacturing and producing these improved catheters.

Table 1-2 The development of technologies in catheter design to curb the problem of CAUTI.

Technology Method	Research targets
Catheter material development	Antifouling material that prevents/repels bacteria/biofilm attachment (anti-bacterial adhesion)
Antibiotic-impregnated catheter/ special metal impregnated catheter	Material with immobilised treatments that stunts/inhibit bacteria/biofilm growth
Catheter design	Minimise contamination of bacteria from the perineal area during insertion. Bigger lumen and eyeholes

1.2.3.2 Pathogenesis of CAUTI

Understanding the complex interaction between the host cell and the pathogen during biofilm infection will support researchers further in finding ways to manage CAUTI. Once established in the urinary bladder, the pathogen attaches to the host mucosal layer, and the host natural defence mechanism will respond to fight and provide resistance towards the pathogen. CAUTI occurs by a continuum pathway by pathogens that usually originate from the perineal on the outer body, which then invade the lower urinary tract, move upwards into the bladder, and multiply once it has arrived at a favourable environment (Shunmugaperumal *et al.* 2015). Using urinary catheters increases the risk for UTI as patients that use catheters for long-term has found to have permanent bacterial colonisation in the urine (Jacobsen *et al.* 2008).

There are two identified typical clinical phases in bacterial infections involving biofilm, which are the initial acute febrile phase and the chronic indolent phase (Figure 1-12). It poses a similar risk of breakage to the mucosal barrier during the indolent infection phase as planktonic bacteria. The infection increases the level of urinary immunoglobulin secretion that reinforces the mucosal barrier along the basement membrane. However, sudden pressure elevation in the urinary collecting system can lead to acute obstruction (e.g., incidental urinary catheter occlusion). This causes the mechanical barrier to break and provide access for bacterial cell into renal parenchyma and blood vessels and cause (recurring) acute febrile infection (Kumon 1996).

In the chronic indolent phase, the use of antimicrobial treatment will be redundant and ineffective, leaving the only possible solution removing the site of biofilm that had caused the infection in the acute febrile phase. The acute pyelonephritis and bacteraemia are primarily treated with the necessary antimicrobial therapy by administering standard or high doses of antibiotics. All planktonic pathogens might have been eradicated with conventional antimicrobial therapy; however, biofilms remain viable due to their high tolerance to antibiotics and are still able to cause bacteriuria after the treatment has ceased. (Kumon 1996; Chua *et al.* 2016).

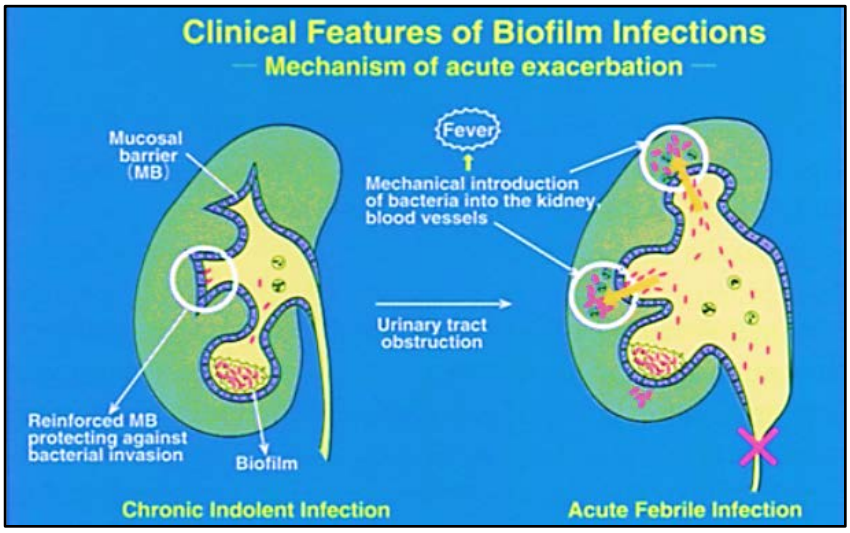

Figure 1-12 Clinical features of biofilm infections on mechanism of the acute exacerbation. Adapted from Kumon (1996).

1.2.3.3 Antimicrobial therapy uses in CAUTI

Antimicrobial therapy is a common CAUTI treatment, as uropathogenic bacteria possess specific virulence factors in their membrane that help them survive host innate immune responses. Therefore, current antimicrobial treatment often targets these virulence factors, and until the recent advocacy to limit the use of therapy when bacteria has developed antimicrobial resistant trait to overcome it (Flores-Mireles *et al.* 2015). This is because biofilms are 1000 times more tolerant to antibiotics than in the same bacteria in the planktonic state (Bonkat *et al.* 2013b; Tolker-Nielsen 2014; Olsen 2015). Other than antibiotic resistance, the frequent use of the antimicrobial treatment in UTI can disrupt the normal microbiota of the lower gastrointestinal tract (Trautner *et al.* 2005; Whiteside *et al.* 2015).

It is vital to identify CAUTI early to avoid the associated risk to the patients. In current practice, blocked catheters or infected catheters from asymptomatic CAUTI patients are removed and treated progressively with systemic antibiotics (Pascual 2002; Henley *et al.* 2007; Shuman and Chenoweth 2010). However, in the case of symptomatic CAUTI, similar antibiotic treatments to complicated UTI were given for ten to fourteen days.

Figure 1-13 shows a representation of a patient that suffers from acute pyelonephritis of bacterial infection (post-operation) known caused by the biofilm of *P. aeruginosa* (Kumon 1996). The patient developed fever despite the treatment with two cephalosporin-type antibiotics, which prompt the removal of urethral stent and catheter as the investigations showed that these were the probable causes of infection. However, the prolonged infection has caused elevated pressure in the renal collecting system and ruptured the infected pelvic mucosa.

This was then followed by continuous medication that includes a combination of two antibiotics targeting systemic and local treatment, which spans over two weeks. It was not until the infected site was removed and nearly two months of overall treatment that the patient gained recovery. This case study is one of many that exhibit the difficulties faced in using antimicrobial therapy for CAUTI. Often seen that antimicrobial therapies were unsuccessful in CAUTI complete eradication due to biofilm, and further developed into complicated UTI, putting the already compromised patient at risk (Ma *et al.* 2007; Bonkat *et al.* 2013a; Chua *et al.* 2016). With the new understanding of biofilm development, it does pose a question whether past experiments that have reported failed in treating the biofilm with the standard dose were caused by the development of antimicrobial treatment that was originally tested against planktonic bacteria.

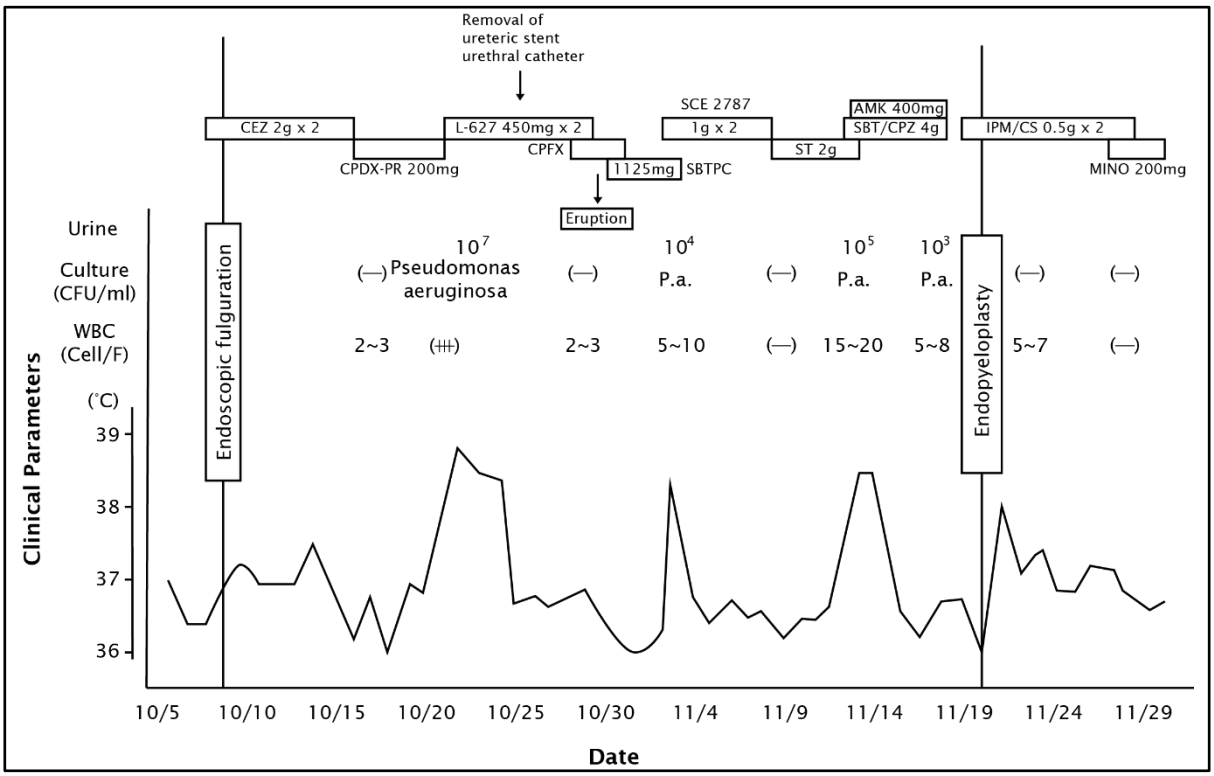

Figure 1-13 Clinical course of a 73-year-old male with biofilm infection caused by *P. aeruginosa*. Adapted from Kumon (1996). (CEZ = cefazolin, CPDX-PR = Cefpodoxime proxetil, L-627 = biapenem, SBTPC = sulbactam/ampicillin, SCE 2787 = cephalosporin, ST = solithromycin, AMK = Amikacin, SBT/CPZ = sulbactam/cefoperazone, IPM/CS = imipenem/colistin, MINO = Minocycline)

To improve the quality of catheter healthcare, we should focus more on giving maximum comfort with effective recuperation process for patients while being responsible for sustaining the management of bacterial infection. Furthermore, we would want to reduce the number of days stay for patients to reduce the exposure risk acquitting nosocomial infection. Other considerations include the cost of antibiotics prescribed and overtreatment from misdiagnosis presumed to be UTI, which need to be considered as these occurrences still happen even after proper prevention framework, adequate staff training, and safety measures have been implemented (Platt *et al.* 1982; Tambyah *et al.* 1999).

1.2.4 Biofilm development on urinary catheter

1.2.4.1 Origin of the term 'Biofilm' and its definition

Present study on biofilm development has been extensive and received increasing medical attention lately. Biofilm caused chronic and persistent infection for bio implant-associated infections, endocarditis, osteomyelitis, operative wound infections including cystic fibrosis and diffuse panbronchiolitis (Kumon 1996; Costerton *et al.* 1999; Bjarnsholt 2013).

Once the biofilm has established its presence, their virulent characteristics protect them from antimicrobial treatment, host defences, and shear forces. This helps them able to overcome any preventive strategies used to combat infections including CAUTI and the search for a successful treatment has yet to be found (Trautner and Darouiche 2004b; Stickler 2008; Trautner *et al.* 2012; Bjarnsholt *et al.* 2013).

Antonie van Leeuwenhoek first observed the aggregations of bacterial cells found on the surface of the teeth and the presence of bacteria as biofilm has been widely studied since then (Bjarnsholt 2013). Our understanding of bacteria presence as our normal flora has included biofilms living on biotic and abiotic inert surfaces within our body. Bacteria existence on and within our bodies has made biofilms a recognised common health problem and is associated with more than eighty per cent (80 %) of human infections. These biofilm-associated bacteria in humans are also the source of recurrent infections as they can withstand host immune defences, antimicrobial treatments, biocides, and hydrodynamic shear forces far better than the corresponding planktonic bacteria form (Hancock *et al.* 2010).

Costerton *et al.* (1978) first described biofilm as sessile bacteria or fungi that have attached and grow onto surfaces, unlike their free-floating and non-adherent planktonic form. The biofilm structure contributed to its survivability and caused problems in the environment, industrial and healthcare (Costerton *et al.* 1978). Once surface attachment is established, these cells aggregate and form various structures depending on the environmental conditions, held together by a glue-like matrix which is the EPS produced by the microorganisms (Bjarnsholt *et al.* 2013). The biofilm matrix consists of a mixture of hydrated polymer proteins, polysaccharides and extracellular DNA, in which its high variability has contributed to the survival of biofilm cells especially in harsh environments (Hall-Stoodley *et al.* 2004). Now after forty years, the "biofilm" definition has not only described its physical form but also included the versatile characteristics in maintaining the cell aggregates and other functional genotype and phenotypes for its survival. Rogers *et al.* (1991) and Rogers and Keevil (1992) were first in describing biofilm as the assembly of microcolonies joined by EPS into stacks or fronds which rise from a basal layer of cells on the substratum.

Costerton *et al.* (1999) later described biofilm as a cluster of bacterial cells that attaches to a surface, aggregates and colonises to form extreme complex structures of cells, extracellular matrix, and other materials when discussing its role in persistent infections. A few years later, Donlan and Costerton (2002) elaborately defined biofilm as "*sessile community characterized by cells that are irreversibly embedded in matrix of extracellular polymeric substances that they have produced, and exhibit an altered phenotype with respect to growth rate and gene transcription.*" This definition is suited to describe the important foundation basis of the microbial ability to form biofilm is as a phenotype that can be transferred or removed genetically along with the added advantages that come with it. These resistant characteristics inherited by the biofilm cell from the parent community is maintained even in the harsh environment due to shear forces (or other stresses) or broken off from the main biofilm while transported to another location in our body (Costerton *et al.* 1999).

1.2.4.2 Biofilm forms and its development process

The main properties of the biofilm form are the cell clusters inside a matrix which many often describe as porous mushroom-like architecture with channels between them to allow bulk fluid flow deep within the biofilm structure providing oxygen, and nutrient access to cells (Donlan and Costerton 2002; Bjarnsholt 2013). However, these studies does not correspond to structure of the aggregated of microcolonies that form stacks or fronds as in Figure 1-14 frequently found in nature and in some laboratory studies using careful microscopy observation (Keevil 2009).

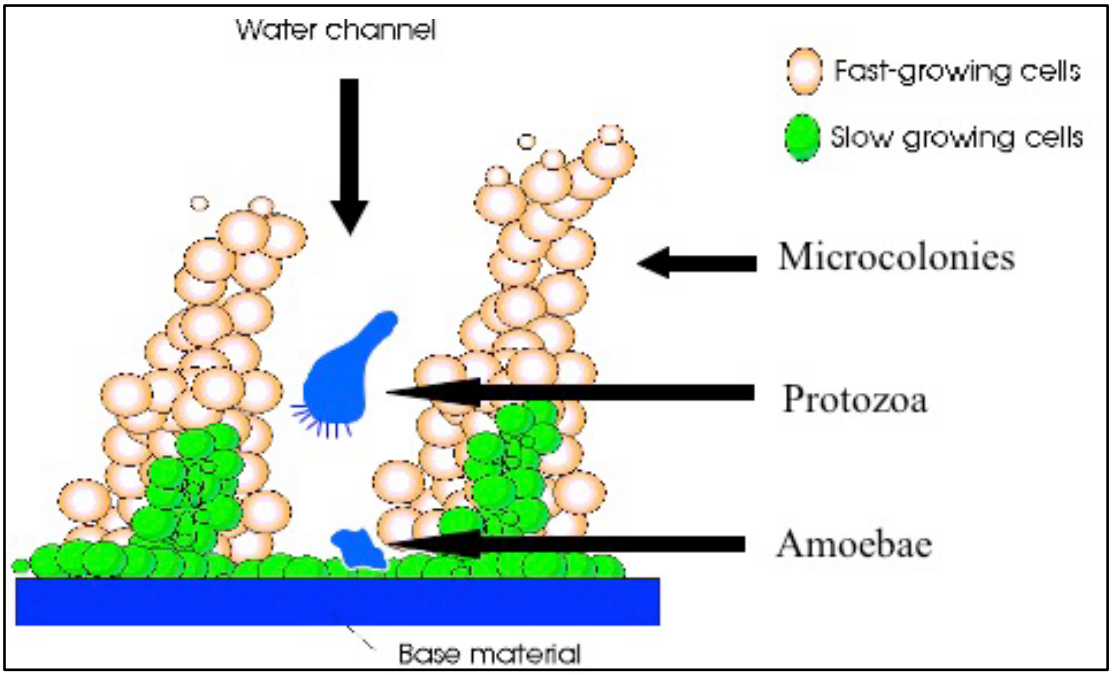

Figure 1-14 Open architecture structure of biofilm with fronds, water channels and grazing eukaryotic predators. Adapted from Keevil (2009).

Nevertheless, the biofilm formation involves several stages that exhibit distinct phenotype before it shapes itself into this complex multicellular biofilm structure. There are external physical factors such as Van der Waals forces, surface electrostatic forces, as well as the hydrophobicity properties of the surface that the cells need to overcome prior to initial stage of biofilm (Marshall *et al.* 1971; Stickler *et al.* 1999b; Pascual 2002; de Melo *et al.* 2013; Azevedo *et al.* 2016b; Gultekinoglu *et al.* 2017). The initial stage (Figure 1-15) in bacterial biofilm formation is the attachment or adherence of bacterial cells onto the surface (Ellwood *et al.* 1982) which is also the first step for bacterial infection and colonisation (Di Martino *et al.* 2002; Coenye and Nelis 2010).

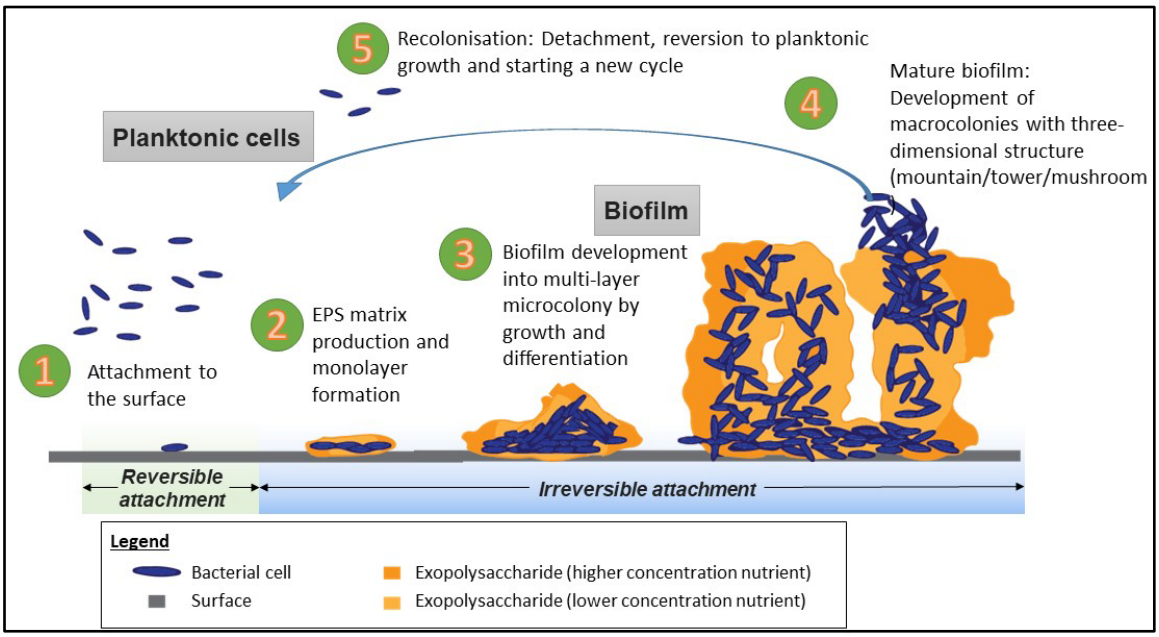

Figure 1-15 The life cycle of biofilm. Progression stages biofilm development, from left to right: Reversible attachment, irreversible attachment, microcolony growth and differentiation, biofilm maturation and recolonisation.

This is known as a reversible attachment as the cell still has the ability to travel in the fluid environment and not bounded to the surface (Habash and Reid 1999; Toutain *et al.* 2004; Romling and Balsalobre 2012). However, once attached, the bacteria produce slime, which was later identified as EPS that are relatively strong and supported by the fluid surrounding it (Kumon 1996; Hall-Stoodley *et al.* 2004; Tenke *et al.* 2006; Wang *et al.* 2012).

The hydrated composition of bacterial community and the EPS structure is affected by the concentration of available nutrients and the flow velocity (Stoodley *et al.,* 1998). At this stage, it is known as biofilm, and the attachment to the surface is considered irreversible. The bacterial cell that is within the slimy EPS matrix continues to grow, especially when surrounded by enriching growth material such as human urine. The bacterial cells grow and develop into mature biofilm through a differentiation process. Upwards growth is observed in mature biofilms, and the shape may be influenced according to the strain and environment.

This complex multicellular structure has been reported true by Klausen *et al.* (2003a) for biofilm formed by bacterial species with motility capabilities and carbon in the nutrient source. Mature biofilm tends to lose fragments of the highest branch and created “flocs” due to shear forces where a section may break off from the main biofilm community or the more loosely attached streamers. These flocs still retains certain biofilm characteristics that enables them to disseminate to another location and can form biofilm once they establish attachment (Costerton *et al.* 1999; Reid 1999; Hall-Stoodley *et al.* 2004). Stoodley *et al.* (1998) concluded that in laminar flow conditions of nutrients, the biofilm structure shows patchy irregular circular clusters (i.e. aggregated microcolonies) with interstitial voids between them. In addition, turbulent conditions presented similar patchy clusters of cells but there are patterns of ripples and streamers following the direction of the flow (Figure 1-16).

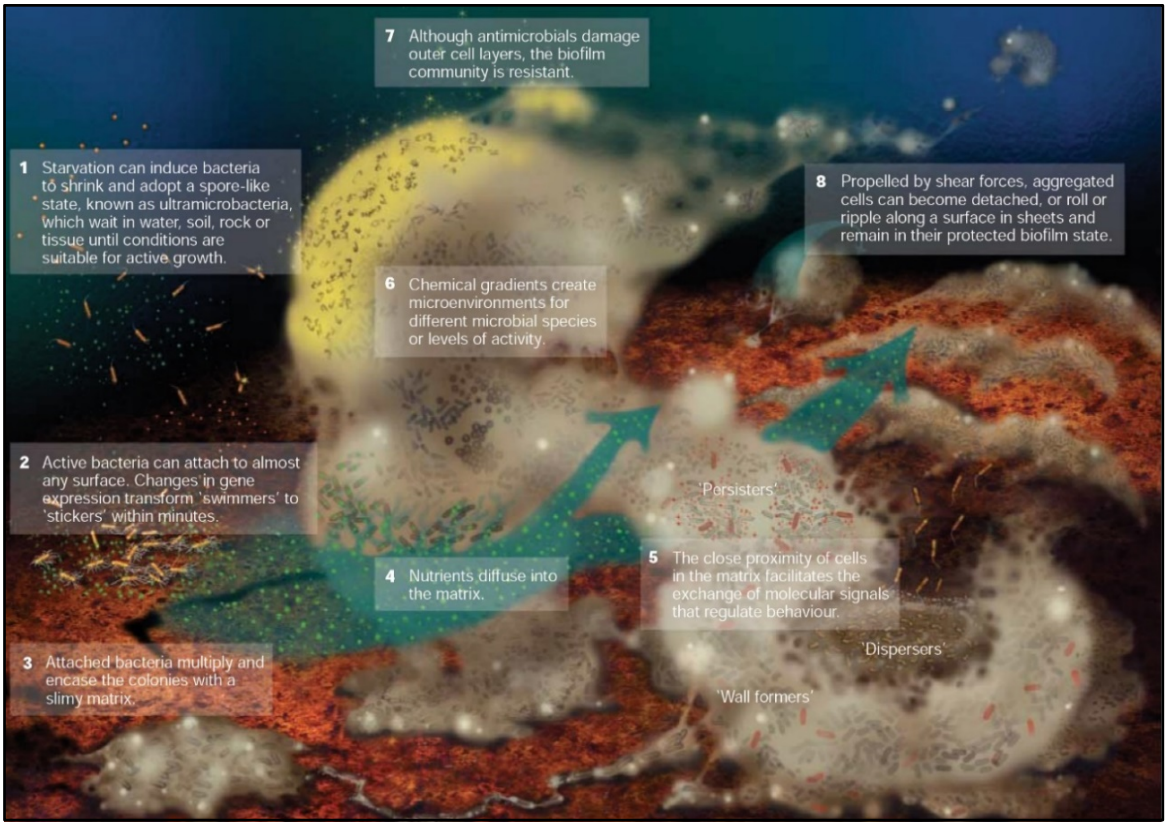

Figure 1-16 Biofilm development and its dynamic growth behaviours influenced by the environment. Adapted by Hall-Stoodley *et al.* (2004). Image by P. Dirckx, MSU Center for Biofilm Engineering, USA.

Many biofilm studies emphasise the importance of bacterial attachment as the crucial initiation to bacterial colonisation in biofilm development process. Various factors are involved in bacterial adherence process, including the bacteria’s capability to attach themselves to a surface by specific cell mechanism function either by producing bacterial adhesins, organelles that assist in adhesion processes such as fimbriae, flagella, or pili, and other assisting proteins such as lipopolysaccharides (Costerton *et al.* 1999; Kikuchi *et al.* 2005).

This can be promoted by the presence of environmental compounds attaching to the substratum forming a conditioning film (Donlan 2002; Wilks *et al.* 2015). Other factors contributing to bacterial adherence is the physicochemical properties and forces existing in the surrounding environment of the interaction between cell and surface (Ellwood *et al.* 1982). In addition, the presence of substances produced by the host body or cell that are involuntary involved in the attachment process such as fibronectins that promote attachment (Di Martino *et al.* 2002).

1.2.4.3 Origin and development of biofilm in CAUTI

The relationship between different species of bacteria in biofilms as complex microbial communities and how they cause infection to the human host are poorly understood. There are several hypotheses on how bacterial contamination occurs with urinary catheterisation and one is the contamination of the catheter tip during the insertion was the way of entry to gain access to the bladder (Barford *et al.* 2008). Possibilities such as lack of personal hygiene or mismanagement of catheter use are the reasons how the pathogen from the perineal area might be contaminating the catheter during the procedure (Maki and Tambyah 2001).

A study by Barford *et al.* (2008) showed there was a higher viability and richer spectrum of the bacterial population in the external catheter compared to the internal catheter. While many studies have been done regarding the CAUTI point of origin, there is still no definite and clear conclusion to it (Barford *et al.* 2008). This is due to the pre-suggested theory that the human bladder and human urine are initially sterile pre-catheterisation and the pathogens from the perineal region are similar to the ones originated from the gut (Hilt *et al.* 2014). The periurethral contamination route starts from the urethra entrance, and subsequently by deeper migration into urethra, which is then followed by bacterial colonisation into the bladder (Flores-Mireles *et al.* 2015).

Migration can be through an extraluminal route that originates from the contamination to the tip during insertion or intraluminal which is caused by ascending biofilm migration from the perineum (Tambyah *et al.* 1999; Maki and Tambyah 2001). Almost ninety per cent (90 %) of CAUTIs are ascending (Czerwonka *et al.* 2014) making it the most common route of infection. Ascending migration is caused by either capillary action or resulted from refluxed contaminated urine inside the catheter due to compromised drainage system or collection bag (Tambyah *et al.* 1999). 16s ribosomal DNA sequence techniques were used to show more than a ninety-eight per cent (98 %) similarity of strain population between the external and internal catheters and the urine (Barford *et al.* 2008). Regardless of the point of entry, once the bacteria reach the urinary tract via the urethra, they first infect the bladder and then the upper part of the urinary tract, leading to serious medical problems (Czerwonka *et al.* 2014).

Bacterial growth detected in urine indicates that there is a diverse bacterial community colonising the urinary tract including potential uropathogens (Hilt *et al.* 2014). Humans' pre-existing urinary normal flora is found similar to organisms that cause UTI from contaminated catheters (Stacy *et al.* 2015; Whiteside *et al.* 2015). A comparison study between microorganisms found in patients with an external catheter and indwelling catheter show that origin from the perineal microflora is possible (Grigoryan *et al.* 2014).

It is only recently that we believe that our bladders may not be sterile and the commensal community existing there might have a role as our natural defence mechanism against infection. Figure 1-17 explains this and how antimicrobial treatment might disrupt the healthy combination of these commensals and thus breach the effect of the defence mechanism that this population provides (Whiteside *et al.* 2015).

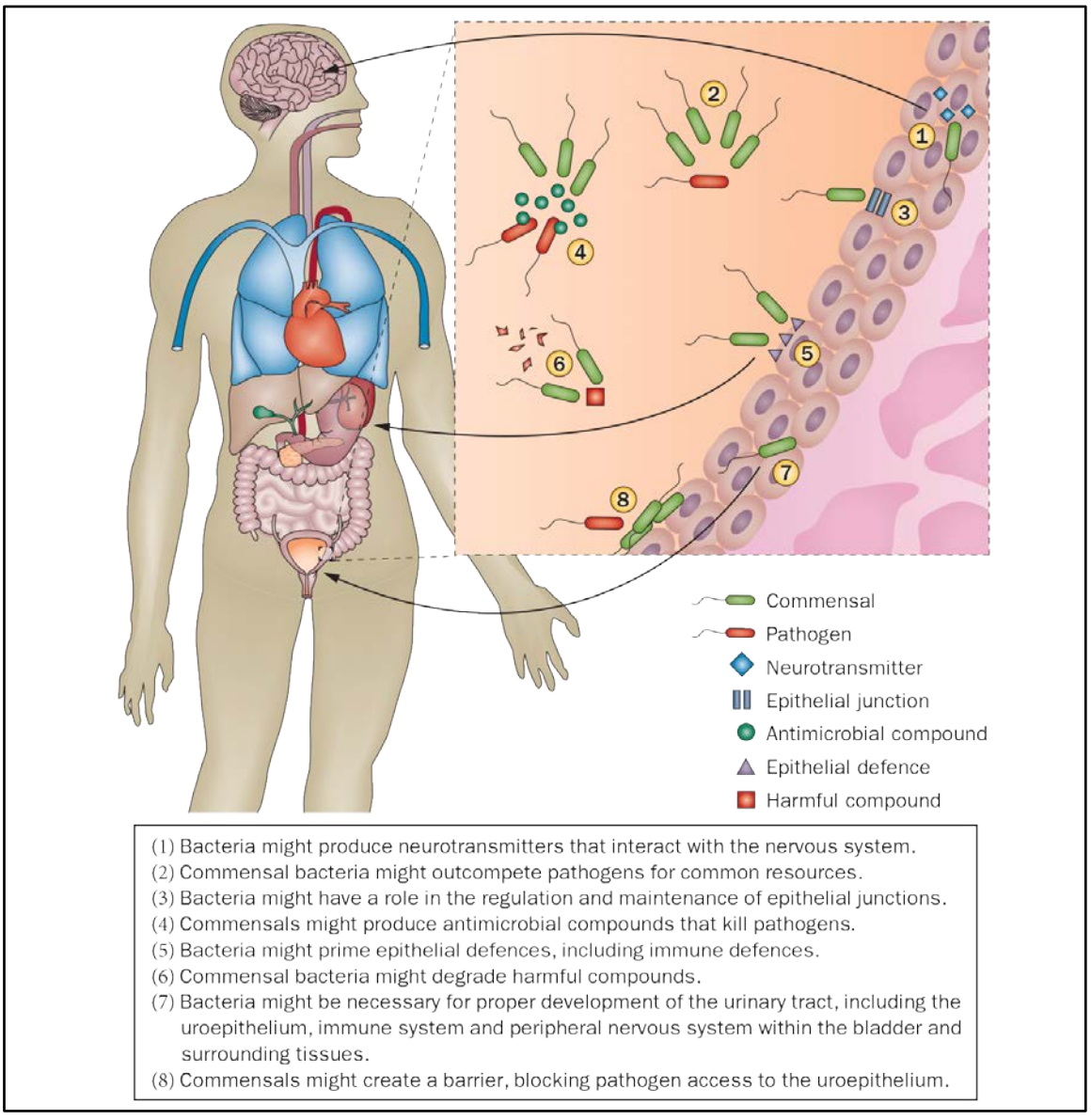

Figure 1-17 Potential roles of the urinary microbiota in homoeostasis of the urinary tract. Adapted from Whiteside *et al.* (2015).

1.2.4.4 Common bacterial species in CAUTI

Escherichia coli is the most common bacterium associated with CAUTI and responsible for more than eighty per cent (80 %) of all cases of UTI (Hancock *et al.* 2008; Watts *et al.* 2010; Cerqueira *et al.* 2013). This Gram-negative bacterium is a common causative agent for both uncomplicated and complicated UTI (Azevedo *et al.* 2014; Flores-Mireles *et al.* 2015). As the most commonly found bacteria in patient samples infected with CAUTI, it is frequently used in biofilm CAUTI research (Tambyah *et al.* 1999).

Studies on *P. aeruginosa* biofilm development from clinical isolates were extensive as *P. aeruginosa* was the most common pathogen found in various infections associated with biofilms (Kumon 1996; Colvin *et al.* 2012; Wesseling 2015). *P. aeruginosa* is a Gram-negative, rod-shaped opportunistic pathogen that has been widely used as the model organism in biofilm research including studies related to nosocomial infections including CAUTI (Lyczak *et al.* 2000; O'Toole *et al.* 2000; Baum *et al.* 2009; Byrd *et al.* 2011; Ghafoor *et al.* 2011; Burrows 2012; Bjarnsholt 2013; Tolker-Nielsen 2014).

P. mirabilis is the most isolated uropathogen in the urine found in nearly forty per cent (40 %) of patients with indwelling catheters which due to its ureolytic activity (Stankowska *et al.* 2012)(Stickler 2008). It also known as the culprit that causes encrustation and catheter blockage, which is usually followed by other complications such as pyelonephritis, septicaemia or endotoxic shock (Stickler 2014). More than half of patients (62 %) with recurrent *P. mirabilis* catheter encrustation develop bladder stones (Jacobsen and Shirtliff 2011).

The survival of *Proteus sp.* biofilm on the catheter relies on its ability to produce microcrystalline material as the foundation layer on the catheter surface (Stickler and Morgan 2008; Morgan *et al.* 2009; Desai *et al.* 2010; Wilks *et al.* 2015). This microcrystalline material is believed to be struvites ($MgNH_4PO_4.6H_2O$) and apatites which have similar properties to bladder stones (McLean *et al.* 1991; Nickel *et al.* 1994; Jacobsen *et al.* 2008).

Struvites are formed as a result of urease activity by urease-producing bacteria such as *P. mirabilis* which increases the pH above neutrality and further making struvite formation more favourable (McLean *et al.* 1991; Morris *et al.* 1999). This crystal formation serves as an excellent protection layer against any antimicrobial treatment available on the catheter and enables the bacteria to attach and proliferate (Stickler and Morgan 2008; Jacobsen and Shirtliff 2011; Tenke *et al.* 2012; Armbruster *et al.* 2017).

1.2.4.5 Single species versus polymicrobial species biofilm studies on catheter

Biofilms in CAUTI are caused by communities of microorganisms that exist on the surface skin of patients and in the urine (Barford *et al.* 2008). Previous studies have shown that CAUTI is often caused by polymicrobial biofilms (Macleod and Stickler 2007; Holá *et al.* 2010). In 1999, a study by Tambyah *et al.* (1999) on patients with UTI reported that *E. coli* was the second most common organism found and single species colonised most of the patients' catheters. Ten years later Holá *et al.* (2010) reported the opposite that there only a small percentage of patients have single species biofilm on the catheters.

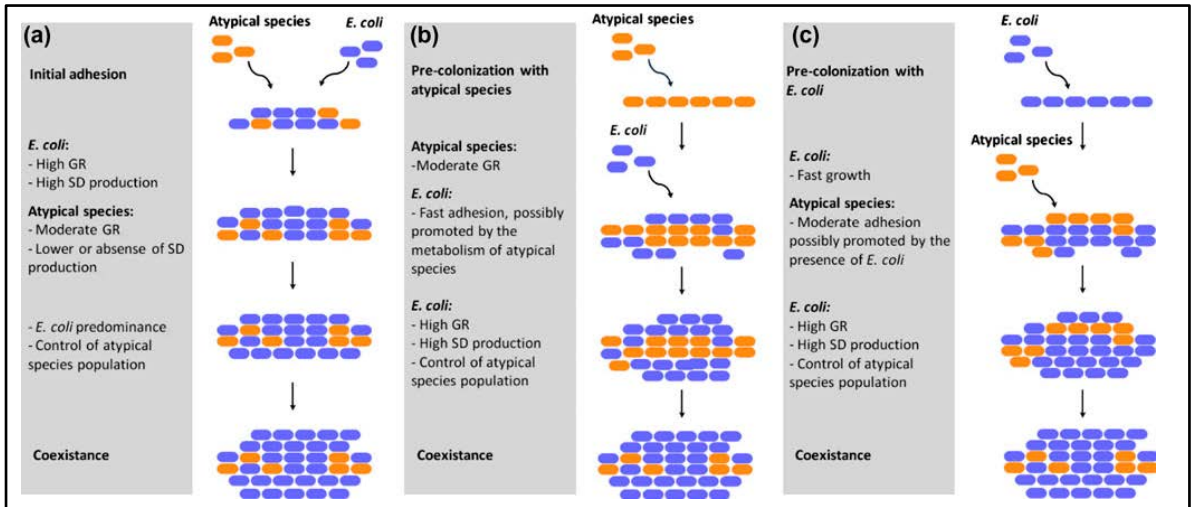

Representation of the interaction between *E. coli* and atypical microorganisms (a) in dual-species biofilm with simultaneous addition of the species; (b) in dual-species biofilm subjected to a pre-colonisation step with the atypical species, followed by the addition of the *E. coli*; and (c) in dual-species biofilms subjected to a pre-colonisation step with *E. coli*, followed by the addition of the atypical species. Regardless of the initial conditions, the dual-species biofilm tended to a final state of coexistence where *E. coli* predominated over the atypical species (GR = growth rate; SD = siderophores).

Figure 1-18 The effects of growth in dual species between *E. coli* and atypical microorganism in different concentration displaying its predominance and coexistence. Image adapted from Azevedo *et al.* (2014).

Both *E. coli* and *P. aeruginosa* are opportunistic uropathogens that possess dominance characteristics over other species due to the favourable microenvironment of our lower urinary tract (Reisner *et al.* 2006; Anderson *et al.* 2007; Hancock *et al.* 2007). Previous studies have reported that these two organisms have the ability to form biofilm that supersede other atypical microorganisms when grown together (Cerqueira *et al.* 2013; Azevedo *et al.* 2014).

While Cerqueira *et al.* (2013) showed that *P. aeruginosa* might have dominance over *E. coli*; a study by Azevedo *et al.* (2014) revealed that *E. coli* biofilm has dominance when grown with other atypical microorganisms due to the advantage of establishing a synergistic cooperation and coexistence with atypical bacteria during multispecies biofilm development on the catheter (Figure 1-18) (Azevedo *et al.* 2014).

The study also showed how the *E. coli* biofilm development as single species or dual species with other atypical microorganisms might provide an explanation for the *E. coli* prevalence in CAUTI. Azevedo *et al.* (2014) concluded that *E. coli* possess a greater ability in forming biofilm when grown in conditions similar to CAUTI regardless of predecessor colonising species.

1.2.4.6 Catheter encrustation by urease-producing biofilm

Encrustation is the accumulation of salt and other organic matter that was found to help the growth of biofilms on the catheter surface. Encrustations were extensively studied as the build-up causes the catheter to be blocked and lead to internal injury in the lining of the bladder and urethra (Stamm 1991; Choong *et al.* 2001; Stickler and Feneley 2010). The blockage will then lead to incontinence and causes extreme pain to the patient, as the bladder and the kidneys become under pressure. Unable to release the urine via the lumen leads to urine leakage and further problems to the patient (Cox *et al.* 1989). Most catheters including silver or nitrofurazone-coated devices are susceptible to encrustation and catheter blockage (Stickler 2014; Wilks *et al.* 2015).

Due to the importance of encrustations, the microorganisms that are prevalent in CAUTI have been divided into catheter blockers and non-blockers depending on the ability of the species to produce urease and form struvites. The main organism that is widely studied and responsible for contamination and encrustation in Foley catheters is the Gram-negative urease-producing *Proteus mirabilis* (Stickler 2014). *Proteus mirabilis* uses the urea in the urine to produce ammonia, thus elevating the pH of urine and the microenvironment of the catheter. The increase of pH above neutral (> pH 7) will cause the magnesium and calcium to become insoluble and precipitate. The aggregation of the precipitates deposit on the catheter and can be seen as encrustation on the catheter surface, which can block the catheter lumen (Morgan *et al.* 2009; Stickler 2014; Wilks *et al.* 2015).

1.2.4.7 Visualisation of biofilm on urinary catheter

Biofilm studies include stages in biofilm development and the different characteristics of biofilm properties. Often these features of biofilm are linked to the genetic mechanism changes required to adapt to the strict environment (Wang *et al.* 2010). However, visualisation of these micro communities has been a challenge in many various methods.

Light microscopy is easy to use and a popular observation technique in the laboratory (Lawrence *et al.* 1991; Walker and Keevil 1994; Azeredo *et al.* 2017). However, in biofilm studies, it has its limitation with hard to image details as well as the stratification of biofilm that consists of different layers of microbes and extracellular polymeric substance. Most biofilm development that occurs, especially on urinary catheters, involves being surrounded by liquid or water where

the biofilm structures are supported in a hydrated environment. In fact, almost more than seventy-three per cent (73 %) of the open biofilm structure is made of extracellular material and fluid (Kumon 1996; Dunne Jr 2002; Davey *et al.* 2003).

This poses a problem for post-processing preparation that requires water to be eliminated, such as prior to scanning electron microscopy (SEM), where the dehydration procedure required will cause the open structure in the biofilm to appear collapsed and alters the visual process (Kumon 1996; Toyofuku *et al.* 2016; Azeredo *et al.* 2017). Another modified version built upon SEM is the environmental SEM (ESEM) that produces an acceptable detailed spatial image of biofilm and requires no dehydration of sample or coating during sample preparation (Holling *et al.* 2014a).

Confocal laser scanning microscopy (CLSM) is widely used and modified in visualising fully hydrated bacterial biofilms (Kumon 1996; Khajotia *et al.* 2013; Swearingen *et al.* 2016). This makes the analysis of living biofilms possible and more preferable than SEM or even conventional phase-contrast microscopy (Kumon 1996). Although very useful, CLSM often disregards out of focused areas and might not be suitable for biofilms on catheters (Donlan and Costerton 2002). Often CLSM is used in combination with a staining technique involving positive staining, negative staining, or combination of both to visualise biofilms and its surrounding material.

An easy-to-use but very powerful method used to visualise biofilm is the EDIC microscopy method as used previously by Keevil (2003). The EDIC microscope is modified from Nomarski DIC (differential interference contrast) light microscope with a Nomarski prism that is able to create a pseudo-3D image of a sample surface. The conventional use of DIC microscopy is to visualise samples to produce high resolution and contrast images using transmitted light. However, EDIC microscopy can further aid observing a sample surface that cannot be visualised with transmitted light.

With the EDIC microscope, the biofilm often can be viewed using an epifluorescence (EF) differential stain applied to the sessile biofilm showing the developing layers on the catheter. For EF microscopy, the EDIC microscope is used together with an excitation and emission filter of a specific wavelength to detect and enhance the fluorophores present in the sample.

Using this advanced EDIC microscopy is very powerful for biofilm study as it is a cost-effective technique, non-destructive; with little to none sample preparation that can capture real-time images of biofilm development. It does not require any modification preparation to the sample and serves as an excellent alternative tool to other visualisation techniques such as Environmental Scanning Electron Microscopy (ESEM) and Scanning Confocal Laser Microscopy (SCLM) (Keevil and Walker 1992; Keevil 2003; Wilks *et al.* 2015).

1.2.4.8 Growth media used in urinary biofilm studies

Present uropathogen biofilm research were reviewed for the common growth media used in past studies. Table A-1 in Appendix A summarises selected biofilm studies categorised according to the growth media used in the *in vitro* biofilm growth method and their characteristics including mode of growth, pH of the media, and the *in vitro* model utilised in the analysis. Common growth media that previous studies have used in urinary biofilm experiments are general nutrient media, ultrafiltered (UF) human urine, and refined artificial urine media (AUM) formulated from urinary related studies. General nutrient media, such as Luria Bertani Broth (LB), Nutrient Broth (NB) or others, were the most commonly used growth media in urinary biofilm research. It is unsurprising as general nutrient media are intended for bacterial growth and are able to guarantee biofilm development.

Past studies have also used UF human urine as a growth medium for uropathogenic biofilms (Anderson *et al.* 1980; Stickler *et al.* 1999a; Morgan *et al.* 2009; Amalaradjou *et al.* 2010; Reisner *et al.* 2014). The UF human urine is an ideal growth medium for uropathogenic biofilms, but there are challenges to using it in *in vitro* studies. It is laborious to obtain large quantities of UF human urine as collecting and sterilising it is an arduous process. Using UF human urine can produce inconsistent and pseudo results caused by the variability of the urine physicochemical properties (Greenwood and O'Grady 1978; Brooks and Keevil 1997).

Urine contains various waste metabolites excreted from the body such as salts, excessive nitrogen, and other nutrients. Different individuals have distinct metabolic needs thus affecting their urine composition. The food consumed, the volume of water intake and various activities contribute to the variability of the urine. The pH level of urine corresponds to changes in the composition of the urine. It can influence certain urease-enzymatic activities of the urine that causes encrustation on the catheter (Edin-Liljegren *et al.* 1992; Getliffe 2004).

It also affects the bacteria virulence factors, which helps with bacterial survivability and induces infection in the human bladder (Shields-Cutler *et al.* 2015). The pH is an important aspect to consider in uropathogenic biofilm studies, as it can influence the topography of a surface material, which affects the bacterial attachment and its pathogenicity (Khan *et al.* 2015; Shields-Cutler *et al.* 2015). A typical range for normal pH urine is approximately between pH 4.6 to pH 8.0. The wide range is due to our daily nutritional intake that varies throughout the day. Our body excretes the urine as a product of the metabolic system that balances the body's pH levels (Rosdahl and Kowalski 2011). The pH of urine is slightly acidic in the morning (pH 6.5 - pH 7.0) due to no intake of food or beverages during sleeping, but then it changes to alkaline (pH 7.5 - pH 8.0) during the evening (Figure 1-19) (Edin-Liljegren *et al.* 1992). The extreme change in diet, precursor indication of kidney disease, kidney failure, loss of water through vomiting or diarrhoea and starvation are all possible causes that affect the pH level to fall within abnormal measurements (Figure 1-20) (Simerville *et al.* 2005; Patel 2006).

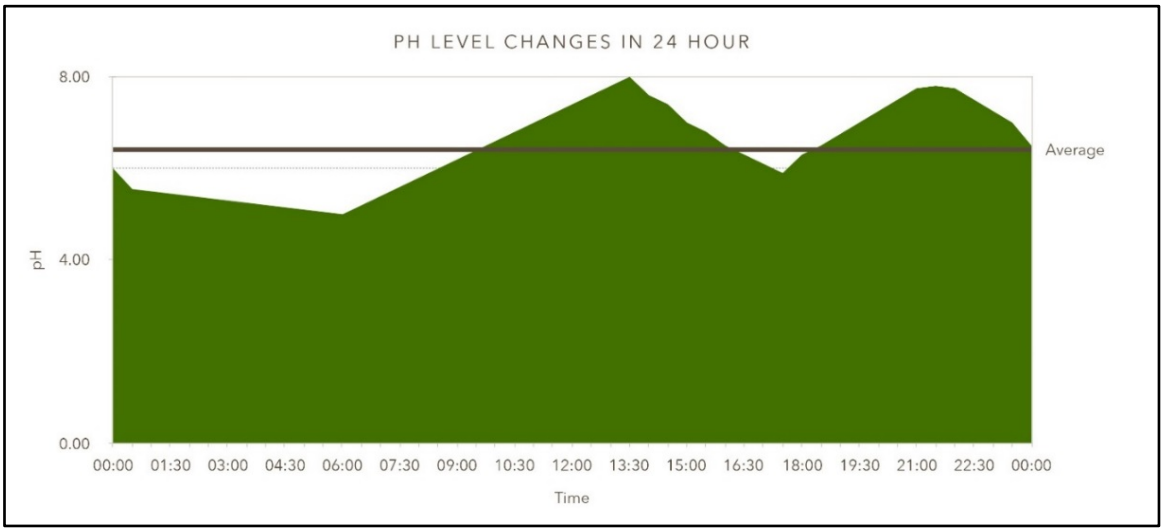

Figure 1-19 Human urine pH level changes throughout the day.

The deteriorating health state of a patient can also influence the abnormal measurements of their urine. Aubron *et al.* (2012) reported the differences in urine characteristics between healthy patients and trauma patients. The report also shows that the urine from the trauma patients facilitates the increased growth of *E. coli* compared to urine from healthy adults. The biochemical composition of urine from trauma patients is different from healthy patients due to inflammation or systemic stress and, for some, the procedure of urinary catheter insertion. The changes in urine composition in trauma patients present a higher level of glycosuria, iron concentration, and several amino acids that promote a favourable growth condition for uropathogenic *E. coli* (UPEC) compared to healthy urine (Aubron *et al.* 2012).

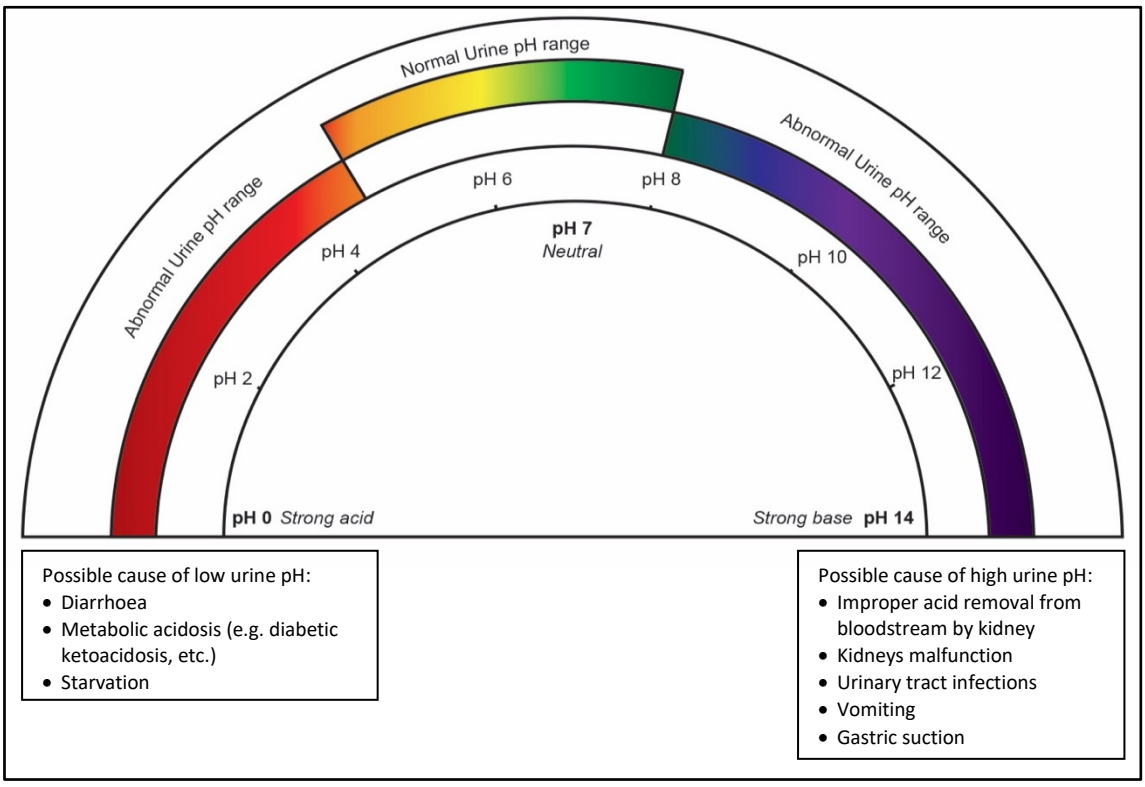

Figure 1-20 Normal and abnormal pH range of the human urine

The current approach for urine substitution is by using an artificial urine medium (AUM). AUM is a refined nutrient medium that is formulated to mimic the physicochemical properties of human urine. AUM is widely used as a urine substitute in investigations related to human bladder and urine, which includes *in vitro* uropathogenic growth studies using a similar experimental environment to the urinary tract.

Careful consideration need to be taken when using any artificial formulation to avoid false representation of the results (Donlan and Costerton 2002). Another concern arises when comparing the result of the studies, as currently there is no standard for uropathogenic growth nutrients; therefore, the similarity to human urine remains unclear. Figure 1-21 shows a pie chart representing the categorised articles according to the growth media used; AUM, UF human urine, or other general growth media.

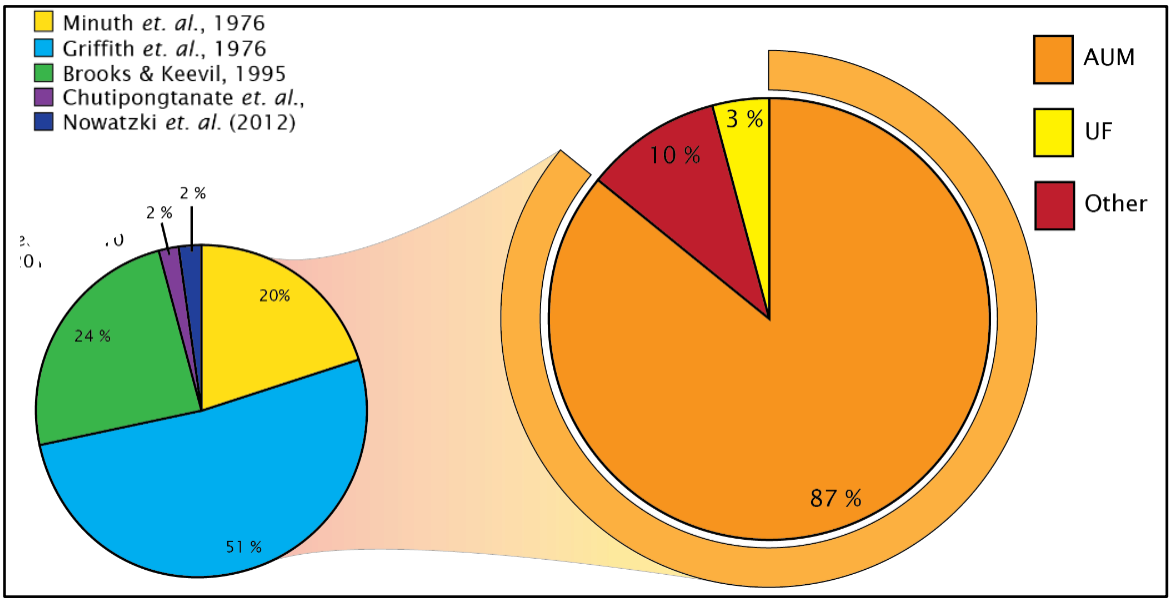

Figure 1-21 Pie chart showing percentages according to the type of growth media and AUM used in selected articles.

Eighty-seven per cent (87 %) of the studies have used AUM as preferred growth nutrient, leaving others with three per cent (3 %) using UF human urine and ten per cent (10 %) using other growth media. The five most common formulations among the studies that were using AUM are Minuth *et al.* (1976), Griffith *et al.* (1976), Brooks and Keevil (1997), Chutipongtanate and Thongboonkerd (2010), and Nowatzki *et al.* (2012).

More than half of the studies used the Griffith *et al.* (1976) formulation (51 %), twenty per cent (20 %) used Minuth *et al.* (1976), twenty-four per cent (24 %) used Brooks and Keevil (1997), and two per cent (2 %) each for Chutipongtanate and Thongboonkerd (2010), and Nowatzki *et al.* (2012). Table C-1 in Appendix C shows the comparison between the AUM formulation, and the differences in chemical composition, concentration, and pH of media.

Minuth *et al.* (1976) published their AUM formulation just before Griffith *et al.* (1976) in the same year and presented a similar chemical composition to Griffith *et al.* (1976). The differences in Griffith *et al.* (1976) were the concentration of urea and ammonium chloride, the omission of creatinine, and the addition of gelatine compared to Minuth *et al.* (1976). Minuth *et al.* (1976) AUM was based on the chemical composition of pooled human urine from healthy volunteers from the study. Griffith *et al.* (1976) AUM was formulated while studying the role of urease in urinary stone formation. The study was a continuation of an earlier study by Musher *et al.* (1974) on the antibacterial effect against urease-producing bacteria, *P. mirabilis*.

Both Musher *et al.* (1974) and Griffith *et al.* (1976) used the work by Robertson *et al.* (1968) for the composition of stone-forming and non-stone-forming urine when formulating the AUM. Griffith *et al.* (1976) research on ureases in urinary stones has influenced the addition of gelatine to increase the AUM matrix. The supersaturation effect induces the precipitation of minerals that occurred similarly in diseased urine. Many studies in CAUTI with mutual interest have used Griffith *et al.* (1976) AUM rather than Minuth *et al.* (1976) since its inception. There was a forty-one year gap since then before the Brooks and Keevil (1997) AUM formulation was published.

Brooks and Keevil (1997) has considered the normal human urine composition published by Altman (1961) and carefully manipulated each of the components to produce an AUM with a stable composition and a balanced electrolyte pH of 6.5. The study was able to produce recoverable clinical isolates which presented favourable bacterial growth (Brooks and Keevil 1997).

Chutipongtanate and Thongboonkerd (2010) created their own AUM formulation from their study by analysing other AUM formulations, which among others, included Brooks and Keevil (1997). A systematic approach was used in comparing six AUM formulations with their own AUM, later referred it as AU-Sririraj. Among the six AUM that were analysed, only Brooks and Keevil (1997) AUM supported bacterial growth, while the others were mostly used for studying calcium crystallisation. Only AU-Sririraj and AUM by Brooks and Keevil (1997) were found to support growth with lower toxicity in Madin-Darby canine kidney (MDCK) cells compared to others. However, AU-Sririraj was targeted for broader use and was not specifically formulated only for bacterial growth. Several essential trace elements were omitted in the AU-Sririraj formulation (Chutipongtanate and Thongboonkerd 2010).

Nowatzki *et al.* (2012) AUM was formulated to study anti-biofilm properties of different manufactured coatings in CAUTI research. The study analysed pooled healthy human urine and used Brooks and Keevil (1997) as a basis for their AUM formulation with certain changes in components and concentration.

Nowatzki *et al.* (2012) used casamino acids in place of bacterial peptone for protein and peptide sources. Casamino acid is one of the chemical components of normal human urine listed in Pschyrembel (2014), although it is in a much lower amount (0.02 g) compared to the amount in Nowatzki *et al.* (2012) AUM (1 g). Nowatzki *et al.* (2012) omitted iron supplementation in the AUM as they thought it was unnecessary for bacterial growth. This was opposite to studies by Hancock *et al.* (2010) and Tielen *et al.* (2013), which highlighted the importance of iron minerals in the nutrient source as it is necessary for bacterial growth. Iron is an essential cofactor in cell metabolism, especially in a limited environment of freely available iron in the mammalian body.

Iron depletion in the environment creates a stressful growth condition that can stimulate the virulence factors in bacteria and affects the biofilm development (Moreira *et al.* 2003; Hancock *et al.* 2010; Tielen *et al.* 2013). Iron has been used in biofilm studies as an anti-fouling material in catheter coating (Trautner and Darouiche 2004b; Flores-Mireles *et al.* 2015). The only AUM in this analysis that includes iron in the formulation is Brooks and Keevil (1997).

Previous studies by Griffith *et al.* (1976) and Brooks and Keevil (1997) have mentioned the importance of pH as an influence on the precipitation of minerals in the AUM. However, only Brooks and Keevil (1997) AUM has a pH which falls within the usual range of a healthy urine (Figure 1-22). Fifty-five per cent (55 %) of the studies analysed used a range of pH in artificial urine medium between pH 6.0 and pH 6.5, while the rest used a lower pH of 5.8 or above pH 6.4.

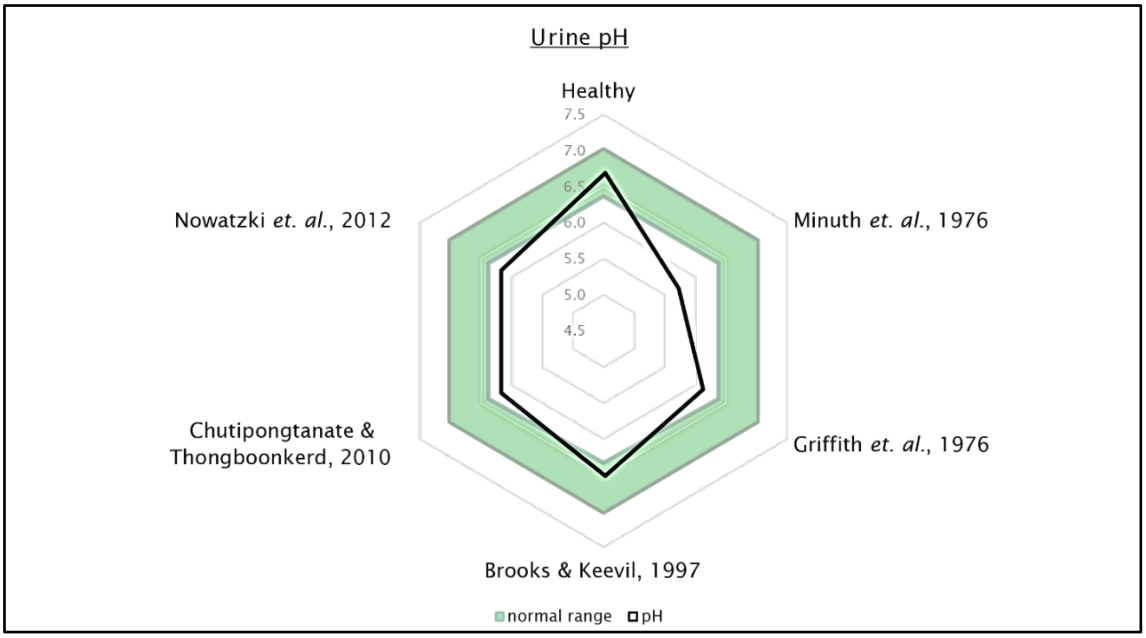

Figure 1-22 Radar graph showing the pH level composition in AUM compared to the usual range of a healthy individual.

Aubron *et al.* (2012) reported that pH level elevation in trauma patients facilitates bacterial infection. This shows similar results to the study by Broomfield *et al.* (2009) using *in vitro* models with urease-producing organisms. It was observed that the catheter blockage happened less than 24 h by *P. mirabilis* and the pH of urine during blockage was above pH 8 (Broomfield *et al.* 2009).

The commonly used media AUM from Griffith *et al.* (1976), and Brooks and Keevil (1997), and the general nutrient TSB were selected to be used in the comparison study of growth nutrient that influences the biofilm development in this research.

1.2.5 *P. aeruginosa* as model organism for urinary biofilm studies

1.2.5.1 Introduction

P. aeruginosa is an established model organism in biofilm studies due to its prevalence in nosocomial biofilm infections (Heydorn *et al.* 2002; Wei and Ma 2013; Wesseling 2015). *P. aeruginosa* was first discovered around 1862 and distinctively known to cause the blue-green coloration of pus of in human infections. However, it was not until twenty years later in 1882 that it was isolated and was previously known as *Bacillus pyocyaneus* (Lyczak *et al.* 2000). Among the reason that made *P. aeruginosa* a prominent model bacterium in biofilm research is because of its comprehensive 6.3-Mbp genome and the availability of a developed transposon mutant library with more than 30,000 sequence-defined mutants (Stover *et al.* 2000; Jacobs *et al.* 2003; Held *et al.* 2012) .

1.2.5.2 *P. aeruginosa* two-allele mutant library

The *P. aeruginosa* two-allele mutant library were developed in 2003 by the team at the Department of Genome Sciences, University of Washington (UWGC, Seattle, Washington, USA). The comprehensive collection was a collaborative initiation between Prof. Maynard Olsen and Prof. Colin Manoil (UWGC) that offers single colony purified isolates of at least two alleles of each PAORF insertion. The library was created using *P. aeruginosa* PAO1 host strain and there are more than nine thousand sequence-defined strains developed in the *P. aeruginosa* two-allele mutant library (Jacobs *et al.* 2003; Held *et al.* 2012). Strains from the *P. aeruginosa* two-allele mutant library have been used for many studies including screening for genotype/phenotype characteristics in biofilm development demonstrate that the library is a useful and invaluable tool for research as it shortens time and reduces cost of conducting experiments (Wu *et al.* 2008; Martinez and Campos-Gomez 2016).

1.2.5.3 *P. aeruginosa* biofilm formation

The developmental life cycle of *P. aeruginosa* biofilm involves multiple stages of biofilm progression with each possessing a unique morphology (Sauer *et al.* 2002). The common initiation of biofilm life cycle begins with the contamination of bacteria in its planktonic state. Upon entering the biofilm state, the first stage of the biofilm life cycle is the reversible attachment of cells to the surface.

The attached cells begin to colonise the surface by aggregating and proliferating to form microcolonies. The microcolonies further distinguishes into macrocolonies involving complex EPS

matrix in the maturation phase. At this point, the attachment of bacteria has become irreversible. The macrocolonies further expand and differentiate into mature biofilm while responding to the environmental factors that affect the biofilm growth and stability. Mature biofilms can be distinctively identified by three-dimensional structures referred to as “mushroom” towers with water channels developed in between *P. aeruginosa* (Costerton *et al.* 1999; Stapper *et al.* 2004; De Kievit 2009; Hay *et al.* 2009).

The last phase of the biofilm life cycle is the dispersal stage where cells are released and return to planktonic state, which then colonises a surface when it is convenient before repeating the biofilm life cycle again (O'Toole *et al.* 2000; Stoodley *et al.* 2002; Rice *et al.* 2009; Musken *et al.* 2010; Rahmani-Badi *et al.* 2014).

1.2.5.4 Regulation of factors affecting biofilm formation in *P. aeruginosa*

P. aeruginosa can form a biofilm on both biotic and abiotic surfaces due to the well-regulated mechanism of its virulence genes (Klausen *et al.* 2003b; Murakami *et al.* 2017). The schematic diagram in Figure 1-23 features the regulation pathway of biofilm formation in *P. aeruginosa* PAO1. There are approximately more than 500 biofilm-related proteins that are mostly regulated by quorum-sensing, polysaccharide production and motility genes (Sauer *et al.* 2002).

Quorum-sensing (QS) in biofilm infections has important implications as it not only controls, but also enhances the virulence factors. Pqs, Rhl and La*s* systems have been identified as the three main QS-controlled mechanisms in *P. aeruginosa*. The QS-controlled mechanism is affected by cell densities, which are detected via the concentration of the QS signal molecules in the biofilm population to activate the relevant gene expression. These QS signal molecules are made of N-acyl-homoserine lactones (AHL) that is used by Las and Rhl, whereas *Pseudomonas* Quinolone Signal is used by the PQS system (Figure 1-24) (De Kievit 2009; Rasamiravaka *et al.* 2015). Approximately ten per cent (10 %) of the *P. aeruginosa* genome consists of QS-related genes mechanism (Miller and Bassler 2001; Kim *et al.* 2015; Newman *et al.* 2017; Abisado *et al.* 2018).

The QS cell-to-cell signalling in biofilms does not only depend on the available cell density but is further affected by various environmental conditions (Musken *et al.* 2010). A study by Allesen-Holm *et al.* (2006) reported that QS-deficient mutants produced thinner biofilms and lacked mushroom morphology compared to wildtype, due to less extracellular DNA (eDNA) available in the biofilm which affects the biofilm phenotype (Allesen-Holm *et al.* 2006). Iron and phosphate positively affect the biofilm formation of *P. aeruginosa* by improving the *pqs* (quinolone signal) system (Musken *et al.* 2010).

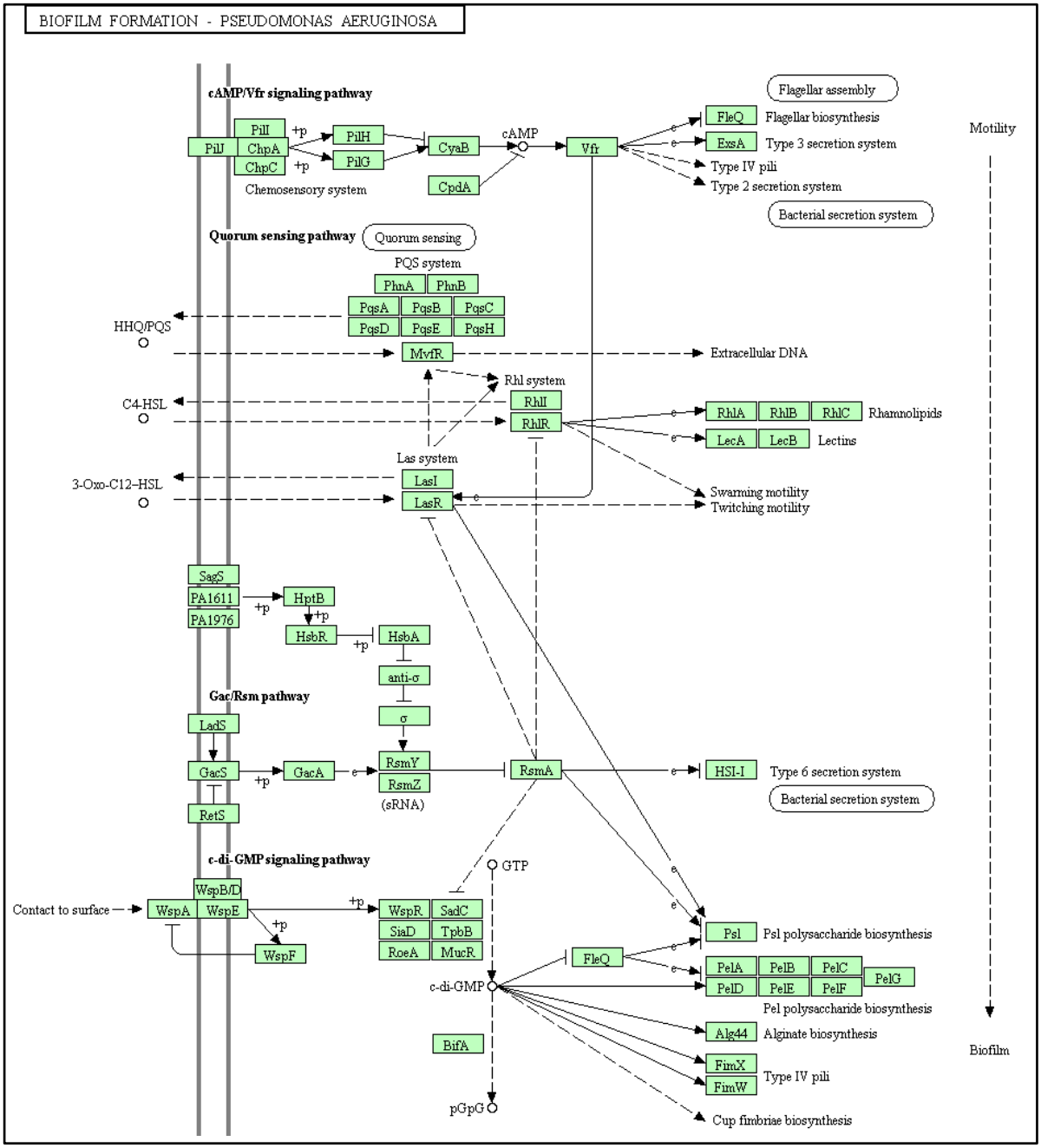

Figure 1-23 *P. aeruginosa* PAO1 biofilm formation pathway (pae02025) according to the KEGG database (www.genome.jp/kegg/).

P. aeruginosa quorum-sensing gene regulation has been reported to influence the properties of the biofilm EPS matrix (Sakuragi and Kolter 2007; Byrd *et al.* 2011). The EPS is the most prominent characteristic in identifying biofilm formation (Stoodley *et al.* 2002). This glue-like EPS glycocalyx slime that envelopes the attached bacteria on a surface is composed of a mixture of extracellular material such as glycoproteins, lipids, polysaccharides and eDNA (Costerton *et al.* 1999; Stoodley *et al.* 2002; Tenke *et al.* 2006).

Polysaccharide-alginate production in the EPS by *P. aeruginosa* biofilm typically has a high sugar-protein ratio and is the fundamental binding property to maintain the stability of the biofilm structure that contributed to the biofilm tolerance toward antimicrobial treatment and host

defence mechanism (Baum *et al.* 2009; Franklin *et al.* 2011). Additionally, it also conditions the surface to mitigate bacterial attachment, as well as catering for micronutrients to the biofilm community (Costerton *et al.* 1999; Rice *et al.* 2009).

Three common polyssacharides of EPS produced by *P. aeruginosa* during biofilm formation have been identified as Psl, Pel and alginate (Ryder *et al.* 2007). *psl* and *pel* are the two most relevant polysaccharide-production gene operons that control the virulence factors in chronic biofilm infection (Jones and Wozniak 2017). The roles of Psl, Pel and alginate production in *P. aeruginosa* urinary biofilm have never been studied before. However, it has been shown that Psl has a significant role in biofilm structures of mucoid strains (Jones and Wozniak 2017).

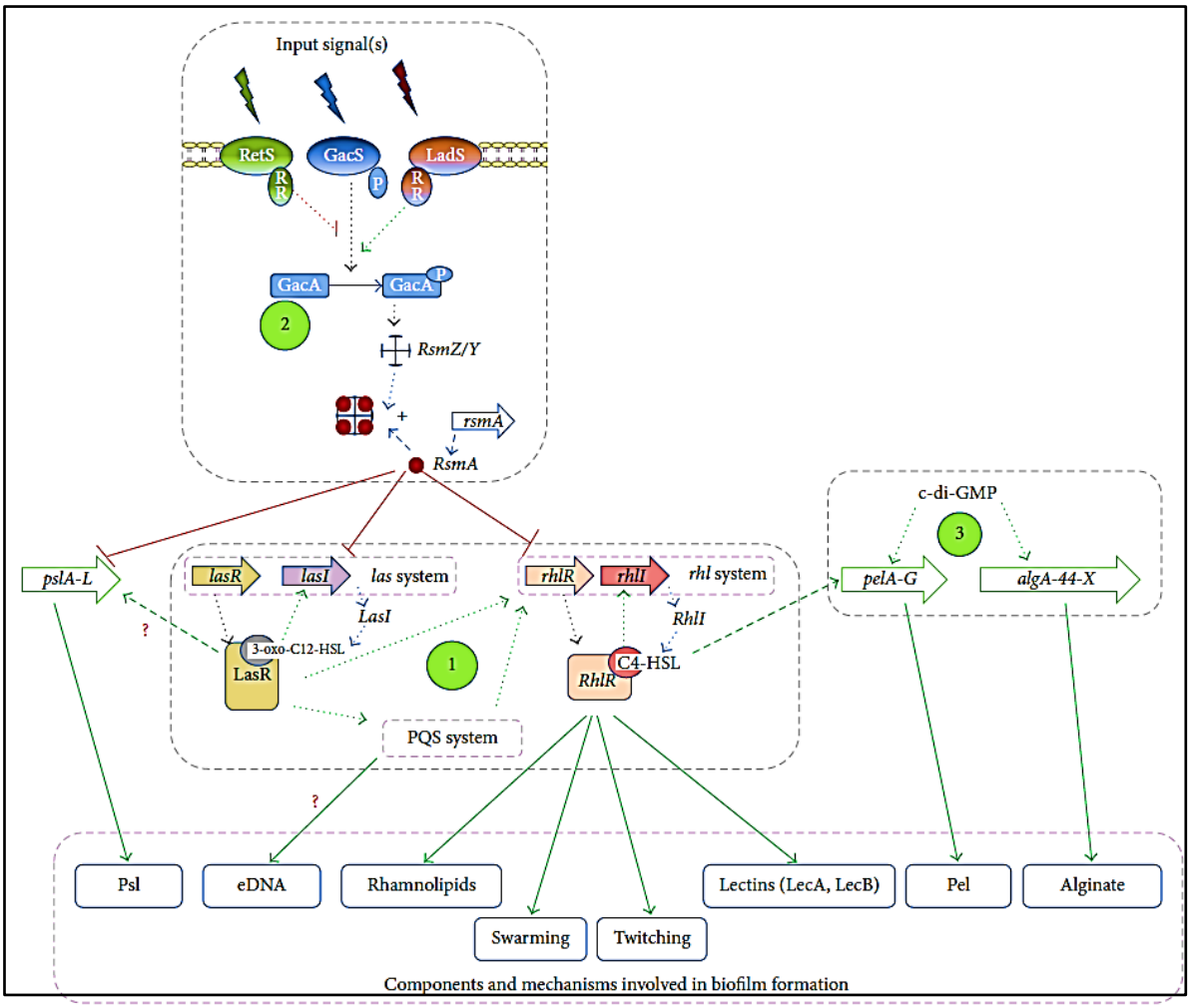

Figure 1-24 Quorum-sensing bacterial system in the regulation of *P. aeruginosa* biofilm formation. Adapted from Rasamiravaka *et al.* (2015).

The mucoid phenotype in *P. aeruginosa* biofilm remains a significant concern in chronic infections especially cystic fibrosis (CF) patients (Costerton *et al.* 1999; Stapper *et al.* 2004; Guttenplan and Kearns 2013; Irie *et al.* 2017). The mucoid phenotype is a result of a mutation in the gene that encodes the anti-sigma factor *mucA* that produced overproduction of alginate that helps the adhesion during the biofilm formation (Flemming and Wingender 2010; Tielen *et al.* 2013; Wesseling 2015; Jones and Wozniak 2017). Alginate is composed of uronic acids and is an

essential component in the biofilm EPS that makes it a key determinant of virulence in biofilm (Pedersen *et al.* 1992; Hay *et al.* 2009; Schurr 2013; Jones and Wozniak 2017).

Previous research has reported on the importance of attachment and motility factors in *P. aeruginosa* biofilm formation, but the current understanding of its role is still not conclusive. Attachment and motility structure, pili and flagella are reported to be involved in the initial attachment stage and microcolony formation in of *P. aeruginosa* biofilms (Whiteley *et al.* 2001; Heydorn *et al.* 2002; Saint and Chenoweth 2003; Burrows 2012; Tolker-Nielsen 2014). However Klausen *et al.* (2003b) have contrastingly reported that both pili and flagella has no role in attachment stage and that the requirement is conditional depending on nutritional factors (Klausen *et al.* 2003b; Wei and Ma 2013).

Sauer *et al.* (2002) has reported the observation of approximately 6-fold change difference in the expression in approximately 800 proteins between biofilm compared to the planktonic state. This means that there are many changes in proteins involved after cells attach to the surface upon entering the initial biofilm formation, which are also known as the reversible attachment.

The study also reported that the change between reversible to irreversible attachment in *P. aeruginosa* biofilm is contributed by the downregulation of motility (flagella) genes and upregulation of attachment appendages (pili) genes instead (Sauer *et al.* 2002). Although this shows that both flagella and pili structure are important to the *P. aeruginosa* biofilm formation, the roles of the attachment and motility genes in urinary biofilm formation on urinary catheter remains unclear.

1.3 Aim and objectives

The aim of this study is to present the variation of factors that influence the three-dimensional structure of urinary biofilms on catheters. This study is focused on answering three key research questions as shown in Figure 1-1, which will be achieved through the completion of the objectives in testing our hypotheses as outlined below.

The first objective is to fundamentally distinguish the physical characteristics observed in *E. coli* and *P. mirabilis* biofilm formation on urinary catheters with different growth media - using episcopic differential interference contrast (EDIC) microscopy and identifying key biofilm development stages. We will test the hypothesis that different nutrients affect urinary biofilm formation.

The second objective is to measure how the growth of *E. coli*, *P. mirabilis* and *P. aeruginosa* biofilms are affected by two different artificial urine media (AUM) and the pH surrounding the

microenvironment on the urinary catheter. These two objectives share a common contribution factor in our hypothesis on the appropriate AUM growth medium for this study.

The third objective is to investigate the biofilm formation in a model system of selected key important mutant genes of *P. aeruginosa,* PAO1, namely urease, quorum-sensing (QS) and attachment/motility (AM) essential genes. After growth in AUM, any phenotypic diversity will be observed and documented in the different mutants, using EDIC microscopy. This will allow the role and relationship of different genes in biofilm formation and development to be determined. This work will hypothesise the identified critical genes that are essential for biofilm growth and formation processes in the PAO1 model.

In achieving these objectives, this study will contribute to the increased depth of understanding of urinary biofilm formation for a number of different bacteria, grown under varying conditions; as well as an insight into the effect of different genes in *P. aeruginosa* PAO1 biofilm formation. This study will then help to inform and improve future treatment regimens and prevention strategies.

Chapter 2 General Methodology

2.1 Bacterial strains

The main bacterial strains used in this study were obtained from the Professor Bill Keevil's Lab (School of Biological Sciences, University of Southampton, UK), and the details are as listed below in Table 2-1. The *P. aeruginosa* PAO1 main reference strain and the transposon mutant strains used in Chapter 5, 6 and 7 were obtained from the *P. aeruginosa* two-allele transposon mutant library (UW Genome Sciences, University of Washington, USA), which were sequenced verified as described previously by Held *et al.* (2012). The knockout mutants used in Chapter 7 were kindly provided by Professor Myron Christodoulides (Molecular Microbiology, University of Southampton, UK). More information on the *P. aeruginosa* strains used in this study are as detailed in Table F-1 in Appendix F.

Table 2-1 Bacteria characteristics and their general growth media

Strain	Characteristics	Reference	General growth media	
			Liquid Broth	Agar
E. coli (UPEC) NCTC 9001	Isolated from: human, urine, cystitis.	ATCC® [a] 11775	TSB [b]	TSA [b], CLED [d]
P. aeruginosa PAO1	Opportunistic human pathogen.	ATCC® [a] 15692	LB [e]	TSA [c]
P. mirabilis NCTC 10975	Isolated from: human, urine.	BS 711	TSB [b]	CLED, TSA [c]

[a] ATCC, American Type Culture Collection.
[b] TSB, Trypticase Soy Broth
[c] TSA, Tryptone Soya Agar
[d] CLED, Cystine lactose electrolyte deficient
[e] LB, Lysogeny broth

2.1.1 Routine bacteria stock preparation

Bacterial stocks of all the strains used in this research were routinely prepared by transferring a single Protect™ glycerol bead (Fisher Scientific, UK) recovered from an existing stock vial into 10 ml of suitable growth culture media (as listed in Table 2-1) in a sterile tube. The culture was incubated overnight at 37 °C in an orbital shaking incubator set at 150 rpm. The overnight culture was harvested following the manufacturer's instructions and transferred into a new vial of Protect™ glycerol beads before being stored at -80 °C.

2.1.2 Inocula preparation

The bacterial inoculum was prepared by firstly making the overnight culture using a single Protect™ glycerol bead (Fisher Scientific, UK) from existing stock. The bacteria were harvested by centrifuging 1 ml of overnight culture at 7500 rpm (5400 × *g*) for 10 min. The supernatant was removed, and the pellet was resuspended using either growth media, sterile distilled water, phosphate-buffered saline (PBS) solution, or artificial urine medium, to form the inoculum. The concentration of bacteria was routinely observed by bacterial enumeration of colony-forming units (CFU) using agar plates. The bacterial inoculum from an overnight culture was serially diluted with PBS. Aliquots of 50 µl from the dilutions were plated onto 5 cm Petri dishes of suitable agar growth media, as listed in Table 2-1. The plates were incubated at 37 °C for 18 - 24 h before formed colonies on the agar plates were enumerated.

2.1.3 Calculation of inoculum concentration

The inoculum concentration was calculated using a statistical formula to be at least 1 × 10^9 cfu/ml, with confidence interval (α = 0.05).

Hypothesis: H_0 : mean initial population = 1 × 10^9 per ml

H_A : mean initial population ≠ 1 × 10^9 per ml

The statistical formula used was:

$$\mu = x \pm t_{(\frac{\alpha}{2}; n-1)}\, s/\sqrt{n}$$

(Paulson 2009)

Where:
- μ = mean population
- x = sample population
- α = significance level
- $t_{\frac{\alpha}{2}}$ = Student's t table value for two-tail α value
- n-1 = degrees of freedom
- n = sample size
- $s/\sqrt{n}$ = SE Mean

The mean (each replicate done at least in duplicate for three serial dilutions) was used for each bacterial inoculum prepared with AUM before the start of the experiment. A two-sample *t*-test was done on the cfu/ml between the two inocula prepared with AUG and AUBK before being used together in an experiment to check there are significance differences in concentration between them.

2.1.4 Growth rate of biofilm

CFU was used to determine the growth profile of each uropathogen grown in the two AUM. The growth rate was calculated from the exponential growth phase by using the following formula:

$$\mu = \frac{(\log_{10} N - \log_{10} N\theta)\ 2.303}{(t - t\theta)}$$

Where:

N = final CFU count (timepoint 6 h)
$N\theta$ = initial CFU count (timepoint 2 h)
t = final time (timepoint 6 h)
$t\theta$ = initial time (timepoint 2 h)
μ = growth rate

2.2 Culture media preparation

2.2.1 Trypticase Soy Broth (TSB)

Trypticase Soy Broth (TSB) (Oxoid, UK) was used as general medium to grow most bacterial cultures. TSB was supplied in the form of dehydrated powdered medium and prepared using deionized water (dH$_2$O). The required amount of dry medium was added to the deionized water, mixed thoroughly, and sterilised at 121 ^{o}C for 15 min as per manufacturer's instructions. The sterilised medium was cooled and maintained sterile before use.

2.2.2 Luria-Bertani broth (LB) Miller

Luria-Bertani broth (LB) Miller (Formedium, UK) is a routine medium which is rich in salt used to grow and for the maintenance of *P. aeruginosa* (LaBauve and Wargo 2012). LB was supplied in the form of dehydrated powdered medium and prepared using deionized water (dH$_2$O). The required amount of dry medium was added to the deionized water, mixed thoroughly, and sterilised at 121 ^{o}C for 15 min as per manufacturer's instructions. The sterilised medium was cooled down and maintained sterile before use.

2.2.3 Tryptone Soya Agar (TSA)

Tryptone Soya agar (TSA) (Oxoid, UK) was used as general medium for bacterial enumeration to determine cell concentration. The required amount of TSA dehydrated powdered medium was added to the deionized water as per manufacturer's instructions, mixed thoroughly, and sterilised at 121 ^{o}C for 15 min. The agar warming function was set 'ON' on the autoclave to maintain the temperature at 50 ^{o}C after the sterilisation cycle had completed. The sterilised agar media was kept warm at 50 ^{o}C in a warming oven until the next step of pouring into Petri plates. A sterile pipette was used to dispensed agar into sterile Petri plates and left until solidified before the lid was placed and kept in storage prior to use.

2.2.4 Cystine Lactose Electrolyte Deficient (CLED) agar

Cystine Lactose Electrolyte Deficient (CLED) agar (Oxoid, UK) was used as differential growth medium for bacterial enumeration of uropathogens. The required amount of dehydrated powdered medium was added to the deionized water as per manufacturer's instructions and sterilised at 121 ^{o}C for 15 min. A sterile pipette was used to dispensed agar into sterile Petri plates and left until solidified before the lid was placed and kept in storage prior to use.

2.2.5 Artificial urine medium Brooks & Keevil, 1997 (AUBK)

The AUBK was prepared as described by Brooks & Keevil (1997). Table 2-2 presents the composition of AUBK medium. A magnetic flea was added to a glass bottle with the required volume of deionized water dispensed using a measuring cylinder, and the contents were autoclaved with the agar warming function set 'ON' to maintain a temperature of 50 ^{o}C after the sterilisation cycle had completed. The autoclaved deionized water was placed on a hot plate stirrer set at the temperature of 50 ^{o}C to help dissolve the chemicals as they were added.

Table 2-2 Composition of Artificial Urine medium by Brooks and Keevil, 1997 (AUBK)

Component	Quantity (g)	Concentration (mmol/l)
Distilled water	to 1 l	
Peptone L37	1	-
Yeast extract	0.005	0.001
Citric acid	0.4	2
Lactic acid	0.1	1.1
Uric acid	0.07	0.4
Creatinine	0.8	7
Urea	10	170
Ammonium chloride	1.3	25
Calcium chloride dihydrate	0.37	2.5
Iron (II) sulphate heptahydrate	0.0012	0.005
Magnesium sulphate heptahydrate	0.49	2
Potassium dihydrogen phosphate	0.95	6.98
Di-potassium hydrogen phosphate	1.2	6.89
Sodium chloride	5.2	90
Sodium bicarbonate	2.1	25
Sodium sulphate decahydrate	3.2	10

Uric acid (0.07 g l^{-1}) was added first to the deionized water and allowed to dissolve. The following were then added: bacteriological peptone (1 g l^{-1}), yeast extract (0.005 g l^{-1}), citric acid (0.4 g l^{-1}), lactic acid (0.1 g l^{-1}), creatinine (0.8 g l^{-1}), ammonium chloride (1.3 g l^{-1}), urea (10.0 g l^{-1}), calcium chloride dihydrate (0.37 g l^{-1}), Iron (II) sulphate heptahydrate (0.0012 g l^{-1}), magnesium sulphate heptahydrate (0.49 g l^{-1}), potassium dihydrogen phosphate (0.95 g l^{-1}), di-potassium hydrogen phosphate (0.2 g l^{-1}), sodium chloride (5.2g l^{-1}), sodium bicarbonate (2.1 g l^{-1}), and sodium sulphate decahydrate (3.2 g l^{-1}). The pH of the artificial medium was then adjusted to pH 6.50. The artificial urine was filtered through a sterile 0.2 µm Sartorius (Göttingen, Germany) filter, and transferred into a pre-sterilised glass bottle for storage. Glassware used were thoroughly washed with hot water and Decon 90 detergent before rinsing with dH_2O.

2.2.6 Artificial urine medium Griffiths *et al.,* 1976 (AUG)

Table 2-3 presents the composition of AUG medium. The AUG was prepared as Griffiths *et al.,* 1976 (AUG) by firstly adding the TSB prior to autoclaving the solution instead of adding it at the end. A magnetic flea was added to the glass bottle with the required volume of deionized water dispensed using a measuring cylinder. TSB was added to the deionized water to a final concentration of 1 g l^{-1}. The contents were autoclaved with the agar warming function set 'ON' to maintain a temperature of 50 ^{o}C after the sterilisation cycle had completed. The autoclaved deionized water was placed on a hot plate stirrer set at the temperature of 50 ^{o}C to help dissolve the chemicals as they were added.

Table 2-3 Composition of artificial urine medium by Griffiths *et al.,* 1976 (AUG)

Component	Quantity (g)	Concentration (mmol/l)
Distilled water	to 1 l	
Gelatine	5	0.9
Urea	25	420
Ammonium chloride	1	19
Calcium chloride	0.49	4.4
Magnesium chloride hexahydrate	0.65	3
Potassium chloride	1.6	21.5
Potassium dihydrogen phosphate	2.8	20.6
Sodium chloride	4.6	0.27
Sodium sulphate	2.3	16.2
Tri-Sodium citrate dihydrate	0.65	2
Di-Sodium oxalate	0.02	0.15

Sodium sulphate (2.30 g l^{-1}) was added to the deionized water and allowed to dissolve. The following were then added: calcium chloride (0.49 g l^{-1}), magnesium chloride hexahydrate (0.65 g l^{-1}), sodium chloride (4.60 g l^{-1}), tri-sodium citrate dihydrate (0.65 g l^{-1}), di-sodium oxalate (0.02 g l^{-1}), potassium dihydrogen phosphate (2.80 g l^{-1}), potassium chloride (1.60 g l^{-1}), ammonium chloride (1.0 g l^{-1}), urea (25.0 g l^{-1}), and gelatine (5 g l^{-1}). The pH of the artificial media was then adjusted to pH 6.10. The artificial urine was filtered through a sterile 0.2 µm Sartorius (Göttingen, Germany) filter, and transferred into a pre-sterilised glass bottle for storage. Glassware used were thoroughly washed with hot water and Decon 90 detergent before rinsing with *d*H_2O.

2.2.7 Phosphate-Buffered Saline (PBS) solution

The solution was prepared using phosphate-buffered saline (PBS) tablets (Oxoid, UK). One PBS tablet for every 100 ml prepared was added to the deionized water according to manufacturer's instructions. The contents were autoclaved at 121°C for 15 min.

2.3 Biofilm assay on urinary catheter

The biofilm was grown as previously described in Wilks *et al.* (2015) using 6-well tissue culture plates in static culture conditions with catheter sections as the growth surface, incubated at 37 °C for a specific predetermined duration according to the experimental plan. This method is the most suitable, efficient and reproducible method for rapid biofilm growth on materials such as silicone catheter in uropathogenic studies. This method is also thought to be the most appropriately mimic the microenvironment of the urinary catheter infection to some extent, especially as short experiments (e.g. 24 h or less) have static to slow urinary nutrient flow within the catheter *in vivo*.

The sterile catheter was removed from packaging and aseptically divided into 1 cm into length pieces using scissors. Each of the 1 cm catheter pieces were then halved aseptically using scissors and placed in the wells with at least two sections for each well (refer to Figure 2-1). Each well was dedicated for one timepoint. The catheter sections in the wells were immersed in 5 ml of growth medium for each well and 100 µl of inoculum (final concentration of 1×10^9 cfu/ml) of test uropathogen overnight culture (prepared as in 2.1.1) was inoculated into each well and then incubated at 37 °C. The unattached or loosely attached bacteria were removed to ensure only sessile biofilm was left on the surface. The catheter sections were removed from the corresponding well at each timepoint, washed in PBS three times, and the excess liquid removed by capillary action on adsorbent tissue paper. The catheter sections subsequently were used in further treatment to study the assayed sessile biofilm.

2.3.1 Determination of colony forming unit of biofilm

To assess the total viable cell counts from the biofilms, the catheter sections (from Section 2.3) were transferred into 10 ml of PBS solution in a sterile tube with glass beads (approximately 2 g of glass beads with diameter of 2 mm). The biofilm cells were harvested by vortexing the tube for 90 seconds. The biofilm culture was serially diluted and 50 µl of the dilution was plated onto corresponding agar media suitable for the uropathogen (as listed in Table 2-1). Each sample dilution was plated in triplicate and incubated at 37 ^{o}C for 18 - 24 h and the colonies counted. Independent biofilm experiments were performed three times for each uropathogen grown in each experiment.

2.4 Biofilm visualization method

2.4.1 Staining biofilm on catheter for microscopy observation

SYTO®9 and 4,6-diamidino-2-phenylindole (DAPI) are both commonly used membrane-permeable fluorescent dyes for cell detection, where SYTO®9 is a green-fluorescent stain and DAPI is a blue fluorescent stain (Johnson and Criss 2013). SYTO®9 and DAPI stains viable and non-viable cells by penetrating both intact and damaged cell membranes and bind to double strand DNA (dsDNA).

Propidium iodide (PI) fluorescent dye also binds to nucleic acid but it is membrane-impermeable and stains cells with a damaged cell membrane or dead cell to red (Johnson and Criss 2013). In LIVE/DEAD® staining, SYTO®9 is used in combination with PI simultaneously to differentiate live from dead cells. As PI displaces the bound SYTO®9, live and viable cells will fluorescence green, viable cells whereas cells that fluorescence red are known as non-viable dead cells (Peeters *et al.* 2008).

Concanavalin A (ConA) is a lectin-based conjugate that binds specifically to α-linked D-mannose-based oligosaccharide in glycoproteins and is commonly used as a differential stain to detect α-D-mannosyl and α-D-glucosyl glycoprotein residues in the extracellular polymeric substances (EPS) biofilm (Leriche *et al.* 2000; Schwartz *et al.* 2003; Wilks *et al.* 2015).

After the biofilms had formed on the catheter in Section 2.3, the catheter sections were placed in an empty sterile plate to be stained with fluorescent differential stains. The solutions for differential stain were prepared from the stock according to the manufacturer's instructions and stored in -20 ^{o}C.

To use SYTO®9, 2 µl was added to 1 ml sterile *d*H_2O in an Eppendorf tube to produce a working solution with final concentration of 10 µg/ml; 100 µl of SYTO®9 working solution was pipetted onto the biofilm on each catheter section and incubated in the dark at room temperature for 15 min.

For DAPI staining (Schwartz *et al.* 2003), 14 µl was added to 1 ml sterile *d*H_2O in an Eppendorf tube to produce a working solution with final concentration of 100 µg/ml. An aliquot of 100µl DAPI working solution was pipetted onto the biofilm on the catheter section and incubated in the dark at room temperature for 15 min.

For tetramethylrhodamine (TRITC)-labelled ConA (Wilks *et al.* 2015), 10 µl was added to 1 ml sterile distilled water in an Eppendorf tube to produce a working solution with final concentration of 50 µg/ml. An aliquot of 100 µl ConA working solution was pipetted onto the biofilm on the catheter section and incubated in the dark at room temperature for 5 min.

After each incubation time, excess dye was removed by capillary action on adsorbent tissue paper, and the catheter was rinsed three times with sterile *d*H_2O. Excess water was then removed by capillary action on adsorbent tissue paper and air dried before microscopy observation.

Table 2-4 Staining methods used for visualisation of biofilm in this study

Method	Usage	Characteristics
4',6-Diamidino-2-phenylindole (DAPI)	Stains all bacterial cells	Binds to the AT-rich regions of DNA from both live and dead cells. Excitation max 358 nm, emission max 461 nm[b.]
SYTO®9[a]	Nucleic acid stain	Excitation max 485 nm, emission max 498 nm[a].
Propidium iodide (PI)[a]	Nucleic acid stain. Cell membrane impermeability for dead cell staining	Excitation max 530 nm, emission max 610 nm[b].
Concanavalin A (ConA)	Background stain for EPS	Binds to α-linked mannose in glycoproteins. Excitation max 495 nm, emission max 515 nm[b].

a Readily available stain in LIVE/DEAD® *Bac*Light™ Bacterial Viability (Peeters *et al.* 2008).

b Data accessed online, http://www.olympusmicro.com/primer/techniques/fluorescence/fluorotable1.html. Last accessed 5th January 2017.

2.4.2 Using episcopic differential interference contrast/epifluorescence (EDIC/EF) microscope

Biofilm development on the catheter surface was observed using a customised Nikon Eclipse LV100D microscope (Best Scientific, UK) equipped for EDIC/EF microscopy (Keevil 2003). The microscope was equipped with long working distance metallurgical objectives (Nikon Plan Achromat) and a high-resolution camera (QImaging Retiga EXi Cooled Digital CCD monochrome camera with RGB colour filter module) and metal halide light source (EXFO X-CITE 120 fluorescence system).

Three low to high magnification objectives (magnification x10, x50, and x100) were used in imaging the biofilm formation taken with ImagePro 6.2 software (Media Cybernetics, UK). Due to the curvature of the catheter, stack images of biofilm were taken for each focal point achieve at the horizontal level during high objective magnification (manual z-scans, one stack image ≈ ± 1 µm). The stack images were processed into a composite image using the extended depth of field plugin (Forster *et al.* 2004) in the open-source image-analysis software, Fiji (Schindelin *et al.* 2012)

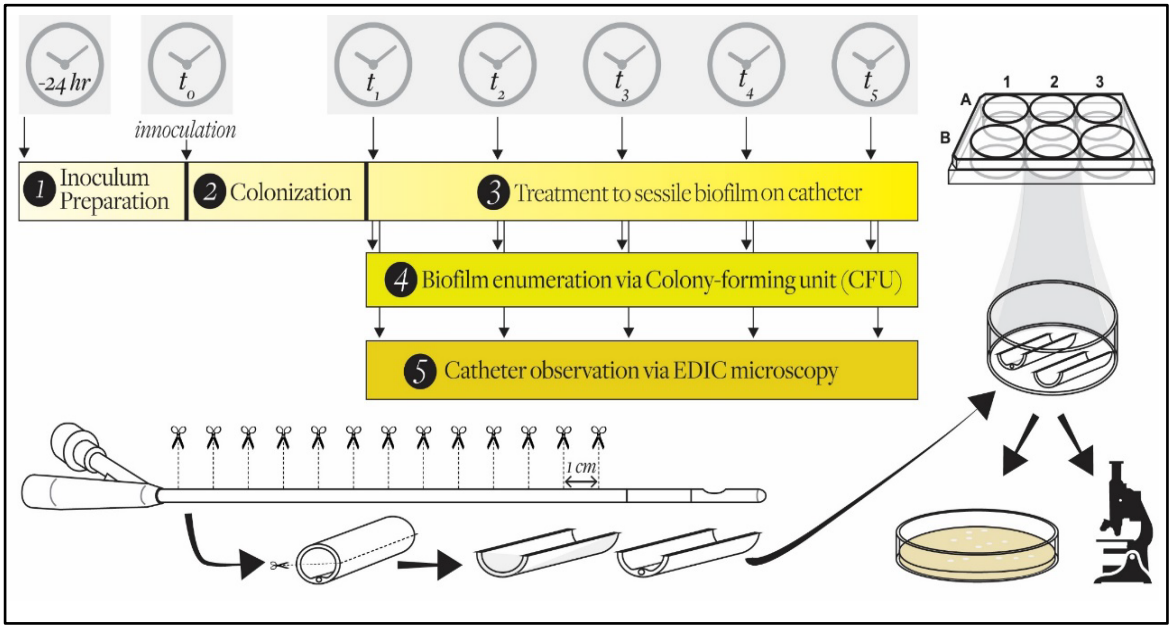

Figure 2-1 General experimental design for growing uropathogenic biofilms on catheter sections using 6-well tissue plate.

Chapter 3 Light Microscopy Analysis of Biofilm Development on Urinary Catheter

3.1 Introduction

This preliminary study will help with the subsequent and future experimental design methods and techniques. The aim of the experiment is to show the distinct characteristics of uropathogenic biofilm development on the silicone catheter surface over time between the different growth media used.

EDIC microscopy was used to visualise the development of uropathogenic biofilms on the urinary catheter (Keevil 2003). Fluorescent differential cell staining dyes were used to characterise the biofilm cells and the extracellular polymeric substances (EPS) of the biofilm during observation under the EDIC/EF microscope. Three growth media were used; a general growth medium, Trypticase Soy Broth (TSB), and two of the most common artificial urine media (AUM) used in urinary biofilm studies, which are Griffith *et al.* (1976), (AUG), and Brooks and Keevil (1997), (AUBK). The first experiment compared development of biofilm grown in TSB to AUBK. The second experiment conducted compared the biofilm development when grown in AUBK or AUG, with the application of various fluorescent dye staining combinations to enhance certain biofilm features when viewed under the EDIC/EF microscope.

3.2 Materials and methods

Escherichia coli (NCTC 9001) and *Proteus mirabilis* (NCTC 10975) inocula were prepared as described in Section 2.1.2. The bacterial inocula were harvested by centrifuging 1 ml of overnight culture at 7500 rpm (5400 × g) for 10 min. The supernatant was removed, and the pellet was suspended using the selected growth medium to form the inoculum. TSB (Oxoid, UK) was prepared by adding the required amount of dry medium to the deionized water, mixed thoroughly, and sterilised at 121 ^{o}C for 15 min as per manufacturer's instructions. AUG and AUBK were prepared as mentioned in Griffith *et al.* (1976) and Brooks and Keevil (1997), respectively. The methods were followed as described in Section 2.3.1 and Section 2.3.2.

The catheter sections for biofilm assay were prepared as described in Section 2.4 prior to the experiment. The silicone catheter (100% silicone, Rüsch Teleflex, UK) was cut into 1 cm catheter sections, which were then also cut longitudinally, and placed in a 6-well tissue culture plate (Nunc, Thermo Scientific, UK) as shown in Figure 3-1.

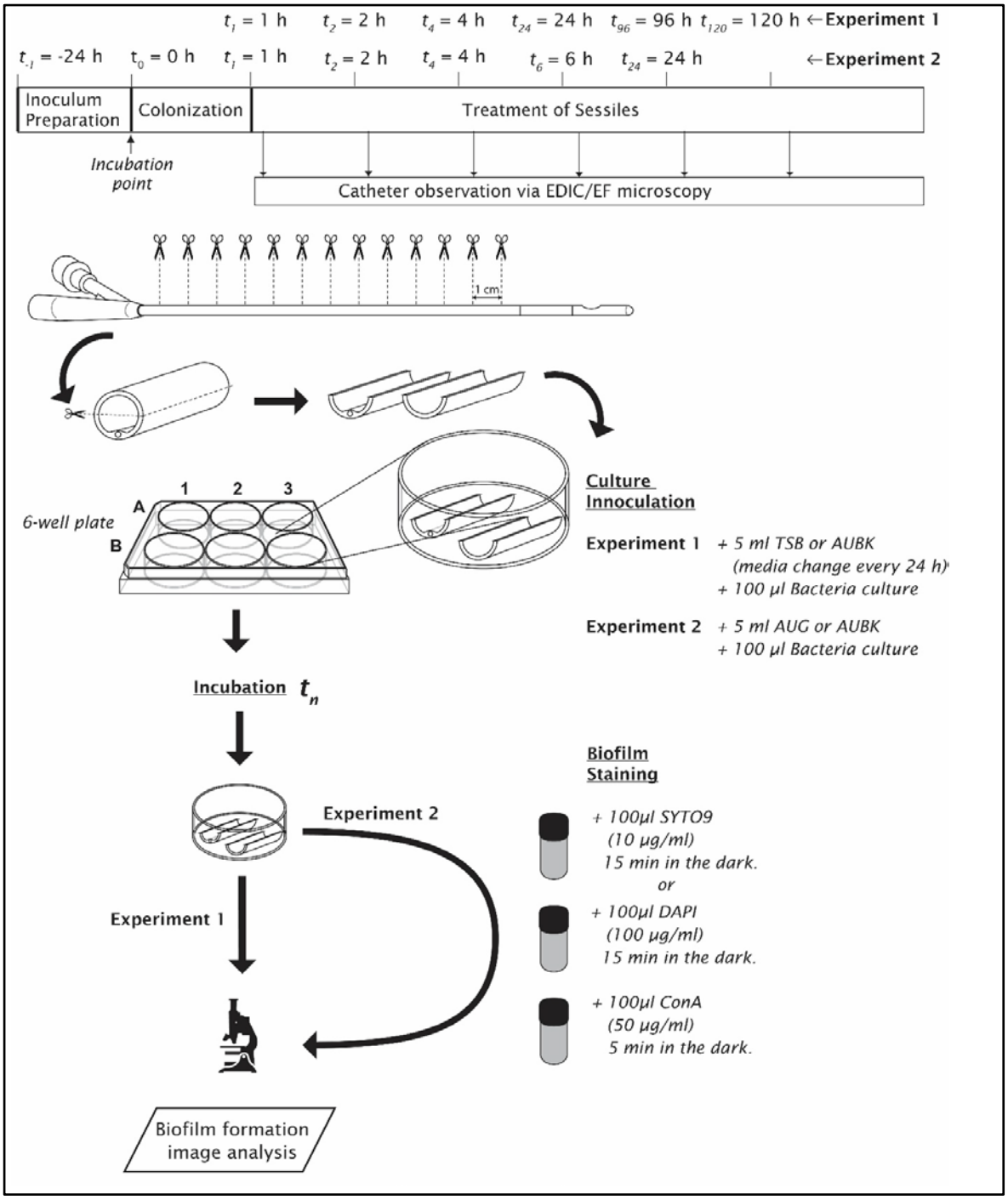

Figure 3-1 Experimental design methods used in this chapter.

For the first temporal biofilm growth experiment, different plates were used for *E. coli* and *P. mirabilis* of each growth media. Each well in the plate was dedicated to time intervals 1, 2, 4, 24, 96 and 120 h with the spare wells as the control. The wells with the catheter sections had either 5 ml TSB or 5 ml AUBK added.

The bacterial inoculum (100 µl) of either *E. coli* or *P. mirabilis* was added to each well in their dedicated plates, except for control wells. The plates were incubated at 37 ^{o}C. After each 24 h timepoint, excess medium was removed from the wells and replaced with the appropriate fresh media. At each time interval, one catheter section was removed and gently washed with PBS

three times. The catheter sections were placed and air-dried in an empty sterile plate before being observed using the EDIC microscope as described in Section 2.5. Images obtained were recorded, analysed and reported as in Section 3.3.2.

For the second experiment, different plates were used for each growth media. Each well in the plate was dedicated to time intervals 1, 2, 4, 6, and 24 h with the spare wells as the controls. The wells with the catheter sections were then added with 5 ml of AUG in each well on the same plate and 5 ml of AUBK in each well on another different plate. The bacterial inoculum (100 µl) of *E. coli* was added to each well, except control. The plates were incubated at 37 ^{o}C. At each time intervals, one catheter section was removed from the well of each plate and washed with PBS three times. The catheter sections were placed in an empty sterile plate to be processed with the fluorescent differential staining dyes.

The working solutions for the differential stains from the freezer were thawed just before use and used to stain the catheter sections as described in Section 3.5.1. The stained catheter sections were air-dried before being observed using the EDIC/EF microscope as described in Section 2.5. Images obtained were recorded, analysed and reported as in Section 3.3.3.

3.3 Results

3.3.1 Surface of an unused silicone catheter

The surface of an unused silicone catheter was first observed to provide information on the surface topography and material characteristics prior to biofilm development. Two EDIC image views are shown (Figure 3-2A and Figure 3-2C) to illustrate the natural topographical surface characteristics of the catheter. Most of the catheter observed had similar characteristics of lateral and longitudinal furrows, with some much deeper than others to create striations lines. Figure 3-2A shows the very rough and imperfect surface of the catheter.

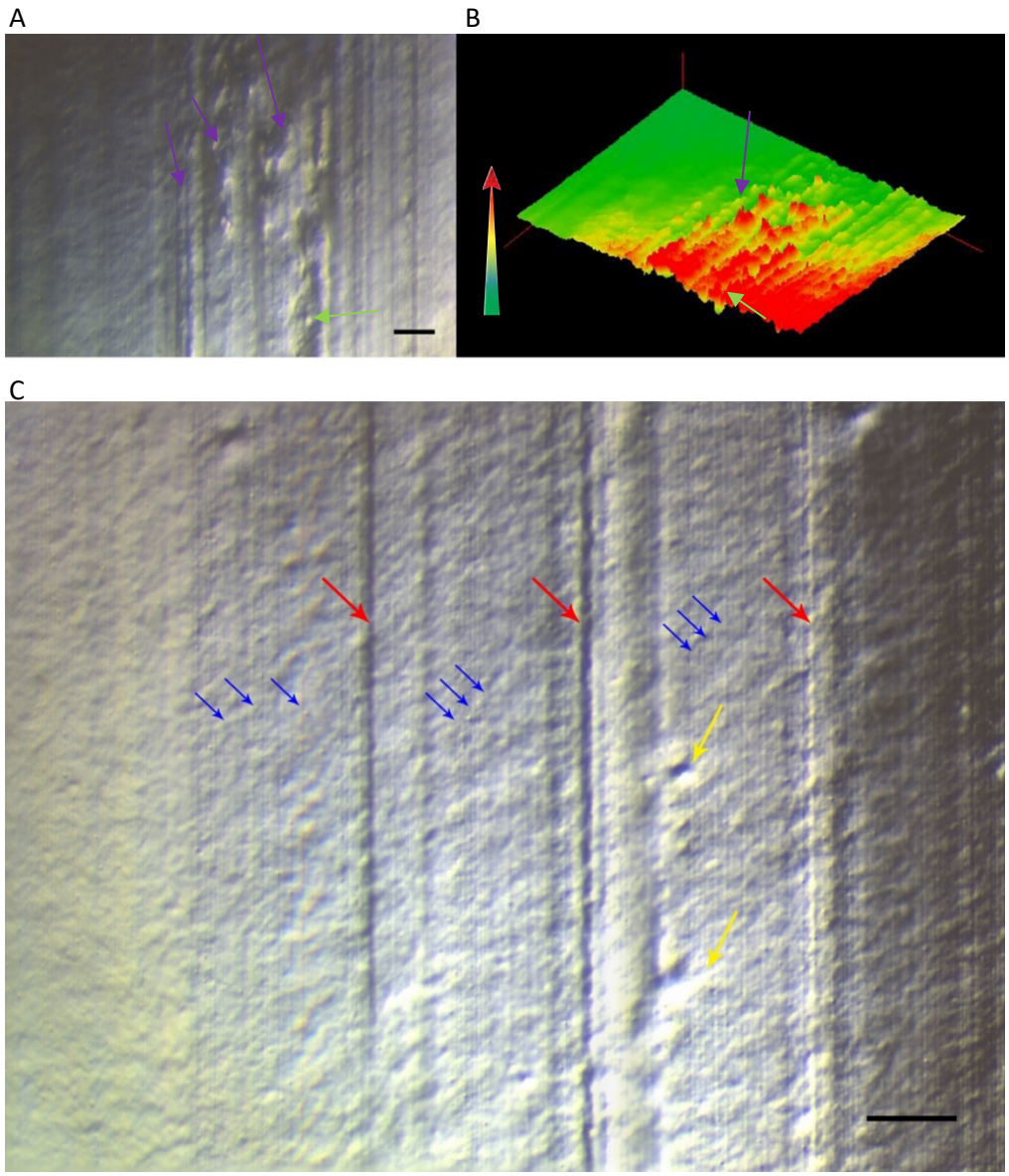

Figure 3-2 An EDIC image of an unused surface of the silicone urinary catheter. A. An example of a rough surface found on the catheter that shows deep striations (indicated by green arrow), and higher bumps (indicated by purple arrows). Magnification × 1000, scale bar = 10 µm. B. Surface plot of image A. Red colour indicates high elevation areas and green colour indicated lower elevation areas of the catheter surface. C. An image view of a different area of the catheter that has the smoothest surface. Blue arrows denote the vertical striation that extends the lengthwise of the catheter. Red arrows denote the deeper striation lines that extend throughout the length of the catheter. Yellow arrows denote the bumps and craters that exist on the catheter surface. Magnification × 1000, scale bar = 5 µm.

Figure 3-2B shows the topography of the catheter surface with red colour indicates high elevation areas and green colour indicated lower elevation areas. The high-elevated areas indicated by red colour on the right side of the image were due to the curvature of the lumen. The visualisation of the biofilm done on the curvature of the surface made it difficult to get a bigger area on the focus plane during low magnifications (× 100 times and × 500 times) compared to a higher magnification (× 1000 times).

Even the smoothest surface observed still shows the presence of vertical striation that extends the lengthwise of the catheter (Figure 3-2C, blue arrows). All these images show the catheter's surface is full of imperfections, such as bumps (indicated by purple and yellow arrows) and deep striations (indicated by red and green arrows) that could be deeper than a cell length.

3.3.2 Temporal biofilm development of *E. coli* and *P. mirabilis* in AUBK and TSB

This first experiment was conducted to see the difference of biofilm between using the general medium, TSB and the specially formulated artificial urine medium, AUBK. The experiment used the uropathogenic *E. coli* and *P. mirabilis*. There were a steady increase and stable build-up of biofilm coverage from 1 h to 24 h for both organisms grown in AUBK (Figure 3-3A to Figure 3-3F and Figure 3-4A to Figure 3-4F) compared to in TSB (Figure 3-3G to Figure 3-3L and Figure 3-4G to Figure 3-4L). The bacterial attachment appeared early within the first hour, which seemed to have facilitated further biofilm development on the catheter. The striations and ridges served as attractive areas for EPS to accumulate, following the parallel striation patterns on the catheter surface (Figure 3-3A and Figure 3-4A).

From 24 h onwards, *E. coli* in AUBK (Figure 3-3D to Figure 3-3F) developed a more complex biofilm compared to *P. mirabilis* (Figure 3-4D to Figure 3-4F), which appeared more uniform except for several microcrystalline structures present on the biofilm.

There were no attached cells seen on the surface for both *E. coli* (Figure 3-3-G and Figure 3-3-H), and *P. mirabilis* (Figure 3-4-G and Figure 3-4-H) in 1 h and 2 h of incubation in TSB. From 4 h until 24 h, the biofilm for both strains was thick with many cells trapped under a sheath of concentrated EPS layer with large voids in between (Figure 3-3-I to Figure 3-3-J and Figure 3-4-I to Figure 30-J).

At 96 h (Figure 3-3-K and Figure 3-4-K), the biofilm was denser compared to 24 h (Figure 3-3-J and Figure 3-4-J). This is similar to how turbidity increases in broth medium, which indicates cell growth. At 120 h (Figure 3-3-L and Figure 3-4-L), there was still a thick matrix biofilm on the catheter with larger voids visible in the biofilm. The biofilm at 96 h for both uropathogen in TSB shows smaller voids, which progressed to bigger voids at 120 h.

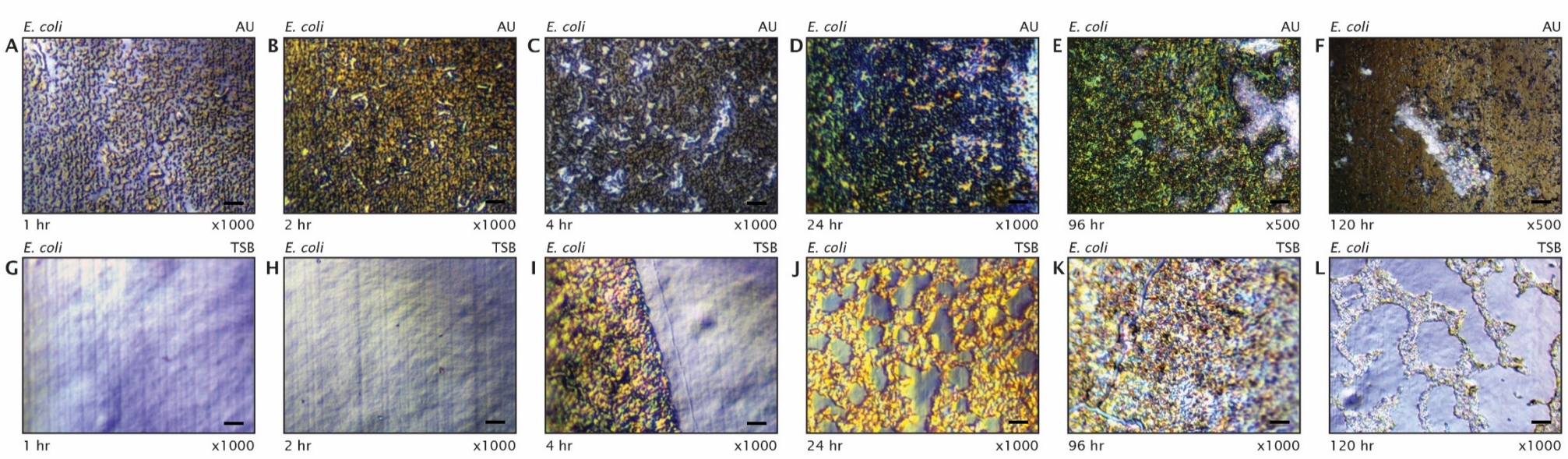

Figure 3-3 EDIC microscopy pictures of *E. coli* biofilm on silicone catheter grew with AUBK (A to F) and TSB (G to L) as growth media. Magnifications × 1000, scale bars = 5 µm.

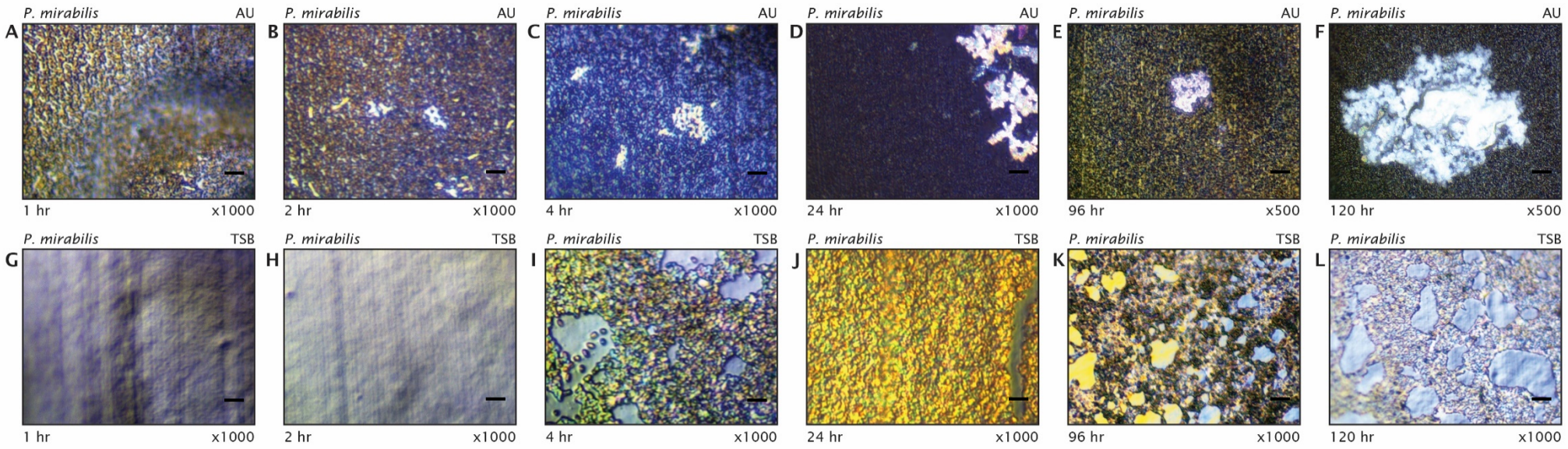

Figure 3-4 EDIC microscopy pictures of *P. mirabilis* biofilm on silicone catheter grown using AUBK (A to F) and TSB (G to L) as growth media. Magnifications × 1000, scale bars = 5 µm.

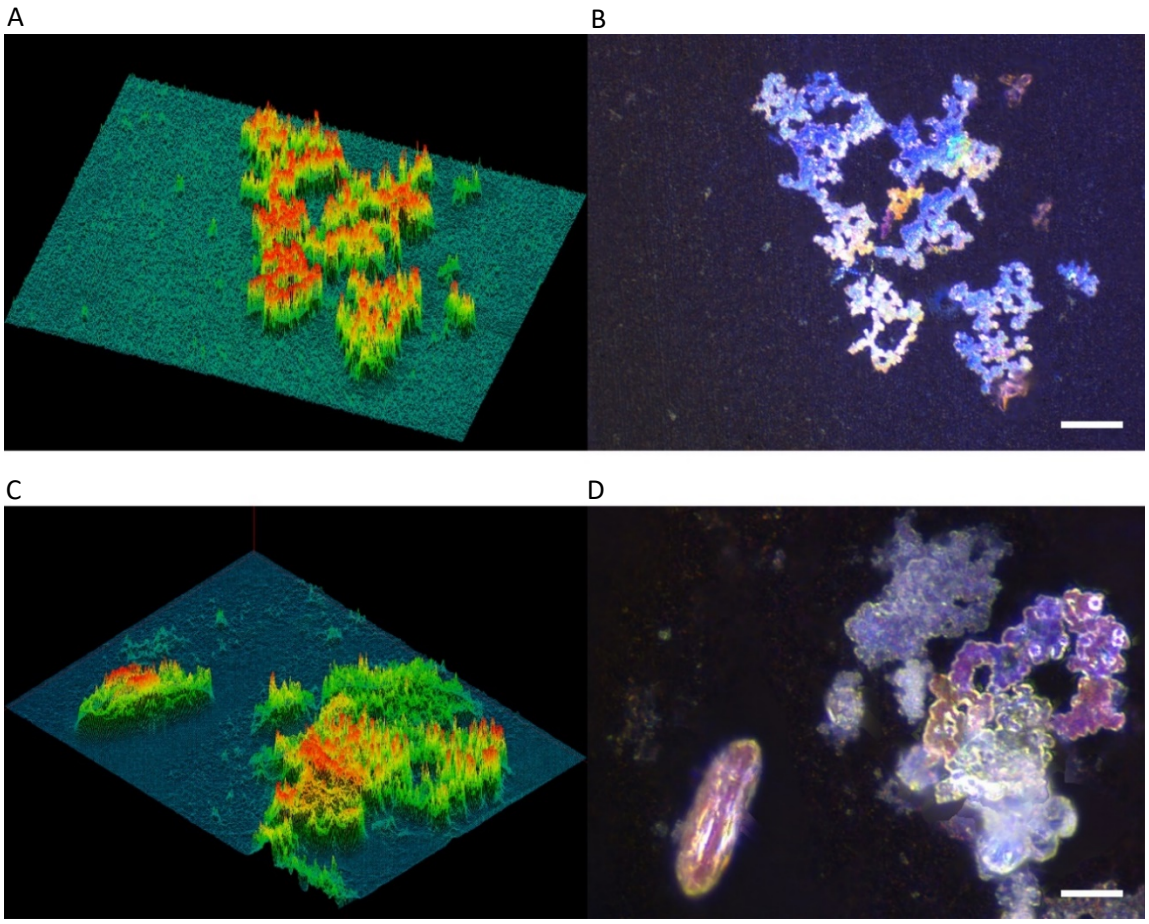

Figure 3-5 Surface plot images (A and C), and EDIC images (B and D) of the microcrystalline formed in *P. mirabilis* biofilm grown with AUBK after 120 h. Magnifications ×1000, scale bars = 5 µm.

There were no microcrystalline structures (neither apatite nor struvite) observed in biofilm grown with TSB for both organisms (Figure 3-3-G to Figure 3-3-L and Figure 3-4-G to Figure 3-4-G-L). However, there was microcrystalline formation present when and *P. mirabilis* was grown in AUBK. These microcrystalline aggregations were larger and more dominantly observed during longer time intervals in *P. mirabilis* (Figure 3-4-E to Figure 3-4-F) than in *E. coli* (Figure 3-3-E to Figure 3-3-F). Close examination of *P. mirabilis* biofilm grown in AUBK at 120 h showed more prominent microcrystalline structures with several large coffin-shaped crystal formed on the catheter (Figure 3-5). The developed microcrystalline structure were also observed in *E. coli* biofilm grown with AUBK in time interval 96 h and 120 h (Figure 3-3E and Figure 3-3F). However, close examination of the *E. coli* biofilm only show presence of amorphous microcrystalline structures with no signs of large crystal formation were observed at 120 h (Figure 3-6).

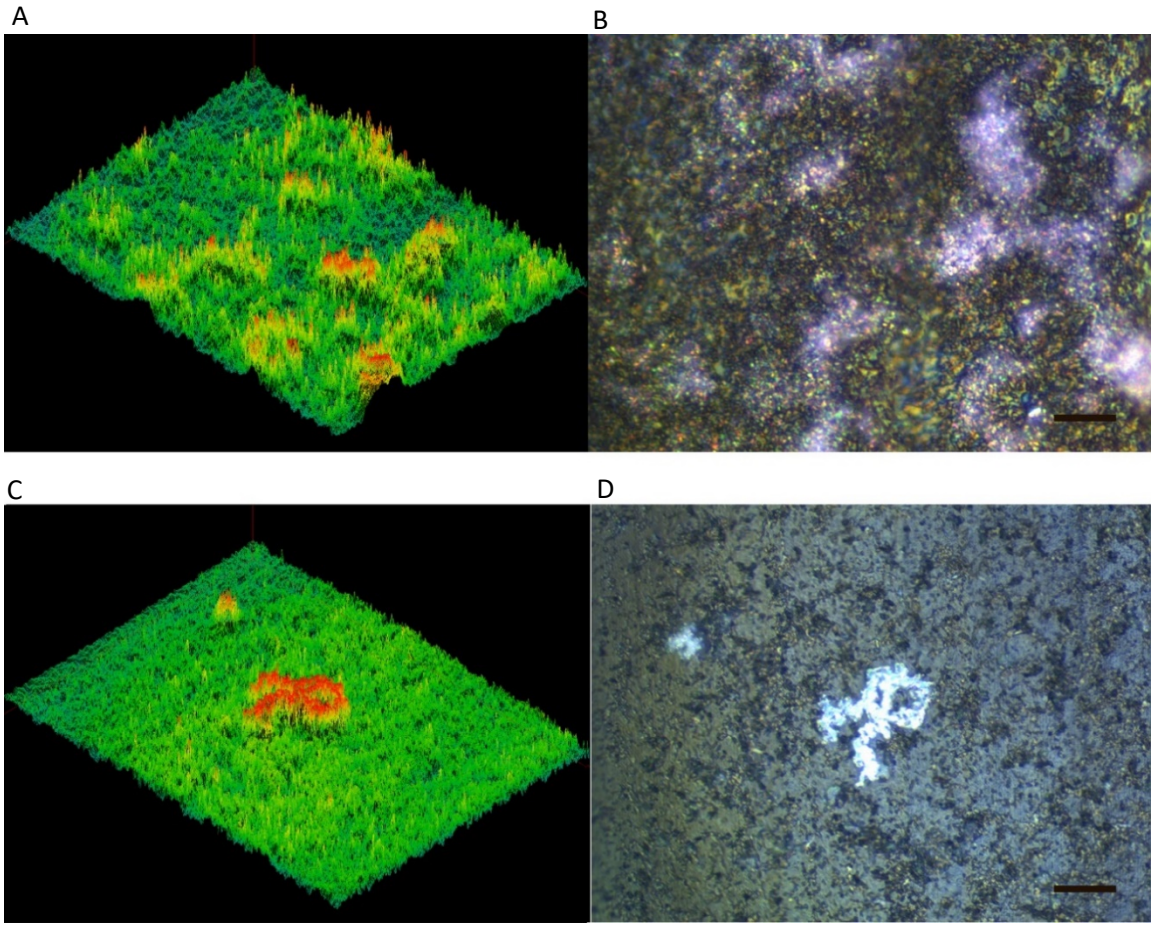

Figure 3-6 Surface plot images (A and C) and EDIC images (B and D) of the microcrystalline formed in *E. coli* biofilm grown with AUBK after 120 h. Magnifications × 1000, scale bars = 5 µm.

3.3.3 Temporal differences of *E. coli* biofilm grown in AUG and AUBK

The common features such as striations and undulations on the catheter surface (as seen earlier in Section 3.3.1) were present (Figure 3-7D, yellow arrow, and Figure 3-11D, blue arrow). The AUG medium was thicker and more viscous when compared to AUBK medium, which was observed during the media preparation. Figure 3-7 to Figure 3-17 show *E. coli* biofilm development over time when grown in AUG and AUBK.

The ConA-stained images of biofilm in AUG presented a smooth layer with a transparent sheen on the surface (Figure 3-7D) that creates visible trailing liquid streaks on the edges (Figure 3-7D, white arrows; Figure 3-9C, yellow arrows; and Figure 3-11D, red arrows). The initial single cell attachment (Figure 3-7D, red arrow) and several small aggregations of cells (Figure 3-7D, blue arrow) were seen after 1 h in AUG.

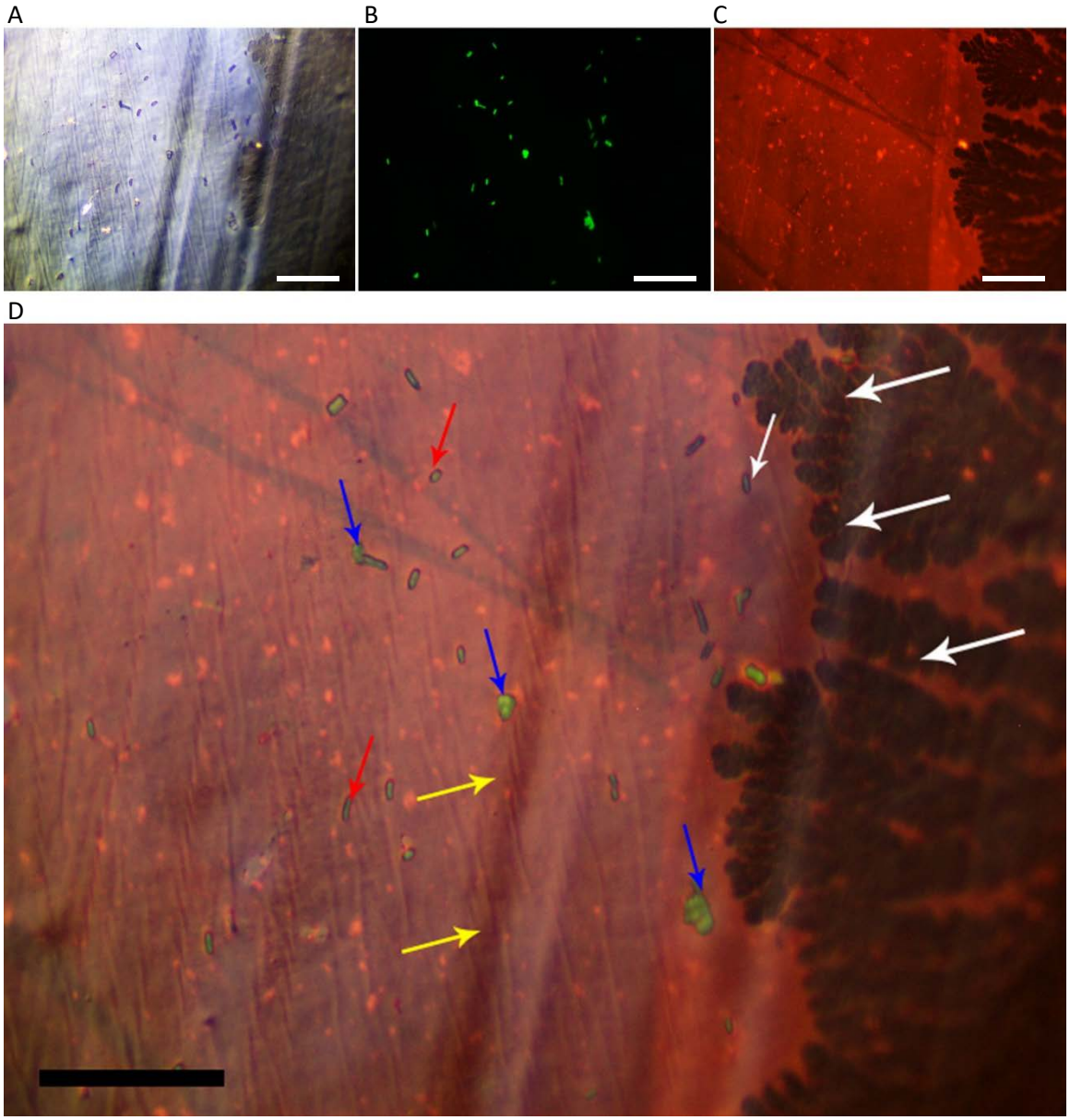

Figure 3-7 1 h *E. coli* biofilm in AUG showing bacterial attachment phase on the urinary catheter when observed using EDIC/EF microscope.

A. An EDIC image that shows the grooves and striation pattern with several visible attached cells on the catheter surface. B. Image shows the SYTO®9-stained *E. coli* cells. C. Image shows the ConA-stained background layer formed on the catheter surface. D. Image composite of A, B and C, the yellow arrows denote the striation furrows, the red arrows denote attached single cells, the blue arrows denote initial cell aggregation forming cell clusters, and the white arrows shows the viscous liquid edges of the AUG media. Magnifications × 1000, scale bars = 10 µm.

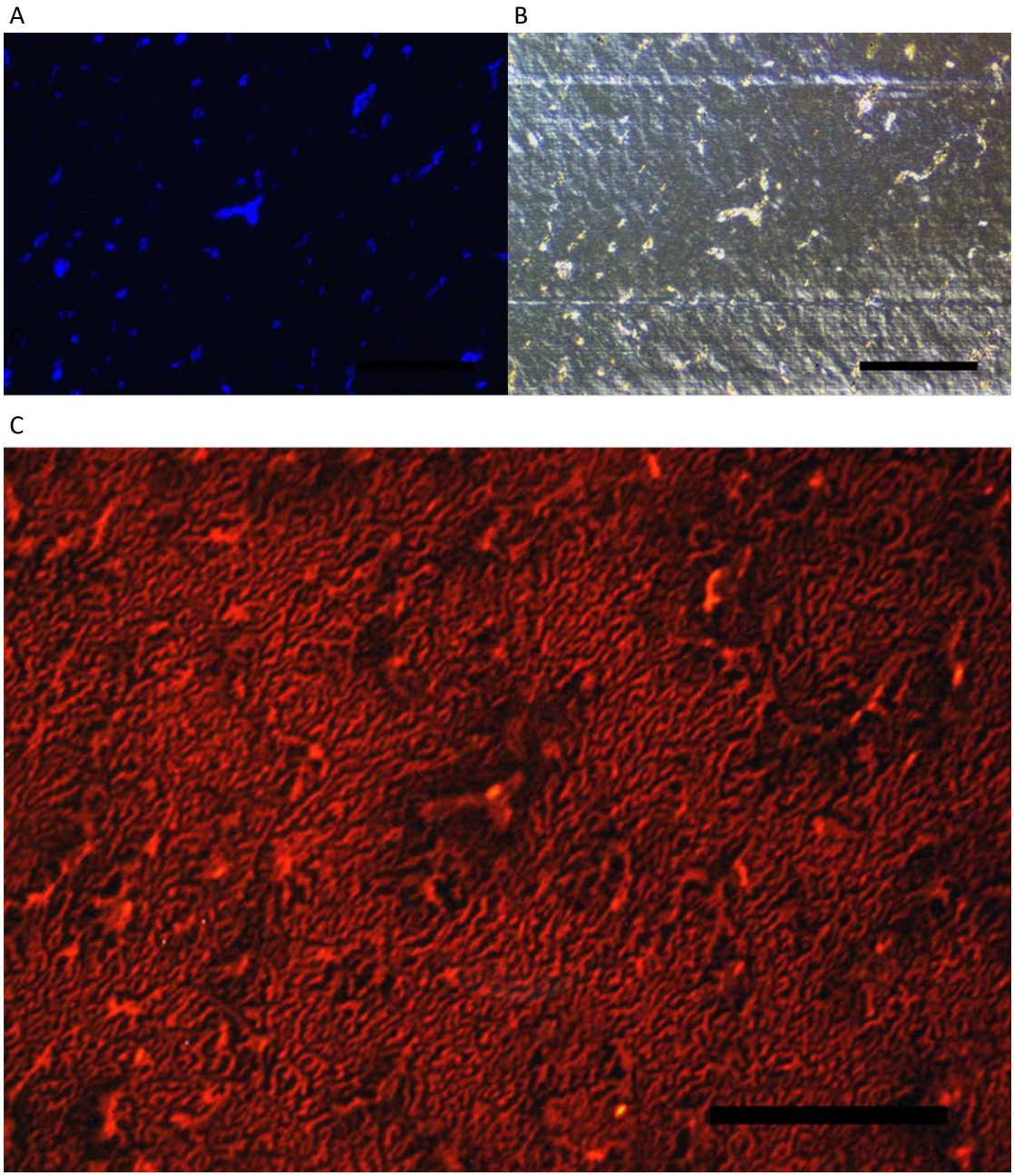

Figure 3-8 1 h *E. coli* biofilm in AUBK showing cell aggregation and EPS layer on the urinary catheter surface with when observed using EDIC/EF microscope.

A. Image shows the DAPI-stained *E. coli* cell aggregates. B. Image shows the EDIC view of the catheter surface. C. Image shows the ConA-stained image of the background EPS conditioning film formed on the catheter, under and around the cells. Magnifications × 1000, scale bars = 10 µm.

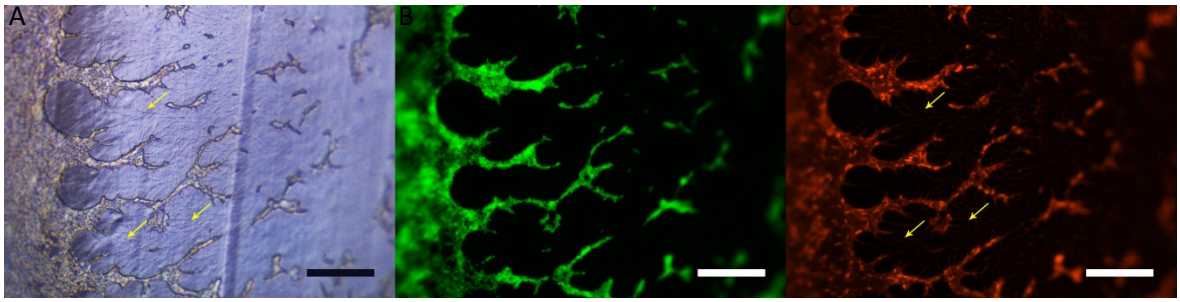

Figure 3-9 2 h *E. coli* biofilm in AUG.
A. Image shows the EDIC view of the catheter surface; yellow arrows denote streaks from the liquid tension between AUG and the catheter surface. B. Image shows the SYTO®9-stained cells appeared bright green with increased intensity in areas with more cells. C. Image shows the ConA-stained image of the background EPS layer. Yellow arrows denote streaks from the liquid tension between AUG and the catheter surface in the same area in A. Magnifications × 1000, scale bars = 5 µm.

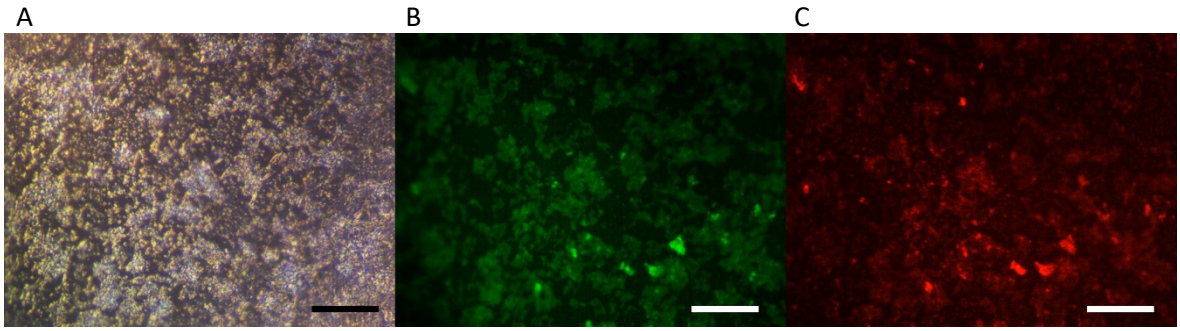

Figure 3-10 2 h *E. coli* biofilm in AUBK.
A. Image shows the EDIC view of more coverage of biofilm on the catheter. B. Image shows the SYTO®9-stained bacterial cell. Biofilm appears green clusters with dark areas of voids in between the biofilm structures. C. Image shows the ConA-stained image of the background EPS layer appeared bright red, with dark areas of void sections. Magnifications × 1000, scale bars = 5 µm.

The SYTO®9 was used in these images to show the single cells and the aggregation of cells. The ConA were staining the AUG medium, which indicates the appearance of a few granules in the medium. In the first hour, the EDIC image of the surface appeared bright with few extracellular materials produced on the catheter surface.

From the DAPI-stained biofilm in AUBK image (Figure 3-8A), there were more bacterial cells aggregates than in AUG. The EDIC image view (Figure 3-8B) showed the catheter surface has more cleared areas between the cell aggregates, but when the ConA-stained image showed there was a copious amount of extracellular conditioning material developed on the catheter surface. The EPS material appeared to have more build-up near and between the bacterial cell aggregates, which helps further bacterial cell attachment to the catheter surface (Figure 3-8C).

The biofilm in AUG appeared thicker and pulled towards the centre lumen at 2 h (Figure 3-9A). In the SYTO®9-stained image showed there were increased cells in the medium (Figure 3-9B). In the ConA-stained image, there was trailing streaks from the viscous medium later (Figure 3-9C, yellow arrow), that showed the medium had a stronger bond than to the catheter surface.

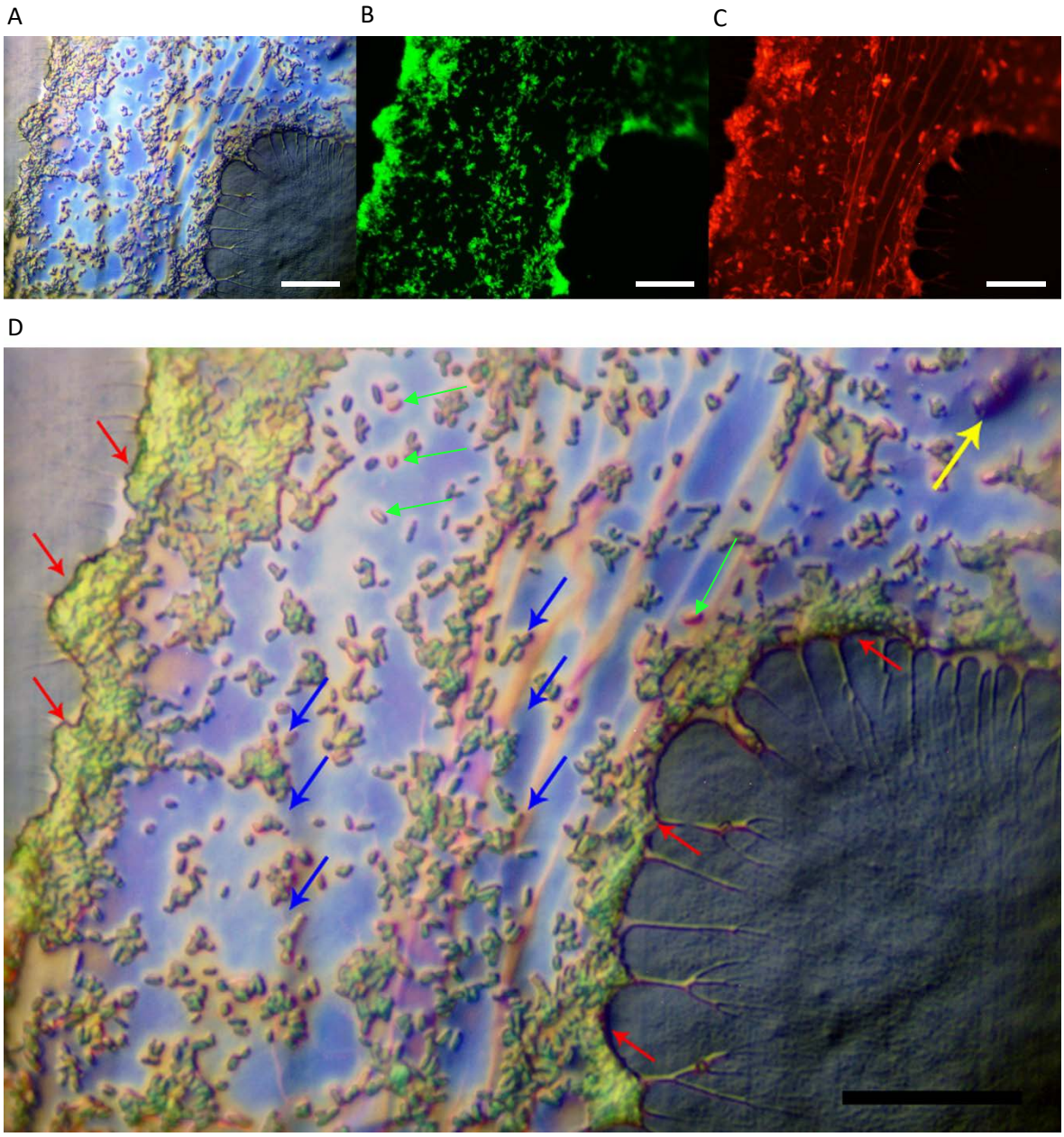

Figure 3-11 4 h *E. coli* biofilm in AUG.

A. Image shows the EDIC view of biofilm on the catheter. B. Image shows the SYTO®9-stained bacterial cell appeared bright green. The concentration of cells is more along the edges of the biofilm layer. C. Image shows the PI-stained image of dead bacterial cells. D. Composite image of A, B and C. Red arrows denote concentrated aggregation of cells at the edges, the yellow arrow denotes a bump present on the catheter surface, blue arrows denote cell aggregations can be seen parallel to striations of the catheter, and green arrows indicate dead cells among the biofilm. Magnification × 1000, scale bars = 10 µm.

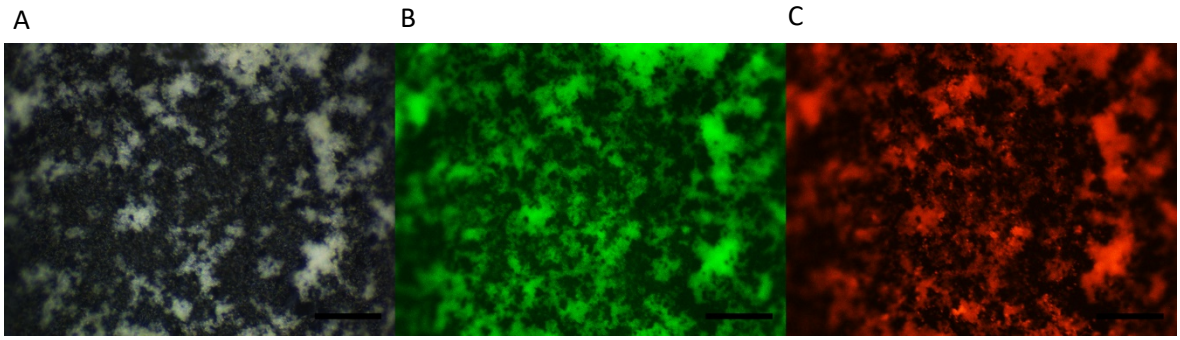

Figure 3-12 4 h *E. coli* biofilm in AUBK.
A. Image shows the EDIC view of biofilm on the catheter. B. SYTO®9-stained bacterial cell appeared bright green. C. Image shows the ConA-stained image of the background EPS layer appeared bright red. White microcrystalline cluster formation in A can be seen autofluorescence green in B and autofluorescence red in C. Magnifications × 1000, scale bars = 5 µm.

The biofilm in AUBK at 2 h (Figure 3-10) appeared as a thin EPS layer which still allowed the underneath layer of the catheter surface can be seen (Figure 3-10A). SYTO®9-stained image showed the bacterial cells in the biofilm (Figure 3-10B), and the ConA-stained image showed the EPS material that was produced and attached to the surface catheter (Figure 3-10C). Some areas have much thicker EPS, showing voids in between.

In AUG at 4 h (Figure 3-11), the EDIC image shows the thickness of the AUG medium on the catheter (Figure 3-11A). Here, the catheter was stained with SYTO®9 (Figure 3-11B) and PI (Figure 3-11C). The SYTO®9 image shows highly concentrated cells on the edges of the liquid barrier (Figure 3-11D, red arrows) and more in the middle. Cell aggregates increased in size and were seen attached to the surface along the striation lines underneath it (Figure 3-11D, blue arrows). Figure 3-11C shows the inactive cells in red colour. In the composite image Figure 3-11D, the green arrows are showing several single inactive cells on the biofilm.

In AUBK at 4 h (Figure 3-12), the biofilm was treated with SYTO®9 (Figure 3-12B) and ConA (Figure 3-12C). From the EDIC image (Figure 3-12A), it appears that the EPS had thickened and resulted with darker surface colour, covering the catheter. There were clusters of white microcrystals formed on the biofilm that also appears to autofluorescence in SYTO®9 and ConA. The autofluorescence makes it harder to differentiate the biofilm layer at this point.

In AUG at the 6 h time stop (Figure 3-13), the biofilm was stained with ConA (Figure 3-13A), and SYTO®9 (Figure 3-13B). The EDIC image (Figure 3-13C) and SYTO®9 image show the bacterial cells in the biofilm layer, scattered and in small clusters except for at the edge below where there is an accumulation of cells can be seen. The composite image (Figure 3-13D) shows clearly that the surface is covered with extracellular layer even when it seemed void from the EDIC and SYTO®9 images.

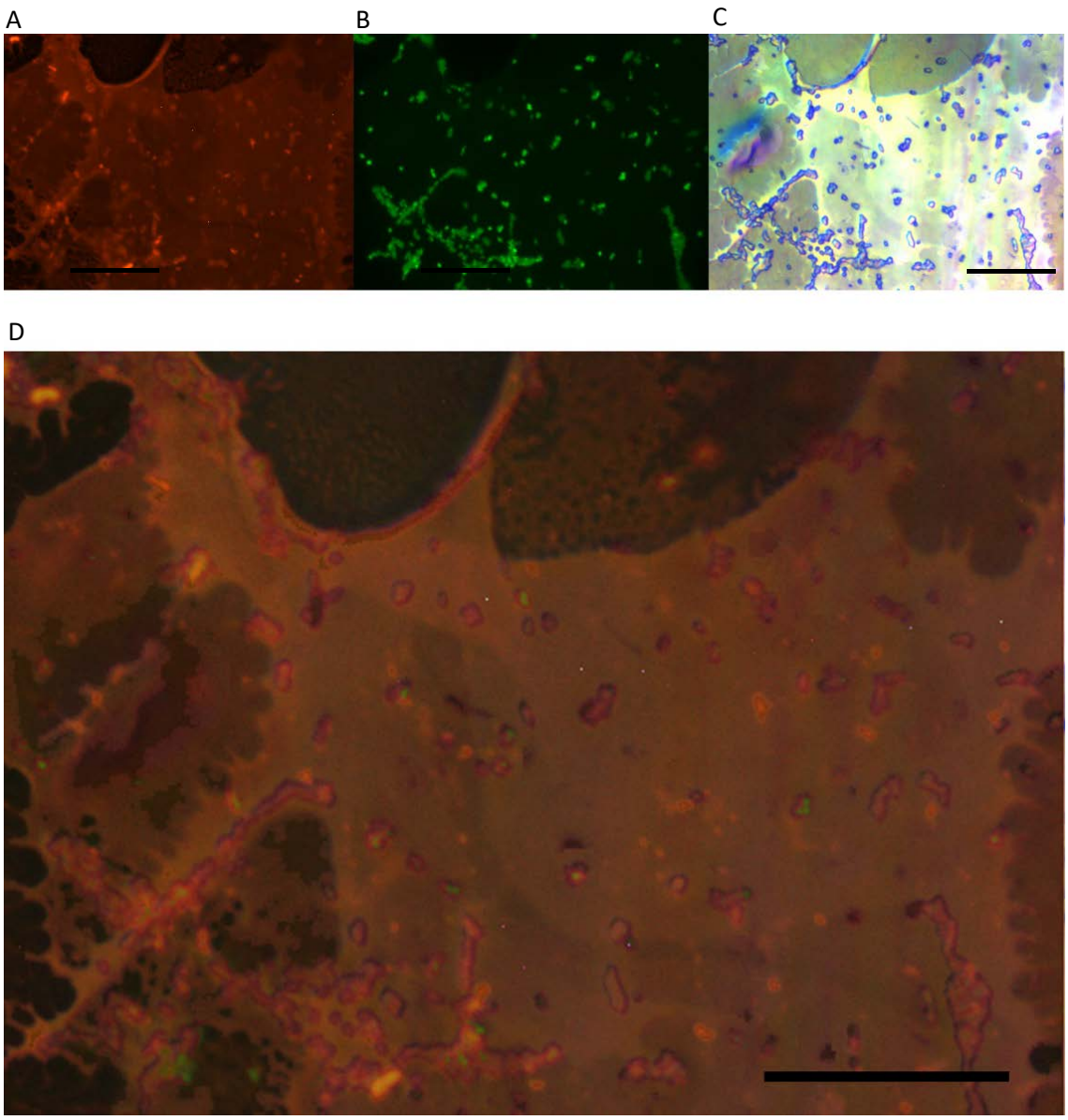

Figure 3-13 6 h *E. coli* biofilm in AUG.
A. Image shows the ConA-stained image of the background EPS layer in red. B. SYTO®9-stained bacterial cell appeared bright green. C. Image shows the EDIC view of biofilm on the catheter. D. Composite image of A, B, and C. Magnifications × 1000, scale bars = 10 µm.

In AUBK at 6 h (Figure 3-14A, Figure 3-14B, and Figure 3-14C), there were increased amount and homogenous layer of extracellular material covering the catheter surface, and in this image, there is a larger form of crystal that autofluorescence in EF filter mode. In AUG at 24 h, there are two image views showing one (Figure 3-15) that is an example of a granulated build-up of EPS layer remaining on the catheter surface even though much of the rest of the biofilm seemed disintegrated, revealing the catheter surface. This is probably because of the white crystal that formed on the EPS (Figure 3-15A) has anchored the EPS layer stronger than the rest of the biofilm. The ConA image (Figure 3-15B) shows that the areas that seemed without any biofilm have a conditioning layer that covered the whole catheter surface.

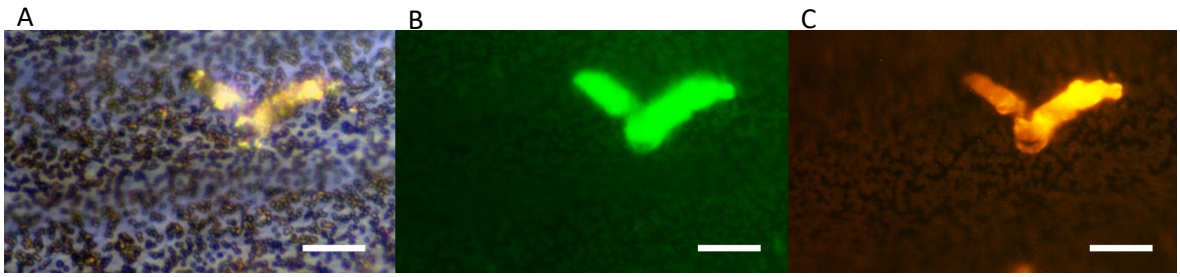

Figure 3-14 6 h *E. coli* biofilm in AUBK.
A. Image shows the EDIC view of biofilm on the catheter. B. SYTO®9-stained bacterial cell appeared bright green. C. Image shows the ConA-stained image of the background EPS layer appeared bright red. Magnifications × 1000, scale bars = 10 µm.

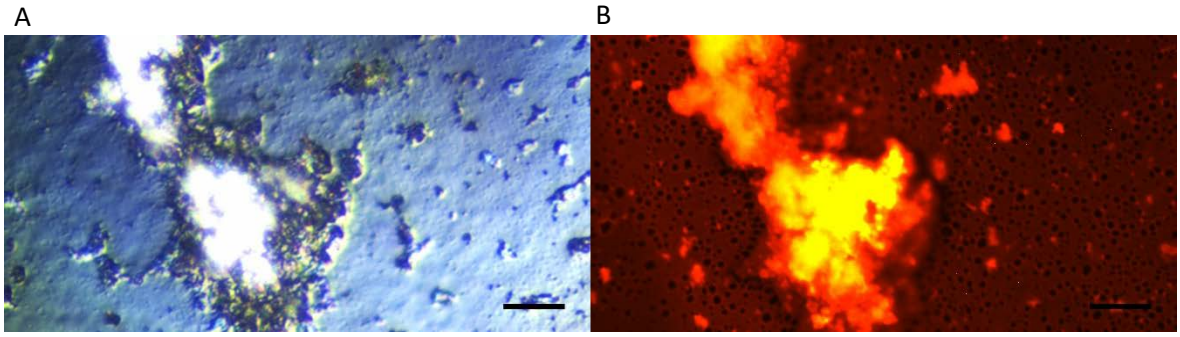

Figure 3-15 24 h *E. coli* biofilm in AUG.
A. Image shows the EDIC view of biofilm on the catheter. B. Image shows the ConA-stained image of the background EPS layer appeared bright red.
White microcrystalline cluster formation in A, can be seen autofluorescence green in B and autofluorescence red in C. Magnifications × 1000, scale bars = 10 µm.

The *E. coli* biofilm grown in AUG at 24 h (Figure 3-16) showed an intact biofilm layer, with several void sections that have disintegrated in between them. The EDIC image (Figure 3-16A) shows the layer of biofilm with visible irregular circular voids. In the SYTO®9 image (Figure 3-16B), it appears that the whole biofilm layer can be seen covering the surface, and the patches of irregular circular voids are clearer with some visible cracks in between because they were unstained. It appears that the layer of biofilm has a varied thickness based on the different intensity of green-coloured material in the image.

The ConA image (Figure 3-16C) shows the background EPS layer, and that the voids we saw in previous images, in fact, have a conditioning film over them, connecting the nearby biofilm communities together. The composite image (Figure 3-16D) shows the biofilm in a matured state and starting to disintegrate, with cracks and voids from removed pieces of biofilm. However, the surface of the catheter still had conditioning film that will continue to facilitate new bacterial attachment to the surface.

The EDIC image of the biofilm grown in AUBK (Figure 3-17A) showed a homogeneous but thick biofilm layer formation after 24 h incubation. There were microcrystals formed on the biofilm that autofluorescence when stained with DAPI (Figure 3-17B) and ConA (Figure 3-17C). The details of the extracellular materials can be seen stacked with various level of thickness and looked granulated (Figure 3-17C). In the DAPI image (Figure 3-17B), the bacterial cells are coloured blue, and one large cell aggregation is seen that corresponds to the yellow arrow in the DAPI/ConA composite image (Figure 3-17D).

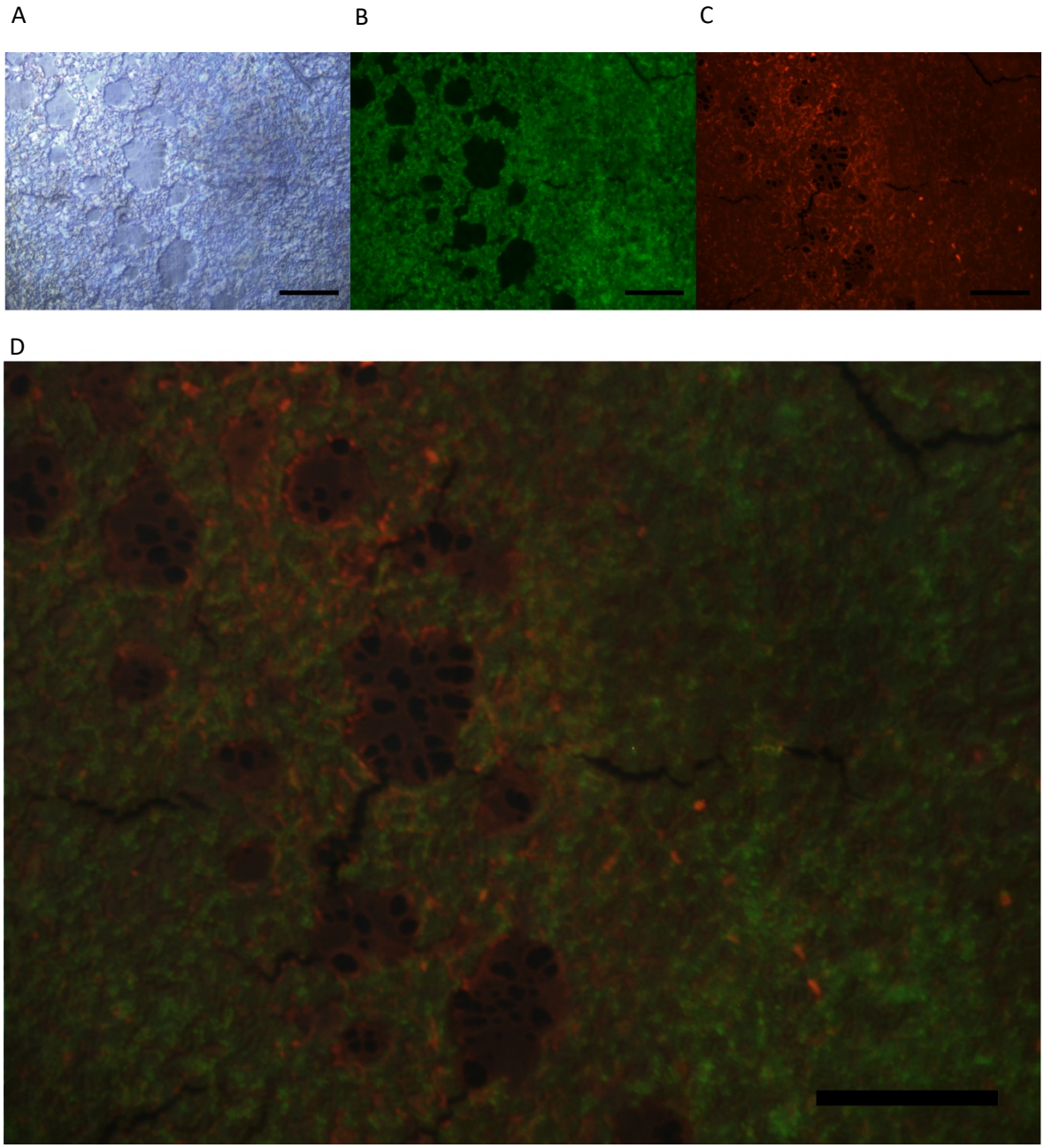

Figure 3-16 *E. coli* in AUG after 24 h incubation.
A. An EDIC image of the catheter surface. B. SYTO®9 image is showing bacterial cells in the biofilm. C. Image shows the ConA-stained background EPS layer appeared bright red that was more in areas that have cell clusters. Conditioning film was present in void cell areas as well. D. Composite image from A, B, and C. Magnifications × 1000, scale bars = 10 µm.

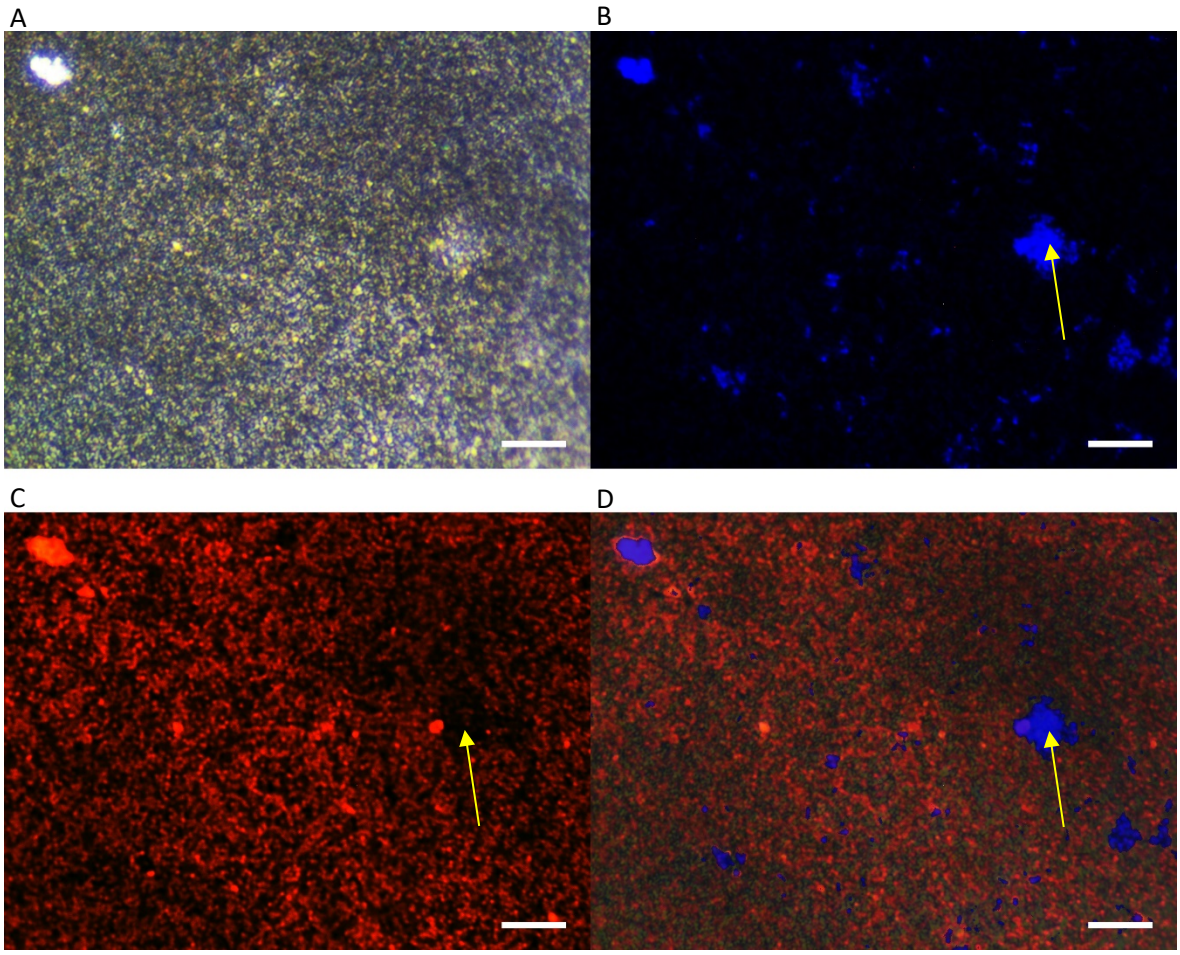

Figure 3-17 *E. coli* in AUBK after 24 h incubation.
A. Image shows the EDIC view of the catheter surface. B. Image shows the DAPI-stained *E. coli* cells in the biofilm. C. Image shows the ConA-stained image of the background EPS conditioning film formed on the catheter, under and around the cells. D. Composite image from A, B and C. Yellow arrow in C and D showing an area of fewer EPS in ConA image is because there are cells on top of it. Magnifications × 1000, scale bars = 10 µm.

3.4 Discussion

The discussion is divided into the following subtopics:

1. Using EDIC for biofilm catheter visualisation and the surface topography of an unused silicone catheters
2. the temporal difference of biofilm grown in AUBK and TSB over a long time-scale
3. the temporal difference of biofilm grown in AUG and AUBK
4. struvite and apatite crystal formation

3.4.1 Using EDIC to visualise the surface topography of an unused silicone catheters

Observation of such thick biofilms, particularly to focus on curved surfaces, is very challenging, as opposed to having one focus plane during biofilm observation on a flat surface. Even though it is even harder to focus on the fluorescent-stained biofilms, using EDIC enables the visualisation of the biofilm without requiring additional complex sample preparation (Keevil 2003).

Undulations and striation lines presented on the urinary catheter were a common feature (Figure 3-2) and were similarly reported previously by Wilks *et al.* (2015). These surface imperfections were likely produced during the manufacturing process of the catheter. Mass manufacturing has always made it challenging to create smooths surface for the silicone catheter as the fabrication of it depends on the mould (Kent and Zeigel 1982; Verran and Boyd 2001; Siddiq and Darouiche 2012; Wilks *et al.* 2015). Using the EDIC microscope, the urinary catheter surface shows a rough facade, longitudinal striation lines, irregular bumps, and craters. These contribute to the surface imperfections that serve as an attractive site for bacterial attachment that could facilitate the colonisation during an infection (Stickler *et al.* 2003; Hola *et al.* 2012; Wilks *et al.* 2015).

3.4.2 The temporal difference of biofilm grown in AUBK and TSB

The results show that the uropathogenic biofilm development in TSB and AUBK were visually contrasting. The different effect on the biofilm development on the catheter was expected based on past biofilm studies (Stoodley *et al.* 1998; Amato and Brynildsen 2014; Kesaano *et al.* 2015). When grown in AUBK, the hydrophobicity on the silicone surface posed no problem for initial bacterial attachment in the first hour. Both strains showed heterogeneous lawn of biofilm growth with the thickness and density of the biofilm increased with time.

There were similarities observed between *E. coli* and *P. mirabilis* biofilm formation in TSB. The biofilm development for both strains was only present at the 4 h incubation time when grown in TSB, which was not suspected due to slow-growing culture. Slow or non-growing biofilm in TSB has been observed previously in Hood and Zottola (1997), which could be due to inadequate nutrient compound for biofilm growth. It could also be due to the presence of inhibitors such as cell surface hydrophobicity that deters bacterial attachment, which is one of the major contributing factors to the formation of biofilms (Blehert *et al.* 2003). At 4 h incubation, a biofilm layer was present that appeared as thick matrix abundant with cells, which could have grown in suspension, and not as a result of a sudden influx of cell growth (Figure 3-3I and Figure 3-4I). The dense but granulated appearance of the biofilm was suspected due to the matrix that traps the bacterial cells are most likely a form of casein. Casein is lumpy in nature and could have thickened during incubation (Belitz *et al.* 2009).

The voids in the biofilm layer were probably due to biofilm dispersion that could be triggered by insufficiency of the required nutrient to maintain a stable biofilm (Stoodley *et al.* 1998). These observations also suggest that the association between the biofilm and the catheter surface was not strong to maintain the whole biofilm structure (Reid and Busscher 1992).

3.4.3 Temporal difference of biofilm grown in AUG and AUBK

This study was aimed to use EDIC/EF microscopy to visualise the influence of different growth media on the uropathogenic biofilm development. EDIC is a powerful microscopy technique to visualise the urinary biofilm grown directly on the catheter without producing artefacts (Keevil 2003; Wilks *et al.* 2015). The results show that the medium composition affects the biofilm development on the catheter surface. It is hard to compare which AUM was better in facilitating bacterial attachment as the bacterial cell appeared in both AUG and AUBK in the first hour of incubation. However, the ConA-stained conditioning layer from AUBK is more developed across the catheter surface compared to AUG, which may be affected by the hydrophobicity of the surface and the internal liquid tension due to the AUG composition.

The interaction between AUM and the surface could change in the micro-environment due to bacterial metabolic processes that subsequently affect the bacterial attachment (Hood and Zottola 1997). The important factors include surface charge, hydrophobicity or hydrophilicity of the catheter, specific adhesion gene ability present in the cell, human proteins and other urine components that may facilitate the attachment process by physicochemical binding to the surface material of the catheter (Holá *et al.* 2010). Most EDIC and ConA images showed an apparent visible biofilm thickness in the AUG medium. The AUG medium also appeared to autofluorescence in most ConA images. During AUG preparation, there was a notably increased viscosity of the media felt compared to AUBK. The viscosity of AUG is probably due to the ingredient gelatine (5 g l^{-1}) which is included in the medium from the original study by Griffith *et al.* (1976) to provide a matrix to the media and create a supersaturation environment to prove it induces crystallisation and encrustation of the AUG in the presence of urease activity.

In comparison to AUBK, the biofilm produces distinct characteristics between bacterial cells and the ConA-stained conditioning film, which is suspected to be EPS. The production of EPS by bacterial cells differs according to the available peptone source (Gray *et al.* 2006). So far, satisfactory observation of the EPS using ConA staining can be seen in AUBK (Figure 3-10), at the initial stages of surface material, and Figure 3-13, where the EPS can be seen as a build-up of granulated mass supporting the biofilm structure. The ConA image of 24 h biofilm in AUBK can be seen areas that were not stained (Figure 3-17C, yellow arrow), meaning that the extracellular materials were surrounding the cell cluster. The same observation was mentioned earlier in (Wilks *et al.* 2015), which explains that the cell clusters are probably primary colonisers on the surface.

3.4.4 Struvites and apatite

The absence of microcrystalline in TSB was expected, as there were no mineral salts in the medium. The appearance of crystal precipitation indicates the increased alkalinity of the environment as calcium and magnesium minerals become insoluble in higher pH (Konieczna *et al.* 2012). In bacterial colonisation, alkalinity relates to urease activity that hydrolyses urea to produce ammonium ions in the environment and induces crystal formation (Shaw *et al.* 2005; Stickler 2008).

Appearances of microcrystalline structures in laboratory studies involving *P. mirabilis* are common as it is a urease-producing bacterium. It induces crystallisation of calcium and magnesium ions in high pH environment (Morris and Stickler 1998; Czerwonka *et al.* 2014; Holling *et al.* 2014b; Wilks *et al.* 2015). The white amorphous microcrystalline structures present in the images were suspected to be apatite, a common structure in a urease-positive uropathogens biofilm, which consists of calcium phosphate mineral (Jacobsen *et al.* 2008; Stickler 2014; Flores-Mireles *et al.* 2015; Wilks *et al.* 2015). Amorphous urate is commonly found in normal human urine and similar crystallisation often presents in long-standing urine analysis (Simerville *et al.* 2005; Patel 2006). However, there was also presence of large coffin-shaped crystal formation observed in *P. mirabilis* biofilm in our study, similar to struvite crystals previous reported by Getliffe (2003), Stickler and Feneley (2010) and Wilks *et al.* (2015). Struvites are crystals consist of magnesium ammonium phosphate which are more resilient to dissolution compared to amorphous apatite and brings more implication to catheter encrustation and blockage (Hedelin 2002; Stickler and Feneley 2010; Wilks *et al.* 2015).

The white aggregations observed were suspected to be amorphous urates that have crystallised in the AUBK and attached to the *E. coli* biofilm. Even though *E. coli* is not a common urease producer, it can utilise urea by using glutamine synthetase. This then alkalizes the urine by releasing ammonia and carbon dioxide which then potentiate urinary struvite formation (Azevedo *et al.* 2016a).Brooks and Keevil (1997) have mentioned that AUBK closely resembled the normal human urine in such that it can form crystals or encrustations, which makes it suitable to be used in wide range of experiments including those related to urinary tract pathogens.

3.5 Conclusion

The study also shows the need to understand the interaction between the bacteria and the catheter material; it needs to have the right media to support the biofilm growth. It also emphasises that the AUM composition that supports the pathogen is also a vital factor when studying the interaction between the bacteria with catheter material.

From these observations, it can be concluded that although TSB is a good general medium for bacterial growth, it affects the biofilm development on the silicone catheter. Using AUM similar to the human urine physicochemical properties is the best choice of medium to conduct an experiment on the uropathogenic biofilm development.

The need and importance of AUM have been emphasised in numerous past studies (Greenwood 1976; Brooks and Keevil 1997; Jones *et al.* 2007; Chutipongtanate and Thongboonkerd 2010; Nowatzki *et al.* 2012; Wilks *et al.* 2015). Prominent CAUTI studies such as by Desai *et al.* (2010) that reported negative results on anti-fouling material might be influenced by the growth media used. Jones *et al.* (2007) also supported the use of AUM over standard media as the study reported more swarmer *P. mirabilis* cells attached to the surface when grown in AUM compared to LB from 12 h to 24 h. This offers a prospective future opportunity to conduct the efficiency of urinary catheters with anti-fouling material using AUM instead.

Compared to AUBK, TSB is found not suitable for uropathogenic biofilm study, as it does not produce the adequate support for the growth of the biofilm on the urinary catheter surface as well as not having similar physicochemical properties of human urine. Based on the results of the experiment, using AUBK achieved the most desirable biofilm growth in contrast to AUG, and will be used in the subsequent studies. AUBK is found to be the best AUM to produce healthy and stronger biofilm development due to possessing refined nutrient components that are very similar to the physicochemistry of human urine.

The limitations of this study are the limited uropathogenic organisms and static growth conditions investigated, which suggest a prospect of expanding the list of test uropathogens in the next study and using a continuous growth condition using a flow catheter model. In order to prevent and minimise the incidental crystallisation during storage, the AUBK pH should be monitored and freshly prepared a day before prior to use.

Overall, EDIC microscopy has proven very instrumental to this study as it manages to visualise the biofilm *in situ* on catheter although it was challenging with the catheter's curved surface. EDIC has also been used in this study together with EF filter to enhance the visualisation of the cells and the EPS matrix to show bacterial attachment and the biofilm.

Chapter 4 Enumeration of Biofilm on Urinary Catheter Grown in Artificial Urine Medium (AUM)

4.1 Introduction

The study in this chapter is conducted concurrently to the study of catheter biofilm observation as described in Chapter 3 to help understand the biofilm development on the urinary catheters. It was discussed in previous chapter that artificial urine media (AUM) is the most suitable growth media used for uropathogenic biofilm studies compared to the general media. There are various published AUM formulations available which feature different constituents or concentration of nutrients between them (Section 1.1.4.8). Therefore, in this experiment, the aim is to observe the biofilm growth of common urinary pathogens in two of the most common AUM formulations used in laboratory studies.

The selected AUM used in this experiment are by Griffith *et al.* (1976), which will be referred as AUG, and another by Brooks and Keevil (1997), which will be referred as AUBK. This study is conducted to show that the two AUM affect the biofilm growth differently. Currently, there are no other similar studies conducted that compared the two AUM as growth nutrient in growing biofilm on urinary catheters.

4.2 Materials and methods

E. coli (9001), *P. mirabilis* (NCTC 10975) and *P. aeruginosa* (PAO1) inocula were prepared as described in Section 2.1.1. The bacterial inocula were harvested by centrifuging 1 ml of overnight culture at 7500 rpm (5400 × *g*) for 10 min. The supernatant was removed, and the pellet was resuspended using the selected growth medium to form the inoculum. The AUG and AUBK media were prepared as described in Section 3.3.1 and Section 3.3.2.

The catheter sections were prepared at the beginning of the experiment as described in Section 2.3. The silicone catheter (100 % silicone, Rüsch Teleflex, UK) was cut into 1 cm catheter sections, which were then also cut longitudinally, and placed in a 6-well tissue culture plate (Nunc) as shown in Figure 4-1. For experiments investigating both short and long duration of biofilm growth, different plates were used for *E. coli*, *P. mirabilis* and *P. aeruginosa* for each growth medium. Each well in the plate was dedicated to time intervals 1, 2, 4, 6, and 24 h for the short experiment and 24, 48, 72, 96, 120 and 144 h for the long experiment, with the spare wells as the control.

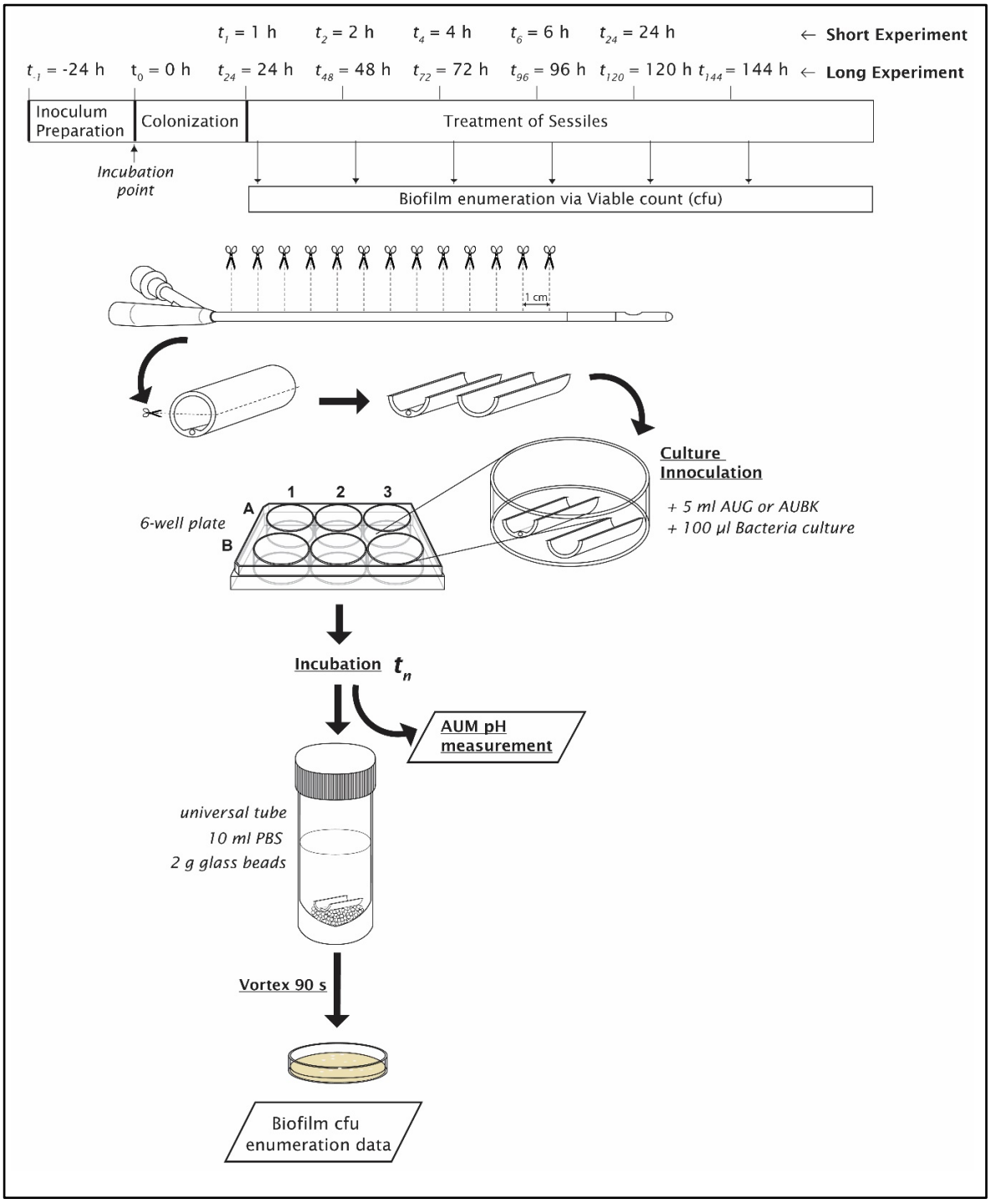

Figure 4-1 Experimental design methods used in this chapter.

The wells with the catheter sections had either 5 ml of AUG or 5 ml of AUBK added. The bacterial inoculum (100 µl) of either *E. coli*, *P. mirabilis*, or *P. aeruginosa* was added to each well in their dedicated plates, except for control wells. The plates were incubated at 37 °C. For the long experiment, excess medium was removed from the wells and replaced with fresh medium at every 24 h interval. The pH measurements were taken by sampling the excess media removed using Orion® pH meter model 520A (Thermo Electron Corp.; Beverly, MA). The biofilm growth in short and long experiments was assessed by bacterial enumeration of viable counts using colony-forming unit (CFU).

At each time interval, the catheter section was removed and gently washed with PBS three times. The catheter section was then placed in 10 ml of PBS solution in a Falcon tube prefilled with 2.00 ± 0.05 g of 2 mm glass beads. The biofilm from catheters was harvested by vortexing the tube for 90 seconds. The biofilm culture was diluted by serial dilution to 10^{-6} and 50 µl was plated onto corresponding agar media suitable for the uropathogen (as listed in Table 2-1). Each sample was plated out in triplicate plates and incubated at 37 ^{o}C for approximately 24 h before the colonies formed were counted for each dilution. The results are expressed as mean value of three independent biofilm experiments performed in a minimum of duplicates for each uropathogen tested in both AUM. All statistical analysis was conducted using Microsoft™ Excel. All comparison data were tested for the equality of variance using the F-test before carrying out a two-sample *t*-test for differences between the biofilm grown in AUG and AUBK. The data were recorded and plotted in the graphs as shown in Figure 4-9, Figure 4-10, and Figure 4-11.

4.3 Results

4.3.1 Standardisation of bacterial inocula concentration

The equality of variances tested for *E. coli* in AUG and AUBK inocula were equal (F = 2.9, *p* = 0.25). The significance threshold was set at *p* = 0.05. The mean for *E. coli* inoculum concentration in AUG (9.65 ± 0.499 $\log_{10}$ cfu/ml) was not significantly different from inoculum in AUBK (9.82 ± 0.293 $\log_{10}$ cfu/ml) when tested using the two-sample *t*-test for equal variances (t (4) = -0.529, *p* = 0.625). The equality of variances tested for *P. aeruginosa* in AUG and AUBK inocula were equal (F = 4.16, p = 0.19). The significance threshold was set at p = 0.05. The mean for *P. aeruginosa* inoculum concentration in AUG (M = 11.15, SD = 1.064, N = 3) was not significantly different from inoculum in AUBK (M = 11.6, SD = 0.522, N = 3) when tested using the two-sample *t*-test for equal variances (t (4) = -0.658, *p* = 0.547). The equality of variances tested for *P. mirabilis* in AUG and AUBK inocula were of unequal variances (F = 0.049, *p* = 0.046). The significance threshold was set at *p* = 0.05. The mean for *P. mirabilis* inoculum concentration in AUG (M = 12.10, SD = 0.218, N = 3) was not significantly different from inoculum in AUBK (M = 11.10, SD = 0.989, N = 3.) when tested using the two-sample *t*-test for unequal variances (t (2) = 1.71, *p* = 0.229).

4.3.2 Bacterial enumeration from 24 h biofilm growth experiment

The 24 h bacterial enumeration data from *E. coli*, *P. aeruginosa,* and *P. mirabilis* biofilm grown in two artificial urine media, AUG and AUBK, were transformed to $\log_{10}$ cfu/ml to represent biofilm growth at each time interval. The data were tested for statistical differences using the two-sample *t*-test with significance threshold set at *p* = 0.05. The results were recorded as shown in Appendix D (Appendices).

The bar graphs for the 24 h biofilm growth comparison between the two AUM for *E. coli*, *P. mirabilis*, and *P. aeruginosa* were as shown in Figure 4-2, Figure 4-3, and Figure 4-4, respectively. For *E. coli* and *P. mirabilis*, biofilm growth between AUG and AUBK were not significantly different, except for in the 2 h point from the 24 h experiment. The mean $\log_{10}$ cfu/ml for the 2 h biofilm growth in AUG was significantly (two-sample *t*-test, $p < 0.05$) less (3.97 $\log_{10}$ cfu/ml ± 0.19, N = 3) compared to AUBK (4.77 $\log_{10}$ cfu/ml ± 0.28, N = 3) for *E. coli*.

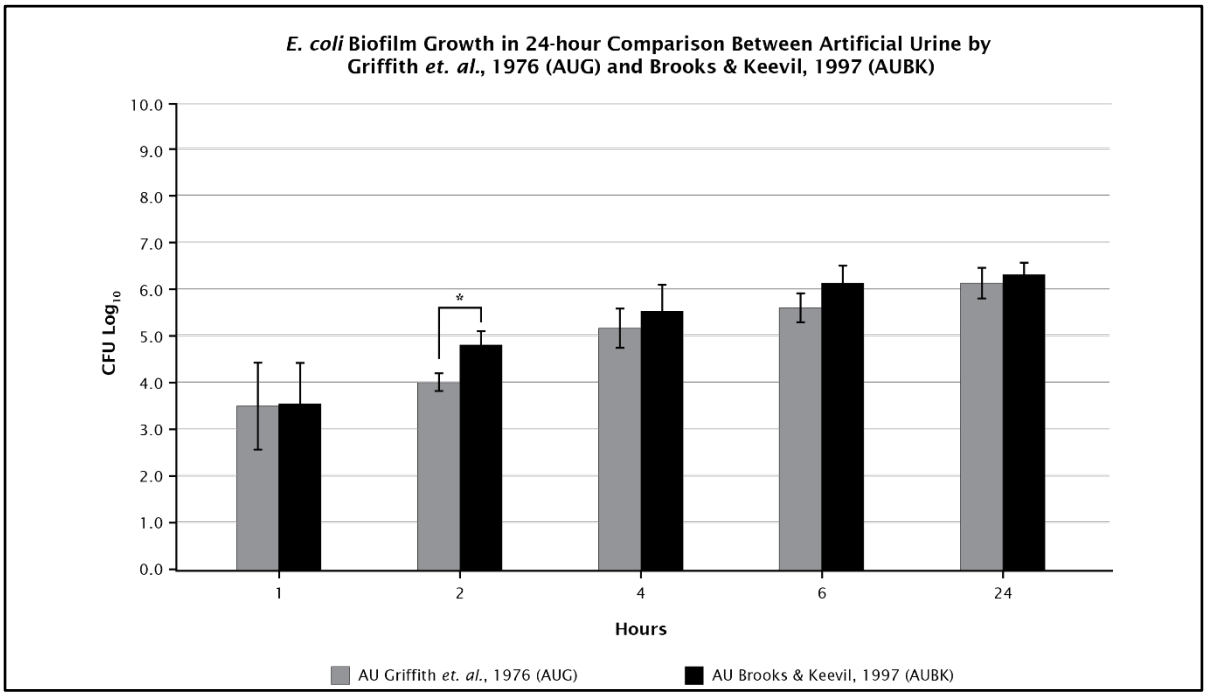

Figure 4-2 Graph of *E. coli* 24 h biofilm grown in AUG and AUBK. Error bars represent standard deviation.

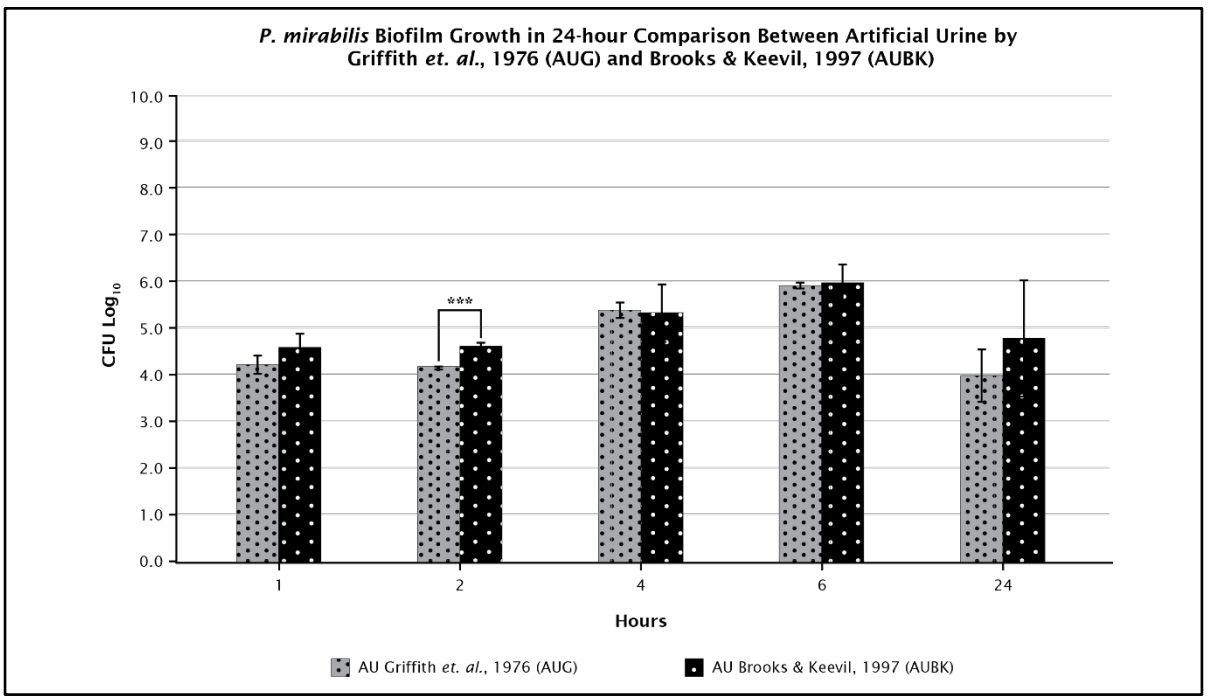

Figure 4-3 Graph of *P. mirabilis* 24 h biofilm grown in AUG and AUBK. Error bars represent standard deviation.

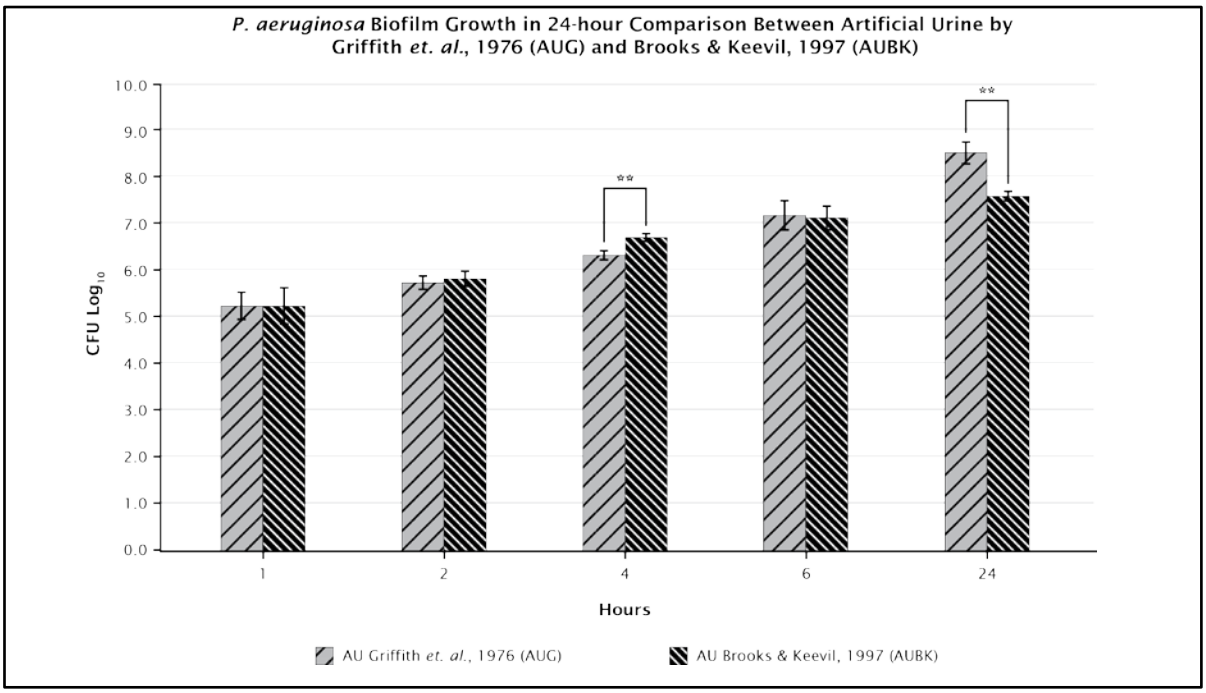

Figure 4-4 Graph of *P. aeruginosa* 24 h biofilm grown in AUG and AUBK. Error bars represent standard deviation.

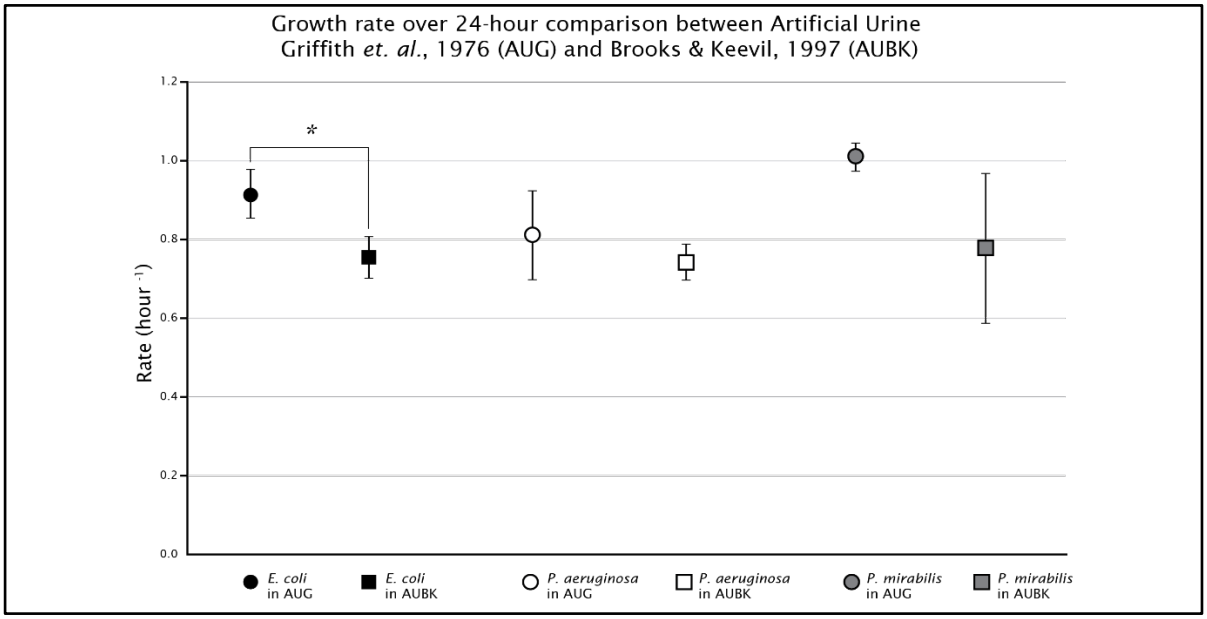

Figure 4-5 Graph is showing the difference in growth rate between the uropathogen when grown in AUG and AUBK. Only *E. coli* shows significant growth rate difference ($p < 0.05$). Error bars represent standard deviation.

Similarly, for *P. mirabilis* biofilm, the mean $\log_{10}$ cfu/ml for the 2 h biofilm growth in AUG was significantly (two-sample *t*-test, $p < 0.001$) less (4.17 $\log_{10}$ cfu/ml ± 0.02, N = 3) compared to AUBK (4.61 $\log_{10}$ cfu/ml ± 0.07, N = 3). For *P. aeruginosa*, the biofilm growth comparisons between AUG and AUBK were significantly different only in the 4 h and 24 h time intervals from the 24 h experiment (two-sample *t*-test, $p < 0.01$). The mean $\log_{10}$ cfu/ml for the 4 h *P. aeruginosa* biofilm growth in AUG was less (6.28 $\log_{10}$ cfu/ml ± 0.09, N = 3) compared to AUBK (6.639 $\log_{10}$ cfu/ml ±

0.09, N = 3). The 24 h biofilm growth in AUG was more (8.44 $\log_{10}$ cfu/ml ± 0.23, N = 3) compared to AUBK (7.53 $\log_{10}$ cfu/ml ± 0.1, N = 3).

The growth rate between the two AUM was analysed using the equation described previously in Section 2.1.4. The 24 h datasets were compared using a two-sample *t*-test. The result showed that there was a significant difference in growth rate between AUG (0.915/hr ± 0.06, N = 3) and AUBK (0.749/hr ± 0.05, N = 3) for *E. coli* (two-sample *t*-test, $p < 0.05$), but not for *P. aeruginosa* and *P. mirabilis* (Figure 4-5).

4.3.3 Bacterial enumeration from 144 h biofilm growth experiment

The 144 h bacterial enumeration data from *E. coli*, *P. aeruginosa*, and *P. mirabilis* biofilm grown in two artificial urine media, AUG and AUBK, were transformed to $\log_{10}$ cfu/ml to compare biofilm growth at each time interval. The data was tested for statistical differences using two-sample *t*-test with significance threshold set at $p = 0.05$. The result was recorded as shown in Appendix E (Appendices). The bar graphs for the 144 h biofilm growth of E. coli, P. aeruginosa, and P. mirabilis comparison between the two AUM were as shown in Figure 4 6, Figure 4 7, and Figure 4 8, respectively. The biofilm growth between AUG and AUBK was not significantly different for *E. coli*, except for in the 96 h time interval (two-sample *t*-test, $p < 0.05$) from the 144 h experiment. The mean $\log_{10}$ cfu/ml for the 96 h biofilm growth in AUG was higher (7.00 $\log_{10}$ cfu/ml ± 0.18, N = 3) compared to AUBK (5.90 $\log_{10}$ cfu/ml ± 0.25, N = 3).

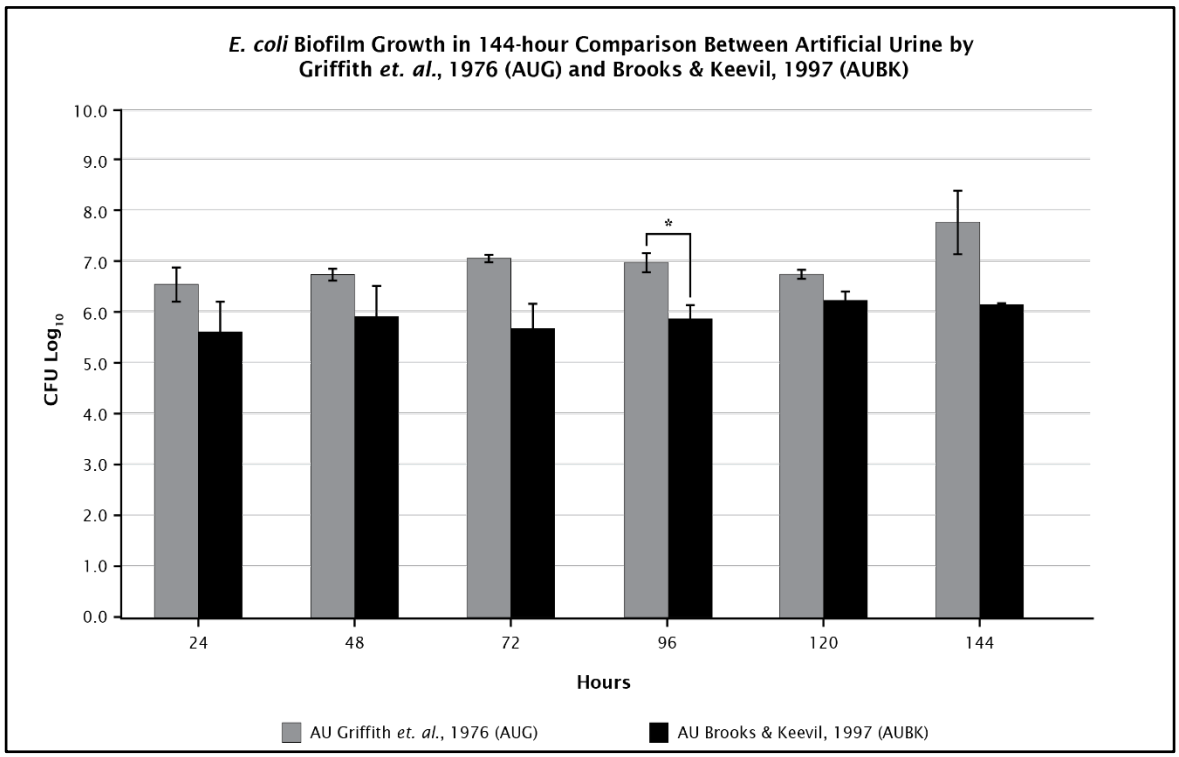

Figure 4-6 Graph of *E. coli* 144 h biofilm grown in AUG and AUBK. Error bars represent standard deviation.

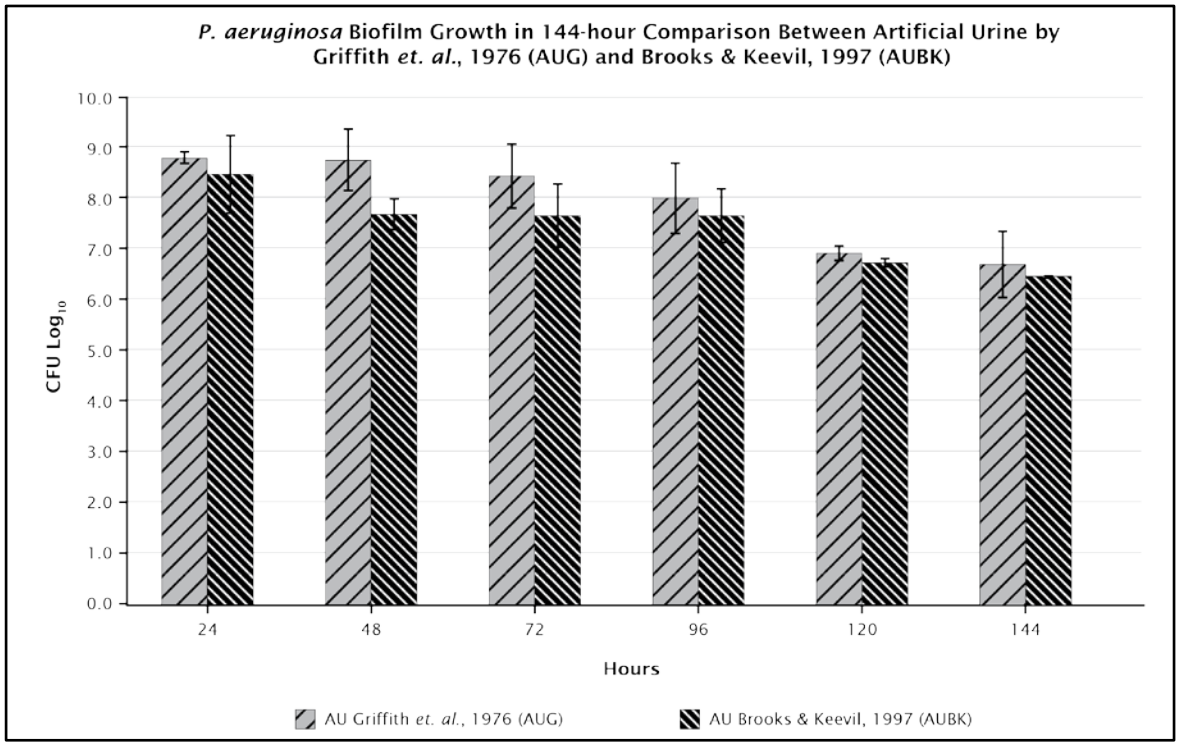

Figure 4-7 Graph of *P. aeruginosa* 144 h biofilm grown in AUG and AUBK. Error bars represent standard deviation.

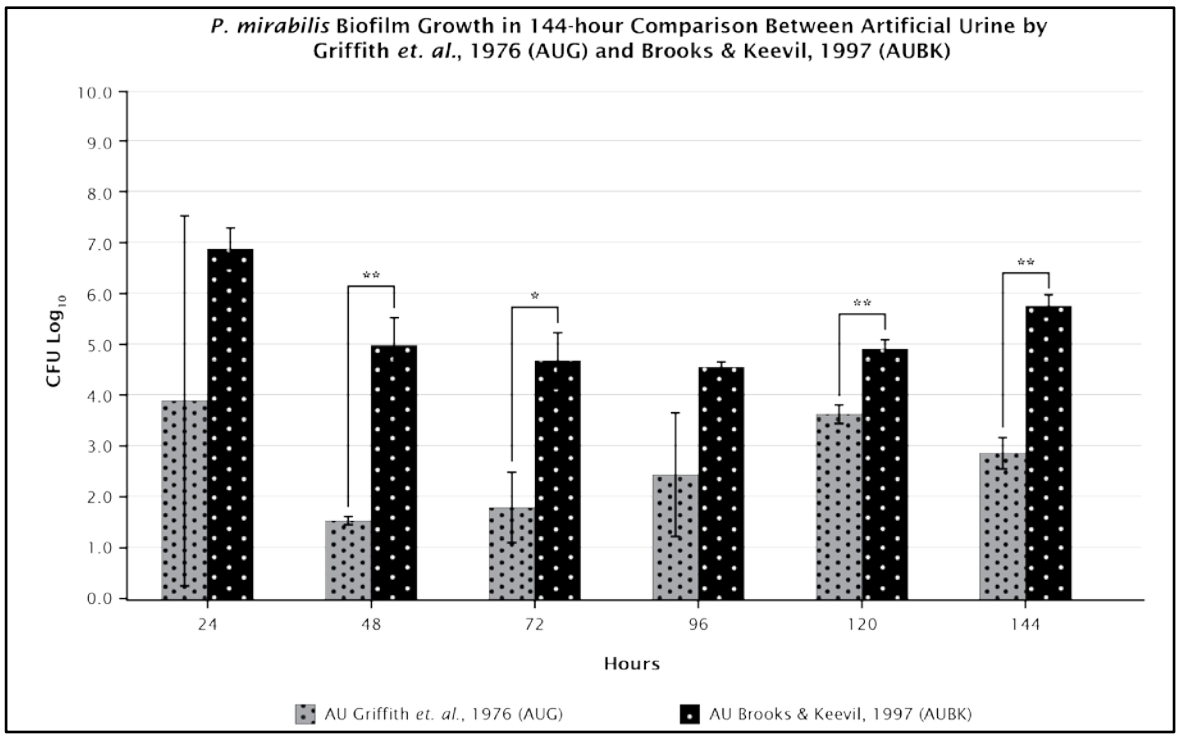

Figure 4-8 Graph of *P. mirabilis* 144 h biofilm grown in AUG and AUBK. Error bars represent standard deviation.

The growth comparison for *P. mirabilis* biofilm between AUG and AUBK was significantly different, except for in the 24 h and 96 h time intervals from the 144 h experiment. The 48 h biofilm growth in AUG was significantly less (1.54 $\log_{10}$ cfu/ml ± 0.09, N = 3) than AUBK (4.98 $\log_{10}$ cfu/ml ± 0.54, N = 3; two-sample *t*-test, $p < 0.01$).

The 72 h biofilm growth in AUG was significantly less (1.80 $\log_{10}$ cfu/ml ± 0.71, N = 3) compared to AUBK (4.69 $\log_{10}$ cfu/ml ± 0.55, N = 3; two-sample *t*-test, $p < 0.05$). The 120 h *P. mirabilis* biofilm growth in AUG was significantly less (3.63 $\log_{10}$ cfu/ml ± 0.21, N = 3) compared to AUBK (4.91 $\log_{10}$ cfu/ml ± 0.19, N = 3; two-sample *t*-test, $p < 0.05$). Lastly, the 144 h biofilm growth in AUG was significantly less (2.85 $\log_{10}$ cfu/ml ± 0.35, N = 3) compared to AUBK (5.73 $\log_{10}$ cfu/ml ± 0.22, N = 3; two-sample *t*-test, $p < 0.01$).

There was no significant difference in mean $\log_{10}$ cfu/ml for the biofilm growth of *P. aeruginosa* between AUG and AUBK throughout the 144 h experiment. The result of both 24 h mean $\log_{10}$ cfu/ml values from the short and long experiment were averaged and showed no significant difference (two-sample *t*-test, $p > 0.06$). The average of the 24 h mean $\log_{10}$ cfu/ml for *E. coli* and *P. mirabilis* showed no significant difference between AUG and AUBK as well (two-sample *t*-test, $p > 0.15$).

4.3.4 AUM pH comparison between AUG and AUBK

The changes in AUM pH from 144 h experiments for *E. coli*, *P. aeruginosa*, and *P. mirabilis* were recorded and plotted in graphs, as shown in Figure 4-9, Figure 4-10, and Figure 4-11, respectively.

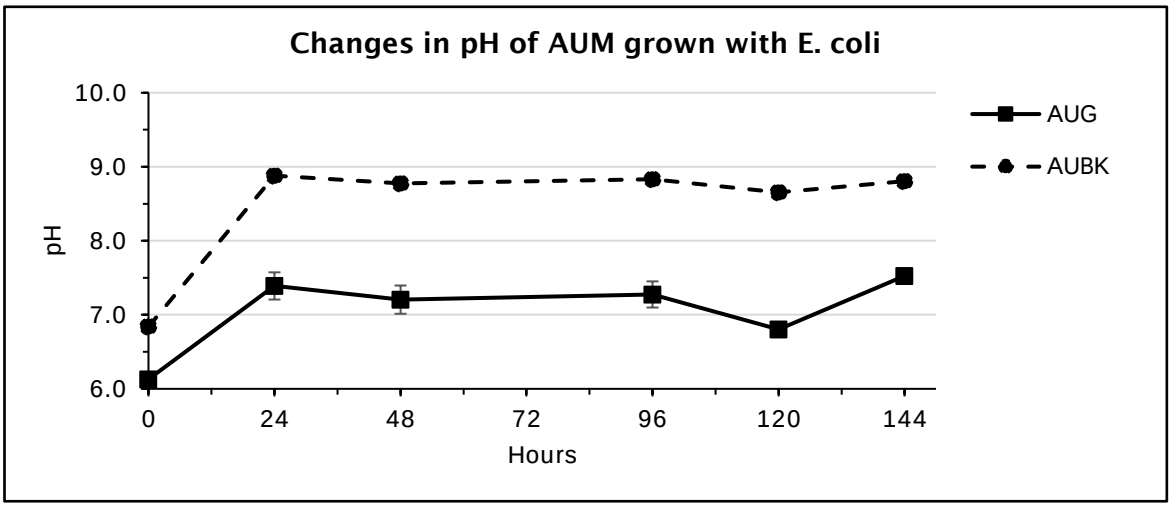

Figure 4-9 Graph of AUM pH changes for *E. coli.* Error bars represent standard deviation.

For *E. coli*, the pH changes in AUG and AUBK appeared differently throughout the experiment, except for the first 24 h, which showed increased of pH for both AUM. For AUBK, the graph for the pH increased from 24 h onwards and stayed within the range of pH 8.5 to pH 9.0 until the 144 h timepoint. For AUG, the pH level was lower than for AUBK and stayed within the range of pH 7.0 to pH 7.5 from 24 h until 96 h timepoint. The pH level dropped to pH 6.8 at the 120 h timepoint and elevated again to pH 7.5 at the 144 h timepoint.

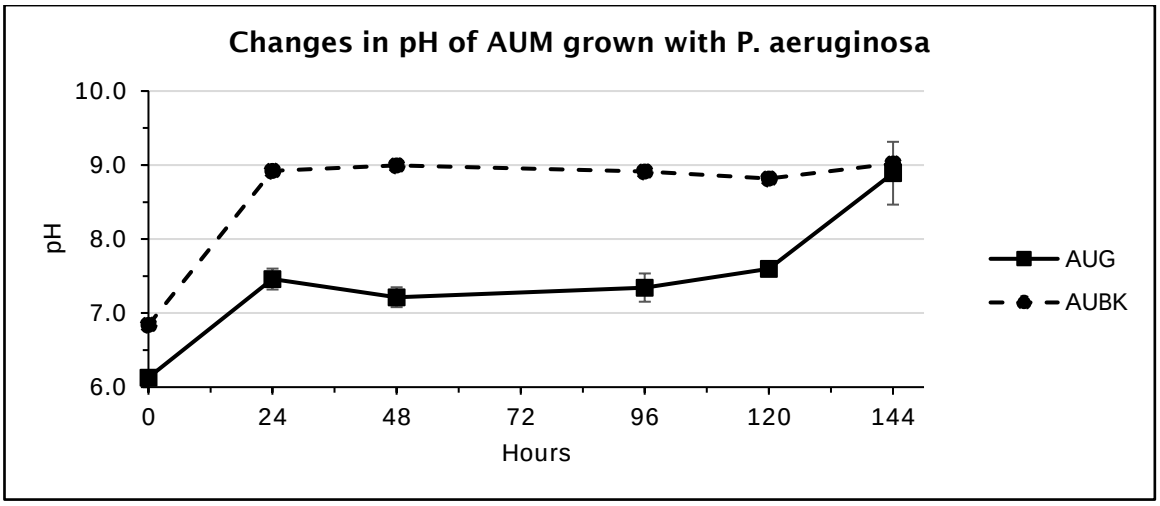

Figure 4-10 Graph of AUM pH changes for *P. aeruginosa.* Error bars represent standard deviation.

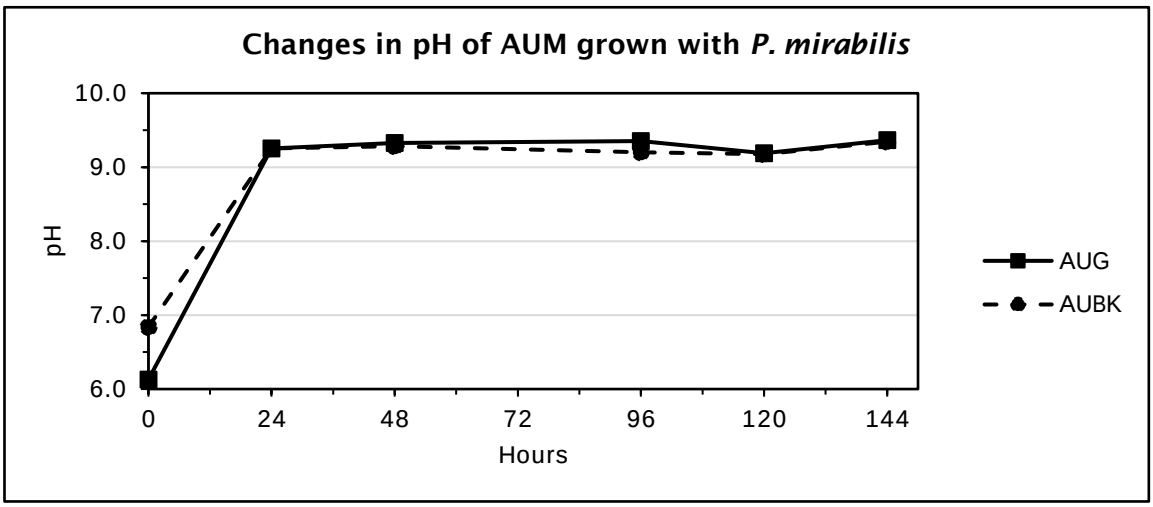

Figure 4-11 Graph of AUM pH changes for *P. mirabilis.* Error bars represent standard deviation.

Similarly, the pH changes for *P. aeruginosa* between AUG and AUBK appeared different as well. However, after the pH increased steadily within the first 24 h, both AUM achieved the same pH range at the end of the 144 h. For AUBK, the pH increased from 24 h onwards and maintained at approximately pH 9 until the 144 h timepoint. For AUG, the pH was lower, which was less than pH 7.5 from 24 h to 120 h timepoints and increased to approximately pH 9 at the 144 h timepoint.

For *P. mirabilis*, the pH profile appears similar for both AUG and AUBK. Both AUM had elevated pH within the first 24 h and reached the same pH range above pH 9. From 24 h to 144 h timepoints, both AUM maintained a high pH level above pH 9.

4.4 Discussion

In this study, all uropathogens tested were able to grow and form biofilms on the catheter under static growth conditions using the method of Wilks *et al.* (2015). The heterogeneous growth characteristics shown were clearly influenced by the differences between AUG and AUBK. Past studies had shown that biofilms are affected by the composition of available nutrients, and some even flourish better in a limited-nutrient environment (Wrangstadh *et al.* 1990; Donlan 2002).

AUBK performed better as an appropriate urine substitute medium in comparison to AUG, as seen in the results from the exponential growth phase for all three tested uropathogens. One reason could be that AUBK contained bacteriological peptone that was easily utilised compared to TSB in AUG with the same concentration. This is also despite the added gelatine in AUG that could serve as an additional peptide source even though it was added with the intention to create a 'supersaturation' effect to the medium.

Gelatine is an irreversibly hydrolysed form of collagen, whose hydrolysis results in the reduction of protein fibrils into smaller peptides, which have a broad molecular weight range based on the process of hydrolysis. Gelatine molecule structure is mainly composed of multiple repetitions of a Gly-X-Y sequence, where X is often proline, and Y is often hydroxyproline.

Conversely, peptone is hydrolysed meat consisting of easily assumable amino acids and short peptides more representative of normal urine (Strong *et al.* 2005). Available nutrients for bacterial uptake play a major role in its growth, and the easily utilised substrates are usually used first (Monod 1949). Past studies have shown that a refined peptone source such as casein or soy produces better bacterial growth than gelatine (Gray *et al.* 2006; Gray *et al.* 2008).

Interestingly, *E. coli* showed significantly higher growth rate with AUG during the short experiment. This could be that while AUBK showed higher biofilm growth at the 2 h time interval for *E. coli*, it was able to utilise AUG in a delayed consumption pattern that benefited culture during the whole duration of the short 24 h experiment (Monod 1949). This simple versus complex nutrient utilisation has been extensively studied in planktonic cultures, but there are very limited studies conducted in the urinary biofilm (Amato and Brynildsen 2014). There is high correlation between nutrient availability and the presence of persister cells (Amato *et al.* 2013). However, it could not be determined that the *E. coli* biofilm in this study was diauxic, non-diauxic or even a co-utilisation growth pattern without conducting a further in-depth study to see the diauxic lag phase in the biofilm growth.

In the long experiment, only once at the 96 h interval was the mean $\log_{10}$ cfu/ml significantly higher in AUG than in AUBK for *E. coli*. At the same time, there was a drop in AUG pH detected at the 120 h time interval, which could perhaps be related to the increase of cell growth. This may be because the media composition and concentration of the nutrients contribute to the interchangeable state from biofilm to planktonic growth (Kim and Frank 1995; Blehert *et al.* 2003).

E. coli is not a common urease producer, but it can utilise urea by using glutamine synthetase, which alkalizes the urea by releasing ammonia and carbon dioxide (Azevedo *et al.* 2016a). Very high pH could induce stress factors that supresses planktonic cell growth (Donlan 2002), but the *E. coli* biofilm showed great tolerance towards high pH that might be one of many survival characteristics adopted throughout the experiment (Donlan and Costerton 2002).

The mean $\log_{10}$ cfu/ml values for *P. aeruginosa* showed no difference between AUG and AUBK in short or long experiments, except for in the 4 h timepoint. However, there was an apparent colour change in the AUBK medium from clear to blue-green colour (not shown) to indicate the pyocyanin production by *P. aeruginosa*.

P. mirabilis showed consistent significant differences where AUBK produced higher mean $\log_{10}$ cfu/ml than AUG, even though there was increasing alkalinity in the AUBK (> pH 9). The increasing pH was due to the urease-producing activity, which releases ammonia and carbon dioxide from the urea and alkalises the AUM (Wilks *et al.* 2015; Azevedo *et al.* 2016a).

The high tolerance of the uropathogenic biofilm formed in AUBK was probably due to the biofilm EPS structures that protect the bacterial cells in the microcolonies from the high pH environment. The biofilm also showed slow but surviving growth, which is probably due to the biofilm EPS structure still allowing diffusion of gaseous change and nutrients to be accessed by the microcolonies (Singh *et al.* 2017).

From the pH graph changes above, the pH for AUG can be seen lower than for AUBK, which follows accordingly to the lower initial pH of AUG compared to AUBK, except for *P. mirabilis*. The pH of AUG for *P. mirabilis* immediately increased to a similar pH to that of AUBK after 24 h. This showed that *P. mirabilis* was able to utilise the higher concentration of urea in AUG (Jacobsen and Shirtliff 2011) and alkalises the medium, in contrast to no changes in *E. coli* and *P. aeruginosa* cultures.

4.5 Conclusion

The different growth effects of nutrients to the uropathogens were expected (Hood and Zottola 1997), and the present study on uropathogenic biofilm formation supports the necessity of using the appropriate AUM similar to human urine to ensure healthy biofilm growth, as well as to ensure experimental reproducibility. The healthy state of a biofilm ultimately depends on a suitable growth medium as a nutrient source. In perspective, biofilm follows true to the maxim 'you are what you eat'. In this study, a healthy biofilm is determined by increased growth, which also withstands high pH environments.

During exponential phase of growth, the nutrients available from the AUM are crucial in helping the bacteria to synthesise appropriate materials to form and survive as a biofilm. Certain chemical components are needed for an adequate source of protein sub-units, while others might be required to trigger certain enzyme production (Donlan 2002).

While this study discussed the biofilm growth related to the source of peptone, gelatine, urea and pH, other chemical components such as sodium bicarbonate can be investigated as to its function in urinary biofilm formation and physiology. Previous studies have found a correlation for bicarbonates in increased cell growth (Kesaano *et al.* 2015), triggering pili formation (Bourgogne *et al.* 2010), as well as the release of eDNA in the biofilm (Rose and Bermudez 2016). This would lead to possible future studies relating the availability of bicarbonates that will affect uropathogenic biofilms.

Chapter 5 The Role of Urease in *Pseudomonas aeruginosa* Biofilm Formation in Artificial Urine Media (AUM)

5.1 Introduction

Ureolytic activity by urease can be found naturally occurring in soil bacteria as well as in human pathogens such as *Staphylococcus aureus*, *Helicobacter pylori*, *Mycobacterium tuberculosis* and *Proteus mirabilis* (Hiron *et al.* 2010; Jacobsen and Shirtliff 2011; Lin *et al.* 2012; Vandecandelaere *et al.* 2017; Graham and Miftahussurur 2018). Urease is also widely studied in *P. mirabilis* as the major virulence factor contributing to urinary tract infections (UTI) and CAUTI due to the encrustation of urethral catheters (Jacobsen and Shirtliff 2011; Lehman and Donlan 2015). The presence of urea in urine is linked to the increased urine pH through the generation of ammonia by the activity of urease. The increased pH is suspected to cause crystal formation in urine that induces catheter encrustation (Jones *et al.* 2005).

Catheter encrustation is a hard mineral deposit biofilm that causes blockage and catheter leakage that causes discomfort to patients (Cox *et al.* 1987; Saint and Chenoweth 2003; Carson *et al.* 2010; Thomsen *et al.* 2011). Removal of encrusted catheters from patients can cause trauma to the urethra (Stickler 2002; Smith 2003; Malic *et al.* 2012). CAUTI related to catheter encrustation often leads to recurrent acute infection and increased morbidity in patients (Cox *et al.* 1987; Saint and Chenoweth 2003; Getliffe 2004).

Urease enzyme has been extensively studied since it was among the earliest enzymes to be crystallised; however, the role of urease in bacterial biofilm is still not well understood (Mulrooney and Hausinger 1990b; Jabri *et al.* 1995; Hedelin 2002; Konieczna *et al.* 2012). The characteristics of urease in *P. aeruginosa* are similar to other bacteria such as *Klebsiella pneumoniae*, *P. mirabilis,* and *Escherichia coli (*Mulrooney and Hausinger 1990b; Clemens *et al.* 1995; Hausinger *et al.* 2001). Bacterial ureases are produced as inactive multimeric apoenzymes that are usually composed of two or three types of the main urease polypeptide subunits UreA, UreB, and UreC, encoded by the corresponding structural genes *ureA*, *ureB* and *ureC*. The urease activation requires the production of additional accessory proteins UreD, UreE, UreF, and UreG by the action of transporting and incorporation of nickel ions to the apoenzyme active site (Figure 5-1) (Mulrooney and Hausinger 1990a; Hausinger *et al.* 2001; Konieczna *et al.* 2012; Fisher *et al.* 2017).

The activity of ureases in urinary pathogens exposes the bacteria to higher-pH environments because of alkalinisation of the infected urine (Clemens *et al.* 1995). Even though the urease function has been studied extensively in *P. mirabilis*, full understanding of the function and roles of urease genes in bacteria and the urinary biofilm remain unknown.

There has been minimal research conducted on the role of urease in the *P. aeruginosa* biofilm growth and development on urinary catheters. The objective of this study was to determine if the urease genes are essential to *P. aeruginosa* biofilm formation when grown in a physiological correct artificial urine media Brooks and Keevil (1997) (AUBK). Deletions or mutations in genes coding for the urease accessory molecules have been found to abolish urease activity (Clemens *et al.* 1995). The *ureC* gene was chosen as it is one of the main alpha subunit components of the urease enzyme that has been found to be strongly conserved throughout eubacteria (Koper *et al.* 2004). The *ureE* gene was chosen as it is an important accessory molecule functioning as a nickel donor to the urease apoprotein (Clemens *et al.* 1995).

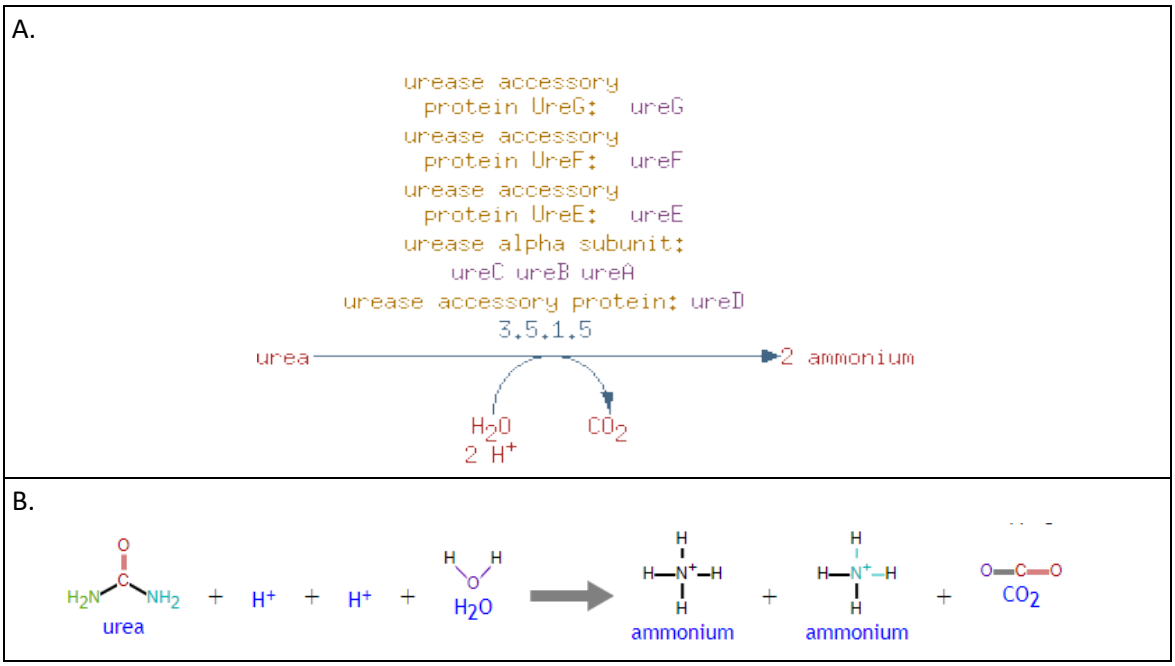

Figure 5-1 The urea degradation pathway summary in *P. aeruginosa* PAO1.
A. The role of urease proteins and their corresponding genes in catalysing the urea degradation. B. Chemical formula equation of the urea hydrolysis into ammonia. Images obtained from http://www.*pseudomonas*.com.

The UreC is a part of urease alpha subunit UreABC and UreE is a part of urease accessory protein. Although it is found that the *ureA* and *ureB* urease subunits are two similar small sizes subunits with each approximately 11,000 Da, the UreC (60.3-kDa peptide) is a large subunit size at 62,000 Da, nearly 5 times bigger compared to *ureE* (17.6-kDa peptide) (Mulrooney and Hausinger 1990a). Little is known about the role of *ureE*, except that it has histidine-rich regions that contributes to the inflammatory response in patients (Mulrooney and Hausinger 1990a).

The role of urease was studied by using an efficient, reliable and repeatable *in vitro* laboratory model system to grow the urease mutant biofilm on urinary catheter pieces (Wilks *et al.* 2015). The expression activity in the formation of biofilm on urinary catheter of *ure*C and *ureE* genes was assessed by analysing the biofilm growth by enumeration and the distinct biofilm morphology characteristics produced by the mutants compared to the PAO1 wildtype. In this study, our hypothesis is that the urease-negative mutants are still able to produce complex biofilm structures on catheter using artificial urine media.

5.2 Materials and methods

This study used the following methods for analysing biofilm formation formed by *P. aeruginosa* PAO1 and screening urease-negative mutants to identify the role of urease in biofilm formation. Figure 5-2 presented the experimental design methods that are used in this chapter, as well as for Chapter 6 and Chapter 7.

5.2.1 Inocula preparation

The inocula preparation for *P. aeruginosa* PAO1 wildtype and urease-negative mutant strains was as described in Section 2.1.2. An aliquot of 1 ml of bacterial inocula from the overnight culture was centrifuged at 7500 rpm (5400 × *g*) for 10 min. After discarding the supernatant, the remaining pellet was resuspended using 1 ml artificial urine medium (Brooks and Keevil 1997) (AUBK) to form the inoculum. Preparation of the AUBK medium used the methods as described in Section 2.3.1.

5.2.2 *P. aeruginosa* PAO1 strains used in this experiment

The details of the main parental *P. aeruginosa* PAO1 wildtype reference strain and the selected urease-negative mutant strains used in this study are as shown inTable 5-1 below. The sequenced verified *P. aeruginosa* PAO1 wildtype and the transposon mutants were obtained from the Seattle *P. aeruginosa* mutant library (University of Washington Genome Sciences, USA) (Jacobs *et al.* 2003; Held *et al.* 2012).

The mutants carrying IS*phoA*/hah transposon insertions are made as previously described by Jacobs *et al.* (2003). Details of the reference *P. aeruginosa* PAO1 wildtype and the mutant strains were also elaborated further in the Appendix F of the Appendices section which were extracted from the accompanying table (PA two-allele library) provided in the *P. aeruginosa* Mutant Library website (https://www.gs.washington.edu/labs/manoil/libraryindex.htm).

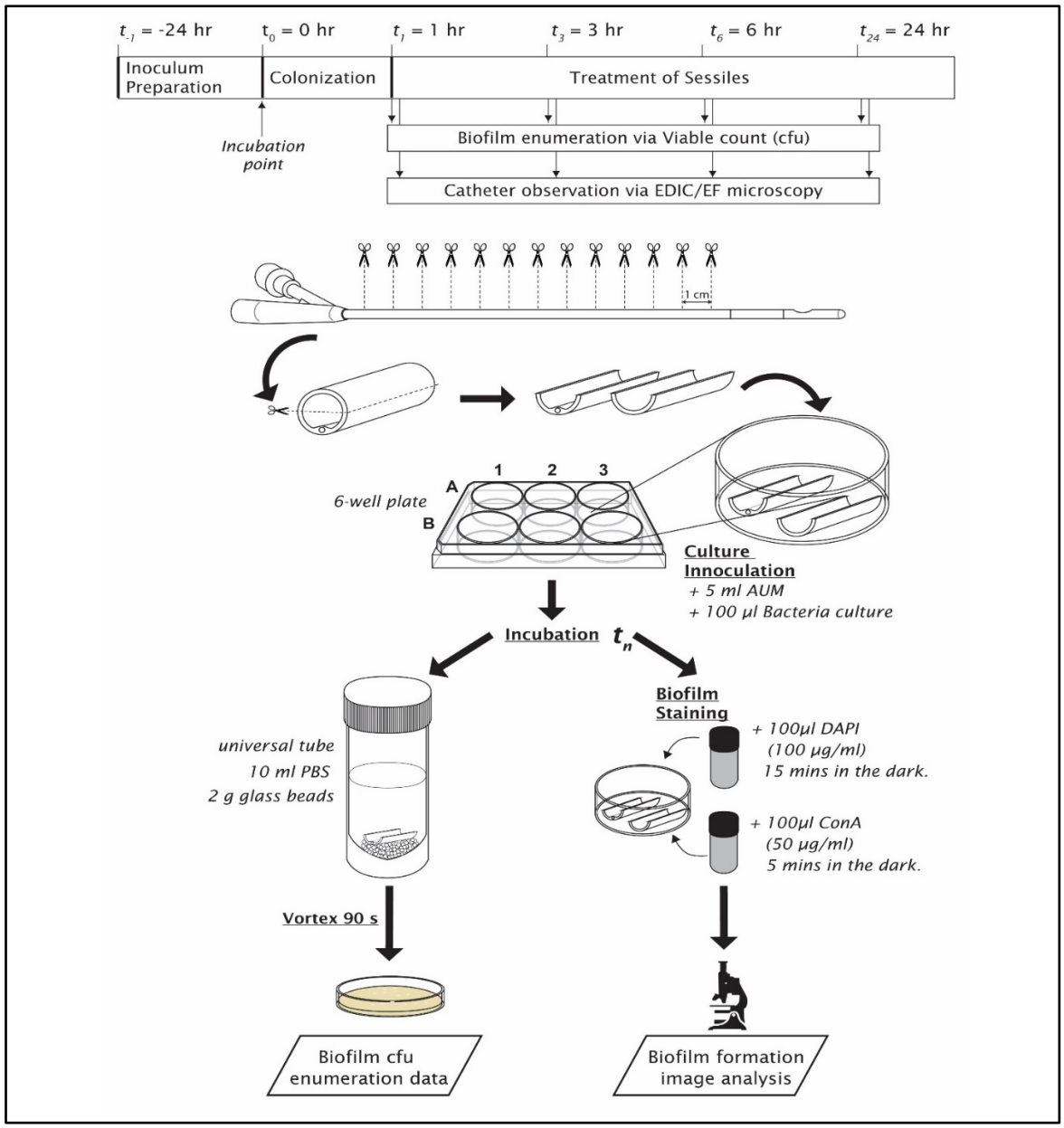

Figure 5-2 Experimental design methods used in Chapter 5, Chapter 6 and Chapter 7.

Table 5-1 *P. aeruginosa* PAO1 strains used in this chapter.

Reference strain

Name	Bacterial strains	Relevant putative ORF function / characteristic(s)	PA ORF
Wildtype	PAO1	Wildtype parental *P. aeruginosa* strain ATCC 15692	MPAO1

Urease-negative mutants

Name	Bacterial strains	Relevant putative ORF function / characteristic(s)	PA ORF
PW9188	ureC-G12::ISphoA/hah	urease alpha subunit mutant	PA4868
PW9189	ureC-C11::ISphoA/hah	urease alpha subunit mutant	PA4868
PW9231	ureE-A01::ISphoA/hah	urease accessory protein UreE mutant	PA4891

5.2.3 Biofilm assay

Biofilm growth assays were conducted as previously described in Wilks *et al.* (2015). Catheter sections were used with AUBK medium in the biofilm growth assay in 6-well plates. Further details of the experiment are as described in Section 2.4. Mono-strain biofilm assay of *P. aeruginosa* wildtype and urease-negative mutants were cultured independently with at least three biological replicates.Approximately 1 cm long silicone catheter (100 % silicone, Rüsch Teleflex, UK) pieces were cut longitudinally to produce two catheter sections and placed in each well in the 6-well plates (Nunc, Thermo Scientific, UK). Each well in the plate represented a separate timepoint of incubation 1 h, 3 h, 6 h, and 24 h with the additional well for the control. One plate was used for each strain in each replication experiment.

The catheter sections in the wells were immersed in 5 ml of AUBK medium and 100 µl of inoculum from Section 5.2.2 (final concentration of approximately 1×10^9 cfu/ml) added into each well and then incubated at 37 ^{o}C. The biofilm was allowed to grow on for 1 h, 3 h, 6 h, and 24 h. At each timepoint, catheter sections from the corresponding well were removed and rinsed with PBS solution three times and dried on tissue paper via capillary action. For every two catheter sections removed at a timepoint, one was subjected to bacterial enumeration, and the other was observed under EDIC/EF microscope for biofilm formation. The pH measurements were taken by sampling the excess media removed using an Orion® pH meter model 520A (Thermo Electron Corp., USA).

5.2.4 Bacterial enumeration from biofilm formed on the catheter

The catheter sections (from Section 5.2.3) were transferred into 10 ml of PBS solution in a sterile tube with approximately 2 g of 2 mm glass beads. The biofilm cells were harvested by vortexing the tube for 90 seconds. The biofilm culture was serially diluted in PBS accordingly. Aliquots of 50 µl of the dilutions were plated onto TSA media plates in triplicate for each selected dilution and incubated at 37 ^{o}C for 18 to 20 h before the colonies were counted. The results of the enumeration data were analysed further using statistics.

5.2.5 Statistical data analysis

The enumeration data obtained by colony forming unit per catheter section (cfu/catheter section) were transformed into logarithmic colony forming unit per catheter section ($\log_{10}$ cfu/catheter section) representing biofilm attached on the catheter at each timepoint. All values (enumeration and pH) are expressed as means ± SD.

The wildtype biofilm enumeration data between timepoints were evaluated for statistical differences using one-way analysis of variance (ANOVA) followed by Bonferroni's multiple comparisons post-hoc test using GraphPad Prism (version 7.05 for Windows, GraphPad Software, La Jolla California USA, www.graphpad.com). Subsequently, using GraphPad Prism, the wildtype and urease-negative mutants biofilm enumeration data were evaluated for statistical differences using one-way analysis of variance (ANOVA) followed by Dunnett's multiple comparisons post-hoc test using GraphPad Prism (probability value of 0.05, $P < 0.05$, was considered statistically significant). The results are reported below in Section 5.3.

5.2.6 Fluorescent differential staining of biofilm on urinary catheter

The catheter sections were prepared for fluorescent differential staining with DAPI and ConA subsequently after the biofilm assay (Section 5.2.3) as described in Section 2.4.1 prior to the microscopy observation. *P. aeruginosa* PAO1 biofilm was stained simultaneously with fluorescent probes to visualise different components of the biofilm using DAPI in blue for cell detection and tetramethylrhodamine (TRITC)-labelled Concanavalin A (ConA) in red to detect α-D-mannosyl and α-D-glucosyl residues (Leriche *et al.* 2000; Schwartz *et al.* 2003; Wilks *et al.* 2015). The biofilm staining method using DAPI and ConA is as detailed further in Section 2.4.1. The stained catheter sections were air-dried before used for EDIC/EF microscopy observation.

5.2.7 Observation using episcopic differential interference contrast/epifluorescence (EDIC/EF) microscope

All strains of *P. aeruginosa* PAO1 biofilm development on the catheter surface were observed using a customised Nikon Eclipse LV100D microscope (Best Scientific, UK) equipped for EDIC/EF microscopy (Keevil, 2003). The microscope was equipped with long working distance metallurgical objectives (Nikon Plan Achromat), a high-resolution camera (QImaging Retiga EXi Cooled Digital CCD monochrome camera with RGB colour filter module) and metal halide light source (EXFO X-CITE 120 fluorescence system). Three low to high magnification view (magnification x 100, x 500, and x 1000) were used in imaging the biofilm formation taken with ImagePro 6.2 software (Media Cybernetics, UK). Due to the curvature of the catheter, stacked images of biofilm were taken for each focal point achieved at horizontal level under high magnification (manual *z*-scans, one stack image ≈ ±1 μm).

5.2.8 Image processing

The stacked images were processed into a composite image using the extended depth of field plugin (Forster *et al.* 2004) in the open-source image-analysis software, Fiji (version 1.42q,

National Institutes of Health, USA) (Schindelin *et al.* 2012). A summary for biofilm images for wildtype (Appendix G) and urease-negative mutants are included in the Appendix H of the Appendices section. The EDIC images presented in the results were converted into grayscale using Adobe Systems Photoshop CS (version CS6) to compensate for the prism's pseudo colouration effects in the EDIC microscope and discussed further in the next section.

5.3 Results

5.3.1 *P. aeruginosa* PAO1 wildtype biofilm growth on urinary catheter using AUBK medium after 1 h, 3 h, 6 h, and 24 h.

The mean values of log10 cfu/catheter section at each timepoints are summarized in Table G-1 (Appendix G) and the growth is illustrated in Figure 5-3. Overall, biofilm growth of *P. aeruginosa* PAO1 wildtype increased at every timepoint. One factor ANOVA with a Bonferroni post-hoc correction showed the mean $\log_{10}$ cfu/catheter section differed significantly between the timepoints ($F(3, 8) = 35.67$, $P < 0.0001$). Bonferroni multiple comparisons post-hoc test revealed that mean $\log_{10}$ cfu/catheter section increased by an average of 0.7 $\log_{10}$ cfu/catheter section after 3 h ($P = 0.0022$).

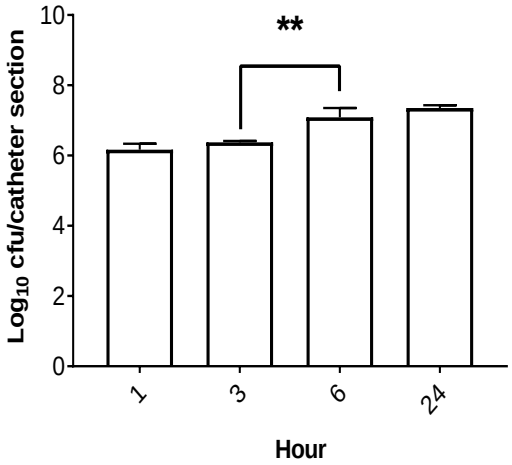

Figure 5-3 Graph of *P. aeruginosa* PAO1 WT biofilm growth at 1 h, 3 h, 6 h and 24 h. Error bars indicates the standard deviation (SD). One factor ANOVA with a Bonferroni post-hoc correction (*, $P < 0.05$; **, $P < 0.01$; ***, $P < 0.001$, and ****, $P < 0.0001$).

However, no statistical differences were observed between 1 h and 3 h indicating that the attached biofilm at 3 h was comparable to 1 h biofilm population ($P = 0.4683$). The biofilm attachment increased from 6 h to 24 h timepoint but no statistically significant differences were observed ($P = 0.2475$).

5.3.2 Microscopy analysis of biofilm formation of *P. aeruginosa* PAO1 wildtype on urinary catheter using AUBK medium in 1 h, 3 h, 6 h, and 24 h.

To assess the differences in biofilm morphology, EDIC/EF microscopy were used to visualize the catheter surface microenvironment during the biofilm colonization stages by *P. aeruginosa* PAO1 wildtype. The biofilm morphologies of *P. aeruginosa* PAO1 wildtype over the time series are as shown in Appendix G.1 (Appendices). The PAO1 wildtype produced sparsely scattered surface microcolonies that consist of closely packed bacterial cells suggesting there were no challenges in establishing attachment on the silicone urinary catheter at the 1 h timepoint (Figure 5-4).

The EDIC image at 1 h showed the early structures of the wildtype biofilm, while the DAPI image at 1 h showed the stained bacterial assembly in the biofilm. Radial structures protruding from the bacterial aggregates were observed indicating the cell flagella tail of *P. aeruginosa*, and that the bacteria came together by twitching motility to form the cell clusters. Respectively, the ConA stained image displayed appearance of the D-mannose component of the EPS surrounding the cell aggregates as well as on the surface. The ConA intensity was more concentrated within the aggregates and on the background surface catheter than the area surrounding the aggregates. This suggests that the extracellular secretion produced by the wildtype conditions the catheter surfaces as well as covers the cell aggregates. Overall observations showed that there were relatively more areas of the catheter that were not covered by biofilm compared to areas of bacterial colonisation.

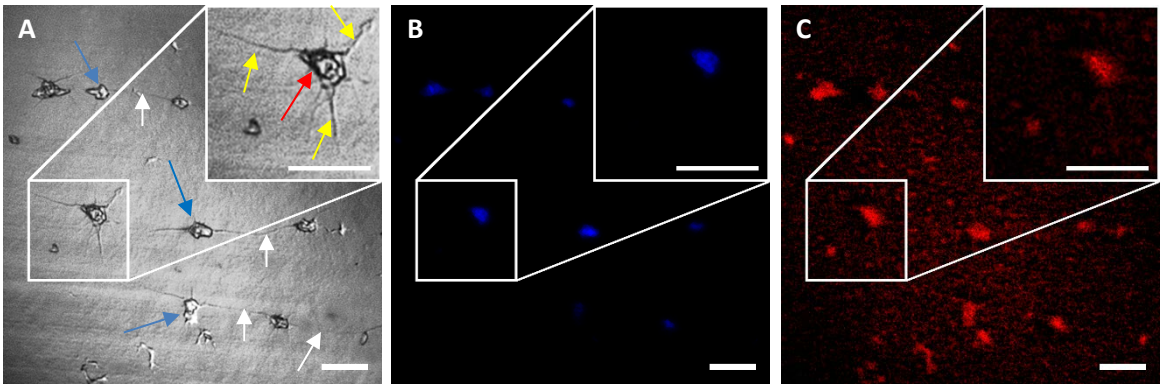

Figure 5-4 The images of representative *P. aeruginosa* PAO1 wildtype biofilm in AUBK at 1 h incubation showing attached bacteria forming assembly of cells on the urinary catheter surface as observed under EDIC/EF microscope.
Insets are the higher magnification (x 1.75) images of the region of interest.

A. EDIC image showing visible scattered assembly of attached bacteria on the catheter surface; blue arrows is showing bacterial aggregation by twitching motility and forming cell clusters; yellow arrows denotes cell flagella and red arrow denotes the vertical stratification indicates occurrence of proliferation creating multilayer aggregates; white arrows shows filamentous structure connecting between the small cell aggregates. B. Image shows the DAPI-stained cells in the biofilm. C. Image shows the ConA-stained background layer formed on the catheter surface. Magnification × 1000, scale bars = 10 µm.

More prominent bacterial aggregates were observed among smaller bacterial aggregates and widely distributed across the catheter surface after 3 h. There were more attached bacterial cells than in 1 h due to the well-conditioned surface. The size difference indicates that the smaller bacterial aggregates are the newly established attached bacteria on the catheter surface and the bigger bacterial aggregates are the formed from the expansion of it as well as by the merging of smaller bacterial aggregates due to twitching motility. The silhouettes of the bacterial cells in the biofilm were identifiable under x 1000 magnification with EDIC microscopy. The microcolonies observed consisted of multi-layered cell aggregates with radial structures made of thin filaments that connects between them, which differed from that observed in 1 h biofilm (Figure 5-4).

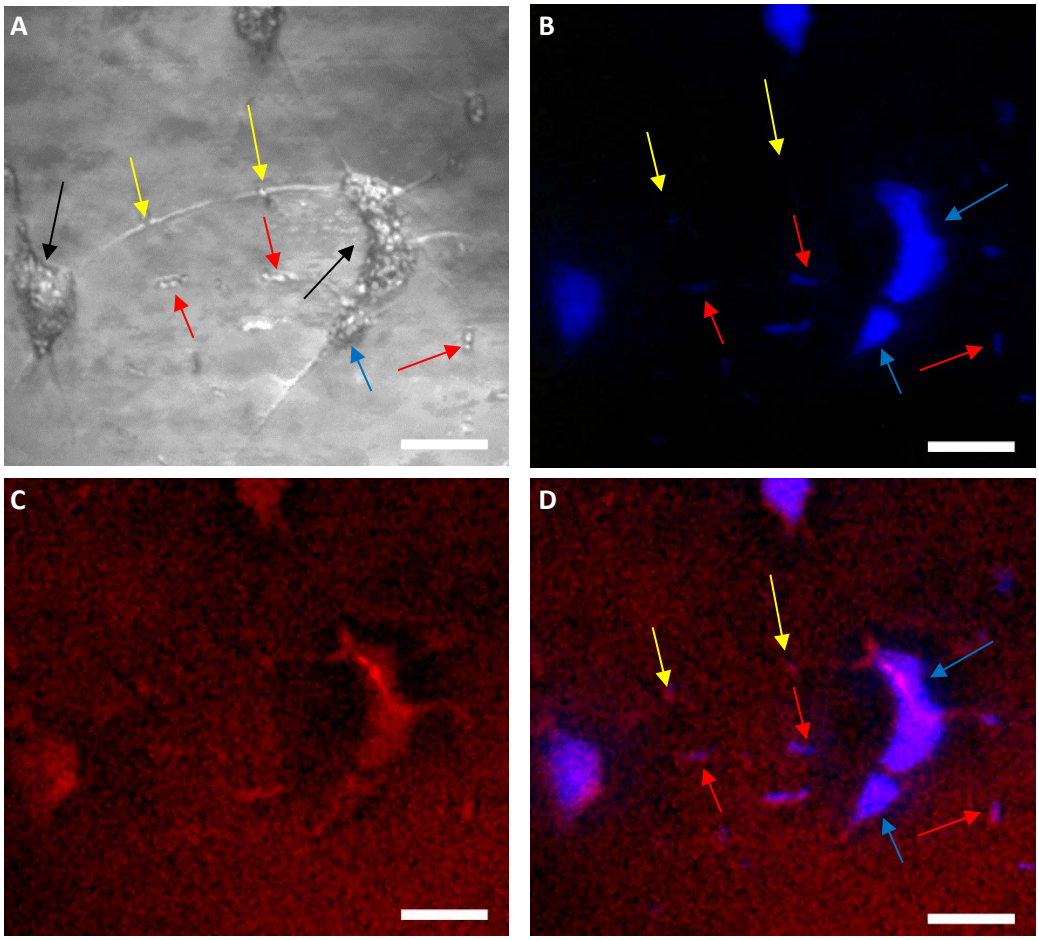

Figure 5-5 *P. aeruginosa* PAO1 wildtype biofilm in AUBK at 3 h incubation showing bigger assembly of cells on the urinary catheter surface than 1 h, as observed under EDIC/EF microscope.

A. EDIC image is showing early structure of bacteria microcolonies on the catheter surface. B. Image shows the DAPI-stained cells in the biofilm. C. Image shows the ConA-stained background layer formed on the catheter surface. D. Composite image of B and C to show the EPS glycolipid surrounds the microcolonies as well as the catheter surface. For all images, red arrows are showing cells dividing, blue arrows are two neighbours of microcolonies that have expanded and can be seen merging, black arrows are bulging cell aggregates and yellow arrow shows single bacterial cells attached on the surface and travelling via the flagella/filament-like tracks. Magnifications × 1000, scale bars = 10 µm.

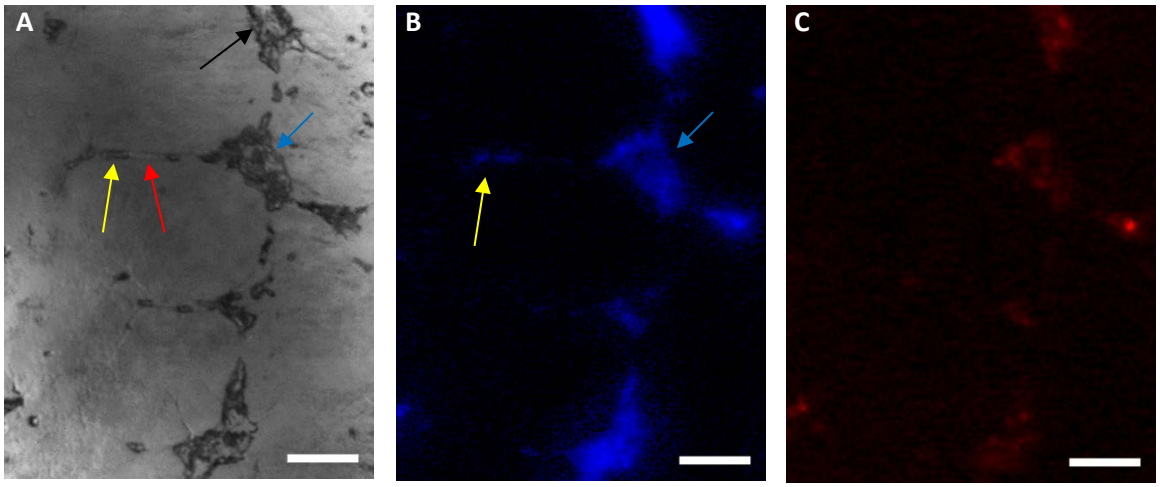

Figure 5-6 *P. aeruginosa* PAO1 wildtype biofilm in AUBK at 6 h showing further differentiation of microcolonies into macrocolonies on the urinary catheter surface as observed under EDIC/EF microscope.

A. EDIC image showing microcolonies of bacteria on the catheter surface which shows a microcolony that has established on the surface (black arrow) in a form of a raised platform. Blue arrow is showing microcolony still under development, as *P. aeruginosa* cells (yellow arrow) are seen twitching following the filament (red arrow) tracks that has been observed previously in earlier hours. B. Image shows the DAPI-stained cells in the biofilm with yellow arrow denotes the twitching cell heading to the nearest microcolony. C. Image shows the ConA-stained background layer formed on the catheter surface. Magnifications × 1000, scale bars = 10 µm.

The biofilm morphology at 6 h timepoint (Figure 5-6) is noticeably different from in the 3 h timepoint (Figure 5-5). There are smaller to medium-sized bacterial aggregates among a network of microcolonies. The biofilm also seems a bit thicker than 3 h timepoint due to closely packed cells in the biofilm. The microcolonies can be seen closer to each other and merging compared to 3 h, which display microcolonies situated individually and distanced apart. Once a microcolony (Figure 5-6A, black arrow) has established, less inbound twitching cells were observed compared to the underdeveloped microcolony (Figure 5-6A, blue arrow) that has cells twitching together to form microcolony. Overall, there are more attached bacteria observed on the catheter surface at 6 h compared to 3 h biofilm that corresponds with the enumeration data.

At the 24 h timepoint (Figure 5-7), clear biofilm differentiation can be seen compared to earlier timepoints. Spatial biofilm coverage increases due to microcolonies expansion forming macrocolonies and three-dimensional structure. The structure of the mature macrocolonies observed were three-dimensional and stratified with amorphous precipitation embedded, giving it an exterior feature similar to “craggy mountain” formation.

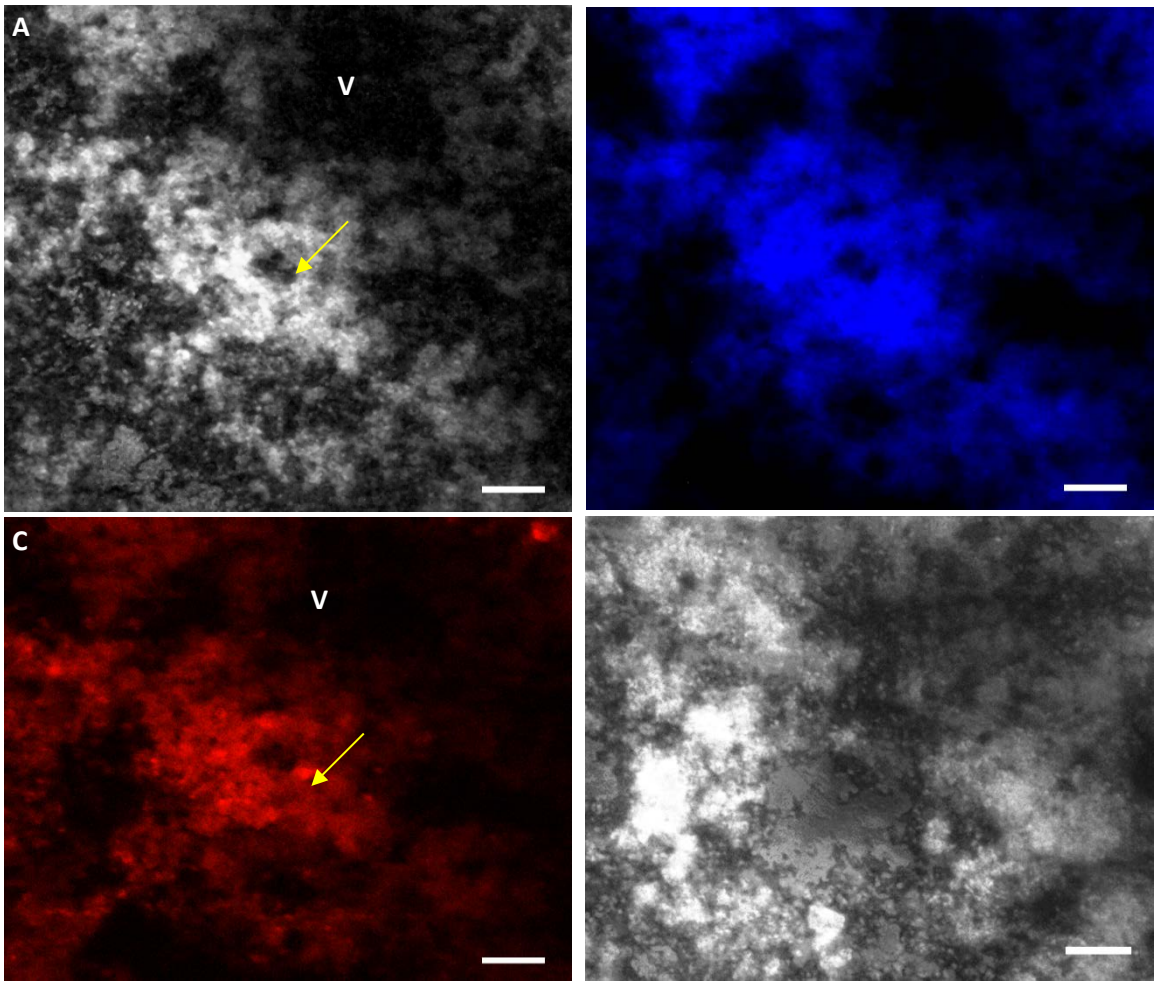

Figure 5-7 *P. aeruginosa* PAO1 wildtype biofilm in AUBK at 24 h showing mature biofilm with evidence of dispersal events via seeding has happened with central hollowing in the biofilm on the urinary catheter surface as observed under EDIC/EF microscope.

A. EDIC image showing mature biofilm formation on the catheter surface with precipitous morphology and obvious vertical stratification development compared to earlier timepoints. B. Image shows the DAPI-stained cells in the biofilm as in image A. C. Image shows the ConA-stained background layer formed on the catheter surface as in image A. D. An EDIC image of the 24 h mature biofilm formation at different location than image A showing more evidence of seeding dispersal events has happened. For all images, yellow arrow denotes the central hollowing observed, indication seeding dispersal event has happened. V = referring to the void areas of catheter surface that are not occluded by the biofilm. Magnifications × 1000, scale bars = 10 µm.

Void spaces were observed forming water channels between macrocolonies, which partially occluded the catheter surface. Dispersion phase of biofilm in the wildtype strain commenced by the 24 h timepoint shown by EDIC images of the biofilm missing peak and crater formation on top of the mature biofilm (Figure 5-7A). Biomineralisation is suspected as uptake of fluorescent dye DAPI and ConA by the crystallisation in the biofilm can be seen in Figure 5-7B and Figure 5-7C, which helps in emphasising the visualisation of the mature biofilm formation at the 24 h timepoint.

5.3.3 Biofilm growth of *P. aeruginosa* PAO1 urease-negative mutants

One-way analysis of variance (ANOVA) was conducted to compare the growth of urease mutant strains with the wildtype. The statistical results obtained are reported in Table 5-2 below. It showed that the mean $\log_{10}$ cfu/catheter section differed significantly between the strains with wildtype only in the 3 h timepoint ($P = 0.0003$) and not significant differences found in other timepoints ($P > 0.05$).

Table 5-2 One-way ANOVA analysis of *P. aeruginosa* PAO1 wildtype and urease-negative mutant biofilm

	One-way ANOVA ($P < 0.05$)					
Time	**ANOVA table**	**SS**	**DF**	**MS**	**F(DFn_3, DFd_{11})**	***P* summary**
1 h	Treatment (between columns)	0.01981	3	0.006602	0.3212	*P* = 0.8101
	Residual (within columns)	0.1644	11	0.02055		ns
	Total	0.1842	14			
3 h	Treatment (between columns)	0.5622	3	0.1874	22.44	*P* = 0.0003
	Residual (within columns)	0.06682	11	0.008352		***
	Total	0.629	14			
6 h	Treatment (between columns)	0.4585	3	0.1528	2.927	*P* = 0.0998
	Residual (within columns)	0.4177	11	0.05221		ns
	Total	0.8762	14			
6 h	Treatment (between columns)	0.1932	3	0.06439	3.039	*P* = 0.0927
	Residual (within columns)	0.1695	11	0.02118		ns
	Total	0.3626	14			

For all significant results shown, $P < 0.05$ (*, $P < 0.05$; **, $P < 0.01$; ***, $P < 0.001$, ****, $P < 0.0001$, and ns, not significant).

Table 5-3 Dunnett's post-hoc multiple comparison test of *P. aeruginosa* PAO1 wildtype and urease-negative mutant biofilm

Strains		**1 h**	**3 h**	**6 h**	**24 h**
WT	**Log_{10} cfu/catheter section**	6.16 ± 0.17	6.38 ± 0.04	7.09 ± 0.27	7.36 ± 0.08
	(%)	(57.82 ± 1.94)	(60.18 ± 0.48)	(68.17 ± 2.97)	(71.15 ± 0.88)
PW9188 -*ureC*	**Log_{10} cfu/catheter section**	6.14± 0.08	6.91 ± 0.10	7.36 ± 0.33	7.04 ± 0.19
	(%)	(57.97 ± 0.94)	(66.68 ± 1.11)	(71.71 ± 3.77)	(68.10 ± 2.19)
	Adjusted *P* value	0.9917 (*ns*)	0.0003 (***)	0.3964 (*ns*)	0.0666 (*ns*)
PW9189 -*ureC*	**Log_{10} cfu/catheter section**	6.14 ± 0.08	6.88 ± 0.09	7.59± 0.09	7.34 ± 0.16
	(%)	(56.96 ± 0.86)	(65.16 ± 0.95)	(72.92 ± 0.94)	(70.21 ± 1.75)
	Adjusted *P* value	0.9941 (*ns*)	0.0004 (***)	0.0708(*ns*)	0.9974 (*ns*)
PW9231 - *ureE*	**Log_{10} cfu/catheter section**	6.06 ± 0.20	6.81 ± 0.12	7.54 ± 0.14	7.24 ± 0.13
	(%)	(57.95 ± 2.28)	(66.59 ± 1.38)	(74.99 ± 1.61)	(71.48 ± 1.46)
	Adjusted *P* value	0.6960 (*ns*)	0.0010 (**)	0.0955 (*ns*)	0.6523 (*ns*)

For all significant results shown, $P < 0.05$ (*, $P < 0.05$; **, $P < 0.01$; ***, $P < 0.001$, ****, $P < 0.0001$, and ns, not significant). Data is expressed as mean ± SD (SD = standard deviation)

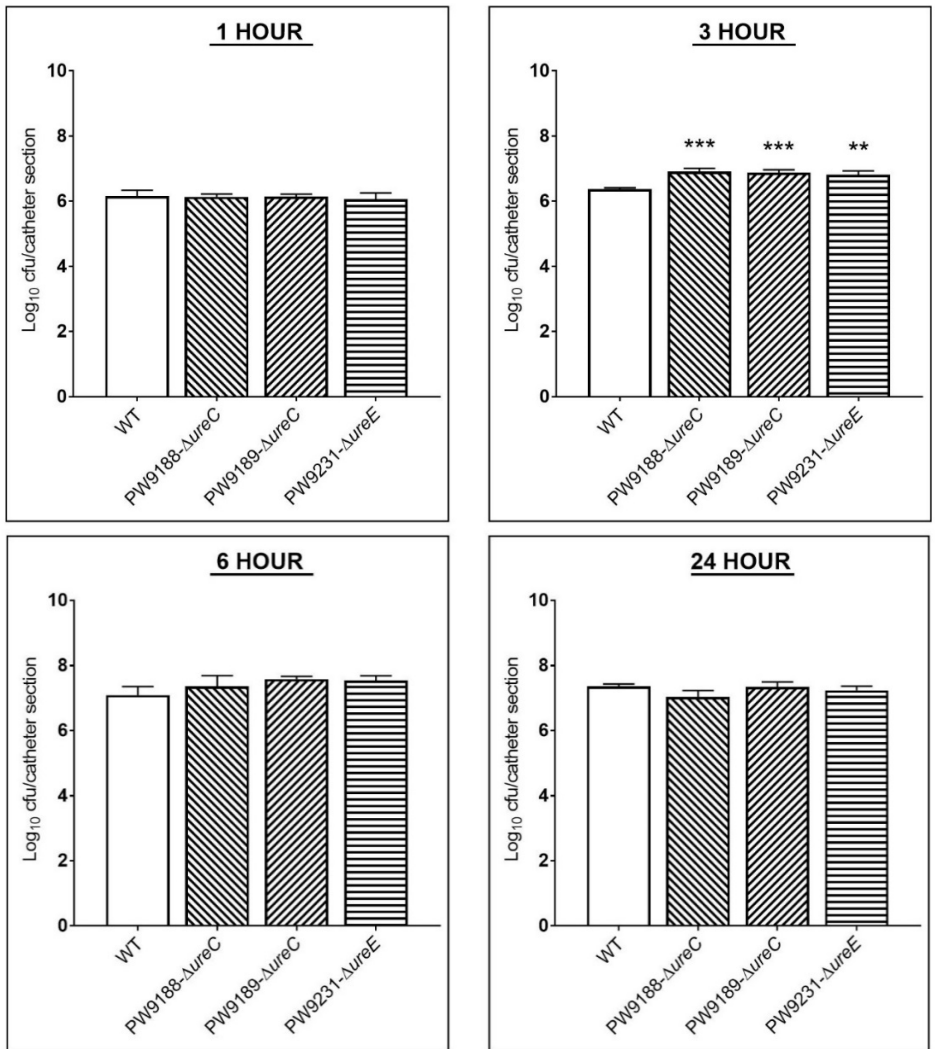

Figure 5-8 Enumeration data (log_{10} cfu/catheter section) of biofilm-derived *P. aeruginosa* PAO1 wildtype and urease mutants at 1 h, 3 h, 6 h and 24 h. Error bars indicates the standard deviation (SD). All of the strains were compared to WT using one-way ANOVA followed by Dunnett's multiple-comparison test (*, $P < 0.05$; **, $P < 0.01$; ***, $P < 0.001$, ****, $P < 0.0001$, and *ns*, not significant).

The mean value of log_{10} cfu/catheter section and Dunnett's multiple comparisons post-hoc test result summary of all urease strain for each timepoints are shown in Table 5-3 and illustrated in graph shown in Figure 5-8. UreC mutant PW9188 biofilm has shown no statistically significant difference in the first hour of incubation (6.14 ± 0.08 log_{10} cfu/catheter section, $P = 0.9917$) compared to wildtype. Only at 3 h that the strain showed significant increased compared to wildtype (6.91 ± 0.10 log_{10} cfu/catheter section, $P = 0.0003$). Contrastingly, subsequent timepoints 6 h and 24 h showed no significant differences compared to wildtype (7.36 ± 0.33 log_{10} cfu/ catheter section, $P = 0.3964$ and 7.04 ± 0.19 log_{10} cfu/ catheter section, $P = 0.0666$, respectively).

Another *ureC* gene mutant PW9189 biofilm has also shown a statistically significant increase only in the 3 h timepoint (6.88 ± 0.09 log_{10} cfu/catheter section, $P = 0.0021$). However, the strain did not show any statistically significant difference of biofilm growth at 1 h, 6 h and 24 h timepoints compared to wildtype (6.14 ± 0.08 log_{10} cfu/catheter section, $P = 0.9941$, 7.59 ± 0.09 log_{10}

cfu/catheter section, $P = 0.0708$ and 7.34 ± 0.16 $\log_{10}$ cfu/catheter section, $P = 0.9974$, respectively). Likewise, the *ureE* gene mutant PW9231 also showed only significant increase in the 3 h timepoint (6.81 ± 0.12 $\log_{10}$ cfu/catheter section, $P = 0.0010$), and no significant difference of biofilm growth at 1 h, 6 h and 24 h timepoints compared to wildtype (6.06 ± 0.20 $\log_{10}$ cfu/catheter section, $P = 0.6960$, 7.54 ± 0.14 $\log_{10}$ cfu/catheter section, p=0.0955 and 7.24 ± 0.13 $\log_{10}$ cfu/catheter section, $P = 0.6523$, respectively).

5.3.3.1 Changes in pH of AUM by *P. aeruginosa* PAO1 wildtype and urease-negative mutants

The Figure 5-9 shows the steadily increasing pH of AUBK by PAO1 wildtype with a final pH value of 8.64 ± 0.05 at 24 h timepoint. To assess differences of pH values between wildtype and the urease mutants, one-way analysis of variance (ANOVA) were conducted and reported in Table 5-4 below. Based on the results, the mean pH values differed significantly between the strains with wildtype in the first and 24 h timepoint ($P = 0.0108$ and $P = 0.0174$, respectively). However, no significant differences were found in the 3 and 6 h timepoints ($P = 0.9984$ and $P = 0.2756$, respectively).

Table 5-4 One-way ANOVA analysis of *P. aeruginosa* PAO1 wildtype and urease-negative mutant pH values

	One-way ANOVA ($P < 0.05$)					
Time	**ANOVA table**	**SS**	**DF**	**MS**	**F(DFn_3, DFd_{11})**	***P* summary**
1 h	Treatment (between columns)	0.0828	3	0.0276	6.0690	$P = 0.0108$
	Residual (within columns)	0.0500	11	0.0045		*
	Total	0.1328	14			
3 h	Treatment (between columns)	0.0002	3	0.0001	0.0107	$P = 0.9984$
	Residual (within columns)	0.0779	11	0.0071		*ns*
	Total	0.0781	14			
6 h	Treatment (between columns)	0.1120	3	0.0373	1.4730	$P = 0.2756$
	Residual (within columns)	0.2788	11	0.0254		*ns*
	Total	0.3908	14			
6 h	Treatment (between columns)	0.0182	3	0.0061	5.2290	$P = 0.0174$
	Residual (within columns)	0.0127	11	0.0012		*
	Total	0.0309	14			

For all significant results shown, $P < 0.05$ (*, $P < 0.05$; **, $P < 0.01$; ***, $P < 0.001$, ****, $P < 0.0001$, and ns, not significant).

Table 5-5 Dunnett's post-hoc multiple comparison test of *P. aeruginosa* PAO1 wildtype and urease-negative mutant pH values

Strain		1 h	3 h	6 h	24 h
WT	**pH**	7.49 ± 0.04	7.72 ± 0.11	8.05 ± 0.16	8.64 ± 0.05
PW9188 ureC	**pH**	7.37± 0.14	7.73 ± 0.03	7.82 ± 0.24	8.58 ± 0.02
	Adjusted *P* value	0.0668 (*ns*)	0.9971 (*ns*)	0.1578 (*ns*)	0.0783 (*ns*)
PW9189 ureC	**pH**	7.31 ± 0.05	7.72 ± 0.05	7.94 ± 0.11	8.58 ± 0.03
	Adjusted *P* value	0.0076 (**)	>0.9999 (*ns*)	0.6638 (*ns*)	0.0990 (*ns*)
PW9231-ureE	**pH**	7.36 ± 0.02	7.72 ± 0.05	7.98 ± 0.07	8.55 ± 0.01
	Adjusted *P* value	0.0525 (*ns*)	0.9991 (*ns*)	0.8563 (*ns*)	0.0115 (*)

For all significant results shown, $P < 0.05$ (*, $P < 0.05$; **, $P < 0.01$; ***, $P < 0.001$, ****, $P < 0.0001$, and ns, not significant). Data is expressed as mean ± SD (SD = standard deviation)

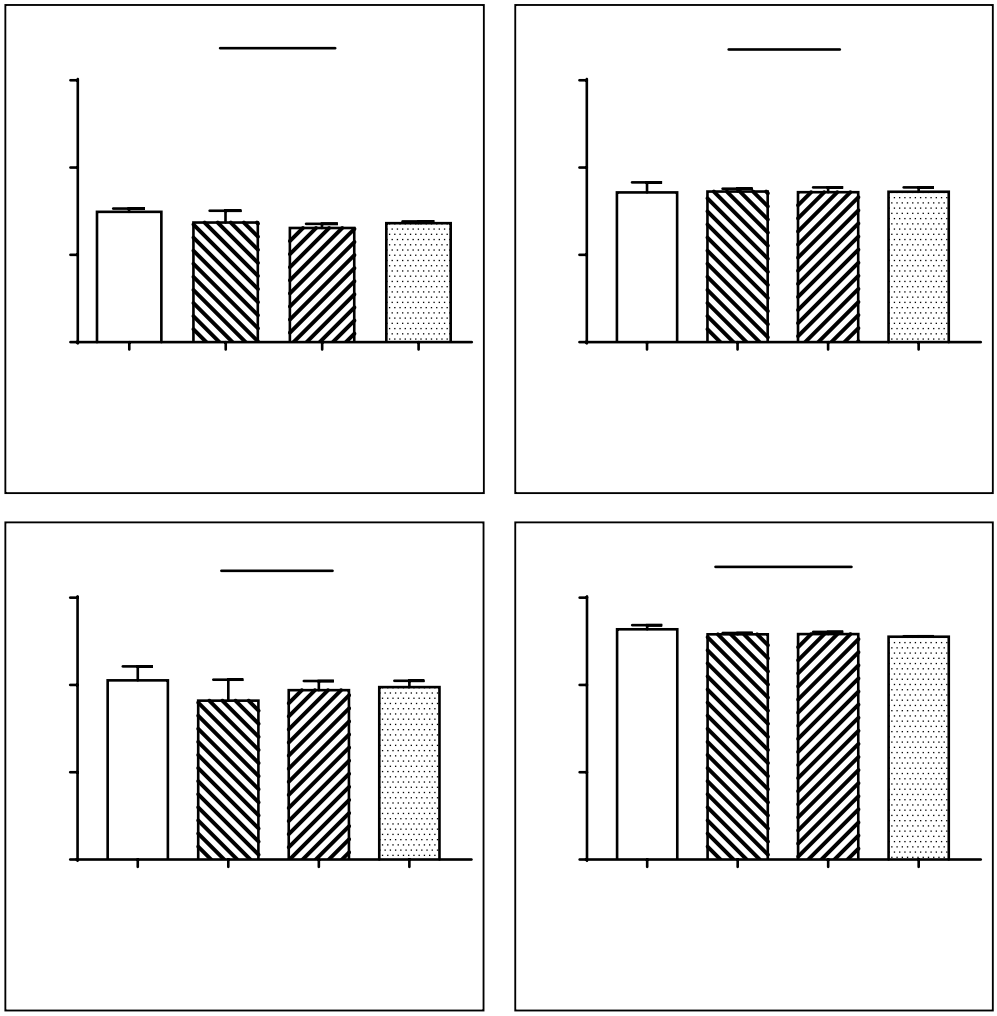

Figure 5-9 pH changes in AUBK by *P. aeruginosa* PAO1 wildtype and urease mutants at 1 h, 3 h, 6 h and 24 h.

Error bars indicates the standard deviation (SD). All of the strains were compared to WT using one-way ANOVA followed by Dunnett's multiple-comparison test (*, $P < 0.05$; **, $P < 0.01$; ***, $P < 0.001$, ****, $P < 0.0001$, and *ns*, not significant).

5.3.4 Microscopy analysis of *P. aeruginosa* PAO1 urease-negative biofilm formation on urinary catheter grown in AUBK medium at 1 h, 3 h, 6 h, and 24 h.

The EDIC microscopy images of the biofilm produced by wildtype and the urease-negative mutants are shown in Figure 5-10. The urease mutants biofilm development showed slight structural differences compared to the wildtype. There was less biofilm build-up in the early hours of incubation, and for ureE, there was less biofilm observed compared to wildtype and ureC mutants. ConA differential stain was used to stain the D-mannose component of the EPS, and there were no structural differences observed compared to the EDIC image (data not shown).

5.4 Discussion

5.4.1 Urease-negative mutants biofilm growth on urinary catheter

This study of using urease mutants aimed to investigate the function of urease genes in *P. aeruginosa* as a uropathogen and their role in urinary biofilm formation. Despite the distinct physicochemical properties and the high level of urea as its main component, urine media has shown to support development of biofilms and provide a suitable environment for growth. *P. aeruginosa* PAO1 wildtype showed a high number of attached biofilm from the first hour of incubation (6.16 ± 0.17 $\log_{10}$ cfu/catheter section) indicating that the strain has no problem in attaching on the catheter. Similarly, urease-negative mutants also showed comparatively high attachment at approximately 6 $\log_{10}$ cfu/catheter section biofilm in the first hour as well.

This agrees with the study by Cole *et al.* (2014) that showed the presence of urea in urine stimulates the biofilm growth in *pel*-negative, psl-negative and *alg*-negative *P. aeruginosa* PA14 mutants. Our biofilm enumeration data were also comparable to the study by Armbruster *et al.* (2017) which demonstrated that urease in *P. stuartii* does not have importance in pathogenicity during *in vivo* coinfection with *P. mirabilis*. Cole *et al.* (2014) studied the effect of DNase I on biofilm grown in urea has negative effect and deduced that the biofilm structure was supported by the released eDNA in the EPS. The study also concluded that biofilm formation in urea was dependant of EPS and alginate production (Cole *et al.* 2014).

Similarly, it is agreed that urease has no critical role in *P. aeruginosa* PAO1 biofilm formation and that there are factors other than urea that induces biofilm growth in urine media. One possible reason that the biofilm formation of the urease-deficient mutants are not affected may be due to the presence of alternative metabolic pathways such as the arginine deiminase (ADI) pathway that does not necessary requires arginine and in certain circumstances are more favoured than urease in pH homeostasis (Mercenier *et al.* 1980; Musken *et al.* 2010).

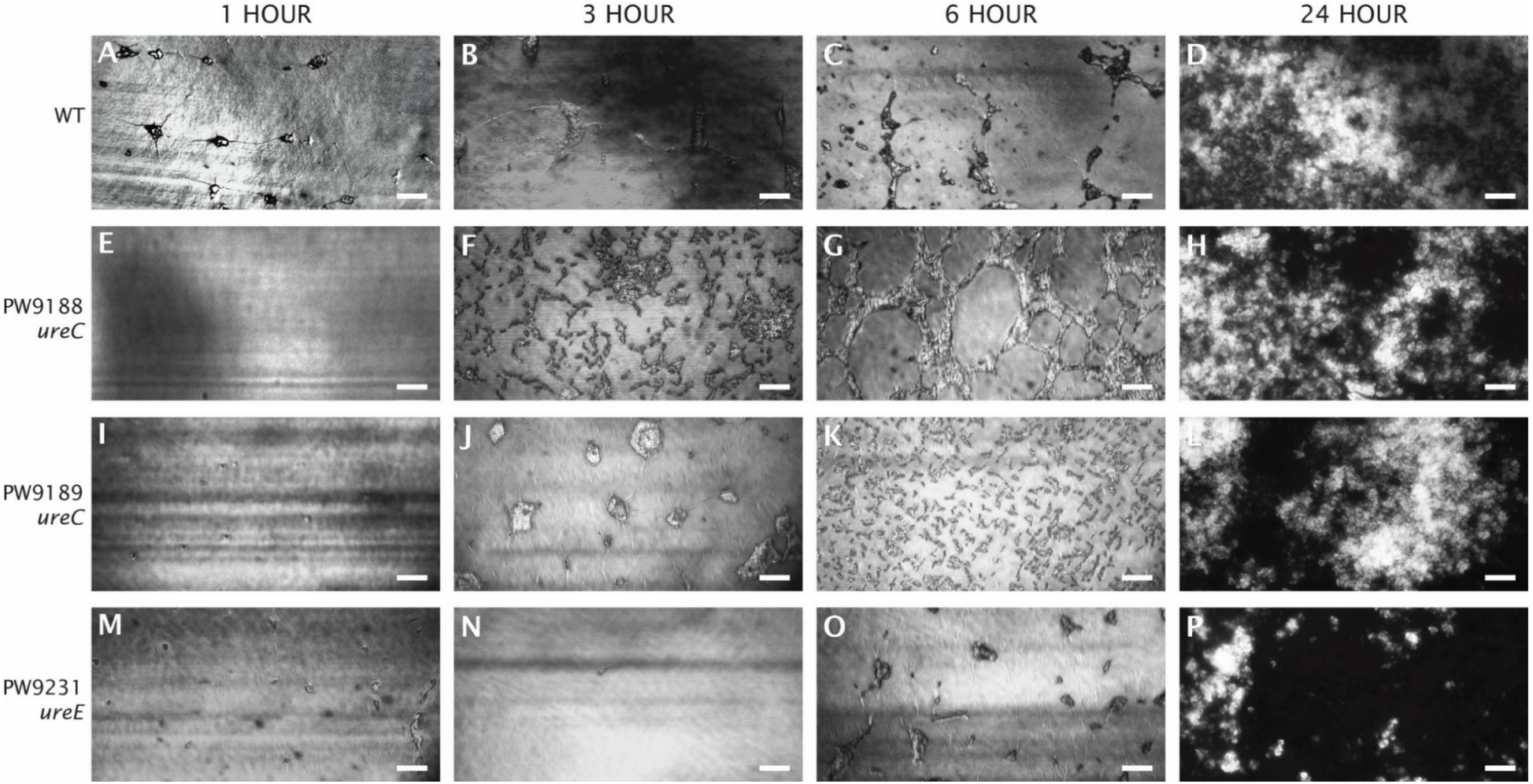

Figure 5-10 EDIC images of *P. aeruginosa* PAO1 wildtype (A-D) and urease mutant biofilm formation on catheters grown in artificial urine media (AUBK) at 1 h, 3 h, 6 h and 24 h incubation (PW9188-*ureC* E-H, PW9189-*ureC* I-L, PW9231-*ureE* M-P). Magnifications × 1000, scale bars = 10 µm

It is possible that even though the biofilm assay was cultured in a normal atmosphere, there are areas in the deep layers within the mature biofilm structure that were deprived of oxygen that would have made the ADI pathway as the alternative route to ammonia production (Sauer *et al.* 2002; Waite *et al.* 2006).

5.4.2 Measurement of pH changes in AUBK

The PAO1 wildtype showed increasing pH changes in AUM in 24 h. The final pH of 8.64 in 24 h is well above the normal urine pH (≈ pH 6.1 - 6.8)(Brooks and Keevil 1997; Aubron *et al.* 2012; Worcester *et al.* 2018), although *P. mirabilis* can achieve even higher pH (pH 9.1 – 9.4) during that time as shown in previous Chapter 4. The increase in pH values over time indicates that urease is not the main contributor in the rise of pH in AUBK. The increased pH is probably due to the production of ammonia that alkalises the urea in the urine media. Similarly, the urease-negative mutants showed increasing pH over time as well, however the pH changes showed little significant differences when compared to the wildtype. This also supports the agreement that urease genes were not important in the alkalisation of the urine media and the bacteria might utilize an alternative metabolism pathway to produce ammonia. The urease mutants must have undergone microbial deamination (McLean *et al.* 1988; Xu *et al.* 2013; Vega *et al.* 2014) that produces substantial amount of ammonia, which affects the pH of the urine media independently of the urea. Although pH measurement alone cannot determine urea hydrolysis over time, the elevated pH shown in the results would normally infer hydrolysis has occurred.

Urine pH is important in treating patients with history of UTI as combined with various factors such as urea, uric acid or creatinine concentration, they are more susceptible to encrustation that leads to blockage of urinary catheter (Stickler *et al.* 1998). The urine pH also useful to determine the pH nucleation that affects the level of precipitation which causes the urolithiasis and encrustation formation on urinary catheter (Wilde and Brasch 2008). Increasing pH in the urine will reduce the solubility of uric acid to form uric acid calculi, or together with ammonium, leads to formation of ammonium acid urate (AAU) urolithiasis in the urine (Chou *et al.* 2012; Abou-Elela 2017).

Uric acid concentration in the AUBK is just below the concentration level of patients with AAU stones (Chou *et al.* 2012) which suggests that there could be a possibility that the uric acid became insoluble as the AUBK pH increases above 7. The pH could reach a plateau at the uric acid dissociation curve (approximately pH 7.2) (Abou-Elela 2017), but the increased pH produced by the PAO1 strains were over this limit strongly supports the existence of other metabolic mechanisms which contributes to the alkalinisation of the urine.

5.4.3 Microscopy analysis of biofilm

Overall observation using the EDIC microscopy images showed that the PAO1 wildtype and urease negative strains were successful in establishing biofilm formation within 24 h as seen in (D, H, L and P). The characteristics presented by P. aeruginosa PAO1 biofilm in this study exhibited distinct phenotype at each biofilm formation stage that conforms to the previously reported biofilm lifecycle stages in past studies, which are the initial attachment, cell aggregation, microcolony formation and early mature biofilm stage with evidence of dispersal event observed (Sauer *et al.* 2002; De Kievit 2009; de Melo *et al.* 2013). The onsets for each biofilm formation stage observed in this study supports previous claims by Sauer *et al.* (2002) from initial attachment to maturation, except for dispersion which the report claimed to begin after 9 days of growth.

All four strains of *P. aeruginosa* PAO1 biofilms were distinctly different compared to *P. mirabilis* (Wilks *et al.* 2015). Wilks *et al.* (2015) reported that the early biofilm formation by *P. mirabilis* was initiated by primary coloniser cells from the observed areas that were not stained by ConA were occupied by the DAPI-stained cells, however our study showed that *P. aeruginosa* produces D-mannose component in the EPS that surrounds the cells and accumulates under and around the microcolony during biofilm formation. Additionally, Wilks *et al.* (2015) also showed that the 24 h mature *P. mirabilis* biofilm were three dimensional and highly reflective, which our study on *P. aeruginosa* also produces three dimensional biofilm but with observed less crystallisation. This could evidently be caused by the low production of urease by *P. aeruginosa* PAO1 strains (Stickler 2014; Cortese *et al.* 2018) as the strains were unaffected by the urea in the AUBK. The ammonia that could be produced from urea hydrolysis was not sufficient in raising the pH to induce apatite and struvite formation (Broomfield *et al.* 2009)

While the wildtype showed cell attachment and consistent characteristics of cell aggregation, the urease-negative mutants showed fewer visible attached cells than wildtype and some timepoints showed the absence of characteristic twitching cells. All urease mutants showed less biofilm in the 1 h panel (E, I, and M). The *ureE*-negative mutant showed slightly less attached biofilm in all the timepoints compared to wildtype (A - D) and *ureC* mutants (M - P). This could mean that the impaired urease genes affect the twitching capability of the cells at certain points. There was abundant presence of ConA stained D-mannose component in the EPS of all the biofilm, showing that these apparent structural changes were not due to the EPS.

From the biofilm morphology produced by the urease-negative mutants, the apparent differences were observed most in the *ureE*-negative mutant, although a lack of twitching movement was also observed in *ureC*-negative mutants. Our observation on the *ureE*-negative mutant suggests that the *ureE*-deficiency might have affected the nickel-requiring urease metalloenzymes

mechanism in the *P. aeruginosa* PAO1 due to the significantly producing attenuation of biofilm structure forming on the catheter. This coincides with the previous study that showed *ureE*-negative mutants affect nearly fifty per cent (50%), as compared to ten per cent (10%) by other mutations in the accessory urease gene *ureD*, *ureF* or *ureG* in the nickel-contents of the wildtype urease (Collins and D'Orazio 1993).

5.5 Conclusion

Since the most critical urinary pathogen *P. mirabilis* relies on urease activity as a virulence factor, the motivation for this study was to investigate if it is similarly true for *P. aeruginosa* PAO1. From the enumeration data and pH results obtained, no considerable distinction was noted when comparing the urease-negative mutants with wildtype. Therefore, it can be concluded that urease does not appear to be important in the biofilm formation of *P. aeruginosa*.

Future studies should be directed at characterising how other urea degradation or ammonia-producing genes are involved in the urinary biofilm formation, including the study of genes related to the ADI pathway in *P. aeruginosa* PAO1 such as *arcA*, *arcB,* and *arcC* (Sauer *et al.* 2002; Waite *et al.* 2006). A study involving *ureB* gene from the main urease enzyme would be interesting to see if it has any role in *P. aeruginosa* PAO1 as it has been previously shown to produce poor biofilm production compared to PA14 wildtype (Musken *et al.* 2010). It has also been previously described that *ureB* is essential for pH homeostasis in other species such as *Streptococcus salivarius* and *Staphylococcus aureus* that it was upregulated during biofilm formation (Musken *et al.* 2010).

The biofilm images of the urease-negative mutants showed a slightly obscure difference in twitching ability suggesting that future work should study the twitching and urease gene capability in the formation of biofilm in detail. This work has also shown that there was no difference in the D-mannose in the EPS constituents that ConA binds to, which suggests further studies should investigate the other constituents of the EPS and how they are involved in any structural changes.

Even though our study did not find the role of urease in *P. aeruginosa* biofilm formation, we hope that this study contributes to the importance of using transposon mutants to screen for potential novel target gene in biofilm formation. It is imperative to identify the essential genes that are able to prevent or disrupt the biofilm formation of *P. aeruginosa* for future development of therapeutic biofilm intervention and maim its pathogenicity that affects CAUTI patients. The next chapter will move towards our attention to the quorum-sensing and polysaccharide genes in the *P. aeruginosa* PAO1 biofilm formation on the urinary catheter.

Chapter 6 The Study of Quorum-Sensing-Negative and Polysaccharide-Negative *Pseudomonas aeruginosa* Mutants Biofilm Formation on Urinary Catheters

6.1 Introduction

In this chapter, we investigate two major factors in biofilm formation; quorum-sensing and polysaccharide production in *P. aeruginosa.* Quorum-sensing (QS) is a cell communication mechanism that is sensitive to and responds to the density of a bacterial population, which in biofilm, is profoundly dependable on the polysaccharide (PS) component in the EPS that forges the biofilm structure and integrity (Stoodley *et al.* 2002; Campisano *et al.* 2006; Yang *et al.* 2011; Wei and Ma 2013). Past research has reported the connection between the QS mechanism and signal diffusion affected by polysaccharide production and impaired structure, which is why these mutant groups are discussed together in this chapter (Sauer *et al.* 2002; Schaber *et al.* 2007; Flemming *et al.* 2016; Mund *et al.* 2017).

Our hyphothesis is that gene regulation in quorum-sensing and polysaccharide production are vital for biofilm development. Since the polysaccharide produced controls the EPS composition, which binds and stabilises the bacterial aggregation in biofilm, it would then affect the density-dependent quorum-sensing signalling.

In general, bacteria release chemical signal molecules called autoinducers (AIs) which in low-density population, diffuse, and in a high-density population, these molecules accumulate and become concentrated. The concentration of the AIs available in the environment provides feedback to the bacteria receptors informing on the density of the population, which then triggers the bacterial gene expression to adjust accordingly to environmental factors. Biofilm research targets the quorum-sensing cell signalling properties to interfere and disrupt the communication within the biofilm communities. Approximately ten per cent (10 %) of the *P. aeruginosa* genome consists of QS-related genes mechanism (Miller and Bassler 2001; Kim *et al.* 2015; Abisado *et al.* 2018).

There are three primary QS systems found in *P. aeruginosa* that form a hierarchical regulation control of the biofilm formation, namely the Las system (*lasI*), the Rhl system together with its virulence factor, rhamnolipids (*rhlI*, *rhlA*, and *rhlB*) and the PQS system (*pqsA* and *pqsE*).

Both LasI and RhlI use N-acyl-homoserine lactone (AHL) as their signal molecules, while the PQS system utilises the 2-heptyl-3-hydroxyl-4-quinolone-based (PQS) signalling system that interacts with the AHL (Kim *et al.* 2005; Tielen *et al.* 2013; Mund *et al.* 2017; Abisado *et al.* 2018).

There are three important polysaccharides in biofilm formation used in this study, namely the Pel polysaccharide (*pelA*), Psl polysaccharide (*pslD, pslG*), and alginate (*algD* and hyper alginate *mucA*)(Stapper *et al.* 2004; Ghafoor *et al.* 2011; Wei and Ma 2013; Cole *et al.* 2014; Baker *et al.* 2016; Irie *et al.* 2017). Limited knowledge is available on the role of polysaccharide alginate production in urinary biofilms but it has shown that it has a very significant role in biofilm structure (Stapper *et al.* 2004; Franklin *et al.* 2011; Cole *et al.* 2014; Jones and Wozniak 2017).

The hypothesis for this study is that both QS and PS gene groups are needed during the same vital events in biofilm development, such as bacterial aggregation or microcolony formation and biofilm maturation stages. However, the individual contributions in crucial events of urinary biofilm formation of the selected genes for this study have not been elucidated. By screening *P. aeruginosa* strains with mutations in the quorum-sensing and polysaccharide genes, we aim to identify which of those critical genes are essential for growth or disrupt the biofilm formation process, as well as to determine their inter-dependence.

The biofilm growth of QS-negative and PS-negative PAO1 mutant strains were compared with the wildtype reference strain using artificial urine medium of Brooks and Keevil (1997) (AUBK). A simple and reproducible *in vitro* laboratory model system for biofilm assay by Wilks *et al.* (2015), described in Chapter 5 was used to conduct biofilm experiments on silicone catheter pieces. Physiological differences in the mutant biofilms were observed under EDIC microscopy. This study hoped to emphasise which genes could be essential in the mechanism for reducing biofilm growth and virulence.

6.2 Materials and methods

This study used the following methods for analysing biofilm formation formed by *P. aeruginosa* PAO1 QS-negative mutants and PS-negative mutants on a urinary catheter. Experimental plan of methods presented earlier in Figure 5-2 (Section 5.2) is used in this chapter.

6.2.1 *Pseudomonas aeruginosa* PAO1 strains used in this experiment

The details of the main *P. aeruginosa* PAO1 wildtype reference strain, QS-negative, and PS-negative mutant strains used in this study are as shown in Table 6-1 below. The sequence-verified *P. aeruginosa* PAO1 wildtype and the transposon mutants were obtained from the Seattle *P.*

aeruginosa mutant library (University of Washington Genome Sciences, USA) (Jacobs *et al.* 2003; Held *et al.* 2012).

Table 6-1 *P. aeruginosa* PAO1 strains used in this chapter

Reference strain			
Name	**Bacterial strains**	**Relevant putative ORF function/characteristic**	**PA ORF**
Wildtype	PAO1	*P. aeruginosa* strain ATCC 15692	MPAO1
QS-negative mutants			
Name	**Bacterial strains**	**Relevant putative ORF function/characteristic**	**PA ORF**
PW3601	*lasI*-F07::IS*lacZ*/hah	Autoinducer synthesis protein LasI mutant	PA1432
PW6886	*rhlA*-E08::IS*phoA*/hah	Rhamnosyltransferase chain A RhlA mutant	PA3479
PW6887	*rhlA*-A01::IS*phoA*/hah	Rhamnosyltransferase chain A RhlA mutant	PA3479
PW6884	*rhlB*-G07::IS*lacZ*/hah	Rhamnosyltransferase chain B RhlB mutant	PA3478
PW6885	*rhlB*-F05:: IS*phoA*/hah	Rhamnosyltransferase chain B RhlB mutant	PA3478
PW6880	*rhlI*-D03::IS*phoA*/hah	Autoinducer synthesis protein RhlI mutant	PA3476
PW6881	*rhlI*-F02::IS*phoA*/hah	Autoinducer synthesis protein RhlI mutant	PA3476
PW2798	*pqsA*-H05::IS*lacZ*/hah	Probable coenzyme A ligase PqsA mutant	PA0996
PW2799	*pqsA*-H04::IS*lacZ*/hah	Probable coenzyme A ligase PqsA mutant	PA0996
PW2806	*pqsE*-G04::IS*lacZ*/hah	Quinolone signal response protein PqsE mutant	PA1000
PW2807	*pqsE*-D03::IS*lacZ*/hah	Quinolone signal response protein PqsE mutant	PA1000
PS-negative mutants			
Name	**Bacterial strains**	**Relevant putative ORF function/characteristic**	**PA ORF**
PW6140	*pelA*-H06::IS*phoA*/hah	PelA mutant	PA3064
PW6141	*pelA*-F09::IS*phoA*/hah	PelA mutant	PA3064
PW4802	*pslD*-H08::IS*lacZ*/hah	PslD mutant	PA2234
PW4803	*pslD*-H09::IS*lacZ*/hah	PslD mutant	PA2234
PW4807	*pslG*-D07::IS*lacZ*/hah	Probable glycosyl hydrolase PslG mutant	PA2237
PW4808	*pslG*-G09::IS*lacZ*/hah	Probable glycosyl hydrolase PslG mutant	PA2237
PW2387	*mucA*-A05::IS*phoA*/hah	anti-sigma factor *mucA* region mutant	PA0763
PW6997	*algD*-C03::IS*phoA*/hah	GDP-mannose 6-dehydrogenase *algD* region mutant	PA3540
PW6998	*algD*-H06::IS*phoA*/hah	GDP-mannose 6-dehydrogenase *algD* region mutant	PA3540

The mutants carrying IS*lacZ*/hah or IS*phoA*/hah transposon insertions are made as previously described by Jacobs *et al.* (2003). Details of the reference *P. aeruginosa* PAO1 wildtype and the mutant strains were also elaborated further in Appendix F of the Appendices section, which was extracted from the accompanying table (PA two-allele library), provided in the *P. aeruginosa* Mutant Library website (https://www.gs.washington.edu/labs/manoil/libraryindex.htm).

6.2.2 Inocula preparation

The inocula preparation for *P. aeruginosa* PAO1 wildtype and mutant strains were prepared as described in Section 2.1.2. The bacterial inocula were harvested by centrifuging 1 ml of overnight culture at 7500 rpm (5400 × g) for 10 min. The supernatant was removed, and the pellet was resuspended using 1 ml artificial urine medium (Brooks and Keevil 1997) (AUBK). The AUBK medium was prepared as described in Section 2.3.1

6.2.3 Biofilm assay

Biofilm growth assay was conducted following as previously described in Wilks *et al.* (2015). Catheter sections are used with AUBK medium in the biofilm growth assay in 6-well plates. Further details of the experiment are as described in Section 2.4. Mono-strain biofilm assay of *P. aeruginosa* wildtype and gene mutants were cultured independently with at least three biological replicates.

Approximately 1 cm long silicone catheter (100 % silicone, Rüsch Teleflex, UK) pieces were cut longitudinally to produce two catheter sections and placed in each well in the 6-well plates (Nunc, Thermo Scientific, UK). Each well in the plate represented a separate timepoint of incubation 1 h, 3 h, 6 h, and 24 h with the additional well for the control. One plate was used for each strain in each replication experiment.

The catheter sections in the wells were immersed in 5 ml of AUBK medium, and 100 µl of inoculum from Section 6.2.2 (final concentration of approximately 1×10^9 cfu/ml) added into each well and then incubated at 37 ^{o}C. The biofilm was allowed to grow on for 1 h, 3 h, 6 h, and 24 h. At each timepoint, catheter sections from the corresponding well were removed and rinsed with PBS solution three times and dried on tissue paper via capillary action. For every two catheter sections removed at a timepoint, one was subjected to bacterial enumeration, and the other was observed under the EDIC/EF microscope for biofilm formation.

6.2.4 Bacterial enumeration from biofilm formed on the catheter

The catheter sections (from Section 6.2.3) were transferred into 10 ml of PBS solution in a sterile tube with approximately 2 g of 2 mm glass beads. The biofilm cells were harvested by vortexing the tube for 90 seconds. The biofilm culture was serially diluted accordingly in PBS. Aliquots of 50 µl of the dilutions were plated onto TSA media plates in triplicates for each selected dilution and incubated at 37 ^{o}C for 18 h to 20 h before the colonies were counted. The results of the enumeration data were analysed further using statistics.

6.2.5 Statistical data analysis

The enumeration data obtained by colony forming unit per catheter section (cfu/catheter section) were transformed into logarithmic colony forming unit per catheter section (log_{10} cfu/catheter section) representing biofilm attached on the catheter at each timepoint. All enumeration values are expressed as means ± SD. The data were evaluated for statistical differences using one-way analysis of variance (ANOVA) followed by Dunnett's multiple comparisons post-hoc test, performed using GraphPad Prism (version 7.05 for Windows, GraphPad Software, La Jolla California USA, www.graphpad.com). A probability value less of 0.05 ($P < 0.05$) was considered statistically significant. The results are reported below in Section 6.3.

6.2.6 Fluorescent differential staining of biofilm on urinary catheter

The catheter sections were prepared for fluorescent differential staining with DAPI and ConA subsequently after the biofilm assay (Section 6.2.3).

P. aeruginosa PAO1 biofilm was stained simultaneously with fluorescent probes to visualise different components of the biofilm using DAPI in blue for cell detection and tetramethylrhodamine (TRITC)-labelled Concanavalin A (ConA) in red to detect α-D-mannosyl and α-D-glucosyl residues (Leriche *et al.* 2000; Schwartz *et al.* 2003; Wilks *et al.* 2015). The biofilm staining method using DAPI and ConA is as detailed further in Section 2.4.1. The stained catheter sections were air-dried before used for EDIC/EF microscopy observation.

6.2.7 Observation using episcopic differential interference contrast/epifluorescence (EDIC/EF) microscope

All strains of *P. aeruginosa* PAO1 biofilm development on the catheter surface were observed using a customised Nikon Eclipse LV100D microscope (Best Scientific, UK) equipped for EDIC/EF microscopy (Keevil, 2003). The microscope was equipped with long working distance metallurgical objectives (Nikon Plan Achromat); a high-resolution camera (QImaging Retiga EXi Cooled Digital CCD monochrome camera with RGB colour filter module) and metal halide light source (EXFO X-CITE 120 fluorescence system). Three low to high magnification objectives (magnification x 10, x 50, and x 100) were used in imaging the biofilm formation taken with ImagePro 6.2 software (Media Cybernetics, UK). Due to the curvature of the catheter, stacked images of biofilm were taken for each focal point achieved at horizontal level high objective magnification (manual z-scans, one stack image ≈ ± 1 µm).

6.2.8 Image processing

The stacked images were processed into a composite image using the extended depth of field plugin (Forster *et al.* 2004) in the open-source image-analysis software, Fiji (Schindelin *et al.* 2012). A summary of the biofilm images for wildtype (Appendix G), QS-negative mutants (Appendix I), and PS-negative mutants (Appendix J) are included in the Appendices section. The images presented in the results were converted into grayscale images to compensate for the prism's pseudo colouration effects in the EDIC microscope and discussed further in the next section.

6.3 Results

6.3.1 Biofilm attachment enumeration analysis of *P. aeruginosa* PAO1 QS-negative mutants on urinary catheters

One-way analysis of variance (ANOVA) was conducted and reported in Table 5-2. The biofilm enumeration data compares the *P. aeruginosa* PAO1 wildtype that has been discussed previously in Chapter 5 with QS-negative mutants. It showed that there were statistically significant differences in mean $\log_{10}$ cfu/catheter section between the strains compared to wildtype for all timepoints measured ($P < 0.0001$). The ANOVA analysis was followed by Dunnett's multiple comparisons post-hoc test and the result summary are shown in Table 5-3. The mean value of $\log_{10}$ cfu/catheter section of the biofilm enumeration data at each timepoints are illustrated in the graph in Figure 6-1.

6.3.1.1 The *lasI*-negative mutant

The *lasI* mutant PW3601 showed no significant difference in growth compared to wildtype at 1 h and 6 h (6.40 ± 0.35 $\log_{10}$ cfu/catheter section, $P = 0.5602$, and 6.86 ± 0.41 $\log_{10}$ cfu/catheter section, $P = 0.8831$, respectively). Only at 3 h did PW3601 showed significantly different results in the number of attached cells (7.20 ± 0.18 $\log_{10}$ cfu/catheter section, $P = 0.0002$) as well as at 24 h (7.92 ± 0.15 $\log_{10}$ cfu/catheter section, $P = 0.0016$) that is higher than wildtype. This strong evidence suggests that Lasl is involved in the irreversible attachment including microcolony formation and biofilm maturation phase, even though it does not seem to affect the initial attachment phase in biofilm development.

Table 6-2 One-way ANOVA analysis of *P. aeruginosa* PAO1 wildtype and QS-negative mutant biofilm between timepoints

	One-way ANOVA ($P < 0.05$)					
Time	**ANOVA table**	**SS**	**DF**	**MS**	**F(DFn_{11}, DFd_{24})**	***P* summary**

1 h	Treatment (between columns)	15.62	11	1.42	44.27	*P* = < 0.0001
	Residual (within columns)	0.7698	24	0.03207		****
	Total	16.39	35			
3 h	Treatment (between columns)	18.87	11	1.716	49.49	*P* = < 0.0001
	Residual (within columns)	0.8321	24	0.03467		****
	Total	19.7	35			
6 h	Treatment (between columns)	6.817	11	0.6197	9.639	*P* = < 0.0001
	Residual (within columns)	1.543	24	0.06429		****
	Total	8.36	35			
6 h	Treatment (between columns)	11.15	11	1.013	41.56	*P* < 0.0001
	Residual (within columns)	0.5851	24	0.02438		****
	Total	11.73	35			

For all significant results shown, $P < 0.05$ (*, $P < 0.05$; **, $P < 0.01$; ***, $P < 0.001$, ****, $P < 0.0001$, and ns, not significant).

6.3.1.2 The *rhl*-negative mutants

In the first hour of biofilm formation, all *rhl*-negative mutants except PW6884-Δ*rhlB* showed no significant differences compared to the wildtype. RhlA mutant PW6886 showed no significant difference at 1 h (5.98 ± 0.16 $\log_{10}$ cfu/catheter section, $P = 0.7746$), but showed very strong evidence of a statistically significant increase at 3 h (7.16 ± 0.21 $\log_{10}$ cfu/catheter section, $P = 0.0003$).

Subsequently at 6 h, PW6886 showed no significant difference again (7.22 ± 0.18 $\log_{10}$ cfu/catheter section, $P = 0.9963$), but then showed strong evidence of increased biofilm growth at 24 h (8.00 ± 0.23 $\log_{10}$ cfu/catheter section, $P = 0.0004$). This showed that the *rhlA* gene might not be important in the initial biofilm formation, and the micro- to macrocolonies biofilm development, but is essential during microcolony formation as well as the maturation phase of biofilm development. Another *rhlA* mutant, PW6887, showed no significant difference compared to wildtype at 1 h (6.35 ± 0.24 $\log_{10}$ cfu/catheter section, $P = 0.8116$), 3 h (6.58 ± 0.19 $\log_{10}$ cfu/catheter section, $P = 0.7595$), and at 6 h (7.26 ± 0.08 $\log_{10}$ cfu/catheter section, $P = 0.9769$). However, PW6887 showed weak evidence of increased biofilm growth at 24 h, suggesting a possible functional role in the background process (7.74 ± 0.04 $\log_{10}$ cfu/catheter section, $P = 0.0422$).

Strain PW6884 showed strong evidence of decreased biofilm growth at 1 h and at 3 h (4.02 ± 0.10 $\log_{10}$ cfu/catheter section, $P < 0.0001$ and 5.37 ± 0.44 $\log_{10}$ cfu/catheter section, $P < 0.0001$, respectively). Subsequently, significant increased biofilm was showed at 6 h (6.21 ± 0.17 $\log_{10}$ cfu/catheter section, $P = 0.0024$) and 24 h (8.35 ± 0.39 $\log_{10}$ cfu/catheter section, $P < 0.0001$). Contrastingly, PW6885 showed significant differences only at 3 h (5.80 ± 0.03 $\log_{10}$ cfu/catheter section, $P = 0.0078$), but no significant differences was observed at 1 h, 6 h and 24 h (5.93 ± 0.13 $\log_{10}$ cfu/catheter section, $P = 0.5620$; 6.91 ± 0.10 $\log_{10}$ cfu/catheter section, $P = 0.9667$; and 7.50 ± 0.12 $\log_{10}$ cfu/catheter section, $P = 0.8564$, respectively).

These results suggest that *rhlB* might not be an essential gene for biofilm development. While wildtype showed microcolonies formation at 3 h, both *rhlB* mutants showed approximately 0.5 to 1 log decreased bacteria cells in biofilm compared to wildtype. Our results showed strong evidence that *rhlB* might be involve in the microcolony formation during biofilm development.

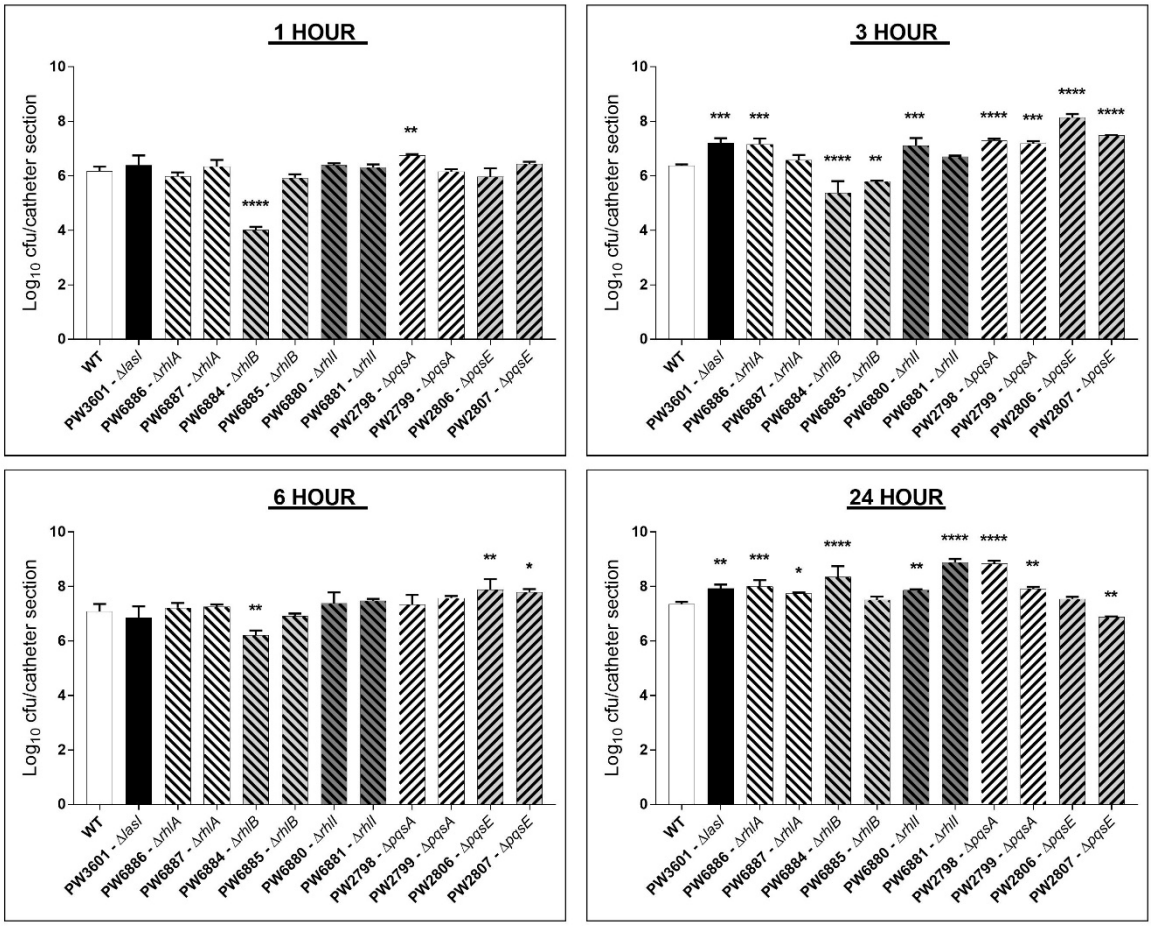

Figure 6-1 Enumeration data (log_{10} cfu/catheter section) of biofilm-derived *P. aeruginosa* PAO1 wildtype (WT) and QS-negative mutants at 1 h, 3 h, 6 h and 6 h. Error bars indicates the standard deviation (SD). All of the strains were compared to WT using one-way ANOVA followed by Dunnett's multiple-comparison test (*, $P < 0.05$; **, $P < 0.01$; ***, $P < 0.001$, ****, and $P < 0.0001$)

Both *rhlI* mutants PW6880 and PW6881 did not show any significant differences of biofilm growth at 1 h compared to wildtype (6.40 ± 0.07 log_{10} cfu/catheter section, $P = 0.5737$ and 6.32 ± 0.10 log_{10} cfu/catheter section, $P = 0.9109$, respectively). At 3 h, only PW6880 showed significant increased biofilm growth (7.11 ± 0.28log_{10} cfu/catheter section, $P = 0.0006$), but no significantly difference was showed by strain PW6881 (6.70 ± 0.04 log_{10} cfu/catheter section, $P = 0.2532$).

Subsequently at 6 h, both PW6880 and PW6881 showed no significantly difference (7.37 ± 0.41 log_{10} cfu/catheter section, $P = 0.7180$; and 7.48 ± 0.07 log_{10} cfu/catheter section, $P = 0.3769$, respectively). At 24 h, both strains showed increased biofilm compared to wildtype (7.86 ± 0.04 log_{10} cfu/catheter section, $P = 0.0049$; and 8.89 ± 0.12 log_{10} cfu/catheter section, $P < 0.0001$, respectively). Both *rhlI* mutants showed approximately 0.5 to 1.5 log of increased bacteria cells in

biofilm compared to wildtype which has shown early biofilm maturation at 24 h. This suggests the possible indication that *rhlI* is essential during early biofilm maturation in *P. aeruginosa* in biofilm development.

Table 6-3 Dunnett's post-hoc multiple comparison tests of *P. aeruginosa* PAO1 wildtype and QS-negative mutant biofilm for each timepoint

Strains		1 h	3 h	6 h	24 h
WT	**Log_{10} cfu/catheter section**	6.16 ± 0.17	6.38 ± 0.04	7.09 ± 0.27	7.36 ± 0.08
	(%)	(57.82 ± 1.94)	(60.18 ± 0.48)	(68.17 ± 2.97)	(71.15 ± 0.88)
PW3601 - Δ*lasI*	**Log_{10} cfu/catheter section**	6.40 ± 0.35	7.20 ± 0.18	6.86 ± 0.41	7.92 ± 0.15
	(%)	(60.93 ± 3.95)	(69.99 ± 2.04)	(66.12 ± 4.63)	(78.10 ± 1.71)
	Adjusted *P* value	0.5602 (*ns*)	0.0002 (***)	0.8831 (*ns*)	0.0016 (**)
PW6886 - Δ*rhlA*	**Log_{10} cfu/catheter section**	5.98 ± 0.16	7.16 ± 0.21	7.22± 0.18	8.00 ± 0.23
	(%)	(55.59 ± 1.75)	(68.86 ± 2.34)	(69.47 ± 1.96)	(78.22 ± 2.60)
	Adjusted *P* value	0.7746 (*ns*)	0.0003 (***)	0.9963 (*ns*)	0.0004 (***)
PW6887 - Δ*rhlA*	**Log_{10} cfu/catheter section**	6.35 ± 0.24	6.58 ± 0.19	7.26 ± 0.08	7.74 ± 0.04
	(%)	(56.98 ± 2.55)	(59.44 ± 2.04)	(66.75 ± 0.85)	(71.90 ± 0.44)
	Adjusted *P* value	0.8116 (*ns*)	0.7595 (*ns*)	0.9769 (*ns*)	0.0422 (*)
PW6884 - Δ*rhlB*	**Log_{10} cfu/catheter section**	4.02 ± 0.10	5.37 ± 0.44	6.21 ± 0.17	8.35 ± 0.39
	(%)	(44.21 ± 1.52)	(63.90 ± 6.43)	(76.21 ± 2.56)	(107.60 ± 5.74)
	Adjusted *P* value	< 0.0001 (****)	< 0.0001 (****)	0.0024 (**)	< 0.0001 (****)
PW6885 - Δ*rhlB*	**Log_{10} cfu/catheter section**	5.93 ± 0.13	5.80 ± 0.03	6.91 ± 0.10	7.50 ± 0.12
	(%)	(55.96 ± 1.48)	(54.51 ± 0.30)	(67.07 ± 1.11)	(73.85 ± 1.38)
	Adjusted *P* value	0.5520 (*ns*)	0.0078 (**)	0.9667 (*ns*)	0.8564 (*ns*)
PW6880 - Δ*rhlI*	**Log_{10} cfu/catheter section**	6.40 ± 0.07	7.11 ± 0.28	7.37 ± 0.41	7.86 ± 0.04
	(%)	(60.78 ± 0.78)	(68.84 ± 3.12)	(71.79 ± 4.58)	(77.29 ± 0.40)
	Adjusted *P* value	0.5737 (*ns*)	0.0006 (***)	0.7180 (*ns*)	0.0049 (**)
PW6881 - Δ*rhlI*	**Log_{10} cfu/catheter section**	6.32 ± 0.10	6.70 ± 0.04	7.48 ± 0.07	8.89 ± 0.12
	(%)	(56.68 ± 1.06)	(60.75 ± 0.46)	(69.07 ± 0.73)	(84.06 ± 1.31)
	Adjusted *P* value	0.9109 (*ns*)	0.2532 (*ns*)	0.3769 (*ns*)	< 0.0001 (****)
PW2798 - Δ*pqsA*	**Log_{10} cfu/catheter section**	6.75 ± 0.05	7.30 ± 0.05	7.34 ± 0.35	8.84 ± 0.11
	(%)	(62.56 ± 0.52)	(68.57 ± 0.55)	(68.96 ± 3.82)	(85.24 ± 1.20)
	Adjusted *P* value	0.0044 (**)	< 0.0001 (****)	0.8262 (*ns*)	< 0.0001 (****)
PW2799 - Δ*pqsA*	**Log_{10} cfu/catheter section**	6.16 ± 0.09	7.18 ± 0.09	7.58 ± 0.07	7.92 ± 0.07
	(%)	(55.27 ± 0.92)	(66.21 ± 1.01)	(70.46 ± 0.78)	(74.15 ± 0.72)
	Adjusted *P* value	> 0.9999 (*ns*)	0.0002 (***)	0.1740 (*ns*)	0.0016 (**)
PW2806 - Δ*pqsE*	**Log_{10} cfu/catheter section**	5.97 ± 0.30	8.14 ± 0.13	7.89 ± 0.38	7.55 ± 0.07
	(%)	(55.06 ± 3.35)	(79.07 ± 1.44)	(76.28 ± 4.22)	(72.49 ± 0.81)
	Adjusted *P* value	0.7654 (*ns*)	< 0.0001 (****)	0.0063 (**)	0.6314 (*ns*)
PW2807 - Δ*pqsE*	**Log_{10} cfu/catheter section**	6.44 ± 0.08	7.48 ± 0.02	7.79 ± 0.11	6.88 ± 0.02
	(%)	(60.25 ± 0.93)	(71.80 ± 0.21)	(75.31 ± 1.25)	(65.16 ± 0.24)
	Adjusted *P* value	0.4007 (*ns*)	< 0.0001 (****)	0.0189 (*)	0.0085 (**)

For all significant results shown, $P < 0.05$ (*, $P < 0.05$; **, $P < 0.01$; ***, $P < 0.001$, ****, $P < 0.0001$, and ns, not significant). Data is expressed as mean ± SD (SD = standard deviation).

6.3.1.3 The *pqs*-negative mutants

PqsA-negative mutant PW2798 biofilm showed a statistically significant difference in the first hour of incubation (6.75 ± 0.05 log_{10} cfu/catheter section, $P = 0.0044$), at 3 h (7.30 ± 0.05 log_{10} cfu/catheter section, $P < 0.0001$), and at 24 h as well (8.84 ± 0.11 log_{10} cfu/catheter section, $P < 0.0001$) compared to wildtype. There was no statistical difference observed at 6 h (7.34 ± 0.34 log_{10} cfu/catheter section, $P = 0.8262$). Another *pqsA* gene mutant PW2799 biofilm has also shown a statistically significant increase at 3 h (7.18 ± 0.09 log_{10} cfu/catheter section, $P = 0.0002$), and at 24 h as well (7.92 ± 0.07 log_{10} cfu/catheter section, $P = 0.0016$). PW2799 showed no statistically significant difference of biofilm growth at 1 h (6.16 ± 0.09log_{10} cfu/catheter section, $P > 0.9999$). Likewise, PW2799 also showed no significant difference at the 6 h (7.58 ± 0.07 log_{10} cfu/catheter section, $P = 0.1740$).

There was no significant difference at 1 h for both PW2806 and PW2807 *pqsE*-negative mutants (5.97 ± 0.30 log_{10} cfu/catheter section, $P = 0.7654$ and 6.44 ± 0.08 log_{10} cfu/catheter section, $P = 0.4007$, respectively). Both PqsE mutants PW2806 and PW2807 showed corresponding statistical differences of approximately one to two log increased biofilm growth at 3 h (8.14 ± 0.13 log_{10} cfu/catheter section, $P < 0.0001$ and 7.48 ± 0.02 log_{10} cfu/catheter section, $P < 0.0001$, respectively). Unlike PqsA mutants, both PqsE mutants also showed statistical significance of approximately 0.7 log_{10} increased biofilm growth at 6 h (7.89 ± 0.38 log_{10} cfu/catheter section, $P = 0.0063$ and 7.79 ± 0.11 log_{10} cfu/catheter section, $P = 0.0189$, respectively). PW2806 showed no statistical difference of biofilm growth in the 24 h (7.55 ± 0.07 log_{10} cfu/catheter section, $P = 0.6314$), whereas PW2807 has shown a statistically significant of approximately 0.48 log decreased in biofilm growth compared to wildtype (6.88 ± 0.02 log_{10} cfu/catheter section, $P = 0.0085$).

6.3.2 Screening of *P. aeruginosa* PAO1 QS-negative mutants for contrasting biofilm characteristics compared to wildtype

To assess the biofilm produced by the wildtype and the QS mutants, the catheter pieces were observed under the EDIC microscope to see for any morphological differences. Overall, the EDIC images obtained of the biofilm formed by QS-negative mutant at 1 and 3 h has fewer observed characteristics compared to longer timepoints, 6 h and 24 h, which the results will be outlaid in detail further below. The distinct characteristics that were observed are the early attachment twitching behaviour of aggregated cells and the formation of stratified 3D tower structure in the early mature biofilm formation. Unless mentioned, all QS-negative mutant strains at 1 h showed similar biofilm morphology to *P. aeruginosa* PAO1 wildtype as described in earlier section in Chapter 5 (Section 5.3.2).

The twitching behaviour in wildtype at the 1 h timepoint showed cell aggregates with near-distanced neighbours and maintained individual groups. This characteristic is highlighted due to the presence of distinct twitching behaviour of cells when coming together forming significantly larger cell groups through microcolony merging. These microcolonies produce different morphology that forms branch-like structures in the early timepoints.

6.3.2.1 The *lasI*-negative mutant (PW3601)

Microscopic observation showed that the PW3601 mutant was able to achieve attachment on the catheter surface and formed cell clusters at 1 h (Figure 6-2). The ConA-stained EPS components (polysaccharides) were more intense in the PW3601 than in wildtype; this could indicate richer D-mannose polysaccharide composition in the EPS. However, the ConA-stained EPS concentrated at the cell clusters observed in the PW3601 is notably similar to wildtype. The fibrinous tracks formed in PW3601 originated from the cell clusters and distended outwards in a dendritic pattern. This unique structure connects two cell clusters in close proximity by forming a fibrinous bridge between them that corresponds to the wildtype.

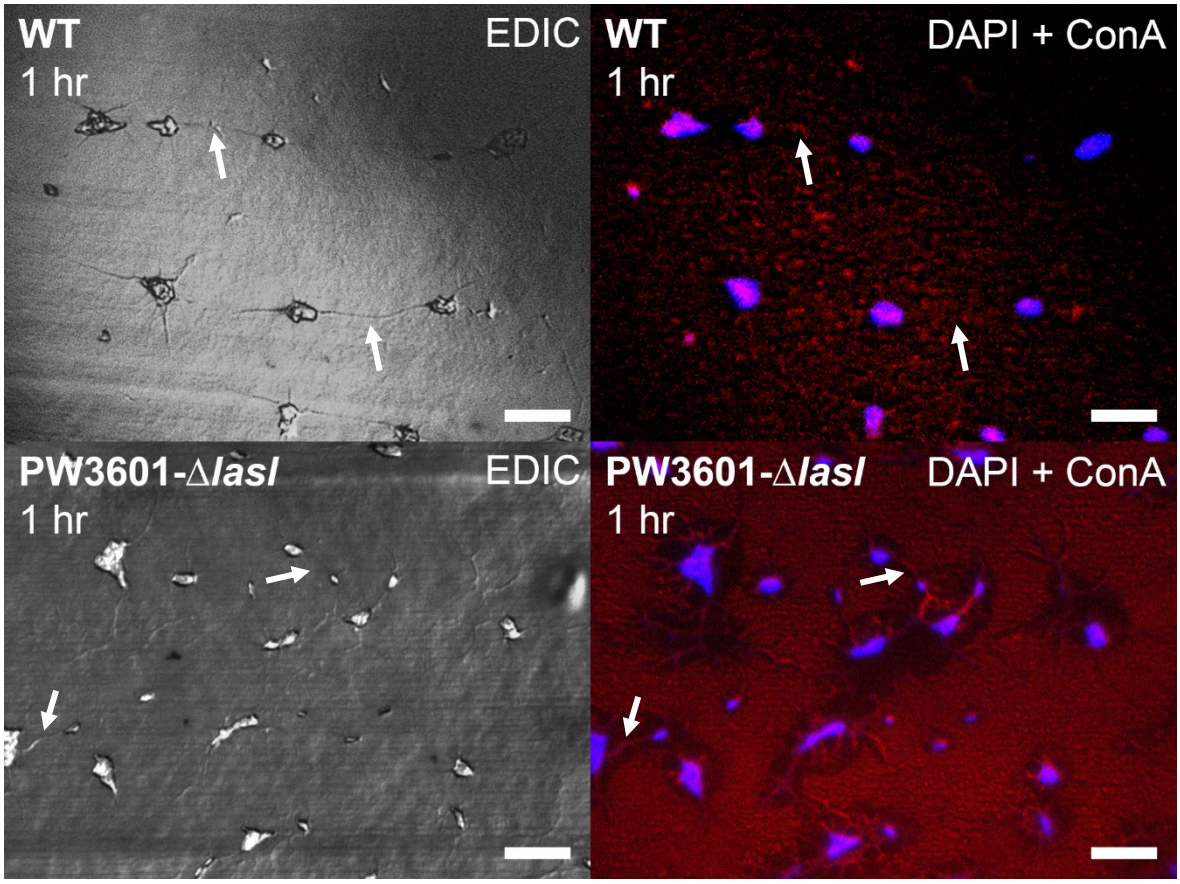

Figure 6-2 PAO1 wildtype and *lasI*-negative mutant (PW3601) share similar formation characteristics at 1 h incubation such as bacterial attachment and cell aggregation. Unique fibrinous track distended from cell clusters in dendritic pattern and formed a bridge (white arrows) between them in transporting cells. Magnification × 1000, scale bars = 10 µm.

Although there was an approximately 0.8 $\log_{10}$ cfu higher at 3 h compared to wildtype, the differences were not distinctively visual from the PW3601 biofilm image. However, the morphological difference was apparent at 24 h as the *lasI*-negative mutant unable to form a wildtype-like stratified 3D structure, but instead formed a lawn mat of biofilm with several crystal structures (Figure 6-3). The PW3601 produced approximately 0.5 $\log_{10}$ cfu higher than wildtype, but the decumbent biofilm means there are no dispersal events via central hollowing, but the presence of dispersal through erosion cannot be excluded.

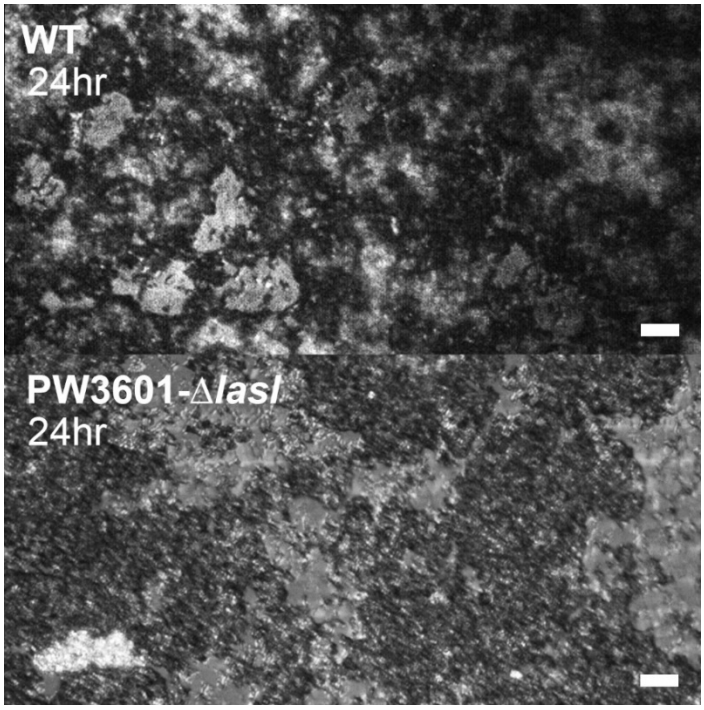

Figure 6-3 EDIC image comparison between wildtype and *lasI*-negative mutant (PW3601) biofilm at 24 h. The lawn mat of biofilm formed by PW3601 is distinct from the 3D stratified tower structure observed in wildtype. Magnification × 500, scale bars = 10 µm.

6.3.2.2 The *rhl*-negative mutants

Although the 1 h image of the RhlA strain PW6886 biofilm showed fewer attached cells, the 3 h biofilm showed microcolonies merging to form a unique geometrical structure on the catheter surface (corresponding to the 0.7 $\log_{10}$ more cfu than wildtype) (Figure 6-4). The image B and D in Figure 6-4 showed the angular biofilm consists of several microcolonies that were in very close proximity merging, which suggests that the mutation in the *rhlA* gene altered the formation.

This geometric structure was also observed in RhlA strain PW6887 (Figure 6-4C and Figure 6-4E) which supports the idea that the effect of the gene mutation was to direct the angular twitching movement. Figure 6-4 also showed the particular fibrinous structure distending from the microcolonies. These may guide the inbound cell navigation; and effect which was similarly observed happening in wildtype.

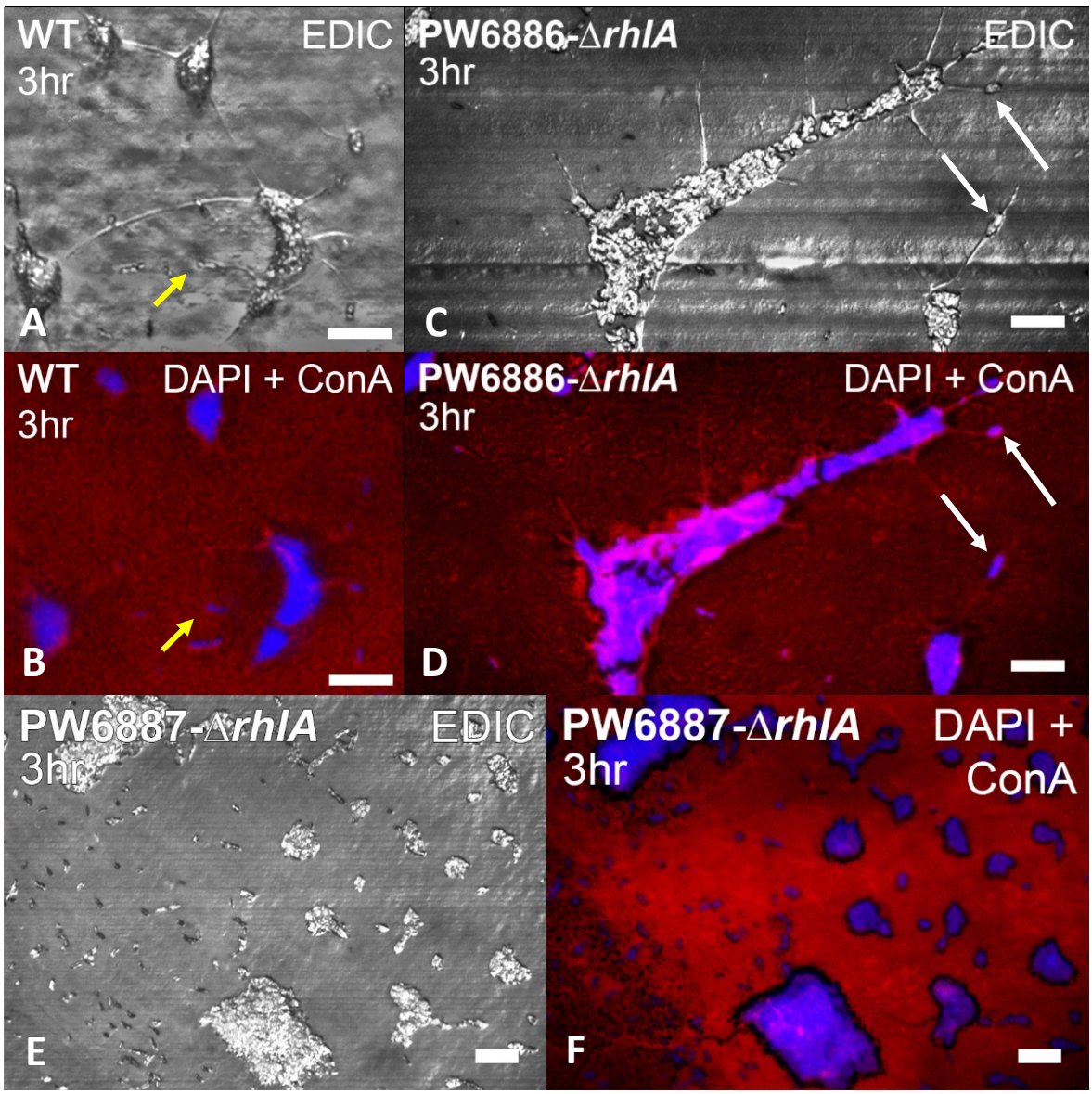

Figure 6-4 EDIC/EF image comparison of biofilm produced by wildtype (A and B) and the *rhlA*-negative mutants at 3 h indicated an effect of directed twitching resulting in an altered shape in angular formations.
PW6886 (C and D) showed the presence of distended fibrinous track that guides the cell movement towards the microcolony (white arrows) similarly observed in wildtype previously (yellow arrow). PW6887 (E and F) microcolony formation produced a geometrical pattern that is affected by the gene mutation. Magnifications × 1000, scale bars = 10 µm.

Subsequently, at 6 h, PW6887 had more biofilm coverage even though the cfu was comparable to wildtype. At 24 h, the PW6886 (Figure 6-5A) and PW6887 (Figure 6-5B) produced similar biofilm morphology to the wildtype; stratified amorphous biofilm formation with more significant voids in between, even though there was evidence of higher $\log_{10}$ cfu compared to wildtype. Both *rhlA*-negative 24 h biofilm appeared to absorb the DAPI and ConA stain due to the crystallisation, and there was no sign of dispersal events although central hollowing was observed.

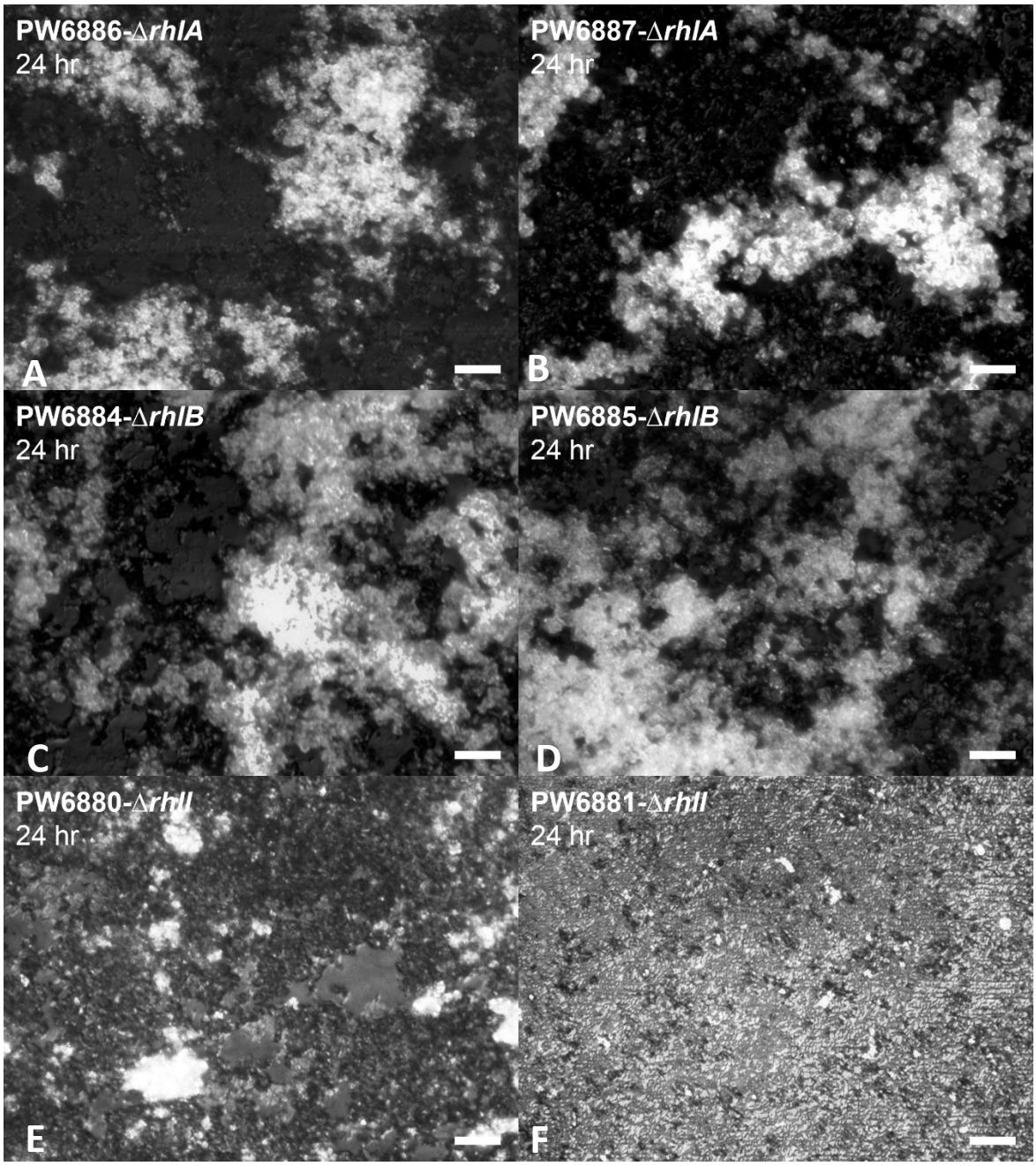

Figure 6-5 Visual inspection of the 24 h biofilm produced by *rhl*-negative mutants showed distinct flatten biofilm formation by the *rhlI*-negative mutants compared to the *rhlA*- and *rhlB*-negative mutants. Magnifications × 1000, scale bars = 10 µm.

Corresponding to the cfu data, both *rhlB* gene mutants (PW6884 and PW6885) showed less attached biofilm at 1 h and 3 h with no apparent signs of cell aggregate forming (Appendix I.5 and I.6 in Appendix I). Strain PW6884 produced bigger amorphous precipitation and crystallisation biofilm formation observed at 3 h that was distinct from wildtype. While both occupy similar surface coverage at 6 h, PW6884 formed crystallised biofilm much earlier than PW6885 that expanded vertically, producing contrasting morphology between them. The attached biofilm at 6 h for PW6884 was comparable to wildtype, but the PW6884 biofilm morphology differs significantly with a crystallised 3D structure already formed since 3 h. Both *rhlB*-negative mutants produced similar amorphous biofilm formation at the 24 h timepoint (Figure 6-5C and Figure

6-5D), with the PW6884 strain producing more crystallisation at 24 h; this corresponds to the substantial evidence of higher cfu compared to wildtype.

The *rhlI*-negative mutants PW6880 and PW6881 showed their ability to establish cell attachment and formed microcolony islands of cell aggregates at 1 h, similar to the biofilm characteristics shown by wildtype. The unique fibrinous track structure was observed present in 1 h, 3 h and 6 h biofilm. Figure 6-6 showed the cell behaviour of transporting across the catheter surface via the fibrinous structure towards the nearest cell groups to form more prominent cell aggregates as similarly described in wildtype. However, these mutant strains were unable to achieve stratified biofilm structure at 24 h and form a more flattened biofilm mat with several exposed areas that serve as void spaces in between (Figure 6-5E and Figure 6-5F). The PW6881 strain produced a more homogenous biofilm compared to PW6880 that occluded the catheter surface as shown in Figure 6-5E, even though not as elevated and stratified as in wildtype. Similarly observed before, the biofilm showed strong fluorescent signals at 24 h suggest that the crystallisation in the biofilm has absorbed the fluorescent dyes.

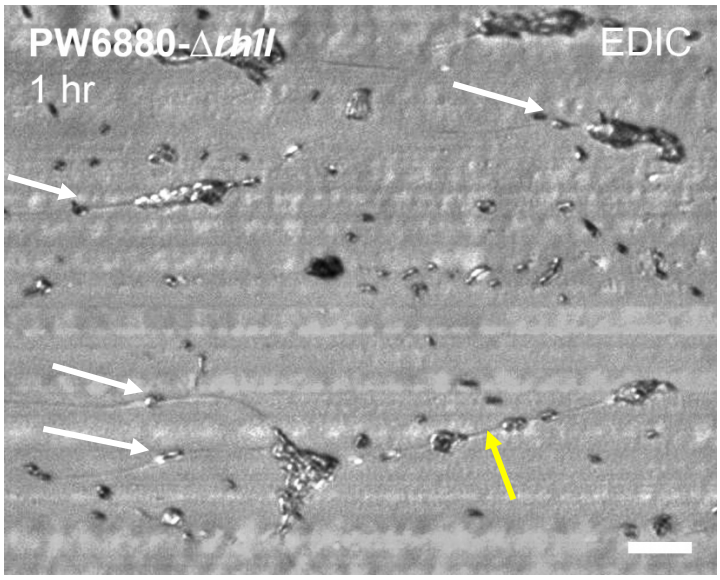

Figure 6-6 EDIC image of attached *rhlI*-negative PW6880 mutant cells on the catheter surface showed aggregation at 1 h with similar wildtype-like traits.
Cell move towards a bigger group of cells guided by the unique fibrinous structure (white arrows). The yellow arrow denotes where a fibrinous bridge was formed instead between cell groups in the transporting cell across the catheter surface. Magnification × 1000, scale bars = 10 µm.

6.3.2.3 The *pqs*-negative mutants

There were no apparent characteristic differences in the biofilm produced by both *pqsA*-negative mutants (PW2798 and PW2799). Both strains showed similar wildtype biofilm phenotype at 1 h, 3 h and 6 h (such as strong bacterial attachment, cell aggregation, microcolony and macrocolonies

formation) except at 24 h, when the strains were unable to achieve biofilm differentiation to produce mature biofilm.

A notable observation was the organisation behaviour presented by both *pqsA*-negative mutants; the formation of a dendritic-like microcolony with visible fibrinous tracks that act as a pathway guide for nearby cells moving towards the microcolony. This unique PqsA microcolony formation was present at 1 h by PW2798 and at 6 h by PW2799, were similar except that PW2799 showed more differentiated EPS compared to PW2798. The EPS differentiation in PW2799 was observed from the visible ConA-stained D-mannose component of the EPS. It was more conditioned on the catheter surface and displayed strong fluorescent signals, showing high absorption of the ConA stain into the biofilm.

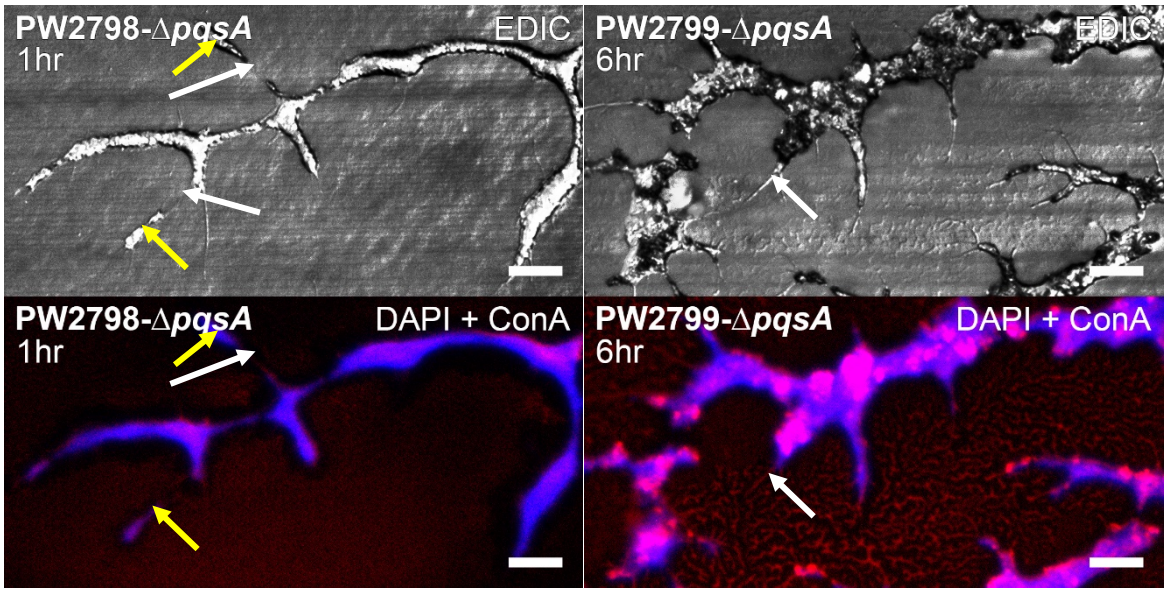

Figure 6-7 Unique characteristic shared by both *pqsA*-negative mutants presenting similar dendritic organisation behaviour in biofilm microcolony formation.
White arrows show the fibrinous track structure that assist in guiding incoming cells towards the microcolony. Yellow arrows show the cells on the fibrinous track. Magnifications ×1000, scale bars = 10 µm.

The *pqsA*-negative mutants produced a biofilm that appeared less developed, despite showing higher cfu count at 24 h compared to wildtype. The biofilm has no amorphous crystallisation with vertical stratification, although the presence of ConA-stained EPS observed on the catheter surface suggests that EPS was not the deterrent factor preventing both *pqsA* mutants from achieving biofilm maturation similar to wildtype.

Both *pqsE*-negative mutants showed similar biofilm characteristics to the wildtype at 1 h. However, close observation of the images at 3 h showed both mutants produced larger and many more microcolonies on the catheter (Figure 6-11). At 6 h, PW2806 formed a large flat microcolony which accumulated at the centre of the catheter, whereas PW2807 biofilm formed a similar flat

biofilm that expanded across the whole catheter surface creating a mat, and both strains produced biofilm with a network of presumably water channels similar to previous reports that formed in between them (Figure 6-9) (Keevil and Walker 1992; Davies 1998; Campanac *et al.* 2002; Donlan and Costerton 2002; Heydorn *et al.* 2002; Stoodley *et al.* 2002; Davey *et al.* 2003; Kikuchi *et al.* 2005; Koseoglu *et al.* 2006; Tenke *et al.* 2006; De Kievit 2009; Burrows 2012). Close observation of the EDIC images as well as from the intensity of signals obtained from the ConA-stained EPS showed that the PW2806 biofilm was thicker than PW2807 and the water channels suggested were wider compared to the water channels produced in PW2807.

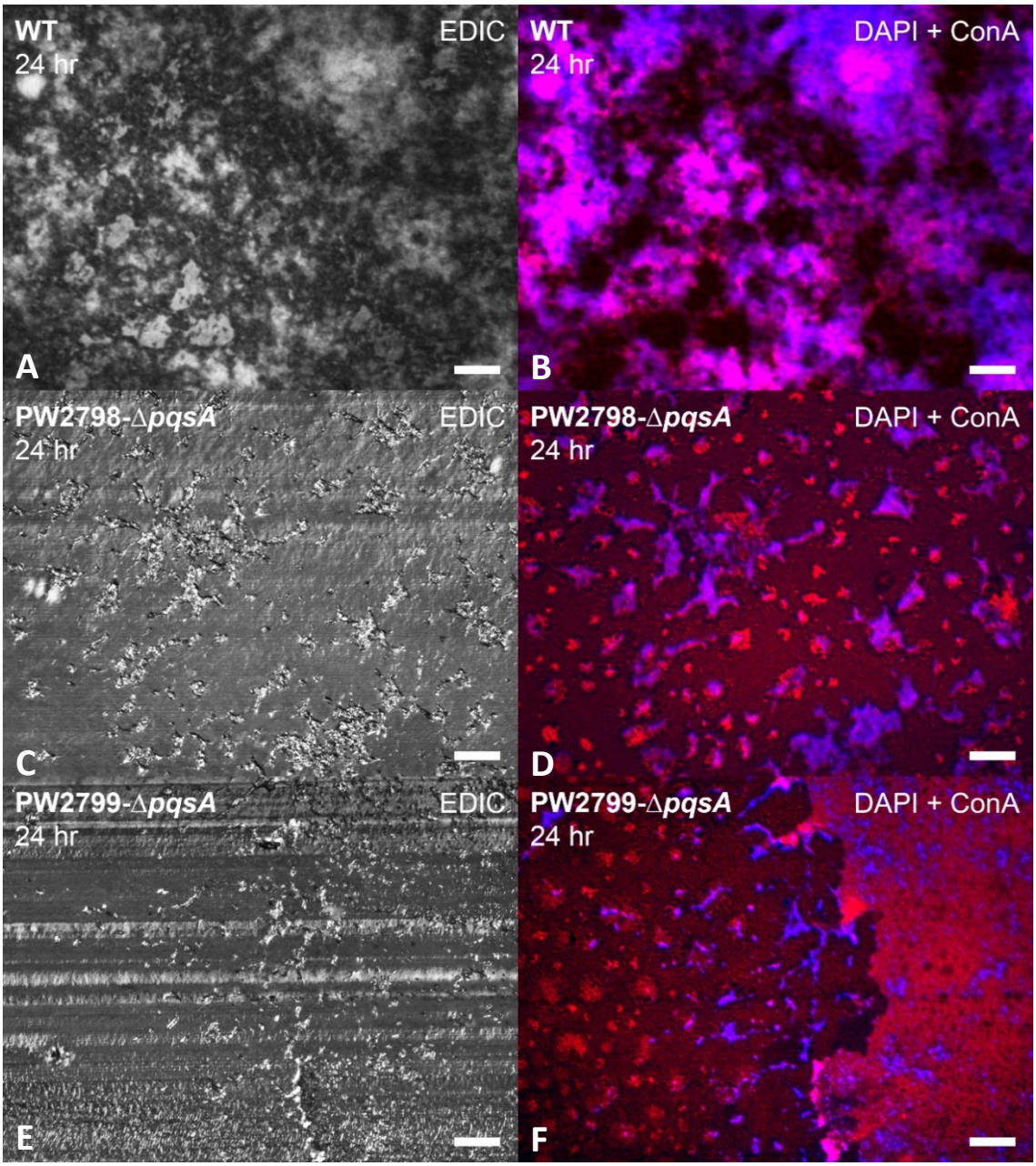

Figure 6-8 Microscopy images of wildtype (A and B) and *pqsA*-negative mutants at 24 h with contrasting biofilm development. PW2798 (C and D) and PW2799 (E and F) biofilm were not the usual multilayer amorphous morphology of 24 h wildtype biofilm even though both mutants had higher cfu count than wildtype. Magnifications × 500, scale bars = 20 µm.

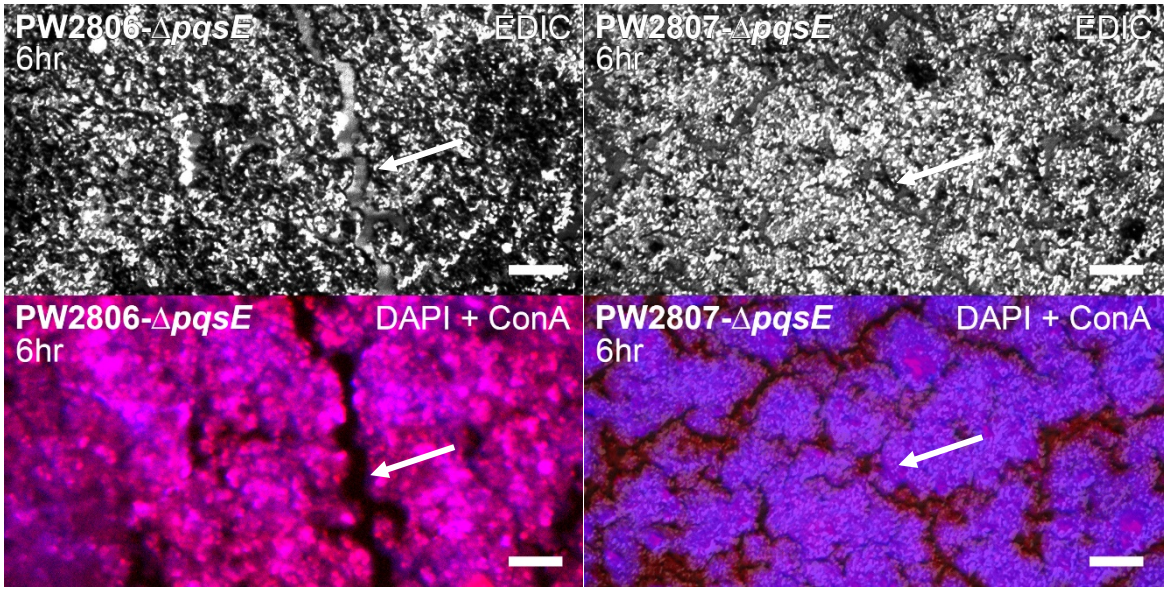

Figure 6-9 Microscopy images of *pqsE*-negative mutant biofilm at 6 h showed flat and undifferentiated biofilm characteristic with presence of a network of water channels (white arrows). Magnifications × 1000, scale bars = 10 µm.

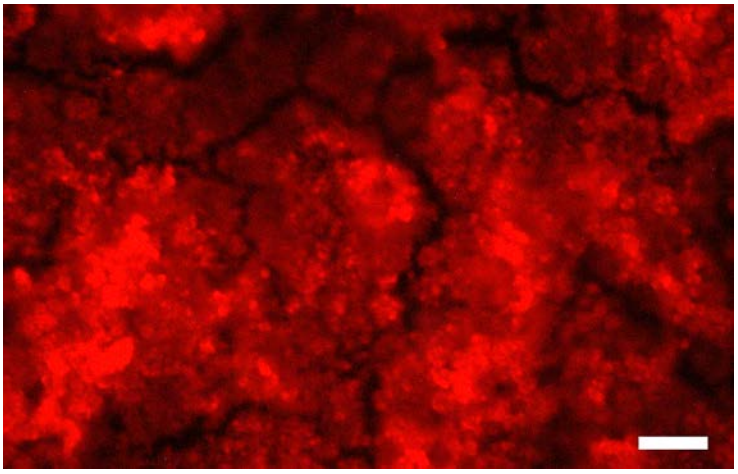

Figure 6-10 ConA-stained 24 h biofilm of *pqsE*-negative strain PW2807 exhibiting the presence of a network of water channels at base of biofilm. Magnification × 1000, scale bars = 10 µm.

At 24 h, both *pqsE*-negative mutants showed fewer but similar to wildtype like three-dimensional stratified amorphous biofilm structure, but with more prominent water channels between the macrocolony towers (Figure 6-11). Close inspection of the area surface between the macrocolonies showed that there was a conditioning film covering the exposed catheter surface areas with a well-detailed water channel network formed at the base of the biofilm. Although less prominent than wildtype, both *pqsE*-negative mutants achieved vertical growth and showed the presence of crystallisation production at 24 h biofilm.

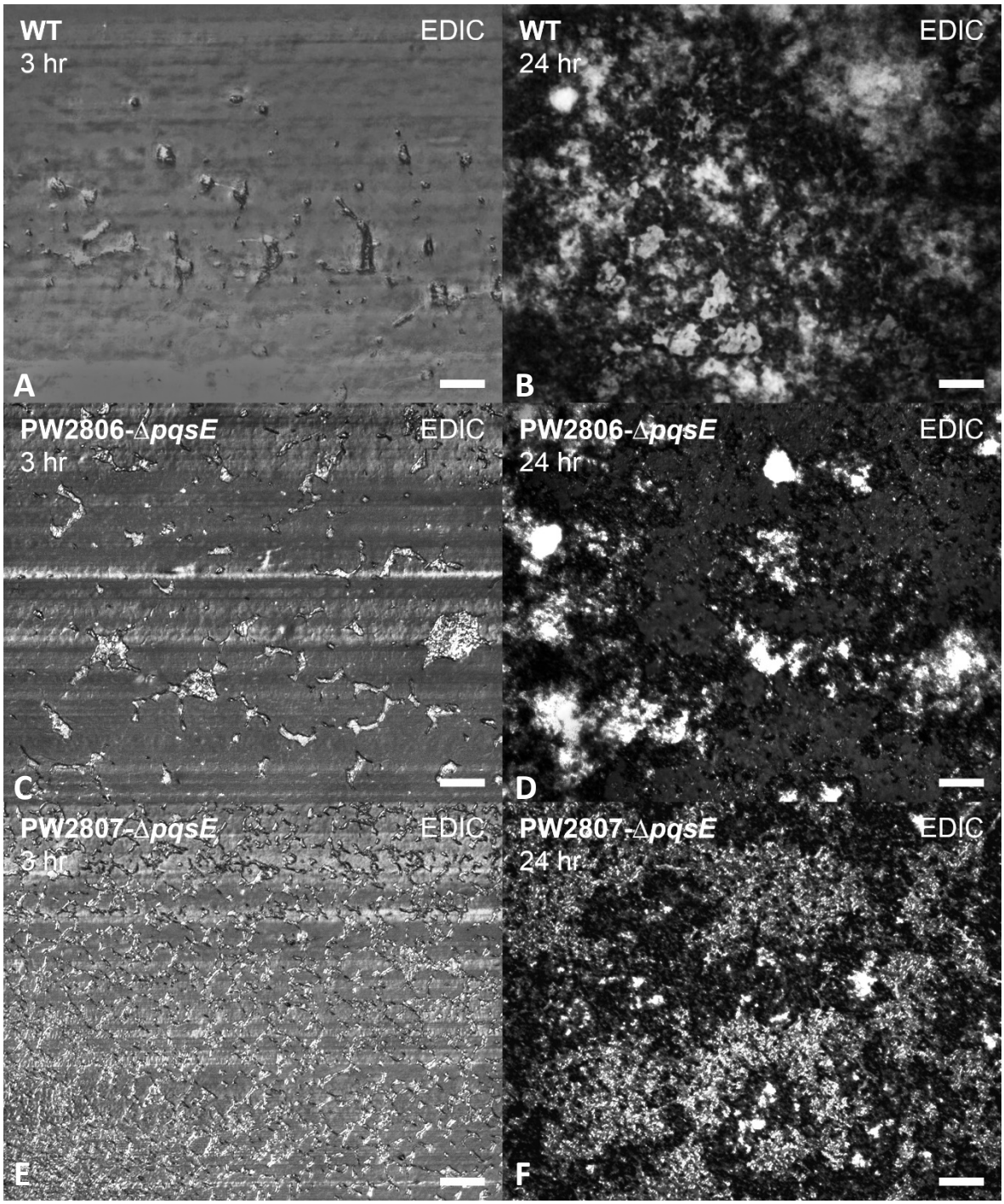

Figure 6-11: EDIC images of biofilm produced by wildtype and *pqsE*-negative mutants at 3 and 24 h. More microcolonies were formed on the catheter surface by the mutants compared to wildtype (A) at 3 h that corresponds to the higher cfu data. The mutants are able to produce mature macro colony towers but not as differentiated as in wildtype. Magnifications × 500, scale bars = 20 µm.

However, there was no evidence of seeding dispersal, but the presence of dispersal through erosion cannot be excluded. Similarly, the ConA image observation at every timepoint for both *pqsE*-negative mutants showed the presence of ConA-stained D-mannose component in the EPS which suggest that the non-involvement of the *pqsE* gene in the production of EPS during biofilm formation.

6.3.3 Biofilm growth of *P. aeruginosa* PAO1 PS-negative mutants

One-way analysis of variance (ANOVA) followed by Dunnett's multiple comparisons post-hoc test was conducted and reported in Table 5-2. It showed that there is a statistically significant difference of mean $\log_{10}$ cfu/catheter section between the strains compared to wildtype for all timepoints measured ($P < 0.0001$).

The mean value of $\log_{10}$ cfu/catheter section and Dunnett's multiple comparisons post-hoc test result summary of all PS-negative mutant strain for each timepoint are shown in Table 5-3.

The mean value of $\log_{10}$ cfu/catheter section of the biofilm enumeration data at each timepoint is illustrated in graph Figure 6-12.

Table 6-4 One-way ANOVA analysis of *P. aeruginosa* PAO1 wildtype and PS-negative mutant biofilm between timepoints

		One-way ANOVA ($P < 0.05$)				
Time	**ANOVA table**	**SS**	**DF**	**MS**	**F(DFn_9, DFd_{20})**	***P* summary**
1 h	Treatment (between columns)	15.92	9	1.769	30.84	$P = < 0.0001$
	Residual (within columns)	1.148	20	0.05738		****
	Total	17.07	29			
3 h	Treatment (between columns)	4.953	9	0.5503	13.32	$P = < 0.0001$
	Residual (within columns)	0.8265	20	0.04133		****
	Total	5.779	29			
6 h	Treatment (between columns)	5.821	9	0.6468	10.05	$P = < 0.0001$
	Residual (within columns)	1.287	20	0.06436		****
	Total	7.108	29			
6 h	Treatment (between columns)	2.086	9	0.2317	3.177	$P = 0.0150$
	Residual (within columns)	1.459	20	0.07294		*
	Total	3.544	29			

For all significant results shown, $P < 0.05$ (*, $P < 0.05$; **, $P < 0.01$; ***, $P < 0.001$, ****, $P <$ 0.0001, and *ns*, not significant).

Table 6-5 Dunnett's post-hoc multiple comparison tests of *P. aeruginosa* PAO1 wildtype and PS-negative mutant biofilm for each timepoint

Strains		1 h	3 h	6 h	24 h
WT	**Log_{10} cfu/catheter section**	6.16 ± 0.17	6.38 ± 0.04	7.09 ± 0.27	7.36 ± 0.08
	(%)	(57.82 ± 1.94)	(60.18 ± 0.48)	(68.17 ± 2.97)	(71.15 ± 0.88)
PW6140 - Δ*pelA*	**Log_{10} cfu/catheter section**	6.46 ± 0.20	6.64 ± 0.12	7.39 ± 0.18	7.79 ± 0.20
	(%)	61.11 ± 2.18	63.11 ± 1.33	71.52 ± 1.98	75.91 ± 2.20
	Adjusted *P* value	0.5661 (*ns*)	0.5115 (*ns*)	0.6045 (*ns*)	0.3118 (*ns*)
PW6141 - Δ*pelA*	**Log_{10} cfu/catheter section**	4.88 ± 0.21	6.56 ± 0.20	7.36 ± 0.20	7.54 ± 0.37
	(%)	45.75 ± 2.49	65.46 ± 2.30	74.87 ± 2.33	77.01 ± 4.37
	Adjusted *P* value	< 0.0001 (****)	0.8470 (*ns*)	0.7290 (*ns*)	0.9601 (*ns*)
PW4802 - Δ*pslD*	**Log_{10} cfu/catheter section**	4.84 ± 0.08	6.17 ± 0.01	7.79 ± 0.44	7.70 ± 0.66
	(%)	41.52 ± 0.84	55.93 ± 0.12	73.45 ± 4.77	72.44 ± 7.19
	Adjusted *P* value	< 0.0001 (****)	0.7812 (*ns*)	0.0192 (*)	0.5452 (*ns*)
PW4803 - Δ*pslD*	**Log_{10} cfu/catheter section**	4.68 ± 0.13	5.70 ± 0.22	6.04 ± 0.36	7.14 ± 0.12
	(%)	42.73 ± 1.49	54.60 ± 2.53	58.53 ± 4.16	71.35 ± 1.44
	Adjusted *P* value	< 0.0001 (****)	0.0043 (**)	0.0005 (***)	0.9140 (*ns*)
PW4807 - Δ*pslG*	**Log_{10} cfu/catheter section**	5.54 ± 0.29	7.16 ± 0.05	7.30 ± 0.18	7.31 ± 0.01
	(%)	51.09 ± 3.31	69.31 ± 0.57	70.94 ± 2.01	71.01 ± 0.14
	Adjusted *P* value	0.0293 (*)	0.0010 (***)	0.8843 (*ns*)	0.9997 (*ns*)
PW4808 - Δ*pslG*	**Log_{10} cfu/catheter section**	6.61 ± 0.10	6.41 ± 0.19	7.48 ± 0.15	7.92 ± 0.08
	(%)	61.41 ± 1.13	59.20 ± 2.07	71.03 ± 1.68	75.76 ± 0.92
	Adjusted *P* value	0.1884 (*ns*)	0.9997 (*ns*)	0.3362 (*ns*)	0.1116 (*ns*)
PW2387 - Δ*mucA*	**Log_{10} cfu/catheter section**	5.21 ± 0.49	6.24 ± 0.48	7.23 ± 0.16	7.67 ± 0.05
	(%)	47.03 ± 5.53	58.65 ± 5.38	69.63 ± 1.76	74.62 ± 0.53
	Adjusted *P* value	0.0007 (***)	0.9701 (*ns*)	0.9902 (*ns*)	0.6330 (*ns*)
PW6997 - Δ*algD*	**Log_{10} cfu/catheter section**	6.69 ± 0.13	7.10 ± 0.06	7.46 ± 0.15	8.00 ± 0.09
	(%)	61.37 ± 1.43	65.82 ± 0.60	69.79 ± 1.60	75.59 ± 0.94
	Adjusted *P* value	0.0888 (*ns*)	0.0023 (***)	0.3883 (*ns*)	0.0517 (*ns*)
PW6998 - Δ*algD*	**Log_{10} cfu/catheter section**	5.76 ± 0.28	6.55 ± 0.20	7.37 ± 0.28	7.43 ± 0.27
	(%)	53.55 ± 3.18	62.40 ± 2.24	71.73 ± 3.15	72.38 ± 3.03
	Adjusted *P* value	0.2588 (*ns*)	0.8969 (*ns*)	0.6731 (*ns*)	0.9995 (*ns*)

For all significant results shown, $P < 0.05$ (*, $P < 0.05$; **, $P < 0.01$; ***, $P < 0.001$, ****, $P < 0.0001$, and ns, not significant). Data is expressed as mean ± SD (SD = standard deviation).

The *pelA*-negative mutant PW6140 showed no significant differences between biofilm and wildtype at every timepoint (1 h, 6.46 ± 0.20 log_{10} cfu/catheter section, $P = 0.5661$; 3 h, 6.64 ± 0.12 log_{10} cfu/catheter section, $P = 0.5115$; 6 h, 7.39 ± 0.18 log_{10} cfu/catheter section, $P = 0.6045$; 24 h, 7.79 ± 0.20 log_{10} cfu/catheter section, $P = 0.3118$).

PW6141 strain of *pelA* gene mutant only showed strong evidence of a statistically significant decrease in the cfu/catheter section at 1 h (4.88 ± 0.21 log_{10} cfu/catheter section, $P < 0.0001$). No significant differences were observed at the 3 h, 6 h, and 24 h compared to wildtype (6.56 ± 0.20 log_{10} cfu/catheter section, $P = 0.8470$; 7.36 ± 0.20 log_{10} cfu/catheter section, $P = 0.7290$; and 7.54

± 0.37 log_{10} cfu/catheter section, $P = 0.9601$, respectively). The 1.2 log_{10} fewer cfu compared to wildtype showed by PW6141 gave solid evidence that the *pelA* gene was involved during the initial biofilm attachment even though it does not affect the subsequent events in biofilm development.

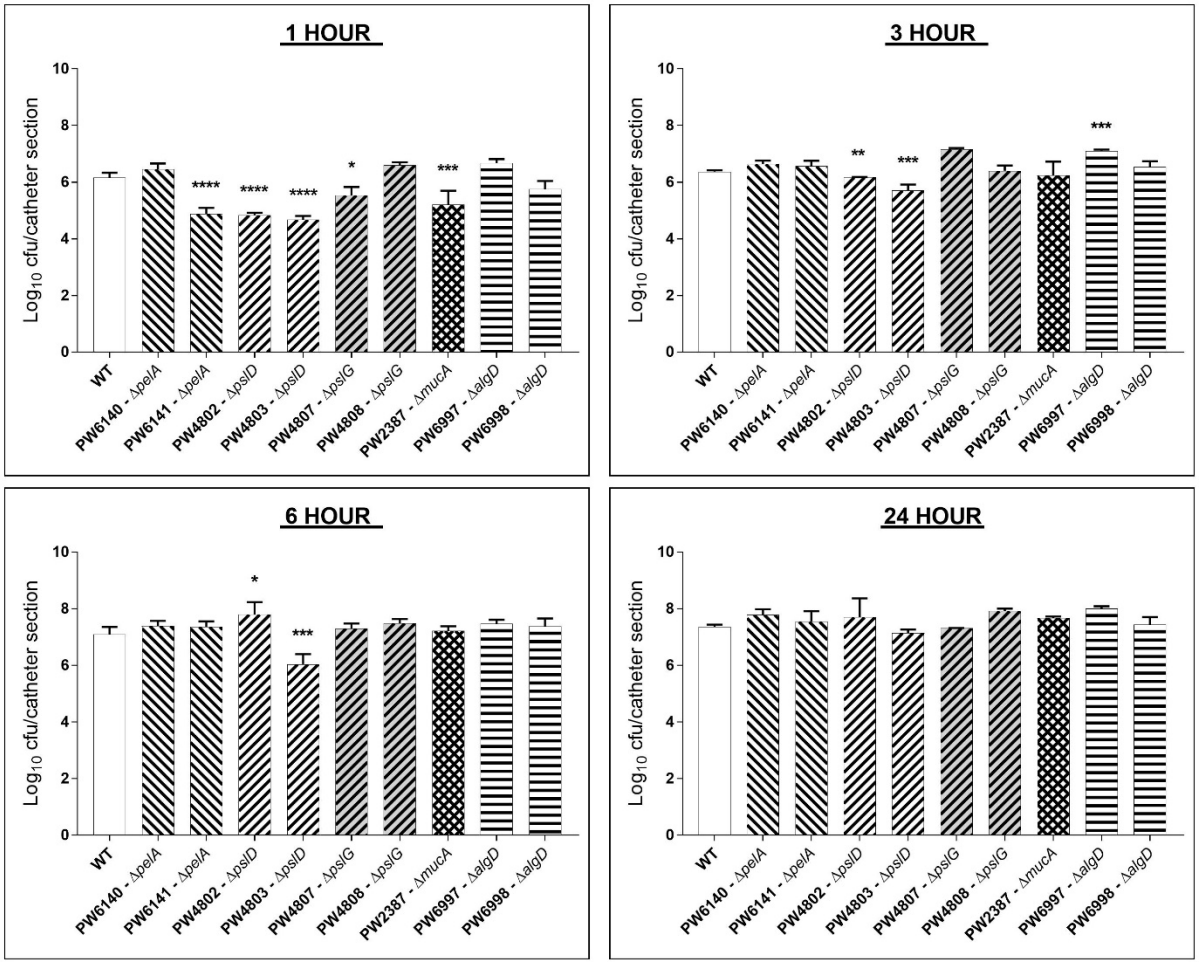

Figure 6-12 Enumeration data (log_{10} cfu/catheter section) of biofilm-derived *P. aeruginosa* PAO1 wildtype (WT) and PS-negative mutants at 1 h, 3 h, 6 h and 24 h. Error bars indicates the standard deviation (SD). All of the strains were compared to WT using one-way ANOVA followed by Dunnett's multiple-comparison test (*, $P < 0.05$; **, $P < 0.01$; ***, $P < 0.001$, ****, and $P < 0.0001$).

PW4802 and PW4803 *pslD*-negative mutants showed strong evidence of significant decrease at 1 h (4.84 ± 0.08 log_{10} cfu/catheter section, $P < 0.0001$; and 4.68 ± 0.13 log_{10} cfu/catheter section, $P < 0.0001$, respectively). The differences compared to wildtype are approximately 1.3 log_{10} less show that the initial attachment of bacterial cells is greatly affected by *pslD*-deficiency.

In subsequent timepoints, PW4802 did not show any apparent differences compared to wildtype (3 h, 6.17 ± 0.01 log_{10} cfu/catheter section, $P = 0.7812$; and 24 h, 7.70 ± 0.66 log_{10} cfu/catheter section, $P = 0.5452$), except at 6 h which showed there was a slight significant increase in biofilm (7.79 ± 0.44 log_{10} cfu/catheter section, $P = 0.192$).

After 1 h, strain PW4803 showed significantly decreased cfu at 3 h and 6 h (5.70 ± 0.22 log_{10} cfu/catheter section, *P* = 0.0043; and 6.04 ± 0.36 log_{10} cfu/catheter section, *P* = 0.0005, respectively). Similar to PW4802, PW4803 did not show a significant difference at 24 h (6.14 ± 0.12 log_{10} cfu/catheter section, *P* = 0.9140) indicating that *pslD* is not important for the biofilm maturation and dispersal phase.

Initially, PW4807 showed weak but significant evidence of less biofilm at 1 h (5.54 ± 0.29 log_{10} cfu/catheter section, *P* = 0.0293), but at 3 h it showed significantly more compared to wildtype (7.16 ± 0.05 log_{10} cfu/catheter section, *P* = 0.0010). However, there were no significant differences observed during the subsequent 6 h and 24 h timepoints (7.30 ± 0.18 log_{10} cfu/catheter section, *P* = 0.8843; and 7.31 ± 0.01 log_{10} cfu/catheter section, *P* = 0.9997, respectively). This evidence shows that *pslG* might have an important role during the initial attachment and microcolony formation but not the maturation phase in the biofilm development.

The PW2387 *mucA*-negative mutant showed significantly less attached biofilm compared to wildtype only at 1 h (5.21 ± 0.49 log_{10} cfu/catheter section, *P* = 0.0007). At subsequent timepoints 3 h, 6 h and 24 h, there were no significant differences observed (6.24 ± 0.48 log_{10} cfu/catheter section, *P* = 0.9701; 7.23 ± 0.16 log_{10} cfu/catheter section, *P* = 0.9902; and 7.67 ± 0.05 log_{10} cfu/catheter section, *P* = 0.6330, respectively).

There was no significant difference shown in the 1 h (6.69 ± 0.13 log_{10} cfu/catheter section, *P* = 0.0888), only at the subsequent 3 h timepoint the PW6997 *algD*-negative mutant showed a significant increase compared to wildtype (7.10 ± 0.06 log_{10} cfu/catheter section, *P* = 0.0023). There were no significant differences observed at 6 h and 24 h (7.46 ± 0.15 log_{10} cfu/catheter section, *P* = 0.3883; and 8.00 ± 0.09 log_{10} cfu/catheter section, *P* = 0.0517, respectively). However, *algD*-negative mutant PW6998 showed no significant differences of attached biofilm compared to wildtype at any timepoints (1 h, 5.76 ± 0.28 log_{10} cfu/catheter section, *P* = 0.2588; 3 h, 6.55 ± 0.20 log_{10} cfu/catheter section, *P* = 0.8969 6 h, 7.37 ± 0.28 log_{10} cfu/catheter section, *P* = 0.6731; 24 h, 7.43 ± 0.27 log_{10} cfu/catheter section, *P* = 0.9995).

6.3.4 Screening of *P. aeruginosa* PAO1 PS-negative mutants for contrasting biofilm characteristics compared to wildtype

The general observation obtained from the microscopy images is that the PS gene mutation affects the initial attachment phase in some PS-negative strains. There was unsubstantial cell adherence at the early timepoint as the mutants were incapable of establishing strong attachment, presenting little or no visible cells attached on the catheter surface. The poor adherence corresponds with the enumeration data obtained from the harvested attached biofilm from the catheter.

Due to the limited cells visualised by EDIC in some images, the merged DAPI and ConA composite images were used to determine the spatial environment of the biofilm (Figure 6-13). The ConA images showed the presence of D-mannose component of the polysaccharide EPS covering the catheter surface, which was also able to capture the gradient of biopolymer adhesives produced by the mutants that creates the 'footprint' of detached cells. The presence of "footprint" on the surface visualised in ConA images suggest the probability of cells detached due to the weak bond to the surface, which could be a contributing factor in reversible attachment.

6.3.4.1 *The pelA*-negative mutant

General observation of the *pelA*-negative mutant PW6140 showed similarity in the progression of biofilm development characteristics compared to wildtype that corresponds to the no significant difference for every timepoint cfu data in Section 6.3.3 as well (Figure 6-13A). At 3 h, networks of microcolonies were observed covering the catheter surface, suggesting that the microcolonies have expanded and merged with the surrounding neighbours to form macrocolonies. At 6 h, most of the biofilm structures differentiated into macrocolonies with evidence of crystallisation production. At 24 h, no apparent differences in the PW6141 mature biofilm characteristic compared to wildtype, except that there were no signs of biofilm dispersal by seeding, as there were no central following feature in the biofilm.

The ConA image visualises the D-mannose in glycoprotein component of the *pelA* mutant EPS showing an extensive interconnecting EPS network mesh that covers above and under the biofilm. The *pelA*-negative mutant PW6141 biofilm had less biofilm attached on the surface at 1 and 3 h, and close examination of the ConA image presented halo patterns on the EPS that suggest the evidence of detached cell thus leaving behind traces of "footprints" (Figure 6-13B).

Compared to PW6140, the onset of initial attachment for PW6141 was delayed caused by the detached cells but did not affect the overall biofilm development, as the mutant is able to form expanding microcolonies at 6 h that is comparable to PW6140 as well as to wildtype. The PW6141 mutant microcolonies were distanced apart, with some were coming together and merging to form more prominent macrocolonies.

There was filamentous structure that form a track recruiting nearby cells towards the microcolonies can be seen at 6 h in PW6141 indicating that the wildtype filamentous track characteristic was retained and not affected by *pelA*-deficiency. High fluorescent signal in the ConA-stained image suggests the EPS was produced with another polysaccharide component other than PelA as the primary component. The 24 h PW6140 biofilm presented a multi-layered amorphous crystallisation biofilm that were similar to wildtype, but there were no central hollowing of the biofilm indicating no seeding dispersal having occurred

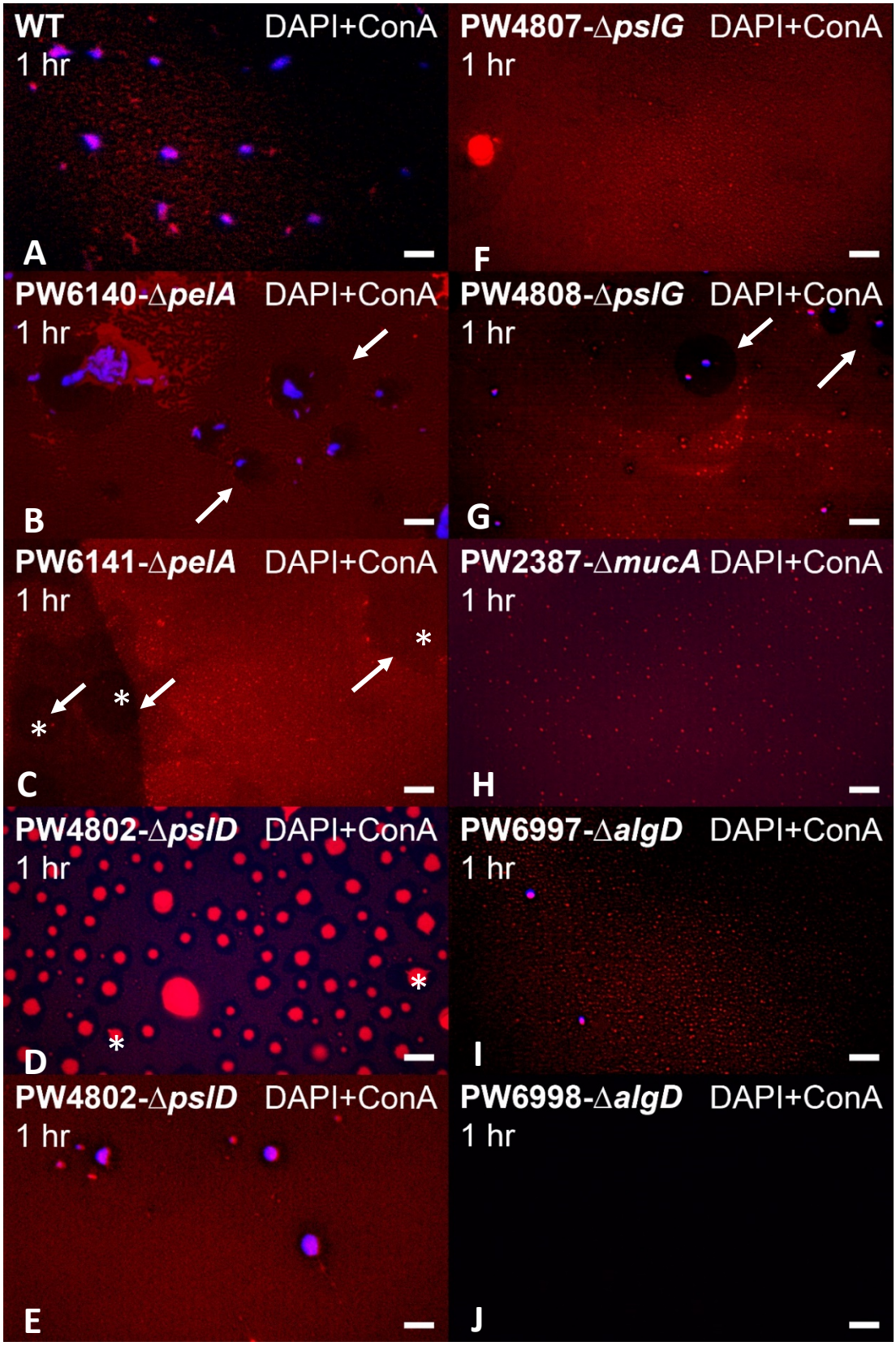

Figure 6-13 DAPI and ConA-stained image showing the surface condition at 1 h for wildtype and PS-negative mutants. White arrows denote the halo patterns in the EPS that exist surrounding a cell aggregate and asterisks denote the detached cell location suggestion. Magnifications × 1000, scale bars = 10 µm.

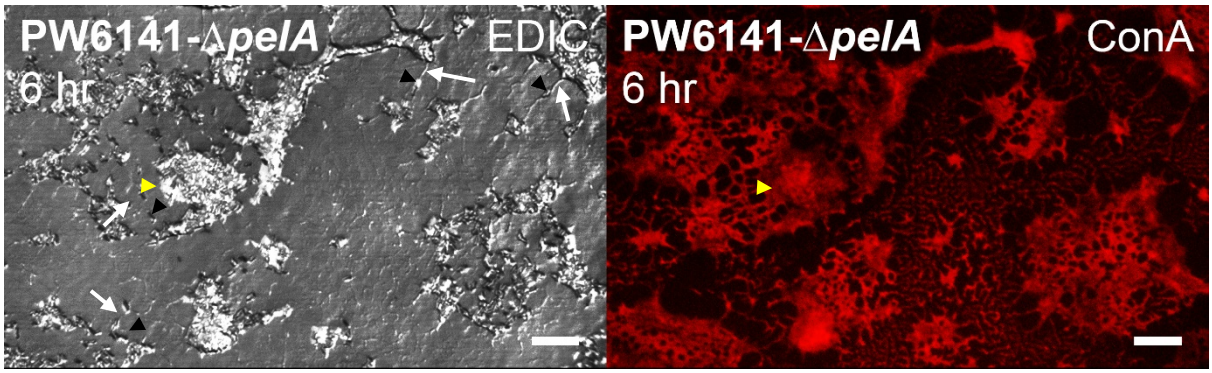

Figure 6-14 Strong fluorescent signal observed in the ConA image of PW6141 mutant biofilm at 6 h indicates the presence of EPS layer that surrounds and forms the adhesive foundation beyond the biofilm periphery (yellow arrowhead).
The ConA image displayed the EPS supports the filamentous structure observed in EDIC (white arrows) that guides the cells (black arrowhead) towards the microcolonies. Magnifications × 1000, scale bars = 10 µm.

6.3.4.2 The *psl*-negative mutants

Both *pslD* mutants showed less biofilm on the catheter surface at 1 h compared to wildtype, which corresponds to the lower cfu data, presented in Section 6.3.3 (Figure 6-15, column 1). However, observation of the ConA image showed the existence of D-mannose-based polysaccharide component in the EPS layer, covering the catheter surface at 1 h with evidence of detached cells from the visible "footprints".

Another characteristic shared by both *pslD*-negative strains was the evidence of crystallisation occurred earlier in the biofilm development during bacterial attachment and microcolony formation.

For PW4802, the microcolony formation can be observed at 3 h, whereas PW4803 strain featured networks of the microcolonies that are far apart at 6 h timepoint. Strong intensity from the ConA image at 3 h onwards that correlates with the biofilm formation showed in EDIC image suggests that the uptake of ConA fluorescent dye by the crystals had occurred. In the absence of PslD, there are other D-mannose-based polysaccharide component that are contained in the EPS that absorbs the ConA.

There are more surface deposits observed in the EDIC image of PW4802 biofilm at 3 h compared to the PW4802 strain that made it hard to see any features that were previously seen in wildtype, such as radials from the cell aggregation or filamentous fibres between the microcolonies. However, in the EDIC image of PW4803 strain biofilm, these features can be seen at the 3 h and 6 h EDIC images.

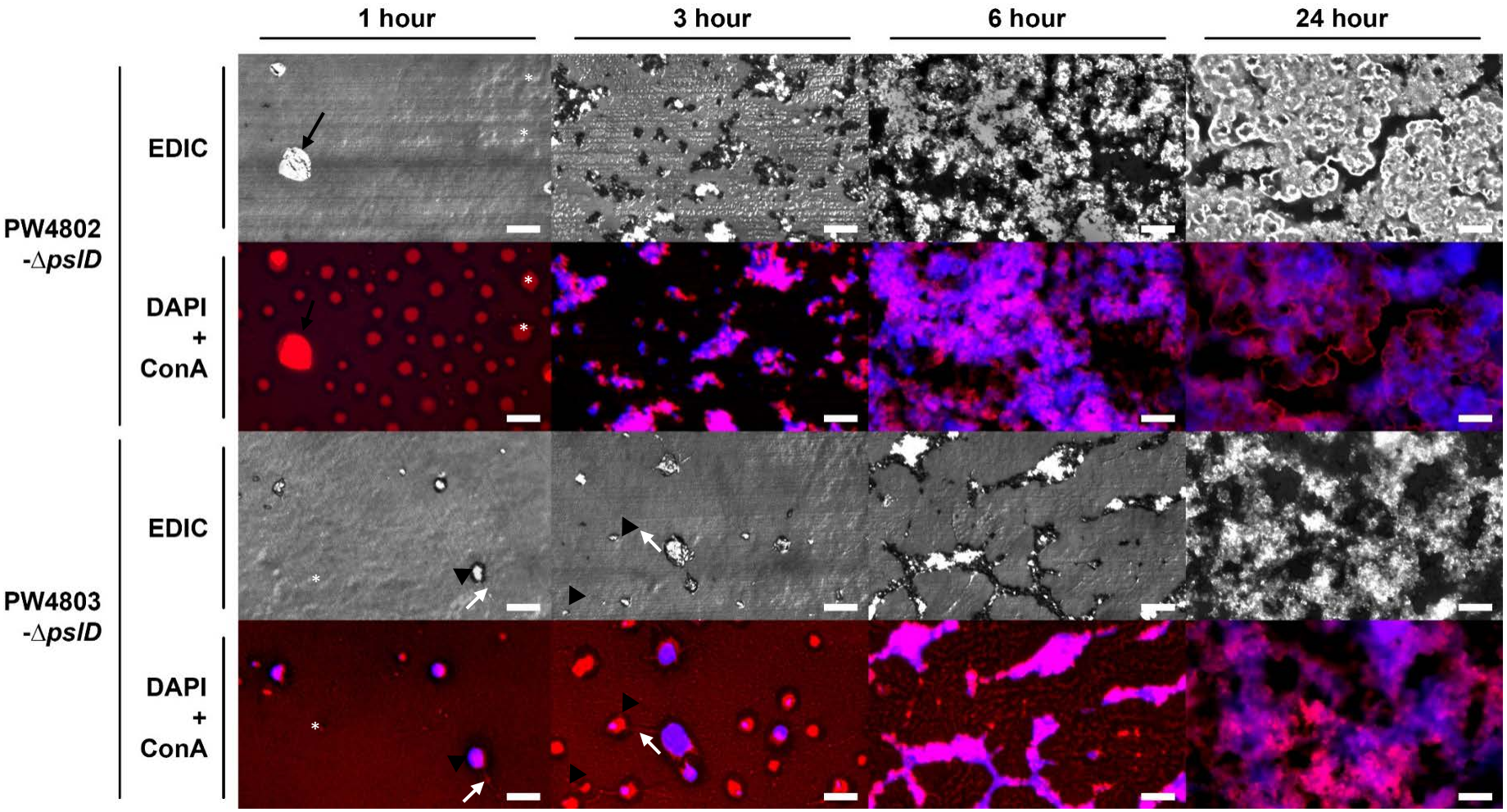

Figure 6-15 EDIC/EF images of *pslD*-negative mutant strain PW4802 (row 1 and 2) and PW4803 (row 3 and 4) at 1 h, 3 h, 6 h and 24 h. Asterisks denote the location of detached cells based on the "footprint" in the ConA stained image. Birefringence were observed from first hour in PW4802 (black arrow, first row, first column). As seen previously, the filamentous structure (white arrows) forms a connecting bridge between nearby microcolonies (black arrowheads).

The PW4802 strain featured the amorphous crystallised multilayer biofilm at the 6 h, which was similar to the PW4803 strain biofilm at 24 h. However, at 24 h, PW4802 biofilm has differentiated with heightened level of crystallised biofilm that looked like canopies. During these times, no central hollowing feature was observed in both strains. Between the two *pslD* mutants, the PW4802 strain showed a faster onset of overall biofilm development compared to strain PW4803.

Other *psl* gene mutants used were the *pslG* mutant pair PW4807 and PW4808. Both *pslG* gene mutant strains showed very few attached cells in the beginning of incubation. For strain PW4807, cell aggregates were observed at the 3 h timepoint with signs of filamentous radials sprouting out the microcolonies. At 6 h, PW4807 biofilm differentiated further to macrocolonies with crystallisation formation and filamentous radials emerging from the sides. Several individual cells were also observed attached to the catheter surface.

The ConA image showed more concentrated EPS production covering the biofilm than the surface. The PW4807 strain showed the familiar amorphous multilayer biofilm characteristics at the 24 h timepoint, with several void areas observed revealing the catheter surface. However, no central hollowing was observed in the biofilm indicating that seeding dispersal has not occurred. Although *pslG* mutant strain PW4808 showed no significant differences in cfu compared to wildtype, the biofilm formation showed characteristic disparity between them. Overall observation of the PW4808 strain showed there was no biofilm differentiation within the 24 h incubation and the biofilm formation lacked multi-layer structures compared to wildtype despite showed evidence of EPS (D-mannose-based polysaccharide) production in the ConA images (Figure J-7, Appendix J).

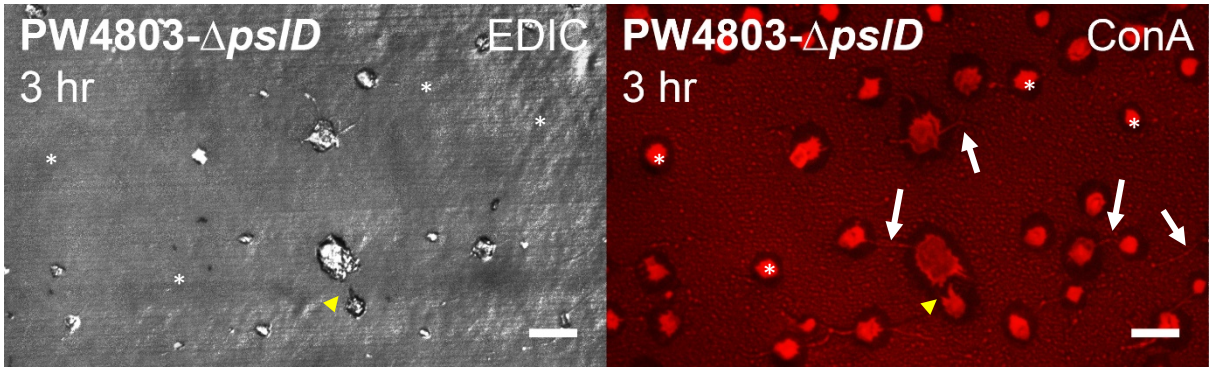

Figure 6-16 The *pslD*-negative microcolony formation mutant biofilm at 3 h.
The ConA image shows the EPS layer produced is distinctly different that the *pelA* mutant biofilm (Figure 6-14) and covers beyond the boundary of the microcolony (yellow arrowhead). The filamentous tracks were clearly visualized in the ConA image white arrows). Magnifications × 1000, scale bars = 10 µm.

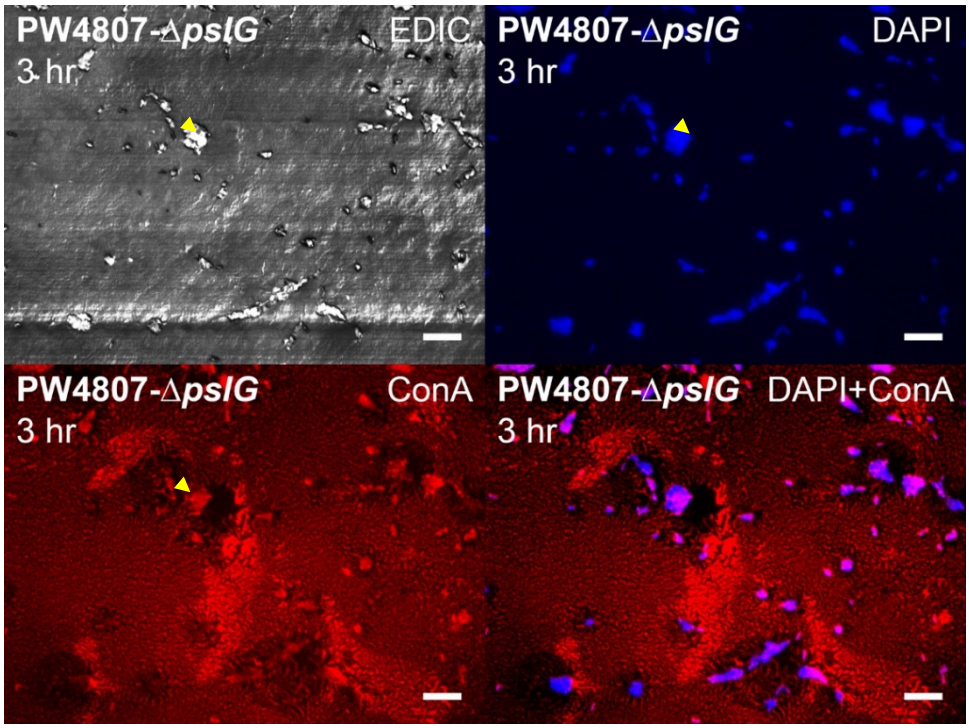

Figure 6-17 The *pslG*-negative strain PW4807 microcolony formation mutant biofilm at 3 h. The ConA image shows the EPS layer produced is distinctly different that the *pelA* mutant biofilm (Figure 6-14) and covers beyond the boundary of the microcolony (yellow arrowhead) and produces a conditioning film on the urinary catheter. Magnifications × 1000, scale bars = 10 µm.

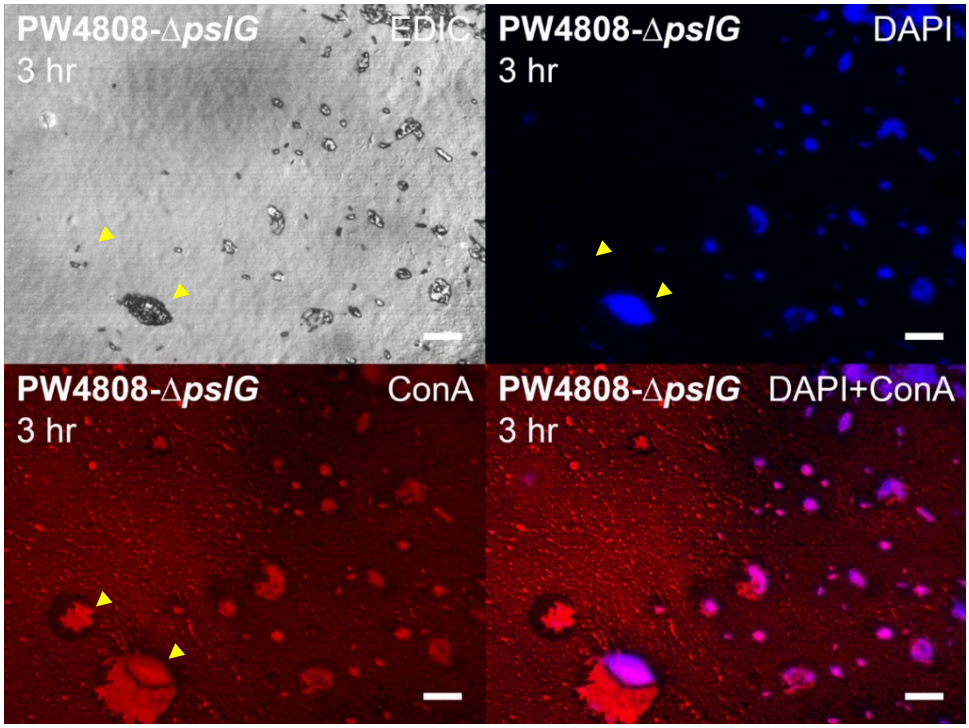

Figure 6-18 The *pslG*-negative strain PW4808 microcolony formation mutant biofilm at 3 h present the formation of aggregated cells and the EPS accumulation that covers the microcolony (yellow arrowhead) and the extended areas around it. Magnifications × 1000, scale bars = 10 µm.

6.3.4.3 The hyper alginate mutant, *mucA* and alginate-negative mutant, *algD*.

The *mucA* mutant PW2387 showed less visible bacterial attachment at the 1 h timepoint that corresponds with the cfu data shown in Section 6.3.3, although there was evidence of material conditioning the catheter surface observed from the ConA image (Figure 6-19). The 3 h biofilm image shows bacterial attachment with some cells aggregating together, with a copious amount of ConA-stained EPS covering the catheter surface. The unique fibrinous track was present and distended from the microcolonies, forming a dendritic pattern and forming a bridge that guides incoming cells towards the microcolonies. There were more merged cell aggregates at the 6 h timepoint, forming the initial microcolony network of biofilm on the surface. The ConA image at 6 h showed obvious concentrated EPS covering the bacterial cells and the catheter surface. The PW2387 biofilm differentiated further at 24 h with wider microcolonies that have merged. Even though at this timepoint the biofilm has proliferated and created multilayers of biofilm on the surface, the structure was distinctly different that the amorphous multilayer biofilm phenotype observed in wildtype at 24 h.

Both *algD* gene mutants, PW6997 and PW6998, showed very few attached cells in the beginning of incubation even though there were no statistical differences found from the cfu/catheter section data compared to wildtype at 1 h. However, the PW6997 strain showed unusual biofilm formation at 3 h that was similar to glue-like that is sticking the cells together, even though the cfu/catheter section data was significantly less than wildtype. There were radial features observed sprouting from the cell aggregates, but these radials bonded with the ConA indicating that the radials here were from the EPS. At 6 h the microcolonies were spread apart covering the catheter surface with signs of filamentous radials sprouting from the microcolonies. Similarly, these radials were also bonded with ConA, which can be clearly seen from the ConA image. The ConA images showed concentrated production of EPS within the bacterial biofilm. However, no filamentous tracks were observed in this strain. The 24 h biofilm of PW6997 strain showed occlusion of catheter surface by biofilm that was in the initial stage producing the amorphous biofilm characteristic.

For the other *algD* mutant, strain PW6998, characteristics were similar to wildtype when comparing the EDIC images across all timepoints. At 3 h timepoint, there were many attachments of individual cells and cell divisions can be observed. Several groups of closely packed cells were seen, but there were no signs of filamentous structure. At 6 h, there were microcolonies formed among many other individual attached cells on the catheter surface. The ConA image at 6 h showed that the EPS covered the catheter surface but more concentrated in the biofilm.

The 24 h biofilm features the amorphous crystalline multilayer three-dimensional biofilm structure that has partial occlusion of the catheter surface. No central hollowing was observed from the biofilm and there were areas of voids that were not covered by biofilm that suggests either the biofilm is in the initial maturation stage or there has been irrigation dispersal of the biofilm instead.

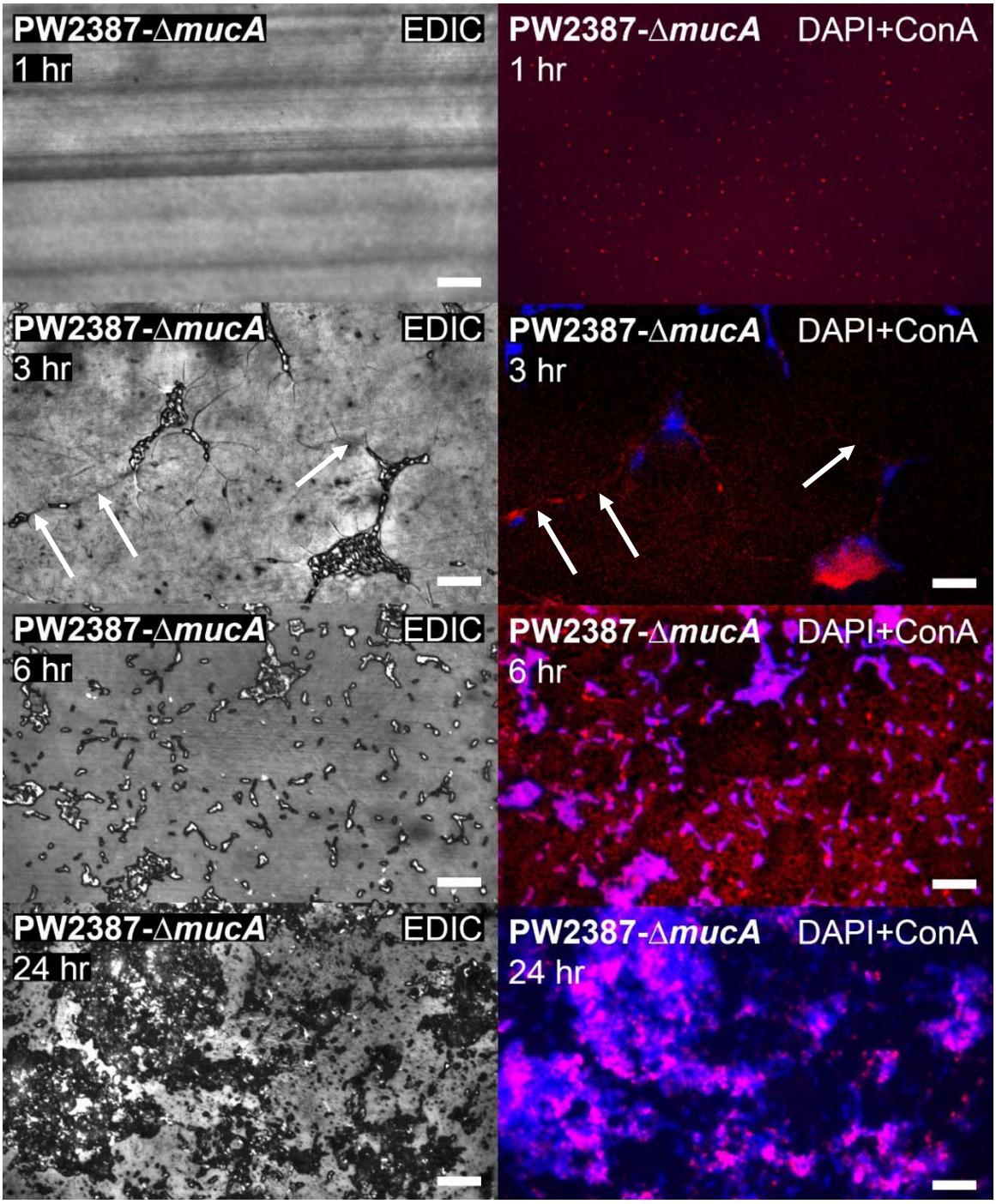

Figure 6-19 EDIC/EF images of *mucA*-negative mutant strain PW2387 at 1 h, 3 h, 6 h and 24 h. Although less attachment observed at 1 h, *mucA*-negative mutant able to form microcolonies at 3 h with the presence of fibrinous structure (white arrows) that forms a connecting bridge between nearby microcolonies. Magnifications × 1000, scale bars = 10 µm.

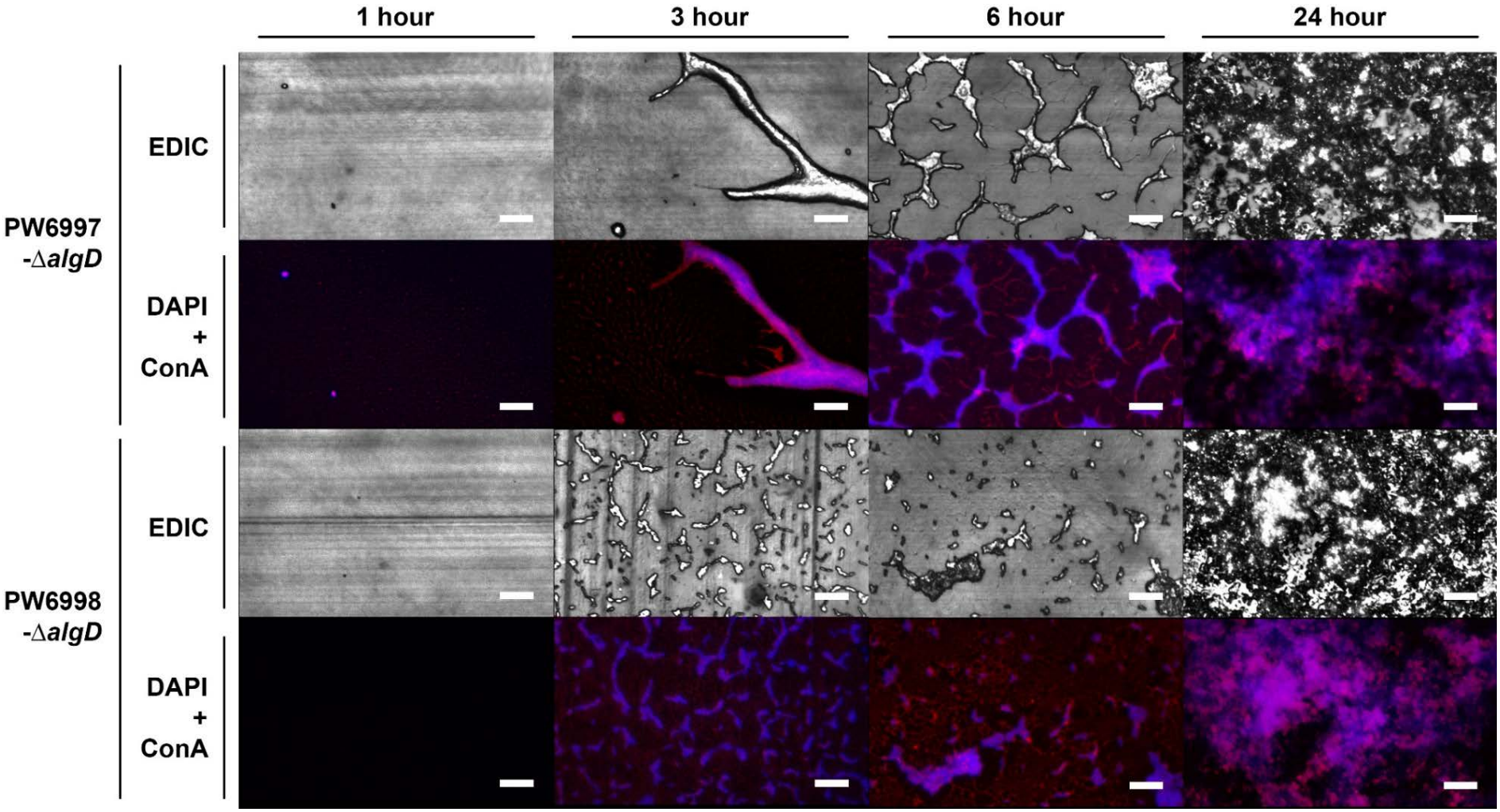

Figure 6-20 Sequential images of *algD*-negative mutant strain PW6997 and PW6998 biofilm development observation at 1 h, 3 h, 6 h, and 24 h using EDIC/EF microscopy. Magnifications × 1000, scale bars = 10 µm.

6.4 Discussion

6.4.1 Overall observation on biofilm enumeration between QS and PS

Overall, the biofilm enumeration data for both QS and PS mutant groups showed that there are abundant cells attached and forming biofilm on the catheter surface even without the QS or PS essential genes when grown in artificial urine media. This indicates that the mutation in the QS or PS genes did not totally abrogate bacterial adherence to the catheter surface. We also found that the artificial urine media from Brooks and Keevil (1997) is a supporting growth media for these mutated uropathogens.

6.4.2 Overall observation on QS-negative mutants biofilm enumeration

Collective observation on the biofilm enumeration data for QS-negative mutants showed no reduced biofilm growth, instead, almost all strains had more significant growth than wildtype at the 3 h and 24 h timepoints. This is because of the density-related events during these times suggesting that *P. aeruginosa* downregulates *lasI*, *rhlI*, *pqsA* and *pqsE* in the QS system. At 3 h was the time when microcolony formation begins, and as we have seen before, neighbouring cells start to migrate towards the nearest biggest microcolony (Heydorn *et al.* 2002; Jennings *et al.* 2015; Ogilvie *et al.* 2015). The next biggest physiological shift in biofilm formation happens at 24 h when microcolonies differentiate and develop further into mature biofilm consisting of macrocolonies (Costerton *et al.* 1999; Heydorn *et al.* 2002; Yang *et al.* 2011). The similar results to wildtype at 1 h and 6 h, is probably due to a compensation mechanism by the mutants as LasI (LasI/R) and RhlI (RhlI/R) work in tandem in controlling various biofilm-related QS regulation in *P. aeruginosa* (Davies 1998; Davey *et al.* 2003; Roy *et al.* 2011).

While other QS-negative mutants were mostly unaffected in the first hour, rhamnolipid mutant PW6884-Δ*rhlB*, showed strong evidence of significantly less (< 2 $\log_{10}$ cfu/catheter section) biofilm compared to wildtype, which it continued to have reduced biofilm subsequently at 3 h and 6 h as well. Our study shows that rhamnolipid is an important biosurfactant that is needed during early biofilm formation events. The *rhlB*-negative mutant biofilm growth was severely affected with the *rhlB* gene deficiency in *P. aeruginosa.* Recent studies conducted on the role of rhamnolipid in biofilm formation show that it is a novel biosurfactant that promotes swarming motility and affects the biofilm formation and its structure (Deziel *et al.* 2003; Zhu and Rock 2008; Kearns 2010; Tolker-Nielsen 2014).

It has also been shown that rhamnolipids improves the PQS signalling system by increasing the solubility and bioactivity (Caiazza *et al.* 2005). At the same time, production of rhamnolipids as biosurfactant in the early biofilm formation is a form of prevention mechanism in facing environmental stress (Deziel *et al.* 2003; Campisano *et al.* 2006). Our findings include that *rhlB* has a more prominent role in biofilm formation compared to *rhlA*. This is also supported by Davey *et al.* (2003) that similarly reported *rhlA* is not required for the initiation of biofilm development, only in macrocolonies.

Zhu and Rock (2008) have reported that rhamnolipids cannot be produced without *rhlA* and *rhlB* genes, which is supported by Kiran *et al.* (2016) that both *rhlA* and *rhlB* are needed to produce rhamnosyl transferase I. However, our earlier understanding about rhamnolipids from Caiazza *et al.* (2005) is that the rhamnolipid precursor, 3-(3-hydroxyalkanoyloxy) alkanoic acids (HAAs), were produced by RhlA but not RhlB. It is further explained that RhlA is required in making HAAs, but RhlB is the assigned rhamnosyl transferase (Deziel *et al.* 2003; Zhu and Rock 2008). The final step in rhamnolipids production involves rhamnosyl transferase RhlB and RhlC to produce monorhamnolipid and dirhamnolipid. However, RhlB can produce both monorhamnolipid and dirhamnolipid, while RhlC only catalyses for dirhamnolipid production (Caiazza *et al.* 2005). This supports our biofilm results for PW6884-Δ*rhlB* mutant that seemed to be more affected by the *rhlB* gene deficiency compared to *rhlA* mutants.

The quinolone signalling system (PQS) is one out of three cell-to-cell signalling systems in *P. aeruginosa* and it is controlled by the *pqsABCDE* operon. Our study includes the two genes from the PQS operon, *pqsA* and *pqsE.* The PQS system requires the *pqsABCDE* gene but can function without the fifth gene *pqsE* as only *pqsA* is involved in the PQS signalling system.

Increased bacteria (> 1 $\log_{10}$ cfu/catheter section) in the first hour by *pqsA* mutants evidently showed that it might be involved in the reversible/irreversible attachment and microcolony formation in the first 3 h. Similarly, our results showed that approximately one log more biofilm growth than wildtype at 24 h timepoint indicates that PqsA might be a necessary gene in the early maturation phase of the biofilm as well.

Compared to *pqsA*, the *pqsE* gene does not have a role in the initial attachment phase and might indicate a complementary relationship with the *pqsA* gene during biofilm formation. Strong evidence of increased biofilm growth in the 3 h timepoint might indicate that PqsE has a role during irreversible attachment and microcolony formation. Evidence of increased growth differences compared to wildtype in the following 6 h timepoint implies that the gene is still relevant during the macrocolony formation in the biofilm development.

Biofilm development of PW2806 in the 24 h is still similar despite the deficiency in *pqsE*; in fact, PW2807 shows evidence that PqsE is possibly responsible for inducing biofilm dispersal. PqsE is also known as the response effector in the PQS system even though it is not required for the PQS biosynthesis. It can independently control PQS system and is responsible in causing multiple virulence factors during an infection (Farrow *et al.* 2008; Wesseling 2015; Viducic *et al.* 2016). The PQS signalling system and the AHL signalling system interface is complex but it is reported that *pqsE* is the link between these two systems (Gallagher *et al.* 2002; Farrow *et al.* 2008; Rasamiravaka *et al.* 2015; Rampioni *et al.* 2016). Thus, the role of *pqsE* has not been well understood, even though its regulation indirectly controls various virulence factor expression, such as pyocyanin, eDNA, phenazine and rhamnolipids (Gallagher *et al.* 2002; Allesen-Holm *et al.* 2006; Wei and Ma 2013; Viducic *et al.* 2016). Schaber *et al.* (2004) also reported that the PQS system is not essential for *P. aeruginosa* to establish infection and goes through a coping mechanism to substitute the loss of the PQS-controlled virulence factors in place.

6.4.3 Microscopy observation of QS-negative mutants biofilm formation

From the EDIC images, we found that not all QS-negative mutants (rhlI, lasII, pqsA, and pqsE) have the capability to form three-dimensional biofilm structure similar to wildtype at 24 h, but produced undifferentiated, flat biofilm instead. Despite the flat undifferentiated biofilm produced by the QS-negative mutants, the corresponding higher enumeration data than wildtype could indicate that without the QS genes, broken down cellular communication prevented biofilm to differentiate, and prevented the dispersal events. Several studies in the past have reported similar undifferentiated and flat biofilm produced by QS mutants that supported our finding (Heydorn *et al.* 2002; Schaber *et al.* 2007; Tolker-Nielsen 2014).

Previous studies also reported similarly to our observation in QS-negative mutant biofilm of loss of three-dimensional microcolony structure as seen in wildtype (Davies 1998; Vega *et al.* 2014). Davies (1998) observed that the loss of microcolony structure and water-channel characteristic in *lasI* mutants mature biofilm could be restored by adding exogenous AHLs, suggesting the importance of QS cell signalling in biofilm development (Davey *et al.* 2003; Vega *et al.* 2014).

Additionally, similar observation by Sakuragi and Kolter (2007) and Wei and Ma (2013) on *las* mutants that also produced flat biofilm that is susceptible to detergents. A study by De Kievit (2009) reported that *pqsA* mutant produced flat and this with very small quantity of eDNA that affected the biofilm integrity and structure.

The defect in mature biofilm formation was probably caused by multifactorial reasons as QS system controls various biofilm mechanism such as swarming, eDNA, and rhamnolipids as well. This means that, in absence of essential QS gene, defective QS system and broken cell-cell communication affects mature biofilm formation and structure in *P. aeruginosa.*

On the other hand, the rhamnolipid-negative mutants, *rhlA* and *rhlB,* showed disparate biofilm development between them even though the mutants are able to produce wildtype-like three-dimensional biofilm structure. Both *rhlA*-negative mutants showed highly ordered geometric microcolonies organisation that could probably be due to the abrogated swarming capability by HAAs as reported by Deziel *et al.* (2003), which were not observed happening in *rhlB*-negative mutants. This is also supported by Caiazza *et al.* (2005) that speculated group behaviours such as swarming will be affected in rhamnolipids mutants.

6.4.4 Overall observation on PS-negative mutants biofilm enumeration

PS-negative mutants showed contrasting biofilm formation compared to QS-negative mutants which most showed reduced biofilm growth at 1 h and some mutants continued having less biofilm than wildtype at 3 h and 6 h timepoints. By 24 h, the biofilm enumeration data for all PS-negative mutants were indifferent to wildtype.

The first hour is a crucial time as the interplay of reversible and irreversible attachment events, depending heavily on the initial bacteria adhesion process to kick off the early biofilm formation on the catheter surface. PW6141-Δ*pelA*, PW4802-Δ*pslD*, PW4803-Δ*pslD*, and PW4807-Δ*pslG* showed significantly less biofilm at 1 h showing that PelA and PslD in polysaccharide production are important during this early biofilm initiation events, to ensure successful attachment of bacteria to the surface. This finding follows a previous study by Jones and Wozniak (2017) which reports the microscopy observation of reduced adhesion in *psl*-negative mutant biofilm formation. This also supported our finding that Psl is most important among the strains tested as the *pslD* gene deficient strain showed reduction effect on biofilm enumeration, observed in 3 and 6 h as well.

However, alginate over production can become a deterrent in biofilm growth, as shown by the hyper alginate mutant PW2387-Δ*mucA* at 1 h timepoint. Contrastingly, both *algD*-negative mutants showed no significantly different biofilm compared to wildtype for all timepoints throughout the 24 h incubation. Flemming and Wingender (2010) reported the involvement of alginate in microcolony formation but our study showed that *algD* is downregulated during microcolony formation at the 3 h timepoint.

Similarly, our finding at 24 h also does not agree with their study that suggested alginate is responsible in maintaining mechanical stability in mature biofilm. This is clear indication that Pel and Psl polysaccharide components in the EPS produced by *P. aeruginosa* is important and that the composition for both are controlled to ensure maintenance of stable biofilm development during the first 24 h.

6.4.5 Microscopy observation of PS-negative mutants biofilm formation

Both PslD and PelA showed importance on early biofilm formation based on biofilm enumeration results however both genes produced different biofilm structure as observed under the EDIC microscope. Aggregated cells induce self-produce EPS that accumulate according to the aggregation size in order to improve the matrix stability and structure (Toutain *et al.* 2004). Psl is a galactose-mannose-rich EPS with relatively lower amounts of glucose and xylose (Ma *et al.* 2006; Ma *et al.* 2007; Byrd *et al.* 2009; Franklin *et al.* 2011; Colvin *et al.* 2012; Wei and Ma 2013; Baker *et al.* 2015). This contributes to the ability to visualise Psl presence in the EPS using the ConA stain. A previous study by Jennings *et al.* (2015) suggested that Pel consists of mainly glucose but its structure remains unknown. However, the ConA-stained EDIC images of both *pelA*- and *pslD*-deficient mutants showed that the D-mannose component in the EPS were formed and concentrated differently from each other.

Both Psl and Pel are important polysaccharides during the initial phase where the cell adheres to the catheter surface, as supported by previous study by Jennings *et al.* (2015). However, similar to precious studies, deletion of *pel* gene did not give any significant impact to the biofilm formation (Yang *et al.* 2011; Colvin *et al.* 2012).

The advantage in our report is the images taken of the D-mannose component in the EPS that added more visual understanding on the biofilm matrix that does not correlate with previous studies. Chew *et al.* (2014) reported that the EPS matrix became more viscous in absence of Psl that facilitates biofilm expansion on the surface. However, our ConA image on *pelA*-deficient and *pslD*-deficient showed that this is otherwise.

The *pelA*-negative mutant showed the self-produced EPS is viscous-like and accumulates around the near parameter but beyond the boundary of the microcolony (Figure 6-14). This is conversely opposite to Chew *et al.* (2014) who reported that without Psl the matrix became more viscous and facilitates the biofilm spreading.

Previous studies also show that the self-produced Psl will surround the *P. aeruginosa* PAO1 cell and increase cell interaction with surface and other cells (Ma *et al.* 2007; Yang *et al.* 2011). This is also supported by a previous study by Colvin *et al.* (2011) that has similarly found that Psl in *P. aeruginosa* PA14 strain is important to maintain the cell to cell interaction.

Our findings also showed that the *pslD*-negative mutant produced distinctly different EPS than the *pelA*-negative mutant*,* which appeared as a thin and less viscous-like conditioning layer, which concentrated more within the boundary of the microcolony (Figure 6-16). Differentiation of EPS that is lacking PslD has also been observed by Campisano *et al.* (2006) in their study using *P. aeruginosa pslD* knockout mutant grown in continuous-culture flow cells with mineral medium. However, even though the EPS biofilm produced were lacking characteristic and structure, they still support our findings that Psl is an important function in biofilm microcolony formation (Campisano *et al.* 2006).

Additionally, comparison of EDIC and ConA images of *pslD* mutant biofilm showed evidence of cell "footprints", or marked presence left by detached cells that is more prominent than in other strains. This could help explain why the consistent less biofilm for *pslD*-negative mutant compared to wildtype could be due to lack of strength in bonding the attached cells to the surface. Among all strains, the *pslD*-negative mutant showed the most EPS observed in the ConA-stained images.

This observation has been discussed previously by Jones and Wozniak (2017) and Colvin *et al.* (2012) that Psl functions as sticky EPS material that aids in adherence, which in infection it mediates adhesion to human airway cells. Our results also agree with previous literature that *pslD* is an essential gene in Psl production in EPS for biofilm formation and development (Campisano *et al.* 2006; Ma *et al.* 2007; Byrd *et al.* 2009).

The reduced biofilm enumeration and the presence of cell "footprints" observed in *pelA*-negative and *pslD*-negative mutants' biofilm were similarly observed in studies by Neu and Marshall (1991) and El-Kirat-Chatel *et al.* (2014), show that these polysaccharides are important during initial cell attachment. El-Kirat-Chatel *et al.* (2014) also reported in their study of *P. fluorescens* LapA-based footprints distribution and adhesion biophysical properties using atomic force microscopy (AFM), suggesting that LapA enables cell attachment to various surfaces. Although this study suggested that the self-produced surface adhesins indicated by cell "footprints" serves as bridging polymers, the role of LapA surface adhesin in *P. aeruginosa* urinary biofilm formation has not yet been determined.

Pel and Psl are both major polysaccharides produced in PAO1, but the preferred primary polysaccharide is Psl, although Pel can be used to compensate where Psl is insufficient (Colvin *et al.* 2012; Jennings *et al.* 2015). A study by Jennings *et al.* (2015) has reported that the predominant role of Psl in maintaining biofilm structure will be compensated with the produced Pel instead in Psl-deficient mutants. Our finding agrees with the report by Jennings *et al.* (2015) that both Psl and Pel are localised in the biofilm periphery, but our report also showed the visualisation of these effects to the biofilm structure in the absence of Psl or Pel.

In absence of Psl, the Pel will structurally form the biofilm periphery, and the Pel-eDNA combination maintained the biofilm stalk in mature biofilm formation (Jennings *et al.* 2015). Our study does not necessary agree with report by Ma *et al.* (2006) that Psl is important in maintaining biofilm structure post attachment as we found this is only true for early biofilm formation and that the mature biofilm development had no problem in progressing by 24 h.

Although Byrd *et al.* (2009) reported that genes *pslACDEFGHIJK*L are essential for biofilm formation, a later study by Winsor *et al.* (2011) reported that deletion to genes *pslA* to *pslD* are sufficient to incapacitate the Psl production in PA14 biofilm formation. Our studies showed strong positive corresponding results where *pslD* mutant has significant decreased biofilm in the first 6 h compared to wildtype.

6.4.6 Alginate showed no importance in biofilm formation in 24 h

We observed the hyper alginate *mucA*-negative mutant biofilm formation resulted in less biofilm enumeration at 1 h compared to wildtype, which was similarly reported by (Caldara *et al.* 2012). As explained in Caldara *et al.* (2012), the overexpression of alginate increases viscosity around the cells that promote cell to cell adhesion and restrict filamentous bridging. Additionally, Ghafoor *et al.* (2011) reported the close link between Pel and alginate; that both are needed to form the mushroom tower structure in mature biofilm, but our finding shows that this is not the case. From our observation at 24 h, the hyper alginate *mucA* is not able to form tower structure biofilm, while our *pelA*, *pslD* and *pslG* mutants are able to form three dimensional structures in mature biofilm. Since our study does not continue beyond the 24 h timepoint, we could not eliminate the possibility that the *mucA* mutant biofilm formation might be delayed.

Even though Lebeaux *et al.* (2014) has identified that alginate is among the important factors in stabilising abiotic and biotic *P. aeruginosa* biofilms, our findings offer a different perspective, namely that alginate might not be a significant component in the urinary biofilm EPS.

Alginate was thought to have a role in biofilm formation as the EPS matrix of mucoid strains were predominantly consisting of alginate that contributes to its antibiotic resistance (Hay *et al.* 2009; Colvin *et al.* 2012). Additionally, *P. aeruginosa* SG81 was reported to have a high content of approximately 2:1 ratio of alginate to protein in its biofilm components, which represents roughly around 0.79 of weight ratios (Baum *et al.* 2009). However, our studies do not show that alginate has an important role in the biofilm formation from our observation within 24 h of study.

6.5 Conclusion

Schaber *et al.* (2007) reported that biofilm formation is independent of quorum-sensing (QS), even though there have been several studies reporting the indirect relationship between QS and polysaccharide (PS) production in *P. aeruginosa* biofilms (Sauer *et al.* 2002; Schaber *et al.* 2007; Flemming *et al.* 2016; Mund *et al.* 2017). Our study provides notable inputs that contribute to the whole picture by conducting biofilm formation capability screening using *P. aeruginosa* mutants that are deficient of QS and PS essential genes.

We also established that gene regulation in QS and PS production are both vital but were not necessarily needed at the same timepoint during biofilm development. Overall, we find that PS plays an important role in aiding cell adhesion during initial attachment, as well as being involved in the structural component of the biofilm microcolony. Our results show that at 1 h, additionally both Pel and Psl polysaccharide production are important, and that Psl is an important adhesive component in the polysaccharide that helps stick the cell to the surface as well as forming the structure of the microcolony in PAO1 biofilm formation. This is from our observation that *pslD* gene mutation produced an adverse biofilm reduction compared to wildtype. It also severely delayed the biofilm formation due to less self-produced EPS matrix. Lack of *pslD* impaired Psl production that causes weak interaction between cells and surface which leaves “footprints” of detached cells in the ConA-stained EPS in the biofilm.

Past studies have described the added benefits of Psl component in EPS other than adhesion and maintaining the three-dimensional biofilm structure such as protection against dehydration, host-cells or environmental stresses, as well as increased antibiotic tolerance (Campisano *et al.* 2006; Ma *et al.* 2006; Irie *et al.* 2017; Murakami *et al.* 2017). We also able to show visual evidence that Pel is able to compensate for the absence of Psl in maintaining biofilm microcolony structure. Conversely, we found that alginate did not play any important role in biofilm formation on the urinary catheter, compared to Psl and Pel.

Our data also show that the effect of these mutational changes at best only delays the onset of the biofilm formation but did not totally abrogate it (Okshevsky *et al.* 2015). Study by Okshevsky *et al.* (2015) using a DNase-based anti-biofilm coating showed promising results in delaying biofilm formation up to 14 h. Biofilm formation life cycle can be expedited or delayed depending on various factors such as surface condition, nutrient availability and strain readiness to transform from planktonic to biofilm state of growth (Ma *et al.* 2007; de Melo *et al.* 2013) (Gloag *et al.* 2013; Chu *et al.* 2018). However, all PS-negative strains used in this study were not able to completely abrogate biofilm formation by 24 h.

Studies on QS are important as it is a unique property that only exists when bacteria in the body form biofilm. Our findings suggest that the QS genes are downregulated during high-populated events such as microcolony and macrocolony formation in *P. aeruginosa* PAO1 biofilm development. This revelation from our results brings concern on common biofilm prevention research themes that focuses on QS inhibitor molecules as a solution (Lebeaux *et al.* 2014).

Among QS inhibitor molecules widely used to combat general as well as urinary biofilm research are catechin (from *Combretum albiflorumbark* extract) and halogenated furanones (from red alga *Delisea pulchra*) that use a competitive binding mechanism to the transcriptional activator protein, interfering with the function of AHL (Kim *et al.* 2005; Siddiq and Darouiche 2012; Tolker-Nielsen 2014; Goncalves *et al.* 2015).

Tannic acid, proanthocyanidins, citrate or other components in cranberry extract were widely used in research for their effect against biofilms, due to their ability to reduce crystalline biofilm in urinary catheter (Stickler 2008; Jones *et al.* 2009; LaPlante *et al.* 2012; Pammi *et al.* 2013; Cai *et al.* 2014; Rane *et al.* 2014; Rasamiravaka *et al.* 2015). Previous study on *P. mirabilis* biofilm showed growth reduction after being exposed to QS inhibitors such as tannic acid (TA) and *p*-nitrophenyl glycerol (PNPG) (Jones *et al.* 2009). However, Jones *et al.* (2009) reported no significant differences were found in biofilm and planktonic growth when exposed to the same concentration of TA, suggesting that QS is only available in the biofilm state. This shows that this study is important in order to understand better the role of QS in controlling biofilm growth on urinary catheters in physiologically relevant, artificial urine.

Additionally, we also studied the role of rhamnolipids as they are expressed together in the Rhl QS system. During the first hour of incubation where initial attachment events are anticipated to occur, only *rhlB* showed approximately 2-log fewer bacteria in biofilm compared to wildtype while the rest of the QS gene deficient strains were unaffected.

Our finding shows that rhamnolipid production is separate to the Rhl system and their expression could have been controlled by other regulatory genes that are involved in the biofilm formation. This also means that rhamnolipids have a role as an important biosurfactant during cell attachment in the urinary biofilm formation.

In this study, biofilm formation was not examined over a longer time period (longer than 24 h), therefore any possible QS or PS gene mutation influences in biofilm development in time period longer than 24 h could not be excluded. This could be considered in planning future studies on observing the biofilm growth of these QS and PS mutants in mature biofilm development (longer than 24 h).

Other future studies that could be conducted following this study include the use of double mutants combining QS and PS gene mutation in biofilm growth on urinary catheter. Additionally, we could extend our findings by studying the Pel and Psl regulation mechanism and their functional and expression profiles for future work in bioremediation of biofilm formation since we observed that Pel could compensate for the preferred Psl produced in the biofilm periphery.

This new information also contributes to the knowledge of which essential genes for urinary biofilm formation in *P. aeruginosa* PAO1. This study provides notable importance, as to the best of our knowledge there is no similar study that describes the morphology of the biofilm formation on the urinary catheter grown during the first 24 h of growth using urine media.

Chapter 7 Study of Essential Genes in Attached/Motility Mutants of *Pseudomonas aeruginosa* Biofilm in Artificial Urine Media (AUM)

7.1 Introduction

This chapter is the continuation of previous chapters and the final chapter of the three-part *P. aeruginosa* biofilm study series, where we investigated the role of cell surface appendages in *P. aeruginosa* PAO1 urinary biofilm formation by utilising the attachment and motility (AM) gene-deficient mutants grown in artificial urine media. *P. aeruginosa* is an ideal model organism for this study as it is the most common opportunistic pathogen that causes acute or chronic infection, including CAUTI, and remains the major pathogen in cystic fibrosis (Ma *et al.* 2007; Burrows 2012; Conrad 2012; Guttenplan and Kearns 2013; Haiko and Westerlund-Wikstrom 2013; Wesseling 2015).

Both flagella and type IV pili have been associated in the early biofilm formation that involves bacterial attachment and microcolony formation, and an important factor in biofilm development (O'Toole and Kolter 1998; Pratt and Kolter 1999; Whiteley *et al.* 2001; Klausen *et al.* 2003b). Focusing on the initial stages of infection, Figure 7-1 shows the five previously identified flagella and pili genes mediating adherence and surface colonisation of bacteria, which are *fliA, fliC, fliM, pilA* and *pilF* (Alm and Mattick 1997; Klausen *et al.* 2003b; Koo *et al.* 2008; Terashima *et al.* 2008; Conrad *et al.* 2011; Burrows 2012; Conrad 2012; Haiko and Westerlund-Wikstrom 2013; Lassek *et al.* 2015; Chua *et al.* 2016; Francis *et al.* 2017). The eleven *P. aeruginosa* PAO1 mutants consist of eight transposon mutants, and three knockout mutants of surface appendage genes involved in attachment/motility (AM), which from here on will be referred to as the AM-negative mutants.

The *in vitro* laboratory model system for biofilm assay previously described by Wilks *et al.* (2015) used in the previous chapter was utilised to grow the mutant biofilm on urinary catheter pieces in artificial urine media, Brooks and Keevil (1997). After several time intervals up until 24 h, the bacterial attachment was observed via colony-forming-unit enumeration of the biofilm, and the biofilm formed on the catheter was visualised using the EDIC microscope.

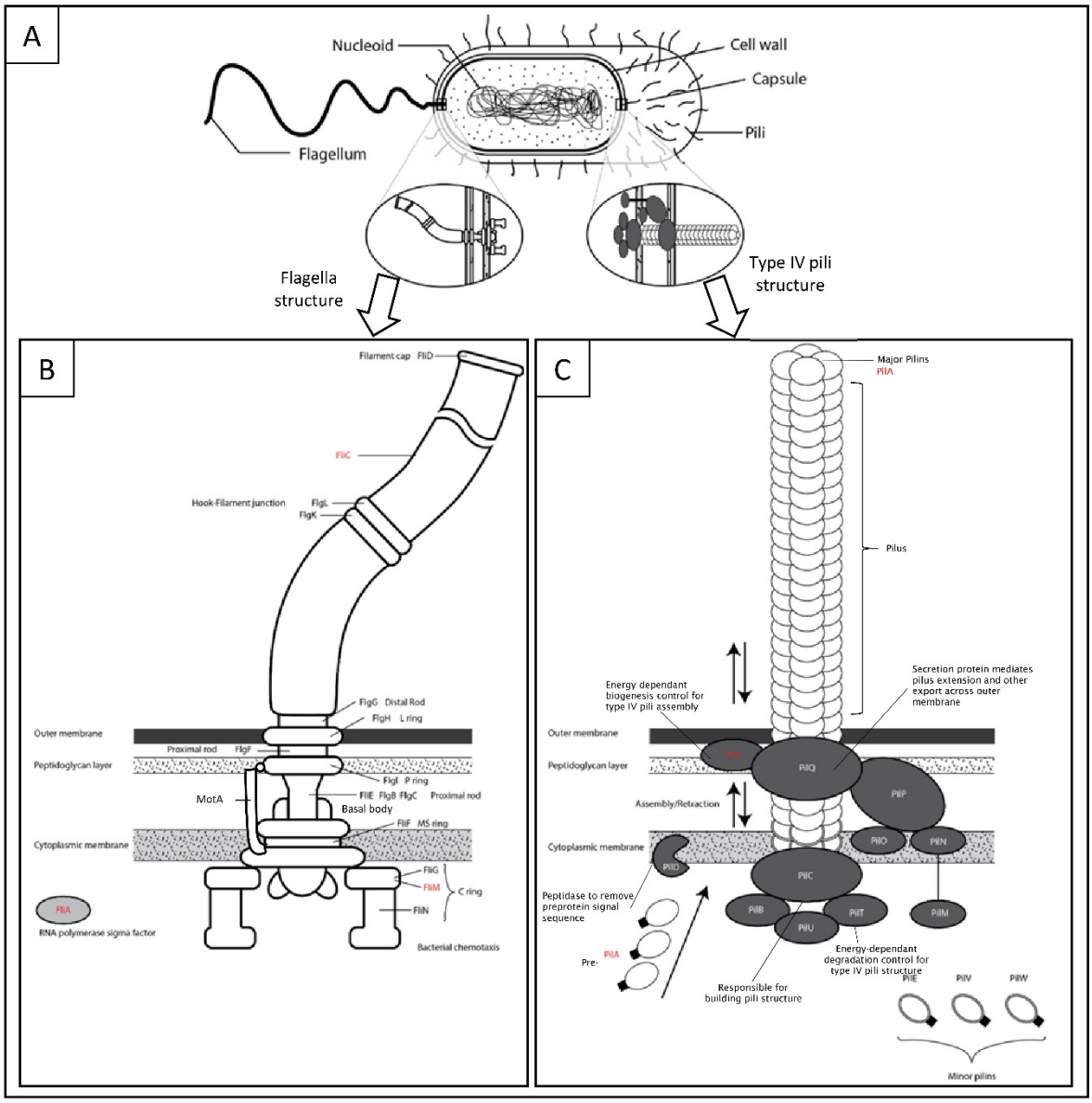

Figure 7-1 Cell-associated surface appendages flagella and pili in *P. aeruginosa*. (A) Typical *P. aeruginosa* cell diagram showing cell structures and the location of the surface appendages. (B) Schematic diagram of the mechanical components of *P. aeruginosa* flagella structure. (C) Schematic diagram of the mechanical assembly of *P. aeruginosa* pili structure. Label with the red font in B and C indicates the proteins of the selected genes used in this study.

The *P. aeruginosa* PAO1 wildtype used as the reference strain for biofilm formation is compared with the AM-negative mutant strains, particularly on the bacterial attachment and the structure of the biofilm. Previous studies had shown that these surface appendages in *P. aeruginosa* are involved in cell locomotion including twitching motility, as well as other virulent factors such as surface attachment, cellular secretion and biofilm formation (O'Toole and Kolter 1998; Klausen *et al.* 2003b; Koo *et al.* 2008; Choi *et al.* 2011; Burrows 2012; Chua *et al.* 2016; de Anda *et al.* 2017).

However, these studies used general laboratory media as the growth media, which brings out the question on how the bacterial attachment in biofilm formation would differ in using artificial media to imitate the effects of AM gene deficiency in bacterial cells in urine.

These virulent factors in *P. aeruginosa* are regulated by its well-characterised genetic pathways, but the specific environmental trigger that controls this regulation remain poorly defined (Persat *et al.* 2015). During this time of writing, the study of biofilm morphological effects that are caused by the absence of surface appendages in the urinary environment has not yet been reported. Therefore, our study will investigate the hypothesis on the biofilm produced by AM-negative mutant strains will be different than wild-type by analysing its biofilm formation on the urinary catheter.

7.2 Materials and methods

This study used the following methods for analysing biofilm formation by screening selected AM-negative mutants from the established bacterial strain *P. aeruginosa* PAO1, to identify essential genes involved in the primary function of surface appendages. Experimental plan of methods presented earlier in Figure 5-2 (Section 5.2) is used in this chapter.

7.2.1 *P. aeruginosa* PAO1 strains used in this experiment

The details of the main parental *P. aeruginosa* PAO1 wildtype reference strain AM-negative mutant strains used in this study are as shown in Table 1. The sequenced verified *P. aeruginosa* PAO1 wildtype and the transposon mutants were obtained from the Seattle *P. aeruginosa* mutant library (University of Washington Genome Sciences, USA) (Jacobs *et al.* 2003; Held *et al.* 2012).

The mutants carrying IS*lacZ*/hah or IS*phoA*/hah transposon insertions are made as previously described by Jacobs *et al.* (2003). The knockout mutant strains were generously provided by Professor Myron Christodoulides (University of Southampton, UK). Details of the reference *P. aeruginosa* PAO1 wildtype and the mutant strains were also elaborated further in Appendix F of the Appendices section which was extracted from the accompanying table (PA two-allele library) provided in the *P. aeruginosa* Mutant Library website (https://www.gs.washington.edu/labs/manoil/libraryindex.htm).

Table 7-1 *P. aeruginosa* PAO1 strains used in this chapter

Reference strain			
Name	**Bacterial strains**	**Relevant putative ORF function**	**PA ORF**
Wildtype	PAO1	*P. aeruginosa* strain ATCC 15692	MPAO1
AM-negative transposon mutants			
Name	**Bacterial strains**	**Relevant putative ORF function**	**PA ORF**
PW3643	*fliA*-E07::IS*lacZ*/hah	alternative sigma factor σ28 for flagella biogenesis mutant	PA1455
PW2970	*fliC*-G03::IS*lacZ*/hah	flagellar filament protein mutant	PA1092
PW2971	*fliC*-G10::IS*phoA*/hah	flagellar filament protein mutant	PA1092
PW3621	*fliM*-B05::IS*lacZ*/hah	flagellar motor protein mutant	PA1443
PW3622	*fliM*-D08::IS*phoA*/hah	flagellar motor protein mutant	PA1443
PW8621	*pilA*-E01::IS*lacZ*/hah	type IV fimbrial pilin protein mutant	PA4525
PW8622	*pilA*-H02::IS*phoA*/hah	type IV fimbrial pilin protein	PA4525
PW7438	*pilF*-E10::IS*phoA*/hah	type IV fimbrial pilin biogenesis lipoprotein mutant	PA3805
AM-negative knockout mutants			
Name	**Source**	**Relevant putative ORF function**	**PA ORF**
Δ***fliC***	Prof Christodoulides lab	Knockout gene flagellar filament protein *fliC* mutant	PA1092
Δ***pilA***	Prof Christodoulides lab	Knockout gene type IV fimbrial pilin protein *pilA* mutant	PA4525
Δ***fliC*Δ*pilA***	Prof Christodoulides lab	Knockout gene flagellar filament protein *fliC* and type IV fimbrial pilin protein *pilA* mutant	-

7.2.2 Inocula preparation

The inocula preparation for *P. aeruginosa* PAO1 wildtype and AM-negative mutant strains were prepared as described in Section 2.1.2. An aliquot of 1 ml of bacterial inocula from the overnight culture was centrifuged at 7500 rpm (5400 × g) for 10 min. After discarding the supernatant, the remaining pellet was resuspended using 1 ml artificial urine medium (Brooks and Keevil 1997) (AUBK) to form the inoculum. Preparation of the AUBK medium used the methods as described in Section 2.3.1.

7.2.3 Biofilm assay

Biofilm growth assay was conducted following as previously described in Wilks *et al.* (2015). Catheter sections are used with AUBK medium in the biofilm growth assay in 6-well plates. Further details of the experiment are as described in Section 2.4. Mono-strain biofilm assay of *P. aeruginosa* wildtype and AM-negative mutants were cultured independently with at least three biological replicates.

Approximately 1 cm long silicone catheter (100 % silicone, Rüsch Teleflex, UK) pieces were cut longitudinally to produce two catheter sections and placed in each well in the 6-well plates (Nunc, Thermo Scientific, UK). Each well in the plate represented a separate timepoint of incubation 1 h, 3 h, 6 h, and 24 h with the additional well for the control. One plate was used for each strain in each replication experiment.

The catheter sections in the wells were immersed in 5 ml of AUBK medium, and 100 µl of inoculum from Section 7.2.2 (final concentration of approximately 1×10^9 cfu/ml) added into each well and then incubated at 37 °C. The biofilm was allowed to grow on for 1 h, 3 h, 6 h, and 24 h. At each timepoint, catheter sections from the corresponding well were removed and rinsed with PBS solution three times and dried on tissue paper via capillary action. For every two catheter sections removed at a timepoint, one was subjected to bacterial enumeration, and the other was observed under the EDIC/EF microscope for biofilm formation.

7.2.4 Bacterial enumeration from biofilm formed on the catheter

The catheter sections (from Section 7.2.3) were transferred into 10 ml of PBS solution in a sterile tube with approximately 2 g of 2 mm glass beads. The biofilm cells were harvested by vortexing the tube for 90 s. The biofilm culture was serially diluted in PBS accordingly. Aliquots of 50 µl of the dilutions were plated onto TSA media plates in triplicate for each selected dilution and incubated at 37 °C for 18 h to 20 h before the colonies were counted. The results of the enumeration data were analysed further using statistics.

7.2.5 Statistical data analysis

The enumeration data obtained by colony forming unit per catheter section (cfu/catheter section) were transformed into logarithmic colony forming unit per catheter section ($\log_{10}$ cfu/catheter section) representing biofilm attached on the catheter at each timepoint. All enumeration values are expressed as means ± SD.

The wildtype and AM-negative mutants biofilm enumeration data analysis for statistical differences were performed using one-way analysis of variance (ANOVA) followed by Dunnett's multiple comparisons post-hoc test with statistical application software, GraphPad Prism (version 7.05 for Windows, GraphPad Software, La Jolla California USA, www.graphpad.com). A probability value less of 0.05 ($P < 0.05$) was considered statistically significant. The results are reported below in Section 7.3.

7.2.6 Fluorescent differential staining of biofilm on urinary catheter

The catheter sections were prepared for fluorescent differential staining with DAPI and ConA subsequently after the biofilm assay (Section 7.2.3). *P. aeruginosa* PAO1 biofilm was stained simultaneously with fluorescent probes to visualise different components of the biofilm using DAPI in blue for cell detection and tetramethylrhodamine (TRITC)-labelled Concanavalin A (ConA) in red to detect α-D-mannosyl and α-D-glucosyl residues (Leriche *et al.* 2000; Schwartz *et al.* 2003; Wilks *et al.* 2015). The biofilm staining method using DAPI and ConA is as detailed further in Section 2.4.1. The stained catheter sections were air-dried before used for EDIC/EF microscopy observation.

7.2.7 Observation using episcopic differential interference contrast/epifluorescence (EDIC/EF) microscope

All strains of *P. aeruginosa* PAO1 biofilm development on the catheter surface were observed using a customised Nikon Eclipse LV100D microscope (Best Scientific, UK) equipped for EDIC/EF microscopy (Keevil, 2003). The microscope was equipped with long working distance metallurgical objectives (Nikon Plan Achromat); a high-resolution camera (QImaging Retiga EXi Cooled Digital CCD monochrome camera with RGB colour filter module) and metal halide light source (EXFO X-CITE 120 fluorescence system). Three low to high magnification objectives (magnification x 10, x 50, and x 100) were used in imaging the biofilm formation taken with ImagePro 6.2 software (Media Cybernetics, UK). Due to the curvature of the catheter, stacked images of biofilm were taken for each focal point achieved at horizontal level during high magnification (manual z-scans, one stack image ≈ ± 1 μm).

7.2.8 Image processing

The stacked images were processed into a composite image using the extended depth of field plugin (Forster *et al.* 2004) in the open-source image-analysis software, Fiji (version 1.42q, National Institutes of Health, USA) (Schindelin *et al.* 2012). A summary of the biofilm images for wildtype (Appendix G) and AM-negative mutants (Appendix K) are included in Appendices section. The EDIC images presented in the results were converted into grayscale using Adobe Systems Photoshop CS (version CS6) to compensate for the prism's pseudo colouration effects in the EDIC microscope and discussed further in the next section.

7.2.9 Comparison of protein structure model between wildtype genes with transposon genes

The reference databases and web-based application tools used in this study are as detailed in Table 7 2 and Table 7 3, respectively. The existing protein structures of the P. aeruginosa PAO1 wildtype AM target genes were first searched in the UniProt website (https://www.uniprot.org) for annotation available in the SWISS-MODEL server (https://swissmodel.expasy.org/)(Schwede et al. 2003; Guex et al. 2009; Bertoni et al. 2017; Bienert et al. 2017; Waterhouse et al. 2018).

Table 7-2 Reference databases used in this study

Database Name	Link	Description
GeneID	https://www.ncbi.nlm.nih.gov/gene	Database of nomenclature, Reference Sequences (RefSeqs), maps, pathways, variations, phenotypes, and links to genome-, phenotype- and locus-specific resources
Pseudomonas Genome DB	http://pseudomonas.com	Updated information of PAO1 genome annotation (Winsor *et al.* 2011)
Kyoto Encyclopedia of Genes and Genomes (KEGG)	https://www.genome.jp/kegg-bin/show_organism?org=pae	Resource database on large-scale molecular datasets generated by genome sequencing and other high-throughput experimental technologies.
UniProt	https://www.uniprot.org	Comprehensive resource for protein information.

Table 7-3 Web-based application tools used to simulate predicted protein model

Database Name	Link	Description
ExPASy: Translate	https://web.expasy.org/cgi-bin/translate/dna_aa	Translation tool for nucleotide (DNA/RNA) sequence into a protein sequence.
SWISS-MODEL	https://swissmodel.expasy.org/	Automated protein structure homology-modelling server

Alternatively, the amino acid sequence of the gene obtained from the gene annotation databases such as GeneID (https://www.ncbi.nlm.nih.gov/gene) or KEGG (Kyoto Encyclopedia of Genes and Genomes, https://www.genome.jp/kegg-bin/show_organism?org=pae) was used with the SWISS-MODEL, a web-based protein structure homology modelling application, to retrieve the reported existing protein structure model exist in the SWISS-MODEL server for the wildtype gene. The SWISS-MODEL built-in automatic modelling mode uses the target protein's amino acid sequence

(or the UniProtKB accession code) as input to produce ranked suitable homology protein model templates according to their quality based on BLAST and HHblits (Schwede et al. 2003; Camacho et al. 2009; Remmert et al. 2011).

The predicted protein structure of the transposon mutants from the Manoil lab (Jacobs *et al.* 2003; Held *et al.* 2012) were compared with the wildtype protein structure by using the predicted acid amino sequence that was input into the SWISS-MODEL protein model simulation web-based application. The predicted acid amino sequence used was translated using another web-based application, ExPASy: Translate (https://web.expasy.org/cgi-bin/translate/dna_aa) from the transposonated gene sequence that was constructed out of the mutant details obtained from the Manoil lab. The predicted protein structure for transposon mutant gene was selected from the results based on the same model template as wildtype for specific comparison. A simple flowchart in Figure 7-2 shows the relevant steps involved in predicted protein structure modelling of mutants to be compared with wildtype using web-based application simulation.

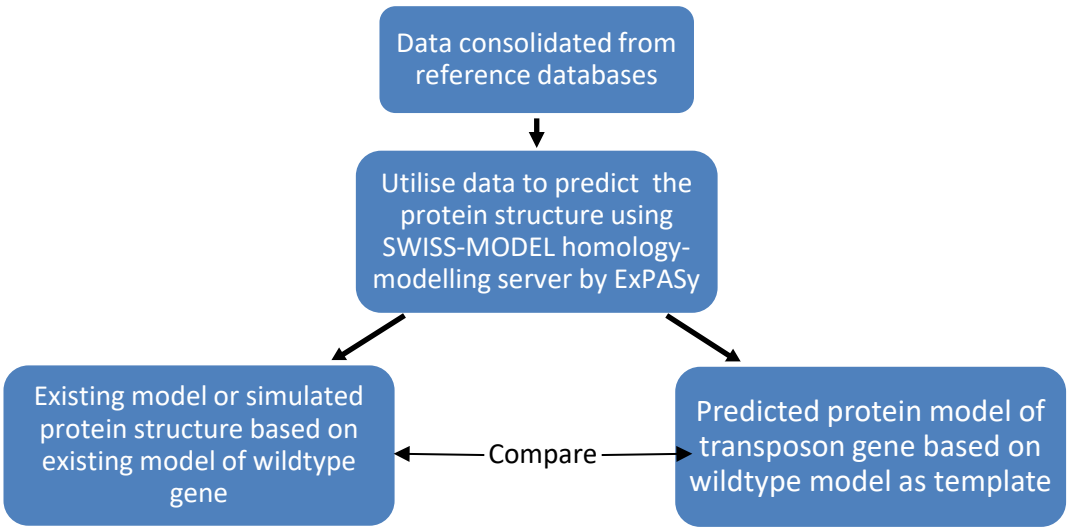

Figure 7-2 Workflow in obtaining the wildtype protein structure and the predicted protein structure of mutants for comparison.

7.3 Results

7.3.1 Biofilm attachment enumeration analysis of *P. aeruginosa* PAO1 AM-negative mutants on urinary catheter

One-way analysis of variance (ANOVA) was conducted and reported in Table 5-2. The biofilm enumeration data compares the *P. aeruginosa* PAO1 wildtype that has been discussed previously

in Chapter 5 with AM-negative mutants. Statistically significant differences of the mean log_{10} cfu/catheter section between the strains compared to wildtype were found at all timepoints; 1 h, 3 h and 6 h ($P < 0.0001$), 24 h ($P = 0.0006$). The ANOVA analysis was followed by Dunnett's multiple comparisons post-hoc test, and the result summary is shown in Table 5-3. The resulting graph using mean value log_{10} cfu/catheter section of the biofilm enumeration data at each timepoint is illustrated in Figure 7-3.

There was only one *fliA* mutant available to be used for this study. The PW3643 mutant showed no significant difference compared to wildtype in the 1 h timepoint (6.68 ± 0.06 log_{10} cfu/catheter section, $P = 0.2957$) but showed significantly higher cfu at 3 h (7.18 ± 0.33 log_{10} cfu/catheter section, $P = 0.0017$) and at 6 h (7.91 ± 0.25 log_{10} cfu/catheter section, $P = 0.0003$). At 24 h there were no significant difference found between PW3643 and wildtype (7.88 ± 0.08 log_{10} cfu/catheter section, $P = 0.1207$).

Table 7-4 One-way ANOVA analysis of *P. aeruginosa* PAO1 AM-negative mutant biofilm

	One-way ANOVA ($P < 0.05$)					
Time	**ANOVA table**	**SS**	**DF**	**MS**	**F(DFn_{11}, DFd_{24})**	***P* summary**
1 h	Treatment (between columns)	19.56	11	1.779	19.14	$P < 0.0001$
	Residual (within columns)	2.138	23	0.09294		****
	Total	21.7	34			
3 h	Treatment (between columns)	20.71	11	1.883	38.01	$P < 0.0001$
	Residual (within columns)	1.139	23	0.04954		****
	Total	21.85	34			
6 h	Treatment (between columns)	6.9	11	0.6273	16.86	$P < 0.0001$
	Residual (within columns)	0.8555	23	0.0372		****
	Total	7.756	34			
24 h	Treatment (between columns)	2.791	11	0.2537	4.983	$P = 0.0006$
	Residual (within columns)	1.171	23	0.05091		***
	Total	3.962	34			

For all significant results shown, $P < 0.05$ (*, $P < 0.05$; **, $P < 0.01$; ***, $P < 0.001$, ****, $P < 0.0001$, and ns, not significant).

FliC mutant PW2970 biofilm has shown a statistically significant less cfu in the first hour of incubation (5.06 ± 0.03 log_{10} cfu/catheter section, $P = 0.0055$) and approximately 1 log less at 3 h timepoint (5.41 ± 0.21 log_{10} cfu/catheter section, $P = 0.0002$) compared to wild type. Even though PW2970 does not show any difference to wildtype at 6 h (6.88 ± 0.23 log_{10} cfu/catheter section, $P = 0.7578$), at 24 h the mutant showed slight significantly more cfu compared to wildtype (8.10 ± 0.11 log_{10} cfu/catheter section, $P = 0.0044$).

Contrastingly, another *fliC* mutant PW2971 showed no significant difference compared to wildtype at 1 h and 24 h (6.45 ± 0.33 log_{10} cfu/ catheter section, P = 0.8714 and 7.83 ± 0.11 log_{10} cfu/ catheter section, P = 0.1212, respectively), but showed a slight difference but significantly more cfu than wildtype in 3 h and 6 h timepoints(6.95 ± 0.25 log_{10} cfu/ catheter section, P = 0.0326 and 7.74 ± 0.05log_{10} cfu/ catheter section, P = 0.0036, respectively).

The *fliM* mutant PW3621 showed a significant 1 log difference less cfu than wildtype in the first hour (4.82 ± 0.18 log_{10} cfu/catheter section, P = 0.0002) and no significant differences in the subsequent timepoints 3 h, 6 h and 24 h (6.14 ± 0.17 log_{10} cfu/catheter section, P = 0.7858, 6.93 ± 0.18 log_{10} cfu/ catheter section, P = 0.9308 and 7.83 ± 0.04 log_{10} cfu/ catheter section, P = 0.1118, respectively).

By contrast, the second *fliM* mutant PW36221 showed only a significantly more cfu than wildtype at 3 h (5.41 ± 0.21 log_{10} cfu/catheter section, P = 0.0002) but no significant differences were found in timepoints 1 h, 6 h and 24 h (6.24 ± 0.10 log_{10} cfu/catheter section, P = 0.9996, 7.37 ± 0.12 log_{10} cfu/ catheter section, P = 0.4446 and 7.76 ± 0.41 log_{10} cfu/catheter section, P = 0.2366, respectively).

Coincidently similarly to PW3621, *pilA* mutant PW8621 showed highly significant poor cfu result at 1 h, with more than 1 log less compared to wildtype (4.63 ± 0.23 log_{10} cfu/catheter section, P < 0.0001). However, the mutant showed no statistically significant difference in the subsequent timepoints 3 h, 6 h and 24 h (6.14 ± 0.17 log_{10} cfu/catheter section, P = 0.7858, 6.93 ± 0.18 log_{10} cfu/ catheter section, P = 0.9308 and 7.83 ± 0.04 log_{10} cfu/ catheter section, P = 0.1118, respectively).

However, the second *pilA* mutant, PW3622, produced a different cfu result in comparison to wildtype with no significant difference in the first and 3 h timepoint (5.83 ± 0.02 log_{10} cfu/ catheter section, P = 0.7463 and 6.43 ± 0.14 log_{10} cfu/ catheter section, P = 0.9996, respectively), and slightly more but significantly different from wildtype at timepoints 6 h and 24 h (7.73 ± 0.36 log_{10} cfu/ catheter section, P = 0.0039 and 8.08 ± 0.51 log_{10} cfu/ catheter section, P = 0.0061, respectively).

Even though the *pilF* mutant PW7438 did not show any significant differences compared to wildtype at timepoints 1 and 6 h (6.37 ± 0.07 log_{10} cfu/ catheter section, P = 0.9799 and 7.30 ± 0.15 log_{10} cfu/ catheter section, P = 0.7700, respectively), the mutant did show weak evidence of significantly higher cfu at 3 h and 24 h timepoints (6.92 ± 0.10 log_{10} cfu/ catheter section, P = 0.0468 and 8.11 ± 0.11 log_{10} cfu/ catheter section, P = 0.0037, respectively).

The biofilm formation of the flagella and pili deficient mutants analysed using the single knockout mutants showed strong evidences of fewer cfu compared to wildtype at the early timepoints 1 and 3 h for Δ*fliC* (4.95 ± 0.06 log_{10} cfu/ catheter section, $P = 0.0006$ and 5.14 ± 0.03 log_{10} cfu/ catheter section, $P < 0.0001$, respectively) and Δ*pilA* (4.80 ± 0.42 log_{10} cfu/ catheter section, $P = 0.0002$ and 5.14 ± 0.03 log_{10} cfu/ catheter section, $P < 0.0001$, respectively).

Table 7-5 Dunnett's post-hoc multiple comparison tests of *P. aeruginosa* PAO1 wildtype and AM-negative mutant biofilm

Strains		1 h	3 h	6 h	24 h
WT	**Log10 cfu/catheter section**	6.16 ± 0.17	6.38 ± 0.04	7.09 ± 0.27	7.36 ± 0.08
	(%)	(57.82 ± 1.94)	(60.18 ± 0.48)	(68.17 ± 2.97)	(71.15 ± 0.88)
PW3643 - Δ*fliA*	**Log10 cfu/catheter section**	6.68 ± 0.06	7.18 ± 0.33	7.91 ± 0.25	7.88 ± 0.08
	(%)	(62.03 ± 0.65)	(67.58 ± 3.57)	(75.46 ± 2.74)	(75.20 ± 0.88)
	Adjusted *P* value	0.2957 (ns)	0.0017 (**)	0.0003 (***)	0.1207 (ns)
PW2970 - Δ*fliC*	**Log10 cfu/catheter section**	5.06 ± 0.03	5.41 ± 0.21	6.88 ± 0.23	8.10 ± 0.11
	(%)	(43.44 ± 0.36)	(47.17 ± 2.27)	(62.85 ± 2.47)	(75.91 ± 1.15)
	Adjusted *P* value	0.0055 (**)	0.0002 (***)	0.7578(ns)	0.0044 (**)
PW2971 - Δ*fliC*	**Log10 cfu/catheter section**	6.45 ± 0.33	6.95 ± 0.25	7.74 ± 0.05	7.83 ± 0.11
	(%)	(60.30 ± 3.61)	(65.89 ± 2.82)	(74.59 ± 0.58)	(75.55 ± 1.26)
	Adjusted *P* value	0.8714 (ns)	0.0326(*)	0.0036 (**)	0.1212 (ns)
PW3621 - Δ*fliM*	**Log10 cfu/catheter section**	4.82 ± 0.18	6.14 ± 0.17	6.93 ± 0.18	7.83 ± 0.04
	(%)	(40.50 ± 1.90)	(54.47 ± 1.85)	(62.83 ± 1.90)	(72.39 ± 0.44)
	Adjusted *P* value	0.0002 (***)	0.7858 (ns)	0.9308 (ns)	0.1118 (ns)
PW3622 - Δ*fliM*	**Log10 cfu/catheter section**	6.24 ± 0.10	7.34 ± 0.05	7.37 ± 0.12	7.76 ± 0.41
	(%)	(56.28 ± 1.05)	(68.05 ± 0.58)	(68.38 ± 1.24)	(72.55 ± 4.36)
	Adjusted *P* value	0.9996 (ns)	0.0002 (***)	0.4446 (ns)	0.2366 (ns)
PW8621 - Δ*pilA*	**Log10 cfu/catheter section**	4.63 ± 0.23	6.03 ± 0.52	7.14 ± 0.11	7.71 ± 0.22
	(%)	(38.91 ± 2.44)	(53.88 ± 5.62)	(65.78 ± 1.21)	(71.97 ± 2.39)
	Adjusted *P* value	<0.0001 (****)	0.3682 (ns)	0.9996 (ns)	0.3506 (ns)
PW8622 - Δ*pilA*	**Log10 cfu/catheter section**	5.83 ± 0.02	6.43 ± 0.14	7.73 ± 0.36	8.08 ± 0.51
	(%)	(52.45 ± 0.26)	(58.95 ± 1.49)	(73.13 ± 3.96)	(76.84 ± 5.59)
	Adjusted *P* value	0.7463 (ns)	0.9996 (ns)	0.0039 (**)	0.0061 (**)
PW7438 - Δ*pilF*	**Log10 cfu/catheter section**	6.37 ± 0.07	6.92 ± 0.10	7.30 ± 0.15	8.11 ± 0.11
	(%)	(59.49 ± 0.77)	(65.63 ± 1.12)	(69.75 ± 1.65)	(78.83 ± 1.23)
	Adjusted *P* value	0.9799 (ns)	0.0468 (*)	0.7700 (ns)	0.0037 (**)
Δ*fliC*	**Log10 cfu/catheter section**	4.95 ± 0.06	5.14 ± 0.03	6.79 ± 0.03	7.84 ± 0.05
	(%)	(42.86 ± 0.61)	(44.96 ± 0.35)	(62.85 ± 0.36)	(74.27 ± 0.51)
	Adjusted *P* value	0.0006 (***)	<0.0001 (****)	0.3636 (ns)	0.1071 (ns)
Δ*pilA*	**Log10 cfu/catheter section**	4.80 ± 0.42	5.10 ± 0.03	6.90 ± 0.10	7.96 ± 0.12
	(%)	(41.06 ± 4.52)	(44.37 ± 0.35)	(63.77 ± 1.04)	(75.26 ± 1.32)
	Adjusted *P* value	0.0002 (***)	<0.0001 (****)	0.8202 (ns)	0.0267 (*)
Δ*fliC*Δ*pilA*	**Log10 cfu/catheter section**	4.92 ± 0.81	5.26 ± 0.11	6.15 ± 0.17	7.15 ± 0.20
	(%)	(41.65 ± 8.58)	(45.21 ± 1.18)	(54.70 ± 1.83)	(65.30 ± 2.15)
	Adjusted *P* value	0.0005 (***)	<0.0001 (****)	0.0002 (***)	0.8759 (ns)

Data is expressed as mean ± SD (SD = standard deviation). For all significant results shown, $P < 0.05$ (*, $P < 0.05$; **, $P < 0.01$; ***, $P < 0.001$, ****, $P < 0.0001$, and ns, not significant).

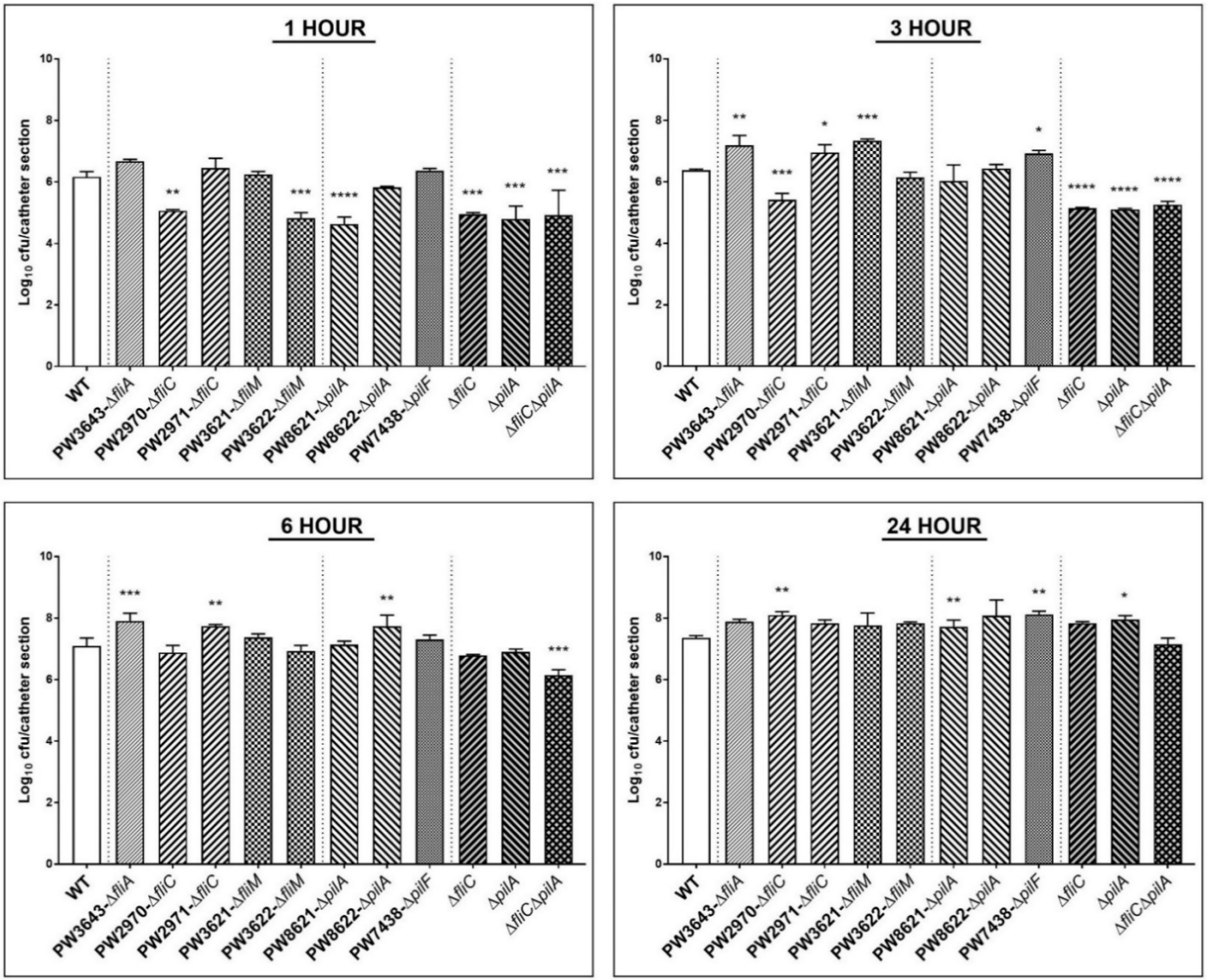

Figure 7-3 Biofilm enumeration in cfu/catheter section of AM-negative mutants at 1 h, 3 h, 6 h and 24 h.

Single knockout mutant Δ*fliC* showed no significant differences compared to wildtype at 6 h and 24 h timepoints (6.79 ± 0.03 $\log_{10}$ cfu/ catheter section, P = 0.3636 and 7.84 ± 0.05 $\log_{10}$ cfu/ catheter section, P = 0.1071, respectively). Even though Δ*pilA* showed no significant difference compared to wildtype at 6 h timepoint (6.90 ± 0.10 $\log_{10}$ cfu/ catheter section, P = 0.8202), there was weak but significant difference shown at 24 h timepoint (7.96 ± 0.12 $\log_{10}$ cfu/ catheter section, P = 0.0267).

Lastly, the double knockout mutant Δ*fliC*Δ*pilA* showed strong significant difference of average 1 log less cfu compared to wildtype at timepoints 1 h, 3 h and 6 h (4.92 ± 0.81 $\log_{10}$ cfu/ catheter section, P = 0.0005, 5.26 ± 0.11 $\log_{10}$ cfu/ catheter section, P < 0.0001, and 6.15 ± 0.17 $\log_{10}$ cfu/ catheter section, P = 0.0002, respectively). However, there was no significant difference shown at 24 h timepoint between the double knockout and wildtype (7.15 ± 0.20 $\log_{10}$ cfu/ catheter section, P = 0.8759).

7.3.1.1 Screening of *P. aeruginosa* PAO1 AM-negative mutants for contrasting biofilm characteristics compared to wildtype

For easier comparison of biofilm structure with PAO1 wildtype, the biofilm EDIC images of AM-negative mutants were divided into three groups, the flagella (*fli*-) transposon mutants' group, the pili (*pil*-) transposon mutants' group and the knockout mutants' group.

7.3.1.2 The flagella (*fli*-) transposon mutant group

EDIC images of biofilm formed by the flagella (*fli*-) transposon mutants compared to wildtype over timepoints 1 h, 3 h, 6 h and 24 h are shown in Figure 7-4.

The *fliA* mutant PW4643 biofilm showed successful surface attachment and colonisation with the presence of small microcolonies, and cell aggregates formation (Figure 7-4A - Figure 7-4D). In terms of structure, all images at every timepoints looked similar, except for in 24 h where the *fliA* mutant biofilm features a lawn-like deflated form with patches of void space (Figure 7-4D), compared to the wildtype that produces a three-dimensional biofilm that looks like a "craggy mountain" with void space in between (Figure 7-4d). Form-wise, biofilm structure of the *fliA* mutant in 3 h and 6 h looked similar to wildtype (Figure 7-4A and Figure 7-4B), the structures were more substantial, which corresponds to the higher than wildtype cfu enumeration data reported earlier in section 7.3.1.

Both fliC mutants studied showed the presence of bacteria attached on the surface in the first hour. Between the two *fliC* mutants, PW2971 strain biofilm (Figure 7-4I - Figure 7-4L) has a more similar form with wildtype compared to strain PW2970 (Figure 7-4E - Figure 7-4H). *FliC* mutant PW2970 cell aggregates were formed but not transformed into microcolonies even though the attached cell were seen distanced apart but spread over the catheter surface at 1 and 3 h (Figure 7-4E and 4F). At timepoints 6 h and 24 h, the PW2970 strain showed the presence of microcolonies formation that has connected to form a network (Figure 7-4, G and H), but it was noticeably different from wildtype's three-dimensional biofilm form. Comparable to wildtype, the *fliC* mutant PW2971 showed cell aggregates and microcolonies formation, although the mutant did not produce a multi-layer three-dimensional form similar to wildtype at 24 h (Figure 7-4L).

The two *fliM* mutants showed similar presence of attached bacteria on the surface at 1 h compared to wildtype even though only strain PW3621 has the correlated data of fewer cells compared to wildtype (Figure 7-4M and Figure 7-4Q). Following that, the 3 h image shows large microcolony formation by PW3621 (Figure 7-4N) that corresponds to the higher cfu data compared to wildtype reported earlier in Section 7.3.1.

The PW3621 strain continues to develop similar wildtype like form in 6 h and 24 h timepoints (Figure 7-4O and Figure 7-4P), producing a multi-layer, three-dimensional "craggy mountain" biofilm formation with the presence of central hollow crater, possibly indicating that dispersal events have happened. Dissimilar to wild type, the *fliM* mutant strain PW3622 showed the inability to form microcolonies and three-dimensional biofilm similar to wildtype within 24 h (Figure 7-4T). All of the flagella (*fli*-) transposon mutants show the presence of fibrinous structure that can be distended from the microcolonies and formed a pathway that navigates cells toward their destinations (Figure 7-5).

ConA-stained images of the flagella (*fli*-) transposon mutant group biofilm show the presence of D-mannose component in the EPS on the catheter surface where there is attached bacteria available. All flagella (*fli*-) mutants showed the apparent presence of D-mannose component in the EPS at all timepoints, except for *fliM* mutants where at timepoints 1 h and 3 h (Figure 7-6) that showed lack of ConA-stained D-mannose component on the catheter surface, as well as no attached cells either. The composite image of DAPI and ConA also reveals the presence of fibrinous track structure that extends from the microcolony that is similarly found in wildtype in all flagella (*fli*-) transposon mutants (Figure 7 6).

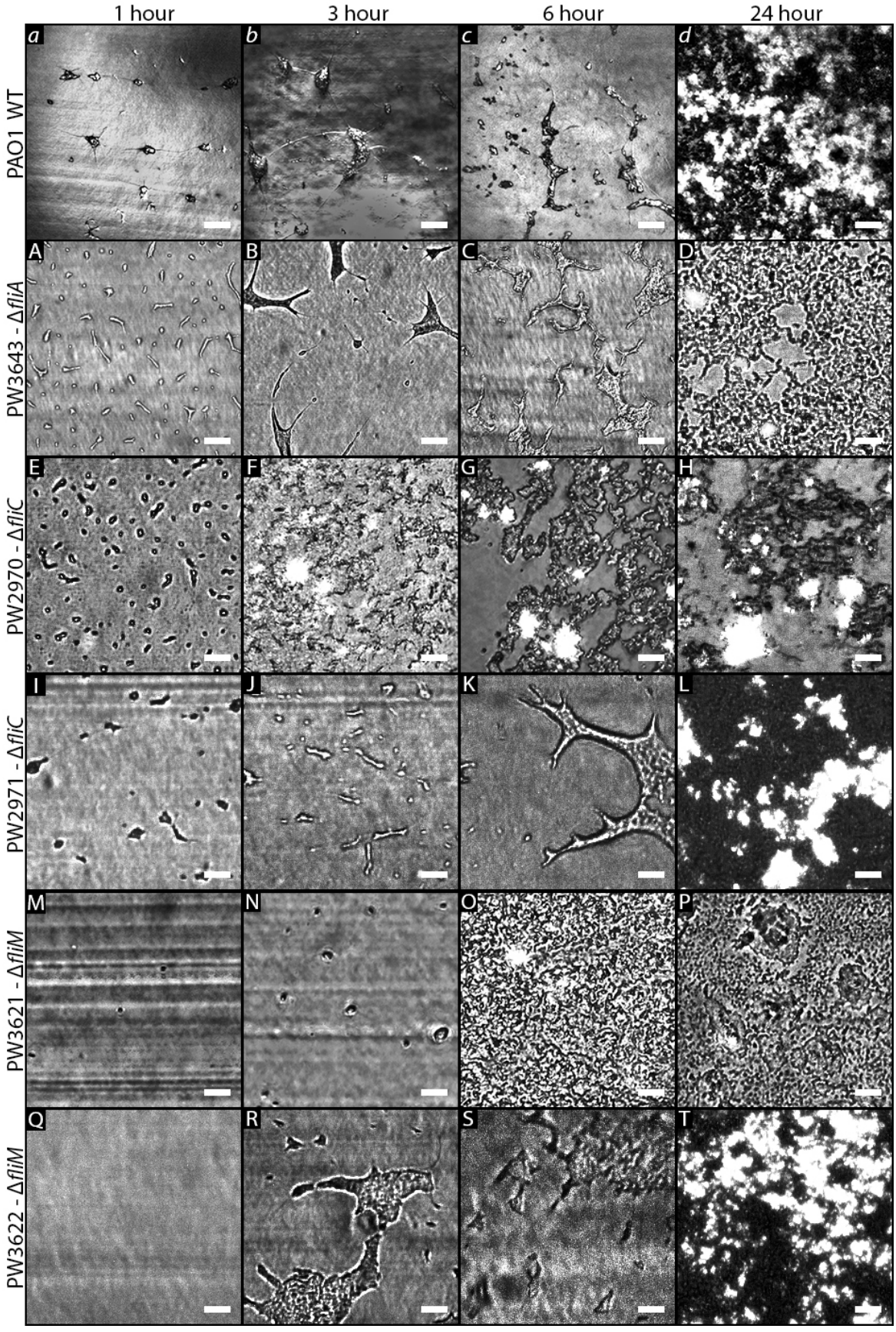

Figure 7-4 Representative EDIC images of AM-negative flagella (*fli*-) transposon mutant group. Magnification × 1000, scale bars = 10 µm.

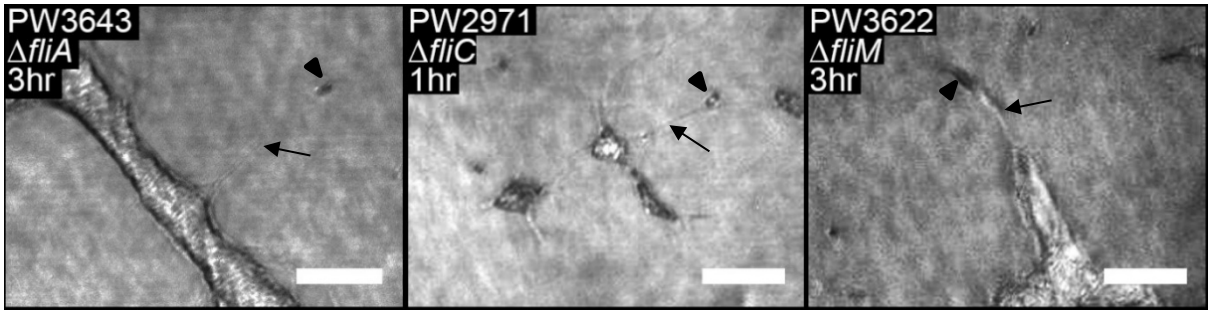

Figure 7-5 Representative images of the fibrinous structure occurred in AM-negative flagella (*fli*-) transposon mutant group.
Black arrows denote the fibrinous structure that creates a pathway for the bacteria cells (black arrowhead). Magnification × 1000, scale bars = 10 µm.

7.3.1.3 The pili (*pil*-) transposon mutant group

Close observation of all the pili (*pil*-) transposon mutant group shows similar features between them, where there is a slightly reduced presence of attached bacteria on the catheter surface in the first hour. All the pili mutants showed attached bacterial cells form small cell groups, as shown in Figure 7-7A, Figure 7-7E and Figure 7-7I).

The PW8621 *pilA* strain showed minimal attachment in the early timepoints that correspond with the cfu enumeration data, but the EDIC image shows the presence of large microcolonies with similar features to wildtype at 6 h (Figure 7-7C). At 24 h, the PW8621 mutant was able to form multi-layer, stratified, three-dimension biofilm structure but with a more prominent macrocolony formation that slightly different to the “craggy mountain” features found in the wildtype strain (Figure 7-7D). There was no visible crater with a central hollowing feature shown at 24 h by the PW8621 mutant, which means the dispersal seeding events did not happen.

Whereas in PW8622, the *pilA* mutant showed wildtype-like features in the biofilm formation at 3 h and 6 h, with microcolonies forming and extending to connect with nearby neighbours to form a network of biofilm network (Figure 7-7F and Figure 7-7G). The PW8622 mutant did achieve in forming three-dimensional macrocolony biofilm structure at 24 h, but the biofilm appeared not differentiated and was not as stratified, which contrastingly different than wildtype and PW8621.

After 1 h, the subsequent timepoints observation shows that the attached *pilF* mutant PW7438 bacterial cells were more than wildtype and form larger microcolonies with higher stratification of biofilm formation. Although the EDIC observation corresponds to the cfu enumeration data at 3 h and 24 h timepoints, the *pilF* mutant’s ability to attach and form macrocolonies was more efficient than the wildtype as observed at 6 h and 24 h images shown in (Figure 7-7K and Figure 7-7L).

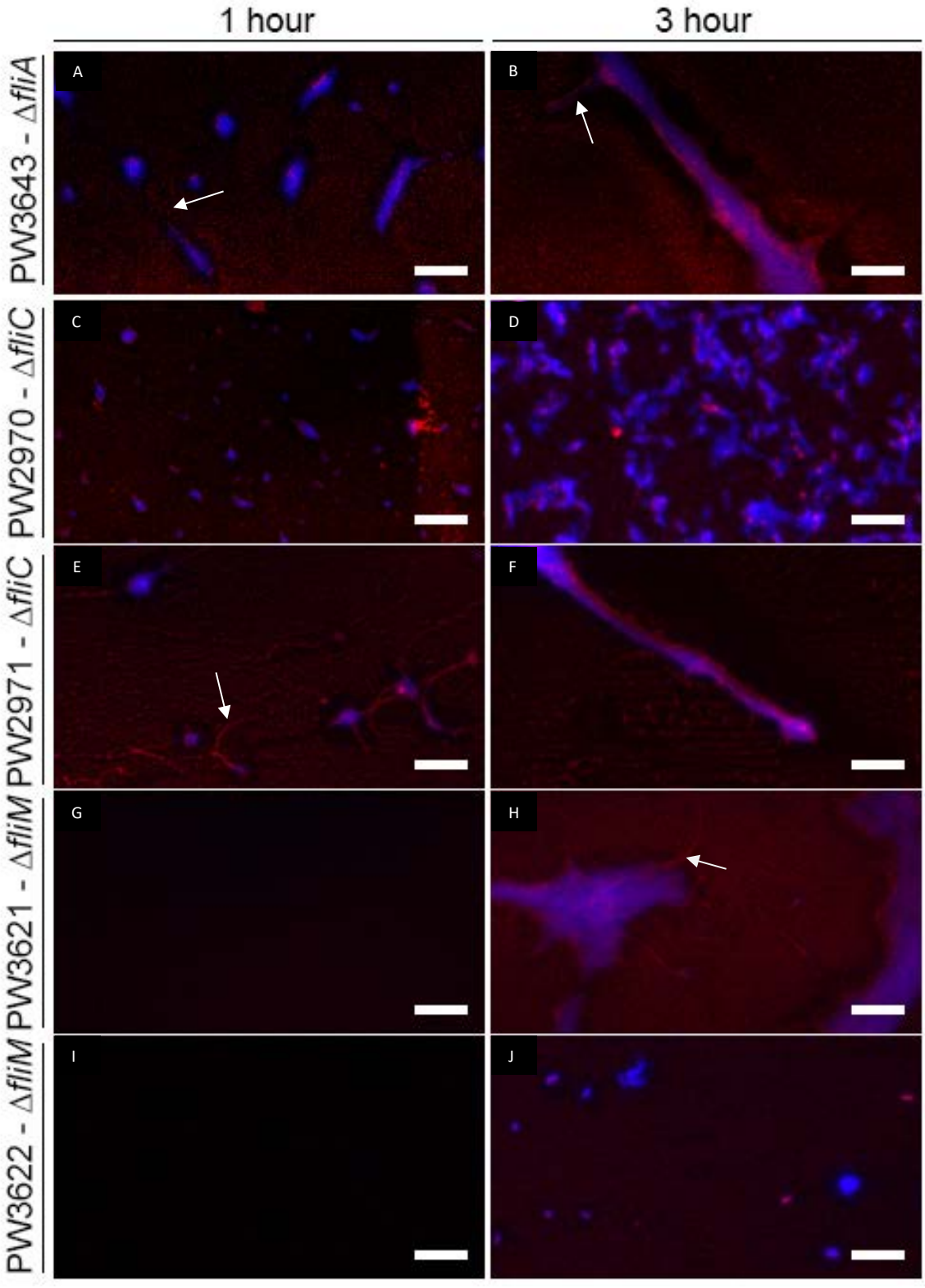

Figure 7-6 Representative composite images of DAPI/ConA-stained AM-negative flagella (*fli-*) transposon mutants' biofilm on a urinary catheter at 1 h and 3 h.

These images show that the ConA-stained EPS produced by the mutants are similar to wildtype. White arrows denote the fibrinous structure that forms on the catheter surface, which was visualised using ConA stain. Magnification × 1000, scale bars = 10 µm.

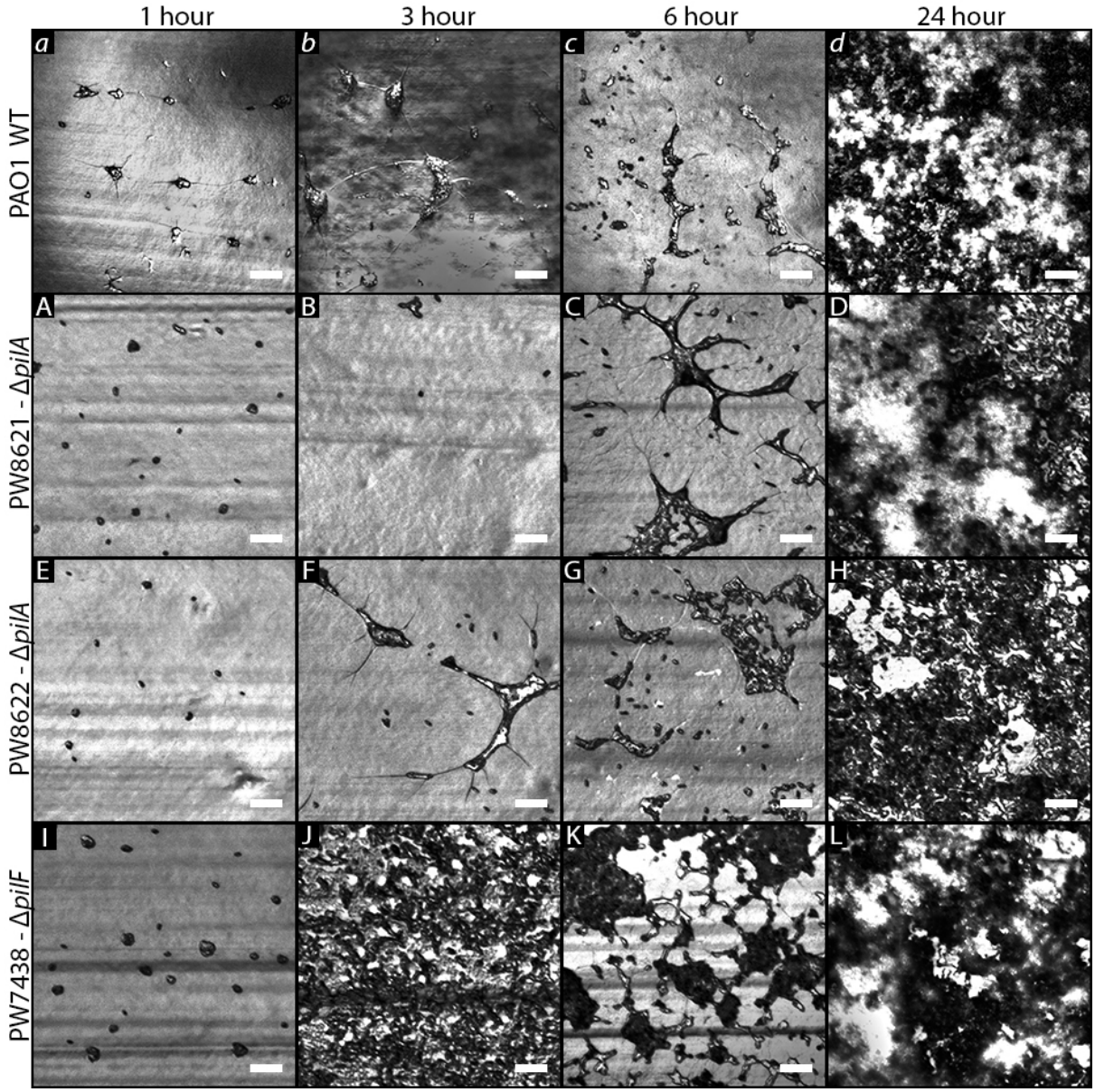

Figure 7-7 Representative EDIC images of AM-negative pili (*pil*-) transposon mutant group. Magnification × 1000, scale bars = 10 µm.

Other notable characteristics that were observed from the pili transposon mutant group are all mutants have areas of void spaces that create a channel in between the biofilm on the catheter at 24 h timepoint, although PW8621 mutant form a more developed biofilm than PW8622 and PW7438 form the most stratified biofilm formation among all three mutants.

However, except for pilA mutant PW8622, pilA mutant PW8621 and pilF mutant PW7438 24 h biofilm showed the presence of amorphous crystallisation formation (Figure 7-7D and Figure 7-7L). The unique fibrinous track structure was also found present in the pili (pil-) transposon mutant biofilm, which was seen, distended from the microcolonies and formed a bridge that navigates cells toward their destinations (Figure 7-8).

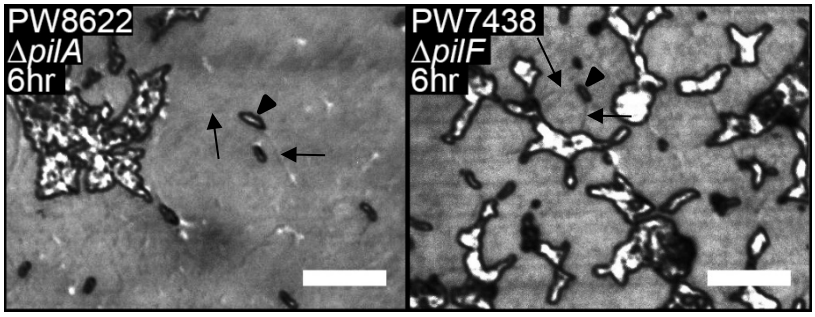

Figure 7-8 Representative images of the fibrinous structure occurred in AM-negative pili (*pil*-) transposon mutant group.
Black arrows denote the fibrinous structure that creates a pathway for the bacteria cells (black arrowhead). Magnification × 1000, scale bars = 10 µm.

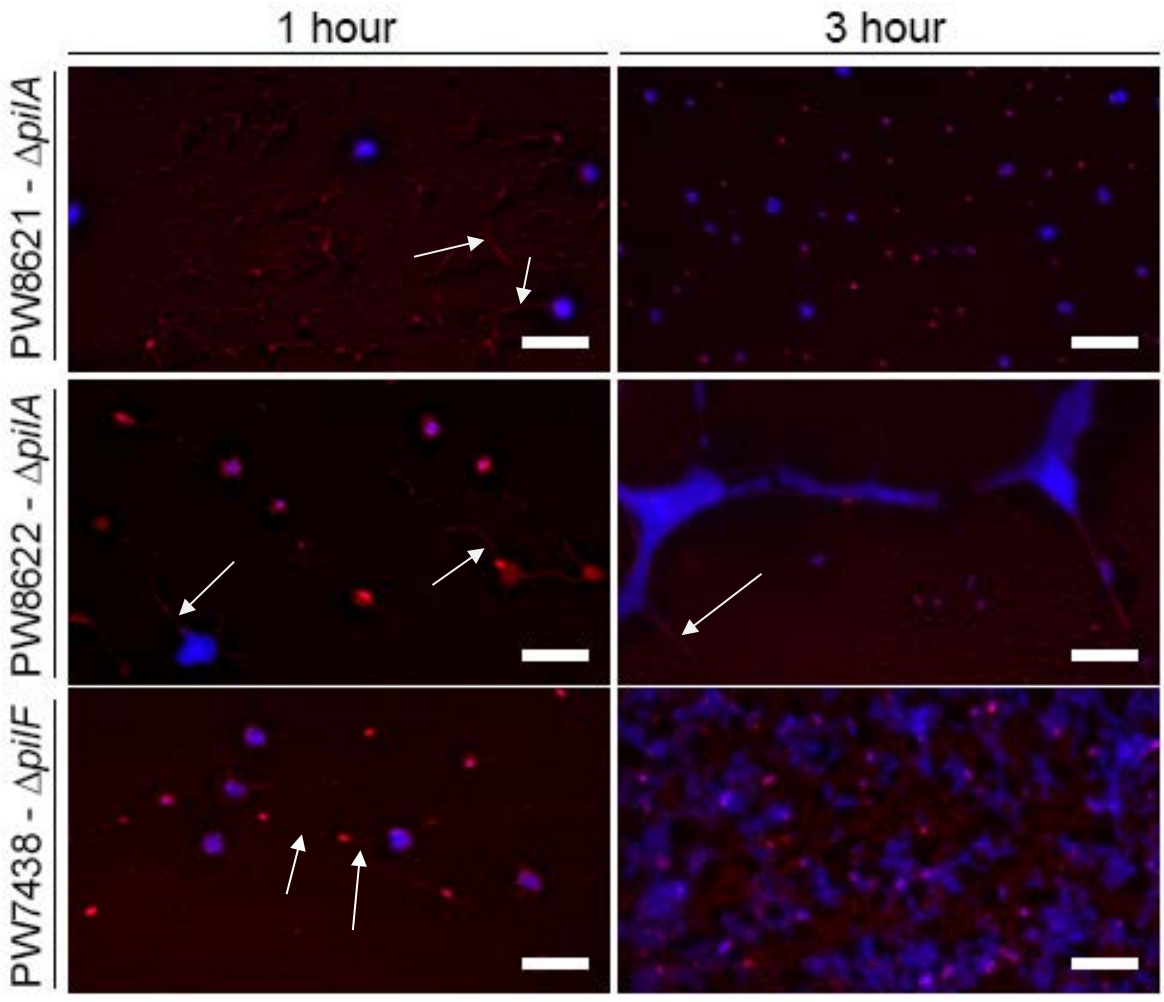

Figure 7-9 Representative composite images of DAPI/ConA-stained AM-negative pili (*pil*-) transposon mutant biofilm on a urinary catheter at 1 h and 3 h.
These images show that the ConA-stained EPS produced by the mutants are similar to wildtype. White arrows denote the fibrinous structure that forms on the catheter surface, which was visualised using ConA stain. Magnification × 1000, scale bars = 10 µm.

7.3.1.4 The knockout mutant group

The EDIC microscopy images of the knockout mutants' group are shown as in Figure 7-10. General observation of the images shows minimal to no presence of attached bacteria on the catheter surface in the first hour that corresponds to the fewer cfu enumeration data compared to wildtype. However, both single gene knockout mutants show the presence of abundant bacteria attachment and biofilm formation in the subsequent timepoints. Overall, the Δ*fliC* knockout mutant showed unusual biofilm characteristics compared to wildtype with low cell aggregation formation observed in timepoints 3 h and 6 h (Figure 7-10B and Figure 7-10C).

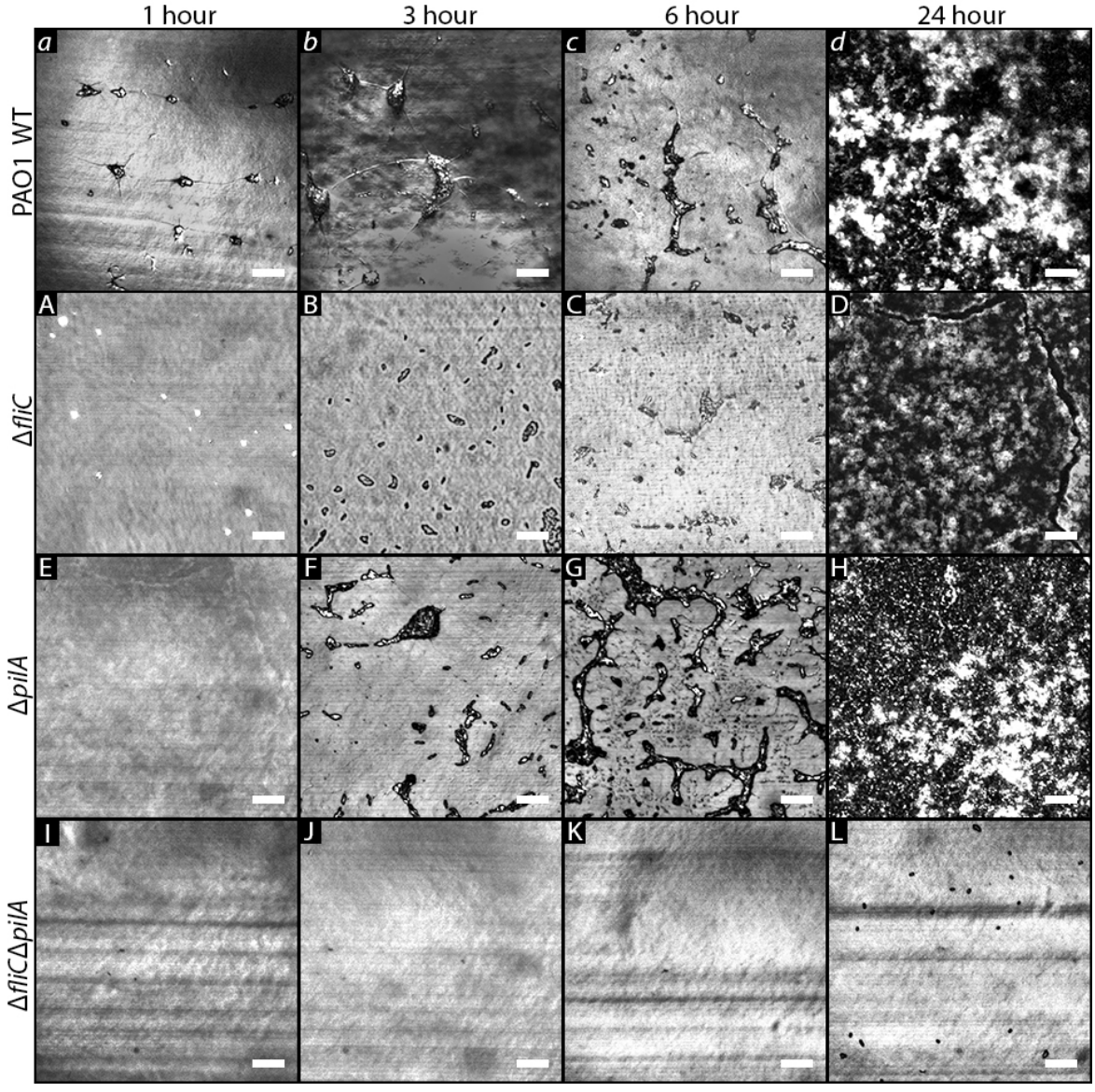

Figure 7-10 Representative EDIC images of knockout AM-negative mutants group. Magnification × 1000, scale bars = 10 µm.

Furthermore, the mutant was unable to produce biofilm with the wildtype-like three-dimensional "craggy and stratified mountain" features in macrocolonies; instead, the biofilm appeared undifferentiated and formed a continuous sheet covering the catheter surface with a narrow gap that creates a channel in between (Figure 7-10D). Instead of a mountain shape, the biofilm has ridges near the channel gap that is made of crystallised material.

Contrastingly, the Δ*pilA* knockout mutant showed the presence of cell aggregation and microcolonies formation during the 3 h and 6 h timepoints (Figure 7-10F and Figure 7-10G). Observation of the 24 h showed that the mutant produced a three-dimensional multi-layered biofilm that has macrocolonies with the shape like a mountain forming on a big continuous sheet that has narrow channels in between (Figure 7-10H).

Lastly, the double knockout Δ*fliC*Δ*pilA* mutant showed no biofilm development at all within the 24 h observation. Although there was no biofilm formation observed on the catheter at 24 h timepoint, there was the presence of attached bacterial cells scattered all over the catheter surface.

Overall mature biofilm terrain structure produced by the AM-negative knockout mutants are shown in the x 100 EDIC images taken at 24 h displayed in Figure 7-11. The representative DAPI/ConA composite images are shown in Figure 7-12, where the presence of D-mannose-based EPS is only available when there are attached bacteria on the surface.

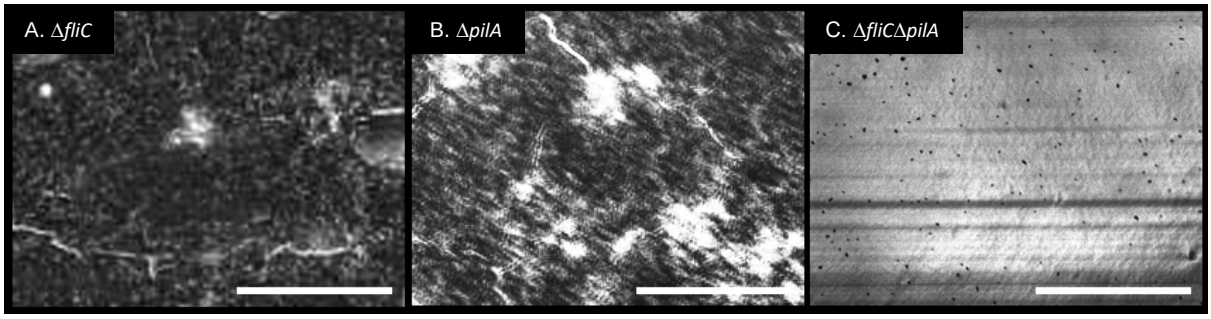

Figure 7-11 Representative EDIC images showing the 24 h biofilm of the knockout mutants of *P. aeruginosa* PAO1. (A)The Δ*fliC* knockout mutant biofilm forms continuous sheet covering the catheter surface with narrow channel formation in between. (B) The Δ*pliA* knockout mutant biofilm observed her are more stratified but forms a big multi-layered mountain-shaped biofilm with patches of void spaces and narrow channel formation in between. (C) The Δ*fliC*Δ*pilA* double knockout biofilm shows no biofilm structure at all, but the presence of attached bacteria were observed scattered all over the catheter surface. Magnification × 100, scale bars = 100 µm.

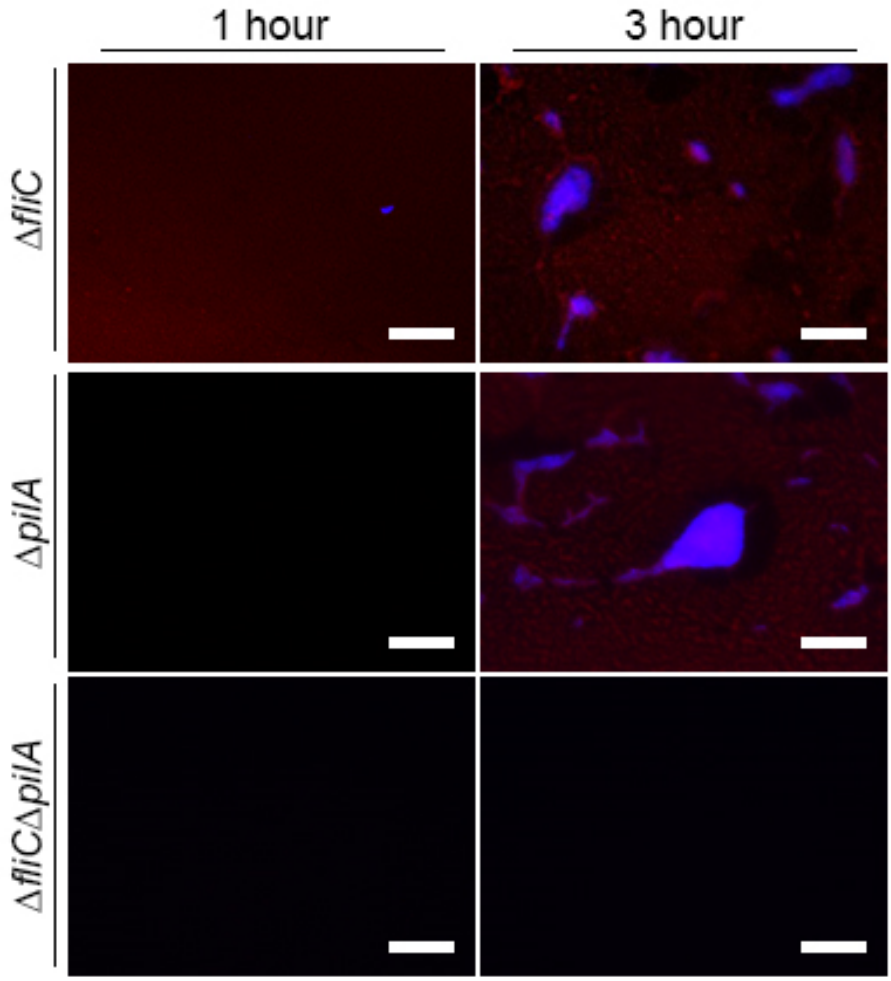

Figure 7-12 Representative composite images of DAPI/ConA-stained AM-negative knockout mutant biofilm on a urinary catheter at 1 h and 3 h. These images show that the ConA-stained EPS produced by the mutants are only present when there is attached bacteria available on the surface. Magnification × 1000, scale bars = 10 µm.

7.3.2 Target protein structure model of *P. aeruginosa* PAO1 wildtype with transposon mutants using SWISS-MODEL

Based on the transposon mutant details extracted from the accompanying table for the PA two-allele library (Appendix G), the transposon location in the mutants in this study is shown in Table 7-6. The comparison between the three-dimensional target protein structures of the *P. aeruginosa* PAO1 wildtype and transposon mutants is shown in Figure 7-13. Data obtained from the homology modelling is detailed further in Appendix L in the Appendices.

Compared to the wildtype FliA protein structure (UniProtKB accession number: P29248), the predicted FliA protein monomer from the PW3643 mutant based on template model 1rp3.1.A is missing the region 4 of the RNA polymerase at the C-terminus end including the helix-turn-helix domain that is involved in the DNA binding.

Table 7-6 List of *P. aeruginosa* PAO1 attachment/motility, AM-negative mutants with the location of the transposon

Strain name	Transposon	Transposon insertion	Transposon location in the PA ORF
PW3643-Δ*fliA*	IS*lacZ*/hah	Near the end (75% ORF)	
PW2970-Δ*fliC*	IS*lacZ*/hah	Middle (56% ORF)	
PW2971-Δ*fliC*	IS*phoA*/hah	Near the front (23% ORF)	
PW3621-Δ*fliM*	IS*lacZ*/hah	Middle (56% ORF)	
PW3622-Δ*fliM*	IS*phoA*/hah	Near the end (86% ORF)	
PW8621-Δ*pilA*	IS*lacZ*/hah	Middle (49% ORF)	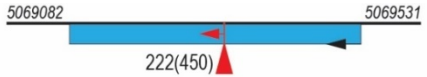
PW8622-Δ*pilA*	IS*phoA*/hah	Near the front (36% ORF)	
PW7438-Δ*pilF*	IS*phoA*/hah	Near the end (83% ORF)	

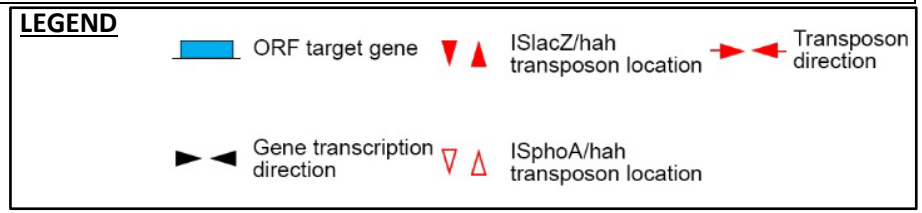

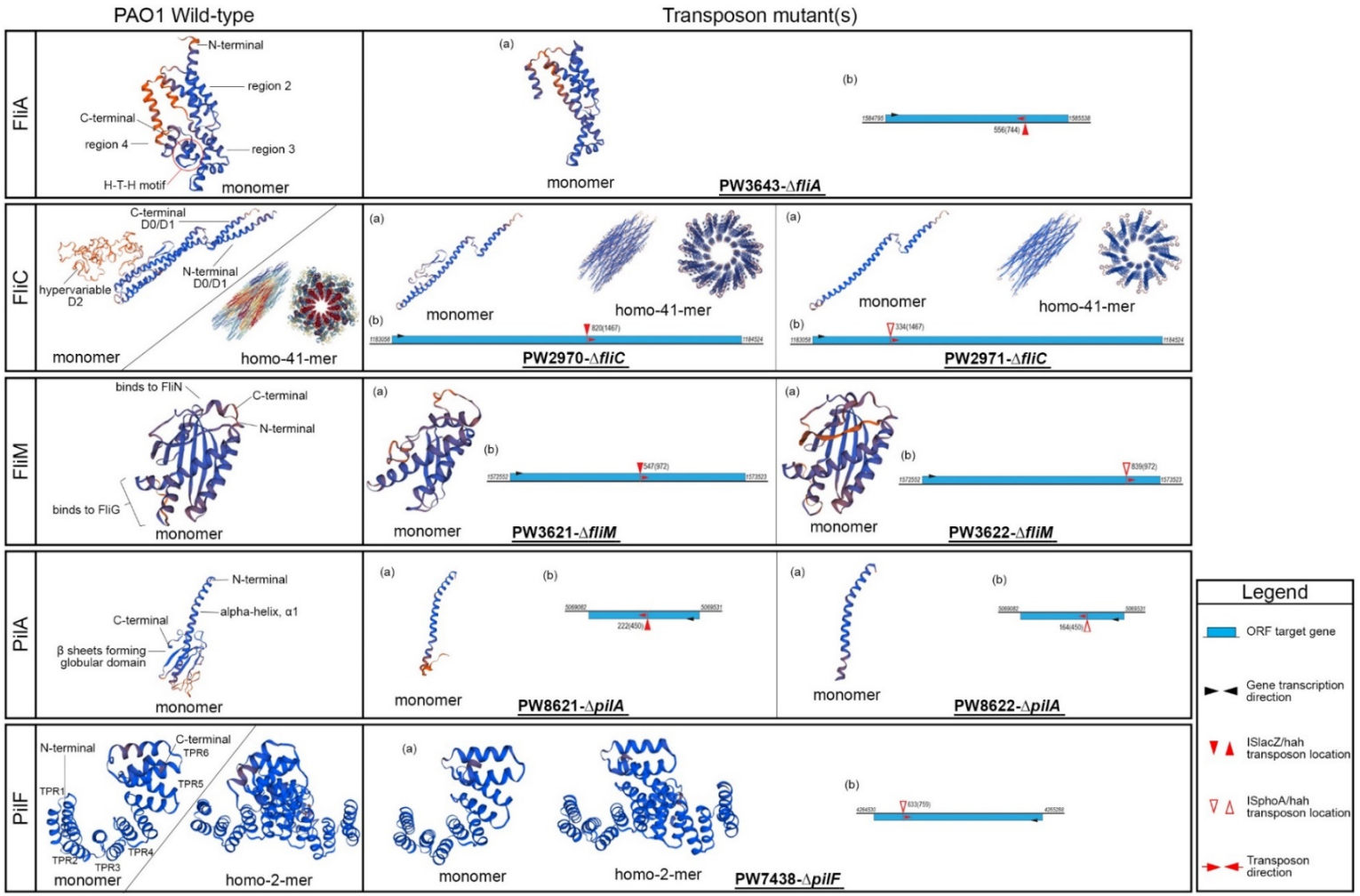

Figure 7-13 Homology modelling of target attachment/motility (AM) protein structures in this study. (a) Protein structures built using SWISS-MODEL. (b) Transposon location in the PA ORF.

As shown in the second row of Figure 7-13, the wildtype FliC monomer flagellin protein structure (UniProtKB accession number: Q9HT84) consists of two D0/D1 alpha-helical regions located at one each terminal end that is linked together to form the pilin and a D2 hypervariable D2 flagellin region that forms the hook structure. The homology modelling also reported the FliC monomer structure assembled in packing orientation to form homo-41-mer flagellar structure. Both *fliC* mutants are predicted to produce only one D0/D1 helical region, except that in PW2970 has a remaining fragment of the hook region at the C-terminal end.

The FliM protein (UniProtKB accession number: Q51465) homology modelling results showed the *fliM* mutant PW3622 predicted FliM protein was similar to wildtype based on the model template 4gc8.1. However, the *fliM* mutant PW3621 predicted FliM protein was smaller and retained the first *β*-sheet structure. The remaining region after the *β*-sheet structure was not predicted to be transcribed for PW3622 FliM protein structure (Figure 7-13, row 3).

The wildtype PilA protein monomer (UniProtKB accession number: P04739) has one alpha helix (α1) pilin with the C-terminal ends after a β-sheet protein structure that forms the globular domain (model template: 1oqw.2). However, the predicted protein monomers for both *pilA* mutants do not have the globular domain and only has the helical pilin structure, α1 (Figure 7-13, row 4). Lastly, the homology modelling of the PilF wildtype protein structure (UniProtKB accession: Q9HXJ2) shows that is made of six tetratricopeptide repeat (TPR) domains and that it is predicted to exists as a homo-dimer PilF protein (model template: 2ho1.1). The simulated predicted protein for *pilF* mutant PW7438 has a similar protein structure with wildtype from TPR1 until TPR5 but does not have TPR6. However, the homology modelling also reported that even with the only TPR1 until TPR5, the PilF protein monomer from the mutant is predicted able to exist as homo-2-mer protein (Figure 7-13, row 5).

7.4 Discussion

7.4.1 Screening of AM-negative mutants from the *Pseudomonas aeruginosa* PAO1 transposon mutant library

The AM-negative mutants were used to study the roles of cell-surface structures, flagella and pili, in *P. aeruginosa* that are involved in the motility and attachment, two most important process in biofilm formation (O'Toole and Kolter 1998; Donlan 2002; Saint and Chenoweth 2003). This work has been able to be conducted with the transposon obtained from the *P. aeruginosa* PAO1 transposon mutant library (Jacobs *et al.* 2003; Held *et al.* 2012).

While the purpose of transposon insertions is to render a gene defective by altering its sequence, the location where the transposon is inserted in the ORF is crucial as it affects the acid amino protein and its structure.

There are at least two transposon types available for most genes in the library, which is the IS*phoA*/hah and IS*lacZ*/hah, that target different sites on the gene (Jacobs *et al.* 2003; Held *et al.* 2012). Held *et al.* (2012) have previously emphasised that using the two available mutants when screening a gene for its corresponding genotype-phenotype relationship will minimise erroneous assignments of phenotype and as at least one will correspond to the correct effect of the mutation when the other is compromised.

Except for *fliA* and *pilF*, two types of transposon mutants, IS*lacZ*/hah and IS*phoA*/hah, for each gene *fliC*, *fliM* and *pilA* were used in this study. From the simulated homology modelling analysis, our finding shows that all AM-negative mutants produce incomplete putative protein structure compared to wildtype (Figure 7-13).

However, from phenotypic analysis, the affected biofilms were observed from the three mutants with IS*lacZ*/hah transposon, namely PW2970-*ΔfliC*, PW3621-*ΔfliM and* PW8621-*ΔpilA*. Coincidently, these three mutants had IS*lacZ*/hah transposon insertion located near the middle area of the gene ORF (49% to 56%, Table 7-6). Screening using more than one mutant per gene in this study confirms the previous suspicion about the association between genotype and phenotype (Held *et al.* 2012).

Future work that should be addressed is to sequence the transposon mutant strains to confirm the insertion sites of the transposon. This is because a previous study by Wu *et al.* (2008) reported that there are instances found which the transposon was inserted at a different, but near, the position stated in the original report. This is to confirm out findings further that the location of the transposon inserted in the gene could affect the resulting phenotype of the biofilm formation.

7.4.2 The role of flagella-mediated motility in urinary biofilm formation stages

In focusing on the role of the flagella in biofilm formation, we first questioned whether the regulation via RNA polymerase sigma factor FliA could suspend the formation of biofilm on urinary catheter using artificial urine media. Past studies have reported that the RNA polymerase sigma factor FliA is essential as the primary regulator in flagellar biosynthesis that affects flagella-mediated swimming and swarming motility (Starnbach and Lory 1992; Ding *et al.* 2009; Wesseling 2015; Lo *et al.* 2016; Francis *et al.* 2017).

In *E. coli*, the sigma factor FliA mediated the bacterial adhesion and the invasion of host intestinal wall in Crohn's disease (Romling and Balsalobre 2012; Haiko and Westerlund-Wikstrom 2013), whereas another study shows, that FliA is an alternative sigma factor complementing the flagellar promoter transcription in *Yersinia pseudotuberculosis* (Ding *et al.* 2009).

Ding *et al.* (2009) reported that the late expression of the *fliA* gene occurred only after the formation of flagellar basal body protein, FliC, together with its anti-sigma factor FlgM. However, the study also reported that deletion of the *fliA* gene significantly reduce the bacteria's swarming motility by downregulating *fliC* by half (Ding *et al.* 2009). One possible explanation for the increased cfu by PW3643-Δ*fliA* mutant in our study may be driven by subjected post-transcriptional regulation of the *fliC* genes as reported similarly in Ding *et al.* (2009).

Despite past studies reporting on reduced motility, a vital biofilm formation factor, in *fliA* mutants, our study shows that the *fliA* mutation did not hinder biofilm growth and was not affected during the initial biofilm formation on the urinary catheter despite not having a functional putative protein FliA. However, microscopy observation of the biofilm structure showed that at 24 h the PW3643-Δ*fliA* mutant was not able to produce a three-dimensional mature biofilm similar to wild type's stratified "craggy mountain" features, formed a continuous sheet with irregular patches of void areas instead (Figure 7-4, second row). This is the first indication that *fliA* is not important in the initial biofilm formation, but without *fliA,* it cannot achieve the stratified "craggy mountain" mature biofilm feature similar to wildtype at 24 h.

The PW3643-Δ*fliA* has IS*lacZ*/hah transposon inserted near the end of the *fliA* ORF at 75% (Table 7-6). Consequently, the resulting incomplete putative FliA protein by the IS*lacZ*/hah transposon caused amino acid alteration within the FliA DNA binding domain (Table 5-3). The affected domain consists of the helix-turn-helix (HTH) motif at the C-terminal end of the putative protein structure that interacts with the DNA helix major groove (Collins and D'Orazio 1993; Miller and Bassler 2001).

Except for *fliM* mutants, all other transposon mutants in the *fli*-mutant group showed the presence of initial adherence to the surface, although the enumeration data shows that PW2970-Δ*fliC* and PW3621-Δ*fliM* biofilm were 1 log less than wildtype at 1 h timepoint. Coincidently, both of these mutants have IS*lacZ*/hah transposon inserted in the middle (56%) of the ORF for both genes (Winsor *et al.* 2011).

In addition to controlling flagellar biosynthesis at the transcriptional level, *fliA*-dependant bacterial motility is also regulated via an independent flagellar biosynthesis mechanism that is controlled by the intracellular c-di-GMP concentrations, but the related gene that is involved in the motility transcription regulation cross-talks remain unclear. (Lo *et al.* 2016; Francis *et al.* 2017). The pathways in intracellular c-di-GMP enzyme-encoding gene regulation are complex and varied, which allows complementation of other genes that restore the motility function in *P. aeruginosa* PAO1 wildtype, such as *bifA* (PA4367) as reported by Lo *et al.* (2016).

The *bifA* were able to complement *fliA*-deficiency, and restore the *fliA*-related motility defect and the pyorubin production observed in the *fliA* PAO1 mutant strain. (Lo *et al.* 2016; Francis *et al.* 2017). However, the *bifA* was found not able to restore the swimming capability suggesting that *fliA*-mediated c-di-GMP concentration modulation only affects the swarming motility but not the swimming motility of *P. aeruginosa* (Lo *et al.* 2016). The resulting continuous flat and homogenous sheet biofilm observed in mature biofilm formation were probably driven by the higher magnitude of swarming motility as similarly concluded by Shrout *et al.* (2006). It was deduced that the different result of mature biofilm forming flat continuous, homogenous sheet is motivated by active swarming cells, as compared to the highly ordered stratified biofilm features has modulated little swarming cells during the initial biofilm formation (Shrout *et al.* 2006; Anderson *et al.* 2007; De Kievit 2009).

Both of the *fliC* transposon mutants showed the disparity of growth in the early hours, but only PW2970-Δ*fliC* coincides with the Δ*fliC* knockout mutant. In addition to that, our homology modelling analysis also predicted that both FliC proteins derived from the Δ*fliC* transposon mutant are lacking one-half of important α-helical region. As shown in Figure 7-13, the PW2970-Δ*fliC* FliC protein monomer only has a fragment of the variable D2 region and one α-helical region, while PW2971-Δ*fliC* mutant FliC protein only has one α-helical region. Wildtype FliC protein structure exhibits typical flagellin structure that has highly conserved two antiparallel α-helical regions which form the hydrophobic spoke that lines the inner core of the polymerised flagella and the variable region exposed to the outside of the structure (Yonekura *et al.* 2003; Forstneric *et al.* 2017).

The predicted homo-41-mer structures in Figure 7-13 shows the defective mutant-derived FliC proteins will form as polymerised structures that are dissimilar to wildtype due to the missing of flagellin D0/D1 region at the C-terminal end. This reason is that the missing amino acids in the mutant-derived FliC flagellin monomer are essential in producing tight-packing flagellum with neighbouring flagellin monomers (Yonekura *et al.* 2003).

The PW2970-Δ*fliC* biofilm formation is affected probably due to a defective FliC monomer. Due to the lack of D0/D1 at the C-terminal end, we presumed that the PW2970-Δ*fliC* retained the hydrophilic variable D2 region that during polymerisation, and form around the outer layer to cover inner core hydrophilic D0/D1 region as shown in the homology simulation. In the other hand, our study shows that the PW2971-Δ*fliC* would not able to polymerise in urinary environment due to the hydrophobic characteristic of the remaining flagellin D0/D1 region (Yonekura *et al.* 2003; Forstneric *et al.* 2017).

Forstneric *et al.* (2017) reported that the missing D0 region in the *S. typhimurium* FliC protein affects the motility of the bacteria as observed in colony formation on soft agar plates. Additionally, the missing D0 domain in the C-terminal spoke region affects the flagella structure and prevents flagella formation, as it is needed for receptor activation (Forstneric *et al.* 2017). As the transposon mutants still have the N-terminal D0 domain, the protein-protein interactions with toll-like receptor 5 (TLR5) heterodimeric complex for flagellin activation are presumably reduced. Our finding similarly supported by the results shown by the knockout Δ*fliC* mutant, which coincides with the results shown by PW2970-Δ*fliC* but significantly reduced cfu showed in 1 and 3 h biofilm. Subsequently in 6 h and 24 h, both transposon mutants PW2970-Δ*fliC* and Δ*fliC* proceed to have similar biofilm enumeration data. The correlation of data between PW2970-Δ*fliC* and Δ*fliC* shows that the different effects between the PW2970-Δ*fliC* and PW2971-Δ*fliC* biofilm was not due to *fliC* deletion pleiotropic effect but instead were mainly affected by the different transposon location of the gene that removes important functional regions of the flagellin.

Previous study has shown that FliC not only serve as motility appendages, it is also involved in innate immunity as well as the release of outer membrane vesicles (OMV) in *P. aeruginosa* that are responsible for the antibiotic resistance transfer as well as packaging the signal molecules in quorum-sensing system (Choi *et al.* 2011; Haiko and Westerlund-Wikstrom 2013). We also studied the role of chemotaxis in the formation of biofilm on the urinary catheter by using the Δ*fliM* transposon mutants. As shown in Figure 7-13, the PW3621-*fliM* mutants with IS*lacZ*/hah inserted in the middle of the ORF produced an incomplete putative FliM protein that lacks *β*-sheets region needed to bind with FliG, to form the C-ring 'switch complex' together with FliN (Terashima *et al.* 2008; Guttenplan and Kearns 2013). The functionality of the FliN-FliM-FliG 'switch complex' were mostly affected by the mutation in FliM because interacts with and triggers the movement activation of the C-terminal domain of FliG. The FliM–FliG interface will then interact with the stator protein, MotA (Terashima *et al.* 2008; Guttenplan and Kearns 2013; Fong and Yildiz 2015). Mutation in the FliM will thereby alter the rotor-stator interaction that controls the swimming speed and rotary direction movement by invoking FliG and MotA in response to the surface as detected by the chemotaxis receptor localised at the pole (Mattick 2002; Terashima *et al.* 2008; Kearns 2010; Guttenplan and Kearns 2013; de Anda *et al.* 2017).

The *P. aeruginosa* surface sensing mechanism in chemotaxis role in biofilm formation is still not well understood, but since both *fliM* mutants in this study showed strong evidence of reduced bacterial attachment in the first hour, it is clear that FliM is essential during the initial attachment in biofilm formation. The *fliM* gene could be a target gene for further study to impede the mechanism of surface sensing, chemotaxis and flagella-related motility in biofilm formation.

7.4.3 The pili (*pil*-) transposon mutant group

From the two *pilA* mutants, the fact that mutant PW8621-Δ*pilA* showed significantly strong evidence of reduced biofilm enumeration of more than 1 log less than wildtype shows the involvement of type IV pili in initial biofilm attachment. To elucidate the PilA deficiency was due to mutated *pilA* gene, the predicted protein structure was shown in Figure 7-13 shows that both *pilA* mutants only retained the single α-helical pilin monomer. However, similarly to previous gene transposon results, only the PW8621-Δ*pilA* mutant with a transposon insertion in the middle of the ORF (49% of the ORF) is a more effective mutant compared to PW8621-Δ*pilA* (36% of the ORF). The biofilm enumeration result of PW8621-Δ*pilA* is also supported by the knockout mutant Δ*pilA.*

Both *pilA* mutants showed a similar presence of cell aggregation features to wildtype at the 1 h, which indicates cells twitching with near-distanced neighbours coming together forming significantly larger cell groups through microcolony merging and maintained as individual cell groups. However, there were less attached cells at 3 h for PW8621-Δ*pilA* as observed from the EDIC images. This is probably an after-effect of the reduced cells at 1 h, which caused cells fail to transition from reversible attachment to irreversible attachment due to lack of type IV pili. This shows the importance of *pilA* in securing an establishing attachment of cells to the surface after that first initial attachment mediated by flagella.

However, at 24 h, both *pilA* mutants showed very different mature biofilm features between them compared to wildtype. Although PW8621-Δ*pilA* mutant showed a stratified three-dimensional structure, the macrocolonies formed are more prominent than wildtype. Whereas PW8622-Δ*pilA* can produce three-dimensional microcolonies albeit smaller than wildtype and the biofilm is distributed covering the catheter surface. This shows that our observation follows the link between the degree of motility in cells during initial biofilm formation influencing the mature biofilm structures as previously reported by Shrout *et al.* (2006), Anderson *et al.* (2007) and De Kievit (2009). The effective mutant PW8621-Δ*pilA* has a lesser motility magnitude compared to PW8622-Δ*pilA* due to lack of PilA.

On the contrary, the PW7438-Δ*pilF* showed no effect on biofilm enumeration implies it is not essential in biofilm formation, even though the mutant showed different behaviour of development compared to wildtype. PilF is a lipoprotein pilotin responsible in pilin assembly by involving in the PilQ outer membrane localisation and multimerisation in order to secrete the major pilin PilA across the outer membrane (Koo *et al.* 2008; Frans *et al.* 2013; Koo *et al.* 2013). Past studies have shown that mutation to PilF abrogated the type IV pilus function by reducing the cell surface piliation and affect attachment (Koo *et al.* 2008; Wesseling 2015).

However, our study shows that there is no effect caused by *pilF* mutation on attachment in biofilm formation. This could be explained by the predicted PilF protein structure of the PW7438-Δ*pilF* mutant in Figure 7-13 that shows the putative protein is missing one tetratricopeptide repeat (TPR), which is the last TPR (TPR6) at the C-terminal end. Koo *et al.* (2013) have reported the functional mapping of PilF that consist of a narrow hydrophobic groove in TPR1 that is important for putative PilG interaction, and TPR2 to TPR4 are required for secretin assembly. Whereas deletion of TPR5 or TPR6 did not reveal to have any effect on the type IV twitching motility (Koo *et al.* 2013). This supports our findings where PW7438-Δ*pilF* showed no importance in biofilm formation on the urinary catheter even though the mutated putative PilF is missing the unimportant TPR6 region.

7.4.4 Differences between transposon and knockout mutants

The knockout mutant enumeration data for Δ*fliC* and Δ*pilA* supports the data obtained from the PW2970-ΔpilC and PW8621-Δ*pilA* showing that these transposons are effective compared to their other IS*phoA*/hah pair. Both Δ*fliC* and Δ*pilA* showed significantly less biofilm compared to wildtype, but the observation of the biofilm showed both knockout mutants have no problems in adherence and microcolony formation. This shows that adherence and microcolony formation can happen with the presence of either *fliC* or *pilA*.

The EDIC observation further supports the transposon result as the Δ*fliC* biofilm at 24 h produced flat, homogenous, continuous sheet and lack of three-dimensional structure compared to Δ*pilA* that produced a slightly bigger three-dimensional macrocolony that is similar to PW8621-Δ*pilA*.

The double knockout mutant Δ*fliC*Δ*pilA* hardly shows any biofilm structure, except for the slight presence of attached cells at 24 h indicates that deletion of both genes abrogates biofilm formation effectively. The previous study by Burrows (2012) reported that mutants that are deficient in both *fliC* and *pilA* adapt to sliding motility instead.

7.4.5 Role of AM-negative mutants in *P. aeruginosa* PAO1 biofilm formation

We deduced that the flagella and type IV pili have an interdependence connection in *P. aeruginosa* motility, especially during attachment and microcolony formation that affects the resulting macrocolony structure in mature biofilm formation. Flagella is essential during cell aggregation and microcolony formation during initial biofilm formation due to its chemotaxis and swimming function. Without it, the cells will be distributed across the catheter surface with no ordered cell organisation (Figure 7-4 and Figure 7-10).

Ong *et al.* (2008) also mentioned how flagella-mediated motility is important in the early attachment phase. Pratt and Kolter (1999) have reviewed previously that the same important roles were also in *E. coli* using Luria Bertani (LB) broth (Pratt and Kolter 1999). However, no actual visualisation on microcolonies formation reported in studies on urinary biofilm, even though O'Toole and Kolter (1998) has emphasised the important role of twitching motility involved (Pratt and Kolter 1999). Our study offers the visualisation of these early events that are affected by flagella-deficiency.

During attachment, the flagella functions in anchoring the cells to the surface, whereas the pili secure the cells to the surface with the help of adequate biosurfactant, making the attachment irreversible, thus prevent the return of the cell to the planktonic form. However, if only flagella is available without pili, it will keep on swimming but not stably attached to the surface, causing the cells to be detached, and causing a phenomenon we refer as a reversible attachment. This means that the type IV pili are important in cell-surface and cell-cell adherence to maintain the biofilm structure. Subsequently, the resulting macrocolony formation without flagella will a flat, continuous, homogenous sheet form, which shows that flagella are essential to achieve the three-dimensional 'craggy mountain' features.

A molecular study on gene expression in *P. aeruginosa* between planktonic and biofilm state by Whiteley *et al.* (2001) revealed that the flagella and pili genes are repressed in biofilms and once completed its function in the attachment and microcolony formation, the subsequent development stages were no longer required for maintenance of a mature biofilm. However, our results show that both flagella and pili are needed to maintain healthy wildtype mature biofilm characteristics.

7.4.6 Different effect in biofilm formation obtained from two transposon mutants of a gene

The different effects obtained from the two transposon mutants of a gene is observed in this study and has been reported before by Wu *et al.* (2008). Wu *et al.* (2008) discussed the mutants obtained from the two-allele library exhibit uncharacterised susceptibility to some antimicrobials could not be attributed to the *phoU* mutation. In our study, we observed that the different biofilm formation behaviour was due to the transposon insertion that affected important putative protein regions that did not render its function useless.

However, in transposon insertions that eliminate the same functional region from the putative protein, it is a coincidence that the effective mutants are from the IS*lacZ*/hah mutant. This is because the insertion location for the two transposon systems is still different.

Therefore, the underlying reason that causes this disparity between the two transposons, (it could be unique to urine media), is still not well understood and needs further research done. These findings contribute to future consideration to use transposon mutants that are preferably inserted in the middle to ensure the effectiveness, or use a knockout mutant instead, especially when studying biofilm using urine media compared to general media.

7.4.7 The unique fibril structure that helps in the translocation of cells but not mediated by *filA*, *filC*, *filM, pilA or pilF*

The unique fibril structure reported found in previous sections was observed to exist throughout all the strains of AM-negative EDIC images, except for the knockout mutant, which when the observation was stopped at 24 h did not form any prominent microcolonies. It could be possible that there is another motility gene that is involved in the unique structure that was seen forming a track to guide incoming cells towards the microcolonies. The reason that it has not been reported elsewhere is probably due to the use of standard lab medium commonly used to study *P. aeruginosa* biofilm, which suggests this characteristic is only displayed in urine media as used in our study. This could additionally suggest that the unique fibril structure could be specific to urine medium.

7.5 Conclusion

Our study shows the close relationship between cell-surface appendages and the affected biofilm formation characteristics. Additionally, this makes the attachment and motility genes the key determinants important to biofilm formation and structure. Among these genes, we found that the mutants that were affected with the gene-deficiency during initial biofilm process are PW2970-*ΔfliC*, PW3621-*ΔfliM, and* PW8621-*ΔpilA* and that their knockout mutants further support both PW2970- Δ*fliC* and PW8621-Δ*pilA* results. We found in this study that it is better to choose mutants with transposon insertion location is in the middle of the target gene, and that it is preferable to use mutants with IS*lacZ*/hah than IS*phoA*/hah transposon.

Our study showed that the *P. aeruginosa* cell attachment to the surface could be via *fliC* or *pilA*, but not without *fliM* (or other chemotaxis sensor mechanism genes) which is needed for surface sensing and rotational movement to get a secure attachment. The rotation of flagella is vital to bring the bacteria near to surface, which powers the movement before it then attaches. We suspect that flagella are important during crucial surface contact and interaction in establishing attachment within the first hour, as shown in our findings.

Close examination of the biofilm structure in our study also shows that the flagella and type IV pili genes are also crucial in maintaining the mature biofilm structure. Previous studies in *P. aeruginosa* motility in biofilm formation were conducted using a carbon-based medium with flow cell growth chambers. Microscopically observed by CLSM showed that both flagella and pili are essential in mature biofilm, as migrating subpopulation motile wildtype cells gives the biofilm its "mushroom"-like feature in biofilm microcolonies (Klausen *et al.* 2003a; Klausen *et al.* 2003b; Allesen-Holm *et al.* 2006; Ghafoor *et al.* 2011; Tolker-Nielsen 2014).

Our findings are significant as it mimics the microenvironment of the biofilm on the urinary catheter closely. Additionally, using EDIC microscopy to analyse the biofilm structure *in situ* has revealed that mature urinary biofilms do not have the "mushroom"-like feature, instead, it is more closely relatable to stratified "craggy mountain"-like description.

The unique fibrinous structure exists in all AM-negative mutant biofilm EDIC images were observed present in the early stages of biofilm formation. This indicates that there could be an external factor other than the AM-negative genes studied that controls this unique structure. This unique structure seems important as it continues to exist in all AM-negative mutant biofilm and support cell translocation across the catheter surface that leads to microcolony formation in biofilm development. It does raise a question as to whether the mutants are not able to produce complete prevention or attachment in biofilm formation was because of this unique structure. As there is very little known about this, therefore this can be later extended using a protein stain such as SYPRO® Ruby stain to show if it is a proteinaceous compound to determine the next target gene of study.

Since this work offers the groundwork on urinary biofilm formation, it is possible that future work includes the study of other target genes that are not covered in our work. One particular gene, *flhF* in *P. aeruginosa*, has not been studied in biofilm formation on the urinary catheter. Previous studies have found the *flhF* function to be flagellin biosynthesis and affected the swarming motility on the agar plate. Murray and Kazmierczak (2006) reported that *flhF* does not increase flagellin synthesis but affects the motility efficiency in *P. aeruginosa* PAK strain in 0.5% M8 swarming media agar. At the time of writing there is one transposon mutant available from the UW Genome Sciences and it has a confirmed IS*lacZ*/hah transposon inserted at 59.6% if the ORF (Winsor *et al.* 2011). Additionally, other future work includes using Western blotting or fluorescence microscopy to show the presence of flagella or type IV pili in this study.

Chapter 8 Overall Discussion and Conclusion

8.1 General discussion

8.1.1 AUBK artificial urine media (Brooks and Keevil 1997) for urinary biofilm studies

The research undertaken has shown the importance of using the appropriate AUM and shown the benefit of comparable results obtained from using AUBK for biofilm growth in our study. The effect of nutrients on biofilm not only affects the metabolic activity of the cells but also affects the EPS production that is needed to maintain the biofilm structure. This can directly concern the proliferation of cells in biofilms and their tolerance to antimicrobial treatment (Gray *et al.* 2008; Singh *et al.* 2017). An overall observation of biofilm formation grown in AUBK in this study produced satisfactory and healthy biofilm development on the urinary catheter. Our study supports the use of AUBK as the preferred artificial urine media formulation in place of urine due to its similar physicochemical properties that support healthy biofilm formation instead of using general laboratory media or other incorrectly formulated media in future urinary biofilm studies.

8.1.2 Repeatable and dependable static biofilm growth model in 6-well plate

The justification of using the static biofilm growth model in 6-well plates with the rationale that it provided a rapid and efficient model for biofilm growth on urinary catheter sections (Wilks *et al.* 2015). Our study also supports this method as prospective growth model assay for future *in vitro* urinary biofilm research. The biofilm growth model proves to be easy to reproduce for comparable biofilm studies and cost-effective. Future applications that can use this method are related urinary biofilm formation studies on the urinary catheter or biofilm formation on other materials for biofouling testing.

8.1.3 EDIC/EF microscopy to image biofilm formation on the catheter

The use of EDIC/EF microscopy in this research allows the *in situ* direct visualisations of the biofilm formed on the catheter has proven to be very useful and avoids artefacts commonly associated with electron microscopy. Unique characteristics that were observed in PAO1 wildtype biofilm suggest valid physiological gene induction observed in the mutants and not an artefact of the urine. Additionally, this work could not have been possible to be conducted with the commonly used observation technique, confocal laser microscopy (CLSM), due to the curvature of the catheter surface. Our study also supports the advantage of using EDIC/EF microscopy due to less sample treatment needed that lessen the preparation time before observation without compromising the quality of visualised images that showed distinct differences in biofilm phenotypes formed on the catheter surface.

8.1.4 Contribution of our findings to the current understanding of urinary biofilm formation in *P. aeruginosa*

The study of *P. aeruginosa* as a model organism for urinary biofilm formation and the associated genetic regulation studied has yielded a wealth of information that contributes to advancing our understanding of the biofilm as a complex, multi-cellular community. (Rice *et al.* 2009; Flemming *et al.* 2016). The use of *P. aeruginosa* PAO1 transposon mutants has shown how associated genes has impacted the different stages in urinary biofilm formation in our study. Table 8-1 summarises the findings in our study that contribute to the understanding of the *P. aeruginosa* urinary biofilm formation and the studied genes associated with it. Each column represents a distinct episode in biofilm development that is observed in our study.

Our finding also shows that the attached cells aggregated upon attachment to catheter surface at 1 h. This is different than what previously reported by Klausen *et al.* (2003b) that suggested that initial microcolonies in *P. aeruginosa* biofilm formation were formed via clonal growth from single cells on the surface and not through cell aggregation. Our finding showed that the cell aggregated at 1 h and 3 h, in addition to the presence of a unique filament trail feature that helps to translocate and navigate cells towards nearby microcolonies that were also present in all mutant' biofilm studied. However, our study was not able to determine the time which the clonal growth occurred in our study, even though division of cells were observed at 3 h, the possibility of it happening concurrently to cell aggregation event before 3 h could not be excluded.

The initial phase of biofilm formation at 1 h can be assessed in two consecutive steps; one is the ability for rapid cell attachment, and two is the ability to remain on the surface with the help of either biosurfactant, polysaccharide or surface appendages. To attach to the surface requires the help of *P. aeruginosa* flagella motility function to swim towards the surface for the cell to interact and tether itself to the surface via the flagella cell pole (O'Toole and Kolter 1998; Mattick 2002; Caiazza and O'Toole 2004; Burrows 2012). This can be seen from our results where attachment was poor for *fliC*, *fliM* and *pilA* deficient mutants at 1 h, thus affecting the initial biofilm formation. The active swimming action needs the flagella motor to propel the flagella so that cells move closer to the surface and tether itself at cell axis, before the cells then transition longitudinally on the surface (Terashima *et al.* 2008; Kearns 2010) (Caiazza and O'Toole 2004).

The rotational action by flagella motor also influences the tethered cell's movements which causes the cell to actively "spin" on it axis while attached to the surface, as reported by Conrad (2012). The rotational spin can either assist the cells transition to longitudinal attachment, or causes the reversible attachment of tethered cells to detach and swim away from the surface, returning to their planktonic state (Lawrence *et al.* 1987; Sauer *et al.* 2002; Conrad *et al.* 2011; Burrows 2012).

Table 8-1 Overall summary on the *P. aeruginosa* urinary biofilm formation and the genes associated with it in our study

***P. aeruginosa* PAO1 strains**	**Biofilm formation timeline**		
	1 h	**3 h to 6 h**	**24 h**
Wildtype biofilm characteristics	**Early reversible attachment stage** • Initial cell attachment to the catheter surface	**Reversible to irreversible stage** • Self-produce EPS • Cell aggregation • Biofilm differentiation towards microcolony formation	**Early mature biofilm stage** • Biofilm differentiation towards mature biofilm formation • Three-dimensional biofilm form • Followed by dispersal stage (more than 24 h)
Urease-negative mutants		Increased cfu/catheter section at 3 h but no effect to biofilm formation	
QS-negative mutants	• *rhlB* - Reduced cfu/catheter section biofilm attachment at 1 h.	• *rhlB* - Reduced cfu/catheter section biofilm attachment at 3 h. • *lasI* • *rhlI* • *pqsA* • *pqsE* } Increased cfu/catheter section but normal microcolony formation at 3 h • *rhlA*- -Produced unique geomatric microcolonies at 3 h.	• *lasI* • *rhlI* • *rhlA* • *rhlB* • *pqsA* } Increased cfu/catheter section biofilm attachment at 24 h. • *lasI* • *rhlI* • *pqsA* • *pqsE* } Produced undifferentiated, flat biofilm with water channels at 24 h.
PS-negative mutants	• *pelA* and *pslD* – Reduced cfu/catheter section biofilm attachment. – Cell "footprints" suggest weak attachment	*pslD* - Reduced cfu/catheter section biofilm attachment. (1 h to 6 h)	• *pslD* – Produced three-dimensional elevated biofilm towers at 24 h.
AM-negative mutants	• *fliC* • *fliM* • *pilA* } Reduced cfu/catheter section biofilm attachment at 1 h.	*fliC* - Reduced cfu/catheter section biofilm attachment at 3 h.	• *fliA* • *fliC* • *fliM* } Produced undifferentiated, flat biofilm with water channels at 24 h.

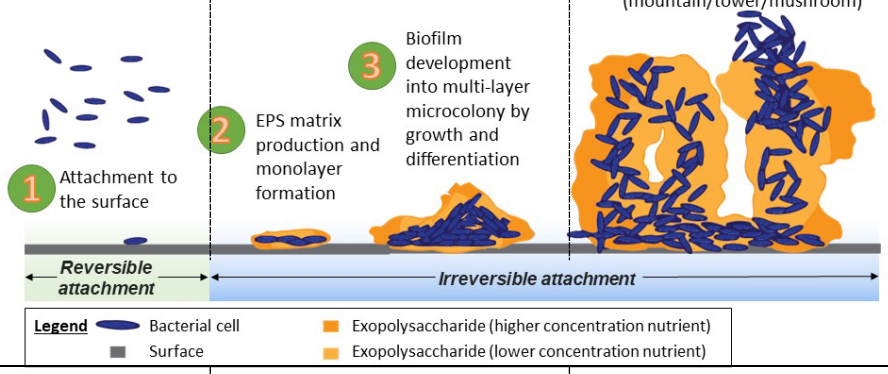

Therefore, our findings also support this as observed in the results shown by *fliM*-negative mutant biofilm formation that presented more biofilm as well as bigger microcolony formation at 3 h, following the successful attachment at 1 h due to the inactivity of the flagellar motor that restricts the cell movement. The first attachment of cell triggers the stimulation of various biofilm proteins' expression which will help with the subsequent phases in biofilm formation (Sauer *et al.* 2002). This can be exemplified in our findings shown by *fliM*-negative mutants where there was no ConA-stained EPS material found at 1 h as there is no apparent cell attached to the surface (Figure 7-6).

Our study showed that the subsequent related step during attachment of cells needed to maintain and secure adherence to the surface is depended on several factors. One of the factors is by the action of surface appendages, as shown in the results by the biofilm growth of *fliC*-negative mutants and *pilA*-negative mutants. Additionally, another critical factor is the surface conditioning properties of the catheter that consists of the self-produced polysaccharide EPS as shown in the results of biofilm formation by the *pelA* and *pslD*-negative mutants, as well as surface biosurfactant as shown in the results by *rhlB*-negative mutant activity.

After 3 h, when cells have attached to the surface and strengthened their adherence with surface appendages and self-produced EPS matrix, the cells aggregate together via flagella-mediated motility. This was shown in the results by the defective *fliC* mutant that did not show organised cell aggregation formation at 1 h and 3 h, which corresponds with the reduced cfu/catheter section biofilm enumeration data. It was not determined in our study that the quorum-sensing genes were involved, as all QS-negative mutants feature cell aggregation in biofilm formation, although the QS mutant group did show increased biofilm enumeration, suggesting that the QS genes were not needed and probably down-regulated during these early events.

Similarly, the twitching motility in *P. aeruginosa* has also been reported to be not regulated by quorum-sensing. (Klausen *et al.* 2003a), suggesting that the cell aggregation migration is independent and not coordinated by QS. This is explained by Martinez and Campos-Gomez (2016) that the microcolony formation was induced by oxypilins, which increases twitching motility but affected by the c-di-GMP that also regulates biofilm formation in *P. aeruginosa*. Cells become more aware when quorum-sensing signal regulation are downregulated during biofilm formation that induces surface motility and motivates cell to be aggregated.

The continuous reduction of *pslD*-negative mutant biofilm shown at 3 h and 6 h suggests that Psl is the preferred polysaccharide in maintaining strong EPS biofilm matrix that confirms the irreversible attachment phase during *P. aeruginosa* biofilm formation. However, no apparent differences to biofilm structure were present in the *pslD*-negative mutant compared to wildtype,

which suggests that the role of Psl is more in maintaining the EPS matrix but not for the structure of microcolonies. This is supported by the towering macrocolonies presented by the *pslD*-negative mutant at 24 h.

The urinary biofilm formed by *P. aeruginosa* wildtype features unique characteristics that differ from the usual macrocolony biofilm description that commonly affiliated to "mushroom with stalk and cap" structures, as reported by past studies (Toutain *et al.* 2004; Allesen-Holm *et al.* 2006; Yang *et al.* 2011; Tolker-Nielsen 2014; Toyofuku *et al.* 2016). This "mushroom" description were related to the "cap" structure formed by the motile cells that have moved towards the top of the macrocolony via type IV pili (Bjarnsholt 2013; Wesseling 2015). However, the description of biofilms has so far been an open interpretation as it has been reported that biofilms can differentiate further into other elaborate forms (Stoodley *et al.* 2002).

Contrastingly, our findings showed that the observed macrocolony in *P. aeruginosa* urinary biofilm formation structure is more affiliated to the "mountain-like" features. At 24 h, the macrocolonies observed featured three-dimensional and stratified with amorphous precipitation at the exterior that is similar to a "craggy mountain" structure. The presence of void spaces in between the macrocolony "mountain" suggested the formation of water channels in between. We were also able to observe the dispersal phase in the wildtype biofilm that features the central "hollow crater" structure in the macrocolony "mountain" suggesting the missing peak was created by released cells from the top of the biofilm macrocolonies.

However, these three-dimensional biofilms were not able produced by the QS-negative mutants, *lasI* , *rhlI*, *pqsA*, and *pqsE,* suggest that broken down cell signalling in QS systems prevents the biofilm differentiation and three-dimensional macrocolony structure in *P. aeruginosa* urinary biofilm formation. Davey *et al.* (2003) and Caiazza *et al.* (2005) has similarly reported that quorum-sensing-controlled production of rhamnolipids were required in the maintenance of three-dimensional macrocolony biofilm in their studies.

Our findings are also supported by previous studies by Tolker-Nielsen (2014) and Yang *et al.* (2011) that QS is important for the "mushroom-cap" structure in macrocolony biofilm formation. This means that, in absence of essential QS gene, a defective QS system causes broken cell-cell communication that affected biofilm differentiation and mature biofilm formation in *P. aeruginosa.* Additionally, we also found that flagella-related mutants were also unable to form three-dimensional macrocolony biofilm. This suggested that flagella-mediated motility has an important role in mature biofilm formation that was similarly reported by Klausen *et al.* (2003b), but contrasting to the report by Wesseling (2015) which indicate that the motility role in mature biofilms were mediated by the type IV pili instead. Our finding shows that the biofilm formed by

pilA-negative mutants were differentiated and formed macrocolony structure at 24 h, compared to the flat and undifferentiated biofilm by *fliC*-negative mutants.

According to Francolini and Donelli (2010), the possible strategies in biofilm treatment and prevention should be based on the bacterial adhesion and surface colonisation, interference to quorum-sensing signal molecules modulation in biofilm development, and the biofilm matrix dispersal phase. Our finding would add the suggestions by Francolini and Donelli (2010) that the bacterial surface appendages showed important attachment/motility roles are more related to most of the strategies mentioned but was not suggested. Additionally, based on our findings, we have demonstrated that quorum-sensing signal deficiency caused no problem in modulating microcolony formation, even though it affects the macrocolony structure significantly in biofilm development.

Our findings also suggest that the dispersal events were not exclusively depending on the biofilm matrix, but it could also be contributed by quorum-sensing, motility or other biofilm virulence factor. It is also emphasized that the motivation in examining the factors contributing to the biofilm structure is to prevent the three-dimensional biofilm formation. Although these strategies suggested were more applicable for biofilm formation in general, in regard to biofilm on the urinary catheter, it is focussed more on the prevention of biofilm formation and eliminate the need for treatments that induce the dispersal phase to disintegrate it.

Lastly, the key processes regulating EPS matrix differentiation and dispersal were not determined from our study although there is a need for more research in the current understanding of it.

8.1.5 Footprints

Using DAPI/ConA differential staining on the biofilm, allows us to analyse the EPS layer of the biofilm based on the visualisation of the D-mannose component of the EPS that absorbs the ConA and cells-stained DAPI against each other or with EDIC for the actual catheter surface condition. We observed instances of cell “footprints” which shows differentiation features of the EPS that indicates cell presence but had no cells visualised in the corresponding DAPI or EDIC images.

This indicates the attachment of cells has been compromised, either by molecular factors such as weak EPS binding cells to surface, or to physical factors such as lack of attachment pili. Due to these factors, even with careful handling during the wash step, the cells can easily be removed and washed away leaving traces of “footprint” on the EPS instead (Neu and Marshall 1991; Gomez-Suarez *et al.* 2002; Toutain *et al.* 2004; El-Kirat-Chatel *et al.* 2014). Gomez-Suarez *et al.* (2002) reported that analysis of the cell “footprints” using x-ray photoelectron spectroscopy

indicated it consisted of uronic acids. Moreover, these "footprints" were also previously reported to be caused by the degeneration of biofilm due to enzymes, cell death or weak biofilm structure that then detached away as aggregated cells into the liquid interface. Detached biofilm is also termed as "flocs" and were reported to still retains certain biofilm characteristics (Hall-Stoodley *et al.* 2004). However, our study was unable to determine further the related characteristics of the bacterial "footprints", other than that it might have influence the unique filament trails that we observed functioning as translocating nearby cells to the nearest microcolonies.

8.1.6 Unique biofilm structure

Among the findings in this study is the presence of a unique structure that resembles a long fibrinous structure. This structure forms long trails that extended from an aggregated cell or microcolonies, which then either forms a bridge between them or seems connected to cells and seemed to help in the translocation of cells towards the microcolonies.

This unique structure was observed in *P. aeruginosa* wildtype urinary biofilm formation as well as in all the transposon mutants studied, suggesting that it is induced by other genes and could possibly be unique for urinary biofilm formation. Closer observation of the unique fibrinous structure revealed it was very different and allows the elimination of other possible explanations for the structure's origin.

The width of the unique fibrinous structure in our study were wider and singular, rather than the filamentous bacteriophage reported in Webb *et al.* (2004) and Secor *et al.* (2015). Although the unique structure in our study was observed connecting between microcolonies, it only forms a singular direct trail/bridge, and differs from the complex network formed by eDNA as reported in Bockelmann *et al.* (2006). We have also eliminated the possibility that this unique structure could be functional amyloid (Zeng *et al.* 2015), even though we had previously described the possibility of links to the biopolymer bridging produced by the bacterial "footprints" mentioned previously.

This also brings our attention to the close but not similar report by Zhao *et al.* (2013) which showed the deposition of Psl by cell migration on the surface, creating a Psl trail that influences the subsequent migration of cells and induces biofilm formation. Another Psl-related report by Wei and Ma (2013), suggested that the presence of Psl can form spider-like fibre matrix created from the pili-mediated cell migration. Seeing that the pslD-negative mutant biofilms still present the unique fibrinous track structure in our study suggests that this unique structure differs than the Psl-mediated structure reported in Zhao *et al.* (2013) and Wei and Ma (2013), or that it consists of Psl and other factors that were not included in our study. It is possible to extend this

finding to future research to provide clearer information on the role and origin of this unique fibrinous track structure.

8.1.7 Limitations of current research

Our study carefully analysed the urinary characteristics by various media as well as the genes affecting the biofilm formation on urinary catheter. This work introduces new knowledge to urinary biofilm research. However, there are limitations to the current work that could be resolved by future studies extending from this thesis.

Overall, the current research was limited by time, which restricted the amount of work conducted that could otherwise be improved and further explored in the future. There are two notable limitations to mention: 1) although the *P. aeruginosa* mutant strains used for this study have been verified elsewhere (Held *et al.* 2012), additional work needs to be conducted to verify further the transposon location in the PAORF upon receiving the strains; and 2) the work conducted is limited to the biofilm phenotype features within 24 h in static culture.

8.2 Proposed future studies as an extension of existing research

The potential investigation is endless as many aspects in the research area can be further explored. This study is important to be continued as it will support and simultaneously extend the foundations of previous literature research in the area of biofilms in general, and specifically the biofilms in urinary catheters. The proposed extension of current research is as below:

8.2.1 Verification of the transposon location in mutants

The verification of the *P. aeruginosa* mutants can be easily resolved as currently the strains are kept in -80^{o}C freezer to ensure culture stability for future verification work. Verification of the transposon location can be conducted as described by Held *et al.* (2012) and following the protocols available on the *P. aeruginosa* two-allele mutant library website by the UWGC (https://www.gs.washington.edu/labs/manoil/libraryindex.htm) (University of Washington, Seattle, Washington, USA) (Jacobs and Manoil 2006). Our study on the genes affecting the urinary biofilm formation were conducted up to 24 h, which meant that further biofilm characteristics that might have presented beyond that point could not be observed.

8.2.2 Studying the biofilm development longer than 24 h

Even though our findings were able to present all five of the distinct biofilm phenotypes by the *P. aeruginosa* PAO1 wildtype within 24 hours, the possibility of additional urinary biofilm characteristics beyond 24 h of growth can be studied as our future work.

8.2.3 Screening for other possible variation of genotype-phenotype relationship in urinary biofilm studies

The work in Chapter 7 shows the advantage of using single and double knockouts in understanding the genotype-phenotype relationship in urinary biofilm formation. With the new genome-editing CRISPR-associated protein 9 (CRISPR-Cas9) system that could provide a promising tool for the generation of the knockout mutants with ease that definitely would benefit the future work (Gupta and Musunuru 2014; Hsu *et al.* 2014; Arora and Narula 2017; Komor *et al.* 2017).

After studying the biofilm development of single uropathogen species, there is a need to consider dual or multi-species of bacteria when existing together as a biofilm. It is crucial to diverge further and look into how these microscale communities of biofilm communicate and live or work together. Potential research includes exploring antimicrobial resistant persister cells and quorum-sensing. There is an immediate need to investigate whether these bacteria in biofilms transfer resistance in biofilm between species, although time will not permit this aspect in the present study.

8.2.4 Nutrients affecting urinary biofilm formation

Bicarbonate is an essential nutrient in the AUBK that was not present in AUG. The effects of bicarbonate to urinary biofilm development can be studied to offer more insights on its function to biofilm regulation. Past studies have found that bicarbonate increases expression of certain virulence genes, increases eDNA and improves biofilm growth (Bourgogne *et al.* 2010; Kesaano *et al.* 2015; Rose and Bermudez 2016).

8.2.5 Biofilm persister cells in the urinary biofilm

The future studies include studying the presence of urinary biofilm persister cells, which pose a risk to antimicrobial treatment and catheter management. In fact, the reported prevalence of resistant strains of bacteria could be a community of biofilm, being tolerant towards the drugs and treatment. The suggested diauxic growth observed in the biofilm of *E. coli* in Chapter 4 was identified in this research and could be further explored in its correlation to persister cells. A past

study by Amato and Brynildsen (2014) has shown that the presence of fluoroquinolone resistant persisters in *E. coli* was induced by the transition of the utilisation of nutrients. With the particular physiochemical properties of the urine that have a dynamic variation among individuals, this makes the study of persister cells an important line of study.

8.3 Concluding remarks and perspectives

The outdated urinary catheter design have contributed to CAUTI prevalence as the material provides an excellent surface area for bacterial adhesion for biofilm development (Wilks *et al.* 2015). Due to the eyelet position above the balloon catheter, it is only capable of syphoning urine that is above the eyelet level, resulting in residual urine in the bladder (Siddiq and Darouiche 2012). The lumen of the urinary catheter is so small and easily become obstructed with biofilm or susceptible to encrustation by urease-producing bacteria. Patients can experience tissue trauma from the removal of encrusted catheter or from rubbing and scratching of the catheter tip with the bladder lining (Getliffe 2003; Flores-Mireles *et al.* 2015).

The background study and literary search were essential to help motivate our pursuit of understanding the factors affecting the three-dimensional structure of biofilms in the urinary catheter. The work contained in this thesis emphasises the need to focus on biofilm development and its role on the urinary catheter as it affects not only new patients but recurrent patients as well. This research aimed to characterise the urinary biofilm formation and the factors affecting its three-dimensional structure, which we have achieved by the presented evidence of well-defined phenotype-genotype relationships of urease, quorum-sensing, polysaccharide as well as attachment and motility genes in urinary biofilm formation.

It is hoped that the additional information provided from this work would benefit the future research in the understanding of the mechanisms of biofilm formation. This work supports and simultaneously extends the background literature on biofilm-related CAUTI and provides the foundation work for future studies in this area of interest.

Future work includes in extending the genotype-phenotype screening of other biofilm-related genes that could have been a valuable tool in understanding different factors that affect the three-dimensional structure of urinary biofilm, which in turn could lead to potential applicable therapeutic and preventive anti-fouling strategies in combating biofilms.

This work is also expected to establish the potential for its findings to have a significant impact on CAUTI studies and improve the quality of patient healthcare and catheter management. Possible application based on our findings could be used for the development of a long-term use catheter

that is effective in preventing biofilm formation by targeting specific genes that hamper the three-dimensional biofilm formation.

This could also forestall the incidences of catheter encrustations and blocked catheter as well as reduced the risk of urinary tract infections. In addition to that, the development of a more cost-effective anti-fouling catheter design or material should also remain the primary focus, which provides more accessibility and benefit to catheter-dependant users worldwide.

In summary, this report has shown an early understanding of the biofilm development on the urinary catheter of substantial importance. Even with the new information gained, and the present knowledge confirmed, there are still much more research needs to be done in for improving the understanding of the science behind the catheter biofilms contributing to CAUTI.

Bibliography

Abisado RG, Benomar S, Klaus JR, Dandekar AA and Chandler JR (2018) Bacterial quorum sensing and microbial community interactions. *MBio* 9(3)

Abou-Elela A (2017) Epidemiology, pathophysiology, and management of uric acid urolithiasis: A narrative review. *J Adv Res* 8(5): 513-527

Allesen-Holm M, Barken KB, Yang L, Klausen M, Webb JS, Kjelleberg S, Molin S, Givskov M and Tolker-Nielsen T (2006) A characterization of DNA release in *Pseudomonas aeruginosa* cultures and biofilms. *Mol Microbiol* 59(4): 1114-28

Alm RA and Mattick JS (1997) Genes involved in the biogenesis and function of type-4 fimbriae in *Pseudomonas aeruginosa*. *Gene* 192(1): 89-98

Altman PL (1961) Physical properties and chemical composition of urine: mammals. Part 1: Man IN: Dittmer DL (ed) *Blood and other bodily fluids.* Washington, D.C.: Federation of American Societies for Experimental Biology 363-369

Amalaradjou MAR, Narayanan A, Baskaran SA and Venkitanarayanan K (2010) Antibiofilm effect of trans-cinnamaldehyde on uropathogenic *Escherichia coli*. *Journal of Urology* 184(1): 358-363

Amato SM and Brynildsen MP (2014) Nutrient transitions are a source of persisters in *Escherichia coli* biofilms. *PLoS One* 9(3): e93110

Amato SM, Orman MA and Brynildsen MP (2013) Metabolic control of persister formation in *Escherichia coli*. *Mol Cell* 50(4): 475-87

Anderson BN, Ding AM, Nilsson LM, Kusuma K, Tchesnokova V, Vogel V, Sokurenko EV and Thomas WE (2007) Weak rolling adhesion enhances bacterial surface colonization. *Journal of Bacteriology* 189(5): 1794-1802

Anderson JD, Johnson KR and Aird MY (1980) Comparison of amoxicillin and ampicillin activities in a continuous culture model of the human urinary bladder. *Antimicrob Agents Chemother* 17(4): 554-7

Armbruster CE, Smith SN, Johnson AO, DeOrnellas V, Eaton KA, Yep A, Mody L, Wu WS and Mobley HLT (2017) The pathogenic potential of *Proteus mirabilis* is enhanced by other uropathogens during polymicrobial urinary tract infection. *Infection and Immunity* 85(2)

Arora L and Narula A (2017) Gene editing and crop improvement using CRISPR-Cas9 system. *Front Plant Sci* 8: 1932

Aubron C, Huet O, Ricome S, Borderie D, Pussard E, Leblanc P-E, Bouvet O, Vicaut E, Denamur E and Duranteau J (2012) Changes in urine composition after trauma facilitate bacterial growth. *BMC infectious diseases* 12(330): 1-10

Azeredo J, Azevedo NF, Briandet R, Cerca N, Coenye T, Costa AR, Desvaux M, Di Bonaventura G, Hebraud M, Jaglic Z, Kacaniova M, Knochel S, Lourenco A, Mergulhao F, Meyer RL, Nychas G, Simoes M, Tresse O and Sternberg C (2017) Critical review on biofilm methods. *Crit Rev Microbiol* 43(3): 313-351

Azevedo AS, Almeida C, Melo LF and Azevedo NF (2014) Interaction between atypical microorganisms and *E. coli* in catheter-associated urinary tract biofilms. *Biofouling* 30(8): 893-902

Azevedo AS, Almeida C, Melo LF and Azevedo NF (2016a) Impact of polymicrobial biofilms in catheter-associated urinary tract infections. *Crit Rev Microbiol*: 1-17

Azevedo AS, Almeida C, Pereira B, Melo LF and Azevedo NF (2016b) Impact of *Delftia tsuruhatensis* and *Achromobacter xylosoxidans* on *Escherichia coli* dual-species biofilms treated with antibiotic agents. *Biofouling* 32(3): 227-241

Bibliography

Baker P, Hill PJ, Snarr BD, Alnabelseya N, Pestrak MJ, Lee MJ, Jennings LK, Tam J, Melnyk RA, Parsek MR, Sheppard DC, Wozniak DJ and Howell PL (2016) Exopolysaccharide biosynthetic glycoside hydrolases can be utilized to disrupt and prevent *Pseudomonas aeruginosa* biofilms. *Sci Adv* 2(5): e1501632

Baker P, Whitfield GB, Hill PJ, Little DJ, Pestrak MJ, Robinson H, Wozniak DJ and Howell PL (2015) Characterization of the *Pseudomonas aeruginosa* glycoside hydrolase PslG reveals that Its levels are critical for Psl polysaccharide biosynthesis and biofilm formation. *J Biol Chem* 290(47): 28374-87

Barford JMT, Anson K, Hu Y and Coates ARM (2008) A model of catheter-associated urinary tract infection initiated by bacterial contamination of the catheter tip. *BJU international* 102(1): 67-74

Baum MM, Kainovic A, O'Keeffe T, Pandita R, McDonald K, Wu S and Webster P (2009) Characterization of structures in biofilms formed by a *Pseudomonas fluorescens* isolated from soil. *BMC Microbiol* 9: 103

Beattie M and Taylor J (2011) Silver alloy vs. uncoated urinary catheters: a systematic review of the literature. *Journal of clinical nursing* 20(15-16): 2098-2108

Belitz H-D, Grosch W and Schieberle P (2009) Milk and dairy products *Food Chemistry*. 498-545

Bjarnsholt T (2013) The role of bacterial biofilms in chronic infections. *APMIS. Supplementum* (136): 1-51

Bjarnsholt T, Alhede M, Alhede M, Eickhardt-Sorensen SR, Moser C, Kuhl M, Jensen PO and Hoiby N (2013) The *in vivo* biofilm. *Trends in microbiology* 21(9): 466-74

Blehert DS, Palmer RJ, Jr., Xavier JB, Almeida JS and Kolenbrander PE (2003) Autoinducer 2 production by *Streptococcus gordonii* DL1 and the biofilm phenotype of a *luxS* mutant are influenced by nutritional conditions. *J Bacteriol* 185(16): 4851-60

Bockelmann U, Janke A, Kuhn R, Neu TR, Wecke J, Lawrence JR and Szewzyk U (2006) Bacterial extracellular DNA forming a defined network-like structure. *FEMS Microbiol Lett* 262(1): 31-8

Bonkat G, Widmer A, Rieken M, van der Merwe A, Braissant O, Müller G, Wyler S, Frei R, Gasser T and Bachmann A (2013a) Microbial biofilm formation and catheter-associated bacteriuria in patients with suprapubic catheterisation. *World Journal of Urology* 31(3): 565-571

Bonkat G, Widmer AF, Rieken M, van der Merwe A, Braissant O, Müller G, Wyler S, Frei R, Gasser TC and Bachmann A (2013b) Microbial biofilm formation and catheter-associated bacteriuria in patients with suprapubic catheterisation. *World Journal of Urology* 31(3): 565-571

Bourgogne A, Thomson LC and Murray BE (2010) Bicarbonate enhances expression of the endocarditis and biofilm associated pilus locus, *ebpR-ebpABC*, in *Enterococcus faecalis*. *BMC Microbiol* 10: 17

Brooks T and Keevil CW (1997) A simple artificial urine for the growth of urinary pathogens. *Lett Appl Microbiol* 24(3): 203-206

Broomfield RJ, Morgan SD, Khan A and Stickler DJ (2009) Crystalline bacterial biofilm formation on urinary catheters by urease-producing urinary tract pathogens: a simple method of control. *Journal of medical microbiology* 58(Pt 10): 1367-1375

Burrows LL (2012) *Pseudomonas aeruginosa* twitching motility: type IV pili in action. *Annu Rev Microbiol* 66: 493-520

Byrd MS, Pang B, Hong W, Waligora EA, Juneau RA, Armbruster CE, Weimer KE, Murrah K, Mann EE, Lu H, Sprinkle A, Parsek MR, Kock ND, Wozniak DJ and Swords WE (2011) Direct evaluation of *Pseudomonas aeruginosa* biofilm mediators in a chronic infection model. *Infect Immun* 79(8): 3087-95

Byrd MS, Sadovskaya I, Vinogradov E, Lu H, Sprinkle AB, Richardson SH, Ma L, Ralston B, Parsek MR, Anderson EM, Lam JS and Wozniak DJ (2009) Genetic and biochemical analyses of the

Pseudomonas aeruginosa Psl exopolysaccharide reveal overlapping roles for polysaccharide synthesis enzymes in Psl and LPS production. *Mol Microbiol* 73(4): 622-38

Cai T, Caola I, Tessarolo F, Piccoli F, D'Elia C, Caciagli P, Nollo G, Malossini G, Nesi G, Mazzoli S and Bartoletti R (2014) Solidago, orthosiphon, birch and cranberry extracts can decrease microbial colonization and biofilm development in indwelling urinary catheter: a microbiologic and ultrastructural pilot study. *World J Urol* 32(4): 1007-14

Caiazza NC and O'Toole GA (2004) SadB is required for the transition from reversible to irreversible attachment during biofilm formation by *Pseudomonas aeruginosa* PA14. *J Bacteriol* 186(14): 4476-85

Caiazza NC, Shanks RM and O'Toole GA (2005) Rhamnolipids modulate swarming motility patterns of *Pseudomonas aeruginosa*. *J Bacteriol* 187(21): 7351-61

Caldara M, Friedlander RS, Kavanaugh NL, Aizenberg J, Foster KR and Ribbeck K (2012) Mucin biopolymers prevent bacterial aggregation by retaining cells in the free-swimming state. *Curr Biol* 22(24): 2325-30

Campanac C, Pineau L, Payard A, Baziard-Mouysset G and Roques C (2002) Interactions between biocide cationic agents and bacterial biofilms. *Antimicrobial Agents and Chemotherapy* 46(5): 1469-1474

Campisano A, Schroeder C, Schemionek M, Overhage J and Rehm BH (2006) PslD is a secreted protein required for biofilm formation by *Pseudomonas aeruginosa*. *Appl Environ Microbiol* 72(4): 3066-8

Cardoso T, Almeida M, Friedman ND, Aragao I, Costa-Pereira A, Sarmento AE and Azevedo L (2014) Classification of healthcare-associated infection: a systematic review 10 years after the first proposal. *BMC Med* 12: 40

Carson L, Gorman SP and Gilmore BF (2010) The use of lytic bacteriophages in the prevention and eradication of biofilms of *Proteus mirabilis* and *Escherichia coli*. *FEMS Immunology And Medical Microbiology* 59(3): 447-455

Cathcart P, van der Meulen J, Armitage J and Emberton M (2006) Incidence of primary and recurrent acute urinary retention between 1998 and 2003 in England. *The Journal of Urology* 176(1): 200-204

Cerqueira L, Oliveira JA, Nicolau A, Azevedo NF and Vieira MJ (2013) Biofilm formation with mixed cultures of *Pseudomonas aeruginosa*/*Escherichia coli* on silicone using artificial urine to mimic urinary catheters. *Biofouling* 29(7): 829-840

Chew SC, Kundukad B, Seviour T, van der Maarel JR, Yang L, Rice SA, Doyle P and Kjelleberg S (2014) Dynamic remodeling of microbial biofilms by functionally distinct exopolysaccharides. *MBio* 5(4): e01536-14

Choi DS, Kim DK, Choi SJ, Lee J, Choi JP, Rho S, Park SH, Kim YK, Hwang D and Gho YS (2011) Proteomic analysis of outer membrane vesicles derived from *Pseudomonas aeruginosa*. *Proteomics* 11(16): 3424-9

Choong S, Wood S, Fry C and Whitfield H (2001) Catheter associated urinary tract infection and encrustation. *International Journal Of Antimicrobial Agents* 17(4): 305-310

Chou Y-H, Huang C-N, Li W-M, Huang S-P, Wu W-J, Tsai C-C, Chang A-W, Chen S-M, Lin Y-L and Lin Y-P (2012) Clinical study of ammonium acid urate urolithiasis. *The Kaohsiung Journal of Medical Sciences* 28(5): 259-264

Chu EK, Kilic O, Cho H, Groisman A and Levchenko A (2018) Self-induced mechanical stress can trigger biofilm formation in uropathogenic *Escherichia coli*. *Nat Commun* 9(1): 4087

Chua SL, Yam JK, Hao P, Adav SS, Salido MM, Liu Y, Givskov M, Sze SK, Tolker-Nielsen T and Yang L (2016) Selective labelling and eradication of antibiotic-tolerant bacterial populations in *Pseudomonas aeruginosa* biofilms. *Nat Commun* 7: 10750

Chutipongtanate S and Thongboonkerd V (2010) Systematic comparisons of artificial urine formulas for *in vitro* cellular study. *Analytical biochemistry* 402(1): 110-112

Clemens DL, Lee BY and Horwitz MA (1995) Purification, characterization, and genetic analysis of *Mycobacterium tuberculosis* urease, a potentially critical determinant of host-pathogen interaction. *J Bacteriol* 177(19): 5644-52

Coenye T and Nelis HJ (2010) *In vitro* and *in vivo* model systems to study microbial biofilm formation. *Journal of Microbiological Methods* 83(2): 89-105

Cole SJ, Records AR, Orr MW, Linden SB and Lee VT (2014) Catheter-associated urinary tract infection by *Pseudomonas aeruginosa* is mediated by exopolysaccharide-independent biofilms. *Infection And Immunity* 82(5): 2048-2058

Collins AS (2008) Preventing health care–associated infections IN: Hughes RG (ed) *Patient Safety and Quality: An Evidence-Based Handbook for Nurses.* Rockville (MD): Agency for Healthcare Research and Quality (US) 547 - 575

Collins CM and D'Orazio SE (1993) Bacterial ureases: structure, regulation of expression and role in pathogenesis. *Mol Microbiol* 9(5): 907-13

Colvin KM, Gordon VD, Murakami K, Borlee BR, Wozniak DJ, Wong GC and Parsek MR (2011) The Pel polysaccharide can serve a structural and protective role in the biofilm matrix of *Pseudomonas aeruginosa*. *PLoS Pathog* 7(1): e1001264

Colvin KM, Irie Y, Tart CS, Urbano R, Whitney JC, Ryder C, Howell PL, Wozniak DJ and Parsek MR (2012) The Pel and Psl polysaccharides provide *Pseudomonas aeruginosa* structural redundancy within the biofilm matrix. *Environ Microbiol* 14(8): 1913-28

Conrad JC (2012) Physics of bacterial near-surface motility using flagella and type IV pili: implications for biofilm formation. *Res Microbiol* 163(9-10): 619-29

Conrad JC, Gibiansky ML, Jin F, Gordon VD, Motto DA, Mathewson MA, Stopka WG, Zelasko DC, Shrout JD and Wong GC (2011) Flagella and pili-mediated near-surface single-cell motility mechanisms in *P. aeruginosa*. *Biophys J* 100(7): 1608-16

Cortese YJ, Wagner VE, Tierney M, Devine D and Fogarty A (2018) Review of catheter-associated urinary tract infections and in vitro urinary tract models. *J Healthc Eng* 2018: 2986742

Costerton JW, Geesey GG and Cheng KJ (1978) How bacteria stick. *Scientific American* 238(1): 86-95

Costerton JW, Stewart PS and Greenberg EP (1999) Bacterial biofilms: a common cause of persistent infections. *Science* 284(5418): 1318-1322

Cox AJ, Hukins DW and Sutton TM (1989) Infection of catheterised patients: bacterial colonisation of encrusted Foley catheters shown by scanning electron microscopy. *Urological Research* 17(6): 349-352

Cox AJ, Hukins DWL, Davies KE, Irlam JC and Sutton TM (1987) An automated technique for *in vitro* assessment of the susceptibility of urinary catheter materials to encrustation. *ARCHIVE: Engineering in Medicine 1971-1988 (vols 1-17)* 16(1): 37-41

Czerwonka G, Arabski M, Wasik S, Jablonska-Wawrzycka A, Rogala P and Kaca W (2014) Morphological changes in *Proteus mirabilis* O18 biofilm under the influence of a urease inhibitor and a homoserine lactone derivative. *Arch Microbiol* 196(3): 169-77

Dave RN, Joshi HM and Venugopalan VP (2011) Novel biocatalytic polymer-based antimicrobial coatings as potential ureteral biomaterial: preparation and *in vitro* performance evaluation. *Antimicrobial Agents And Chemotherapy* 55(2): 845-853

Davey ME, Caiazza NC and O'Toole GA (2003) Rhamnolipid surfactant production affects biofilm architecture in *Pseudomonas aeruginosa* PAO1. *J Bacteriol* 185(3): 1027-36

Davies DG (1998) The involvement of cell-to-cell signals in the development of a bacterial biofilm. *Science* 280(5361): 295-298

de Anda J, Lee EY, Lee CK, Bennett RR, Ji X, Soltani S, Harrison MC, Baker AE, Luo Y, Chou T, O'Toole GA, Armani AM, Golestanian R and Wong GCL (2017) High-speed "4D" computational microscopy of bacterial surface motility. *ACS Nano* 11(9): 9340-9351

De Kievit TR (2009) Quorum sensing in *Pseudomonas aeruginosa* biofilms. *Environ Microbiol* 11(2): 279-88

de Melo WCMA, Avci P, de Oliveira MN, Gupta A, Vecchio D, Sadasivam M, Chandran R, Huang Y-Y, Yin R, Perussi LR, Tegos GP, Perussi JR, Dai T and Hamblin MR (2013) Photodynamic inactivation of biofilm: taking a lightly colored approach to stubborn infection. *Expert Review Of Anti-Infective Therapy* 11(7): 669-693

Denstedt JD and Cadieux PA (2009) Eliminating biofilm from ureteral stents: the Holy Grail. *Current opinion in urology* 19(2): 205-210

Desai DG, Liao KS, Cevallos ME and Trautner BW (2010) Silver or nitrofurazone impregnation of urinary catheters has a minimal effect on uropathogen adherence. *Journal of Urology* 184(6): 2565-2571

Deziel E, Lepine F, Milot S and Villemur R (2003) *rhlA* is required for the production of a novel biosurfactant promoting swarming motility in *Pseudomonas aeruginosa*: 3-(3-hydroxyalkanoyloxy)alkanoic acids (HAAs), the precursors of rhamnolipids. *Microbiology* 149(Pt 8): 2005-13

Di Martino P, Merieau A, Phillips RS, Orange N and Hulen C (2002) Isolation of an *Escherichia coli* strain mutant unable to form biofilm on polystyrene and to adhere to human pneumocyte cells: involvement of tryptophanase. *Canadian Journal of Microbiology* 48(2): 132-137

Ding L, Wang Y, Hu Y, Atkinson S, Williams P and Chen S (2009) Functional characterization of FlgM in the regulation of flagellar synthesis and motility in *Yersinia pseudotuberculosis*. *Microbiology* 155(Pt 6): 1890-900

Donlan RM (2002) Biofilms: Microbial life on surfaces. *Emerging infectious diseases* 8(9): 881-890

Donlan RM and Costerton JW (2002) Biofilms: Survival mechanisms of clinically relevant microorganisms. *Clin. Microbiol. Rev.* 15(2): 167-193

Dunne Jr WM (2002) Bacterial adhesion: Seen any good biofilms lately? *Clin. Microbiol. Rev.* 15(2): 155-166

Edin-Liljegren A, Grenabo L, Hedelin H, Pettersson S and Wang YH (1992) The influence of pH and urine composition on urease enzymatic activity in human urine. *Urol Res* 20(1): 35-9

El-Kirat-Chatel S, Boyd CD, O'Toole GA and Dufrene YF (2014) Single-molecule analysis of *Pseudomonas fluorescens* footprints. *ACS Nano* 8(2): 1690-8

Ellwood DC, Keevil CW, Marsh PD, Brown CM and Wardell JN (1982) Surface-associated growth. *Philos Trans R Soc Lond B Biol Sci* 297(1088): 517-32

Farrow JM, 3rd, Sund ZM, Ellison ML, Wade DS, Coleman JP and Pesci EC (2008) PqsE functions independently of PqsR-*Pseudomonas* quinolone signal and enhances the *rhl* quorum-sensing system. *J Bacteriol* 190(21): 7043-51

Feneley RC, Hopley IB and Wells PN (2015) Urinary catheters: history, current status, adverse events and research agenda. *J Med Eng Technol* 39(8): 459-70

Feneley RCL, Kunin CM and Stickler DJ (2012) An indwelling urinary catheter for the 21st century. *BJU international* 109(12): 1746-1749

Fisher KA, Yarwood SA and James BR (2017) Soil urease activity and bacterial ureC gene copy numbers: Effect of pH. *Geoderma* 285: 1-8

Flemming H-C and Wingender J (2010) The biofilm matrix. *Nat Rev Microbiol* 8(9): 623-33

Flemming HC, Neu TR and Wingender J (2016) *The perfect slime: Microbial extracellular polymeric substances (EPS)*.

Flores-Mireles AL, Walker JN, Caparon M and Hultgren SJ (2015) Urinary tract infections: epidemiology, mechanisms of infection and treatment options. *Nat Rev Microbiol* 13(5): 269-84

Fong JN and Yildiz FH (2015) Biofilm matrix proteins. *Microbiol Spectr* 3(2)

Forster B, Van De Ville D, Berent J, Sage D and Unser M (2004) Complex wavelets for extended depth-of-field: a new method for the fusion of multichannel microscopy images. *Microsc Res Tech* 65(1-2): 33-42

Forstneric V, Ivicak-Kocjan K, Plaper T, Jerala R and Bencina M (2017) The role of the C-terminal D0 domain of flagellin in activation of Toll like receptor 5. *PLoS Pathog* 13(8): e1006574

Francis VI, Stevenson EC and Porter SL (2017) Two-component systems required for virulence in *Pseudomonas aeruginosa*. *FEMS Microbiol Lett* 364(11)

Francolini I and Donelli G (2010) Prevention and control of biofilm-based medical-device-related infections. *FEMS Immunology And Medical Microbiology* 59(3): 227-238

Franklin MJ, Nivens DE, Weadge JT and Howell PL (2011) Biosynthesis of the *Pseudomonas aeruginosa* extracellular polysaccharides, Alginate, Pel, and Psl. *Front Microbiol* 2: 167

Frans I, Busschaert P, Dierckens K, Michiels CW, Willems KA, Lievens B, Bossier P and Rediers H (2013) Are type IV pili involved in *Vibrio anguillarum* virulence towards sea bass (*Dicentrarchus labrax L.*) larvae? *Agricultural Sciences* 04(06): 30-38

Gallagher LA, McKnight SL, Kuznetsova MS, Pesci EC and Manoil C (2002) Functions required for extracellular quinolone signaling by *Pseudomonas aeruginosa*. *Journal of Bacteriology* 184(23): 6472-6480

Getliffe K (2003) Managing recurrent urinary catheter blockage: problems, promises, and practicalities. *Journal Of Wound, Ostomy, And Continence Nursing: Official Publication Of The Wound, Ostomy And Continence Nurses Society / WOCN* 30(3): 146-151

Getliffe K (2004) The effect of acidic maintenance solutions on catheter longevity. *Nursing Times* 100(16): 32-4

Ghafoor A, Hay ID and Rehm BH (2011) Role of exopolysaccharides in Pseudomonas aeruginosa biofilm formation and architecture. *Appl Environ Microbiol* 77(15): 5238-46

Gich F, Janys MA, Konig M and Overmann J (2012) Enrichment of previously uncultured bacteria from natural complex communities by adhesion to solid surfaces. *Environ Microbiol* 14(11): 2984-97

Gloag ES, Turnbull L, Huang A, Vallotton P, Wang H, Nolan LM, Mililli L, Hunt C, Lu J, Osvath SR, Monahan LG, Cavaliere R, Charles IG, Wand MP, Gee ML, Prabhakar R and Whitchurch CB (2013) Self-organization of bacterial biofilms is facilitated by extracellular DNA. *Proc Natl Acad Sci U S A* 110(28): 11541-6

Gomez-Suarez C, Pasma J, van der Borden AJ, Wingender J, Flemming HC, Busscher HJ and van der Mei HC (2002) Influence of extracellular polymeric substances on deposition and redeposition of *Pseudomonas aeruginosa* to surfaces. *Microbiology* 148(Pt 4): 1161-9

Goncalves I, Abreu AS, Matama T, Ribeiro A, Gomes AC, Silva C and Cavaco-Paulo A (2015) Enzymatic synthesis of poly(catechin)-antibiotic conjugates: an antimicrobial approach for indwelling catheters. *Applied Microbiology and Biotechnology* 99(2): 637-651

Graham DY and Miftahussurur M (2018) *Helicobacter pylori* urease for diagnosis of *Helicobacter pylori* infection: A mini review. *J Adv Res* 13: 51-57

Gray VL, Muller CT, Watkins ID and Lloyd D (2008) Peptones from diverse sources: pivotal determinants of bacterial growth dynamics. *J Appl Microbiol* 104(2): 554-65

Gray VL, O'Reilly M, Muller CT, Watkins ID and Lloyd D (2006) Low tyrosine content of growth media yields aflagellate *Salmonella enterica* serovar Typhimurium. *Microbiology* 152(Pt 1): 23-8

Greene L, Marx J and Oriola S (2008) *Guide to the elimination of catheter-associated urinary tract infections(CAUTIs)*. Washington, D.C.: Association for Professionals in Infection Control and Epidemiology

Greenwood D (1976) Use of an *in vitro* model of the urinary bladder in the investigation of bacterial response to antibiotics IN: Williams JD and Geddes AM (eds) *Laboratory Aspects of Infections*. New York: Springer US 241-247

Greenwood D and O'Grady F (1978) An in vitro model of the urinary bladder. *Journal of Antimicrobial Chemotherapy* 4(2): 113-20

Griffith DP, Musher DM and Itin C (1976) Urease. The primary cause of infection-induced urinary stones. *Investigative urology* 13(5): 346-50

Grigoryan L, Abers MS, Kizilbash QF, Petersen NJ and Trautner BW (2014) A comparison of the microbiologic profile of indwelling versus external urinary catheters. *American Journal of Infection Control* 42(6): 682-684

Gultekinoglu M, Kurum B, Karahan S, Kart D, Sagiroglu M, Ertaş N, Haluk Ozen A and Ulubayram K (2017) Polyethyleneimine brushes effectively inhibit encrustation on polyurethane ureteral stents both in dynamic bioreactor and *in vivo*. *Mater. Sci. Eng. C* 71: 1166-1174

Gupta RM and Musunuru K (2014) Expanding the genetic editing tool kit: ZFNs, TALENs, and CRISPR-Cas9. *J Clin Invest* 124(10): 4154-61

Guttenplan SB and Kearns DB (2013) Regulation of flagellar motility during biofilm formation. *FEMS Microbiol Rev* 37(6): 849-71

Habash M and Reid G (1999) Microbial biofilms: Their development and significance for medical device-related infections. *J. Clin. Pharmacol.* 39(9): 887-898

Haiko J and Westerlund-Wikstrom B (2013) The role of the bacterial flagellum in adhesion and virulence. *Biology (Basel)* 2(4): 1242-67

Hall-Stoodley L, Costerton JW and Stoodley P (2004) Bacterial biofilms: from the natural environment to infectious diseases. *Nature reviews. Microbiology* 2(2): 95-108

Hancock V, Dahl M and Klemm P (2010) Abolition of biofilm formation in urinary tract *Escherichia coli* and *Klebsiella* isolates by metal interference through competition for fur. *Appl Environ Microbiol* 76(12): 3836-41

Hancock V, Ferrières L and Klemm P (2007) Biofilm formation by asymptomatic and virulent urinary tract infectious *Escherichia coli* strains. *FEMS Microbiology Letters* 267(1): 30-37

Hancock V, Ferrières L and Klemm P (2008) The ferric yersiniabactin uptake receptor FyuA is required for efficient biofilm formation by urinary tract infectious *Escherichia coli* in human urine. *Microbiology (Reading, England)* 154(Pt 1): 167-175

Hausinger RP, Colpas GJ and Soriano A (2001) Urease: a paradigm for protein-assisted metallo center assembly. *ASM News* 67: 78-84

Hay ID, Gatland K, Campisano A, Jordens JZ and Rehm BH (2009) Impact of alginate overproduction on attachment and biofilm architecture of a supermucoid *Pseudomonas aeruginosa* strain. *Appl Environ Microbiol* 75(18): 6022-5

Hedelin H (2002) Uropathogens and urinary tract concretion formation and catheter encrustations. *Int J Antimicrob Agents* 19(6): 484-7

Held K, Ramage E, Jacobs M, Gallagher L and Manoil C (2012) Sequence-verified two-allele transposon mutant library for *Pseudomonas aeruginosa* PAO1. *J Bacteriol* 194(23): 6387-9

Henley D, Nguyen H and Inderjeeth CA (2007) Ward-based protocols can improve assessment and management of urinary tract infections in hospitalised patients. *Australas J Ageing* 26(3): 125-130

Heydorn A, Ersboll B, Kato J, Hentzer M, Parsek MR, Tolker-Nielsen T, Givskov M and Molin S (2002) Statistical analysis of *Pseudomonas aeruginosa* biofilm development: Impact of mutations in genes involved in twitching motility, cell-to-cell signaling, and stationary-phase sigma factor expression. *Applied and Environmental Microbiology* 68(4): 2008-2017

Hilt EE, McKinley K, Pearce MM, Rosenfeld AB, Zilliox MJ, Mueller ER, Brubaker L, Gai X, Wolfe AJ and Schreckenberger PC (2014) Urine is not sterile: Use of enhanced urine culture techniques to detect resident bacterial flora in the adult female bladder. *J Clin Microbiol* 52(3): 871-6

Hiron A, Posteraro B, Carriere M, Remy L, Delporte C, La Sorda M, Sanguinetti M, Juillard V and Borezee-Durant E (2010) A nickel ABC-transporter of *Staphylococcus aureus* is involved in urinary tract infection. *Mol Microbiol* 77(5): 1246-60

Hola V, Peroutkova T and Ruzicka F (2012) Virulence factors in *Proteus* bacteria from biofilm communities of catheter-associated urinary tract infections. *FEMS Immunology And Medical Microbiology* 65(2): 343-349

Holá V, Ruzicka F and Horka M (2010) Microbial diversity in biofilm infections of the urinary tract with the use of sonication techniques. *FEMS Immunology And Medical Microbiology* 59(3): 525-528

Holling N, Dedi C, Jones CE, Hawthorne JA, Hanlon GW, Salvage JP, Patel BA, Barnes LM and Jones BV (2014a) Evaluation of environmental scanning electron microscopy for analysis of *Proteus mirabilis* crystalline biofilms *in situ* on urinary catheters. *FEMS Microbiol Lett* 355(1): 20-7

Holling N, Lednor D, Tsang S, Bissell A, Campbell L, Nzakizwanayo J, Dedi C, Hawthorne JA, Hanlon G, Ogilvie LA, Salvage JP, Patel BA, Barnes LM and Jones BV (2014b) Elucidating the genetic basis of crystalline biofilm formation in *Proteus mirabilis*. *Infect Immun* 82(4): 1616-26

Hood SK and Zottola EA (1997) Adherence to stainless steel by foodborne microorganisms during growth in model food systems. *Int J Food Microbiol* 37(2-3): 145-53

Hsu PD, Lander ES and Zhang F (2014) Development and applications of CRISPR-Cas9 for genome engineering. *Cell* 157(6): 1262-78

Irie Y, Roberts AEL, Kragh KN, Gordon VD, Hutchison J, Allen RJ, Melaugh G, Bjarnsholt T, West SA and Diggle SP (2017) The *Pseudomonas aeruginosa* PSL polysaccharide is a social but noncheatable trait in biofilms. *MBio* 8(3)

Jabri E, Carr M, Hausinger R and Karplus P (1995) The crystal structure of urease from *Klebsiella aerogenes*. *Science* 268(5213): 998-1004

Jacobs MA, Alwood A, Thaipisuttikul I, Spencer D, Haugen E, Ernst S, Will O, Kaul R, Raymond C, Levy R, Chun-Rong L, Guenthner D, Bovee D, Olson MV and Manoil C (2003) Comprehensive transposon mutant library of *Pseudomonas aeruginosa*. *Proc Natl Acad Sci U S A* 100(24): 14339-44

Jacobs MA and Manoil C (2006) A genome-wide mutant library of P*seudomonas aeruginosa* IN: J.L. R and R.C. L (eds) *Pseudomonas*. Boston, MA: Springer, 121-138

Jacobsen SM and Shirtliff ME (2011) *Proteus mirabilis* biofilms and catheter-associated urinary tract infections. *Virulence* 2(5): 460-465

Jacobsen SM, Stickler DJ, Mobley HLT and Shirtliff ME (2008) Complicated catheter-associated urinary tract infections due to *Escherichia coli* and *Proteus mirabilis*. *Clin. Microbiol. Rev.* 21(1): 26-59

Jahn P, Preuss M, Kernig A, Seifert-Huhmer A and Langer G (2007) Types of indwelling urinary catheters for long-term bladder drainage in adults. *Cochrane Database Syst Rev* (3): CD004997

Jennings LK, Storek KM, Ledvina HE, Coulon C, Marmont LS, Sadovskaya I, Secor PR, Tseng BS, Scian M, Filloux A, Wozniak DJ, Howell PL and Parsek MR (2015) Pel is a cationic exopolysaccharide that cross-links extracellular DNA in the *Pseudomonas aeruginosa* biofilm matrix. *Proc Natl Acad Sci U S A* 112(36): 11353-8

Johnson JR, Berggren T and Conway AJ (1993) Activity of a nitrofurazone matrix urinary catheter against catheter-associated uropathogens. *Antimicrobial Agents and Chemotherapy* 37(9): 2033-2036

Johnson MB and Criss AK (2013) Fluorescence microscopy methods for determining the viability of bacteria in association with mammalian cells. *J Vis Exp* (79)

Jones BV, Mahenthiralingam E, Sabbuba NA and Stickler DJ (2005) Role of swarming in the formation of crystalline *Proteus mirabilis* biofilms on urinary catheters. *Journal of medical microbiology* 54(Pt 9): 807-813

Jones CJ and Wozniak DJ (2017) Psl produced by mucoid *Pseudomonas aeruginosa* contributes to the establishment of biofilms and immune evasion

MBio 8(3)

Jones SM, Dang TT and Martinuzzi R (2009) Use of quorum sensing antagonists to deter the formation of crystalline *Proteus mirabilis* biofilms. *International Journal Of Antimicrobial Agents* 34(4): 360-364

Jones SM, Yerly J, Hu Y, Ceri H and Martinuzzi R (2007) Structure of *Proteus mirabilis* biofilms grown in artificial urine and standard laboratory media. *FEMS Microbiology Letters* 268(1): 16-21

Kearns DB (2010) A field guide to bacterial swarming motility. *Nat Rev Microbiol* 8(9): 634-44

Keevil B (2009) Biofilms in water systems - origins and treatment. *Culture* 30(1): 13-16

Keevil CW (2003) Rapid detection of biofilms and adherent pathogens using scanning confocal laser microscopy and episcopic differential interference contrast microscopy. *Water Sci Technol* 47(5): 105-116

Keevil CW and Walker JT (1992) Nomarski DIC microscopy and image analysis. *Binary*: 92-95

Kent K and Zeigel RF (1982) Surface topography of silicone rubber prosthetic materials fabricated using conventional processing techniques. *The Journal of Prosthetic Dentistry* 48(6): 698-702

Kesaano M, Gardner RD, Moll K, Lauchnor E, Gerlach R, Peyton BM and Sims RC (2015) Dissolved inorganic carbon enhanced growth, nutrient uptake, and lipid accumulation in wastewater grown microalgal biofilms. *Bioresour Technol* 180: 7-15

Khajotia SS, Smart KH, Pilula M and Thompson DM (2013) Concurrent quantification of cellular and extracellular components of biofilms. *J Vis Exp* (82): e50639

Khan AA, Siddiqui AZ, Al-Kheraif AA, Zahid A and Divakar DD (2015) Effect of different pH solvents on micro-hardness and surface topography of dental nano-composite: An *in vitro* analysis. *Pak J Med Sci* 31(4): 854-9

Kikuchi T, Mizunoe Y, Takade A, Naito S and Yoshida SI (2005) Curli fibers are required for development of biofilm architecture in *Escherichia coli* K-12 and enhance bacterial adherence to human uroepithelial cells. *Microbiol. Immunol.* 49(9): 875-884

Kim HY, Choe HS, Lee DS, Yoo JM and Lee SJ (2015) A novel rat model of catheter-associated urinary tract infection. *International Urology and Nephrology* 47(8): 1259-1263

Kim KY and Frank JF (1995) Effect of nutrients on biofilm formation by *Listeria monocytogenes* on stainless steel. *J Food Protect* 58(1): 24-28

Kim YH, Kim YH, Kim JS and Park S (2005) Development of a sensitive bioassay method for quorum sensing inhibitor screening using a recombinant *Agrobacterium tumefaciens*. *Biotechnol. Bioprocess Eng.* 10(4): 322-328

King C, Alvarez LG, Holmes A, Moore L, Galletly T, Aylin P and Garcia Alvarez L (2012) Risk factors for healthcare-associated urinary tract infection and their applications in surveillance using hospital administrative data: A systematic review. *Journal of Hospital Infection* 82: 219-226

Kiran GS, Ninawe AS, Lipton AN, Pandian V and Selvin J (2016) Rhamnolipid biosurfactants: evolutionary implications, applications and future prospects from untapped marine resource. *Crit Rev Biotechnol* 36(3): 399-415

Klausen M, Aaes-Jørgensen A, Molin S and Tolker-Nielsen T (2003a) Involvement of bacterial migration in the development of complex multicellular structures in *Pseudomonas aeruginosa* biofilms. *Molecular Microbiology* 50(1): 61-68

Klausen M, Heydorn A, Ragas P, Lambertsen L, Aaes-Jørgensen A, Molin S and Tolker-Nielsen T (2003b) Biofilm formation by *Pseudomonas aeruginosa* wild type, flagella and type IV pili mutants. *Molecular Microbiology* 48(6): 1511-1524

Kohler-Ockmore J and Feneley RC (1996) Long-term catheterization of the bladder: prevalence and morbidity. *British journal of urology* 77: 347-51

Komor AC, Badran AH and Liu DR (2017) CRISPR-based technologies for the manipulation of eukaryotic genomes. *Cell* 169(3): 559

Konieczna I, Zarnowiec P, Kwinkowski M, Kolesinska B, Fraczyk J, Kaminski Z and Kaca W (2012) Bacterial urease and its role in long-lasting human diseases. *Current Protein and Peptide Science* 13(8): 789-806

Koo J, Tammam S, Ku SY, Sampaleanu LM, Burrows LL and Howell PL (2008) PilF is an outer membrane lipoprotein required for multimerization and localization of the *Pseudomonas aeruginosa* type IV pilus secretin. *J Bacteriol* 190(21): 6961-9

Koo J, Tang T, Harvey H, Tammam S, Sampaleanu L, Burrows LL and Howell PL (2013) Functional mapping of PilF and PilQ in the *Pseudomonas aeruginosa* type IV pilus system. *Biochemistry* 52(17): 2914-23

Koper TE, El-Sheikh AF, Norton JM and Klotz MG (2004) Urease-encoding genes in ammonia-oxidizing bacteria. *Applied and Environmental Microbiology* 70(4): 2342-2348

Koseoglu H, Aslan G, Esen N, Sen BH and Coban H (2006) Ultrastructural stages of biofilm development of *Escherichia coli* on urethral catheters and effects of antibiotics on biofilm formation. *Urology* 68(5): 942-946

Kumon H (1996) Pathogenesis and management of bacterial biofilms in the urinary tract. *Journal of Infection and Chemotherapy* 2(1): 18-28

Kunin CM, Douthitt S, Dancing J, Anderson J and Moeschberger M (1992) The association between the use of urinary catheters and morbidity and mortality among elderly patients in nursing homes. *American journal of epidemiology* 135(3): 291-301

LaBauve AE and Wargo MJ (2012) Growth and laboratory maintenance of *Pseudomonas aeruginosa*. *Curr Protoc Microbiol* Chapter 6: Unit 6E 1

LaPlante KL, Sarkisian SA, Woodmansee S, Rowley DC and Seeram NP (2012) Effects of cranberry extracts on growth and biofilm production of *Escherichia coli* and *Staphylococcus* species. *Phytotherapy research : PTR* 26(9): 1371-4

Lassek C, Burghartz M, Chaves-Moreno D, Otto A, Hentschker C, Fuchs S, Bernhardt J, Jauregui R, Neubauer R, Becher D, Pieper DH, Jahn M, Jahn D and Riedel K (2015) A metaproteomics approach to elucidate host and pathogen protein expression during catheter-associated urinary tract infections (CAUTIs). *Mol. Cell. Proteomics* 14(4): 989-1008

Lawrence EL and Turner IG (2005) Materials for urinary catheters: a review of their history and development in the UK. *Medical engineering & physics* 27(6): 443-53

Lawrence JR, Delaquis PJ, Korber DR and Caldwell DE (1987) Behavior of *Pseudomonas fluorescens* within the hydrodynamic boundary layers of surface microenvironments. *Microb Ecol* 14(1): 1-14

Lawrence JR, Korber DR, Hoyle BD, Costerton JW and Caldwell DE (1991) Optical sectioning of microbial biofilms. *J Bacteriol* 173(20): 6558-67

Lebeaux D, Ghigo JM and Beloin C (2014) Biofilm-related infections: bridging the gap between clinical management and fundamental aspects of recalcitrance toward antibiotics. *Microbiol Mol Biol Rev* 78(3): 510-43

Lehman SM and Donlan RM (2015) Bacteriophage-mediated control of a two-species biofilm formed by microorganisms causing catheter-associated urinary tract infections in an *in vitro* urinary catheter model. *Antimicrob Agents Chemother* 59(2): 1127-37

Leriche V, Sibille P and Carpentier B (2000) Use of an enzyme-linked lectinsorbent assay to monitor the shift in polysaccharide composition in bacterial biofilms. *Applied and Environmental Microbiology* 66(5): 1851-1856

Lim K, Chua RRY, Ho B, Tambyah PA, Hadinoto K and Leong SSJ (2015) Development of a catheter functionalized by a polydopamine peptide coating with antimicrobial and antibiofilm properties. *Acta Biomater* 15: 127-138

Lin W, Mathys V, Ang EL, Koh VH, Martinez Gomez JM, Ang ML, Zainul Rahim SZ, Tan MP, Pethe K and Alonso S (2012) Urease activity represents an alternative pathway for *Mycobacterium tuberculosis* nitrogen metabolism. *Infect Immun* 80(8): 2771-9

Lo YL, Shen L, Chang CH, Bhuwan M, Chiu CH and Chang HY (2016) Regulation of motility and phenazine pigment production by FliA is cyclic-di-GMP dependent in *Pseudomonas aeruginosa* PAO1. *PLoS One* 11(5): e0155397

Lyczak JB, Cannon CL and Pier GB (2000) Establishment of *Pseudomonas aeruginosa* infection: lessons from a versatile opportunist. *Microbes and Infection* 2(9): 1051-1060

Ma L, Jackson KD, Landry RM, Parsek MR and Wozniak DJ (2006) Analysis of *Pseudomonas aeruginosa* conditional Psl variants reveals roles for the Psl polysaccharide in adhesion and maintaining biofilm structure postattachment. *J Bacteriol* 188(23): 8213-21

Ma L, Lu H, Sprinkle A, Parsek MR and Wozniak DJ (2007) *Pseudomonas aeruginosa* Psl is a galactose- and mannose-rich exopolysaccharide. *J Bacteriol* 189(22): 8353-6

Macleod SM and Stickler DJ (2007) Species interactions in mixed-community crystalline biofilms on urinary catheters. *Journal of medical microbiology* 56(Pt 11): 1549-1557

Maki DG and Tambyah PA (2001) Engineering out the risk for infection with urinary catheters. *Emerging infectious diseases* 7(2): 342-7

Malic S, Jordan RPC, Waters MGJ, Stickler DJ and Williams DW (2014) Biocide activity against urinary catheter pathogens. *Antimicrobial Agents And Chemotherapy* 58(2): 1192-1194

Malic S, Waters MGJ, Basil L, Stickler DJ and Williams DW (2012) Development of an "early warning" sensor for encrustation of urinary catheters following *Proteus* infection. *Journal of Biomedical Materials Research Part B-Applied Biomaterials* 100B(1): 133-137

Marshall KC, Stout R and Mitchell R (1971) Selective sorption of bacteria from seawater. *Canadian Journal of Microbiology* 17(11): 1413–1416

Martinez E and Campos-Gomez J (2016) Oxylipins produced by *Pseudomonas aeruginosa* promote biofilm formation and virulence. *Nat Commun* 7: 13823

Mattick JS (2002) Type IV pili and twitching motility. *Annu Rev Microbiol* 56: 289-314

McLean RJ, Lawrence JR, Korber DR and Caldwell DE (1991) *Proteus mirabilis* biofilm protection against struvite crystal dissolution and its implications in struvite urolithiasis. *The Journal Of Urology* 146(4): 1138-1142

McLean RJC, Nickel JC, Cheng KJ, Costerton JW and Banwell JG (1988) The ecology and pathogenicity of urease-producing bacteria in the urinary tract. *Crit. Rev. Microbiol.* 16(1): 37-79

Mercenier A, Simon J-P, Vander Wauven C, Haas D and Stalon V (1980) Regulation of enzyme synthesis in the arginine deiminase pathway of *Pseudomonas aeruginosa*. *Journal of Bacteriology* 144(1)

Miller MB and Bassler BL (2001) Quorum sensing in bacteria. *Annu Rev Microbiol* 55: 165-99

Minuth JN, Musher DM and Thorsteinsson SB (1976) Inhibition of the antibacterial activity of gentamicin by urine. *The Journal of infectious diseases* 133(1): 14-21

Mittal R, Sharma S, Chhibber S, Aggarwal S, Gupta V and Harjai K (2010) Correlation between serogroup*, in vitro* biofilm formation and elaboration of virulence factors by uropathogenic *Pseudomonas aeruginosa*. *FEMS Immunology And Medical Microbiology* 58(2): 237-243

Monod J (1949) The growth of bacterial cultures. *Annual Reviews in Microbiology* 3(1): 371-394

Moreira LO, Andrade AF, Vale MD, Souza SM, Hirata R, Jr., Asad LM, Asad NR, Monteiro-Leal LH, Previato JO and Mattos-Guaraldi AL (2003) Effects of iron limitation on adherence and cell surface carbohydrates of *Corynebacterium diphtheriae* strains. *Appl Environ Microbiol* 69(10): 5907-13

Morgan SD, Rigby D and Stickler DJ (2009) A study of the structure of the crystalline bacterial biofilms that can encrust and block silver Foley catheters. *Urological Research* 37(2): 89-93

Morris NS and Stickler DJ (1998) Encrustation of indwelling urethral catheters by *Proteus mirabilis* biofilms growing in human urine. *Journal of Hospital Infection* 39(3): 227-234

Morris NS, Stickler DJ and McLean RJ (1999) The development of bacterial biofilms on indwelling urethral catheters. *World Journal Of Urology* 17(6): 345-350

Morris NS, Stickler DJ and Winters C (1997) Which indwelling urethral catheters resist encrustation by Proteus mirabilis biofilms? *British journal of urology* 80(1): 58-63

Mulrooney SB and Hausinger RP (1990a) Sequence of the *Klebsiella aerogenes* urease genes and evidence for accessory proteins facilitating nickel incorporation. *J Bacteriol* 172(10): 5837-43

Mulrooney SB and Hausinger RP (1990b) Sequence of the *Klebsiella aerogenes* urease genes and evidence for accessory proteins facilitating nickel incorporation. *J Bacteriol* 172(10): 5837-43

Mund A, Diggle SP and Harrison F (2017) The fitness of *Pseudomonas aeruginosa* quorum sensing signal cheats is influenced by the diffusivity of the environment. *MBio* 8(3)

Murakami K, Ono T, Viducic D, Somiya Y, Kariyama R, Hori K, Amoh T, Hirota K, Kumon H, Parsek MR and Miyake Y (2017) Role of *psl* genes in antibiotic tolerance of adherent *Pseudomonas aeruginosa*. *Antimicrob Agents Chemother* 61(7)

Murray TS and Kazmierczak BI (2006) FlhF is required for swimming and swarming in *Pseudomonas aeruginosa*. *J Bacteriol* 188(19): 6995-7004

Musher DM, Griffith DP, Tyler M and Woelfel A (1974) potentiation of the antibacterial effect of methanamine by acetohydroxamic acid. *Antimicrobial Agents and Chemotherapy* 5(2): 101-105

Musken M, Di Fiore S, Dotsch A, Fischer R and Haussler S (2010) Genetic determinants of *Pseudomonas aeruginosa* biofilm establishment. *Microbiology* 156(Pt 2): 431-41

National Patient Safety Agency (2004) The economic case: Implementing near-patient alcohol handrub in your trust.

Neu TR and Marshall KC (1991) Microbial “footprints” - A new approach to adhesive polymers. *Biofouling* 3(2): 101-112

Newman DK and Willson MM (2011) Review of intermittent catheterization and current best practices. *Urologic nursing* 31(1): 12-28

Newman JW, Floyd RV and Fothergill JL (2017) The contribution of *Pseudomonas aeruginosa* virulence factors and host factors in the establishment of urinary tract infections. *FEMS Microbiol Lett* 364(15)

Nickel JC, Costerton JW, McLean RJC and Olson M (1994) Bacterial biofilms: influence on the pathogenesis, diagnosis and treatment of urinary tract infections. *Journal of Antimicrobial Chemotherapy* 33 Suppl A: 31-41

Nicolle LE (2014) Catheter associated urinary tract infections. *Antimicrob Resist Infect Control* 3: 23

Nowatzki PJ, Koepsel RR, Stoodley P, Min K, Harper A, Murata H, Donfack J, Hortelano ER, Ehrlich GD and Russell AJ (2012) Salicylic acid-releasing polyurethane acrylate polymers as anti-biofilm urological catheter coatings. *Acta Biomater* 8(5): 1869-1880

Nzakizwanayo J, Hanin A, Alves DR, McCutcheon B, Dedi C, Salvage J, Knox K, Stewart B, Metcalfe A, Clark J, Gilmore BF, Gahan CG, Jenkins AT and Jones BV (2015) Bacteriophage can prevent encrustation and blockage of urinary catheters by *Proteus mirabilis*. *Antimicrob Agents Chemother* 60(3): 1530-6

O'Toole G, Kaplan HB and Kolter R (2000) Biofilm formation as microbial development. *Annu Rev Microbiol* 54: 49-79

O'Toole GA and Kolter R (1998) Flagellar and twitching motility are necessary for *Pseudomonas aeruginosa* biofilm development. *Mol Microbiol* 30(2): 295-304

Ogilvie AT, Brisson BA, Singh A and Weese JS (2015) In vitro evaluation of the impact of silver coating on *Escherichia coli* adherence to urinary catheters. *Can. Vet. J.* 56(5): 490-494

Okshevsky M, Regina VR and Meyer RL (2015) Extracellular DNA as a target for biofilm control. *Curr Opin Biotech* 33: 73-80

Olsen I (2015) Biofilm-specific antibiotic tolerance and resistance. *Eur J Clin Microbiol Infect Dis* 34(5): 877-86

Ong C-LY, Ulett GC, Mabbett AN, Beatson SA, Webb RI, Monaghan W, Nimmo GR, Looke DF, McEwan AG and Schembri MA (2008) Identification of type 3 fimbriae in uropathogenic *Escherichia coli* reveals a role in biofilm formation. *Journal Of Bacteriology* 190(3): 1054-1063

Pammi M, Liang R, Hicks J, Mistretta TA and Versalovic J (2013) Biofilm extracellular DNA enhances mixed species biofilms of *Staphylococcus epidermidis* and *Candida albicans*. *BMC Microbiol* 13: 257

Pascual A (2002) Pathogenesis of cathether-related infections: Lessons for new designs. *Clinical Microbiology and Infection* 8(5): 256-264

Patel HP (2006) The abnormal urinalysis. *Pediatr Clin North Am* 53(3): 325-37, v

Paulson DS (2009) *Biostatistics and microbiology: A survival manual*. New York: Springer-Verlag

Pedersen SS, Hoiby N, Espersen F and Koch C (1992) Role of alginate in infection with mucoid *Pseudomonas aeruginosa* in cystic fibrosis. *Thorax* 47(1): 6-13

Peeters E, Nelis HJ and Coenye T (2008) Comparison of multiple methods for quantification of microbial biofilms grown in microtiter plates. *Journal of Microbiological Methods* 72(2): 157-65

Persat A, Inclan YF, Engel JN, Stone HA and Gitai Z (2015) Type IV pili mechanochemically regulate virulence factors in *Pseudomonas aeruginosa*. *Proc Natl Acad Sci U S A* 112(24): 7563-8

Pickard R, Lam T, MacLennan G, Starr K, Kilonzo M, McPherson G, Gillies K, McDonald A, Walton K, Buckley B, Glazener C, Boachie C, Burr J, Norrie J, Vale L, Grant A and N'Dow J (2012) Antimicrobial catheters for reduction of symptomatic urinary tract infection in adults requiring short-term catheterisation in hospital: a multicentre randomised controlled trial. *The Lancet* 380(9857): 1927-1935

Platt R, Polk BF, Murdock B and Rosner B (1982) Mortality associated with nosocomial urinary-tract infection. *The New England journal of medicine* 307(11): 637-642

Platt R, Polk BF, Murdock B and Rosner B (1986) Risk factors for nosocomial urinary tract infection. *American journal of epidemiology* 124(6): 977-985

Pomfret I (2007) Urinary catheterization: selection and clinical management. *Br J Community Nurs* 12(8): 348-54

Pratt LA and Kolter R (1999) Genetic analyses of bacterial biofilm formation. *Curr. Opin. Microbiol.* 2(6): 598-603

Pratt RJ, Pellowe CM, Wilson JA, Loveday HP, Harper PJ, Jones SRLJ, McDougall C and Wilcox MH (2007) epic2: National evidence-based guidelines for preventing healthcare-associated infections in NHS hospitals in England. *Journal of Hospital Infection* 65: S1-S59

Prinjha S and Chapple A (2013) Living with an indwelling urinary catheter. *Nursing times* 109(44): 12-14

Pschyrembel W (2014) *Pschyrembel klinisches wörterbuch*. German: Walter de Gruyter

Rahmani-Badi A, Sepehr S, Mohammadi P, Soudi MR, Babaie-Naiej H and Fallahi H (2014) A combination of cis-2-decenoic acid and antibiotics eradicates pre-established catheter-associated biofilms. *Journal of medical microbiology* 63(Pt 11): 1509-1516

Ramakrishnan K and Mold JW (2004) Urinary catheters: A review. *The Internet Journal of Family Practice* 3(2)

Ramanathan R and Duane TM (2014) Urinary tract infections in surgical patients. *The Surgical clinics of North America* 94(6): 1351-1368

Rampioni G, Falcone M, Heeb S, Frangipani E, Fletcher MP, Dubern JF, Visca P, Leoni L, Camara M and Williams P (2016) Unravelling the genome-wide contributions of specific 2-alkyl-4-quinolones and PqsE to quorum sensing in *Pseudomonas aeruginosa*. *PLoS Pathog* 12(11): e1006029

Rane HS, Bernardo SM, Howell AB and Lee SA (2014) Cranberry-derived proanthocyanidins prevent formation of *Candida albicans* biofilms in artificial urine through biofilm- and adherence-specific mechanisms. *The Journal Of Antimicrobial Chemotherapy* 69(2): 428-436

Rasamiravaka T, Labtani Q, Duez P and El Jaziri M (2015) The formation of biofilms by *Pseudomonas aeruginosa*: a review of the natural and synthetic compounds interfering with control mechanisms. *Biomed Res Int* 2015: 759348

Reid G (1999) Biofilms in infectious disease and on medical devices. *International Journal of Antimicrobial Agents* 11(3-4): 223-226

Reid G and Busscher HJ (1992) Importance of surface properties in bacterial adhesion to biomaterials, with particular reference to the urinary tract. *Int Biodeterior Biodegrad* 30(2-3): 105-122

Reisner A, Krogfelt KA, Klein BM, Zechner EL and Molin S (2006) *In vitro* biofilm formation of commensal and pathogenic *Escherichia coli* strains: impact of environmental and genetic factors. *Journal Of Bacteriology* 188(10): 3572-3581

Reisner A, Maierl M, Jörger M, Krause R, Berger D, Haid A, Tesic D and Zechner EL (2014) Type 1 fimbriae contribute to catheter-associated urinary tract infections caused by *Escherichia coli*. *Journal Of Bacteriology* 196(5): 931-939

Rice SA, Tan CH, Mikkelsen PJ, Kung V, Woo J, Tay M, Hauser A, McDougald D, Webb JS and Kjelleberg S (2009) The biofilm life cycle and virulence of *Pseudomonas aeruginosa* are dependent on a filamentous prophage. *ISME J* 3(3): 271-82

Robertson WG, Peacock M and Nordin BE (1968) Activity products in stone-forming and non-stone-forming urine. *Clinical science* 34(3): 579-594

Rogers J and Keevil CW (1992) Immunogold and fluorescein immunolabelling of *Legionella pneumophila* within an aquatic biofilm visualized by using episcopic differential interference contrast microscopy. *Applied and Environmental Microbiology* 58(7): 2326 - 2330

Rogers J, Lee JV, Dennis PJ and Keevil CW (1991) Continuous culture biofilm model for the survival and growth of *Legionella pneumophila* and associated protozoa in potable water systems IN: Morris R, Alexander LM, Wyn-Jones P and Sellwood J (eds) *Proceedings of the UK Symposium on Health-Related Water Microbiology*. London: IAWPRC 192 - 200

Romling U and Balsalobre C (2012) Biofilm infections, their resilience to therapy and innovative treatment strategies. *Journal of internal medicine* 272(6): 541-61

Rosdahl CB and Kowalski MT (2011) *Textbook of basic nursing* (10 Edition). Lippincott Williams & Wilkins

Rose SJ and Bermudez LE (2016) Identification of bicarbonate as a trigger and genes involved with extracellular DNA export in mycobacterial biofilms. *MBio* 7(6)

Roy V, Adams BL and Bentley WE (2011) Developing next generation antimicrobials by intercepting AI-2 mediated quorum sensing. *Enzyme Microb. Technol.* 49(2): 113-123

Ryder C, Byrd M and Wozniak DJ (2007) Role of polysaccharides in *Pseudomonas aeruginosa* biofilm development. *Curr Opin Microbiol* 10(6): 644-8

Saint S (2000) Clinical and economic consequences of nosocomial catheter-related bacteriuria. *American journal of infection control* 28(1): 68-75

Saint S and Chenoweth CE (2003) Biofilms and catheter-associated urinary tract infections. *Infect Dis Clin North Am* 17(2): 411-432

Sakuragi Y and Kolter R (2007) Quorum-sensing regulation of the biofilm matrix genes (*pel*) of *Pseudomonas aeruginosa*. *J Bacteriol* 189(14): 5383-6

Sauer K, Camper AK, Ehrlich GD, Costerton JW and Davies DG (2002) *Pseudomonas aeruginosa* displays multiple phenotypes during development as a biofilm. *Journal of Bacteriology* 184(4): 1140-1154

Schaber JA, Carty NL, McDonald NA, Graham ED, Cheluvappa R, Griswold JA and Hamood AN (2004) Analysis of quorum sensing-deficient clinical isolates of Pseudomonas aeruginosa. *Journal of medical microbiology* 53(9): 841-853

Schaber JA, Triffo WJ, Suh SJ, Oliver JW, Hastert MC, Griswold JA, Auer M, Hamood AN and Rumbaugh KP (2007) Pseudomonas aeruginosa forms biofilms in acute infection independent of cell-to-cell signaling. *Infect Immun* 75(8): 3715-21

Schindelin J, Arganda-Carreras I, Frise E, Kaynig V, Longair M, Pietzsch T, Preibisch S, Rueden C, Saalfeld S, Schmid B, Tinevez JY, White DJ, Hartenstein V, Eliceiri K, Tomancak P and Cardona A (2012) Fiji: an open-source platform for biological-image analysis. *Nat Methods* 9(7): 676-82

Schmiemann G, Kniehl E, Gebhardt K, Matejczyk MM and Hummers-Pradier E (2010) The diagnosis of urinary tract infection: a systematic review. *Dtsch Arztebl Int* 107(21): 361-7

Schumm K and Lam TB (2008) Types of urethral catheters for management of short-term voiding problems in hospitalised adults. *Cochrane Database Syst Rev* (2): CD004013

Schurr MJ (2013) Which bacterial biofilm exopolysaccharide is preferred, Psl or alginate? *J Bacteriol* 195(8): 1623-6

Schwartz T, Hoffmann S and Obst U (2003) Formation of natural biofilms during chlorine dioxide and u.v. disinfection in a public drinking water distribution system. *Journal of Applied Microbiology* 95(3): 591-601

Secor PR, Sweere JM, Michaels LA, Malkovskiy AV, Lazzareschi D, Katznelson E, Rajadas J, Birnbaum ME, Arrigoni A, Braun KR, Evanko SP, Stevens DA, Kaminsky W, Singh PK, Parks WC and Bollyky PL (2015) Filamentous bacteriophage promote biofilm assembly and function. *Cell Host Microbe* 18(5): 549-59

Shaw GL, Choong SK and Fry C (2005) Encrustation of biomaterials in the urinary tract. *Urological Research* 33(1): 17-22

Shields-Cutler RR, Crowley JR, Hung CS, Stapleton AE, Aldrich CC, Marschall J and Henderson JP (2015) Human urinary composition controls antibacterial activity of siderocalin. *J Biol Chem* 290(26): 15949-60

Shrout JD, Chopp DL, Just CL, Hentzer M, Givskov M and Parsek MR (2006) The impact of quorum sensing and swarming motility on *Pseudomonas aeruginosa* biofilm formation is nutritionally conditional. *Mol Microbiol* 62(5): 1264-77

Shuman EK and Chenoweth CE (2010) Recognition and prevention of healthcare-associated urinary tract infections in the intensive care unit. *Critical Care Medicine* 38(8 SUPPL.): S373-S379

Shunmugaperumal T, Kaur V and Thenrajan RS (2015) Lipid- and polymer-based drug delivery carriers for eradicating microbial biofilms causing medical device-related infections. *Advances in experimental medicine and biology* 831: 147-89

Siddiq DM and Darouiche RO (2012) New strategies to prevent catheter-associated urinary tract infections. *Nature Reviews. Urology* 9(6): 305-314

Simerville JA, Maxted WC and Pahira JJ (2005) Urinalysis: A comprehensive review. *American family physician* 71(6): 1153-62

Simhi E, van der Mei HC, Ron EZ, Rosenberg E and Busscher HJ (2000) Effect of the adhesive antibiotic TA on adhesion and initial growth of *E. coli* on silicone rubber. *FEMS Microbiology Letters* 192(1): 97-100

Singh S, Singh SK, Chowdhury I and Singh R (2017) Understanding the mechanism of bacterial biofilms resistance to antimicrobial agents. *Open Microbiol J* 11: 53-62

Smith L (2003) Which catheter? Criteria for selection of urinary catheters for children. *Paediatr Nurs* 15(3): 14-8

Stacy A, McNally L, Darch SE, Brown SP and Whiteley M (2015) The biogeography of polymicrobial infection. *Nat Rev Microbiol*

Stahlhut SG, Struve C, Krogfelt KA and Reisner A (2012) Biofilm formation of Klebsiella pneumoniae on urethral catheters requires either type 1 or type 3 fimbriae. *FEMS Immunology and Medical Microbiology* 65(2): 350-359

Stamm WE (1991) Catheter-associated urinary tract infections: epidemiology, pathogenesis, and prevention. *The American Journal Of Medicine* 91(3B): 65S-71S

Stamm WE and Norrby SR (2001) Urinary tract infections: disease panorama and challenges. *The Journal of infectious diseases* 183 Suppl 1: S1-4

Stapper AP, Narasimhan G, Ohman DE, Barakat J, Hentzer M, Molin S, Kharazmi A, Hoiby N and Mathee K (2004) Alginate production affects *Pseudomonas aeruginosa* biofilm development and architecture, but is not essential for biofilm formation. *J Med Microbiol* 53(Pt 7): 679-90

Starnbach MN and Lory S (1992) The *filA* (rpoF) gene of *Pseudomonas aeruginosa* encodes an alternative sigma factor required for flagellin synthesis. *Molecular Microbiology* 6(4): 459-469

Stickler D, Morris N, Moreno MC and Sabbuba N (1998) Studies on the formation of crystalline bacterial biofilms on urethral catheters. *European Journal of Clinical Microbiology & Infectious Diseases* 17(9): 649-652

Stickler D, Young R, Jones G, Sabbuba N and Morris N (2003) Why are Foley catheters so vulnerable to encrustation and blockage by crystalline bacterial biofilm? *Urological Research* 31(5): 306-311

Stickler DJ (2002) Susceptibility of antibiotic-resistant Gram-negative bacteria to biocides: a perspective from the study of catheter biofilms. *Journal Of Applied Microbiology* 92 Suppl: 163S-170S

Stickler DJ (2008) Bacterial biofilms in patients with indwelling urinary catheters. *Nature clinical practice. Urology* 5(11): 598-608

Stickler DJ (2014) Clinical complications of urinary catheters caused by crystalline biofilms: Something needs to be done. *Journal of internal medicine* 276(2): 120-129

Stickler DJ and Feneley RCL (2010) The encrustation and blockage of long-term indwelling bladder catheters: a way forward in prevention and control. *Spinal Cord* 48(11): 784-790

Stickler DJ and Morgan SD (2008) Observations on the development of the crystalline bacterial biofilms that encrust and block Foley catheters. *The Journal of hospital infection* 69(4): 350-60

Stickler DJ, Morris NS and Winters C (1999a) Simple physical model to study formation and physiology of biofilms on urethral catheters *Methods Enzymol.*: Elsevier 494-501

Stickler DJ, Morris NS and Winters C (1999b) Simple physical model to study formation and physiology of biofilms on urethral catheters. *Methods Enzymol.* 310: 494-501

Stoodley P, Dodds I, Boyle JD and Lappin-Scott HM (1998) Influence of hydrodynamics and nutrients on biofilm structure. *J Appl Microbiol* 85 Suppl 1: 19S-28S

Stoodley P, Sauer K, Davies DG and Costerton JW (2002) Biofilms as complex differentiated communities. *Annual Review of Microbiology* 56: 187-209

Stover CK, Pham XQ, Erwin AL, Mizoguchi SD, Warrener P, Hickey MJ, Brinkman FS, Hufnagle WO, Kowalik DJ, Lagrou M, Garber RL, Goltry L, Tolentino E, Westbrock-Wadman S, Yuan Y, Brody LL, Coulter SN, Folger KR, Kas A, Larbig K, Lim R, Smith K, Spencer D, Wong GK, Wu Z, Paulsen IT, Reizer J, Saier MH, Hancock RE, Lory S and Olson MV (2000) Complete genome sequence of *Pseudomonas aeruginosa* PAO1, an opportunistic pathogen. *Nature* 406(6799): 959-64

Strong KJ, Osicka TM and Comper WD (2005) Urinary-peptide excretion by patients with and volunteers without diabetes. *J Lab Clin Med* 145(5): 239-46

Swearingen MC, Mehta A, Mehta A, Nistico L, Hill PJ, Falzarano AR, Wozniak DJ, Hall-Stoodley L and Stoodley P (2016) A novel technique using potassium permanganate and reflectance confocal microscopy to image biofilm extracellular polymeric matrix reveals non-eDNA networks in *Pseudomonas aeruginosa* biofilms. *Pathog Dis* 74(1): ftv104

Tambyah PA, Halvorson KT and Maki DG (1999) A prospective study of pathogenesis of catheter-associated urinary tract infections. *Mayo Clinic Proceedings* 74(2): 131 - 6

Tatem AJ, Klaassen Z, Lewis RW and Terris MK (2013) Frederick Eugene Basil Foley: his life and innovations. *Urology* 81(5): 927-31

Tenke P, Kovacs B, Jäckel M and Nagy E (2006) The role of biofilm infection in urology. *World Journal Of Urology* 24(1): 13-20

Tenke P, Köves B, Nagy K, Hultgren SJ, Mendling W, Wullt B, Grabe M, Wagenlehner FME, Cek M, Pickard R, Botto H, Naber KG and Bjerklund Johansen TE (2012) Update on biofilm infections in the urinary tract. *World Journal Of Urology* 30(1): 51-57

Terashima H, Kojima S and Homma M (2008) Flagellar motility in bacteria. *International Review of Cell and Molecular Biology* 270: 39-85

Thomsen TR, Hall-Stoodley L, Moser C and Stoodley P (2011) The role of bacterial biofilms in infections of catheters and shunts. *Biofilm Infections*: 91-109

Tielen P, Rosin N, Meyer A-K, Dohnt K, Haddad I, Jänsch L, Klein J, Narten M, Pommerenke C, Scheer M, Schobert M, Schomburg D, Thielen B and Jahn D (2013) Regulatory and metabolic networks for the adaptation of *Pseudomonas aeruginosa* biofilms to urinary tract-like conditions. *Plos One* 8(8): e71845-e71845

Tolker-Nielsen T (2014) Pseudomonas aeruginosa biofilm infections: from molecular biofilm biology to new treatment possibilities. *APMIS. Supplementum* (138): 1-51

Toutain CM, Caiazza NC and O'Toole GA (2004) Molecular basis of biofilm development by Pseudomonads IN: Ghannoum M and O'Toole GA (eds) *Microbial Biofilms*.

Toyofuku M, Inaba T, Kiyokawa T, Obana N, Yawata Y and Nomura N (2016) Environmental factors that shape biofilm formation. *Biosci Biotechnol Biochem* 80(1): 7-12

Trautner BW and Darouiche RO (2004a) Catheter-associated infections: pathogenesis affects prevention. *Archives Of Internal Medicine* 164(8): 842-850

Trautner BW and Darouiche RO (2004b) Role of biofilm in catheter-associated urinary tract infection. *American journal of infection control* 32(3): 177-183

Trautner BW, Hull RA and Darouiche RO (2005) Prevention of catheter-associated urinary tract infection. *Current opinion in infectious diseases* 18(1): 37-41

Trautner BW, Lopez AI, Kumar A, Siddiq DM, Liao KS, Li Y, Tweardy DJ and Cai C (2012) Nanoscale surface modification favors benign biofilm formation and impedes adherence by pathogens. *Nanomedicine: Nanotechnology, Biology, And Medicine* 8(3): 261-270

Vandecandelaere I, Van Nieuwerburgh F, Deforce D and Coenye T (2017) Metabolic activity, urease production, antibiotic resistance and virulence in dual species biofilms of *Staphylococcus epidermidis* and *Staphylococcus aureus*. *PLoS One* 12(3): e0172700

Vega LM, Alvarez PJ and McLean RJ (2014) Bacterial signaling ecology and potential applications during aquatic biofilm construction. *Microb Ecol* 68(1): 24-34

Velraeds MMC, Van De Belt-Gritter B, Van Der Mei HC, Reid G and Busscher HJ (1998) Interference in initial adhesion of uropathogenic bacteria and yeasts to silicone rubber by a *Lactobacillus acidophilus* biosurfactant. *Journal of medical microbiology* 47(12): 1081-1085

Verran J and Boyd RD (2001) The relationship between substratum surface roughness and microbiological and organic soiling: A review. *Biofouling* 17(1): 59-71

Viducic D, Murakami K, Amoh T, Ono T and Miyake Y (2016) RpoN modulates carbapenem tolerance in *Pseudomonas aeruginosa* through *Pseudomonas* quinolone signal and PqsE. *Antimicrob Agents Chemother* 60(10): 5752-64

Waite RD, Paccanaro A, Papakonstantinopoulou A, Hurst JM, Saqi M, Littler E and Curtis MA (2006) Clustering of *Pseudomonas aeruginosa* transcriptomes from planktonic cultures, developing and mature biofilms reveals distinct expression profiles. *BMC Genomics* 7: 162

Walker JT and Keevil CW (1994) Study of microbial biofilms using light microscope techniques. *Int Biodeter Biodegr* 34(3-4): 223-236

Wang R, Neoh KG, Kang ET, Tambyah PA and Chiong E (2015) Antifouling coating with controllable and sustained silver release for long-term inhibition of infection and encrustation in urinary catheters. *Journal of Biomedical Materials Research - Part B Applied Biomaterials* 103(3): 519-528

Wang R, Neoh KG, Shi Z, Kang ET, Tambyah PA and Chiong E (2012) Inhibition of *Escherichia coli* and *Proteus mirabilis* adhesion and biofilm formation on medical grade silicone surface. *Biotechnology and Bioengineering* 109(2): 336-345

Wang X, Lünsdorf H, Ehrén I, Brauner A and Römling U (2010) Characteristics of biofilms from urinary tract catheters and presence of biofilm-related components in *Escherichia coli*. *Current microbiology* 60(6): 446-453

Watts RE, Hancock V, Ong C-LY, Vejborg RM, Mabbett AN, Totsika M, Looke DF, Nimmo GR, Klemm P and Schembri MA (2010) *Escherichia coli* isolates causing asymptomatic bacteriuria in catheterized and noncatheterized individuals possess similar virulence properties. *Journal Of Clinical Microbiology* 48(7): 2449-2458

Webb JS, Lau M and Kjelleberg S (2004) Bacteriophage and phenotypic variation in *Pseudomonas aeruginosa* biofilm development. *J Bacteriol* 186(23): 8066-73

Wei Q and Ma LZ (2013) Biofilm matrix and its regulation in *Pseudomonas aeruginosa*. *Int J Mol Sci* 14(10): 20983-1005

Wesseling W (2015) Beneficial biofilms in marine aquaculture? Linking points of biofilm formation mechanisms in *Pseudomonas aeruginosa* and *Pseudoalteromonas* species. *AIMS Bioengineering* 2(3): 104-125

Whiteley M, Bangera MG, Bumgarner RE, Parsek MR, Teitzel GM, Lory S and Greenberg EP (2001) Gene expression in *Pseudomonas aeruginosa* biofilms. *Nature* 413(6858): 860-4

Whiteside SA, Razvi H, Dave S, Reid G and Burton JP (2015) The microbiome of the urinary tract - a role beyond infection. *Nat Rev Urol* 12(2): 81-90

Wilde MH and Brasch J (2008) A pilot study of self-monitoring urine flow in people with long-term urinary catheters. *Research in Nursing & Health* 31(5): 490-500

Wilks SA, Fader MJ and Keevil CW (2015) Novel insightsinto the *Proteus mirabilis* crystalline biofilm using real-time imaging. *PLoS One* 10(10): e0141711

Winsor GL, Lam DK, Fleming L, Lo R, Whiteside MD, Yu NY, Hancock RE and Brinkman FS (2011) Pseudomonas Genome Database: improved comparative analysis and population genomics capability for *Pseudomonas* genomes. *Nucleic Acids Res* 39(Database issue): D596-600

Worcester EM, Bergsland KJ, Gillen DL and Coe FL (2018) Mechanism for higher urine pH in normal women compared with men. *Am J Physiol Renal Physiol* 314(4): F623-F629

World Health Organization (2011) *Report on the burden of endemic health care-associated infection worldwide*. Geneva, Switzerland

Wrangstadh M, Szewzyk U, Ostling J and Kjelleberg S (1990) Starvation-specific formation of a peripheral exopolysaccharide by a marine *Pseudomonas* sp., strain S9. *Appl Environ Microbiol* 56(7): 2065-72

Wu X, Wang H and Zhao X (2008) Antimicrobial studies with the *Pseudomonas aeruginosa* two-allele library require caution. *Antimicrob Agents Chemother* 52(10): 3826-7

Xu Z, Fang X, Wood TK and Huang ZJ (2013) A systems-level approach for investigating *Pseudomonas aeruginosa* biofilm formation. *PLoS One* 8(2): e57050

Yang L, Hu Y, Liu Y, Zhang J, Ulstrup J and Molin S (2011) Distinct roles of extracellular polymeric substances in *Pseudomonas aeruginosa* biofilm development. *Environ Microbiol* 13(7): 1705-17

Yonekura K, Maki-Yonekura S and Namba K (2003) Complete atomic model of the bacterial flagellar filament by electron cryomicroscopy. *Nature* 424(6949): 643-50

Zeng G, Vad BS, Dueholm MS, Christiansen G, Nilsson M, Tolker-Nielsen T, Nielsen PH, Meyer RL and Otzen DE (2015) Functional bacterial amyloid increases *Pseudomonas* biofilm hydrophobicity and stiffness. *Front Microbiol* 6: 1099

Zhao K, Tseng BS, Beckerman B, Jin F, Gibiansky ML, Harrison JJ, Luijten E, Parsek MR and Wong GCL (2013) Psl trails guide exploration and microcolony formation in *Pseudomonas aeruginosa* biofilms. *Nature* 497(7449): 388-391

Zhu K and Rock CO (2008) RhlA converts beta-hydroxyacyl-acyl carrier protein intermediates in fatty acid synthesis to the beta-hydroxydecanoyl-beta-hydroxydecanoate component of rhamnolipids in *Pseudomonas aeruginosa*. *J Bacteriol* 190(9): 3147-54

Appendices

Appendix A Experimental approaches used in uropathogenic biofilm studies

Table A-1 Evaluation of experimental approaches in uropathogenic biofilm studies

	Bacteria used					AUM				Culture type		AUM pH				*In vitro* model method used with catheter						
Mono Sp. Biofilm	*E. coli*	*P. aeruginosa*	*P. mirabilis*	Fungi	Other	M	G	BK	FU	Stat.	Con.	5.8	6 - 6.5	6.5 <	Other	96-well plate	MRD	Catheter section	Flow cell	Flow-thru catheter	Lab. Bladder	**Notes**
Anderson *et al.,* 1980	√								√		√				√						√	
Nickel *et al.,* 1985a		√				√					√				√		√					
Nickel *et al.,* 1985b		√				√					√				√		√					
Liedberg *et al.,* 1989		√				√					√				√		√					
Liedberg *et al.,* 1990		√				√					√				√		√					
Mclean *et al.,* 1991			√				√				√	√							√			c
Nickel *et al.,* 1992		√				√					√				√					√		
Rogers *et al.,* 1996	√							√			√		√							√		c
Morris *et al.,* 1997			√				√				√		√								√	
Goto *et al.,* 1999a		√					√				√		√							√		
Goto *et al.,* 1999b		√				√					√				√					√		c
Hashimoto, 2001		√				√					√				√		√					
Morris & Stickler, 2001			√				√				√		√								√	

(continue to next page)

(continued)

Mono Sp. Biofilm	Bacteria used					AUM				Culture type		AUM pH				*In vitro* model method used with catheter						Notes
	E. coli	*P. aeruginosa*	*P. mirabilis*	Fungi	Other	M	G	BK	FU	Stat.	Con.	5.8	6 - 6.5	6.5 <	Other	96-well plate	MRD	Catheter section	Flow cell	Flow-thru catheter	Lab. Bladder	
Chakravarti *et al.,* 2005			√				√				√		√								√	
Mikuniya *et al.,* 2005		√				√					√				√		√					
Burton *et al.,* 2006	√	√			√			√		√			√					√					
Jain *et al.,* 2007				√			√			√		√				√						
Jones *et al.,* 2007			√					√			√		√						√			
Barford *et al.,* 2008	√										√										√	a
Darouiche *et al.,* 2008	√	√			√			√		√			√					√				
Schulz *et al.,* 2008			√				√				√		√								√	
Stickler & Morgan, 2008			√				√				√		√								√	
Broomfield *et al.,* 209	√	√	√		√		√				√		√								√	
Percival *et al.,* 2009			√				√				√		√								√	
Soriano *et al.,* 2009					√		√			√			√			√						c
Amalaradjou *et al.,* 2010	√								√	√					√	√						
Desai *et al.,* 2010	√				√					√					√			√				a
Gilmore *et al.,* 2010			√																			

(continue to next page)

(continued)

Mono Sp. Biofilm	Bacteria used					AUM				Culture type		AUM pH				*In vitro* model method used with catheter						Notes
	E. coli	*P. aeruginosa*	*P. mirabilis*	Fungi	Other	M	G	BK	FU	Stat.	Con.	5.8	6 - 6.5	6.5 <	Other	96-well plate	MRD	Catheter section	Flow cell	Flow-thru catheter	Lab. Bladder	
Watts *et al.,* 2010	√						√			√		√				√		√				
Dohnt *et al.,* 2011		√						√			√		√								√	
Gabi *et al.,* 2011			√				√				√		√						√			
Negri *et al.,* 2011				√			√				√	√								√		
Narten *et al.,* 2012		√						√		√			√									b
Negri *et al.,* 2012				√			√			√		√						√				
Tielen *et al.,* 2013		√						√		√			√									b
Blanco *et al.,* 2014		√			√					√	√				√			√			√	a
Cole *et al.,* 2014		√								√			√					√				a
Rahmani-Badi *et al.,* 2014	√						√			√	√		√			√		√	√			
Rane *et al.,* 2014				√			√			√		√						√				
Sako *et al.,* 2014		√				√				√					√	√						
Wang *et al.,* 2015a			√				√				√		√								√	
Wang *et al.,* 2015b	√	√	√				√			√			0					√				
Wilks *et al.,* 2015			√					√		√			√					√				

(continue to next page)

(continued)

Dual Sp. Biofilm	**Bacteria used**					**AUM**				**Culture type**		**AUM pH**				***In vitro* model method used with catheter**						**Notes**
	E. coli	*P. aeruginosa*	*P. mirabilis*	Fungi	Other	M	G	BK	FU	Stat.	Con.	5.8	6 - 6.5	6.5 <	Other	96-well plate	MRD	Catheter section	Flow cell	Flow-thru catheter	Lab. Bladder	
Lellouche *et al.,* 2012	√	√								√	√			√				√				a
Nowatzki *et al.,* 2012	√				√					√	√		√					√	√	√		a, b
Cerqueira *et al.,* 2013	√	√						√		√			√									
Reisner *et al.,* 2014	√				√		√				√		√								√	
Lehman & Donlan, 2015		√	√					√			√			√						√		

Polymicrobial Sp. Biofilm	**Bacteria used**					**AUM**				**Culture type**		**AUM pH**				***In vitro* model method used with catheter**						**Notes**
	E. coli	*P. aeruginosa*	*P. mirabilis*	Fungi	Other	M	G	BK	FU	Stat.	Con.	5.8	6 - 6.5	6.5 <	Other	96-well plate	MRD	Catheter section	Flow cell	Flow-thru catheter	Lab. Bladder	
Silva *et al.,* 2010				√			√			√		√						√				
Kishikawa *et al.,* 2013	√	√	√		√		√				√				√						√	
Azevedo *et al.,* 2014	√				√			√		√			√			√						
Malic *et al.,* 2014	√	√	√		√		√			√			√			√						
Samaranayake *et al.,* 2014	√	√		√						√			√			√						a

a using other non-urine related media

b using other in-vitro models

c using other temperature than 37 ºC

Appendix B Comparison of AUM formulation in CAUTI research

Table B-1 Chemical comparison between selected AUM formulation in CAUTI research

		Minuth *et al*, 1976		Griffith *et al*, 1976		Brooks & Keevil, 1997		Chutipongtanate & Thongboonkerd 2010		Nowatzki, *et al,* 2012	
Compound	**Chemical Formula**	**Quantity (g)**	**Concentration (mmol/l)**	**Quantity (g)**	**Concentration (mmol/l)**	**Quantity (g)**	**Concentration (mmol/l)**	**Quantity (g)**	**Concentration (mmol/l)**	**Quantity (g)**	**Concentration (mmol/l)**
Distilled water	H_2O	1 L		1 L		1 L		200ml		1 L	
Peptone media				1[a]		1[b]				1[c]	
Yeast extract	$C_{19}H_{14}O_2$					0.005	*0.001*				
Citric acid	$C_6H_8O_7$					0.4	*2.00*			0.33	*1.71*
Lactic acid	$C_2H_4OHCOOH$					0.1	*1.10*				
Uric acid	$C_5H_4N_4O_3$					0.07	*0.40*	0.17	*1.01*		
Creatinine	$C_4H_7N_3O$	1.1	*9.72*			0.8	*7.00*	0.45	*3.98*		
Gelatine	$C_6H_{12}O_6$			5	*0.90*						
Urea	$CO(NH_2)_2$	12	*199.80*	25	*420.00*	10	*170.00*	12	*199.80*	18.62	*310*
Ammonium chloride	NH_4Cl	2	*37.39*	1	*19.00*	1.3	*25.00*	0.805	*15.05*	1.5	*28*
Calcium chloride	$CaCl_2$			0.49	*4.42*					0.24	*2.2*
Calcium chloride dihydrate	$CaCl_2 \bullet 2H_2O$	0.65	*4.42*			0.37	*2.50*	0.445	*3.03*		
Iron (II) sulphate heptahydrate	$FeSO_4 \bullet 7H_2O$					0.0012	*0.01*				
Magnesium chloride hexahydrate	$MgCl_2 \bullet 6H_2O$	0.651	*3.20*	0.65	*3.00*						
Magnesium sulphate	$MgSO_4$									0.31	*2.6*

(continue to next page)

(continued)

Compound	Chemical Formula	Minuth, *et al*, 1976		Griffith, *et al,* 1976		Brooks & Keevil, 1997		Chutipongtanate & Thongboonkerd 2010		Nowatzki, *et al*, 2012	
		Quantity (g)	Concentration (mmol/l)	Quantity (g)	Concentration (mmol/l)	Quantity (g)	Concentration (mmol/l)	Quantity (g)	Concentration (mmol/l)	Quantity (g)	Concentration (mmol/l)
Magnesium sulphate heptahydrate	$MgSO_4 \bullet 7H_2O$					0.49	*2.00*	0.5	*2.03*		
Potassium chloride	KCl	1.6	*21.46*	1.6	*21.50*			2.25	*30.18*	2.91	*39.1*
Potassium dihydrogen phosphate	KH_2PO_4	2.8	*20.57*	2.8	*20.57*	0.95	*6.98*				
Di-potassium hydrogen phosphate	K_2HPO_4					1.2	*6.89*				
Sodium chloride	NaCl	4.6	*78.71*	4.6	*0.27*	5.2	*90.00*	3.17	*54.24*	3.41	*58.4*
Sodium bicarbonate	$NaHCO_3$					2.1	*25.00*	0.17	*2.02*		
Sodium sulphate	Na_2SO_4	2.3	*16.19*	2.3	*16.19*			1.29	*9.08*	1.87	*13.2*
Sodium sulphate decahydrate	$Na_2SO_4 \bullet 10H_2O$					3.2	*10.00*			4.25	*13.2*
Sodium dihydrogen phosphate	NaH_2PO_4							0.5	*4.17*	1.04	*8.7*
Di-Sodium hydrogen phosphate	Na_2HPO_4							0.011	*0.39*		
Tri-Sodium citrate	$Na_3C_6H_5O_7$	0.65	*2.52*								
Tri-Sodium citrate dihydrate	$Na_3C_6H_5O_7 \bullet 2H_2O$			0.65	*2.00*			1.485	*5.05*		
Di-Sodium oxalate	$Na_2C_2O_4$	0.02	*0.15*	0.02	*0.15*			0.015	*0.11*		
pH		5.7-5.8		6.1		6.5		6.2		6.2	

[a] Griffith, *et al*. (1976) uses TSB

[b] Brooks & Keevil (1997) uses Peptone L37

[c] Nowatzki, *et al.* (2012) uses Casamino acid

Appendix C Analysis of biofilm data values in 24 h experiment

Table C-1 Colony forming unit (log_{10} cfu/ml) enumeration analysis of 24 h biofilm in the two artificial urine medium, AUG and AUBK.

	E. coli				
	AU Griffith, *et al*. (1976)		AU Brooks & Keevil (1997)		*t*-test
Hours	**Mean**	**SD**	**Mean**	**SD**	
1	3.500	0.915	3.506	0.841	*ns*
2	3.966	0.192	4.769	0.283	$P < 0.05$
4	5.120	0.409	5.500	0.556	*ns*
6	5.555	0.299	6.069	0.375	*ns*
24	6.087	0.309	6.258	0.254	*ns*

	P. aeruginosa				
	AU Griffith, *et al.* (1976)		AU Brooks & Keevil (1997)		*t*-test
Hours	**Mean**	**SD**	**Mean**	**SD**	
1	5.197	0.274	5.205	0.379	*ns*
2	5.682	0.140	5.790	0.160	*ns*
4	6.283	0.090	6.639	0.089	$P < 0.01$
6	7.091	0.335	7.084	0.239	*ns*
24	8.442	0.232	7.534	0.099	$P < 0.01$

	P. mirabilis				
	AU Griffith, *et al.* (1976)		AU Brooks & Keevil (1997)		*t*-test
Hours	**Mean**	**SD**	**Mean**	**SD**	
1	4.199	0.192	4.578	0.297	*ns*
2	4.165	0.018	4.610	0.066	$P < 0.001$
4	5.349	0.191	5.328	0.630	*ns*
6	5.917	0.080	5.964	0.397	*ns*
24	3.968	0.577	4.772	1.274	*ns*

For all significant results shown, $P < 0.05$.

Appendix D Analysis of biofilm data values in 144 h experiment

Table D-1 Colony forming unit (log_{10} cfu/ml) enumeration analysis of 144 h biofilm in the two artificial urine medium, AUG and AUBK.

E. coli

	AU Griffith, *et al.* (1976)		AU Brooks & Keevil (1997)		*t*-test
Hours	**Mean**	**SD**	**Mean**	**SD**	
24	6.58	0.308	5.62	0.618	*ns*
48	6.75	0.121	5.94	0.586	*ns*
72	7.06	0.092	5.70	0.501	*ns*
96	7.00	0.184	5.90	0.253	$P < 0.05$
120	6.76	0.111	6.25	0.187	*ns*
144	7.79	0.601	6.16	0.024	*ns*

P. aeruginosa

	AU Griffith, *et al.* (1976)		AU Brooks & Keevil (1997)		*t*-test
Hours	**Mean**	**SD**	**Mean**	**SD**	
24	8.81	0.132	8.49	0.782	*ns*
48	8.78	0.607	7.72	0.309	*ns*
72	8.45	0.633	7.68	0.617	*ns*
96	8.01	0.695	7.67	0.524	*ns*
120	6.93	0.157	6.70	0.084	*ns*
144	6.72	0.648	6.46	0.011	*ns*

P. mirabilis

	AU Griffith, *et al.* (1976)		AU Brooks & Keevil (1997)		*t*-test
Hours	**Mean**	**SD**	**Mean**	**SD**	
24	3.88	3.646	6.88	0.399	*ns*
48	1.54	0.088	4.98	0.537	$P < 0.01$
72	1.80	0.707	4.69	0.550	$P < 0.05$
96	2.45	1.201	4.54	0.108	*ns*
120	3.63	0.209	4.91	0.192	$P < 0.05$
144	2.85	0.346	5.73	0.224	$P < 0.01$

For all significant results shown, $P < 0.05$.

Appendix E Details of *P. aeruginosa* PAO1 strains used

Table E-1 List of *P. aeruginosa* PAO1 strains described in Chapter 5, 6 and 7

Reference strain

Name	Bacterial strains	Putative ORF function / characteristic(s)	PA ORF
Wild type (WT)	PAO1	Wild-type parental *P. aeruginosa* strain ATCC 15692	MPAO1

Urease mutants

Mutant	Bacterial strains	Putative ORF function / characteristic(s)	PA ORF
PW9188-Δ*ureC*	ureC-G12::ISphoA/hah‡	urease alpha subunit UreC	PA4868
PW9189-Δ*ureC*	ureC-C11::ISphoA/hah‡	urease alpha subunit UreC	PA4868
PW9231-Δ*ureE*	ureE-A01::ISphoA/hah‡	urease accessory protein UreE	PA4891

Quorum-sensing mutants

Name	Bacterial strains	Putative ORF function / characteristic(s)	PA ORF
PW6887-Δ*rhlA*	*rhlA*-A01::ISphoA/hah‡	Rhamnosyltransferase chain A RhlA	PA3479
PW6884-Δ*rhlB*	*rhlB*-G07::ISlacZ/hah†	Rhamnosyltransferase chain B RhlB	PA3478
PW6885-Δ*rhlB*	*rhlB*-F05:: ISphoA/hah‡	Rhamnosyltransferase chain B RhlB	PA3478
PW6880-Δ*rhlI*	*rhlI*-D03::ISphoA/hah‡	Autoinducer synthesis protein RhlI	PA3476
PW6881-Δ*rhlI*	*rhlI*-F02::ISphoA/hah‡	Autoinducer synthesis protein RhlI	PA3476
PW3601-Δ*lasI*	*lasI*-F07::ISlacZ/hah†	Autoinducer synthesis protein LasI	PA1432
PW2798-Δ*pqsA*	*pqsA*-H05::ISlacZ/hah†	Probable coenzyme A ligase PqsA	PA0996
PW2799-Δ*pqsA*	*pqsA*-H04::ISlacZ/hah†	Probable coenzyme A ligase PqsA	PA0996
PW2806-Δ*pqsE*	*pqsE*-G04::ISlacZ/hah†	Quinolone signal response protein PqsE	PA1000
PW2807-Δ*pqsE*	*pqsE*-D03::ISlacZ/hah†	Quinolone signal response protein PqsE	PA1000

Polysaccharide mutants

Name	Bacterial strains	Putative ORF function / characteristic(s)	PA ORF
PW6140-Δ*pelA*	*pelA*-H06::ISphoA/hah‡	PelA	PA3064
PW6141-Δ*pelA*	*pelA*-F09::ISphoA/hah‡	PelA	PA3064
PW4802-Δ*pslD*	*pslD*-H08::ISlacZ/hah†	PslD	PA2234
PW4803-Δ*pslD*	*pslD*-H09::ISlacZ/hah†	PslD	PA2234
PW4807-Δ*pslG*	*pslG*-D07::ISlacZ/hah†	Probable glycosyl hydrolase PslG	PA2237
PW4808-Δ*pslG*	*pslG*-G09::ISlacZ/hah†	Probable glycosyl hydrolase PslG	PA2237
PW2387-Δ*mucA*	*mucA*-A05::ISphoA/hah‡	*P. aeruginosa PAO1 mutant strain PW2387* of anti-sigma factor *mucA* region	PA0763
PW6997-Δ*algD*	*algD*-C03::ISphoA/hah‡	*P. aeruginosa PAO1 mutant strain PW2387* of GDP-mannose 6-dehydrogenase *algD* region	PA3540
PW6998-Δ*algD*	*algD*-H06::ISphoA/hah‡	*P. aeruginosa PAO1 mutant strain PW2387* of GDP-mannose 6-dehydrogenase *algD* region	PA3540

(continued to next page)

(continue)

Attachment/Motility (AM)-negative group

Name	Bacterial strains	Relevant putative ORF function / characteristic(s)	PA ORF
PW3643-Δ*fliA*	*fliA*-E07::IS*lacZ*/hah†	sigma factor FliA mutant	PA1455
PW2970-Δ*fliC*	*fliC*-G03::IS*lacZ*/hah†	flagellin type B mutant	PA1092
PW2971-Δ*fliC*	*fliC*-G10::IS*phoA*/hah‡	flagellin type B mutant	PA1092
PW3621-Δ*fliM*	*fliM*-B05::IS*lacZ*/hah†	flagellar motor switch protein FliM mutant	PA1443
PW3622-Δ*fliM*	*fliM*-D08::IS*phoA*/hah‡	flagellar motor switch protein FliM mutant	PA1443
PW8621-Δ*pilA*	*pilA*-E01::IS*lacZ*/hah†	type 4 fimbrial precursor PilA mutant	PA4525
PW8622-Δ*pilA*	*pilA*-H02::IS*phoA*/hah‡	type 4 fimbrial precursor PilA mutant	PA4525
PW7438-Δ*pilF*	*pilF*-E10::IS*phoA*/hah‡	type 4 fimbrial biogenesis protein PilF mutant	PA3805
Δ*fliC*	Δ*fliC*α	Knock out mutant strain for flagellin type B	PA1092
Δ*pilA*	Δ*pilA*α	Knock out mutant strain for type 4 fimbrial precursor PilA	PA4525
Δ*fliC*Δ*pilA*	Δ*fliC*Δ*pilA*α	flagellin type B & type 4 fimbrial precursor PilA double knockout mutant strain	PA1092 + PA4525

† Transposon insertion using primer *lacZ* 148 primer (5'-gggtaacgccagggttttcc-3')
‡ Transposon insertion presence using primer Hah minus 138 (5'cgggtgcagtaatatcgccct-3')
α Knock-out strain obtained from Professor Myron Christodoulides lab, University of Southampton

Table E-2 List of transposons used in *P. aeruginosa* PAO1 mutant

Transposon

Transposable elements	Vectors	Delivery method	Selection marker	Deletion method
T5 (IS*phoA*/hah-cm)	pCM638 pCM665	Conjugation	chloramphenicol	*loxP*
T6 (IS*phoA*/hah-tc)	pCM639	Conjugation	tetracycline	*loxP*
T7 (IS*lacZ*/hah-cm)	pIT1	Conjugation	chloramphenicol	*loxP*
T8 (IS*lacZ*/hah-tc)	pIT2	Conjugation	tetracycline	*loxP*

Table E-3 List of primer details for verification of presence of transposon by PCR in *P. aeruginosa* PAO1 mutant

Strain Name	F Primer Name	F Primer Seq	F Primer Position	F Primer T_m	Insert - F	R Primer Name	R Primer Seq	R Primer Position	R Primer T_m	R - Insert	WT PCR Len	Seq.
PW2387	32854F.f	CACGCCCTGAAGGACATC	831631	60.205	578	32854F.r	TGTCTCTCCTCAGCGGTTTT	832507	59.989	298	876	Yes
PW2798	1932F.f	CGCCTCGAACTGTGAGATTT	1078064	60.397	557	1932F.r	GAGAAATCGTCGAGCAAAGG	1078865	59.955	244	801	Yes
PW2799	19744F.f	GCCGTGATCAATCCCAAGT	1078702	60.887	569	19744F.r	AGCAGGATCTGGTTGTCGTC	1079837	60.269	566	1135	Yes
PW2806	1308F.f	CATGTGATCTGCCATCAACC	1082701	59.925	566	1308F.r	TCCAGGTAAGCCTCCATGTC	1083556	60.073	289	855	Yes
PW2807	17750F.f	CTGCTGCCCTACCTGTGTC	1083177	59.43	580	17750F.r	CTTCCAGTCGATAGCCAACC	1084020	59.694	263	843	Yes
PW2970	245F.f	TGCAGCAGTCCACCAATATC	1183302	59.679	575	245F.r	GTTGGTAGCGTTTTCCGAGA	1184383	60.249	506	1081	Yes
PW2971	45281F.f	CGATATTGGCGAGTCCTCTT	1182862	59.292	529	45281F.r	GCTTCGACGAGTTGGAGTTC	1183910	59.997	519	1048	Yes
PW3601	11174F.f	GGGAGAAGGAAGTGTTGCAG	1558709	59.844	588	11174F.r	ATCATCATCTTCTCCACGCC	1559711	60.042	414	1002	
PW3621	1374F.f	TGCTTTCCCAGGATGAAATC	1572568	60.014	530	1374F.r	TCCTCGGTGGTCACTTTTTC	1573582	60.088	484	1014	
PW3622	55256F.f	AACCTGGTGAAGATGAAGCC	1572858	59.141	532	55256F.r	GGGATGTCCAGGATCACATC	1573795	60.145	405	937	Yes
PW3643	21187R.f	CGTATGTATAGCAAGGCGCA	1584816	59.886	534	21187R.r	TATTGGTGAAGCCCAAGTCC	1585721	59.933	371	905	
PW4802	11184F.f	GAAGAACTCGCCAGGCTACC	2457621	61.287	591	11184F.r	TGATCTCTATCGGCAGGGTC	2458484	60.181	272	863	
PW4803	11184F.f	GAAGAACTCGCCAGGCTACC	2457621	61.287	591	11184F.r	TGATCTCTATCGGCAGGGTC	2458484	60.181	272	863	
PW4807	5204R.f	CGGTGGTCTGGAAAGACTTC	2461578	59.697	568	5204R.r	GTAGTCCAGCGCACTCATCA	2462398	60.016	252	820	Yes
PW4808	11363F.f	TACTGCTGCTGGTGTTCTGG	2461512	60.049	531	11363F.r	GAAGATCCGGTCGTAGTCCA	2462410	60.073	367	898	Yes
PW6140	39219R.f	ACGGATCGAGGATCCAGC	3432402	61.171	534	39219R.r	GGACAGCTTCCAGCTACAGG	3433405	60.012	469	1003	Yes
PW6141	51892F.f	CCCTGCCAGAGATTGGTGTA	3431696	61.055	567	51892F.r	GAAACTCAAGGTCAAGCCGA	3432658	60.375	395	962	Yes
PW6880	32454R.f	ACGAGATGGCGGAATGACT	3888958	60.639	662	32454R.r	TTCCACCACAAGAACATCCA	3890010	59.935	390	1052	Yes
PW6881	55473R.f	ACGAGATGGCGGAATGACT	3888958	60.639	538	55473R.r	TTCCACCACAAGAACATCCA	3890010	59.935	514	1052	Yes
PW6884	21357R.f	CTGTGCGGTTGTGACAATTC	3890856	60.16	696	21357R.r	TTGCATAACGCACGGAGTAG	3892078	59.895	526	1222	Yes
PW6885	42183R.f	CCCGTAGTTCTGCATCTGGT	3890416	60.134	548	42183R.r	AACTGCAACGCTTTCTCGAT	3891330	60.022	366	914	Yes
PW6997	53079F.f	CTGGACTCCGACGTATCGTT	3963046	60.134	582	53079F.r	GGAGACCAGCAGTGAGGAGA	3963969	60.55	341	923	Yes
PW6998	53212F.f	TTAACGGAAAGGCCATCAAG	3962343	60.067	532	53212F.r	GTCTCGATGTAGCCCAGGTC	3963125	59.685	250	782	Yes
PW7438	40584F.f	CTCCTGCCACCAGAAGTAGC	4264122	60.012	534	40584F.r	GCCCGGGTACTGAACAACTA	4264975	59.993	319	853	Yes
PW8621	20501R.f	GGAATCAACGAGGGCACC	5068763	61.454	547	20501R.r	ACCCAGTTTCCTTGATCGTG	5069628	59.966	318	865	Yes
PW8622	33348R.f	ACTACATCTCCATCGGCACC	5068809	59.957	559	33348R.r	ACCCAGTTTCCTTGATCGTG	5069628	59.966	260	819	Yes
PW9188	40132F.f	CGCTGATCCTCGACCACT	5465034	59.936	583	40132F.r	GGGTTGATGGTGTACTTGGC	5466048	60.24	431	1014	Yes
PW9189	45440F.f	ACCGCCGACAAGATGAAG	5465945	59.787	565	45440F.r	TCACGTCCTTCTTGCTGATG	5466789	59.984	279	844	Yes
PW9231	35481R.f	CGCGCTGCAATATTTTGTTA	5487087	59.872	562	35481R.r	CTCCAGAACCAGGCACTCAG	5488174	60.997	525	1087	Yes

Appendix F *P. aeruginosa* PAO1 wildtype (WT)

F.1 Biofilm data values of *P. aeruginosa* PAO1 wildtype (WT)

Table F-1 *P. aeruginosa* PAO1 wildtype strain biofilm enumeration data expressed as mean ± SD (SD = standard deviation)

Reference strain		**1 h**	**3 h**	**6 h**	**24 h**
Wildtype (WT)	**Log_{10} cfu/catheter section**	6.16 ± 0.17	6.38 ± 0.04	7.09 ± 0.27	7.36 ± 0.08
	(%)	(57.82 ± 1.94)	(60.18 ± 0.48)	(68.17 ± 2.97)	(71.15 ± 0.88)

Table F-2 One-way ANOVA analysis of *P. aeruginosa* PAO1 wildtype biofilm enumeration between timepoints

One-way ANOVA ($P < 0.05$)

ANOVA table	**SS**	**DF**	**MS**	$F_{(3, 8)}$	***P* summary**	**R^2**
Treatment (between columns)	2.894	3	0.9645	35.62	$P < 0.0001$	0.9304
Residual (within columns)	0.2163	8	0.02704		(****)	
Total	3.11	11				

Table F-3 *P. aeruginosa* PAO1 WT Bonferroni's post-hoc multiple comparison test of *P. aeruginosa* PAO1 wildtype biofilm enumeration between timepoints

	1 h	**3 h**	**6 h**	**24 h**
Log_{10} cfu/catheter section	6.16 ± 0.17	6.38 ± 0.04	7.09 ± 0.27	7.36 ± 0.08
(%)	(57.82 ± 1.94)	(60.18 ± 0.48)	(68.17 ± 2.97)	(71.15 ± 0.88)
		1 h *vs* 3 h	3 h *vs* 6 h	6 h *vs* 24 h
Adjusted *P* value		$P = 0.4661$	$P = 0.0021$	$P = 0.2470$
Significant summary		*ns*	**	*ns*

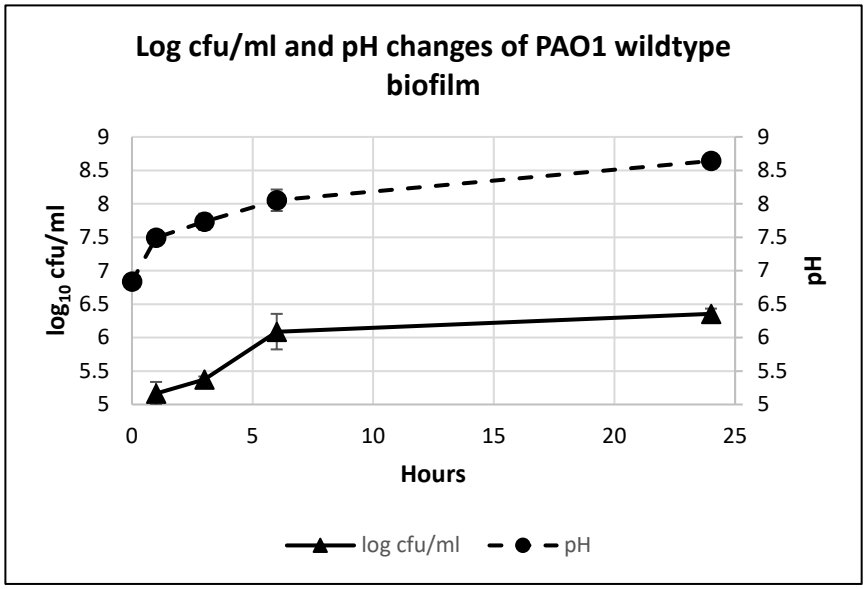

Figure F-1 Graph shows the log_{10} cfu/ml and AUBK pH data of *P. aeruginosa* PAO1 wildtype biofilm. Error bar indicates the standard deviation (SD).

F.2 Biofilm images of *P. aeruginosa* PAO1 wildtype (WT)

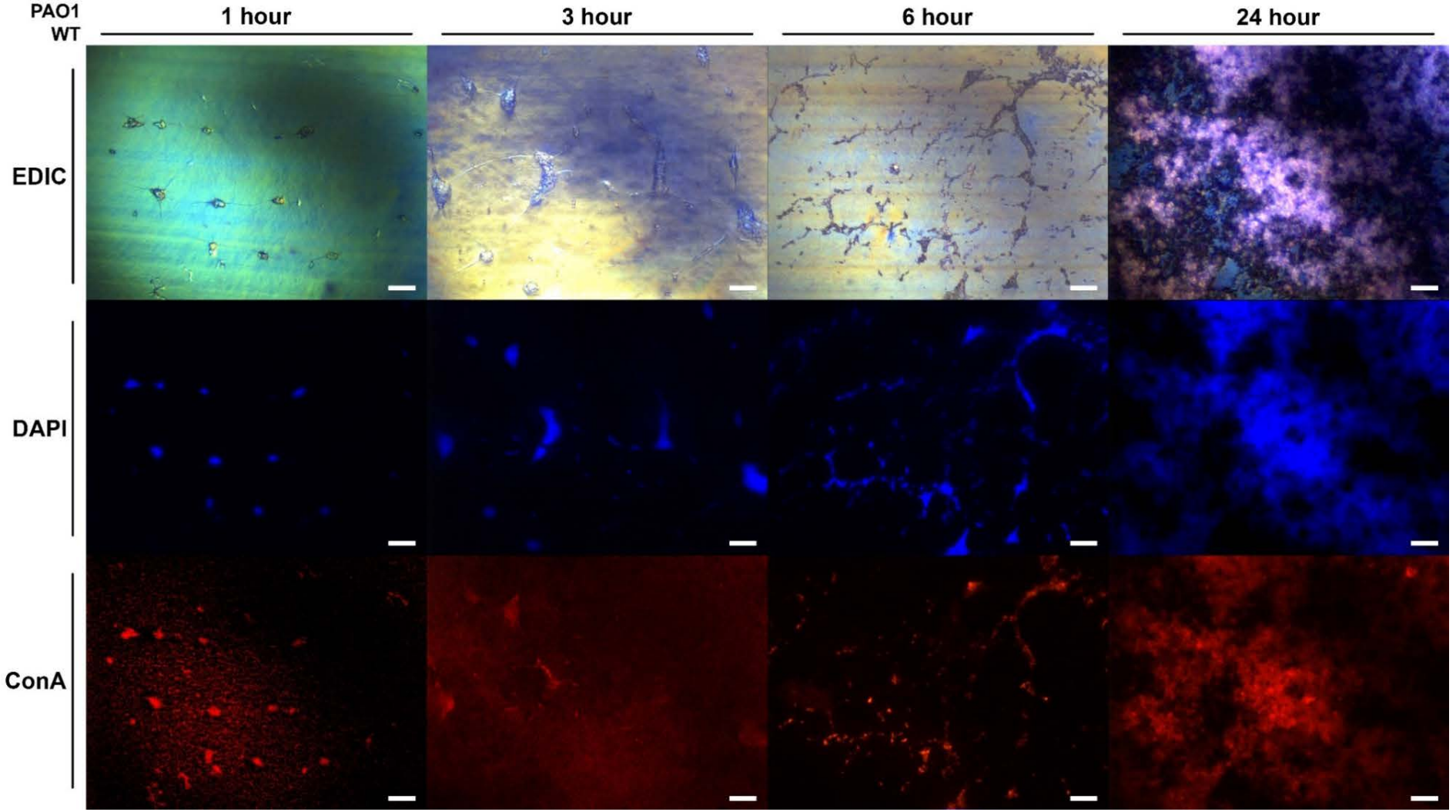

Figure F-2 *P. aeruginosa* PAO1 reference strain wildtype (WT) biofilm morphology on urinary catheter grown in AUBK at 1 h, 3 h, 6 h and 24 h time point as observed under EDIC/EF microscope. Magnification x 1000. Scale bar = 10 µm.

Appendix G Urease-negative *P. aeruginosa* PAO1 mutant group

G.1 Biofilm enumeration data analysis of urease-negative *P. aeruginosa* PAO1 mutant group

Table G-1 Brown-Forsythe one-way ANOVA analysis of *P. aeruginosa* PAO1 wildtype and urease-negative mutant biofilm enumeration data between timepoints

Time	ANOVA table	SS	DF	MS	F(DFn_3, DFd_8)	P value	P summary	R^2	F(DFn_{11}, DFd_{24})	P value	P summary
1 h	Treatment (between columns)	0.01981	3	0.006602	0.3212	P=0.8101	No	0.1075	0.6318	0.6149	No
	Residual (within columns)	0.1644	8	0.02055		*ns*					
	Total	0.1842	11								
3 h	Treatment (between columns)	0.5622	3	0.1874	22.44	P=0.0003	Yes	0.8938	0.28	0.8385	No
	Residual (within columns)	0.06682	8	0.008352		***					
	Total	0.629	11								
6 h	Treatment (between columns)	0.4585	3	0.1528	2.927	P=0.0998	No	0.5233	0.315	0.8143	No
	Residual (within columns)	0.4177	8	0.05221		*ns*					
	Total	0.8762	11								
6 h	Treatment (between columns)	0.1932	3	0.06439	3.039	P=0.0927	No	0.5327	0.3475	0.7922	No
	Residual (within columns)	0.1695	8	0.02118		*ns*					
	Total	0.3626	11								

For all significant results shown, $P < 0.05$ (*, $P < 0.05$; **, $P < 0.01$; ***, $P < 0.001$, ****, $P < 0.0001$, and *ns*, not significant).

G.2 Biofilm images of *P. aeruginosa* PAO1 mutant strain PW9188-Δ*ureC* (ureC-G12::IS*phoA*/hah)

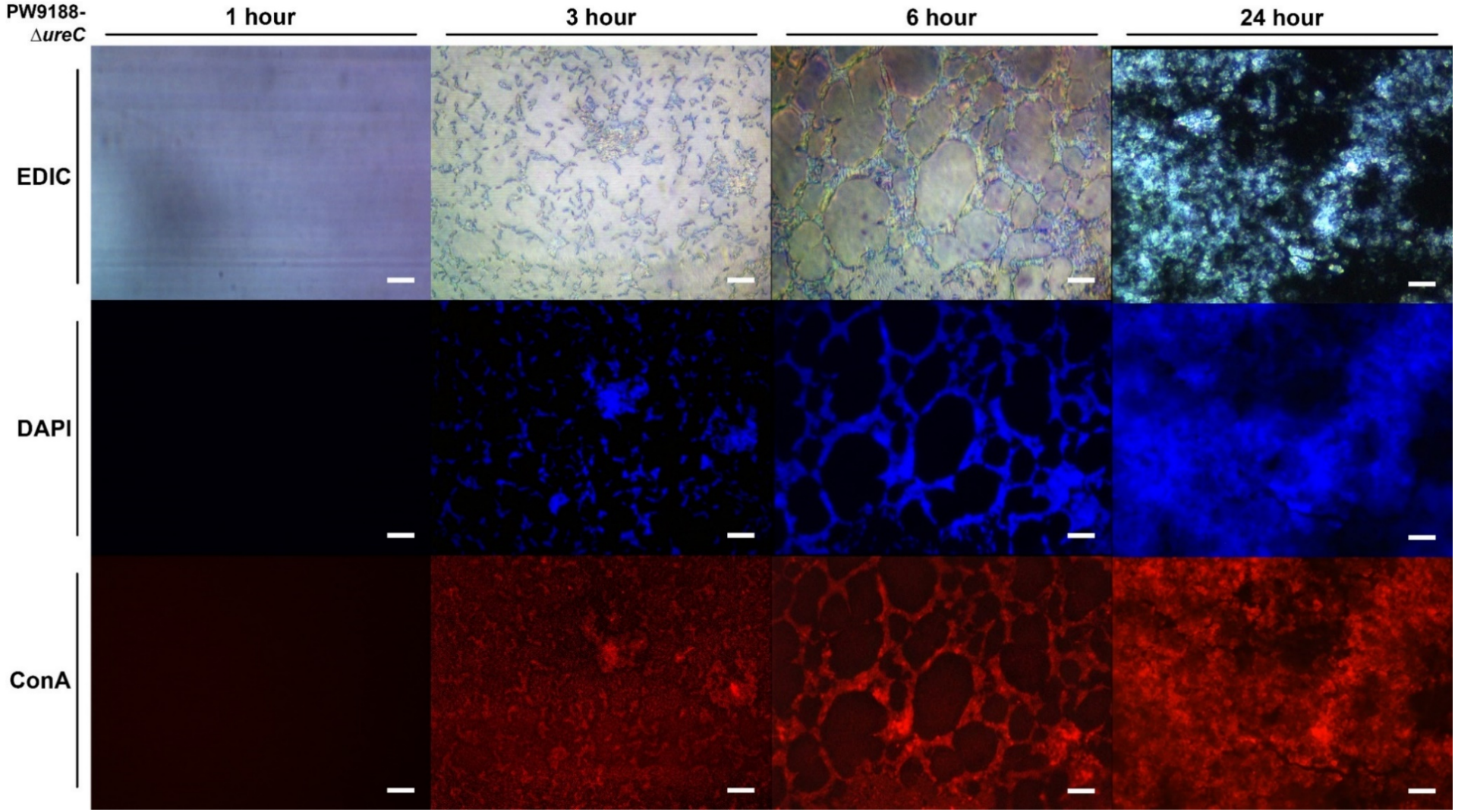

Figure G-2 *P. aeruginosa* PAO1 mutant strain PW9188-Δ*ureC* biofilm morphology on urinary catheter grown in AUBK at 1 h, 3 h, 6 h and 24 h timepoint as observed under EDIC/EF microscope. Magnification x 1000. Scale bar = 10 µm.

G.3 Biofilm images of *P. aeruginosa* PAO1 mutant strain PW9189-Δ*ureC* (ureC-C11::IS*phoA*/hah)

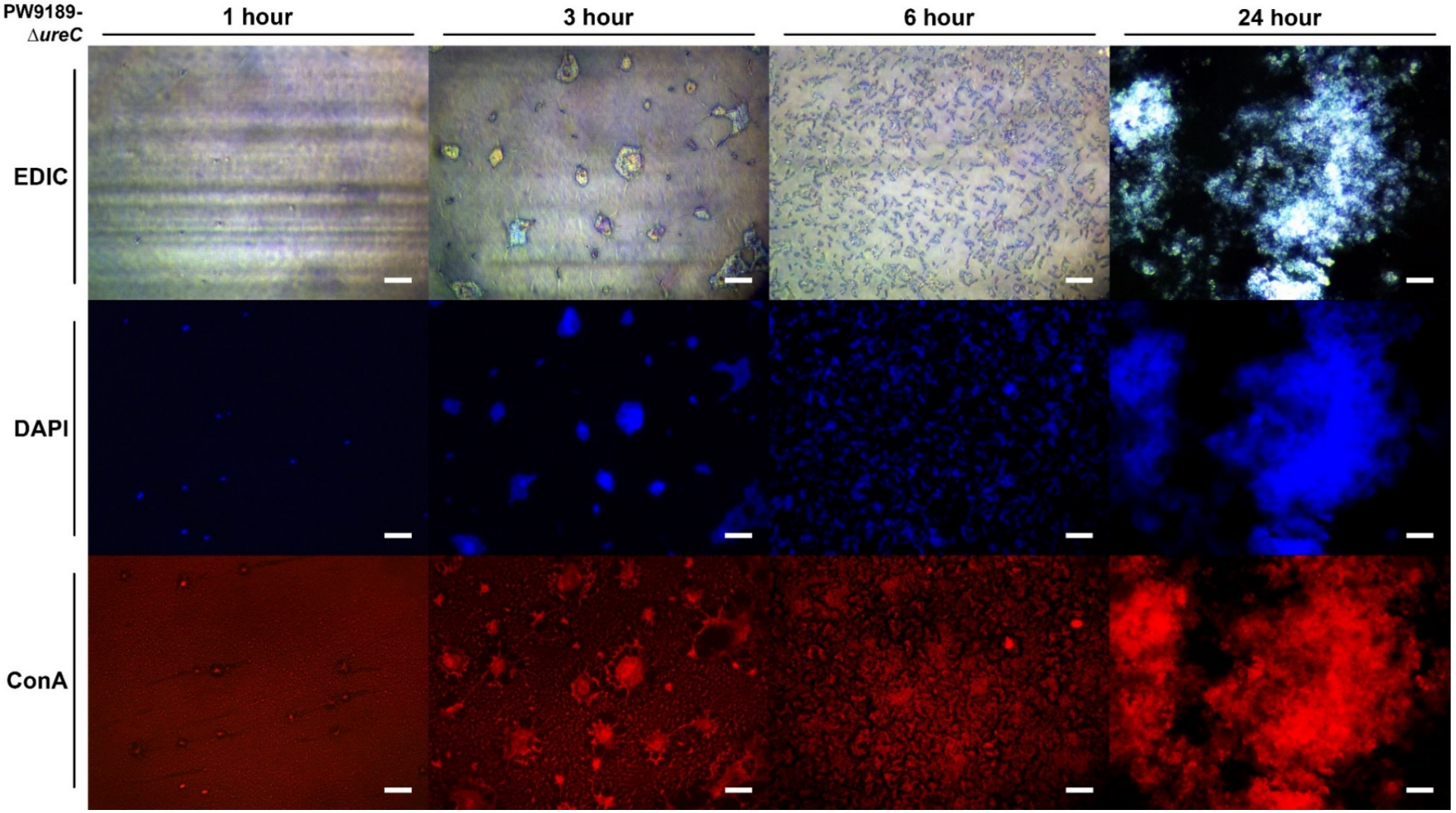

Figure G-3 *P. aeruginosa* PAO1 mutant strain PW9189-Δ*ureC* biofilm morphology on urinary catheter grown in AUBK at 1 h, 3 h, 6 h and 24 h timepoint as observed under EDIC/EF microscope. Magnification x 1000. Scale bar = 10 µm.

G.4 Biofilm images of *P. aeruginosa* PAO1 mutant strain PW9231-Δ*ureE* (ureE-A01::IS*phoA*/hah)

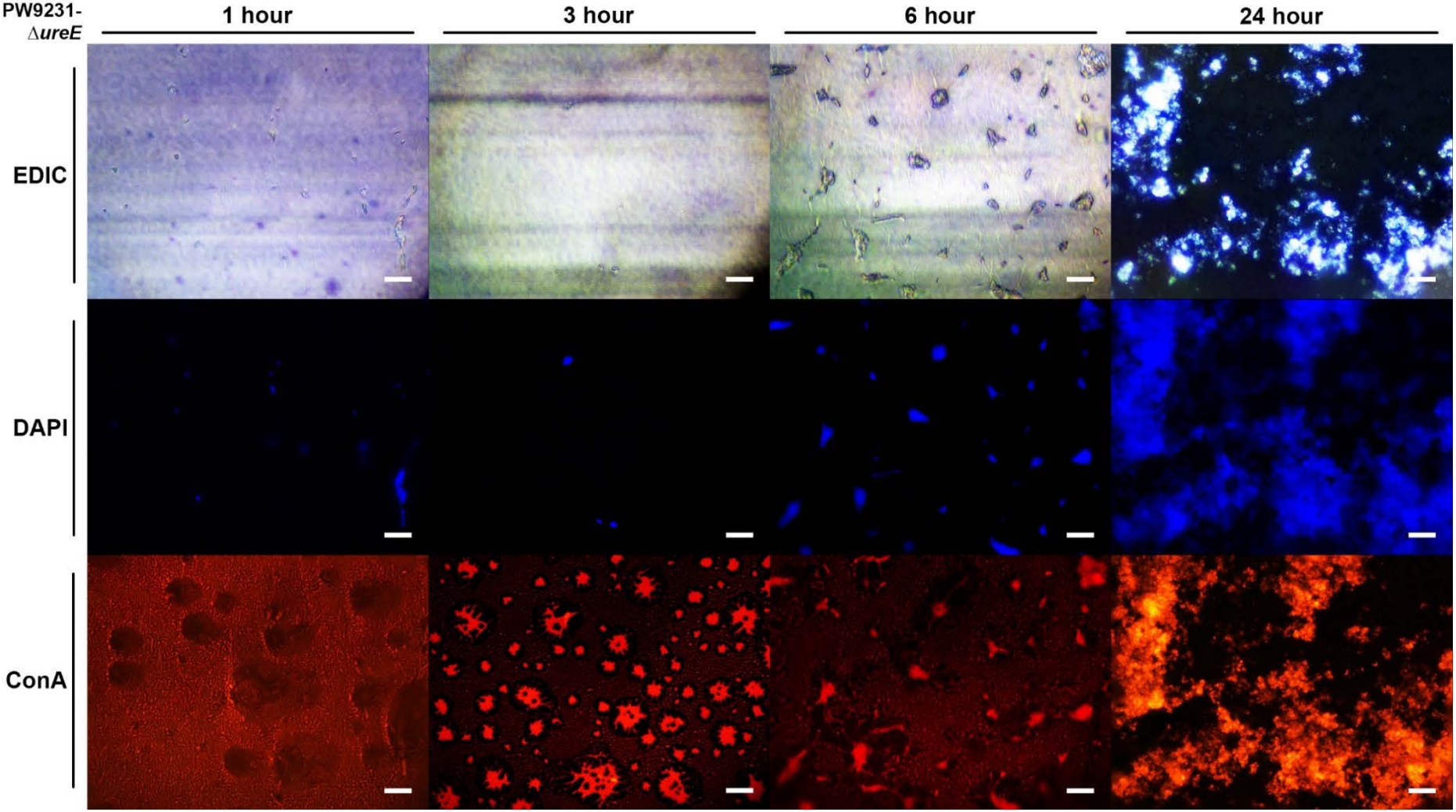

Figure G4 *P. aeruginosa* PAO1 mutant strain PW9231-Δ*ureE* biofilm morphology on urinary catheter grown in AUBK at 1 h, 3 h, 6 h and 24 h timepoint as observed under EDIC/EF microscope. Magnification x 1000. Scale bar = 10 µm.

Appendix H Quorum-sensing (QS)-negative *P. aeruginosa* PAO1 mutant group

H.1 Biofilm enumeration data analysis of QS-negative *P. aeruginosa* PAO1 mutant group

Table H-1 Brown–Forsythe one-way ANOVA analysis of *P. aeruginosa* PAO1 wildtype and QS-negative mutant biofilm enumeration data between timepoints

	One-way ANOVA ($P < 0.05$)								Brown-Forsythe test ($P < 0.05$)		
Time	**ANOVA table**	**SS**	**DF**	**MS**	**F(DFn_{11}, DFd_{24})**	***P* value**	***P* summary**	**R^2**	**F(DFn_{13}, DFd_{28})**	***P* value**	***P* summary**
1 h	Treatment (between columns)	15.62	11	1.42	44.27	P = < 0.0001 ****	Yes	0.9537	0.5286	0.8869	No
	Residual (within columns)	0.7698	24	0.03207							
	Total	16.39	35								
3 h	Treatment (between columns)	18.87	11	1.716	49.49	P = < 0.0001 ****	Yes	0.9578	0.9285	0.6216	No
	Residual (within columns)	0.8321	24	0.03467							
	Total	19.7	35								
6 h	Treatment (between columns)	6.817	11	0.6197	9.639	P = < 0.0001 ****	Yes	0.814	0.626	0.8121	No
	Residual (within columns)	1.543	24	0.06429							
	Total	8.36	35								
24 h	Treatment (between columns)	11.15	11	1.013	41.56	P < 0.0001 ****	Yes	0.9579	0.8676	0.5927	No
	Residual (within columns)	0.5851	24	0.02438							
	Total	11.73	35								

For all significant results shown, $P < 0.05$ (*, $P < 0.05$; **, $P < 0.01$; ***, $P < 0.001$, ****, $P < 0.0001$, and *ns*, not significant).

H.2 Biofilm images of *P. aeruginosa* PAO1 mutant strain PW3601-Δ*lasI* (*lasI*-F07::IS*lacZ*/hah)

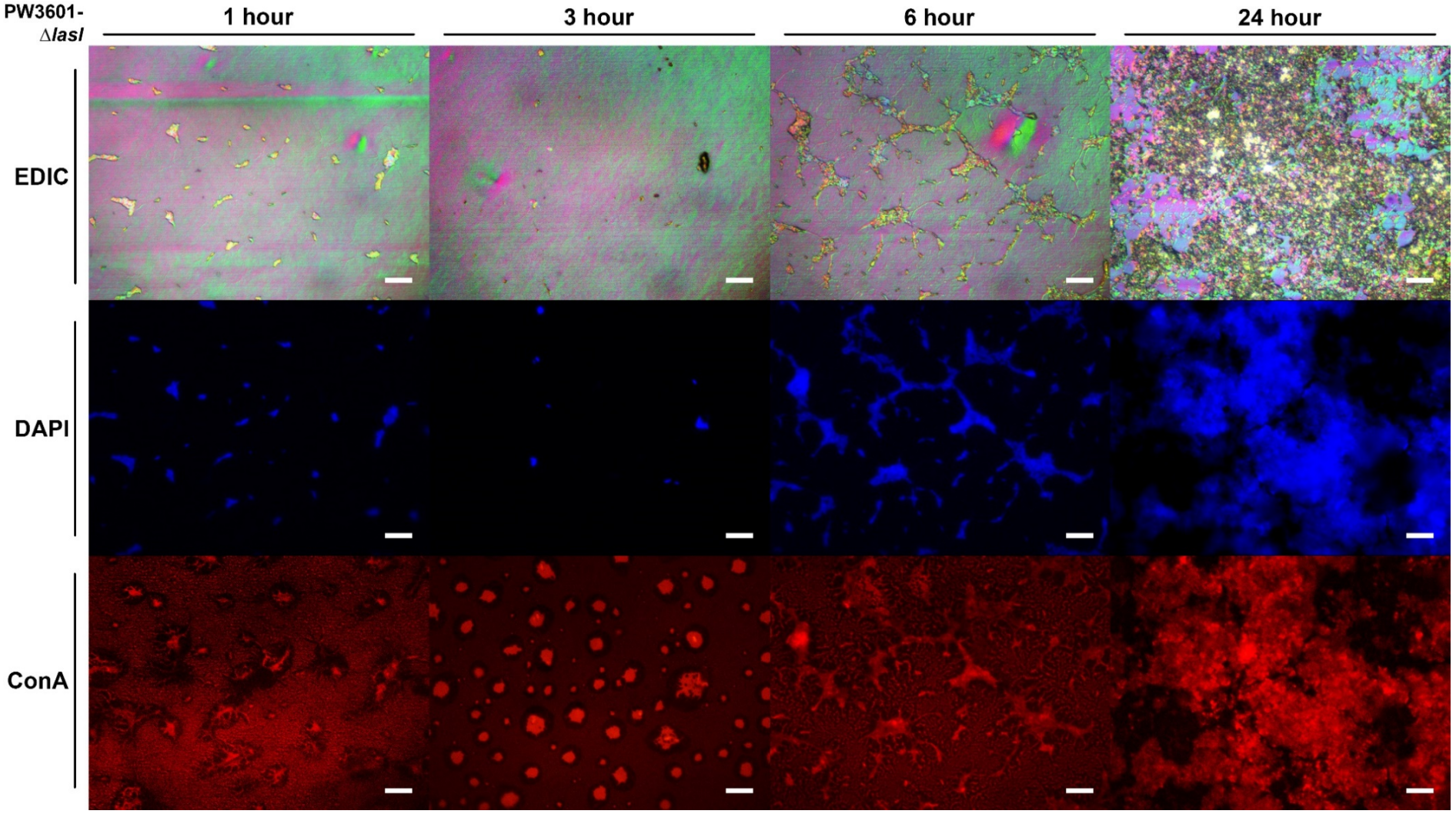

Figure H2 *P. aeruginosa* PAO1 mutant strain PW3601-Δ*lasI* biofilm morphology on urinary catheter grown in AUBK at 1 h, 3 h, 6 h and 24 h timepoint as observed under EDIC/EF microscope. Magnification x 1000. Scale bar = 10 µm.

H.3 Biofilm images of *P. aeruginosa* PAO1 mutant strain PW6886-Δ*rhlA* (*rhlA*-E08::IS*phoA*/hah)

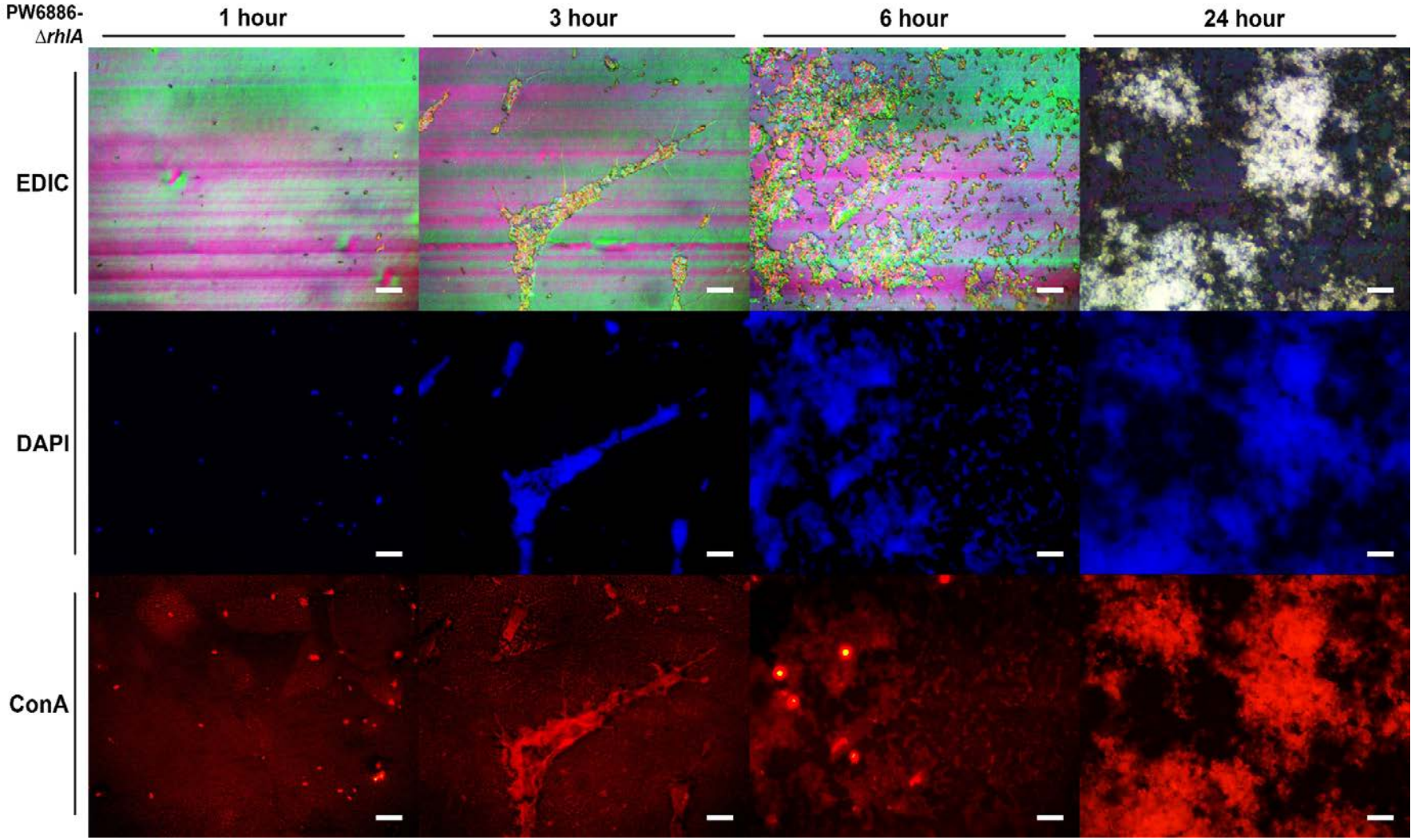

Figure H3 *P. aeruginosa* PAO1 mutant strain PW6886-Δ*rhlA* biofilm morphology on urinary catheter grown in AUBK at 1 h, 3 h, 6 h and 24 h timepoint as observed under EDIC/EF microscope. Magnification x 1000. Scale bar = 10 µm.

H.4 Biofilm images of *P. aeruginosa* PAO1 mutant strain PW6887-Δ*rhlA* (*rhlA*-A01::IS*phoA*/hah)

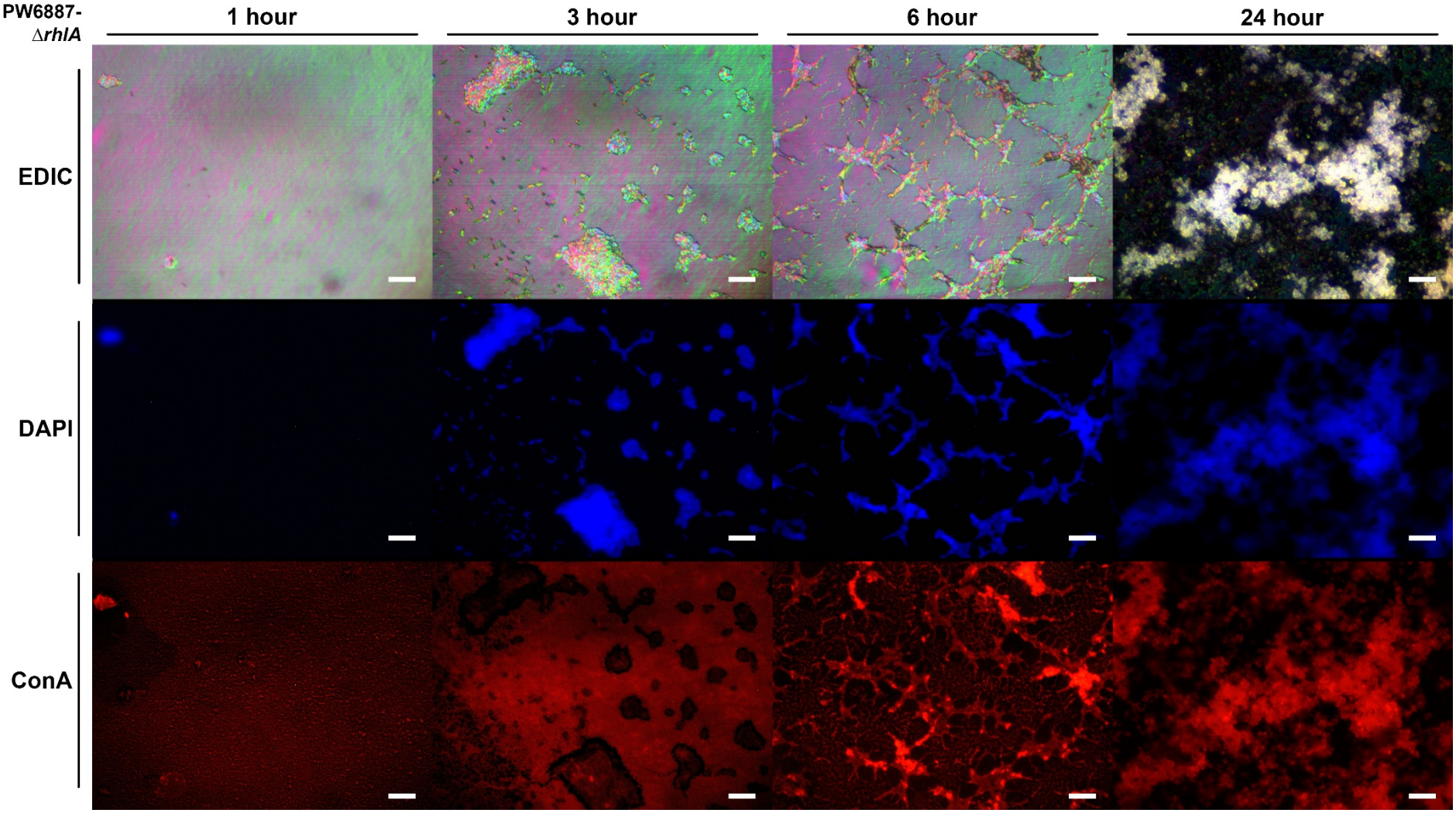

Figure H4 *P. aeruginosa* PAO1 mutant strain PW6887-Δ*rhlA* biofilm morphology on urinary catheter grown in AUBK at 1 h, 3 h, 6 h and 24 h timepoint as observed under EDIC/EF microscope. Magnification x 1000. Scale bar = 10 µm.

H.5 Biofilm images of *P. aeruginosa* PAO1 mutant strain PW6884-Δ*rhlB* (*rhlB*-G07::IS*lacZ*/hah)

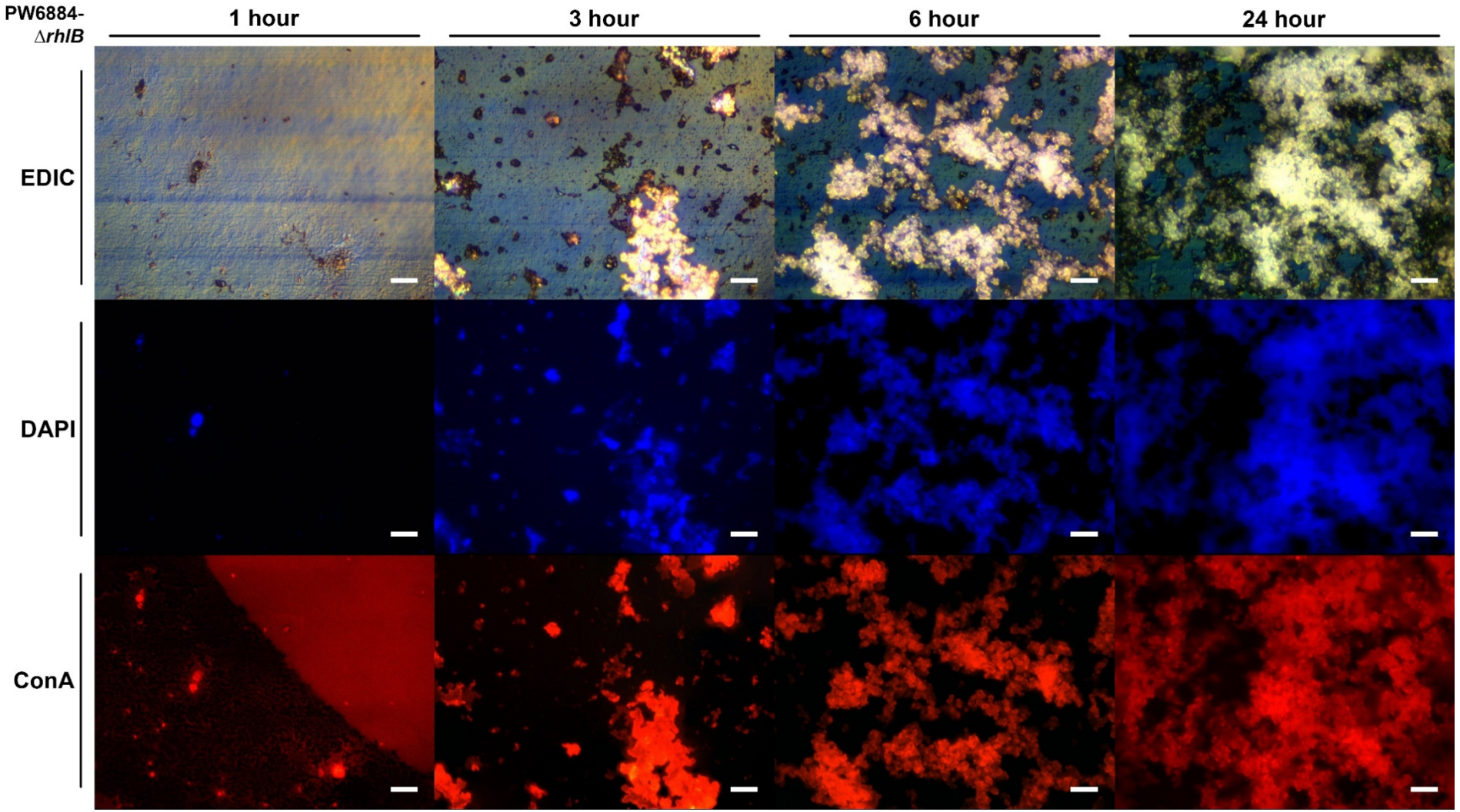

Figure H5 *P. aeruginosa* PAO1 mutant strain PW6884-Δ*rhlB* biofilm morphology on urinary catheter grown in AUBK at 1 h, 3 h, 6 h and 24 h timepoint as observed under EDIC/EF microscope. Magnification x 1000. Scale bar = 10 µm.

H.6 Biofilm images of *P. aeruginosa* PAO1 mutant strain PW6885-Δ*rhlB* (*rhlB*-F05::IS*phoA*/hah)

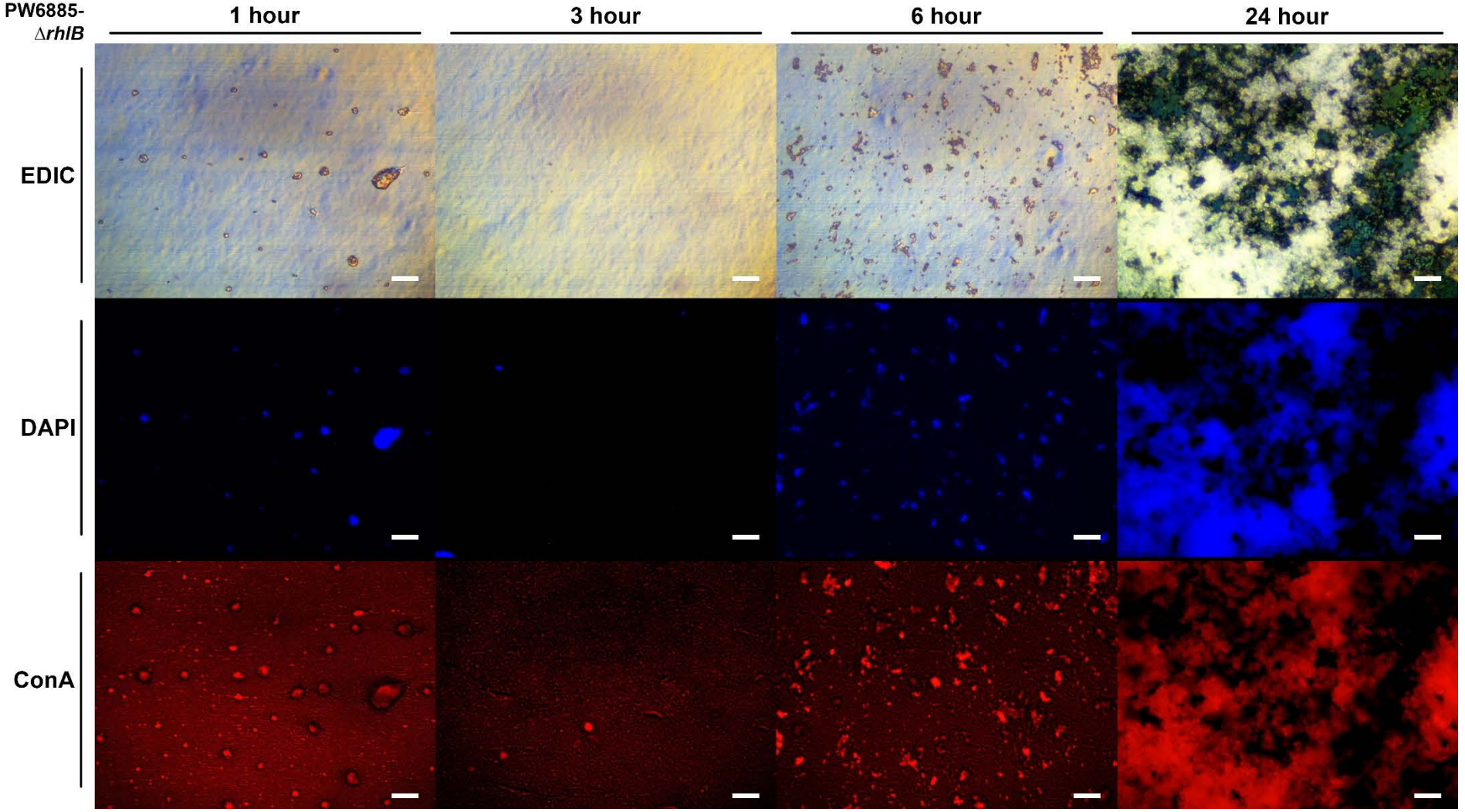

Figure H6 *P. aeruginosa* PAO1 mutant strain PW6885-Δ*rhlB* biofilm morphology on urinary catheter grown in AUBK at 1 h, 3 h, 6 h and 24 h timepoint as observed under EDIC/EF microscope. Magnification x 1000. Scale bar = 10 µm.

H.7 Biofilm images of *P. aeruginosa* PAO1 mutant strain PW6880-Δ*rhlI* (*rhlI*-D03::IS*phoA*/hah)

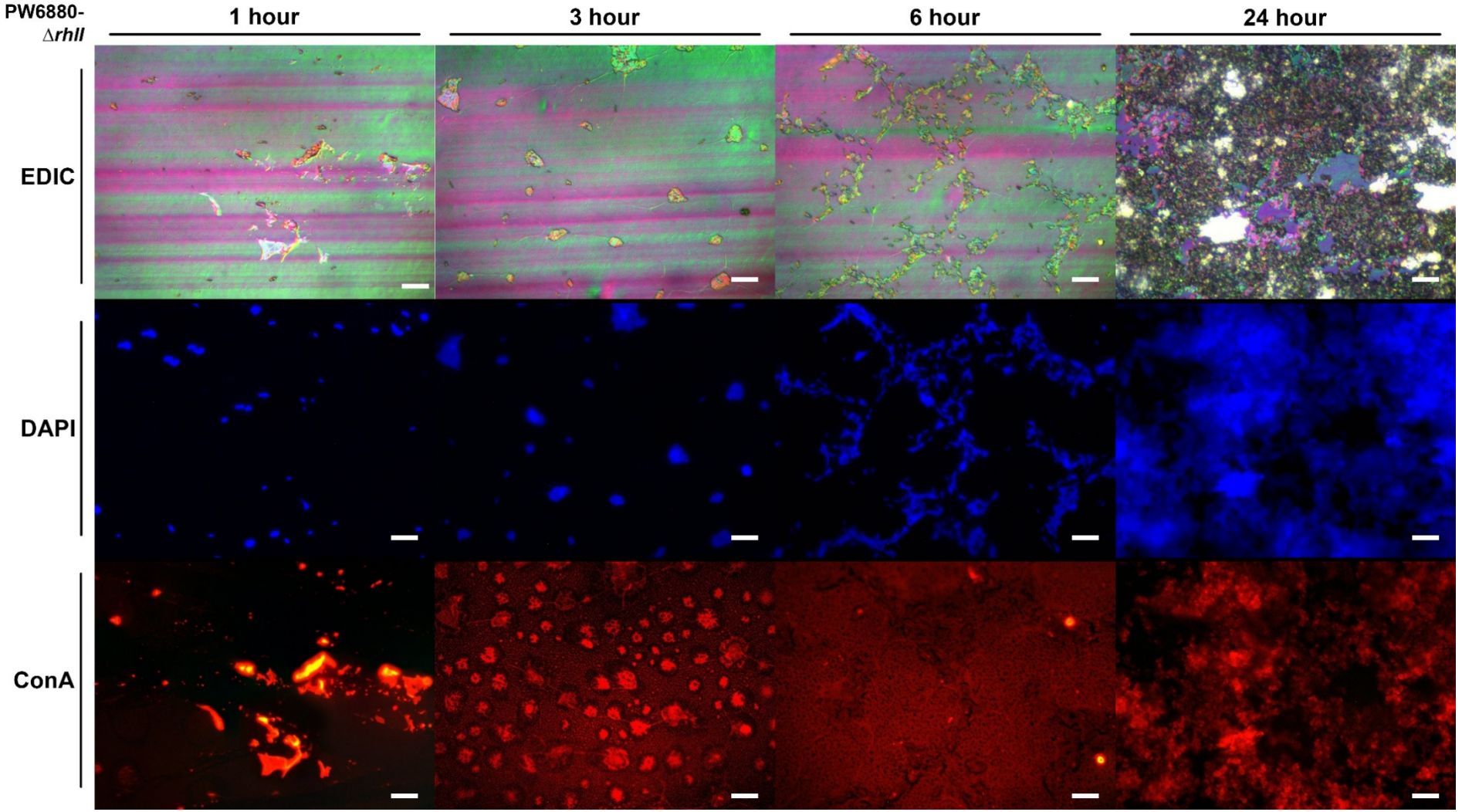

Figure H7 *P. aeruginosa* PAO1 mutant strain PW6880-Δ*rhlI* biofilm morphology on urinary catheter grown in AUBK at 1 h, 3 h, 6 h and 24 h timepoint as observed under EDIC/EF microscope. Magnification x 1000. Scale bar = 10 µm.

H.8 Biofilm images of *P. aeruginosa* PAO1 mutant strain PW6881-Δ*rhlI* (*rhlI*-F02::IS*phoA*/hah)

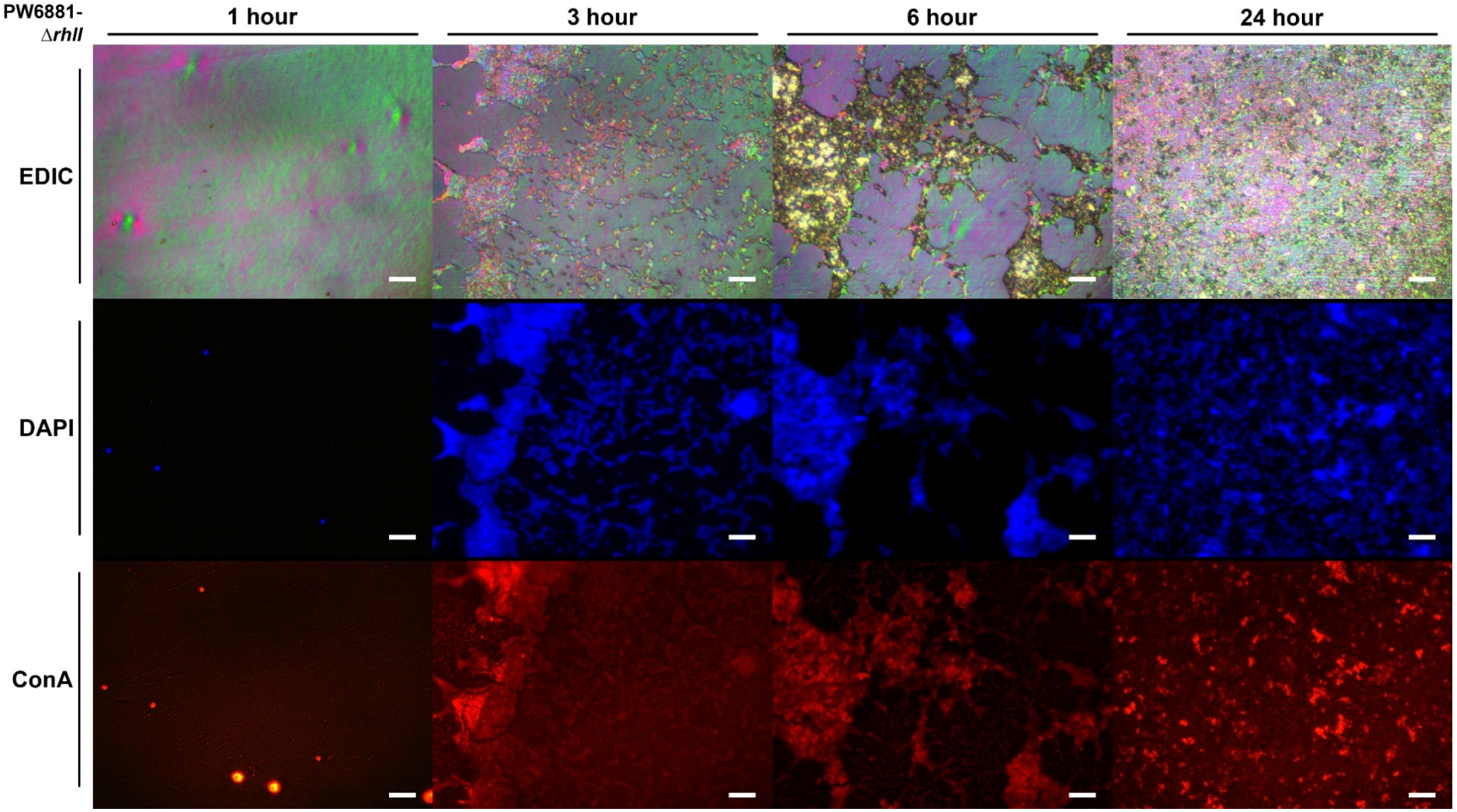

Figure H8 *P. aeruginosa* PAO1 mutant strain PW6881-Δ*rhlI* biofilm morphology on urinary catheter grown in AUBK at 1 h, 3 h, 6 h and 24 h timepoint as observed under EDIC/EF microscope. Magnification x 1000. Scale bar = 10 µm.

H.9 Biofilm images of *P. aeruginosa* PAO1 mutant strain PW2798-Δ*pqsA* (*pqsA*-H05::IS*lacZ*/hah)

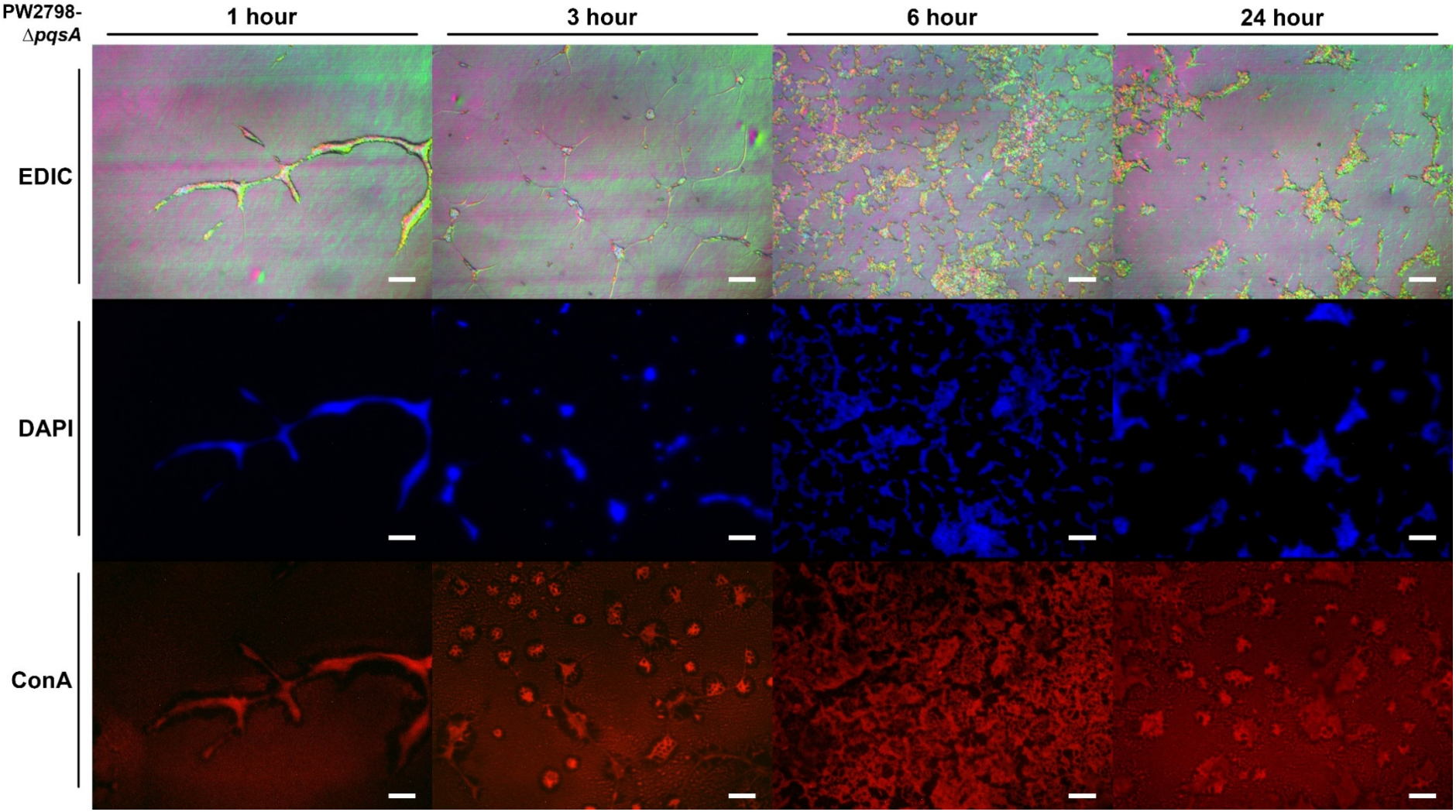

Figure H9 *P. aeruginosa* PAO1 mutant strain PW2798-Δ*pqsA* biofilm morphology on urinary catheter grown in AUBK at 1 h, 3 h, 6 h and 24 h timepoint as observed under EDIC/EF microscope. Magnification x 1000. Scale bar = 10 µm.

H.10 Biofilm images of *P. aeruginosa* PAO1 mutant strain PW2799-Δ*pqsA* (*pqsA*-H04::IS*lacZ*/hah)

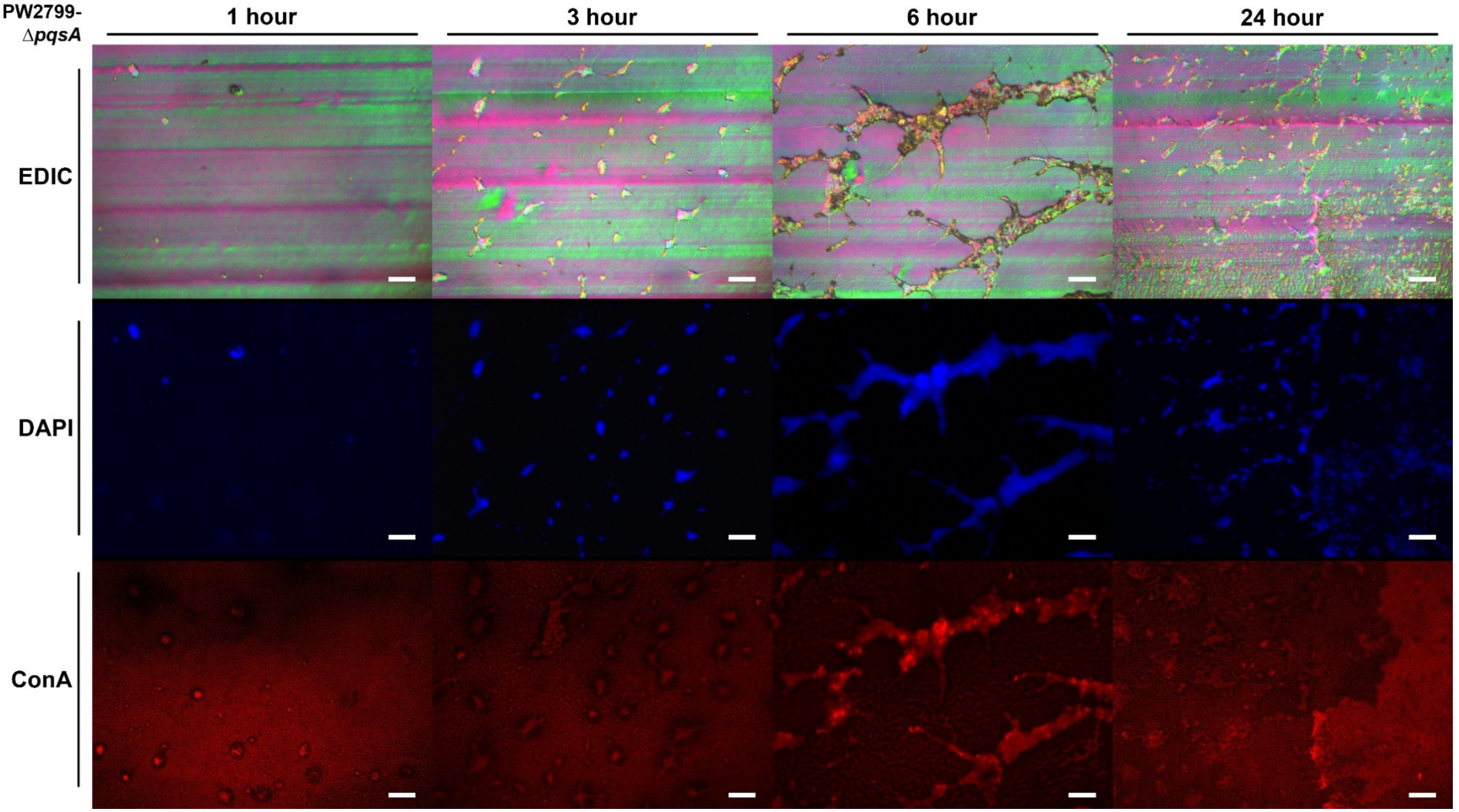

Figure H10 *P. aeruginosa* PAO1 mutant strain PW2799-Δ*pqsA* biofilm morphology on urinary catheter grown in AUBK at 1 h, 3 h, 6 h and 24 h timepoint as observed under EDIC/EF microscope. Magnification x 1000. Scale bar = 10 µm.

H.11 Biofilm images of *P. aeruginosa* PAO1 mutant strain PW2806-Δ*pqsE* (*pqsE*-G04::IS*lacZ*/hah)

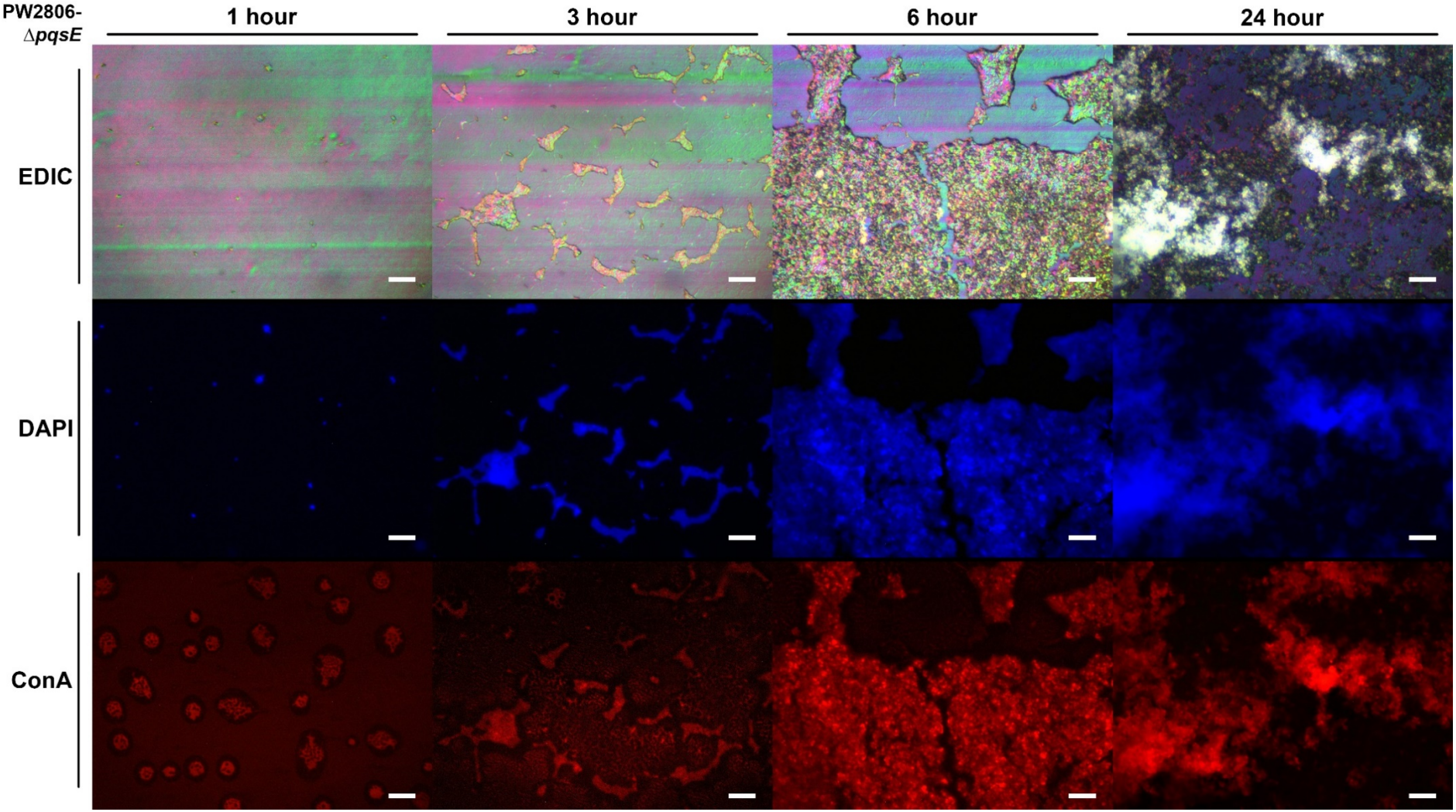

Figure H11 *P. aeruginosa* PAO1 mutant strain PW2806-Δ*pqsE* biofilm morphology on urinary catheter grown in AUBK at 1 h, 3 h, 6 h and 24 h timepoint as observed under EDIC/EF microscope. Magnification x 1000. Scale bar = 10 µm.

H.12 Biofilm images of *P. aeruginosa* PAO1 mutant strain PW2807-Δ*pqsE* (*pqsE*-G04::IS*lacZ*/hah)

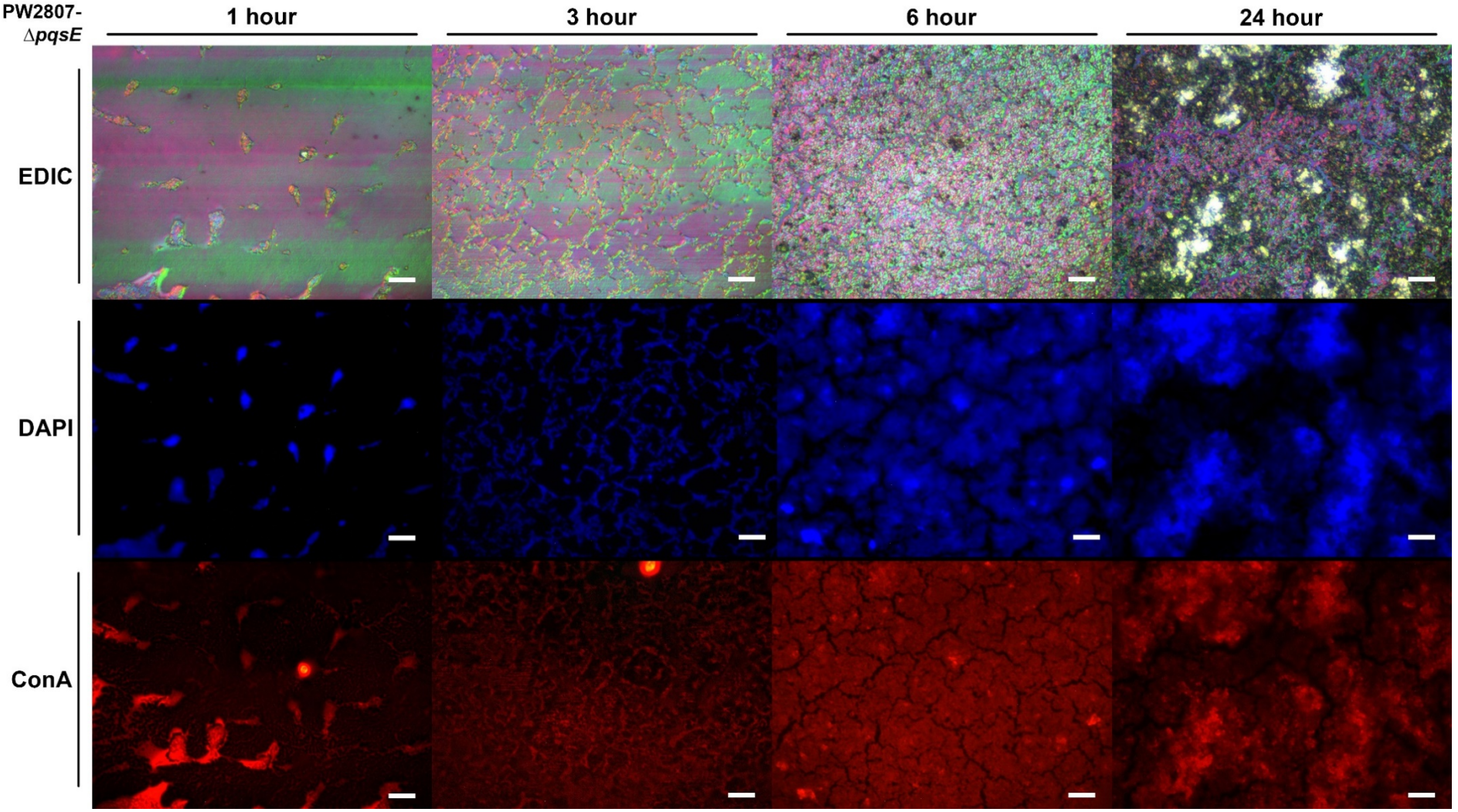

Figure H12 *P. aeruginosa* PAO1 mutant strain PW2807-Δ*pqsE* biofilm morphology on urinary catheter grown in AUBK at 1 h, 3 h, 6 h and 24 h timepoint as observed under EDIC/EF microscope. Magnification x 1000. Scale bar = 10 µm.

Appendix I Polysaccharide (PS)-negative *P. aeruginosa* PAO1 mutant group

I.1 Biofilm enumeration data analysis of PS-negative *P. aeruginosa* PAO1 mutant group

Table J-1 Brown–Forsythe one-way ANOVA analysis of *P. aeruginosa* PAO1 wildtype and PS-negative mutant strains between timepoints.

		One-way ANOVA ($P < 0.05$)							Brown-Forsythe test ($P < 0.05$)		
Time	**ANOVA table**	**SS**	**DF**	**MS**	**F(DFn_9, DFd_{20})**	**P value**	**P summary**	**R^2**	**F(DFn_9, DFd_{20})**	**P value**	**P summary**
1 h	Treatment (between columns)	15.92	9	1.769	30.84	P<0.0001	Yes	0.9328	0.5629	0.8110	No
	Residual (within columns)	1.148	20	0.05738							
	Total	17.07	29								
3 h	Treatment (between columns)	4.953	9	0.5503	13.32	P<0.0001	Yes	0.857	1.08	0.4181	No
	Residual (within columns)	0.8265	20	0.04133							
	Total	5.779	29								
6 h	Treatment (between columns)	5.821	9	0.6468	10.05	P<0.0001	Yes	0.8189	0.3802	0.9310	No
	Residual (within columns)	1.287	20	0.06436							
	Total	7.108	29								
6 h	Treatment (between columns)	2.086	9	0.2317	3.177	P=0.0150	Yes	0.5884	0.7103	0.6934	No
	Residual (within columns)	1.459	20	0.07294							
	Total	3.544	29								

For all significant results shown, $P < 0.05$ (*, $P < 0.05$; **, $P < 0.01$; ***, $P < 0.001$, ****, $P < 0.0001$, and *ns*, not significant).

I.2 Biofilm images of *P. aeruginosa* PAO1 mutant strain PW6140-Δ*pelA* (*pelA*-H06::IS*phoA*/hah)

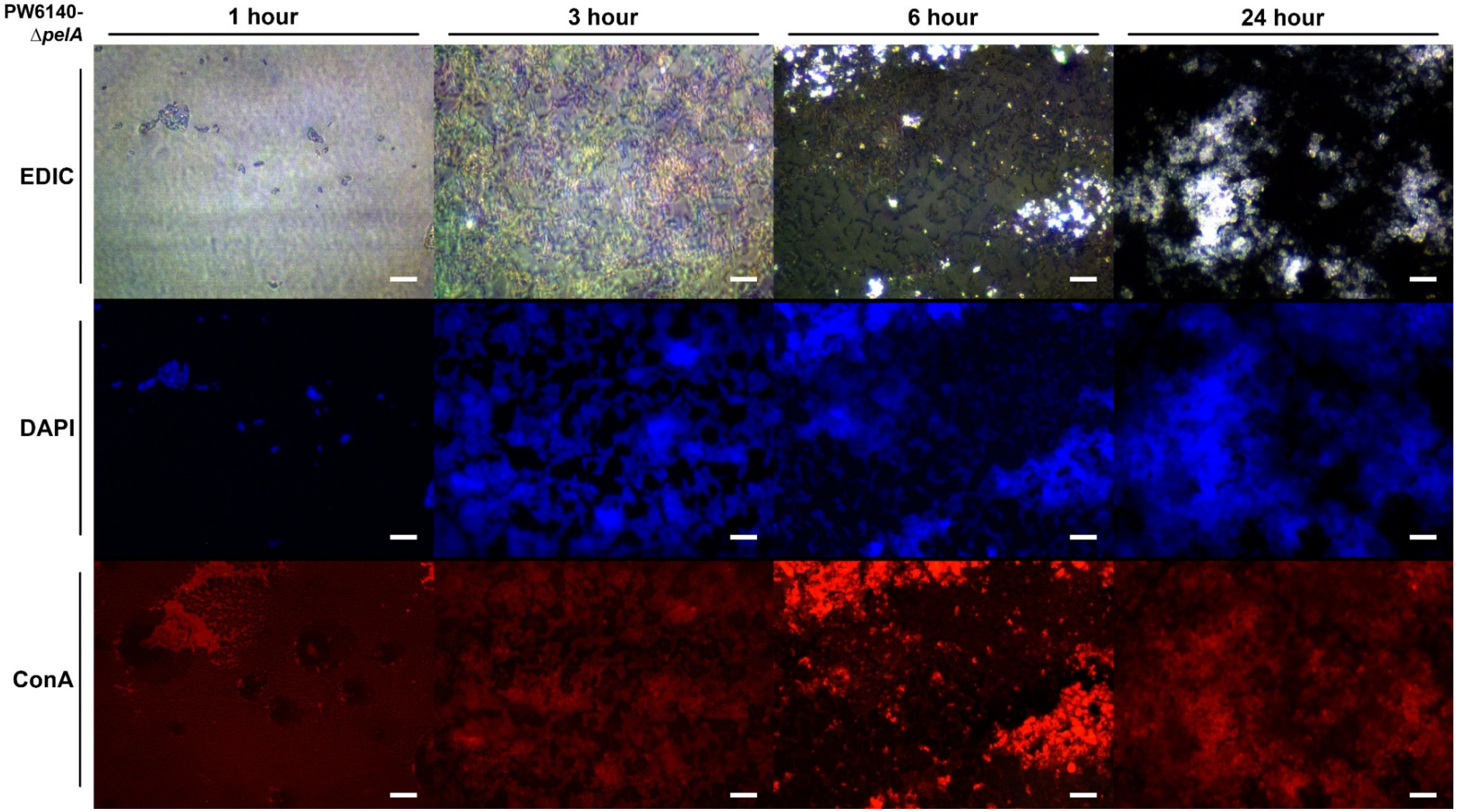

Figure I2 *P. aeruginosa* PAO1 mutant strain PW6140-Δ*pelA* biofilm morphology on urinary catheter grown in AUBK at 1 h, 3 h, 6 h and 24 h timepoint as observed under EDIC/EF microscope. Magnification x 1000. Scale bar = 10 µm.

I.3 Biofilm images of *P. aeruginosa* PAO1 mutant strain PW6141-Δ*pelA* (*pelA*-F09::IS*phoA*/hah)

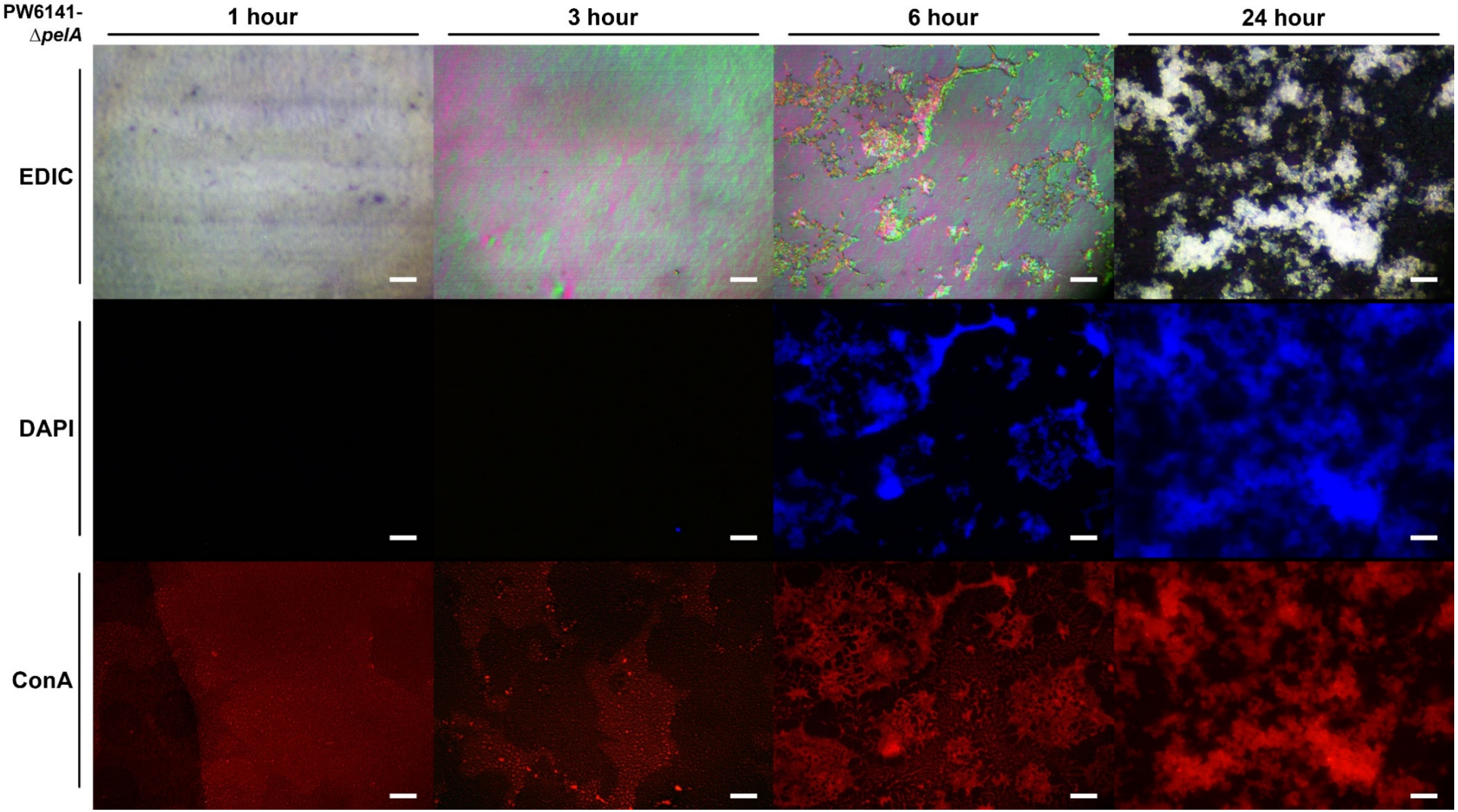

Figure I3 *P. aeruginosa* PAO1 mutant strain PW6141-Δ*pelA* biofilm morphology on urinary catheter grown in AUBK at 1 h, 3 h, 6 h and 24 h timepoint as observed under EDIC/EF microscope. Magnification x 1000. Scale bar = 10 µm.

I.4 Biofilm images of *P. aeruginosa* PAO1 mutant strain PW4802-Δ*pslD* (*pslD*-H08::IS*lacZ*/hah)

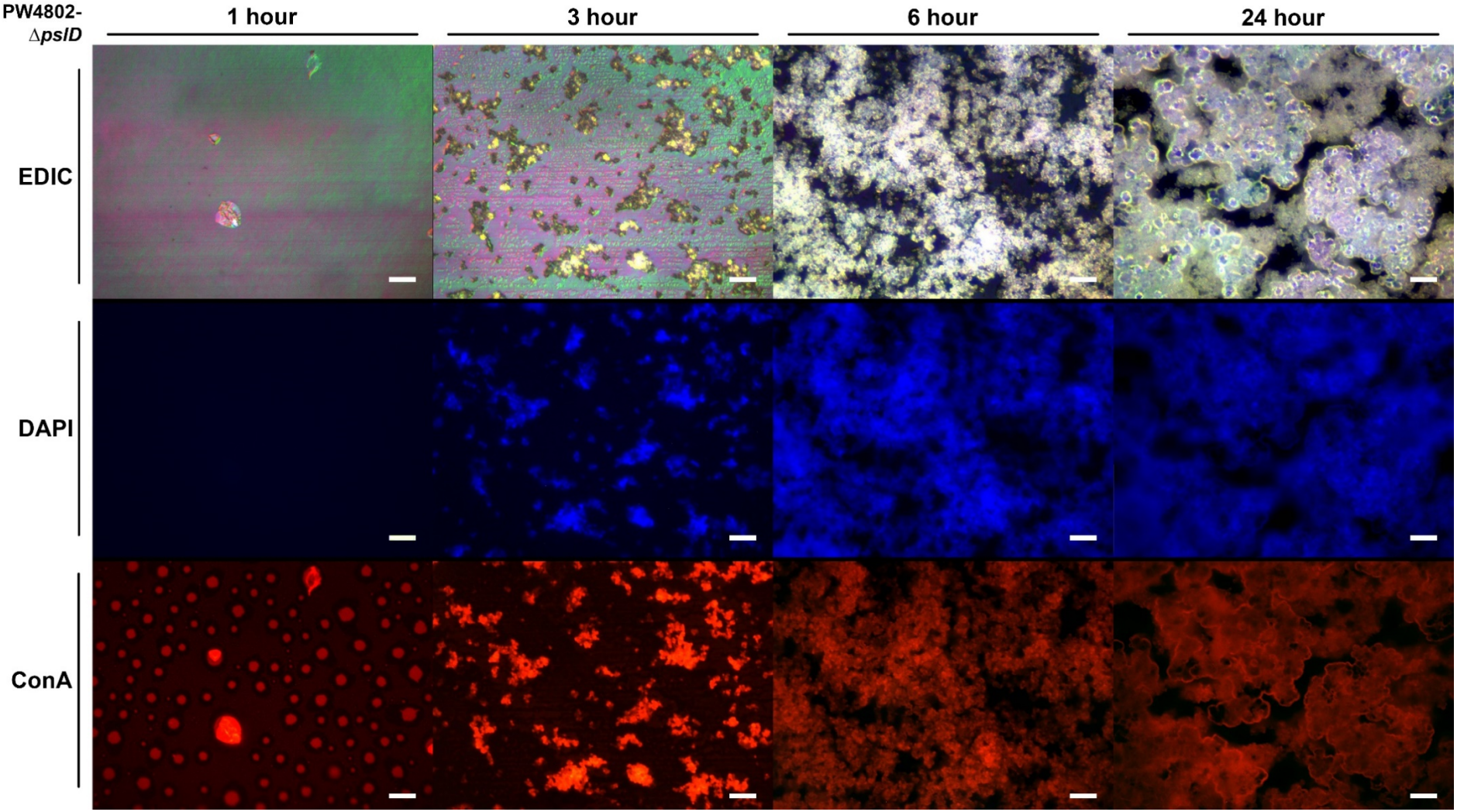

Figure I4 *P. aeruginosa* PAO1 mutant strain PW4802-Δ*pslD* biofilm morphology on urinary catheter grown in AUBK at 1 h, 3 h, 6 h and 24 h timepoint as observed under EDIC/EF microscope. Magnification x 1000. Scale bar = 10 µm

I.5 Biofilm images of *P. aeruginosa* PAO1 mutant strain PW4803-Δ*pslD* (*pslD*-H09::IS*lacZ*/hah)

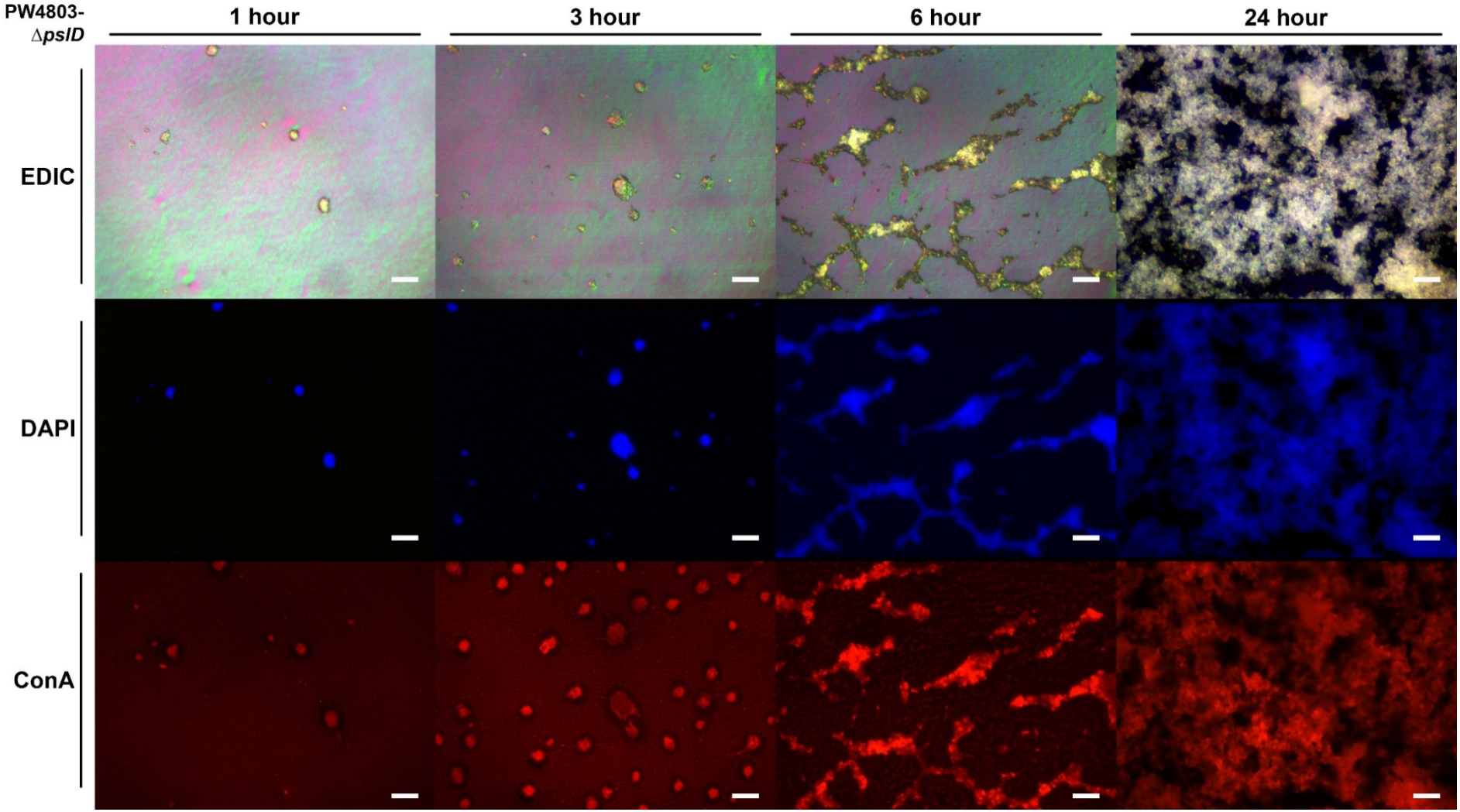

Figure I5 *P. aeruginosa* PAO1 mutant strain PW4803-Δ*pslD* biofilm morphology on urinary catheter grown in AUBK at 1 h, 3 h, 6 h and 24 h timepoint as observed under EDIC/EF microscope. Magnification x 1000. Scale bar = 10 µm

I.6 Biofilm images of *P. aeruginosa* PAO1 mutant strain PW4807-Δ*pslG* (*pslG*-D07::IS*lacZ*/hah)

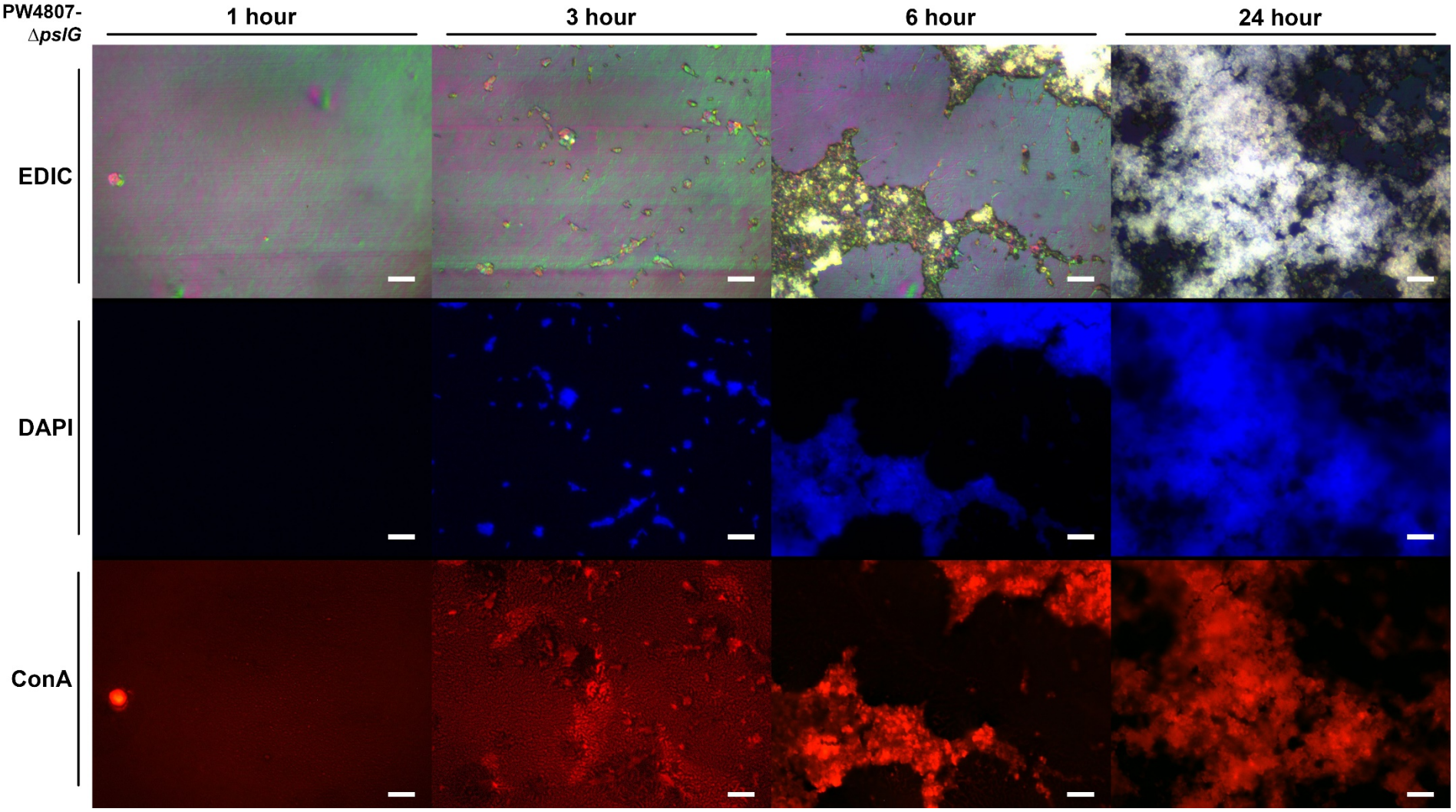

Figure I6 *P. aeruginosa* PAO1 mutant strain PW4807-Δ*pslG* biofilm morphology on urinary catheter grown in AUBK at 1 h, 3 h, 6 h and 24 h timepoint as observed under EDIC/EF microscope. Magnification x 1000. Scale bar = 10 µm.

I.7 Biofilm images of *P. aeruginosa* PAO1 mutant strain PW4808-Δ*pslG* (*pslG*-G09::IS*lacZ*/hah)

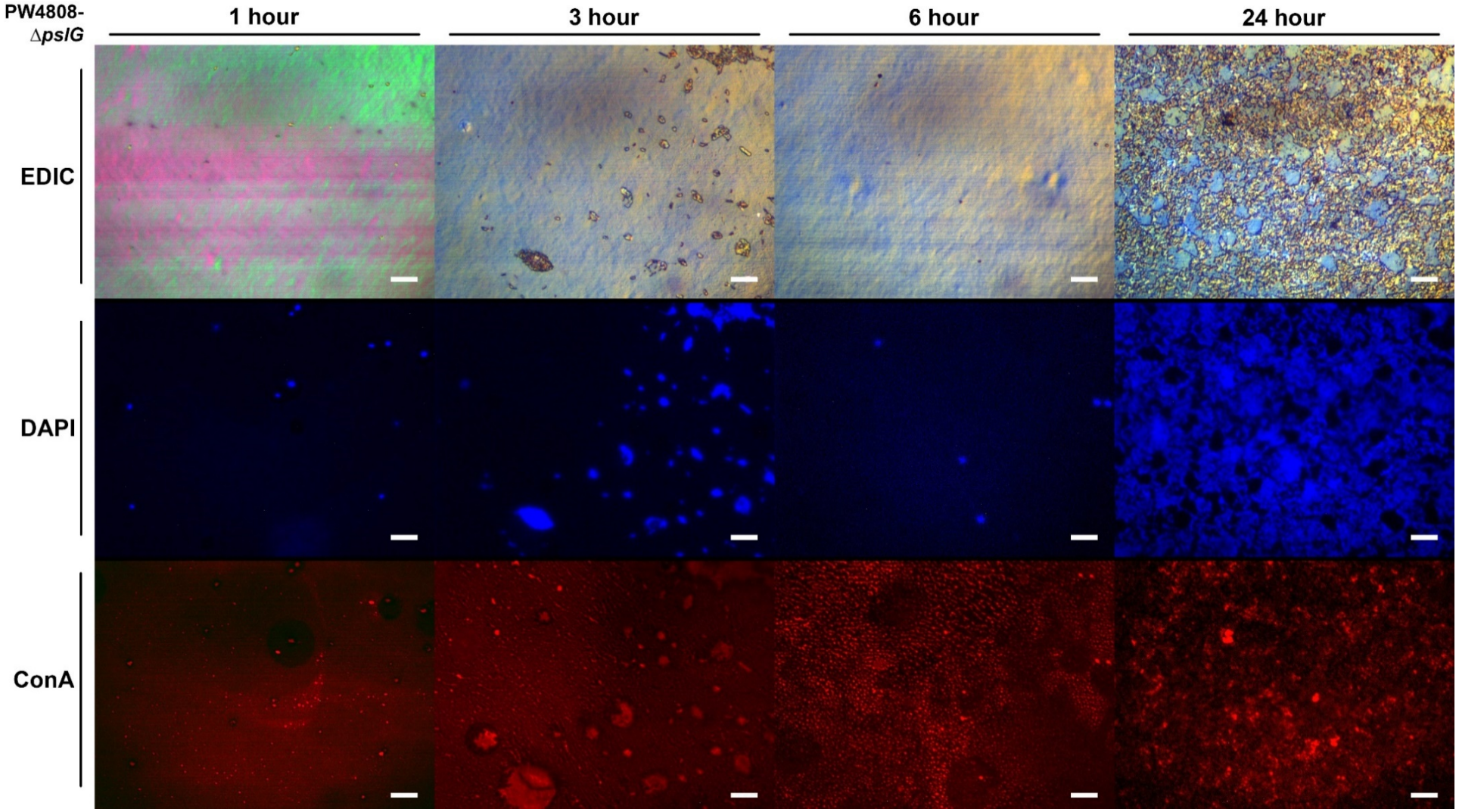

Figure J7 *P. aeruginosa* PAO1 mutant strain PW4808-Δ*pslG* biofilm morphology on urinary catheter grown in AUBK at 1 h, 3 h, 6 h and 24 h timepoint as observed under EDIC/EF microscope. Magnification x 1000. Scale bar = 10 µm.

I.8 Biofilm images of *P. aeruginosa* PAO1 mutant strain PW2387-Δ*mucA* (*mucA*-A05::IS*phoA*/hah)

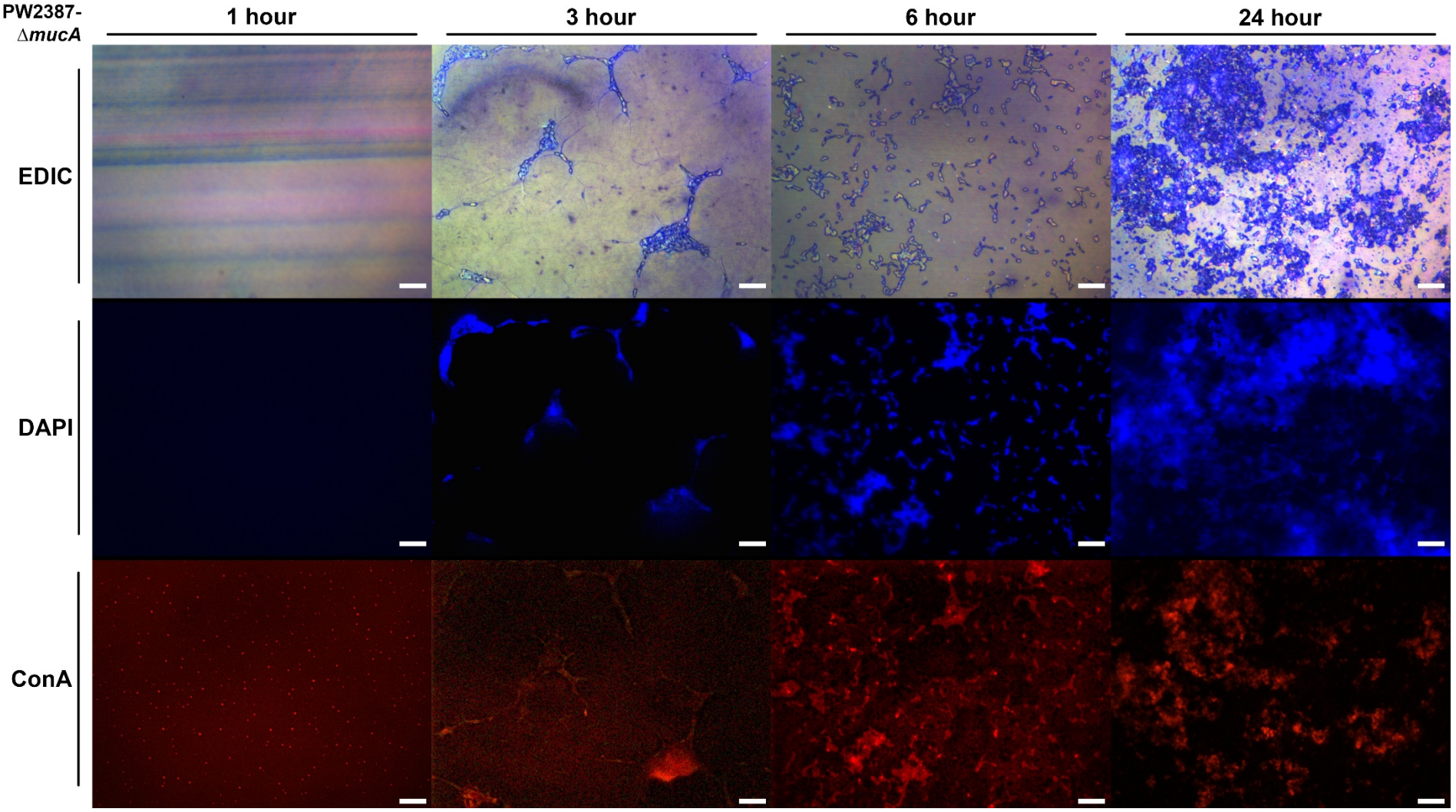

Figure I8 *P. aeruginosa* PAO1 mutant strain PW2387-Δ*mucA* biofilm morphology on urinary catheter grown in AUBK at 1 h, 3 h, 6 h and 24 h timepoint as observed under EDIC/EF microscope. Magnification x 1000. Scale bar = 10 µm.

I.9 Biofilm images of *P. aeruginosa* PAO1 mutant strain PW6997-Δ*algD* (*algD*-C03:IS*phoA*/hah)

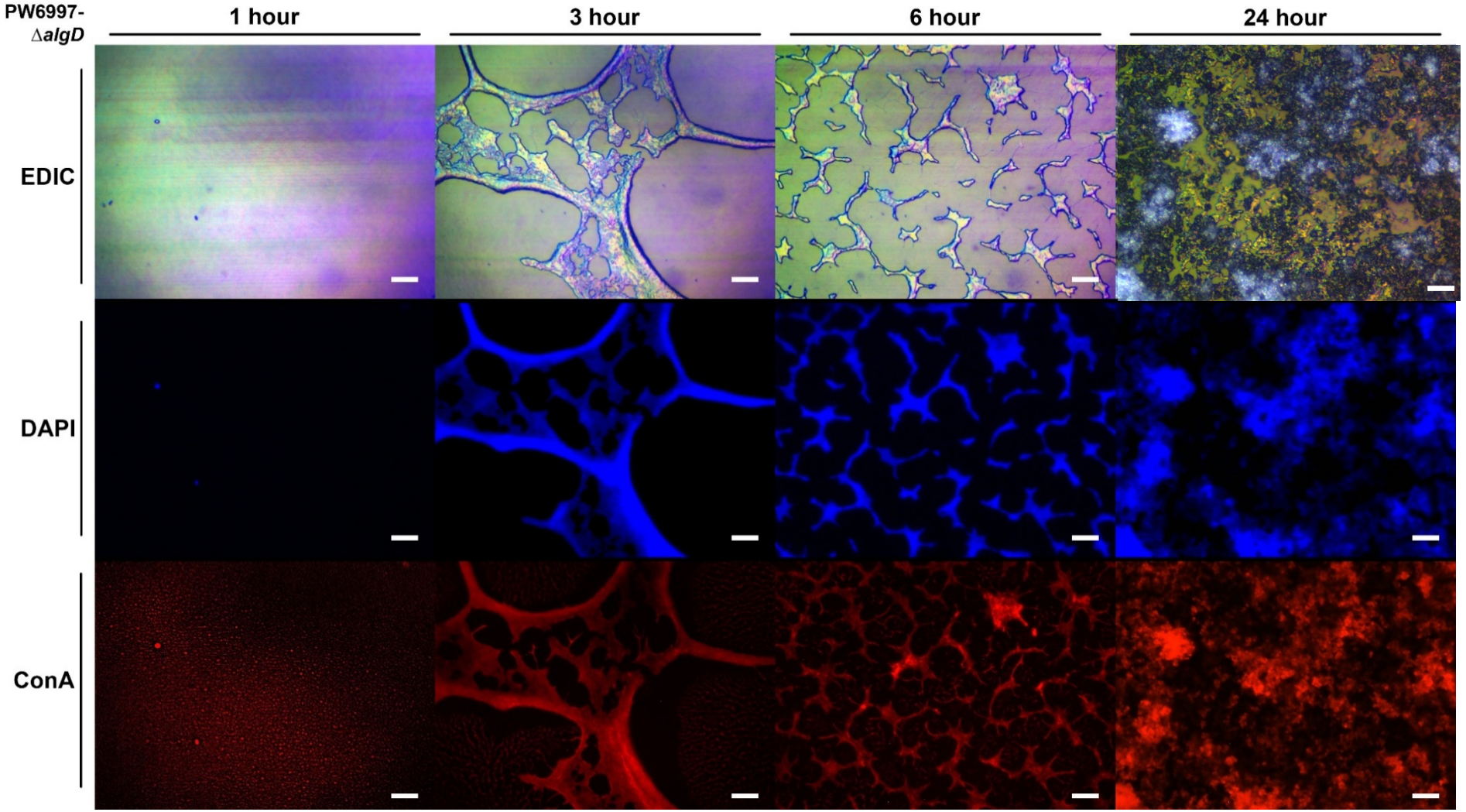

Figure J9 *P. aeruginosa* PAO1 mutant strain PW6997-Δ*algD* biofilm morphology on urinary catheter grown in AUBK at 1 h, 3 h, 6 h and 24 h timepoint as observed under EDIC/EF microscope. Magnification x 1000. Scale bar = 10 µm.

I.10 Biofilm images of *P. aeruginosa* PAO1 mutant strain PW6998-Δ*algD* (*algD*-H06:IS*phoA*/hah)

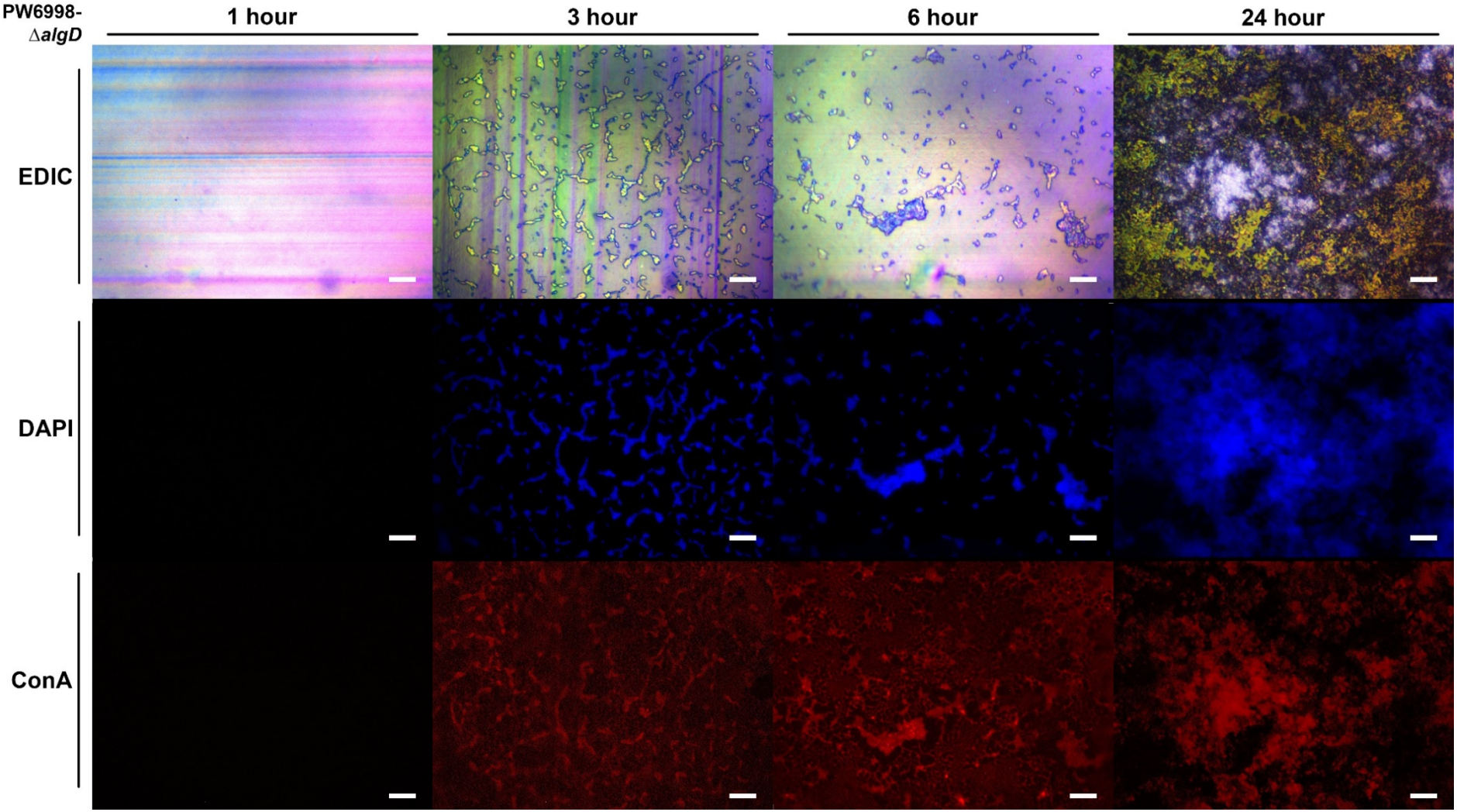

Figure J10 *P. aeruginosa* PAO1 mutant strain PW6998-Δ*algD* biofilm morphology on urinary catheter grown in AUBK at 1 h, 3 h, 6 h and 24 h timepoint as observed under EDIC/EF microscope. Magnification x 1000. Scale bar = 10 µm.

Appendix J Attachment/Motility (AM)-negative *P. aeruginosa* PAO1 mutant group

J.1 Biofilm growth of attachment/motility (AM)-negative *P. aeruginosa* PAO1 mutant group

Table K-1 Brown–Forsythe one-way ANOVA analysis of *P. aeruginosa* PAO1 appendages-related mutant strains and wildtype

		One-way ANOVA ($P < 0.05$)							Brown-Forsythe test ($P < 0.05$)		
Time	**ANOVA table**	**SS**	**DF**	**MS**	**F(DFn_{14}, DFd_{29})**	**P value**	**P summary**	**R^2**	**F(DFn_{14}, DFd_{29})**	**P value**	**P summary**
1 h	Treatment (between columns)	21.03	14	1.502	18.52	P<0.0001	Yes	0.8994	0.6483	0.8025	No
	Residual (within columns)	2.352	29	0.08109							
	Total	23.38	43								
3 h	Treatment (between columns)	23.9	14	1.707	42.44	P<0.0001	Yes	0.9535	1.094	0.4025	No
	Residual (within columns)	1.166	29	0.04022							
	Total	25.06	43								
6 h	Treatment (between columns)	9.467	14	0.6762	14.01	P<0.0001	Yes	0.8712	0.4241	0.9536	No
	Residual (within columns)	1.4	29	0.04826							
	Total	10.87	43								
6 h	Treatment (between columns)	6.446	14	0.4604	13.05	P<0.0001	Yes	0.7201	1.668	0.0824	No
	Residual (within columns)	2.506	29	0.03529							
	Total	8.951	43								

For all significant results shown, $P < 0.05$ (*, $P < 0.05$; **, $P < 0.01$; ***, $P < 0.001$, ****, $P < 0.0001$, and *ns*, not significant).

J.2 Biofilm images of *P. aeruginosa* PAO1 mutant strain PW3643-Δ*fliA* (*fliA*-E07::IS*lacZ*/hah)

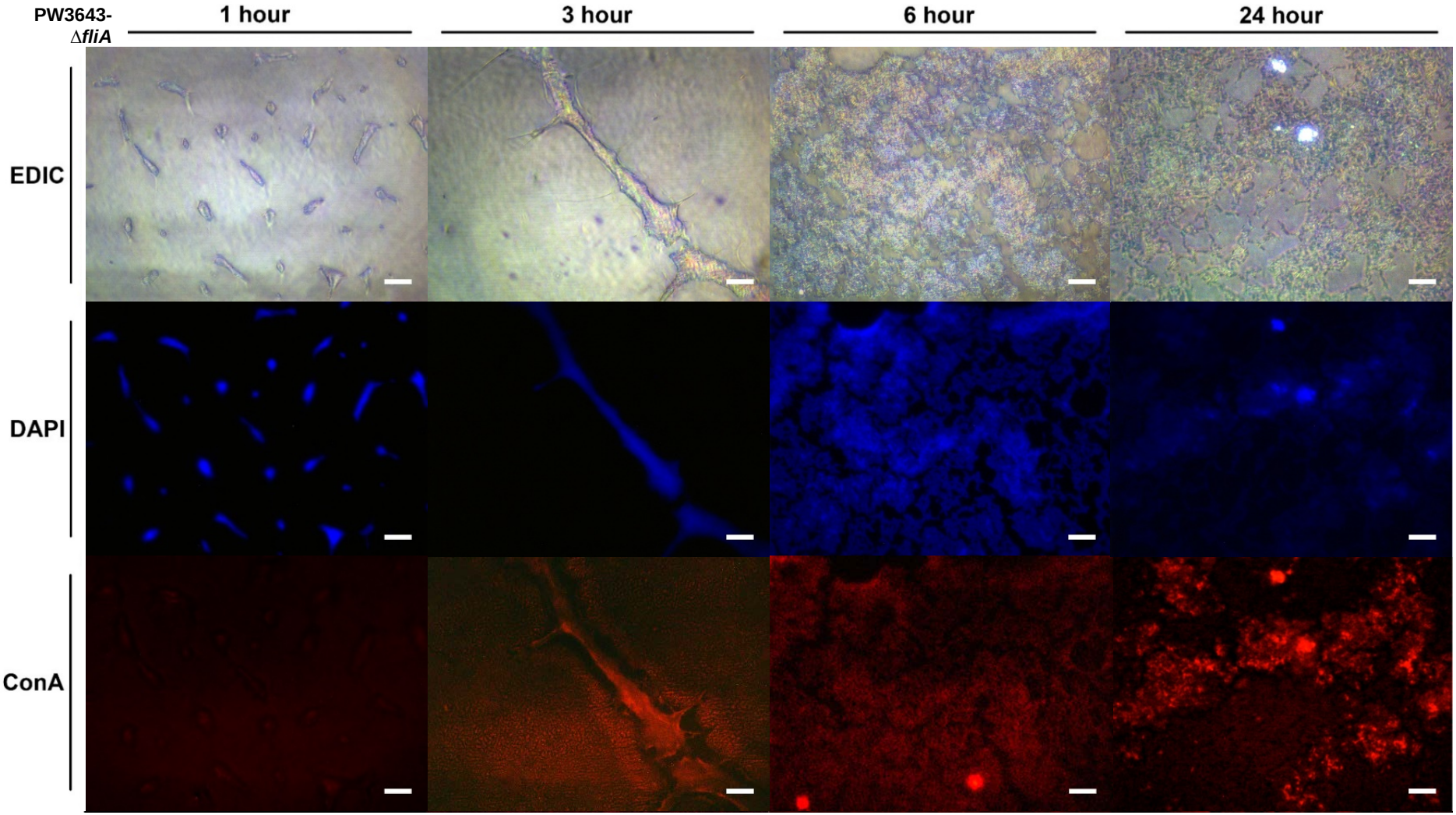

Figure K2 *P. aeruginosa* PAO1 mutant strain PW3643-Δ*fliA* biofilm morphology on urinary catheter grown in AUBK at 1 h, 3 h, 6 h and 24 h timepoint as observed under EDIC/EF microscope. Magnification x 1000. Scale bar = 10 µm.

J.3 Biofilm images of *P. aeruginosa* PAO1 mutant strain PW2970-Δ*fliC* (*fliC*-G03::IS*lacZ*/hah)

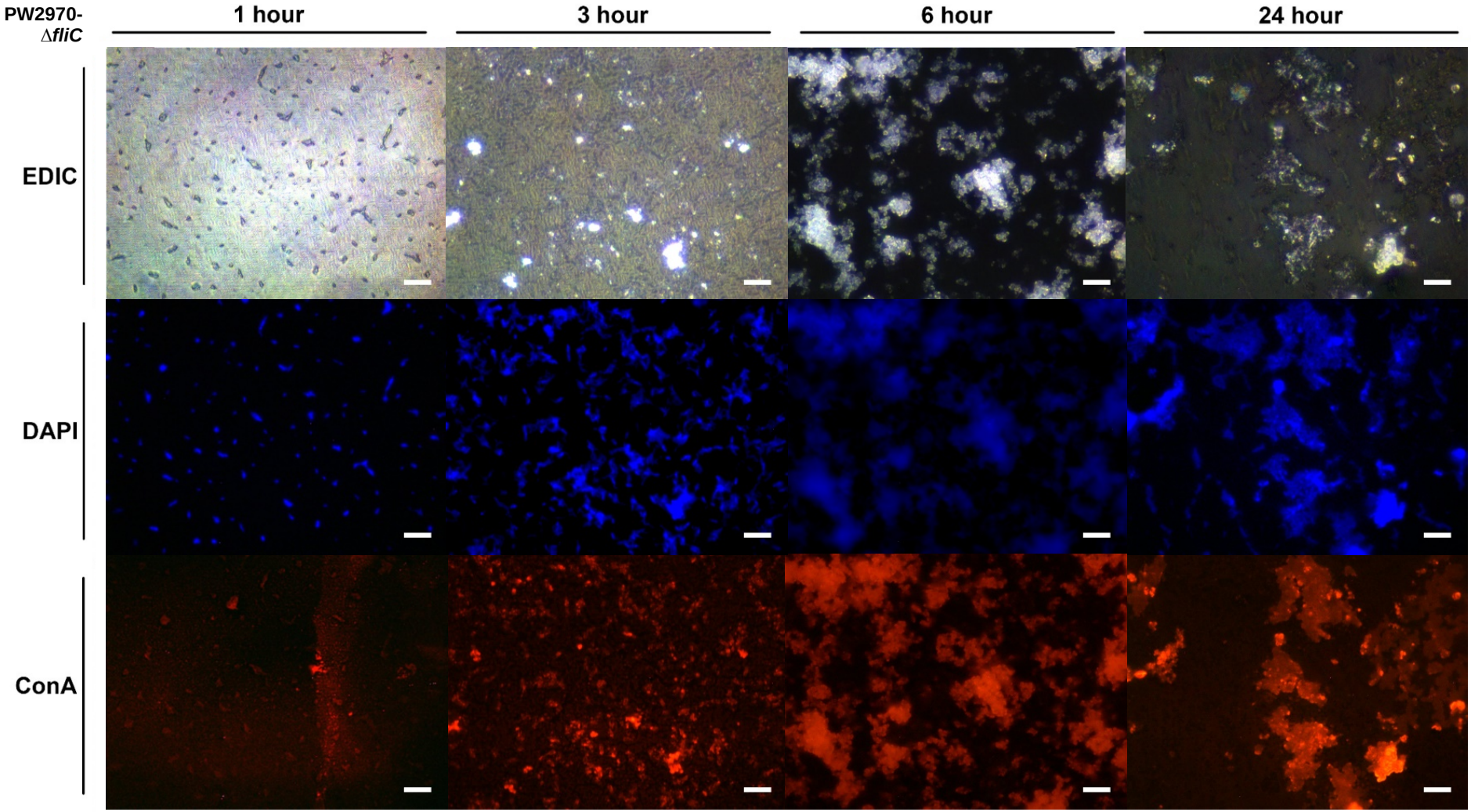

Figure K3 *P. aeruginosa* PAO1 mutant strain PW2970-Δ*fliC* biofilm morphology on urinary catheter grown in AUBK at 1 h, 3 h, 6 h and 24 h timepoint as observed under EDIC/EF microscope. Magnification x 1000. Scale bar = 10 µm.

J.4 Biofilm images of *P. aeruginosa* PAO1 mutant strain PW2971-Δ*fliC* (*fliC*-G10::IS*phoA*/hah)

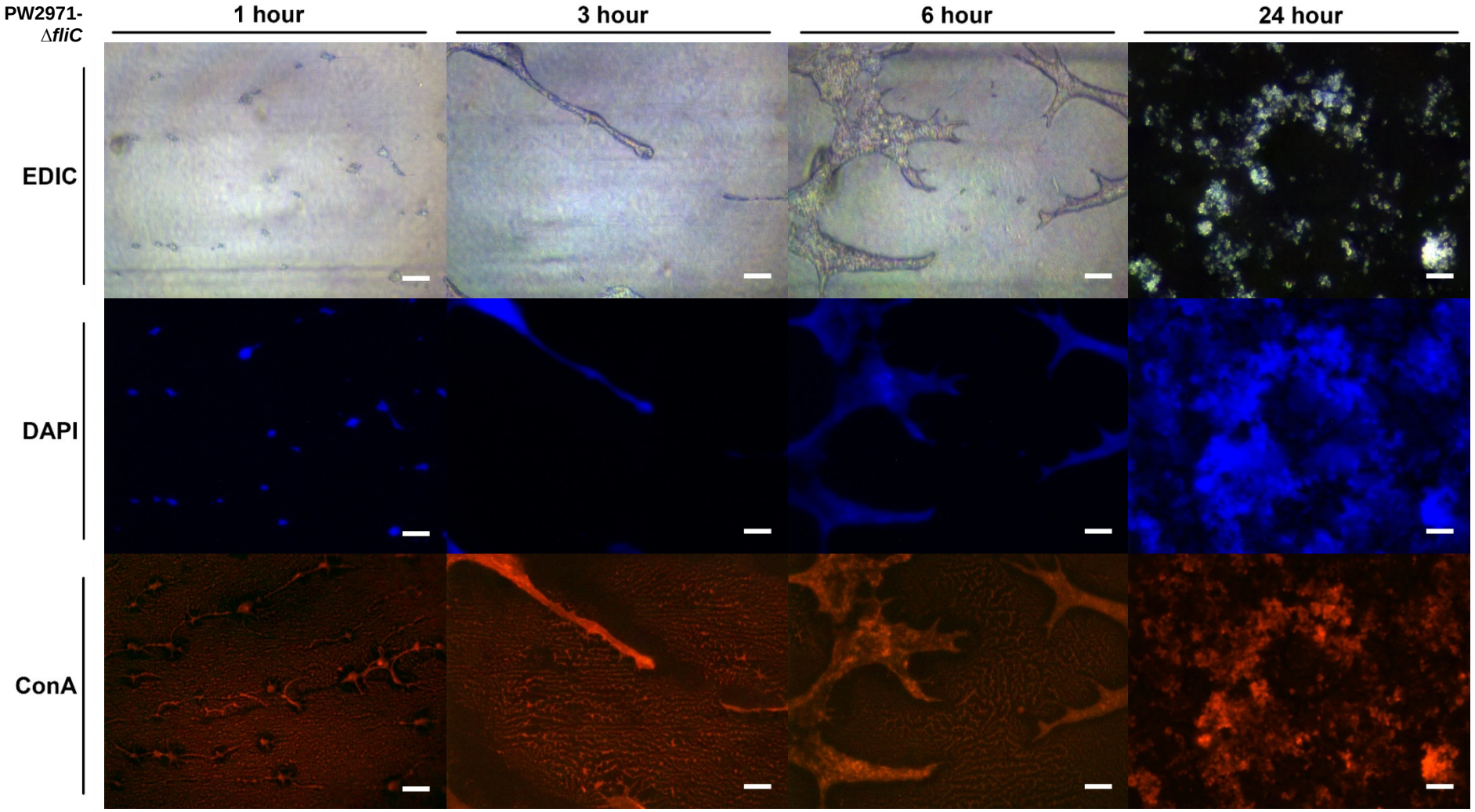

Figure J4 *P. aeruginosa* PAO1 mutant strain PW2971-Δ*fliC* biofilm morphology on urinary catheter grown in AUBK at 1 h, 3 h, 6 h and 24 h timepoint as observed under EDIC/EF microscope. Magnification x 1000. Scale bar = 10 µm.

J.5 Biofilm images of *P. aeruginosa* PAO1 mutant strain PW3621-Δ*fliM* (*fliM*-B05::IS*lacZ*/hah)

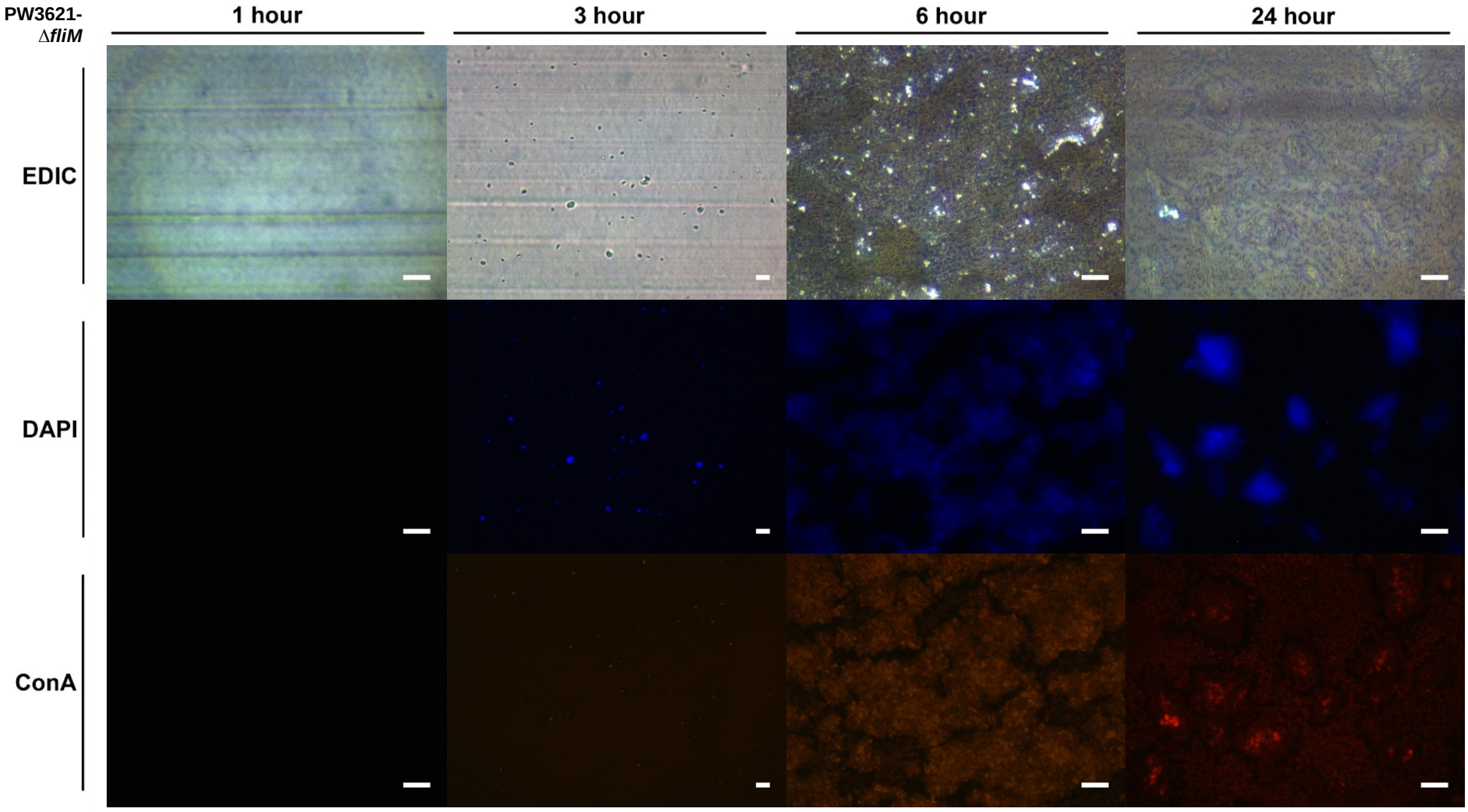

Figure K5 *P. aeruginosa* PAO1 mutant strain PW3621-Δ*fliM* biofilm morphology on urinary catheter grown in AUBK at 1 h, 3 h, 6 h and 24 h timepoint as observed under EDIC/EF microscope. Magnification x 1000 for 1 h, 6 h and 24 h. Magnification x 500 for 3 h. Scale bar = 10 µm.

J.6 Biofilm images of *P. aeruginosa* PAO1 mutant strain PW3622-Δ*fliM* (Δ*fliM*-D08::IS*phoA*/hah)

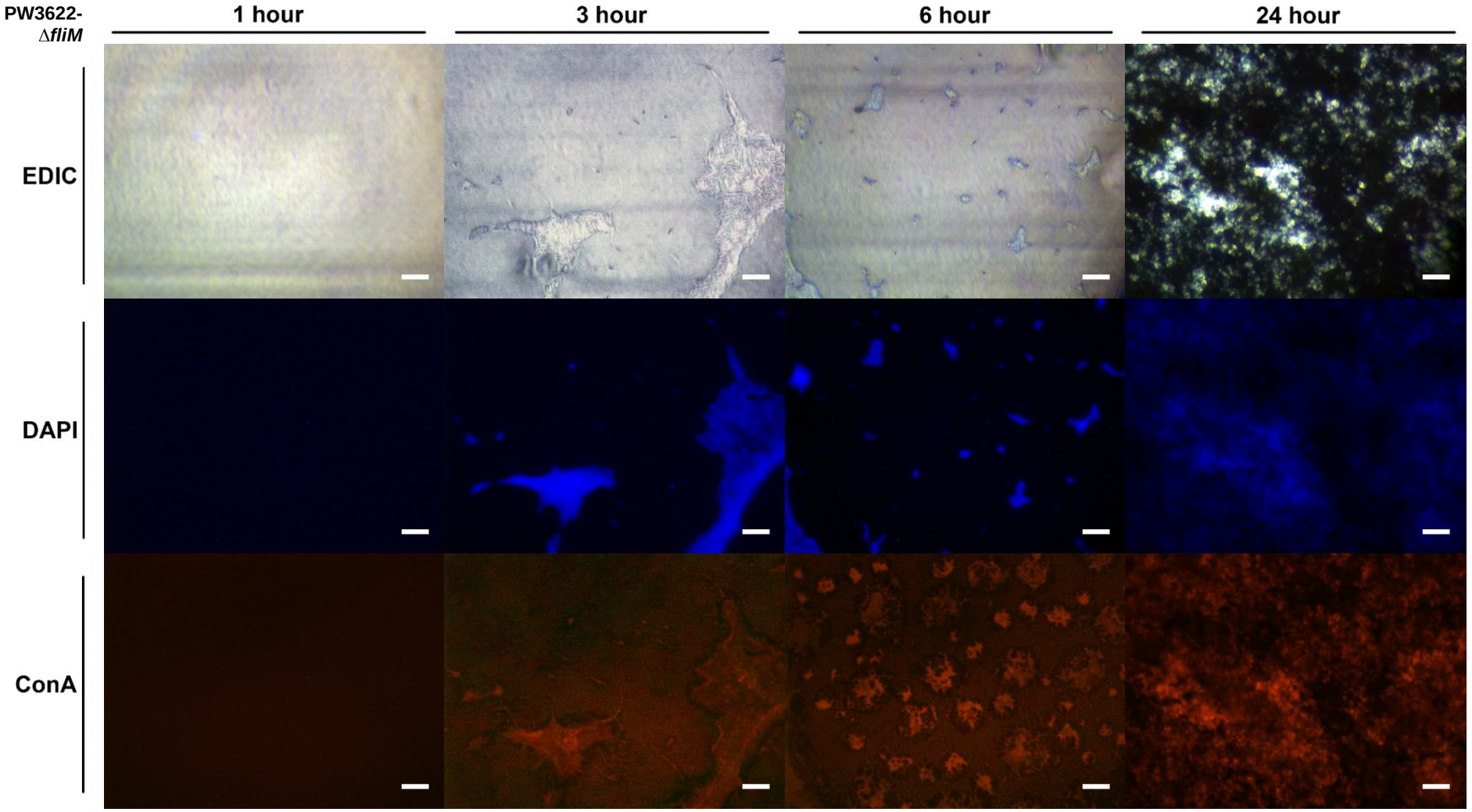

Figure K6 *P. aeruginosa* PAO1 mutant strain PW3622-Δ*fliM* biofilm morphology on urinary catheter grown in AUBK at 1 h, 3 h, 6 h and 24 h timepoint as observed under EDIC/EF microscope. Magnification x 1000. Scale bar = 10 µm.

J.7 Biofilm images of *P. aeruginosa* PAO1 mutant strain PW8621-Δ*pilA* (*pilA*-E01::IS*lacZ*/hah)

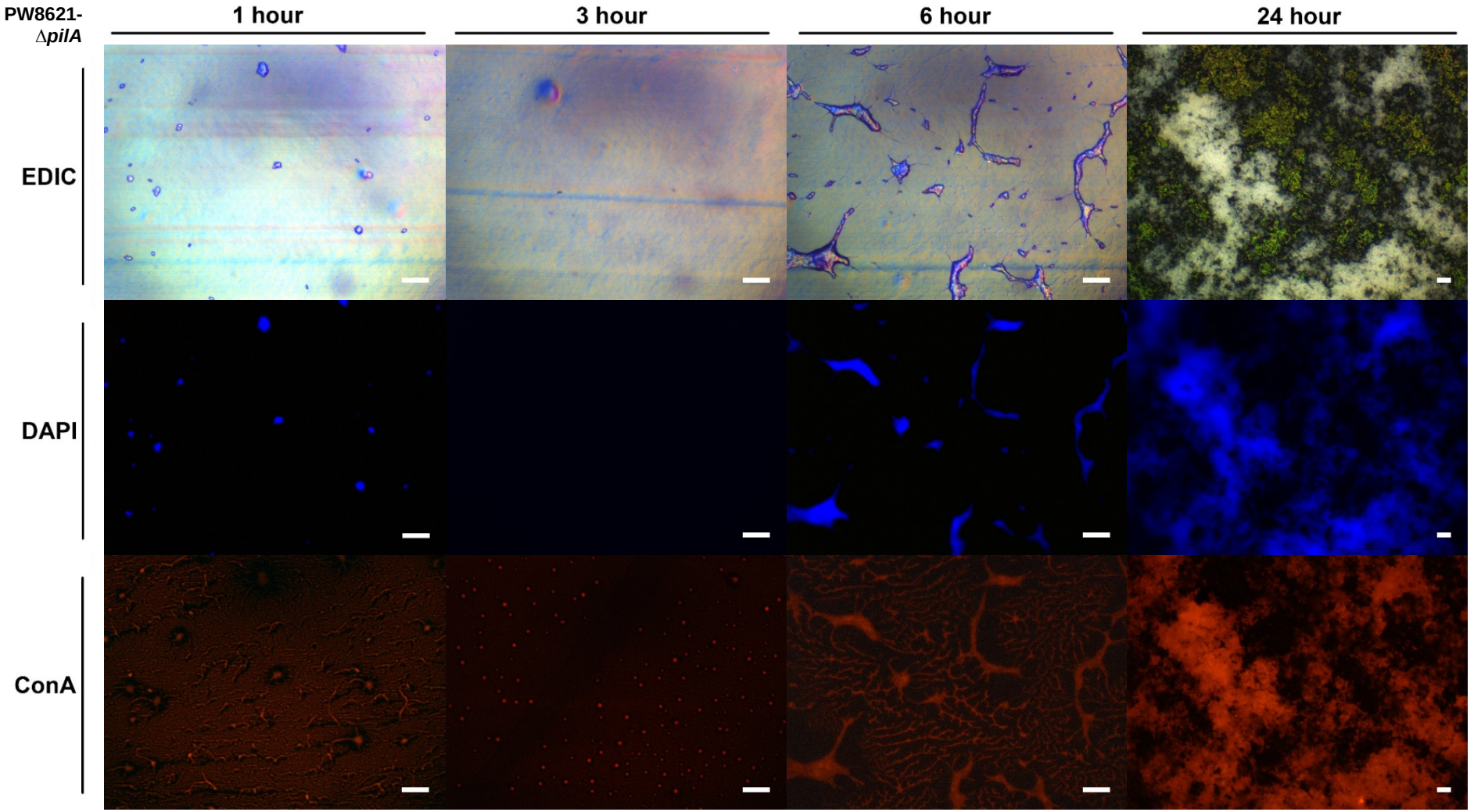

Figure K7 *P. aeruginosa* PAO1 mutant strain PW8621-Δ*pilA* biofilm morphology on urinary catheter grown in AUBK at 1 h, 3 h, 6 h and 24 h timepoint as observed under EDIC/EF microscope. Magnification x 1000 for 1 h, 3 h and 6 h. Magnification x 500 for 24 h Scale bar = 10 µm.

J.8 Biofilm images of *P. aeruginosa* PAO1 mutant strain PW8622-Δ*pilA* (*pilA*-H02::IS*phoA*/hah)

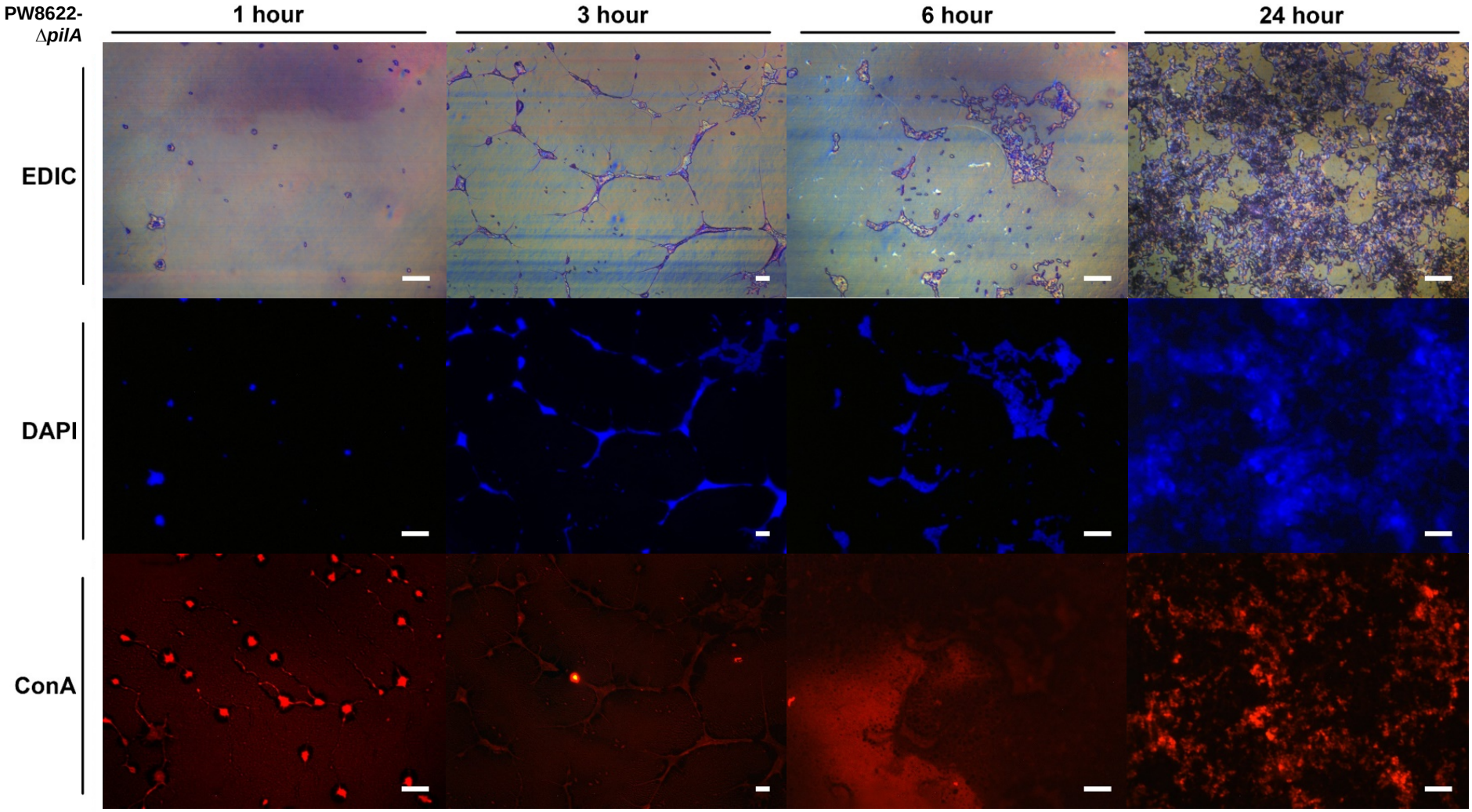

Figure K8 *P. aeruginosa* PAO1 mutant strain PW8622-Δ*pilA* biofilm morphology on urinary catheter grown in AUBK at 1 h, 3 h, 6 h and 24 h timepoint as observed under EDIC/EF microscope. Magnification x 1000 for 1 h, 6 h and 24 h. Magnification x 500 for 3 h. Scale bar = 10 µm.

J.9 Biofilm images of *P. aeruginosa* PAO1 mutant strain PW7438-Δ*pilF* (*pilF*-E10::IS*phoA*/hah)

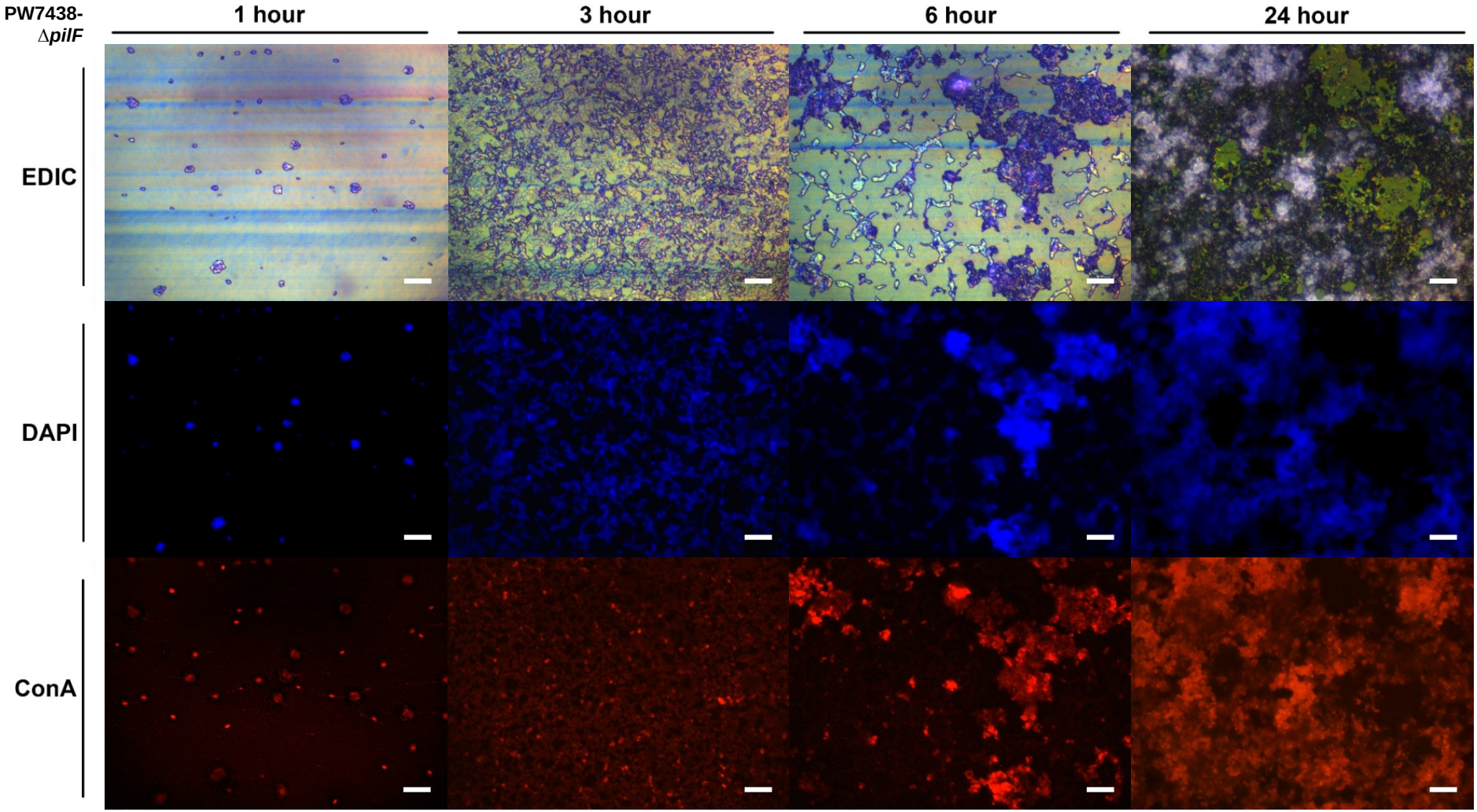

Figure J9 *P. aeruginosa* PAO1 mutant strain PW7438-Δ*pilF* biofilm morphology on urinary catheter grown in AUBK at 1 h, 3 h, 6 h and 24 h timepoint as observed under EDIC/EF microscope. Magnification x 1000. Scale bar = 10 µm.

J.10 Biofilm images of *P. aeruginosa* PAO1 knockout mutant strain Δ*fliC*

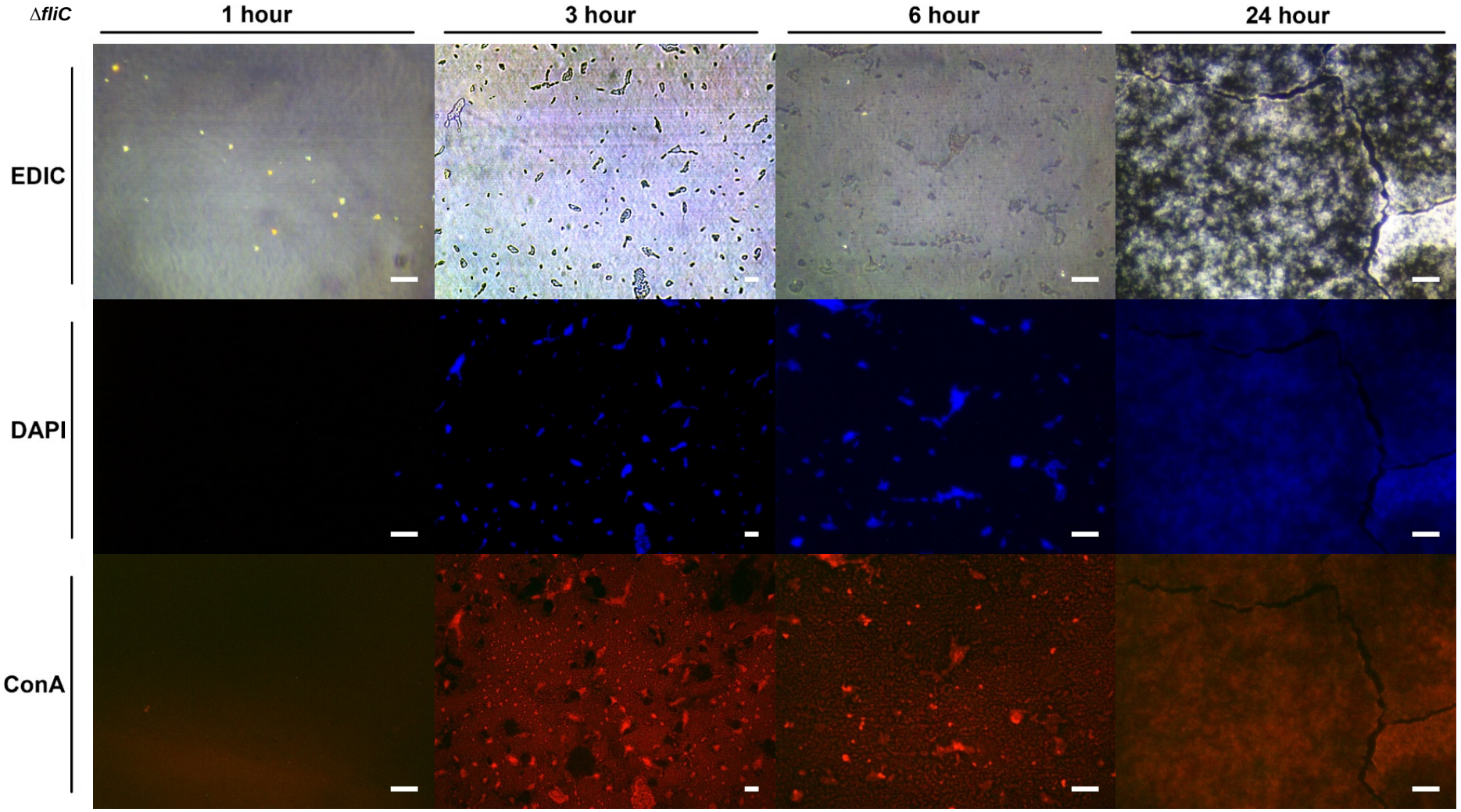

Figure J10 *P. aeruginosa* PAO1 knockout mutant strain Δ*fliC* biofilm morphology on urinary catheter grown in AUBK at 1 h, 3 h, 6 h and 24 h timepoint as observed under EDIC/EF microscope. Magnification x 1000 for 1 h, 6 h and 24 h. Magnification x 500 for 3 h. Scale bar = 10 µm.

J.11 Biofilm images of *P. aeruginosa* PAO1 knockout mutant strain Δ*pilA*

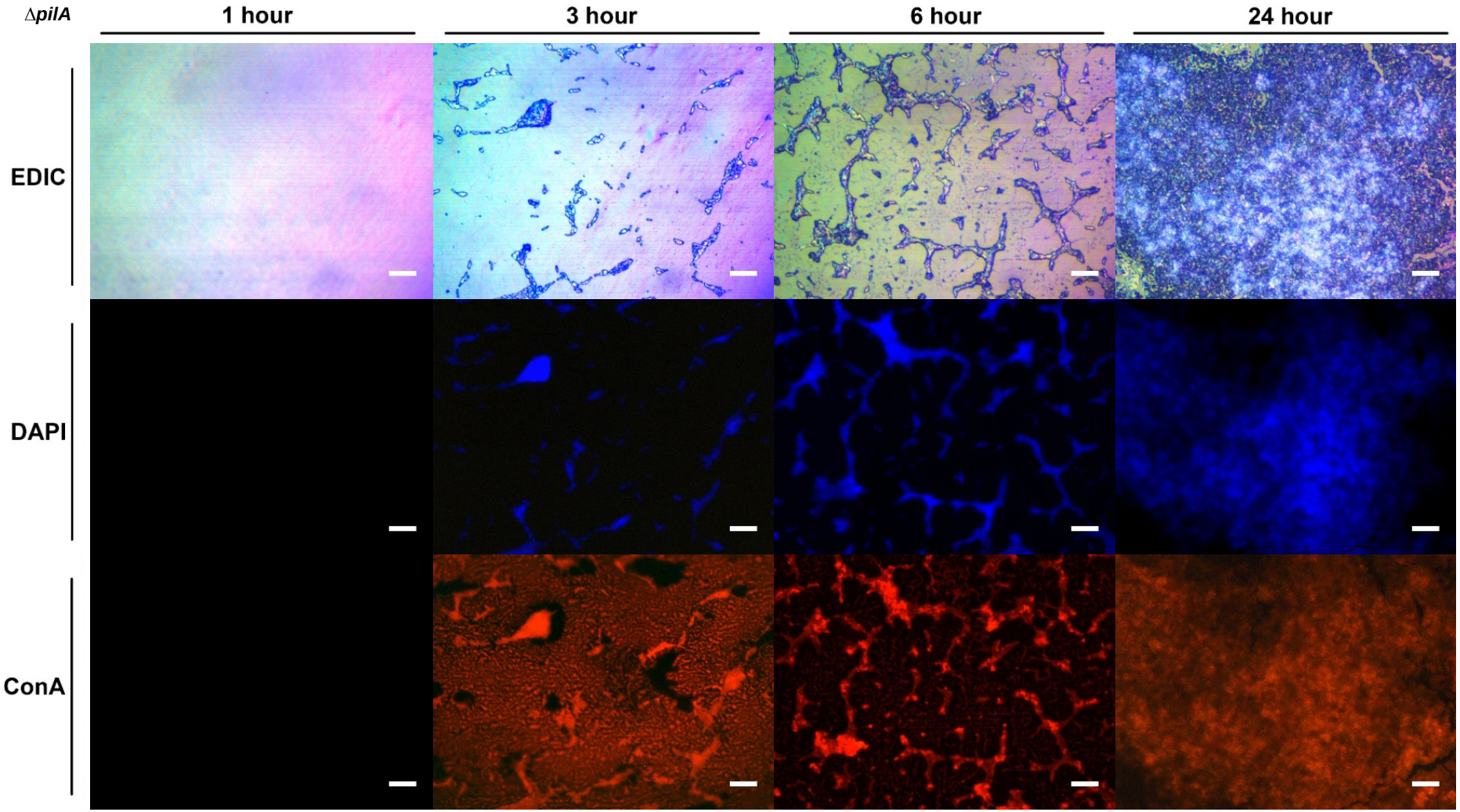

Figure J11 *P. aeruginosa* PAO1 knockout mutant strain Δ*pilA* biofilm morphology on urinary catheter grown in AUBK at 1 h, 3 h, 6 h and 24 h timepoint as observed under EDIC/EF microscope. Magnification x 1000. Scale bar = 10 µm.

J.12 Biofilm images of *P. aeruginosa* PAO1 double knockout mutant strain Δ*fliC*Δ*pilA*

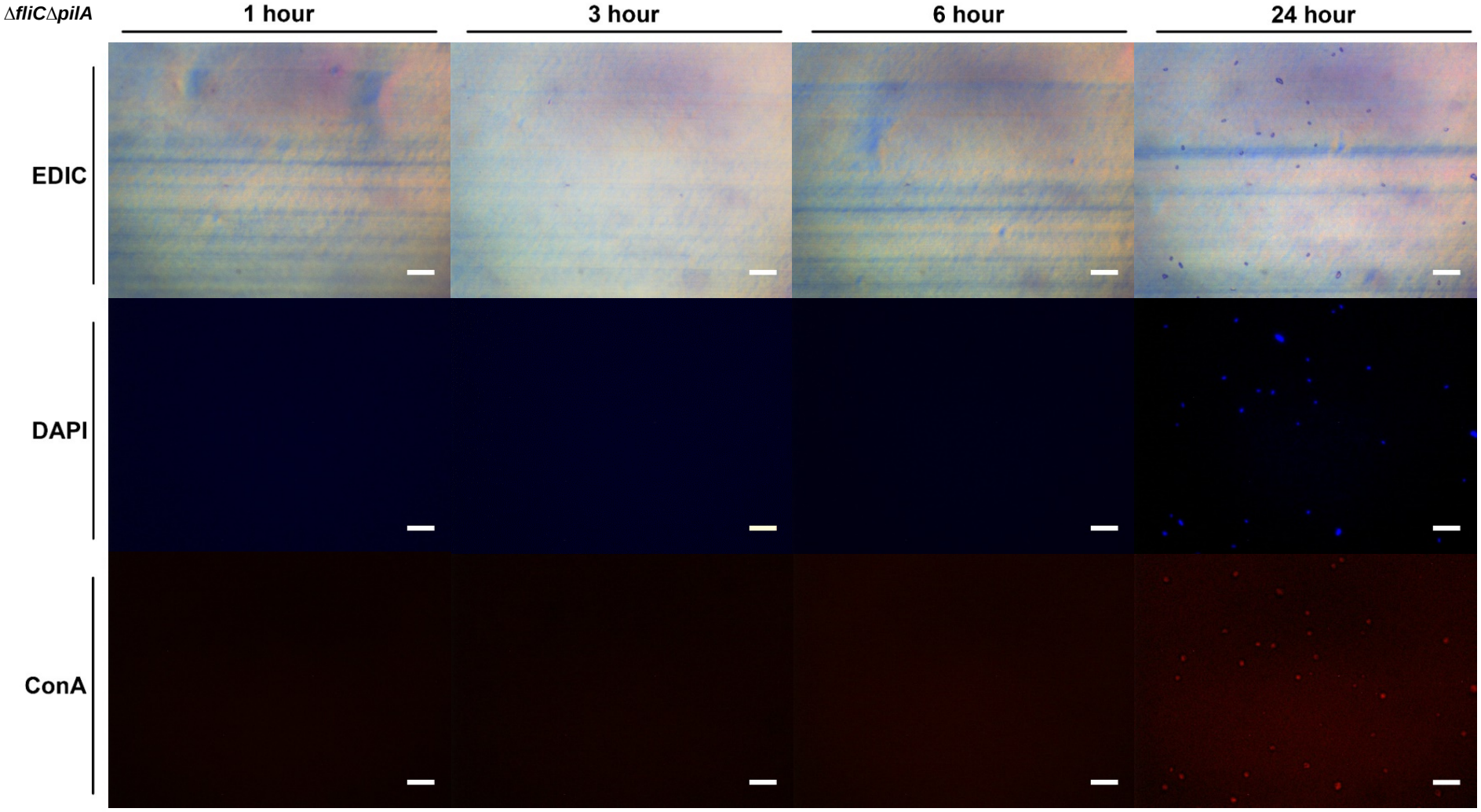

Figure J12 *P. aeruginosa* PAO1 double knockout mutant strain Δ*fliC*Δ*pilA* biofilm morphology on urinary catheter grown in AUBK at 1 h, 3 h, 6 h and 24 h timepoint as observed under EDIC/EF microscope. Magnification x 1000. Scale bar = 10 µm.

Appendix K Protein homology structure model simulation

Table K-1 Homology structure modelling simulation details

									Main oligo-structure		Other oligo-structure	
No.	**Target Protein**	**Strain**	**Transposon (Position)**	**SWISS-MODEL template**	**Total AA**	**Coverage**	**Seq. Identity**	**Seq Similarity**	**Oligo-state**	**Range**	**Oligo-state**	**Range**
1.	FliA	WT	-	1rp3.1.A	247	0.89	35.91%	0.89	RNA polymerase sigma factor FliA	9-233 (247)	-	-
2.		PW3643-Δ*fliA*	IS*lacZ*/hah[†] 556 (744)		191	0.87	27.14%	0.35	RNA polymerase sigma factor FliA	18-186 (191)	-	-
3.	FliC	WT	-	5wk6.1.A	488	1.00	99.80%	0.58	B-type flagellin FliC	5-488 (488)	-	-
4.		PW2970-Δ*fliC*	IS*lacZ*/hah 820 (1467)		1330	0.21	100.00%	0.58	B-type flagellin FliC	5-168 (1330)	Beta galactosidase	316-1330 (1330)
5.		PW2971-Δ*fliC*	IS*phoA*/hah 334 (1467)		116	0.97	100.00%	0.58	B-type flagellin FliC	5-112 (116)	-	-
6.	FliM	WT	-	4gc8.1.A	323	0.63	26.60%	0.34	Flagellar motor switch protein FliM	45-229 (323)	Flagellar motor switch protein FliN fragment	243-320 (323)
7.		PW3621-Δ*fliM*	IS*lacZ*/hah[†] 547(972)		188	0.83	28.21%	0.35	Flagellar motor switch protein FliM	45-187 (188)	-	-
8.		PW3622-Δ*fliM*	IS*phoA*/hah 839 (972)		762	0.25	29.47%	0.36	Flagellar motor switch protein FliM	45-225 (762)	Putative flagellar motor switch protein FliN Alkaline phosphatase	246-318 (762) 318-762 (762)
9.	PilA	WT	-	1oqw.2.A	149	0.94	67.86%	0.48	Type 4 fimbrial precursor PilA	7-147 (149)	-	-
10.		PW8621-Δ*pilA*	IS*lacZ*/hah 222 (450)		74	0.81	88.52%	0.55	Type 4 fimbrial precursor PilA	7-70 (74)	-	-
11.		PW8622-Δ*pilA*	IS*phoA*/hah 164 (450)		537	0.09	95.83%	0.57	Type 4 fimbrial precursor PilA	7-54 (537)	Alkaline phosphatase	93-537 (537)
12.	PilF	WT	-	2ho1.1.A	252	0.92	100.00%	0.60	Type 4 fimbrial biogenesis protein PilF	31-252 (252)	-	-
13.		PW7438-Δ*pilF*	IS*phoA*/hah 633 (759)		269	0.71	100.00%	0.60	Type 4 fimbrial biogenesis protein PilF	31-213 (269)	-	-